The influence of nitrogen inputs on the oxygen dynamics of the North Sea

Dissertation
with the aim of achieving
a doctoral degree
at the Faculty of Mathematics,
Informatics and Natural Sciences
Department of Earth Sciences
of Universität Hamburg

submitted by
Fabian Große
Hamburg, January 2017

1. Reviewer: Dr. habil. Thomas Pohlmann
Institute of Oceanography
Universität Hamburg

2. Reviewer: Prof. Dr. Myron Peck
Institute for Hydrobiology and Fisheries Science
Universität Hamburg

The defence took place on 12 May 2017.

Corrected version.

"La science, mon garçon, est faite d'erreurs,
mais d'erreurs qu'il est bon de commettre,
car elles mènent peu à peu à la vérité."

"Science, my lad, is made up of mistakes,
but they are mistakes which it is useful to make,
because they lead little by little to the truth."

'La voyage au centre de la terre'
Jules Verne (1828–1905)

Abstract

This study presents a detailed, model-based analysis of the North Sea oxygen (O_2) dynamics in recent years. Special focus is put on the physico-biochemical interactions controlling the evolution of O_2 deficiency (i.e., O_2 concentrations $<6\,\mathrm{mg\,O_2\,L^{-1}}$) during seasonal stratification and the role of nitrogen (N) inputs from external sources. A three-dimensional model system, consisting of the physical model HAMSOM and the biogeochemical model ECOHAM, is applied to the North Sea region for the period 2000–2014 using realistic forcing data ('reference run').

Furthermore, a nutrient tracing method, called 'trans-boundary nutrient transports' (TBNT), is applied to N originating from different riverine and non-riverine sources. The TBNT method is expanded by a direct link of O_2-consuming processes to individual N sources. By this, for the first time a detailed, quantitative analysis of the influences of individual N sources on the O_2 conditions in the North Sea is presented. This is especially useful for a reliable estimation of the potential of riverine N reductions as a measure for mitigating eutrophication and O_2 deficiency in the North Sea.

The validation against *in situ* observations demonstrates that the model provides reasonable skill in representing the main features of the North Sea physics and biochemistry. However, seasonal stratification is slightly underestimated, resulting in a slight overestimation of bottom O_2 concentrations in some regions.

The qualitative analysis of summer O_2 concentrations and potential influencing factors identifies the following key factors controlling O_2: (sufficiently long) seasonal stratification as a prerequisite, high net primary production (NPP) as the major source of organic matter, and the size of the sub-thermocline volume (V_{sub}). Consequently, the North Sea can be subdivided into three different types in terms of O_2: (1) a highly productive, non-stratified coastal zone, (2) a productive, seasonally stratified zone with a small $V_{\mathrm{sub},}$ and (3) a productive, seasonally stratified zone with a large $V_{\mathrm{sub.}}$ Type 2 is identified to be most susceptible to O_2 deficiency and extends over wide parts of the southern and eastern central North Sea.

Lowest simulated O_2 concentrations of less than $5.2\,\mathrm{mg\,O_2\,L^{-1}}$ occur in the eastern central North Sea (about 56 °N, 6 °E; O_2 deficiency zone: ODZ) in 2002. O_2 mass balances show that aerobic remineralisation accounts for roughly 85 % of gross O_2 consumption (GOC) in the pelagic bottom layer of this region. The comparison to other regions suggests that the relative contributions of the different O_2-consuming processes in the bottom layer at a certain location depend on the water column depth, independent of the overall GOC.

It is further shown that NPP controls the year-to-year variability in the bottom O_2 conditions. Increased NPP enhances directly and indirectly (due to enhanced zooplankton

growth/mortality) organic matter export below the thermocline. Enhanced zooplankton growth additionally increases GOC due to respiration. The overall increase in organic matter export results in stronger bacterial remineralisation which in turn triggers nitrification. Although counter-intuitive, even events of strong mixing, that cause a complete renewal of bottom O_2, can result in a net decrease in bottom O_2 (in the sequel of the event) due to the enhancement of NPP and downward mixing of organic matter.

The TBNT analysis reveals that GOC in the entire northern North Sea and most of the central regions is dominated by the North Atlantic N supply across the northern shelf edge. In contrast, the southern North Sea underlies a strong influence of the large Dutch (NL-1; Rhine and Meuse) and German (DE; Elbe, Ems, Weser), but also British rivers (UK-2; at the British east coast). Here, atmospheric N deposition also constitutes a remarkable source strongly affected by anthropogenic emissions.

Consequently, most of the GOC in the ODZ of the North Sea can be attributed to these N sources (roughly 85 %). The North Atlantic accounts for the major contribution of about 41 % averaged over 2000–2014. Atmospheric deposition and the main riverine sources contribute about 16 %, 10 % (NL-1), 11 % (DE) and 7 % (UK-2), respectively. The overall riverine contribution to GOC in the ODZ results in about 38 %. This suggests that riverine N reductions may have a relevant positive effect on O_2 in the ODZ, provided carefully defined reduction targets.

This is confirmed by a model scenario using N reductions ('reduction run') compliant with the European Union's Water Framework Directive (WFD). According to WFD implementation plans, zero and 5 % reductions in N are applied to the British and Dutch rivers, respectively, relative to the loads of the reference run. High N reductions (consistent with a concentration of total N of $2.8\,\mathrm{mg\,N\,L^{-1}}$) are applied to the German rivers. Also, high reductions are applied to the French rivers and the Scheldt (50 % and 37 %, respectively).

Due to the only minor reductions in the NL-1 and UK-2 rivers, minimum O_2 concentrations increased by only $0.3\,\mathrm{mg\,O_2\,L^{-1}}$ in the ODZ relative to the reference run. This increase results mainly from the high reductions in the German rivers. In the 'Oyster Grounds' (about 54.5 °N, 3 °E) – a region well known for being susceptible to O_2 deficiency – the improvements are even less due to the large influence of the NL-1 and UK-2 rivers and the only minor N reductions. This suggests that WFD-compliant N reduction targets require revision.

However, the results demonstrate the principally high potential of optimised riverine N reductions for improving the O_2 conditions of the North Sea. Thus, these efforts likely constitute a potent means to support the improvement or mitigate the degradation of O_2 conditions induced by still uncertain effects of climate change. Especially, in combination with the expected future reduction in atmospheric N deposition.

Zusammenfassung

Die vorliegende Arbeit stellt eine detaillierte, modellgestützte Analyse der Sauerstoffdynamik (O_2) der Nordsee in der jüngeren Vergangenheit dar. Der Fokus liegt dabei auf der Analyse des Zusammenwirkens der physikalischen und biochemischen Prozesse, die zur Ausbildung eines O_2-Defizits (d.h., O_2-Konzentration $<6\,\mathrm{mg\,O_2\,L^{-1}}$) während saisonaler Schichtung führen, sowie der Rolle von Stickstoffeinträgen (N) äußerer Quellen, wie z.B. Flüssen. Hierzu wird ein dreidimensionales Modellsystem – bestehend aus dem physikalischen Modell HAMSOM und dem biogeochemischen Modell ECOHAM – unter Verwendung realistischer Antriebsdaten für den Zeitraum 2000–2014 auf die Nordsee angewendet (‚Referenzlauf').

Zudem wird eine Methode zur Verfolgung von Nährstoffeinträgen – genannt ‚transboundary nutrient transports' (TBNT; dt.: ‚grenzüberschreitende Nährstofftransporte') – auf N angewendet, welcher durch Flüsse und andere Quellen in die Nordsee eingetragen wird. Die TBNT-Methode wird dahingehend erweitert, die O_2 verbrauchenden Prozesse an die einzelnen N-Einträge zu koppeln. Damit ist es erstmals möglich, die Einflüsse individueller N-Einträge auf die O_2-Dynamik der Nordsee zu quantifizieren. Dies ist insbesondere für die zuverlässige Abschätzung der Wirksamkeit von N-Reduktionen in Flüssen relevant.

Die Validation mit *In-situ*-Messungen zeigt, dass das Modellsystem die wesentlichen Strukturen der Physik und Biochemie der Nordsee gut abbildet. Lediglich die saisonale Schichtung wird etwas unterschätzt, was in einigen Regionen zu einer Überschätzung der bodennahen O_2-Konzentrationen führt.

Die qualitative Analyse sommerlicher O_2-Konzentrationen und möglicher Einflussgrößen identifiziert folgende Größen als ausschlaggebend für die Entwicklung des O_2: (hinreichend lang anhaltende) saisonale Schichtung als Grundvoraussetzung, hohe Nettoprimärproduktion (NPP) als die wesentliche Quelle für organische Substanz sowie die Größe des Volumens unterhalb der Sprungschicht (V_{sub}). Daraus ergibt sich eine regionale Unterteilung der Nordsee in drei verschiedene Typen in Bezug auf O_2: (1) eine sehr produktive, nicht geschichtete Küstenzone, (2) eine produktive, saisonal geschichtete Zone mit einem kleinen V_{sub} und (3) eine produktive, saisonal geschichtete Zone mit einem großen V_{sub}. Typ 2 erweist sich als besonders anfällig für die Bildung eines O_2-Defizits und erstreckt sich über weite Teile der südlichen und östlichen, zentralen Nordsee.

Die Simulation weist die geringsten O_2-Konzentrationen ($<5{,}2\,\mathrm{mg\,O_2\,L^{-1}}$) in der östlichen, zentralen Nordsee (bei etwa 56 °N, 6 °O; O_2-Defizitzone: ODZ) im Jahr 2002 auf. O_2-Massenbilanzen zeigen, dass die aerobe Remineralisierung für etwa 85 % des Bruttosauerstoffverbrauchs (GOC; engl.: gross O_2 consumption) in der pelagischen Bodenschicht dieser Region verantwortlich ist. Der Vergleich mit anderen Regionen legt nahe, dass die

relativen Beiträge der verschiedenen O_2 verbrauchenden Prozesse in der Bodenschicht einer bestimmten Region von deren Wassertiefe abhängen und unabhängig vom Absolutwert des GOC sind.

Weiterhin wird gezeigt, dass die NPP die jährlichen Schwankungen in den bodennahen O_2-Bedingungen steuert. Die erhöhte NPP verstärkt auf direkte und indirekte Weise (aufgrund verstärkten Zooplanktonwachstums/-sterbens) den Export organischer Substanz in die Regionen unterhalb der Sprungschicht. Das verstärkte Zooplanktonwachstum bewirkt zudem eine Zunahme des GOC aufgrund höherer Veratmung. Diese Gesamtzunahme im Export organischer Substanz resultiert in erhöhter bakterieller Remineralisierung, welche wiederum die Nitrifizierung anregt. Zudem zeigt sich der unerwartete Effekt, dass selbst Ereignisse starker Vermischung, welche zunächst eine vollständige Erneuerung des Boden-O_2 herbeiführen, aufgrund der erhöhten NPP und des zusätzlichen Exports von organischer Substanz in einer Nettoabnahme des Boden-O_2 resultieren können.

Die TBNT-Analyse offenbart, dass der N-Eintrag des Nordatlantiks über die nördliche Schelfkante den GOC in der gesamten nördlichen Nordsee und den meisten zentral gelegenen Regionen dominiert. Hingegen unterliegt die südliche Nordsee einem starken Einfluss der Einträge aus den großen niederländischen (NL-1; Rhein und Maas) und deutschen (DE; Elbe, Ems, Weser), aber auch britischen Flüssen (UK-2; an der britischen Ostküste). Hier spielt zudem die atmosphärische N-Deposition, welche stark anthropogen beeinflusst ist, eine wesentliche Rolle.

Folglich ist der Großteil des GOC in der ODZ der Nordsee den genannten N-Quellen zuzuordnen (etwa 85 %). Der nordatlantische Eintrag trägt gemittelt über 2000–2014 etwa 41 % bei. Die atmosphärische Deposition und die Einträge der wichtigsten Flüsse tragen jeweils etwa 16 %, 10 % (NL-1), 11 % (DE) und 7 % (UK-2) bei. Der Gesamtbeitrag der N-Einträge aus Flüssen zum GOC in der ODZ beläuft sich auf ungefähr 38 %. Dies zeigt, dass N-Reduktionen in den Flusseinträgen durchaus einen relevanten, positiven Effekt auf die O_2-Bedingungen der ODZ haben können – sorgsam definierte Reduktionsziele vorausgesetzt.

Dies wird durch ein Modellszenario untermauert, welches N-Reduktionen (‚Reduktionslauf‘) entsprechend der Wasserrahmenrichtlinie (WFD; engl.: Water Framework Directive) der Europäischen Union anwendet. Nach den geplanten WFD-Maßnahmen werden in den britischen Flüssen keine und in den niederländischen Flüssen nur geringe (5 %) N-Reduktionen gegenüber dem Referenzlauf vorgenommen. Im Vergleich dazu sind die Reduktionen in den deutschen Flüssen, welche sich aus einer Zielkonzentration für Gesamt-N im Fluss von $2{,}8\,\mathrm{mg\,N\,L^{-1}}$ ergeben, relativ hoch. Ebenfalls hohe Reduktionen werden in den französischen Flüssen (50 %) und der Schelde (37 %) vorgenommen.

Infolge der nur geringen Reduktionen in den NL-1- und UK-2-Flüssen erhöhen sich

die minimalen O_2-Konzentrationen in der ODZ nur um maximal $0{,}3\,\mathrm{mg\,O_2\,L^{-1}}$ verglichen zum Referenzlauf. Diese Zunahme ist im Wesentlichen auf die hohen Reduktionen in den deutschen Flüssen zurückzuführen. In den ‚Oyster Grounds' (etwa 54,5 °N, 3 °O) – eine Region, die bekanntermaßen anfällig für ein O_2-Defizit ist – fällt die Verbesserung aufgrund des noch höheren Einflusses der NL-1- und UK-2-Flüsse und der geringen N-Reduktionen sogar noch geringer aus. Dies legt nahe, dass eine Überarbeitung der WFD-konformen N-Reduktionsziele erforderlich ist.

Die Ergebnisse veranschaulichen dennoch das grundsätzlich hohe Potenzial abgestimmter N-Reduktionen in Flüssen für die Verbesserung der O_2-Bedingungen der Nordsee. Daher stellen diese Bestrebungen mit hoher Wahrscheinlichkeit ein wirksames Mittel dar, um die Verbesserung der O_2-Bedingungen zu unterstützen oder ihre Verschlechterung abzuschwächen, welche sich durch die weiterhin unsicheren Auswirkungen des Klimawandels ergeben können. Dies gilt insbesondere im Zusammenspiel mit der zu erwartenden, zukünftigen Reduktion der atmosphärischen N-Deposition.

Contents

Chapter 1

Introduction

The availability of dissolved oxygen (O_2) in marine waters is crucial for the metabolism of many marine species, including fishes and invertebrates (e.g., Rosenberg et al., 1991; Díaz and Rosenberg, 1995). Low O_2 conditions with concentrations of less $2\,\mathrm{mg\,O_2\,L^{-1}}$, often referred to as hypoxia (e.g., Tyson and Pearson, 1991; Rabalais et al., 2002a), constitute a major stressor to marine species and can have a severe impact on the biodiversity of an ecosystem (Gray et al., 2002; Vaquer-Sunyer and Duarte, 2008; Friedrich et al., 2014). Several studies show that the O_2 conditions in the global ocean aggravated during the past decades (e.g., Díaz and Rosenberg, 2008; Stramma et al., 2008; Falkowski et al., 2011; Helm et al., 2011). Therefore, the assessment of the O_2 conditions and the investigation of the processes, that influence the O_2 dynamics in the different regions of the global ocean, is essential in order to detect regions susceptible to low O_2 conditions, and to develop potential management strategies to maintain or improve the status of these regions in terms of O_2.

In principle, the availability of O_2 in marine waters is controlled by both, physical and biochemical processes and factors. On the side of the physical factors, the solubility of O_2 in seawater depends on the water temperature (T) and salinity (S) and decreases with increasing T or S (e.g., Benson and Krause, 1984). Furthermore, the exchange of O_2 at the interface between atmosphere and ocean influences the O_2 availability in the ocean surface layer. It is driven by the local winds and the difference between the O_2 saturation concentration of the atmosphere and the O_2 concentration at the surface (e.g., Wanninkhof, 1992). In the interior ocean, advection of oxygenated (i.e., O_2-rich) and deoxygenated water masses affects the spreading of high- and low-O_2 waters, respectively, as well as the vertical mixing of O_2 from the oxygenated surface waters into the deeper layers. In regions, where (seasonal or perennial) stratification occurs, the mixing-induced diapycnal, vertical exchange of O_2 can be reduced significantly due to less strong mixing. While the latter two processes only affect the spreading of O_2 within the ocean interior, the exchange between the atmosphere and the ocean constitutes the only physical source process for O_2 within the marine system.

Considering the biochemical processes affecting O_2, photosynthesis by autotroph organisms (e.g., phytoplankton) represents a major source process for O_2 in marine waters. In

contrast, other biochemical processes, like respiration by bacteria, zooplankton or higher trophic species, as well as nitrification, consume O_2. As photosynthesis only occurs in the euphotic upper layer of the ocean while respiratory processes also take place in the aphotic zone, the O_2 concentration of a water body principally tends to decrease the longer it is away from the sea surface. Here, aerobic remineralisation of dead organic matter is considered the major O_2-consuming process (e.g., Díaz and Rosenberg, 2008). A summary of the physical and biochemical processes affecting O_2 concentrations is provided by Peña et al. (2010).

The spatial distribution of sub-surface O_2 in the global ocean reveals distinct spatial patterns with regions of high and low O_2 concentrations (Falkowski et al., 2011, therein Fig. 1). High sub-surface O_2 concentrations can be found in high latitudes in regions of deep water formation (e.g., Labrador Sea). In contrast, lowest O_2 concentrations of even less than $0.3\,\mathrm{mg\,O_2\,L^{-1}}$ occur in the northern Indian Ocean (around 800 m depth) and the tropical East Pacific Ocean (in 100 m–400 m depth) (Stramma et al., 2010). These regions are often referred to as oxygen minimum zones (OMZ). The very low sub-surface O_2 concentrations in these regions result from the combination of high upper-ocean productivity, resulting in high O_2 consumption due to aerobic organic matter remineralisation, and only weak advective ventilation (Stramma et al., 2008). Trends of decreasing O_2 were found for these regions over the past 50–60 years (Stramma et al., 2008; Falkowski et al., 2011).

Helm et al. (2011) also report a decrease in the average O_2 concentration of the global ocean by roughly $0.03\,\mathrm{mg\,O_2\,L^{-1}}$ between 1970 and 1990. They attribute about 15 % of this global O_2 decrease to an increase in mixed layer T, which reduces the surface ocean's O_2 storage capacity, and suggest that the remainder can be explained by an overall decrease in the exchange between surface waters and the ocean interior due to enhanced stratification caused by warmer surface waters. The continuation of this decrease (Stramma et al., 2008; Frölicher et al., 2009; Falkowski et al., 2011) implies the expansion of the OMZs in the global ocean, which may have significant impact on a global scale as anoxic conditions (i.e., the complete depletion of O_2) support the marine production of nitrous oxide (N_2O; Naqvi et al., 2000), a greenhouse gas with high global warming potential. Consequently, the decrease in marine O_2 concentrations due to global warming could result in a positive feedback on the global T increase.

The expansion of the OMZs and the overall decrease in the average O_2 concentration of the global ocean will possibly also affect the O_2 conditions on shelf ecosystems influenced by deep-water upwelling (Stramma et al., 2010). However, at the present day coastal and shelf ecosystems across the entire globe already experience low O_2 condition, partly driven naturally and partly due to direct and indirect anthropogenic pressures (Díaz and Rosenberg, 2008; Rabalais et al., 2010). These changes in the O_2 conditions in the shelf

seas are reported to be significantly stronger than in the open ocean (about 10 times faster during 1976–2000; Gilbert et al., 2010).

Therefore, the investigation of the drivers and processes controlling O_2 conditions in coastal and shelf seas constitutes an important subject, especially in the context of anthropogenic influences and potential changes under a changing climate.

1.1 Low oxygen conditions in shelf seas

Like in the open ocean, the evolution of O_2 concentrations in shelf seas is controlled by the balance between O_2 supply, due to exchange with the atmosphere and internal ventilation as well as primary production (PP), and O_2 consumption due to biochemical processes. Shelf sea hypoxia can form naturally in upwelling regions (e.g., Dugdale et al., 1977; Chapman and Shannon, 1985), isolated deep basins and fjords (Levin et al., 2009; Rabalais et al., 2010) or estuaries (e.g., Cooper and Brush, 1993; Zimmerman and Canuel, 2002). In most shelf seas affected by hypoxia, seasonal or perennial stratification has a strong influence on the evolution of these low O_2 conditions (Díaz, 2001; Díaz and Rosenberg, 2008; Friedrich et al., 2014), as it separates the oxygenated surface waters from the sub-pycnocline waters, dominated by O_2 consumption (e.g., Díaz, 2001; Greenwood et al., 2010; O'Boyle and Nolan, 2010).

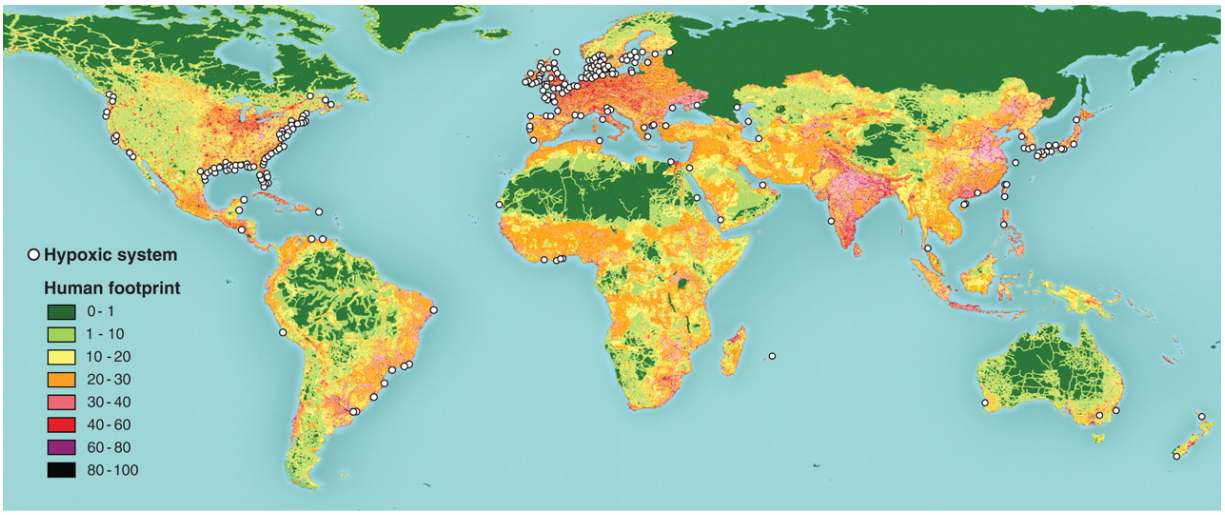

Figure 1.1: Global distribution of scientifically reported eutrophication-associated O_2 minimum zones (white circles), and human footprint (coloured map; in %) according to Sanderson et al. (2002). From Díaz and Rosenberg (2008). Reprinted with permission from the American Association for the Advancement of Science (AAAS).

Historic occurrences of hypoxia – before industrialisation gathered pace in the mid-19$^{\text{th}}$

century – are reported for only a few ecosystems, e.g., the Baltic Sea (Zillén et al., 2008) or Chesapeake Bay (Cooper and Brush, 1993; Zimmerman and Canuel, 2002). In most coastal ecosystems, hypoxia can be considered as a symptom of more recent decades (which, however, may also relate to a lack of studies in other ecosystems affected by hypoxia). Díaz and Rosenberg (2008) reported an exponential increase in hypoxia in marginal seas since the 1960s and found more than 400 coastal marine ecosystems, that are scientifically reported to be affected by hypoxia (see Fig. 1.1, white dots). They attributed this increase to increasing eutrophication, i.e., the riverine input of excess nutrients, nitrogen (N) and phosphorus (P), resulting in enhanced PP (Jickells, 1998) and, consequently, increased O_2 consumption. Díaz (2001) summarised the eutrophication-associated process chain, that leads to the evolution of hypoxia in shelf seas, as follows: PP is increased by excess nutrient input, resulting in additional amounts of organic matter. Due to the shallow water depth, much of this organic matter then sinks to the bottom. In case of stratification, hypoxia evolves as the result of enhanced O_2 consumption during the bacterial degradation of organic matter near the seafloor and the limited ventilation of the sub-pycnocline layers.

In the last decades, world's largest eutrophication-associated hypoxic zones in shelf seas were found in the Baltic Sea (up to 100,000 km^2; Rosenberg, 1985), the northwestern shelf of the Black Sea (up to 40,000 km^2; Mee, 2006) and in the northern Gulf of Mexico (up to 22,000 km^2; Rabalais and Turner, 2001). While Black Sea hypoxia has almost vanished since the early 1990s due to strong reductions in riverine nutrient loads (Mee, 2006), no clear reduction in the hypoxic area is reported for the Gulf of Mexico until 2013 (Mississippi River Gulf of Mexico Watershed Nutrient Task Force, 2013), and even an increase is found for the Baltic Sea since the early 1990s (Carstensen et al., 2014a,b).

Besides eutrophication, higher carbon dioxide (CO_2) emissions and associated climate change impacts may additionally influence the future O_2 conditions in these marine ecosystems (e.g., Justić et al., 1996, 2003; Stigebrandt and Gustafsson, 2003; Neumann, 2010). Because of the negative implications of hypoxia for the marine fauna (e.g., Díaz and Rosenberg, 1995; Vaquer-Sunyer and Duarte, 2008; Topcu et al., 2009; Friedrich et al., 2014) it is important to foster the understanding of the physico-biochemical interactions and anthropogenic influences that cause the evolution of hypoxia, in order to anticipate potential future changes in these ecosystems. This is of special importance in the context of the ecological management of marine ecosystems affected by hypoxia as nutrient reductions measures in major tributaries may positively influence future O_2 conditions in eutrophic shelf seas (e.g. Paerl, 2006; Conley et al., 2009; Kemp et al., 2009; Paerl, 2009; Laurent and Fennel, 2014).

1.1.1 Oxygen conditions of the North Sea

In the North Sea – a northwestern European shelf sea – severe hypoxia was also observed in the German Bight in late summer 1982 resulting in death among benthic and demersal species, including fish (von Westernhagen and Dethlefsen, 1983). von Westernhagen and Dethlefsen (1983) also found this hypoxic event to coincide with pronounced stratification. Further occurrences of low O_2 conditions, although non-hypoxic (i.e., O_2 concentrations $\geq 2\,mg\,O_2\,L^{-1}$), in the early 1980s were reported by other studies (Rachor and Albrecht, 1983; Brockmann and Eberlein, 1986), observing O_2 concentrations of partly less than $3\,mg\,O_2\,L^{-1}$. These observations of low O_2 conditions, for the first time, raised the public awareness of low O_2 conditions in the North Sea. Further studies related these occurrences of low O_2 conditions in the German Bight to excess nutrient loads by the German rivers Elbe and Weser (Brockmann and Eberlein, 1986; Brockmann et al., 1988), but suggested that nutrient inputs from adjacent North Sea regions may also have contributed to these events of low O_2 conditions. Peeters et al. (1995) also found that low O_2 concentrations of about $4\,mg\,O_2\,L^{-1}$ in the Oyster Grounds in the late 1980s partly related to high riverine nutrient loads in combination with persistent stratification.

In consequence of the hypoxic conditions in the 1980s, the 2nd International Conference on the Protection of the North Sea (ICNS-2) declared in 1987 to "aim to achieve a substantial reduction (of the order of 50 %) in inputs of P and N to these areas between 1985 and 1995" (ICNS-2, 1988), in order to mitigate the effects of eutrophication in the North Sea. In 1992, the Oslo-Paris Convention for the Protection of the Marine Environment of the North-East Atlantic ('OSPAR convention'; OSPAR, 1992) was signed by all North Sea neighbouring countries (and others), which agreed that reduction measures should be applied to N and P compounds from land-based sources (including rivers; OSPAR, 1992). Since that, the P loads have been reduced by more than 50 % in most continental North Sea tributaries (including Rhine and Elbe), which also resulted in an improvement of the North Sea O_2 conditions and thus the benthic communities (e.g., Duineveld et al., 1991). However, riverine N loads were reduced to a clearly lesser extent (e.g., Artioli et al., 2008; Claussen et al., 2009; OSPAR, 2013a) and the North Sea O_2 conditions are still perturbed (Topcu and Brockmann, 2015).

In the context of the ecological management of the North Sea and other European shelf seas, OSPAR introduced a subdivision of low O_2 conditions into different degrees of severity within the so-called 'Common Procedure' (OSPAR, 2003, 2013b). According to this Common Procedure, marine waters are defined as 'O_2-deficient' in case of O_2 concentrations of less than $6\,mg\,O_2\,L^{-1}$ (OSPAR, 2005; Best et al., 2007; Claussen et al., 2009; OSPAR, 2013b) as negative effects on marine species can occur already at O_2 concentrations below this threshold (Gray et al., 2002). Following this definition, the term 'O_2

deficiency' is used in this thesis when referring to low O_2 conditions in the North Sea. The occurrence of O_2 deficiency constitutes a major indicator of eutrophication (category 3 indicator, i.e., "evidence of undesirable disturbance"; OSPAR, 2003) and directly results in the classification as a so-called 'problem area' in terms of eutrophication (Claussen et al., 2009).

The adoption of the European Union's (EU) Water Framework Directive (WFD; EU, 2000) in 2000 provided a legislative frame for the achievement or maintenance of a good status in limnic surface waters (i.e., in rivers and lakes) and in a narrow band of 12 nautical miles along the coasts. However, without specifying this good status and without considering the marine regions affected by O_2 deficiency. Therefore, the EU's Marine Strategy Framework Directive (MSFD; EU, 2008) was adopted in 2008. This legislation aims for the achievement or maintenance of a so-called 'good environmental status' in European marine waters. According to descriptor 5 'Eutrophication' of the MSFD, the good environmental status is – among other criteria – defined by the absence of O_2 deficiency in the considered marine ecosystem, following the definition of O_2 deficiency used by OSPAR (OSPAR, 2012).

Despite the significant reductions in riverine nutrient (especially P) loads since the early 1990s (Artioli et al., 2008; Claussen et al., 2009; OSPAR, 2013a), Topcu and Brockmann (2015) report the regular occurrence of seasonal O_2 deficiency in the southeastern North Sea up to recent years (see Fig. 1.2). Weston et al. (2008) even report almost hypoxic conditions in the Oyster Grounds region in late September/early October 2003. Thus, O_2 deficiency remains a persistent problem. According to Kemp et al. (2009) these events can be classified as 'persistent seasonal'. O_2 deficiency in the North Sea was less pronounced in recent years compared to the early 1980s. However, the potential negative, ecological impacts of O_2 deficiency on the marine fauna (Díaz and Rosenberg, 1995; Vaquer-Sunyer and Duarte, 2008; Topcu et al., 2009; Friedrich et al., 2014), require a comprehensive assessment of the current North Sea state in terms of O_2 deficiency.

However, O_2 measurements are sparse and either temporally or spatially limited (Große et al., 2016). Spatially resolved O_2 measurements give insight in the distributions of O_2 concentrations and in the spatial extent of O_2 deficiency, though, only in case of the appropriate timing of the measurements (Friedrich et al., 2014). In contrast, they do not provide information on the preceding evolution of O_2 concentrations in relation to physical and biochemical controls. Temporally resolved O_2 observations reveal the temporal evolution of O_2 concentrations, but require additional measurements of such quantities influencing the O_2 dynamics (e.g., hydrographic parameters like T and S) in order to allow for the interpretation of the physico-biochemical interactions that lead to the evolution of the observed O_2 concentrations.

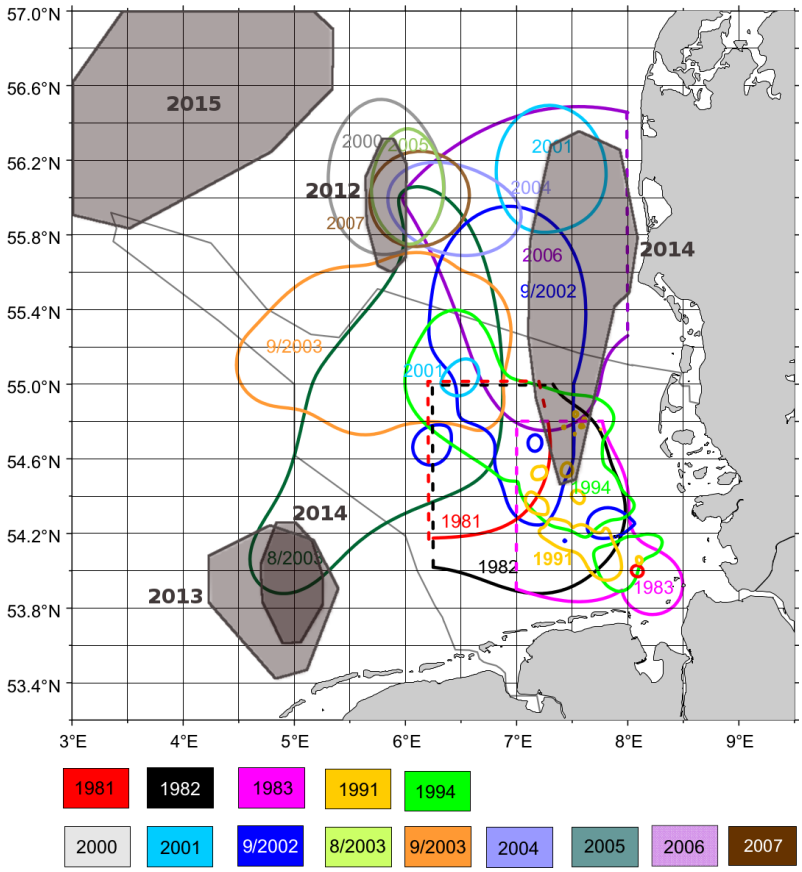

Figure 1.2: Spatial extent of observed O_2 deficiency (O_2 concentrations $<6\,\mathrm{mg\,O_2\,L^{-1}}$) in the southeastern North Sea during 1980–2015. Dotted lines indicate geographical limits of the individual surveys. Light grey line marks German exclusive economic zone. Main figure from Topcu and Brockmann (2015) (courtesy of Uwe Brockmann). Grey overlays derived from recent O_2 observations (courtesy of Sieglinde Weigelt-Krenz).

Only in recent years continuous measurements for the North Sea have become available, e.g., by the SmartBuoy programme of the Centre for Environment, Fisheries and Aquaculture Science (Cefas, UK; Mills et al., 2003) or the MARNET programme (MARine Monitoring NETwork in the North Sea and Baltic Sea) of the Federal Maritime and Hydrographic Agency (BSH, Germany). These monitoring programmes provide temporally highly resolved (at least daily) time series of O_2 and related parameters (e.g., T, S, chlorophyll) in different depths and allow for the analysis of the temporal evolution of stratification and O_2 concentrations at the monitoring site.

Greenwood et al. (2010) published the first data from continuous measurements of bottom O_2 concentrations (and supplemental parameters) at two North Sea sites ('North Dogger' and 'Oyster Grounds'). These time series constitute the first continuous measure-

ments in regions potentially affected by O_2 deficiency in a European shelf sea (Greenwood et al., 2010). They allowed for the first detailed analysis of the processes controlling the evolution of low bottom O_2 under stratified conditions in the North Sea, as well as the rapid recovery of bottom O_2 concentrations after the breakdown of stratification in autumn. However, even these temporally highly resolved measurements did not provide sufficient information to fully understand the physico-biochemical interactions that caused the observed O_2 evolution. Queste et al. (2013), who extended the locally confined findings by Greenwood et al. (2010) to the spatial scale using survey data from August 2010 and ICES historical data, refer to "plausible mechanisms" like vertical mixing or advection when the measurements could not be explained in detail. In consequence, Greenwood et al. (2010) stated, that the observations provided insight into the processes affecting the O_2 dynamics, but that "models are required to further elucidate the relative significance of the seasonal drivers".

Numerical ecosystem models provide a valuable tool to analyse the O_2 dynamics of the marine environment as they describe the physical and biochemical processes affecting O_2 and allow for their quantification. Thus, they can help to understand and interpret measurements of O_2 and related parameters and can further describe the history of events of low O_2 conditions in the North Sea (Große et al., 2016). Thus, they provide a temporally and spatially consistent image of O_2 conditions which facilitates the detection of regions potentially susceptible to O_2 deficiency, which is especially relevant for the development of a cost-efficient O_2 monitoring strategy for the North Sea. This is of great importance for the marine ecosystem management and the mitigation of low O_2 conditions, e.g., by eutrophication abatement measures (OSPAR, 1992; EU, 2000, 2008).

The capability of these models to represent the physics and biochemistry of the North Sea (e.g., Baretta et al., 1995; Lancelot et al., 1997; Skogen et al., 2004; Pätsch and Kühn, 2008; Lenhart et al., 2010; Lorkowski et al., 2012; van der Molen et al., 2013; van Leeuwen et al., 2013; Troost et al., 2014) allows for the better estimation of potential future responses in the ecosystem dynamics. This is especially relevant in relation to climate change impacts (e.g., Clark et al., 2003; Attrill et al., 2007; Gröger et al., 2013; Meire et al., 2013), such as changing weather (Woth et al., 2006; Beniston et al., 2007; Rabalais et al., 2010), increasing atmospheric CO_2 levels (Justić et al., 1996, 2003; Melzner et al., 2013) and increasing T (Lowe et al., 2009; van der Molen et al., 2013; Mathis and Pohlmann, 2014).

However, quantitative studies on the current state of the O_2 conditions of the North Sea and the physico-biochemical interactions controlling the evolution of O_2 concentrations are sparse (Greenwood et al., 2010; Meire et al., 2013; Queste et al., 2013, 2016; Rovelli et al., 2016). In addition, they either focus only on selected processes, e.g., vertical mixing

(Rovelli et al., 2016), or are spatially (Greenwood et al., 2010; Meire et al., 2013) or temporally (Queste et al., 2013, 2016; Rovelli et al., 2016) limited.

Therefore, the temporally and spatially consistent, quantitative analysis of the current state of the North Sea O_2 dynamics in relation to its physical and biochemical characteristics and external influences (e.g., riverine nutrients) is key for the estimation of potential future changes related to eutrophication abatement policies or climate change.

1.2 Research objective and structure of this thesis

This thesis aims for the comprehensive description and analysis of the North Sea O_2 dynamics in recent years. Special focus is put on the elucidation of the physico-biochemical interactions driving the O_2 dynamics of the North Sea during seasonal stratification, and on the role of N inputs from external sources. In order to achieve this objective a physical-biogeochemical North Sea model is applied to the North Sea and analysed with regard to the individual physical and biochemical processes controlling O_2. In addition, a numerical method for the tracing of nutrients from individual sources within biogeochemical models is implemented and expanded by the creation of a direct link to the O_2 dynamics. The results obtained from the application of this method to the model results are analysed with regard to the influence of the different N sources in the O_2 dynamics of the North Sea. The following specific questions shall be answered by this thesis:

Q1 Which regional differences in North Sea O_2 dynamics can be detected under the recent environmental conditions?

Q2 What are the physical and biochemical factors controlling the evolution of O_2 deficiency in the regions most susceptible to low O_2 conditions?

Q3 What drives the year-to-year variability in bottom O_2 concentrations in the regions of lowest O_2 concentrations?

Q4 Which role play riverine and non-riverine sources for the evolution of O_2 deficiency in the North Sea?

Q5 What is the potential of N reductions in North Sea tributaries for improving the North Sea O_2 conditions?

Q6 What changes in the O_2 dynamics can be expected due to climate change?

In order to address these questions the remaining part of this thesis is structured as follows: Chapter 2 provides a brief description of the North Sea system, followed by a description of the applied model system in Ch. 3. Chapter 4 gives an overview of the North Sea hydrography as simulated by the hydrodynamical model used in this thesis. Further-

more, it presents a new criterion for the determination of stratification characteristics in relation to O_2 dynamics. A detailed analysis of the North Sea O_2 dynamics is given in Ch. 5. The focus of the chapter is on a general characterisation of North Sea regions in relation to their O_2 dynamics and the quantitative analysis of the physico-biochemical interactions controlling the evolution of O_2 deficiency under stratified conditions. Chapter 6 presents the method applied for the tracing of N from various external sources, including a comparison with existing studies. It further provides a more detailed analysis of different N-related quantities relevant to the O_2 dynamics. Due to the various different aspects addressed in these three chapters, where applicable, the discussion of the results comes along with the different result sections. A conclusion of the main findings is provided at the end of each chapter.

Subsequently, Ch. 7 presents the approach for linking to the O_2 cycle to the N tracing method, that allows for the quantification of the influence of individual N sources on the O_2 dynamics of the North Sea. Based on this, the current state of North Sea O_2 deficiency in relation to riverine and non-riverine N sources is analysed, followed by an analysis of riverine N reductions and their impact on the O_2 conditions in the North Sea. Different to the other chapters, a discussion of the results is provided at the end of this chapter, right before the conclusions. Finally, Ch. 8 provides a summary of the main conclusions drawn from this study.

Chapter 2

The North Sea system

The North Sea is a semi-enclosed, temperate shelf sea in northwestern Europe (Ducrotoy et al., 2000). Depending on the definition of its outer boundaries its area encompasses about 575,300 km^2 (ICES, 1983; Otto et al., 1990) to 750,000 km^2 (Ducrotoy et al., 2000) with an average depth of 74 m to 90 m, respectively. In the Northeast, it is directly connected to the Northeast Atlantic Ocean via two narrow channels (Pentland Firth and Fair Isle Channel) and by a shelf break zone of roughly 400 km zonal extent. In the Southwest, it is connected to the Northeast Atlantic via the English Channel ending in the narrow Strait of Dover. In the East it is connected to the Baltic Sea via the Skagerrak/Kattegat region and the Danish Straits/Belt sea.

In the following, an overview of the main features of the North Sea physics and biochemistry is provided, in relation to the different nutrient sources.

2.1 General circulation and hydrography

The general circulation of the North Sea is well described and studied (e.g., Lee, 1980; Backhaus, 1985; Otto et al., 1990; Huthnance, 1991; Turrell et al., 1992; Pohlmann, 1996; Smith et al., 1996; Lenhart and Pohlmann, 1997; Hainbucher and Backhaus, 1999; Ducrotoy et al., 2000; Skogen et al., 2002; Winther and Johannessen, 2006) and here, only a brief description of the main features will be provided. For this purpose, Fig. 2.1 shows the schematic presentation of the North Sea general circulation according to Turrell et al. (1992). In the North, the North Atlantic Current transports warm and high-saline water northeast along the northern shelf break. Branches of North Atlantic water (NAW) enter the North Sea across the shelf break, mainly between the Orkney Islands and the Norwegian coast, and the Fair Isle Channel. The largest part of the NAW enters the North Sea across the northeastern shelf edge where it follows the western slope of the Norwegian Trench, a deep channel off the Norwegian coast. The NAW entering the North Sea in this region was reported to have S of 35.2–35.4 [1] and T of 7 °C–9 °C (Furnes et al., 1986). However, a T increase of about 0.8 °C–1 °C has been reported for this inflow during the

1. In this thesis, S is reported in the (dimensionless) practical salinity scale (PSS-78; Lewis and Perkin, 1978).

last decades (Holliday et al., 2009; Huthnance et al., 2016; Larsen et al., 2016). For the NAW entering the North Sea through the Fair Isle Channel, average T of 9.67±0.34 °C and average S of 34.88±0.08 were found by Holliday et al. (2009) for the period 1971–2000. To a lesser extent NAW also enters the North Sea through the Pentland Firth between the Scottish coast and the Orkney Islands, where it mixes with the North Sea water and freshwater from the Scottish rivers.

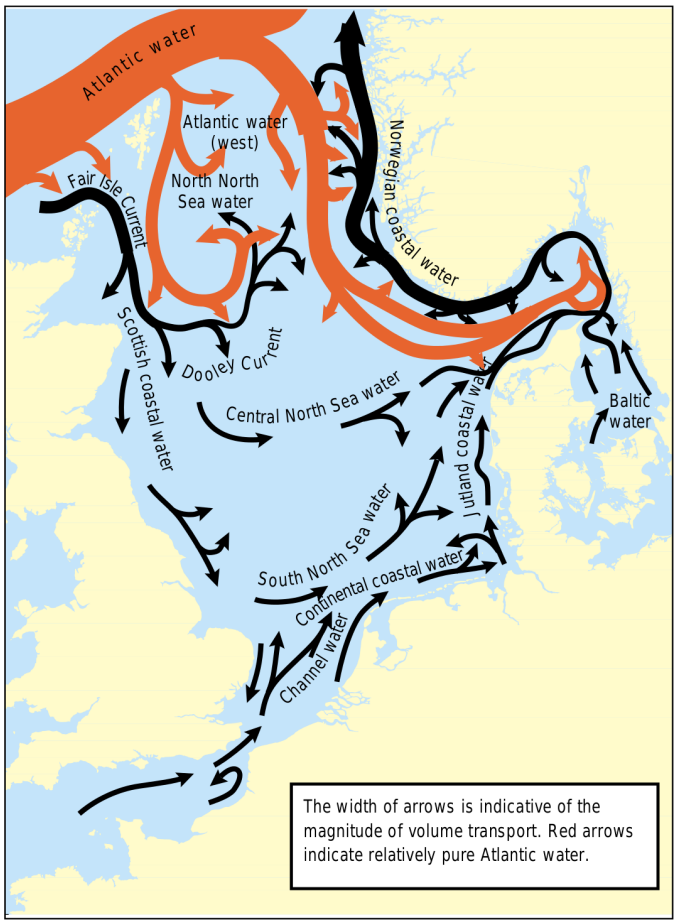

Figure 2.1: Schematic view of the general circulation of the North Sea (OSPAR, 2000, after Turrell et al. (1992); reprinted with permission from the OSPAR Secretariat).

In the northwestern North Sea, the NAW basically follows the Scottish northeast coast, along which it is additionally driven by and mixed with riverine freshwater discharge. It is partly recirculated as the Dooley Current at about 57 °N–58 °N (Dooley, 1974). The water masses, that are not recirculated with the Dooley Current continue flowing south, before they are again partly recirculated directly north of the Dogger Bank, a shallow bank in the western North Sea with bottom depths of 18 m–40 m (Kröncke and Knust, 1995). The recirculated water continues east towards the northern tip of Denmark. Only

about 5 % of the NAW reach those parts of the North Sea south of Dogger Bank (Lenhart and Pohlmann, 1997). During its southward flow, the NAW is further mixed with North Sea water and freshwater inputs from the British east coast. In the Southern Bight, the region between Dogger Bank and the Strait of Dover, the southward flow encounters the northwestward inflow of Channel Water coming through the Strait of Dover.

The circulation in the southern North Sea is dominated by northeastward flow of the recirculated NAW and the English Channel inflow. The latter drives the continental coastal current (Hofmann et al., 2005), together with the high continental riverine freshwater discharges (Ducrotoy et al., 2000; Hofmann et al., 2005). In the German Bight, the continental coastal current is diverted north and follows the Danish west coast as the Jutland Current. At the northern tip of Denmark, the latter turns east into the Skagerrak, where it is recirculated and mixed with low-S water coming from the Baltic Sea. Subsequently, the currents follow the Norwegian coast as the Norwegian Coastal Current. The latter is additionally driven by freshwater discharges from Norwegian rivers, and finally leaves the North Sea across the northeastern shelf break Huthnance (1991); Turrell et al. (1992). The overall turnover time of the North Sea circulation is about one year (Otto et al., 1990).

Besides this general, cyclonic circulation, the surface currents of the central North Sea are strongly affected by westerly winds and eastward moving weather systems (Otto et al., 1990), which are the dominant meteorological feature in the North Sea region. Consequently, the surface currents are highly variable due to changing wind directions in these weather systems (Lee, 1980).

Another important aspect of the North Sea is the seasonal (and locally perennial) stratification, which occurs in large parts of the North Sea (see Fig. 2.2). While most parts of North Sea are well-mixed during winter, mainly due to surface cooling. The spatial distribution of seasonal stratification is strongly affected by the tides, with the semi-diurnal, lunar M_2 tide as the dominant tidal component (Otto et al., 1990). Pingree et al. (1978) provided a first characterisation of stratification in the North Sea Simpson and Hunter (1974), based on the tidal current velocity and bottom depth. By this, they could differentiate between three regimes of summer stratification in the North Sea: (1) a well-mixed (central and northern North Sea), (2) a well-stratified (coastal southern North Sea) and (3) a transitional frontal zone between the former two (see grey overlays in Fig. 2.2).

This first characterisation already showed that most parts of the Southern Bight and the coastal waters of the southern North Sea are well-mixed throughout the entire year due to strong tides and shallow bottom depth. In contrast, basically the entire northern and central North Sea, and parts of the southern North Sea, are seasonally well-stratified due to the greater bottom depth and less strong tides. This stratification characterisation was refined by van Leeuwen et al. (2015) based on a statistical analysis of a 51-year, hydro-

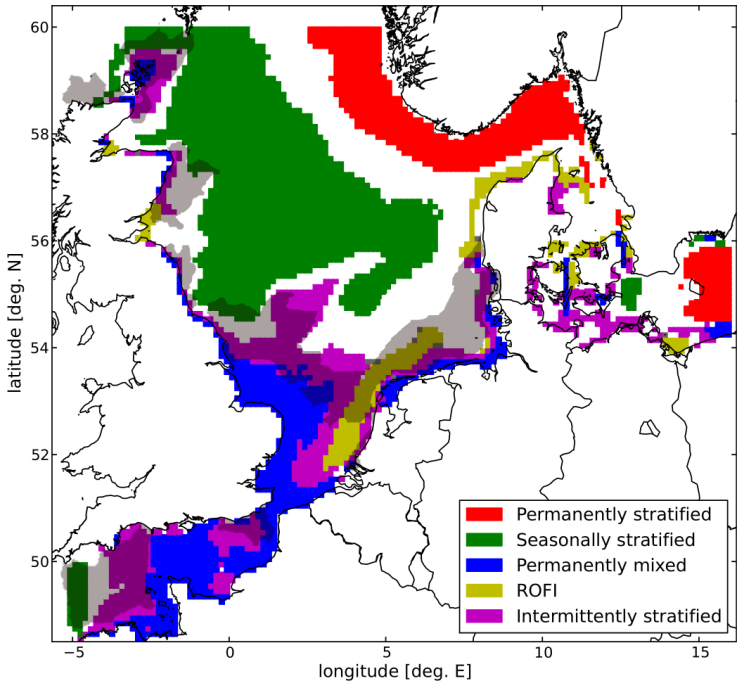

Figure 2.2: Classification of density stratification regimes (colours) in the North Sea as described by van Leeuwen et al. (2015) (Fig. 5 therein; UK Crown Copyright), white areas indicate non-classified areas. Grey overlays indicate 'transitional frontal zones' between seasonally stratified (central and northern North Sea) and permanently well-mixed areas (coastal southern North Sea and most parts of English Channel) according to Pingree et al. (1978) (see Fig. 2 therein).

dynamical simulation of the North Sea. They found that the North Sea can be subdivided into five different stratification regimes (see coloured patches in Fig. 2.2): (1) permanently stratified (red), (2) seasonally stratified (green), (3) permanently mixed (blue), (4) so-called 'regions of freshwater influence' (olive; ROFI; Latinopoulos et al., 1970), and (5) intermittently stratified (violet). Some regions could not be classified as one of the previously mentioned types of stratification according to their analysis (white areas in Fig. 2.2). This also applies to some regions for which O_2 deficiency is regularly reported (see Fig. 1.2).

The transitional zone defined by the Pingree et al. (1978) matches the intermittently stratified regions found by van Leeuwen et al. (2015) very well in most regions, and only partly overlaps with the ROFIs (in the Rhine plume) and non-classified areas (in the German Bight). High freshwater inflow from the Baltic Sea and the Norwegian rivers results in permanent haline stratification in the Norwegian Trench (van Leeuwen et al., 2015).

In combination with the annual cycle of solar radiation, both, general circulation and

tides, influence the annual cycle of T and S in the North Sea. The annual cycle of T in the North Sea is also well described (e.g., Lee, 1980; Otto et al., 1990; Elliott et al., 1991; Janssen et al., 1999) and again only the main features will be mentioned based on the climatology (1900–1996) by Janssen et al. (1999). During winter, the entire North Sea is well-mixed (except for the Norwegian Trench) with lowest T of about 3 °C in the inner German Bight during February/March, and highest T of 7 °C–7.5 °C in the northwestern North Sea due to the warm North Atlantic inflow. SST starts to increase in the southern and central North Sea in March/April, and slightly delayed in the northern North Sea.

During summer, overall highest SST of above 18 °C is reached in the well-mixed coastal zone of the southern North Sea, while maximum SST in the seasonally well-stratified, central North Sea results in 14 °C–16 °C. At the same time, bottom T shows values of 7 °C–9 °C north of 50 m-isobath, which extends roughly from the British coast at 54 °N, 0 °E to the northern tip of Denmark. In the northern North Sea maximum SST shows values of 12 °C–13 °C, accompanied by bottom T of about 7 °C–8 °C in the Northeast and 10 °C–11 °C in the Northwest. In September, SST starts to decline in the entire North Sea due to decreasing solar radiation. In combination with the onset of autumn storms, this results in the decline of stratification and, finally, again well-mixed conditions in the entire North Sea (excluding the Norwegian Trench).

It should be noted that, due to the observed changes in North Sea SST during the last decades (Wiltshire et al., 2008; Holliday et al., 2009; Dye et al., 2013; Larsen et al., 2016), the absolute T values mentioned above may differ from more recent T measurements, however, the general spatial patterns are still the same.

The annual cycle of S is much less pronounced than that of T and here only the main spatial patterns will be described based on the climatology by Janssen et al. (1999). Haline stratification plays only a minor role in most parts of the North Sea, except for the Norwegian Trench (van Leeuwen et al., 2015). From spring to autumn, weak haline stratification can also evolve along the British east coast and in the vicinity of the mouths of Rhine and Elbe (see sea surface S (SSS) and bottom S maps in Janssen et al. (1999)), due to riverine freshwater discharges. However, in most regions seasonal stratification is T-driven and can be observed by a distinct thermocline (i.e., a strong vertical T gradient).

In the Norwegian Trench, SSS ranges between 30 and 33 with the lowest values in June. Only in the eastern Skagerrak SSS reaches even lower values of 28 and less. This relates to the inflow of low-S water from the Baltic Sea. Bottom S ranges between 34.6 along the Norwegian coast and 35.2 in the offshore regions of the Norwegian Trench. Along the British coast, SSS varies between 34–34.5, without any clear seasonal signal. Bottom S shows values of 34.2–34.6. In the coastal zone of the southern North Sea, SSS ranges between about 29 near the Elbe mouth and 33 in regions less affected by river discharges.

Bottom S is only slightly higher than SSS in the regions affected by freshwater discharge. For both, no clear seasonality can be found, except in the Elbe mouth where bottom S is lowest in April due to high discharge in succession of the snow melt.

In the offshore regions of the North Sea the general spatial distributions of SSS and bottom S are very similar (differences $\leq$0.1) and show only minor variability during the annual cycle. Highest S values of 35.2 occur in the northern North Sea east of the Shetland Islands, due to the North Atlantic inflow. S stays above 34.75–35 until about 56 °N with higher surface values West due to the cyclonic circulation, which transports slightly less saline water from the Southeast northward. While seasonal variations in bottom S in the central and northern North Sea are negligible, SSS shows minor seasonal variations with slightly higher values during winter and lower values during summer (Janssen et al., 1999). In the offshore regions of the southern North Sea, SSS and bottom S range between 34 in the outer German Bight and about 34.75 around the Dogger Bank, with only minor seasonal variations.

As the O_2 dynamics of the North Sea are strongly related to the seasonal dynamics of phytoplankton, the following section describes the main aspects of the North Sea biogeochemistry in relation to the hydrodynamics and hydrography delineated above.

2.2 Biochemistry

The annual cycle of inorganic nutrients, phytoplankton and zooplankton in the North Sea is strongly affected by the annual cycle of solar radiation as it affects both, light availability and thermal stratification. Another major controlling factor is the availability of inorganic nutrients that are utilised by primary producers (e.g., phytoplankton) for building up biomass. Both, light and nutrient availability, control jointly the annual cycle of PP. A detailed review of the annual cycle of the North Sea phytoplankton dynamics is provided by Reid et al. (1990). Here, only a brief summary of the main features in relation to nutrient and (micro-/meso-) zooplankton is given. The diurnal cycle of PP (e.g., van Haren et al., 1998) or vertical zooplankton migration (e.g., Krause and Radach, 1989) are not described.

During winter, the entire water body of the North Sea is enriched with inorganic nutrients as a result of low PP rates (due to light limitation), remineralisation of organic matter and mixing-induced overturning of the water column. Besides this, the input of inorganic nutrients by external sources, e.g., rivers, the atmosphere, from the Atlantic and Baltic Sea, support the replenishment of the nutrient inventory of the North Sea (e.g., Brockmann et al., 1988; Radach and Lenhart, 1995; Jickells, 1998; Hydes et al., 1999; Brion et al., 2004; Artioli et al., 2008).

When light availability increases in spring and the onset of stratification inhibits the mixing of phytoplankton out of the euphotic zone (i.e., the light-flooded upper water column) (Sharples et al., 2006), PP is enhanced and a so-called phytoplankton 'spring bloom' is initiated (Gieskes and Kraay, 1975). This spring bloom is characterised by a rapid increase in phytoplankton biomass – often expressed in chlorophyll-a (Chl-a) concentrations as a proxy for phytoplankton biomass. The spring bloom is usually initiated in March/April and first occurs in the shallower coastal waters of the southern North Sea and the perennially stratified Norwegian Trench (e.g., McQuatters-Gollop et al., 2007). Maximum Chl-a concentrations during the spring bloom are observed in the coastal southern North Sea, e.g., in the German Bight ($16\,\mathrm{mg\,Chl\text{-}a\,m^{-3}}$ and higher; Joint and Pomroy, 1993) or in the Rhine plume (up to $80\,\mathrm{mg\,Chl\text{-}a\,m^{-3}}$; Gieskes and Kraay, 1975). Primary production rates during the spring bloom can reach values up to $2.4\,\mathrm{g\,C\,m^{-2}\,d^{-1}}$ in the German Bight (Joint and Pomroy, 1993), but show a general decrease to the offshore regions of the southern and central North Sea.

The phytoplankton spring bloom is usually initiated by diatoms (Gieskes and Kraay, 1975, 1983; McQuatters-Gollop et al., 2007), that utilise silicate (SiO_4^-), phosphate (PO_4^{3-}) and, preferably, nitrate (NO_3^-) for PP. When the NO_3^- or SiO_4^- pools in the euphotic surface mixed layer (SML) are depleted (except for regions with continuous inorganic nutrient supply, e.g., by rivers), the relative importance of flagellates, that utilise PO_4^{3-} and ammonium (NH_4^+) during PP, increases (Gieskes and Kraay, 1975, 1983; McQuatters-Gollop et al., 2007).

After the spring bloom maximum (i.e., the time of maximum Chl-a concentration), the phytoplankton biomass (and Chl-a concentration) shows a clear decrease in most North Sea regions as a result of nutrient limitation and increasing zooplankton grazing, in response to increasing phytoplankton concentrations. Only in the tidally well-mixed coastal regions, where nutrients are continuously provided by rivers, PP and thus phytoplankton biomass stays high. In the stratified regions, phytoplankton biomass remains low during summer, due to ongoing nutrient limitation and zooplankton grazing. This so-called summer standing stock (Colebrook, 1979) is dominated by flagellates (McQuatters-Gollop et al., 2007) which utilise the inorganic nutrients released during remineralisation of the previously produced organic matter. This standing stock prevails mainly in the vicinity of the thermocline, where light and nutrient availability are sufficiently high to allow for PP. This feature is often referred to as deep chlorophyll maximum (Weston et al., 2005). Weston et al. (2005) reported Chl-a concentrations of about $6\,\mathrm{mg\,Chl\text{-}a\,m^{-3}}$ and PP rates of about $0.4\,\mathrm{g\,C\,m^{-2}\,d^{-1}}$ within the deep chlorophyll maximum.

During events of enhanced wind-induced mixing during the stratified period, the nutrient pool of the euphotic SML is replenished by nutrient supply from the deeper layers.

These nutrients are immediately utilised by the primary producers and can result in short-term increases in phytoplankton biomass, and subsequent increases in zooplankton. The decreasing solar radiation in combination with the onset of the autumn storms causes a degradation of stratification from late August/early September onwards. This results in a deepening of SML and enables an autumn phytoplankton bloom due to enhanced nutrient availability (Colebrook, 1979; Moll, 1998; McQuatters-Gollop et al., 2007).

After this autumn bloom, phytoplankton biomass decreases in both, seasonally stratified and well-mixed regions, due to increasing light limitation and zooplankton grazing. At the same time, inorganic nutrient levels start to increase again, mainly as a result of phyto- and zooplankton mortality and subsequent organic matter remineralisation.

As indicated, rivers can play an important role for the nutrient supply to specific North Sea regions and thus on the seasonal dynamics of the biochemistry in these regions. Therefore, a short overview of the influence of riverine nutrient input on the North Sea will be given in the following.

2.2.1 External nutrient sources

The availability of nutrients in the North Sea system is strongly influenced by the inflow of nutrients from adjacent seas, especially the North Atlantic (e.g., Artioli et al., 2008; Gröger et al., 2013). In addition, riverine and – in case of N – atmospheric inputs play an important role (Brockmann et al., 1988; Emeis et al., 2015).

The catchment area of the North Sea has a spatial extent of 841,500 km^2 (Buser et al., 1998; OSPAR, 2000) with an annual freshwater discharge of about 300 $km^3\,a^{-1}$–350 $km^3\,a^{-1}$ (OSPAR, 2000). The most important rivers in the North Sea catchment area are the large continental rivers (Elbe, Weser, Rhine, Meuse, Scheldt and Seine) as well as Thames and Humber at the British east coast (OSPAR, 2000). Due to the cyclonic circulation of the North Sea, these rivers have a strong impact on the biochemistry, especially, of the southern North Sea (Brockmann and Eberlein, 1986; Brockmann et al., 1988; Kemp et al., 2009).

Artioli et al. (2008) calculated mass balances for total nitrogen (TN) and total phosphorus (TP) for three different decades ('pre-eutrophication' directly after the Second World War, 'eutrophication' in the 1980s and 'contemporary' around 2000). They found that average annual riverine TN input into the southern North Sea was about 720 kt N a^{-1} during the contemporary period, compared to only 97 kt N a^{-1} in the pre-eutrophication period and 912 kt N a^{-1} during the period of the highest eutrophication. This indicates the strong anthropogenic influence on riverine N inputs. For TP, they calculated corresponding values of 45 kt P a^{-1}, 21 kt P a^{-1} and 113 kt P a^{-1}, respectively.

The comparison to the TN input into the southern North Sea from adjacent marine

regions of 1126 kt N a^{-1} (Artioli et al., 2008) implies that the contemporary riverine supply accounts for almost two thirds of the TN input across marine boundaries. In fact, this riverine contribution can be expected to be even higher as the marine contribution calculated by Artioli et al. (2008) includes additional riverine inputs from outside the mass balance area. For TP, the riverine input adds up to only about 25 % of the input from adjacent marine regions. This illustrates the importance of riverine (inorganic and organic) nutrient input, especially in terms of TN.

The riverine inputs into the North Sea underlie strong inter-annual to intra-seasonal variations, e.g., due to the snow melt in early spring (e.g., Pinto et al., 2007) or events like heavy rainfall (e.g., Peperzak, 2003; Ulbrich et al., 2003; Kienzler et al., 2015; Mudersbach et al., 2016) causing higher freshwater and thus nutrient discharges. Although rivers constitute a continuous source of nutrients for the marine system, the timing of periods of high nutrient loads may be crucial for the actual influence of such loads on the marine ecosystem. As PP requires sufficient light availability, high loads outside the growing season may only have a minor impact on PP.

In addition to the variations in loads of TN or TP, the riverine systems also underlie an annual cycle of phytoplankton (i.e., organic matter) and inorganic nutrients (e.g., Schuchardt and Schirmer, 1990). Consequently, the seasonally varying input of inorganic and organic nutrients can have different effects on the different North Sea regions affected by riverine nutrient input (Kemp et al., 2009), as inorganic nutrients are directly available to primary consumers while organic nutrients need to be remineralised first.

The atmospheric deposition of inorganic N constitutes another relevant source of N in the North Sea. Troost et al. (2013) found that up to 20 % of TN in the southern North Sea originate from atmospheric deposition. According to Artioli et al. (2008), the contemporary atmospheric contribution is about 199 kt N a^{-1} compared to 31 kt N a^{-1} during the pre-eutrophication period. Thus, atmospheric deposition adds up to about 28 % of the riverine N inputs into the southern North Sea. In addition, this implies a remarkable increase in atmospheric N deposition since the mid-1940s, which mainly relates to increased anthropogenic emissions (Paerl, 1997; Schöpp et al., 2003). However, Schöpp et al. (2003) also report a distinct reduction in European N emissions since the 1980s, which also resulted in reduced atmospheric inputs into the North Sea (Artioli et al., 2008). The complex interactions between the physical (general circulation and stratification) and biochemical features of the North Sea, in combination with the variations in different nutrient inputs likely have a strong impact on the seasonal and year-to-year variability of the O_2 dynamics of the North Sea. Therefore, a detailed analysis of the interplay of these individual factors is urgently required.

Chapter 3

The Ecosystem Model

This chapter provides an overview of the physico-biogeochemical model system used for the analyses presented in this thesis. First, the three-dimensional (3D), baroclinic ocean model HAMSOM (HAMburg Shelf Ocean Model; Backhaus (1985); Pohlmann (1991, 1996)) is described briefly focusing on the features relevant for the O_2 dynamics. This model is used for the simulation of the physical quantities (i.e., T and S), volume transports and vertical turbulent mixing coefficients. Second, the 3D biogeochemical model ECOHAM (ECOsystem model, HAMburg; e.g., Moll, 1998; Pätsch and Kühn, 2008; Kühn et al., 2010; Lorkowski et al., 2012; Große et al., 2016) is presented, which constitutes the basis for the simulation of the biochemical cycles, e.g., of N. At the beginning of this second part, a more general description of ECOHAM is provided, followed by a detailed description of the O_2 cycle as implemented in ECOHAM. Finally, the applied model setup is presented, including a description about the simulation sequence and the coupling of HAMSOM and ECOHAM as well as information about the model domain and grid.

3.1 The hydrodynamical model HAMSOM

The hydrodynamical model HAMSOM (Backhaus, 1985) constitutes a baroclinic, primitive equation model with a free surface and applies the hydrostatic and Boussinesq approximations (Pohlmann, 1991). It is defined on an Arakawa C-grid (Arakawa and Lamb, 1977) and applies z-coordinates for resolving the vertical dimension. The horizontal advective flow field is calculated using the component upstream scheme, the vertical advective flow results from the continuity equation (Lamb, 1879). The vertical turbulent mixing follows Kochergin (1987) and is described in Sect. 3.1.1. In the interior model domain T and S are treated as prognostic state variables. At the open boundaries certain boundary conditions are prescribed which are discussed briefly in Sect. 3.1.2. For a detailed description of HAMSOM the reader is referred to Backhaus and Hainbucher (1987) and Pohlmann (1991, 1996).

3.1.1 Parameterisation of vertical mixing in HAMSOM

The focus of this thesis is on the physico-biochemical interactions controlling the O_2 dynamics of the North Sea. As seasonal density stratification is considered as a key factor for the O_2 dynamics it is essential to show how vertical mixing is parametrised within HAMSOM. According to Mellor and Yamada (1974) the vertical mixing coefficient A_v under stationary conditions can be described as follows:

$$A_v = (c_{\mathrm{ml}} \cdot h_{\mathrm{ml}})^2 \cdot \sqrt{\left(\frac{\partial u}{\partial z}\right)^2 + \left(\frac{\partial v}{\partial z}\right)^2 + \frac{1}{S_M}\frac{g}{\rho}\frac{\partial \rho}{\partial z}}. \tag{3.1}$$

The constant $c_{\mathrm{ml}} = 0.05$ constitutes a constant was determined by Kochergin (1987). h_{ml} represents the mixed layer thickness. $\partial u/\partial z$ and $\partial v/\partial z$ represent the vertical gradient of the zonal and meridional current velocities, respectively. The last term under the square root is the squared Brunt-Väisälä-frequency or stratification frequency N divided by the negative Schmidt number S_M. It is defined as (Haurwitz et al., 1959):

$$N^2 = -\frac{g}{\rho}\frac{\partial \rho}{\partial z}, \tag{3.2}$$

with g representing the standard gravity ($9.80665\,\mathrm{m\,s^{-2}}$), and density ρ according to the equation of state (EOS) by Jackett and McDougall (1995) [1]. The EOS by Jackett and McDougall (1995) represents a newer formulation of the EOS according to Fofonoff and Millard (1983), which utilises the (dimensionless) practical salinity scale (PSS-78; Lewis and Perkin, 1978). Therefore, S is reported according to PSS-78 in this thesis.

The Brunt-Väisälä-frequency is an indicator for stable ($N^2 > 0$) or unstable ($N^2 < 0$) conditions within the water column. If unstable conditions occur HAMSOM reinforces the Brunt-Väisälä-frequency by factor 15 which increases the vertical mixing coefficient A_v. HAMSOM uses a maximum vertical mixing coefficient of $A_{v,\max} = 0.08\,\mathrm{m^2\,s^{-1}}$.

3.1.2 Initialisation, boundary conditions and forcing data

HAMSOM uses monthly climatological distributions of T and S based on the World Ocean Atlas 2001 (Conkright et al., 2002) for initialisation. At the open boundaries, sea surface elevation is calculated as the combined effect of so-called dynamic heights, the 'inverted barometer effect' (Doodson, 1924) and the principal lunar semi-diurnal tide (M_2),

1. Very shortly before the submission of this thesis a bug was found in the EOS in the HAMSOM code. This bug caused that the EOS by Jackett and McDougall (1995) was applied using *in situ* T instead of potential temperature (Θ). For this reason Appendix A.1 was added to this thesis in order to demonstrate that this bug does not affect the basic results and conclusions.

which constitutes the dominant tidal component in the North Sea (e.g., Otto et al., 1990). In HAMSOM the dynamic height is calculated relative to a layer of no motion of 500 m or relative to the bottom depth in case of shallower water. For the horizontal transport velocities radiation open boundary conditions (Orlanski, 1976) are applied, while radiation and radiative-nudging OBCs are used for tracers (T and S) in the case of inflow and outflow conditions, respectively. A detailed description of the open boundary conditions for advective flow as well as T and S is provided in Chen et al. (2013).

The meteorological forcing is derived from NCEP/NCAR reanalysis data (Kalnay et al., 1996; Kistler et al., 2001) and provides 6-hourly information on air temperature, cloud coverage, relative humidity, wind speed and direction. Short-wave radiation is calculated from astronomical insolation and cloud coverage applying a correction factor of 0.9 (Lorkowski et al., 2012). The data are interpolated to the model grid and time step according to O'Driscoll et al. (2013) and Chen et al. (2014). Daily freshwater run-off data for 254 rivers were provided by Sonja van Leeuwen from the Centre of Environment, Fisheries and Aquaculture Science (Cefas) and represent an updated data set of that used by Lenhart et al. (2010) covering the period 1977–2014. As this run-off data is part of the same data set providing the nutrient load data, a more detailed description of the individual data sources is given in Sect. 3.2.2.2.

3.2 The biogeochemical model ECOHAM

This study applies the biogeochemical model ECOHAM (e.g., Moll, 1998; Pätsch and Kühn, 2008; Lorkowski et al., 2012; Große et al., 2016) for the simulation of the North Sea biogeochemistry. It is a 3D, biogeochemical model utilising the same spatial grid as HAMSOM. It uses the T and S distributions as well as the advective flow fields and vertical mixing coefficients calculated by HAMSOM as physical forcing for the biogeochemical simulation. ECOHAM includes all parameter groups of a so-called NPZD-type model (nutrients-phytoplankton-zooplankton-detritus) to represent the lower trophic layer dynamics. In addition, it includes a parametrisation of the so-called 'microbial loop' (Azam et al., 1983). ECOHAM simulates the cycles of N, P, carbon (C), silicon (Si) and O_2.

The ECOHAM version used for this thesis is a successor of former model versions described by Pätsch and Kühn (2008), Kühn et al. (2010) and Lorkowski et al. (2012). Its major difference to these earlier model versions is the different model grid described in Sect. 3.3. The present model ECOHAM version includes the following state variables:

- 4 nutrients (NO_3^-, NH_4^+, PO_4^{3-}, SiO_4^-),
- 2 phytoplankton groups (diatoms, flagellates),

- 2 zooplankton groups (micro-, mesozooplankton),
- bacteria,
- 2 fractions of detritus (fast and slowly sinking),
- labile dissolved organic matter,
- semi-labile organic carbon,
- calcite,
- dissolved inorganic carbon,
- total alkalinity,
- benthic calcite and
- benthic particulate organic matter.

The complete set of equations and process parametrisations describing the change of the individual state variables with time is given in Lorkowski et al. (2012). In the following only the molar ratios of the different state variables are provided as they partly differ from those used by Lorkowski et al. (2012). For both phytoplankton groups a C:N:P ratio of 132.5:20:1 is used (Lorkowski et al., 2012), which implies a C:N ratio of 6.625 identical to Redfield (1934), but C:P and N:P ratios higher than Redfield (1934) according to the findings of Quigg et al. (2003). For diatoms a C:Si ratio of 5.76 is applied. In addition, the Chl-a content of diatoms and flagellates is calculated diagnostically following Cloern et al. (1995). For the two zooplankton groups a C:N:P ratio of 110:20:1 is used, while for bacteria a ratio of 50:10:1 is applied. The elemental ratios of detrital matter can evolve freely.

3.2.1 The oxygen cycle in ECOHAM

In general, the change of the concentration C of a model state variable, such as O_2, with time t is described by the convection-diffusion equation:

$$\frac{dC}{dt} = \underbrace{\nabla \cdot \left(\overline{\overline{d}} \nabla C\right)}_{diffusion} \quad \underbrace{- \nabla \cdot (\vec{v} C)}_{convection/advection} \quad \underbrace{+ R.}_{sources/sinks} \tag{3.3}$$

The diffusive transport is calculated according to Fick's first law with the second order diffusion tensor (or diffusivity) $\overline{\overline{d}}$. In the convective/advective transport term, $\vec{v}$ represents the 3D velocity vector. R represents the sources and sinks of X (i.e., biochemical processes, input from external sources). As this thesis focuses on the O_2 dynamics of the North Sea its implementation to ECOHAM (Müller, 2008) is presented in the following in more detail.

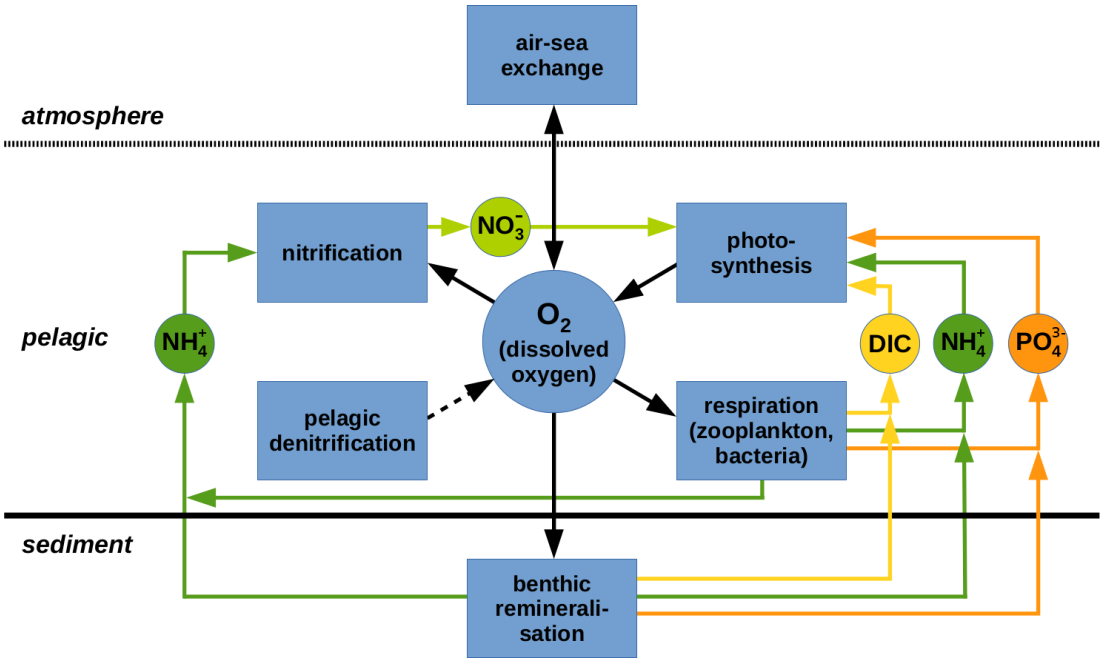

Figure 3.1: Schematic view on the oxygen cycle as implemented in ECOHAM, including the links to the carbon, nitrogen and phosphorus cycles. Linking state variables are: dissolved inorganic C (DIC), NH_4^+, NO_3^- and PO_4^{3-}. Adapted from Müller (2008).

A conceptual view of the O_2 cycle implemented to ECOHAM is provided in Fig. 3.1, including the links to the biogeochemical cycles of C (yellow), N (green) and P (orange). The arrows indicate the direction of a process, e.g., NH_4^+ is released during benthic remineralisation and consumed by nitrification. The exchange of O_2 between atmosphere and ocean is parametrised according to Wanninkhof (1992). In the interior water column, photosynthesis (i.e., primary production) constitutes a source process for O_2 and links the O_2 cycle to the cycles of C, N and P. All other biochemical processes, namely respiration by zooplankton and aerobic bacteria, and nitrification, represent O_2-consuming processes. While the former processes also constitute a link of the O_2 cycle to the cycles of C, N and P, nitrification is only linked to the N cycle. Pelagic denitrification is implemented to ECOHAM, but is negligible as it only occurs under anaerobic conditions, which do not occur in the North Sea. Pelagic anaerobic NH_4^+ oxidation (anammox) is not implemented for the same reason. Except for NPP, the biological processes involved in the O_2 cycle are not T-dependent in the applied model setup.

Net primary production (NPP), i.e., the uptake of inorganic nutrients and dissolved inorganic C (DIC) by phytoplankton (minus respiration), constitutes an important O_2 production process within the water column. Phytoplankton can conduct NPP under the use of two different types of chemically active N molecules, NO_3^- and NH_4^+. The former

can be described by the following chemical equation (following Richards (1965)):

$$x \cdot CO_2 + y \cdot H^+ + y \cdot NO_3^- + H_3PO_4 + (x+y) \cdot H_2O \Leftrightarrow \\ \Leftrightarrow (CH_2O)_x(NH_3)_yH_3PO_4 + (x+2y) \cdot O_2. \tag{3.4}$$

Here, x and y represent the mols of C and N relative to P within phytoplankton, i.e., in ECOHAM $x = 132.5$ and $y = 20$ according to the C:N:P ratio of 132.5:20:1 Lorkowski et al. (2012). Following Neumann (2000), NPP based on NH_4^+ can be described by the following chemical equation:

$$x \cdot CO_2 + y \cdot NH_4^+ + H_3PO_4 + x \cdot H_2O \Leftrightarrow (CH_2O)_x(NH_3)_yH_3PO_4 + x \cdot O_2. \tag{3.5}$$

Equations (3.4) and (3.5) show that O_2 production relative to N uptake (O_2/N) is more efficient in case of NO_3^--based NPP. For NO_3^--based NPP it results in $x/y + 2$ in case of NO_3^--based NPP, while it only yields x/y in case of NH_4^+-based NPP, with x/y representing the C:N of phytoplankton. In ECOHAM, the ratios result in 8.625 and 6.625 for NO_3^-- and NH_4^+-based NPP, respectively (Müller, 2008). The uptake of NO_3^- and NH_4^+ by phytoplankton is parametrised in ECOHAM as follows:

$$\mathrm{NPP}_{ij} = C_{\mathrm{phn}_i} \cdot \mu_{10,i} \cdot f_{T,\mathrm{phy}} \cdot f_{\mathrm{par}} \cdot f_{\mathrm{nut},i}. \tag{3.6}$$

Here, NPP_{ij} represents the NPP by phytoplankton group phn_i (in N units) using chemically active N of type j. Phytoplankton group phn_1 refers to diatoms, while phn_2 refers to flagellates. C_{phn_i} and $\mu_{10,i}$ represent the phytoplankton concentration and the growth rate at 10 °C of the corresponding phytoplankton group. The latter equals $1.1\,\mathrm{d}^{-1}$ for diatoms and $0.9\,\mathrm{d}^{-1}$ for flagellates. $f_{T,\mathrm{phy}}$ constitutes a T-dependent factor for phytoplankton ($f_{T,\mathrm{phy}} = 1.5^{(T-10)/10}$, with T in °C), while f_{par} is the light limitation factor depending on the available photosynthetically active radiation according to Steele (1962). The last term $f_{\mathrm{nut},ij}$ represents the nutrient limitation of phytoplankton group phn_i depending on the availability of NO_3^-, NH_4^+, PO_4^{3-} and SiO_4^- (in case of diatoms). Nutrient limitation follows Liebig's law of the minimum (Liebig, 1841).

While NPP constitutes the only biochemical O_2 production process, a couple of O_2 consumption processes exist and are parametrised by ECOHAM. The transformation of NH_4^+ to NO_3^- by bacteria ('nitrifiers') is called **nitrification**. This process takes place under aerobic conditions and is conducted by two groups of bacteria: NH_4^+ oxidisers and nitrite oxidisers. The first group oxidises NH_4^+ to nitrite, while the second group oxidises nitrite to NO_3^- (Müller, 2008). In ECOHAM nitrification is implemented according to Fennel et al. (2006), who describe this two-step process by the following simplified chemical equation:

$$NH_4^+ + 2 \cdot O_2 \rightarrow NO_3^- + 2 \cdot H^+ + H_2O. \tag{3.7}$$

In ECOHAM, the O_2 consumption due to nitrification is formulated as follows:

$$P_{\mathrm{O_2,nit}} = \begin{cases} 0 & \text{for } C_{\mathrm{O_2}} \leq 0 \text{ (anoxic)} \\ 2 \cdot r_{\mathrm{nit}}(I,z) \cdot C_{\mathrm{NH_4^+}}(z) & \text{otherwise (oxic),} \end{cases} \tag{3.8}$$

with the nitrification rate r_{nit} being a function of light intensity I and depth z, showing higher values under low light conditions. $C_{\mathrm{NH_4^+}}$ represents the NH_4^+ concentration in depth z (in $\mathrm{mmol\,N\,m^{-3}}$). The factor 2 results from the uptake ratio $O_2/NH_4^+ = 2\,\mathrm{mmol\,O_2/mmol\,N}$, according to the left-hand side of Eq. (3.7). $C_{\mathrm{O_2}}$ represents the concentration of dissolved oxygen in $\mathrm{mmol\,O_2\,m^{-3}}$.

Under oxic conditions, the pelagic and benthic O_2 consumption due to **bacterial remineralisation of organic matter** is described by the following chemical equation:

$$\begin{aligned} &(CH_2O)_x(NH_3)_yH_3PO_4 + x \cdot O_2 + y \cdot H^+ \Leftrightarrow \\ &\Leftrightarrow\ x \cdot CO_2 + y \cdot NH_4^+ + H_3PO_4 + x \cdot H_2O. \end{aligned} \tag{3.9}$$

The elemental ratios between C, N and P in the organic matter may differ from the Redfield ratios of C:N:P=106:16:1 (Redfield, 1934), indicated by the variables x and y. C oxidation takes place with a ratio of $C/O_2 = 1$ (Neumann, 2000). Due to the latter, the formulation of O_2 consumption due to **pelagic remineralisation** under oxic conditions within ECOHAM can be described by the net release of C by bacteria:

$$P_{\mathrm{O_2,bac}} = P^{\mathrm{base}}_{\mathrm{O_2,bac}_i} + P^{\mathrm{cor}}_{\mathrm{O_2,bac}_i}. \tag{3.10}$$

Here, $P^{\mathrm{base}}_{\mathrm{O_2,bac}_i}$ describes the uncorrected C uptake, and $P^{\mathrm{cor}}_{\mathrm{O_2,bac}_i}$ represents the correction term for the bacterial C uptake. The uncorrected C uptake $P^{\mathrm{base}}_{\mathrm{O_2,bac}_i}$ is calculated as:

$$P^{\mathrm{base}}_{\mathrm{O_2,bac}_i} = \mu_{\mathrm{bac}} \cdot C_{\mathrm{bac}}, \tag{3.11}$$

with the C excretion rate of bacteria $\mu_{\mathrm{bac}} = 0.1\,\mathrm{d^{-1}}$ and the bacteria-C concentration C_{bac} (in $\mathrm{mmol\,C\,m^{-3}}$). The correction term $P^{\mathrm{cor}}_{\mathrm{O_2,bac}_i}$ in Eq. (3.10) is calculated as:

$$\begin{aligned} P^{\mathrm{cor}}_{\mathrm{O_2,bac}_i} =& \Delta P_{\mathrm{bap}} \cdot r_{\frac{\mathrm{bac}}{\mathrm{bap}}} + \\ &+ \begin{cases} \Delta P_{\mathrm{bac}} + \Delta P_{\mathrm{ban}} \cdot r_{\frac{\mathrm{bac}}{\mathrm{ban}}} & \text{for } \frac{\Delta P_{\mathrm{bac}}}{\Delta P_{\mathrm{ban}}} > r_{\frac{\mathrm{bac}}{\mathrm{ban}}} \wedge C_{\mathrm{NH_4^+}} \leq C^{\mathrm{thres}}_{\mathrm{NH_4^+}} \\ \max\left(0, \Delta P_{\mathrm{bac}} + \Delta P_{\mathrm{ban}} \cdot r_{\frac{\mathrm{bac}}{\mathrm{ban}}}\right) & \text{for } \frac{\Delta P_{\mathrm{bac}}}{\Delta P_{\mathrm{ban}}} \leq r_{\frac{\mathrm{bac}}{\mathrm{ban}}} \\ 0 & \text{otherwise.} \end{cases} \end{aligned} \tag{3.12}$$

Here, ΔP_{bac}, ΔP_{ban} and ΔP_{bap} represent the net uptake of C, N and P by bacteria, respectively. The molar C:N ratio for bacteria equals $r_{\frac{\mathrm{bac}}{\mathrm{ban}}} = 5$ while that for C:P equals

$r_{\frac{\text{bac}}{\text{bap}}} = 50$. $C^{\text{thres}}_{\text{NH}_4^+} = 0.1\,\text{mmol N}\,\text{m}^{-3}$ describes the threshold concentration for bacterial NH_4^+ uptake. The net C uptake is calculated as:

$$\Delta P_{\text{bac}} = P_{\text{doc}\to\text{bac}} - \sum_{i=1}^{2} P_{\text{bac}\to\text{zoc}_i} - P^{\text{base}}_{\text{O}_2,\text{bac}_i}, \tag{3.13}$$

where $P_{\text{doc}\to\text{bac}}$ represents the bacterial uptake of dissolved organic C (DOC), and $P_{\text{bac}\to\text{zoo}_i}$ describe the grazing of zooplankton on bacteria (in C units; $i = 1, 2$ refer to micro- and mesozooplankton, respectively). The net N uptake by bacteria is formulated as:

$$\Delta P_{\text{ban}} = P_{\text{don}\to\text{ban}} + P_{\text{NH}_4^+\to\text{ban}} - P_{\text{ban}\to\text{NH}_4^+} - \sum_{i=1}^{2} P_{\text{ban}\to\text{zon}_i}, \tag{3.14}$$

with the uptake of dissolved organic N (DON), $P_{\text{don}\to\text{ban}}$, and the uptake and excretion of NH_4^+, $P_{\text{NH}_4^+\to\text{ban}}$ and $P_{\text{ban}\to\text{NH}_4^+}$, respectively. $P_{\text{ban}\to\text{zon}_i}$ describes the grazing of zooplankton on bacteria (in N units). The net uptake of P by bacteria is calculated as:

$$\Delta P_{\text{bap}} = \max\left(P^{\text{req}}_{\text{bap}} - P^{\text{max}}_{\text{bap}}\right), \tag{3.15}$$

with the required and the maximum P uptake, $P^{\text{req}}_{\text{bap}}$ and $P^{\text{max}}_{\text{bap}}$, respectively. The required P uptake reads as:

$$P^{\text{req}}_{\text{bap}} = \left(P_{\text{don}\to\text{ban}} + P_{\text{NH}_4^+\to\text{ban}} - P_{\text{ban}\to\text{NH}_4^+}\right) \cdot r_{\frac{\text{bap}}{\text{ban}}} - P_{\text{dop}\to\text{bap}}, \tag{3.16}$$

where $r_{\frac{\text{bap}}{\text{ban}}} = 1/10$ represents the molar ratio of P:N of bacteria. $P_{\text{dop}\to\text{bap}}$ describes the bacterial uptake of dissolved organic P (DOP). The maximum P uptake is calculated as:

$$P^{\text{max}}_{\text{bap}} = P_{\text{NH}_4^+\to\text{ban}} \cdot \frac{C_{\text{PO}_4^{3-}}}{C_{\text{NH}_4^+}}, \tag{3.17}$$

with the PO_4^{3-} concentration $C_{\text{PO}_4^{3-}}$ in $\text{mmol P}\,\text{m}^{-3}$.

In addition to pelagic remineralisation, benthic O_2 consumption due to **bacterial remineralisation of sedimented organic matter** is represented in ECOHAM. The model version applied for this study uses a relatively simple sediment module represented by a single layer of no vertical extent below the deepest pelagic layer, in which the sinking organic matter is collected and remineralised (Moll, 1998; Pätsch et al., 2009). Benthic remineralisation is described similar to Fennel et al. (2006) allowing no year-to-year accumulation of organic matter in the sediment. The corresponding benthic O_2 consumption is formulated based on C remineralisation:

$$P_{\text{O}_2,\text{sed}} = \mu_{\text{spoc}} \cdot C_{\text{spoc}}, \tag{3.18}$$
$$\text{for } C_{\text{O}_2} > 0 \;\vee\; \left(C_{\text{O}_2} \le 0 \wedge C_{\text{NO}_3^-} \le C^{\text{thres}}_{\text{NO}_3^-}\right).$$

Here, the benthic remineralisation rate of sedimented particulate organic C (SPOC) is set to $\mu_{\mathrm{spoc}} = 0.028\,\mathrm{d}^{-1}$ and C_{spoc} represents the concentration of SPOC (in $\mathrm{mmol\,C\,m^{-3}}$). According to Eq. (3.18), benthic remineralisation only takes place under oxic conditions ($C_{\mathrm{O_2}} > 0$) or anoxic conditions coinciding with $\mathrm{NO_3^-}$ concentrations ($C_{\mathrm{NO_3^-}}$) equal or below the threshold concentration of $C^{\mathrm{thres}}_{\mathrm{NO_3^-}} = 0.1\,\mathrm{mmol\,N\,m^{-3}}$). In ECOHAM, $\mathrm{O_2}$ concentrations may become negative representing reduced end products (e.g., hydrogen sulphides; Seitzinger and Giblin, 1996).

Finally, **zooplankton respiration** constitutes another $\mathrm{O_2}$ consumption process. It is parametrised by ECOHAM following Sterner and Elser (2002):

$$P_{\mathrm{O_2,zoc}_i} = P^{\mathrm{base}}_{\mathrm{O_2,zoc}_i} + P^{\mathrm{cor}}_{\mathrm{O_2,zoc}_i}, \tag{3.19}$$

with the uncorrected C excretion $P^{\mathrm{base}}_{\mathrm{O_2,zoc}_i}$ and the correction term for the zooplankton C uptake, $P^{\mathrm{cor}}_{\mathrm{O_2,zoc}_i}$. The index $i = 1$ refers to the microzooplankton-C ($\mathrm{zoc_1}$), while $i = 2$ refers to mesozooplankton-C ($\mathrm{zoc_2}$). The uncorrected C excretion is calculated as:

$$P^{\mathrm{base}}_{\mathrm{O_2,zoc}_i} = \left(P^{\mathrm{loss}}_{\mathrm{zoc}_i} + (1 - r_{\mathrm{det}}) \cdot P^{\mathrm{mort}}_{\mathrm{zoc}_i}\right) \cdot (1 - r_{\mathrm{dic}}). \tag{3.20}$$

Here $P^{\mathrm{loss}}_{\mathrm{zoc}_i}$ represents the metabolic losses of C by zooplankton and $P^{\mathrm{mort}}_{\mathrm{zoc}_i}$ depicts the zooplankton mortality (in C units). $r_{\mathrm{det}} = 0.33$ and $r_{\mathrm{dic}} = 0.5$ constitute the fractions of the C losses going into detritus and DIC, respectively. ECOHAM parametrises the metabolic losses $P^{\mathrm{loss}}_{\mathrm{zoc}_i}$ as follows:

$$P^{\mathrm{loss}}_{\mathrm{zoc}_i} = \max\left(0, P^{\mathrm{up}}_{\mathrm{zoc}_i} - P^{\mathrm{faec}}_{\mathrm{zoc}_i} - \mu^{\mathrm{max}}_{\mathrm{zoc}_i} \cdot C_{\mathrm{zoc}_i}\right). \tag{3.21}$$

The gross uptake of C by zooplankton is described by $P^{\mathrm{up}}_{\mathrm{zoc}_i}$. $P^{\mathrm{faec}}_{\mathrm{zoc}_i}$ represents the loss of zooplankton-C due to faecal pellet production, while $\mu^{\mathrm{max}}_{\mathrm{zoc}_i}$ and C_{zoc_i} are the maximum zooplankton growth rate related to the least available food element (C, N or P) and the zooplankton-C concentration, respectively. The zooplankton gross uptake of C is calculated as:

$$P^{\mathrm{up}}_{\mathrm{zoc}_i} = \sum_{j=1}^{2} P_{\mathrm{phc}_j \to \mathrm{zoc}_i} + P_{\mathrm{dec}_1 \to \mathrm{zoc}_i} + P_{\mathrm{zoc}_1 \to \mathrm{zoc}_i}, \tag{3.22}$$

with $P_{\mathrm{phc}_j \to \mathrm{zoc}_i}$ representing the grazing of zooplankton group i on phytoplankton group j and the ingestion of slowly sinking detritus by zooplankton ($P_{\mathrm{dec}_1 \to \mathrm{zoc}_i}$; both in C units). $P_{\mathrm{zoc}_1 \to \mathrm{zoc}_i}$ indicates the grazing of zooplankton group i on microzooplankton, which is zero in case of $i = 1$ as microzooplankton does not feed on itself.

The faecal pellet production ($P^{\mathrm{faec}}_{\mathrm{zoc}_i}$; in C units) is defined as:

$$P^{\mathrm{faec}}_{\mathrm{zoc}_i} = (1 - r_{\mathrm{faec}}) \cdot P^{\mathrm{up}}_{\mathrm{zoc}_i}, \tag{3.23}$$

with the assimilation coefficient of zooplankton $r_{\text{faec}} = 0.75$.

The maximum growth rate ($\mu^{\max}_{\text{zoc}_i}$) in Eq. 3.21 is calculated as:

$$\mu^{\max}_{\text{zoc}_i} = \min\left(\frac{P^{\text{up}}_{\text{zoc}_i} - P^{\text{faec}}_{\text{zoc}_i}}{C_{\text{zoc}_i}}, \frac{P^{\text{up}}_{\text{zon}_i} - P^{\text{faen}}_{\text{zon}_i}}{C_{\text{zon}_i}}, \frac{P^{\text{up}}_{\text{zop}_i} - P^{\text{faep}}_{\text{zop}_i}}{C_{\text{zop}_i}}\right) - \mu^{\min}_{\text{zoo}}. \tag{3.24}$$

Here, $P^{\text{up}}_{\text{zon}_i}$ and $P^{\text{up}}_{\text{zop}_i}$ represent the zooplankton gross uptake of N and P, respectively, analogous to Eq. (3.22). Accordingly, $P^{\text{faen}}_{\text{zon}_i}$ (in N units) and $P^{\text{faep}}_{\text{zop}_i}$ (in P units) are the faecal pellet production analogous to Eq. (3.23). C_{zon_i} and C_{zop_i} indicate the zooplankton-N and -P concentration, respectively. $\mu^{\min}_{\text{zoo}}$ is the minimum zooplankton loss rate of $0.01\,\text{d}^{-1}$ due to basic maintenance.

The zooplankton mortality in Eq. (3.20) is defined as:

$$P^{\text{mort}}_{\text{zoc}_i} = r_{\frac{\text{zoc}_i}{\text{zon}_i}} \cdot f_{T,\text{zoo}} \cdot \left(\frac{\mu^{\text{lin}}_{\text{zoo}} \cdot C_{\text{zon}_i}}{k_{\text{zoo}} + C_{\text{zon}_i}} + \mu^{\text{qua}}_{\text{zoo}} \cdot C_{\text{zon}_i}\right) \cdot C_{\text{zon}_i}. \tag{3.25}$$

The stoichiometric ratio of zooplankton-C to zooplankton-N of 5.5 is represented by $r_{\frac{\text{zoc}_i}{\text{zon}_i}}$. The T-dependency of zooplankton mortality is given by $f_{T,\text{zoo}} = 1^{(T-10)/10)}$ (with T in °C) and the half-saturation constant of zooplankton mortality k_{zoo} is set to $0.2\,\text{mmol N}\,\text{m}^{-3}$. $\mu^{\text{lin}}_{\text{zoo}} = 0.15\,\text{d}^{-1}$ and $\mu^{\text{qua}}_{\text{zoo}} = 0.02\,\text{d}^{-1}$ represent the linear and quadratic zooplankton mortality rate, respectively. With Eqs. (3.20)–(3.25), the uncorrected zooplankton excretion of C ($P^{\text{base}}_{\text{O}_2,\text{zoc}_i}$), i.e., uptake of O_2 can be calculated. The correction term $\Delta P^{\text{cor}}_{\text{O}_2,\text{zoc}_i}$ (see Eq. (3.19)) is calculated as follows:

$$P^{\text{cor}}_{\text{O}_2,\text{zoc}_i} = \begin{cases} \Delta P_{\text{zoc}_i} - \Delta P_{\text{zon}_i} \cdot r_{\frac{\text{zoc}_i}{\text{zon}_i}} & \text{for } \frac{\Delta P_{\text{zoc}_i}}{\Delta P_{\text{zon}_i}} \geq r_{\frac{\text{zoc}_i}{\text{zon}_i}} \wedge \frac{\Delta P_{\text{zon}_i}}{\Delta P_{\text{zop}_i}} \leq r_{\frac{\text{zon}_i}{\text{zop}_i}} \\ \Delta P_{\text{zoc}_i} - \Delta P_{\text{zop}_i} \cdot r_{\frac{\text{zoc}_i}{\text{zop}_i}} & \text{for } \frac{\Delta P_{\text{zoc}_i}}{\Delta P_{\text{zop}_i}} \geq r_{\frac{\text{zoc}_i}{\text{zop}_i}} \wedge \frac{\Delta P_{\text{zon}_i}}{\Delta P_{\text{zop}_i}} \geq r_{\frac{\text{zon}_i}{\text{zop}_i}} \\ 0 & \text{otherwise.} \end{cases} \tag{3.26}$$

Here, ΔP_{zoc_i}, ΔP_{zon_i} and ΔP_{zop_i} represent the net uptake of C, N and P by zooplankton, respectively. $r_{\frac{\text{zoc}_i}{\text{zop}_i}} = 110$ and $r_{\frac{\text{zon}_i}{\text{zop}_i}} = 20$ are the stoichiometric ratios of C:P and N:P for zooplankton applied in ECOHAM. The net uptake of C is calculated as:

$$\Delta P_{\text{zoc}_i} = P^{\text{up}}_{\text{zoc}_i} - \sum_{j=1}^{2} P_{\text{zoc}_i \to \text{dec}_j} - P_{\text{zoc}_i \to \text{dic}} - P_{\text{zoc}_i \to \text{doc}}. \tag{3.27}$$

The different loss processes given in this equation are the release of detrital matter ($P_{\text{zoc}_i \to \text{dec}_j}$; $j = 1, 2$ refer to slowly and fast sinking detritus, respectively) and the excretion of DIC ($P_{\text{zoc}_i \to \text{dic}}$) and DOC ($P_{\text{zoc}_i \to \text{doc}}$). The net uptakes of N and P by zooplankton are defined analogously to Eq. (3.27) with the only difference in the excretion of DIC and DOC, which are replaced by the excretion of NH_4^+ and DON in case of N and excretion of PO_4^{3-} and DOP for P.

3.2.2 Boundary conditions and forcing data

ECOHAM uses the daily fields of T and S as well as advective flow and vertical diffusion coefficients calculated and stored during the HAMSOM simulation as its physical background. For the initialisation of the biogeochemical state variables results from the ECOHAM simulation conducted by Lorkowski et al. (2012) are used as basis. These results are interpolated to the current ECOHAM grid (from 24 to 31 vertical layers) and improved values for the Kattegat/Skagerrak region are incorporated. For the prescription of the concentrations of the biogeochemical model state variables at the open boundaries ECOHAM utilises a depth-dependent, monthly climatology; only for DIC annually varying monthly fields are used (Lorkowski et al., 2012). The photosynthetically active radiation at the sea surface is calculated as 43 % of the overall incoming short-wave radiation (see Sect. 3.1.2). In order to include the effect of suspended particulate matter (SPM) on the light climate a daily SPM climatology is used (Heath et al., 2002).

3.2.2.1 Atmospheric nitrogen deposition

The inclusion of N input by atmospheric deposition is crucial when investigating the influence of N on the North Sea O_2 dynamics. In this thesis, the same atmospheric deposition fields are applied as described briefly in Große et al. (2016). The data preparation was conducted by Markus Kreus from the Institute of Oceanography, Universität Hamburg, who developed a hybrid approach allowing for the extrapolation of the available data set to longer time periods. The application of this hybrid approach was necessary due to the overall simulation period (1977–2014) exceeding the period of data availability (1995–2012).

The basic deposition data originate from the European Monitoring and Evaluation Programme (EMEP; `www.emep.int`) model and cover the period 1995–2012. First, the EMEP data for total deposition of oxidised (NO_x) and reduced nitrogen (NH_3) are interpolated to the model grid. In a second step a spatial anomaly field of the deposition rates of NO_x and NH_3 is calculated. This is done for both quantities by first calculating the average deposition during 1995–2012 for each individual grid cell, based on the interpolated EMEP data, and subsequent subtraction of the spatial average deposition rate over the entire domain.

Spatially and annually averaged deposition rates are than calculated for the year 2005 based on the EMEP data. In order to obtain spatially and annually averaged deposition rates for different years, these 2005 average deposition fields are multiplied with the long-term trends (normalised with respect to 2005) in European atmospheric deposition found by Schöpp et al. (2003, their Fig. 2). Finally, the previously calculated anomaly fields are

added to these average deposition rates yielding the spatially varying annual atmospheric N deposition rates used as ECOHAM forcing.

3.2.2.2 River forcing

The river load data for the biogeochemical state variables is part of the same data set containing the freshwater discharge. This data set contains daily resolved data for 3300 rivers in total, of which 254 lie inside the ECOHAM domain. The input locations of the rivers inside the domain are defined as the surface grid cell of that water column nearest to the actual geographic location of the corresponding river mouth. The data set principally includes time series of freshwater discharge and the following biochemical quantities: TN, NO_3^-, NH_4^+, dissolved inorganic N (DIN), TP, PO_4^{3-}, SiO_4^-, alkalinity, DIC, DOC, SPM and nitrite. However, the latter three are not used as input for ECOHAM. Biochemical loads provided in the data are always calculated as the product of freshwater discharge and the concentration of the difference biochemical quantities.

The river raw data for the different countries, which was compiled to the composite data set used in this thesis, originate from different sources. The data acquisition and preparation as well as the compilation of the composite data set is the work of Sonja van Leeuwen. The only exception is the data of the Belgian, Dutch and German rivers which were acquired and prepared by Pätsch et al. (2016), and incorporated in unchanged form to this composite data set. This data includes all the above mentioned quantities required by ECOHAM for the Scheldt, 5 Dutch and 3 German rivers. A description of the other river data is given in the following as no detailed description of the data is currently publicly available.

The data of six Swedish rivers entering the ECOHAM model domain (and 69 Swedish, Finnish and Estonian rivers not entering the domain) is based on monthly data provided by Miguel Alberto Rodriguez Medina from the Baltic Nest Institute (BNI) and can be obtained from the Baltic Environmental Database (BED; `http://nest.su.se/bed/`). These monthly data cover the period 1970–2014 and include all the above mentioned quantities required by ECOHAM. Daily data for this period was derived by linear interpolation between the monthly values and subsequent adjustment to annual data from the BED in order to obtain the correct sum of annual loads.

Daily discharge as well as TN and TP data for 25 Danish rivers were provided by Jens Bøgestrand from the former National Environmental Research Institute of Denmark (DMU) covering the period 1989–2007. For these quantities the years 1977–1988 were filled with daily 10-year climatologies of the years 1989–1998, while daily 10-year climatologies of the years 1998–2007 were used to fill the data of the years 2008–2014.

Daily freshwater discharge data for eight French rivers (four inside the ECOHAM do-

main) were obtained from the Banque Hydro (www.hydro.eaufrance.fr) and – for the Seine – from the Groupement d'Intérêt Public Seine-Aval (http://seine-aval.crihan.fr). The different freshwater data cover the entire period 1971–2015 and partly also early years. Daily time series of the concentrations biochemical quantities also originate from different sources. Biochemical data for Authie, Canche and Somme were obtained from the Agence de l'Eau Artois-Picardie (www.eau-artois-picardie.fr). For Dordogne and Garonne biochemical data were acquired from the Système d'Information sur l'Eau du Bassin Adour Garonne (http://adour-garonne.eaufrance.fr). Daily biochemical data for Loire and Vilaine were obtained from the OSUR portal of the Agence de l'Eau Loire-Bretagne (http://osur.eau-loire-bretagne.fr/exportosur). For the Seine daily biochemical data were acquired from the Agence de l'Eau Seine-Normandie (www.eau-seine-normandie.fr). The biochemical data of all French rivers, except for the Loire, cover the period 1971–2015, some also contain data for earlier years. Biochemical data for the Loire are only available from year 2000. Therefore, biochemical data for the years prior to 2000 are calculated as the product of daily 10-year climatologic concentrations during 2000–2009 and the available freshwater discharge. The French biochemical river data contain all the above mentioned quantities required by ECOHAM, except for DIC. For the Dordogne SiO_4^- and alkalinity are additionally missing; for the Garonne SiO_4^- is not present in the data.

Daily freshwater discharge of 12 Norwegian rivers were obtained from the Norwegian Water Resources and Energy Directorate (www.nve.no) covering the period 1980–2014. Discharges prior to 1980 were filled with a daily 10-year climatology of the period 1980–1989. Daily time series of the biochemical quantities in these rivers were obtained from the Norwegian Institute for Water Research (www.niva.no/). This data covers the period 1990–2014. For the period 1980–1989 the actual discharge data is multiplied with daily 10-year climatologic concentrations of the biochemical quantities during 1990–1999. For the years prior to 1980, the daily discharge climatology of 1980–1989 is multiplied with the daily climatologies of the concentrations of the different biochemical quantities of 1990–1999. The Norwegian river data contain data for all quantities required by ECOHAM except for DIN, DIC and alkalinity.

For the UK (excl. Northern Ireland) monthly freshwater discharge and biochemical data for the period 1974–2015 was acquired from the Environment Agency (www.gov.uk/environment-agency) for England and Wales and the Scottish Environment Protection Agency (www.sepa.org.uk) for a total of 160 rivers. Additionally, daily freshwater discharge data was obtained from National River Flow Archive (NRFA; http://nrfa.ceh.ac.uk). This daily data is corrected depending on the size of the catchment area of the individual rivers and the gauge station (i.e., distance between gauge

station and river mouth) in order to include ungauged tributaries to the considered river. Monthly average concentrations are calculated based on the monthly data and multiplied with this corrected daily freshwater discharge data yielding daily resolved time series of the biochemical quantities. The resulting UK river data shows varying quality with respect to biochemical data availability in different rivers. For the major rivers (e.g., Thames and Humber) only DIC and TN are missing, while for some very small rivers only freshwater discharge is available.

For five Northern Irish rivers daily freshwater discharge data was obtained from the NRFA covering the period 1972–2009. Daily biochemical data was acquired from the Northern Irish Rivers Agency (`www.infrastructure-ni.gov.uk/rivers-agency`) covering 1990–2006. The gap filling of the data for the years after 2009 (discharge) and 2006 (biochemical quantities) is also done based on daily 10-year climatologies analogously to, e.g., the Norwegian rivers. With respect to biochemical quantities, only four of the five resulting river data contain information on NO_3^-, NH_4^+, TP, PO_4^{3-} and SiO_4^-. For the fifth river only freshwater discharge is available. The other biochemical quantities required by ECOHAM are generally not available for the Northern Irish rivers.

For 33 Irish rivers daily freshwater discharge data for the period 1952–2011 were obtained from the HydroNet of the Irish Environment Protection Agency (`www.epa.ie/hydronet`). Annual data for the biochemical quantities for 1997–2009 are obtained from the annual OSPAR reports on Riverine Inputs and Direct Discharges to Convention Waters (RID; e.g., OSPAR, 2011). Annual average concentrations from the RID data are multiplied with the daily freshwater discharge yielding daily resolved biochemical loads. The biochemical data availability varies between different rivers, with some containing information on TN, NO_3^-, NH_4^+, TP, PO_4^{3-} and SiO_4^-, while for others no biochemical data are available at all. The other biochemical quantities required by ECOHAM are generally not available for the Irish rivers.

It has to be noted that the river data set compiled by Sonja van Leeuwen constitutes a comprehensive data set for riverine freshwater and nutrient input into the North Sea and adjacent regions of the northwestern European continental shelf. Especially for the North Sea no comparable data set including such a large number of rivers from the different neighbouring countries is available. Therefore, this data set provides a valuable basis for this thesis which focuses particularly on the influence of riverine nitrogen input on the North Sea O_2 dynamics, despite its minor restrictions with respect to data availability for some mainly small rivers.

As ECOHAM utilises riverine input of inorganic and organic matter – with the latter not explicitly included in the river data provided by Sonja van Leeuwen – riverine input of organic N and P has to be derived from total (TN, TP) and inorganic N and P input,

respectively. The riverine input of particulate organic N (PON) is calculated as:

$$\mathrm{PON} = \mathrm{TN} - \begin{cases} \mathrm{DIN} & \text{for } \mathrm{TN} > 0 \wedge \mathrm{DIN} > 0 \\ \left(\mathrm{NO_3^-} + \mathrm{NH_4^+}\right) & \text{for } \mathrm{TN} > 0 \wedge \mathrm{DIN} < 0 \wedge \mathrm{NO_3^-} > 0 \wedge \mathrm{NH_4^+} > 0 \end{cases} \tag{3.28}$$

Particulate organic P (POP) is calculated accordingly, subtracting $\mathrm{PO_4^{3-}}$ from TP (in case of both being greater than zero). In case that exactly one of the two organic quantities, PON or POP, cannot be calculated from its corresponding total and inorganic quantities, it is calculated using an N:P ratio of 16:1 according to Redfield (1934) and the previously calculated organic quantity (e.g., $\mathrm{POP} = 1/16 \cdot \mathrm{PON}$ [mol]). Particulate organic C (POC) has to be calculated directly from PON (or POP) as total C is not included in the data. Thus, POC is calculated from POP and a C:N ratio of 106:16 (Redfield, 1934) after the calculation of PON as previously described. PON, POP and POC are added to the fast sinking detritus pool when entering the model domain, Organic Si is not included as river input in this thesis.

The resulting biochemical river data may still contain gaps in time series of individual quantities, or may even lack entire time series for individual rivers as described previously. In any of these cases ECOHAM applies an intrinsic gap filling algorithm that utilises the available freshwater discharge data and the biochemical state variable concentration in the river input cell to calculate a river load such that the concentration of the state variable in the input cell is not diluted by the freshwater discharge. This algorithm is applied in any occasion when freshwater discharge data are available, but input data for individual state variables are missing. In addition, the same algorithm is applied to model state variables that are generally not included in the river data, e.g., bacteria-N, in order to avoid dilution of these quantities. In case of gaps in the discharge data the riverine input of both, freshwater and biochemical quantities, is considered to be zero.

3.3 Model grid and simulation sequence

HAMSOM and ECOHAM utilise the same grid, which is shown in Fig. 3.2 including the bottom topography (grey areas indicate land). The model domain covers the area from 47 ° 35' N to 63 ° 59' N and 15 ° 15' W to 14 ° 5' E. The latitudinal direction has a resolution of 1/5 ° which implies 82 grid cells. The longitudinal direction has a resolution of 1/3 ° resulting in 88 grid cells. The vertical dimension is resolved by 31 z-layers with the following depth levels (in m): 10, 15, 20, 25, 30, 35, 40, 45, 50, 60, 70, 80, 90, 100, 120, 140, 160, 180, 200, 250, 300, 350, 400, 500, 600, 800, 1000, 1500, 2000, 3000, 4000. In total, the domain encompasses 4455 water columns and 83558 wet cells.

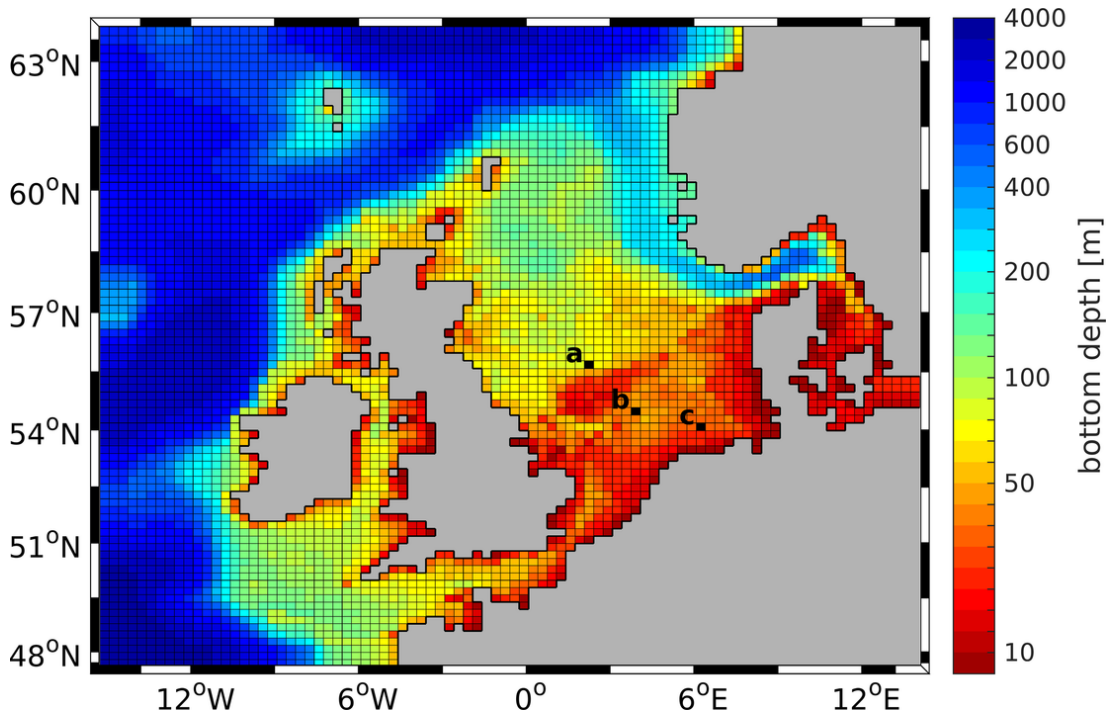

Figure 3.2: Model domain and bathymetry as used by HAMSOM and ECOHAM. Colour scale increments are equidistant between two labelled depth levels. Grey areas indicate land. Black markers indicate locations of time series observations: a) Cefas North Dogger, b) Cefas Oyster Grounds, c) MARNET Ems (see Sect. 3.4.2.1.

The HAMSOM model is run over the period 1976–2014 with a time step of 10 minutes and generates daily (24-hour averages) output for the entire model domain (T, S, advective flow, vertical diffusion coefficient, sea surface elevation). The first year of this simulation represents the spin-up period of HAMSOM. The river freshwater discharge data of 1977 are used for this spin-up year. ECOHAM is run off-line, i.e., de-coupled from HAMSOM, over the period 1977–2014 using a time step of 30 minutes. It utilises the daily output fields provided by HAMSOM and applies linear interpolation between the daily information originating from HAMSOM. The off-line procedure in combination with the daily output of HAMSOM implies that diurnal cycles of stratification or currents, e.g., due to tides, are not considered in ECOHAM. For spin-up, the year 1977 is re-run two times. As the period of interest of this study is 2000–2014, this spin-up procedure does not affect the presented model results. During the simulation, ECOHAM applies a dynamic time step subdivision in cases of state variable concentrations becoming negative or state variable rates of change exceeding 40 % of the current state variable concentration.

Due to the off-line simulation of ECOHAM an influence of the biochemical model on the thermal structure by enhanced light attenuation due to SPM or phytoplankton is not taken

into account. In addition, short wave radiation is attributed to the first layer (surface) only in HAMSOM. However, a sensitivity study allowing for deeper light penetration and feedback on the thermal structure confirmed this effect to be only of minor importance (Große et al., 2016).

3.4 Validation data

In order to demonstrate that the applied hydrodynamical and biogeochemical models, HAMSOM and ECOHAM are capable of reproducing well the North Sea dynamics different data sets are used for model validation. The validation of HAMSOM focuses on stratification related quantities, namely summer T and S. The validation of ECOHAM focuses on the representation of inorganic nutrient concentrations and Chl-a (as a proxy for phytoplankton biomass), and more specifically on spatial and temporal patterns of O_2. The used data sets are described in the following.

3.4.1 Hydrographic data

The data set used for the validation of the North Sea hydrography as simulated by HAMSOM (see Sect. 4.2) constitutes a data set of transect measurements of summer T and S provided by the BSH. The data can be accessed via the Copernicus Marine Environment Monitoring Service (CMEMS; `http://marine.copernicus.eu`; product identifier: INSITU_NWS_TS_REP_OBSERVATIONS_013_043).

This data set consists of zonal transect measurements of T and S between 54 °N and 60 °N with a 1 °-interval basically covering the entire North Sea (7 transects in total) over the period 1998–2010. From 1998 to 2006, measurements were taken from R/V Gauss, while from 2007 to 2010 data were collected from R/V Pelagia. An undulating device equipped with sensors measuring conductivity, T and depth (CTD) was used for the measurements of the years 1998–2009. In 2010, CTD sensors were placed on a ScanFish device, a vehicle with flaps controlling the up- and downward movement within the water column. The measuring depth ranges from the near-surface (2 m–3 m) to about 85 m or less, depending on the water depth. The recording duration of each single transect ranges between 1 and 3 days depending on the distance covered. The equipped CTD sensors have a sampling frequency of 32 Hz resulting in spatially and temporally high-resolved measurements. Calibration of the CTD sensors was conducted before and after each year's observation campaign. Data errors were found to be less than 0.01 units of both, T (°C) and S (PSS-78).

Before using the data for model validation a data filtering is applied, removing the

data measured during the transfer between the different zonal transects. In addition, very short continuous data sections (less than 6 subsequent data points) are removed in order to exclude data potentially affected by sensor failure. Last, data measured south of 53.8 °N are removed as south of this latitude no transect measurements were conducted. In the following, the resulting data product is referred to as 'ScanFish' data.

3.4.2 Biogeochemical data

The validation of the North Sea biogeochemistry, and particularly O_2, as simulated by ECOHAM is based on multiple different data sets. For the validation of the upper layer biogeochemistry (see Sect. 5.1), a composite data set is used, which contains (inorganic) nutrient, Chl-a and O_2 data from different data sources. One part of the data is obtained from the 'Meeresumweltdatenbank' (MUDAB; `http://geoportal.bafg.de/MUDABAnwendung`). This data includes individual point measurements of NO_3^-, NH_4^+, PO_4^{3-}, SiO_4^-, Chl-a and O_2 from various originators covering the period 2000–2008. A second subset of data was provided by Uwe Brockmann and Monika Schütt (Division of Biogeochemistry and Marine Chemistry, Institute for Geology, Universität Hamburg) and represents a data set that was also used in several projects funded by the German Federal Environment Agency (UBA). This data also contains individual point measurements from different originators, covering the period 2000–2014. Furthermore, data collected during the North Sea programme, carried out by the Royal Netherlands Institute for Sea Research (NIOZ), are included in the composite data set. This data contains individual profile measurements covering the entire North Sea with a grid of approximately $1\,^\circ \times 1\,^\circ$. Data added to the composite data set were collected during cruises with R/V Pelagia during the following periods: August, September and November 2001, February, March and May 2002, and August and September 2005. For a detailed description of the data the reader is referred to Thomas et al. (2012) (2001 and 2002 cruises) and Thomas and Borges (2012) (2005 cruise) which include both, the data itself and the cruise reports with detailed information on the instrumentation.

3.4.2.1 Bottom oxygen measurements

The different observation data sets described in the following and used for the validation of simulated bottom O_2 are identical to that applied by Große et al. (2016). For the validation of the spatial distribution of simulated summer bottom O_2 concentrations, the bottom O_2 measurements of August and September 2001 and 2005 of the data set just described are used (Thomas et al., 2012; Thomas and Borges, 2012). In addition, bottom O_2 collected during R/V Pelagia cruises in August and September 2008 are included (Zemmelink, 2008). The resulting data set encompasses data sampled from 18 August to 13 September 2001, and from 17 August to 5 September 2005 and 2008. Each year the North Sea was sampled on an approximate $1\,^\circ \times 1\,^\circ$ grid with about 90 stations (Bozec et al., 2005, 2006; Salt et al., 2013). During each cruise, a total of 750 water samples were collected for dissolved O_2. In 2001, the O_2 concentrations were determined by the Winkler titration using a potentiometric end-point determination with an accuracy of $\pm\,2\,\mu\mathrm{mol\,O_2\,kg^{-1}}$ (less than $\pm\,0.07\,\mathrm{mg\,O_2\,L^{-1}}$ depending on T and S). In 2005 and 2008, the O_2 concentrations were obtained applying the spectrophotometric Winkler approach with a precision of less than $0.03\,\mathrm{mg\,O_2\,L^{-1}}$. A detailed description of the measurement system used is given in Reinthaler et al. (2006).

For the validation of the temporal evolution of bottom O_2 concentration data from two different providers is used. Cefas operates a network of so-called SmartBuoys to provide autonomous *in situ* measurements of physical, chemical and biological parameters (Mills et al., 2003). One SmartBuoy was located directly north of the Dogger Bank ('North Dogger') at 55°41' N, 2°16.80' E; see marker a in Fig. 3.2) between 24 February 2007 to 15 September 2008 in 85 m water depth (Greenwood et al., 2010). Another SmartBuoy was located in 45 m depth at 54 ° 24.84' N, 4 ° 2.50' E in the Oyster Grounds area south of Dogger Bank ('Oyster Grounds'; see marker b in Fig. 3.2). O_2 concentrations were continuously recorded with a frequency of 5 Hz at 31 m and 85 m at North Dogger, and at 35 m and 45 m at Oyster Grounds. These autonomous O_2 measurements were corrected for drift using O_2 concentrations determined from discrete water samples to give an accuracy of 0.5 % (Greenwood et al., 2010). For validation purposes the O_2 data derived from the near-bottom sensors are used. This data can be accessed via: `http://cefasmapping.defra.gov.uk/Smartbuoy`.

The BSH operates a continuous monitoring station at 54°10' N, 6°21' E ('MARNET Ems'; see marker c in Fig. 3.2). The O_2 saturation is measured hourly using opto-chemical sensors (optodes). Sensors are located in 6 and 30 m depth, respectively, and the bottom depth is 33 m. O_2 concentration is calculated from observed O_2 saturation and the O_2 saturation concentration derived from observed T and S according to Benson and Krause (1984). The applied sensors have a resolution of $0.03\,\mathrm{mg\,O_2\,L^{-1}}$ and an accuracy better

than $0.26\,\mathrm{mg\,O_2\,L^{-1}}$. Before deploying the sensors a 0 %–100 % calibration is conducted, and they are re-calibrated after operation to quantify any drift. In addition, a regular on-site validation takes place using a calibrated fast optode (accuracy of $\pm\,2$ %) or by applying the Winkler titration (accuracy better than $\pm\,1$ %). This data can be obtained from: `http://www.bsh.de/en/Marine_data/Observations/MARNET_monitoring_network/`.

Chapter 4

Hydrography and stratification of the North Sea

Stratification, i.e., the vertical structure of T and S, plays a crucial role in the North Sea O_2 dynamics as it controls the turbulent exchange of O_2 between the oxygenated surface waters and the less saturated deeper waters below the mixed layer depth (MLD). Therefore, the reasonable representation of the main hydrographic features, i.e., distribution of T and S as well as stratification, by the applied hydrodynamical model constitutes the fundamental basis for the investigation of North Sea biogeochemistry in relation to O_2 dynamics (see Ch. 5).

In order to demonstrate that the HAMSOM model is capable of reproducing well these features and thus provides a reliable basis for the investigation of the North Sea O_2 dynamics, this chapter first provides a general overview of the North Sea hydrography (T and S) simulated by the HAMSOM model (see Sect. 3.1). Multi-year monthly averages of simulated sea surface T (SST) and S (SSS) are shown in order to describe the annual cycle of these quantities in the North Sea. These 17-year averages are calculated over the period 1998–2014 for two reasons. First, the analysis of the O_2 dynamics (see Ch. 5) focuses on the years 2000–2014. Second, high-resolution *in situ* ScanFish data of T and S along certain zonal transects during the summers 1998–2010 are available from the BSH. After the description of seasonal cycles of SST and SSS, these data are used for the validation of summer T and S in the North Sea. By this, a detailed description of the features of summer T and S, with a special focus on their vertical structure and regional differences, is provided. In addition to this qualitative validation, the model performance is assessed quantitatively to further evaluate the capabilities of HAMSOM with respect to summer stratification.

4.1 Sea surface temperature and salinity

In order to provide insight in the average annual cycle of SST and SSS of the North Sea as simulated by HAMSOM, Fig. 4.1 and Fig. 4.2 show the 17-year, monthly climatology of simulated SST and SSS, respectively. In this study, SST and SSS refer to the first model

layer which encompasses the uppermost 10 m. The averaging period encompasses the years 1998–2014, the corresponding standard deviations (STD) are provided in Appendix A.2. The term 'sea surface' here refers to the surface layer of the model which represents the uppermost 10 m of the water column (or less in case of a shallower bathymetry).

Figure 4.1 shows that lowest SST in the eastern North Sea and the adjacent Kattegat and Danish straits is reached in February (Fig. 4.1b) while in the central and western North Sea lowest SST is reached in March (Fig. 4.1c). Minimum SST of the 17-year climatology goes down to 0 °C in the Skagerrak, Kattegat and Danish straits and can even fall below 0 °C in individual years as indicated by the high STD of up to 2 °C in these regions (see Appendix A.2, Fig. A.2). In the North Sea, lowest SST is reached in the German Bight, reaching a minimum of about 4 °C, but can go down to about 1 °C for individual years in this region (not shown). In most parts of the central and western North Sea, average SST in March shows values of 6 to 7 °C. In the northwesternmost part of the North Sea, SST exceeds values of 7 °C due to the inflow of relatively warm NAW (compared to the inner North Sea) through the Pentland Firth and Fair Isle Channel, and east of the Shetlands. The same applies to the southwestern North Sea (near the Strait of Dover) resulting from the inflow of Atlantic water through the English Channel.

SST gradually increases from March/April (Fig. 4.1c and d) to August (Fig. 4.1h), when maximum SST is reached in the entire North Sea region. The highest average SST is reached in the Danish straits with values of up to 21 °C. Along the continental North Sea coast from Belgium in the Southwest to Denmark in the Northwest a band with SST of up to 19 °C can be seen. From June to September (Fig. 4.1f–i), the SST in the North Sea shows a steady decrease from this coastal area in the Southeast towards the Atlantic inflow region around Fair Isle in the Northwest, where an average SST of 12 °C to 13 °C is present. On the one hand, this relates to the increase in depth from only 10 m to 20 m along the continental coast to about 200 m in the North. The shallower depth allows for an earlier onset of surface warming in spring as the heat from solar radiation is distributed over a smaller water body. On the other hand, the northern part is strongly influenced by the inflow of NAW branching off the North Atlantic Current and advecting relatively cold water compared to the southern coastal zone. For the same reasons, an SST gradient inverse to that during summer can be seen from January to March (Fig. 4.1a–c). This relates to the NAW, which enters the northwestern North Sea, being warm compared to the water masses in the southern North Sea. In October (Fig. 4.1j), this gradient starts to diminish as SST starts to decrease in the shallow coastal areas due to surface cooling, leaving a warm-water tongue which extends from the Strait of Dover in the Southwest to approximately 7 °E, 54.5 °N in the Northwest. This signal remains visible in November (Fig. 4.1k), however, to a lesser extent and characterised by generally lower SST within

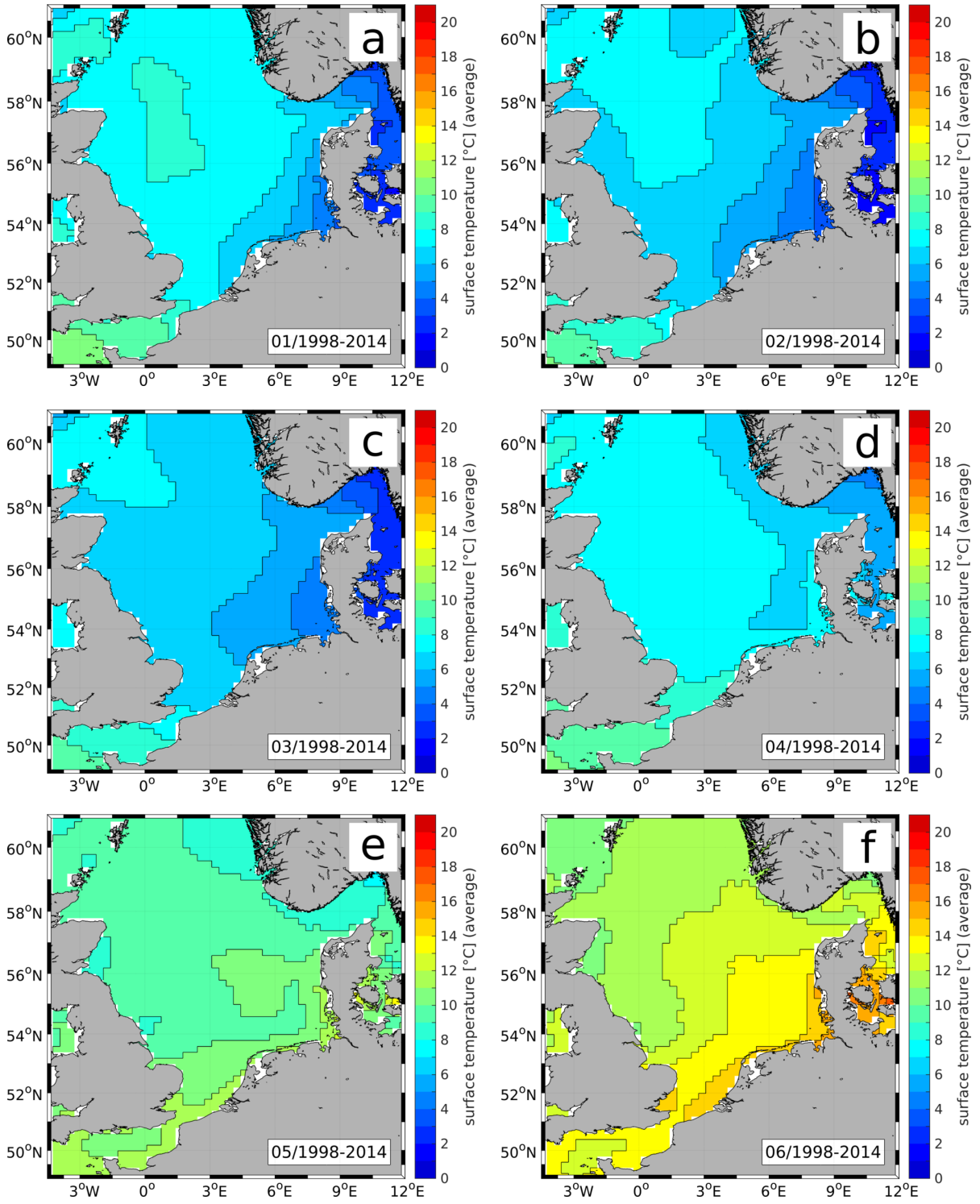

Figure 4.1: Monthly climatology of simulated sea surface temperature during the 17-year period 1998–2014. Months are indicated by numbers in bottom-right corner of each panel: (a) January to (f) June. For corresponding standard deviation see Fig. A.2.

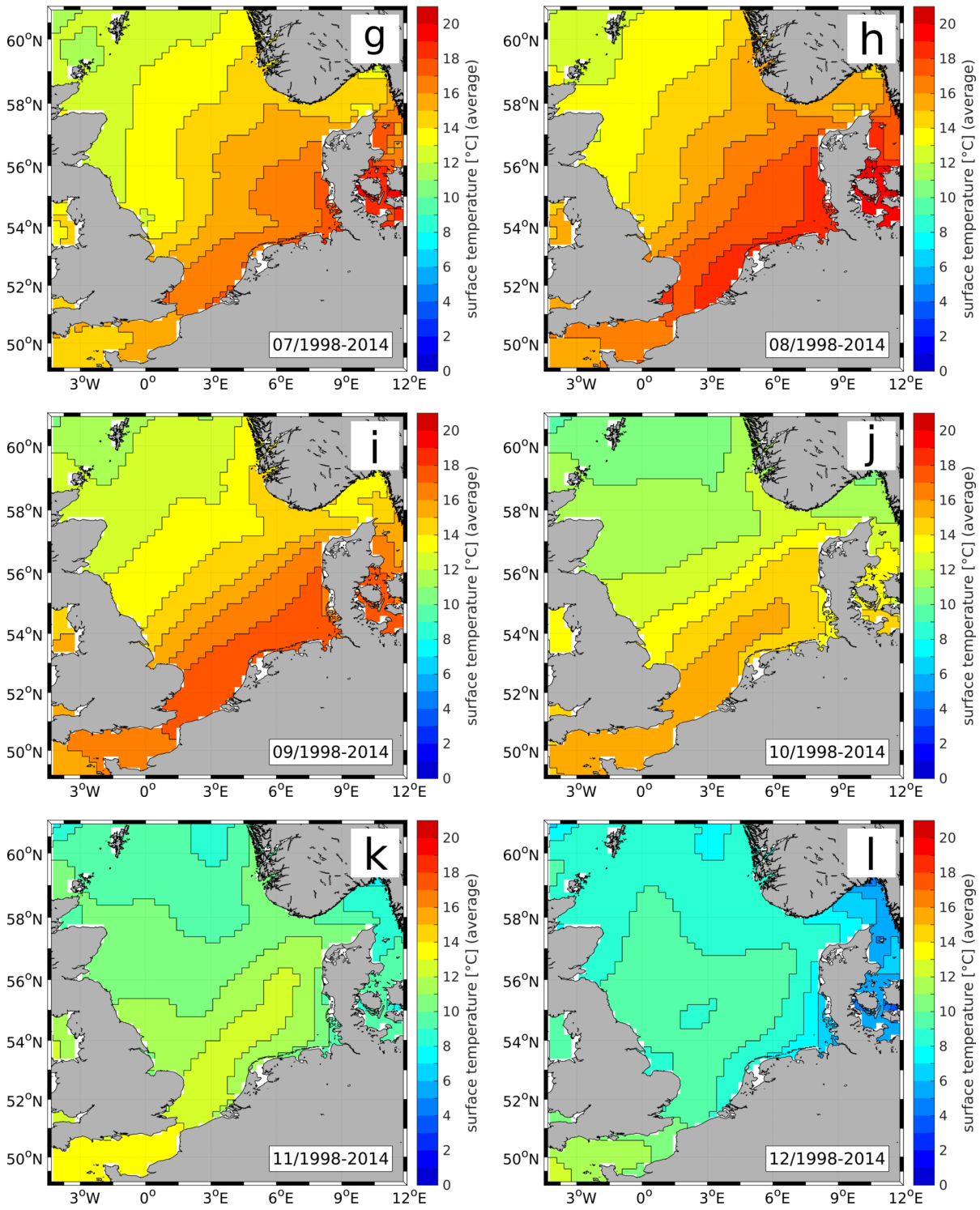

Continued: (g) July to (l) December.

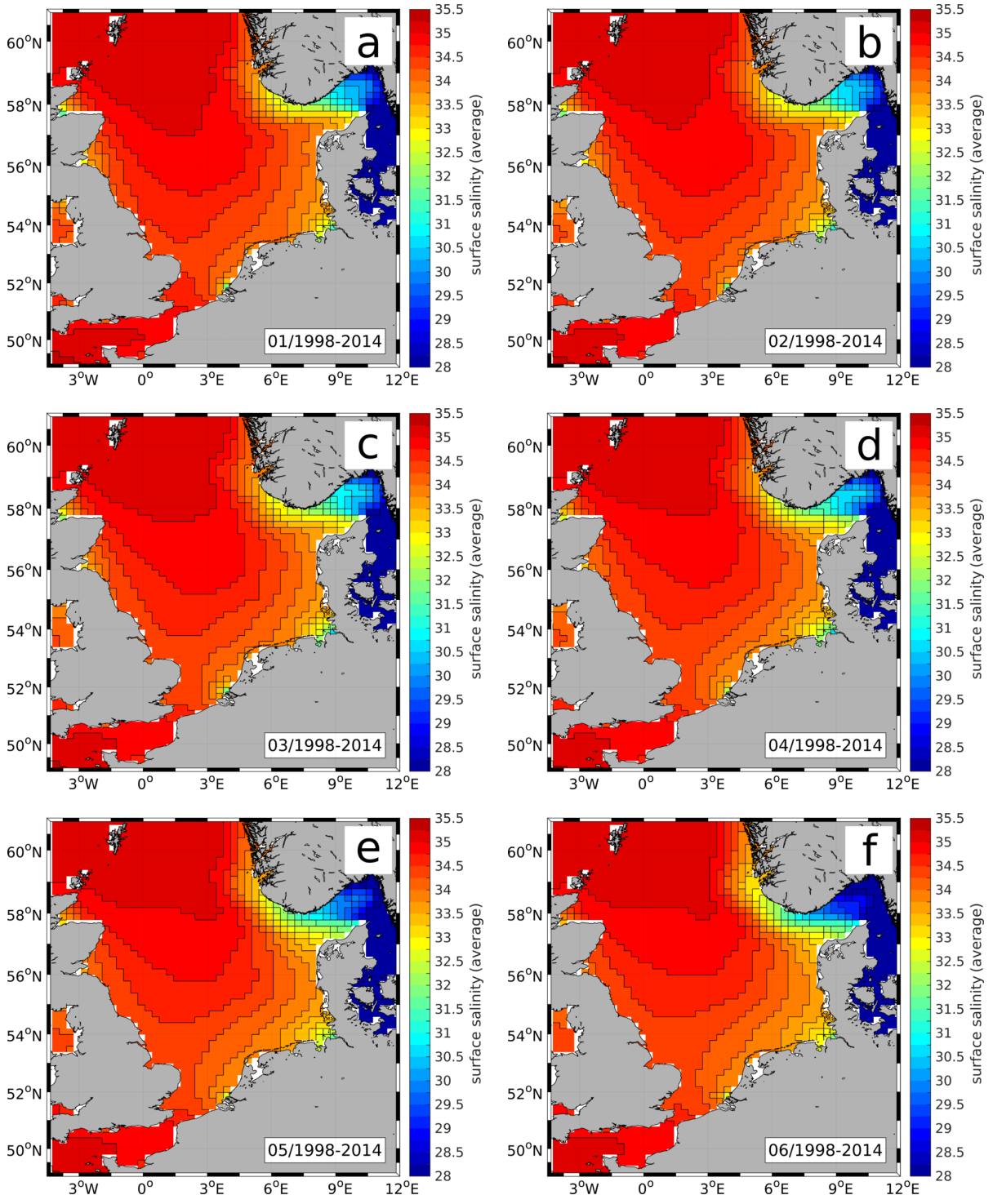

Figure 4.2: Monthly climatology of simulated sea surface salinity during the 17-year period 1998–2014. Colour scale cut at lower end. Months are indicated by numbers in bottom-right corner of each panel: (a) January to (f) June. For corresponding standard deviation see Fig. A.3.

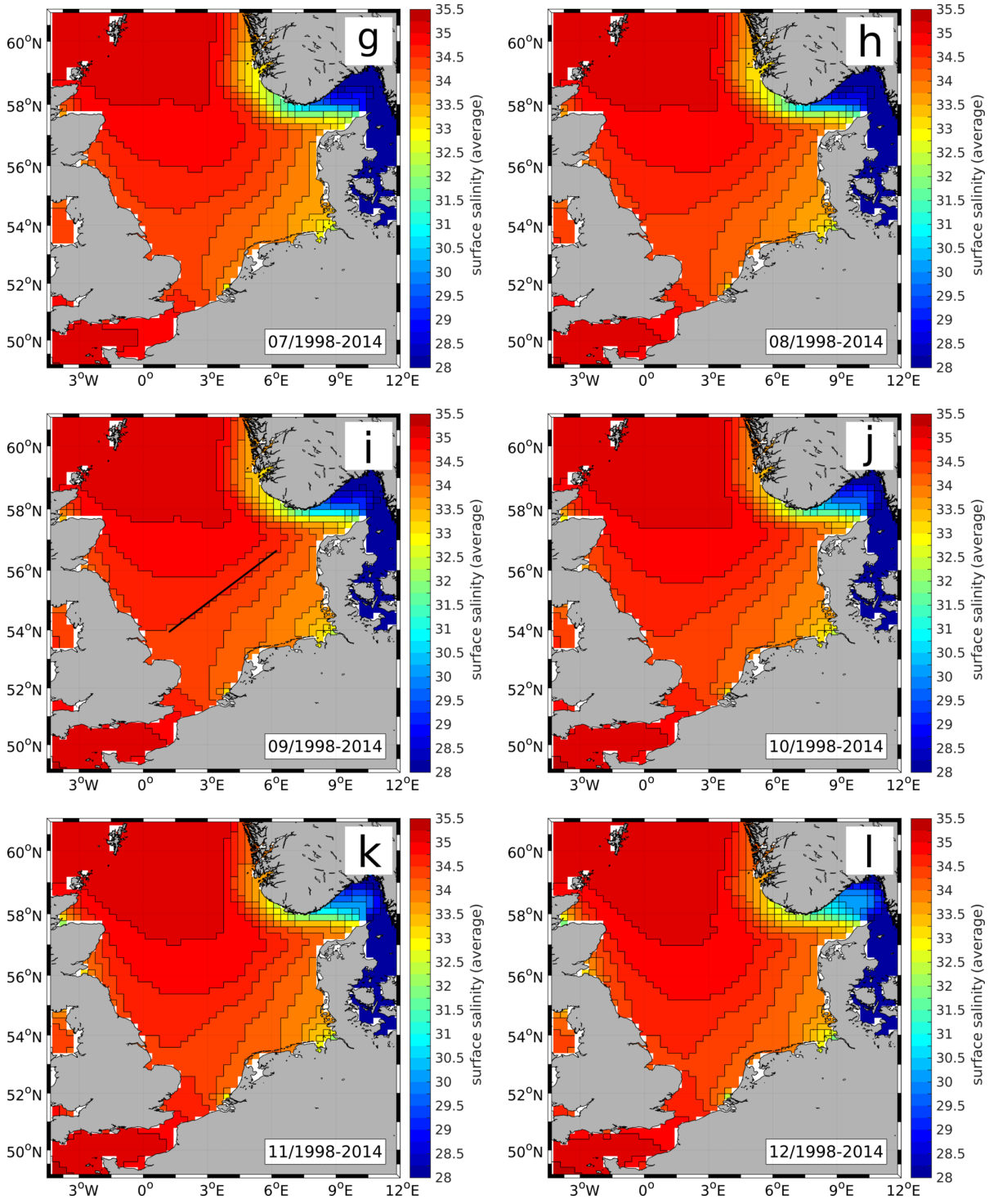

Continued: (g) July to (l) December. Black line in panel i marks the approximate location of the 34.74-isohaline referred to in the text.

the entire North Sea with maximum values of up to 13 °C. In December (Fig. 4.1l), this tongue has vanished and almost the entire North Sea shows SST between 8 °C and 10 °C.

The annual cycle of SSS, presented in Fig. 4.2 (lower end of colour scale cut at 28), shows a less pronounced seasonal signal than SST. In general, a North-South gradient in SSS can be seen throughout the entire year with high SSS around the Shetland Islands in the Northwest and lower SSS near the continental coast of the southern North Sea. Only along the British east coast SSS shows generally low values due to riverine freshwater discharge. The northwestern part of the North Sea (north of 58 °N, west of 4 °E) consistently shows average SSS above 35, except for the regions near the British coast. North of 54 °N, most parts of the central and western North Sea show average SSS between 34.75 and 35, except for the British coastal zone where riverine freshwater discharge causes a reduction in SSS with minimum values of approximately 32 in the Moray Firth (northwest Scotland). The 34.75g kg^{-1}-isohaline basically follows a line from 1 °E, 54 °N to 6.5 °E, 57 °N (see black line in Fig. 4.2i), which roughly corresponds to the 50 m-isobath, with only slight zonal or meridional shifts during the annual cycle. This relates to the fact that this northern part of the North Sea is dominated by high-saline water originating from the Atlantic inflow across the northern shelf edge. Most of this water is recirculated north of the shallow Dogger Bank, which extends approximately from 1.5 °E, 54.5 °N to 5 °E, 55.5 °N and constitutes a natural barrier for the NAW originating from the North (e.g., Kröncke and Knust, 1995; Lenhart and Pohlmann, 1997).

In the Southern Bight, the Atlantic inflow through the English Channel has a stronger influence, however, its high-S signal is less pronounced than that in the northern North Sea. This results from the riverine freshwater discharge from southern UK and northern France resulting in a dilution of the high-saline signal within the English Channel, before it enters the North Sea through the Strait of Dover. In addition, the freshwater discharge from river Thames at the southeast coast of the UK and, even more important, from the Dutch and Belgian rivers Rhine, Meuse and Scheldt further dilute the SSS signal originating from the English Channel. At the mouths of Rhine and Meuse (at approximately 4 °E, 54 °N in the model) average SSS varies between 31.5 and 33.5 during the annual cycle. Here, the lowest SSS occurs in March/April (Fig. 4.2c and d), visible in the low-S signal in and around the river mouth, when the snowmelt on the continent causes an increase in riverine freshwater discharge. The Atlantic inflow from the English Channel together with the riverine discharge from southern UK and the continental rivers constitute the main drivers of the continental coastal current in this region.

Along the continental coastal current between the mouths of Rhine and Meuse and the northwestern tip of Denmark monthly averaged SSS consistently stays below 34.25 during the annual cycle and even below 34 from March to July (Fig. 4.2c–f) due to the

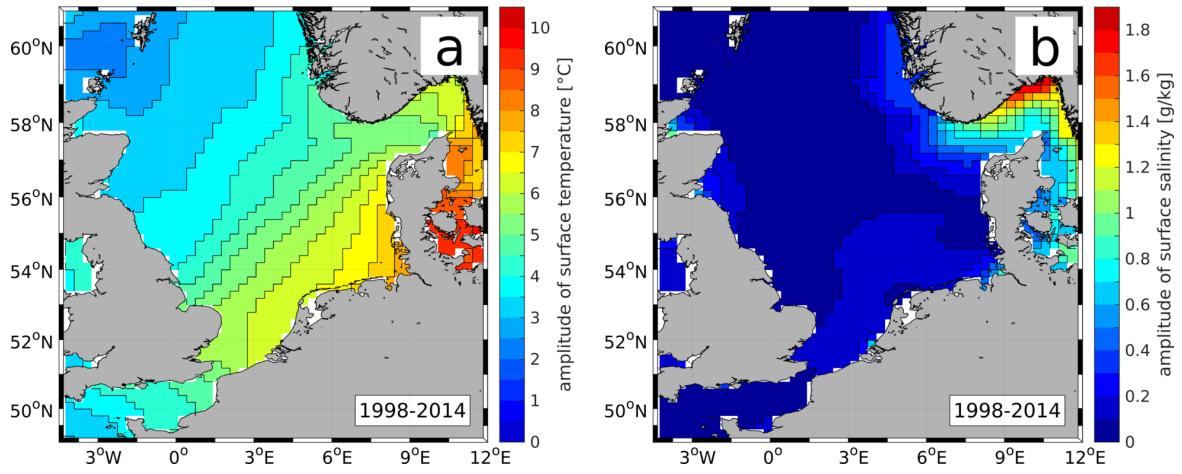

Figure 4.3: Amplitude of the annual cycle of sea surface (a) temperature and (b) salinity during 1998–2014.

increased riverine discharge in spring. The German Bight represents the area of lowest SSS along the continental coast. On the one hand, this relates to the already less saline water downstream of Rhine and Meuse and, on the other hand, to the high discharges of the rivers Elbe and Weser into this area, adding up to about $1000\,\mathrm{m^3\,s^{-1}}$ on average (Pätsch et al., 2016). Similar to the Rhine and Meuse area, the lowest SSS of 31 and even less occur during March and April (Fig. 4.2c and d) due to the high freshwater discharge caused by the snowmelt. The high STD of up to 1.6 at the mouths of Rhine and Meuse and in the Elbe estuary from February to April (see Appendix A.2, Fig. A.3b–d) illustrates the high year-to-year variability in riverine freshwater discharge. It further indicates that SSS of less than 30 can occur during years of particularly high river run-off during the melting period.

West of the northern tip of Denmark the Jutland current, which is the extension of the continental coastal current, first enters the Skagerrak before it joins the Norwegian coastal current. The latter is driven by the water originating from the Jutland current as well as the Baltic inflow and riverine freshwater discharge at the south coast of Norway. The Baltic inflow brings low-S water with SSS of about 10 and less around the Danish straits (e.g., Alheit et al., 2005), which mixes with the high-saline North Sea water in the Kattegat/Skagerrak region resulting in SSS between 28 (and less) and 31 in the Skagerrak. The Norwegian coastal current consequently follows the Norwegian coast northwestward and finally leaves the North Sea across the shelf edge, with its pathway clearly detectable by the lower SSS along the Norwegian south and west coast relative to the higher SSS farther offshore. Except for this region in the vicinity of the Baltic inflow, where STD of up to 4 occur during the analysed period 1998–2014 (see Fig. A.3), and the above mentioned

river locations most North Sea areas show only minor variations in SSS throughout the annual cycle and the analysed period. On the one hand, this indicates the important role of the Atlantic inflow across the northern shelf edge on the northern North Sea SSS, and on the other hand, demonstrates the strong influence of the continental rivers on the southeastern North Sea and, especially, that of the Baltic inflow on the northeastern North Sea.

In order to summarise the variation of SST and SSS during the annual cycle, Fig. 4.3a and b, respectively, show the amplitudes of SST and SSS of the annual cycle during 1998–2014. The amplitude for each model grid cell was calculated by applying a Fourier transformation to the daily time series of simulated SST and SSS, respectively. It can be seen that in most parts of the North Sea, except for the areas influenced by the Baltic inflow the amplitude of SST is much higher than that of SSS. Especially in the central North Sea, SST amplitude reaches values between 5 °C and 7 °C which is 25 to 50 times higher than that of SSS ranging between 0 and 0.2. S has an about 5–10 times stronger influence on density than T (according to the 'thermodynamic equation of seawater 2010'; TEOS-10 IAPWS, 2008; IOC et al., 2010). Consequently, the large relative difference in amplitude is a strong indicator that T constitutes the main driver for the evolution of seasonal stratification in the central North Sea. In contrast, in the Skagerrak and at the southern tip of Norway – the region of the strongest influence of the Baltic inflow –, SSS amplitude reaches values between 0.7 and 1.8, while SST amplitude ranges from 5 to 6.5 °C. This indicates that in this area S is of equal or even greater importance for surface water density and thus can have a major influence on seasonal stratification.

4.2 Summer temperature and salinity

The previous section gave insight in the spatial and seasonal patterns of SST and SSS as simulated by HAMSOM, and showed that in most North Sea regions, T constitutes the major impacting factor for seasonal stratification. As O_2 deficiency in the North Sea evolves during summer, the period of strongest stratification, it is important to reproduce well the spatial (horizontal and vertical) patterns of summer T in particular, but also S.

For this purpose, high-resolution ScanFish observations of T and S along seven basically zonal transects, covering the entire North Sea (see Fig. 4.4), are presented in Fig. 4.5 and Fig. 4.6, respectively. Such transect measurements have been carried out in summer of the years 1998 to 2010. Here, 2005 is chosen as it provides the best data coverage across all seven transects and thus gives a good overview over the horizontal and vertical distribution of T and S in the North Sea during summer. For most other years, either data for entire transects or large parts of individual transects (extending over more than 2 °E) are missing.

With respect to the representativity of the year 2005 it has to be noted, that especially in the eastern part of the central North Sea some specific features are visible in the S observations, which do not occur during all years. These features will be discussed in more detail during the following comparison.

The ScanFish measurements presented have been carried out from 16 to 27 August 2005, with an observation period of 2 to 3 days per transect (see bottom-right corner of each figure panel). The displayed simulation data represent temporal averages over the observation period of each transect, based on daily model output. The corresponding STDs are not presented as they show only very small values.

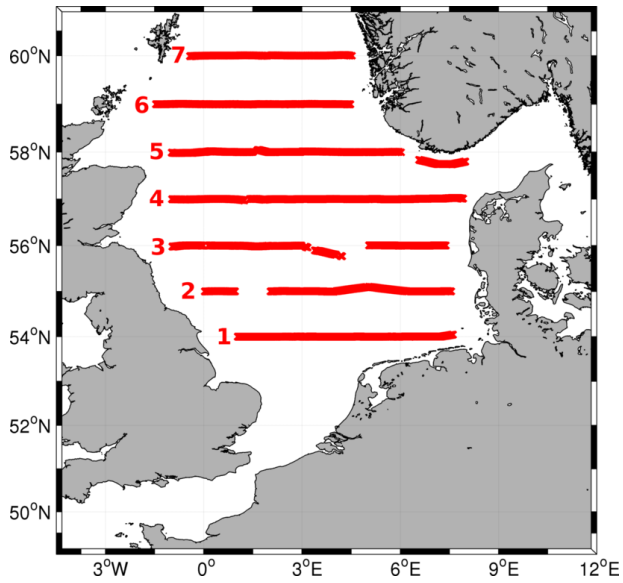

Figure 4.4: Trajectories of ScanFish transects in 2005 after filtering the raw data. Transect numbering as used in Fig. 4.5–Fig. 4.7.

Before comparing the individual transects a more general description of the observed and simulated T patterns is provided. The observations (Fig. 4.5; left) show a decrease in near-surface (upper 20 m) T from South (transect #1; Fig. 4.5a) to North (transect #7; Fig. 4.5m). An eastward increase in near-surface T can also be seen along all transects, except for transect #7. Besides this, the transects #2 to #7 show a distinct thermal stratification in most parts of each transect which is characterised by a distinct T difference between surface and bottom and by a pronounced vertical T gradient in 30 to 40 m depth. For transect #1 only weak thermal stratification can be seen in the deeper regions roughly between 2 °E and 3 °E. These basic features are principally well reproduced by HAMSOM (Fig. 4.5; right), however, not to their full extent. In the following a more detailed analysis of the observed summer T structures will be given in relation to the simulated T fields.

At the western edge of transect #1 (Fig. 4.5a), which is located at about 54 °N, 1 °E to

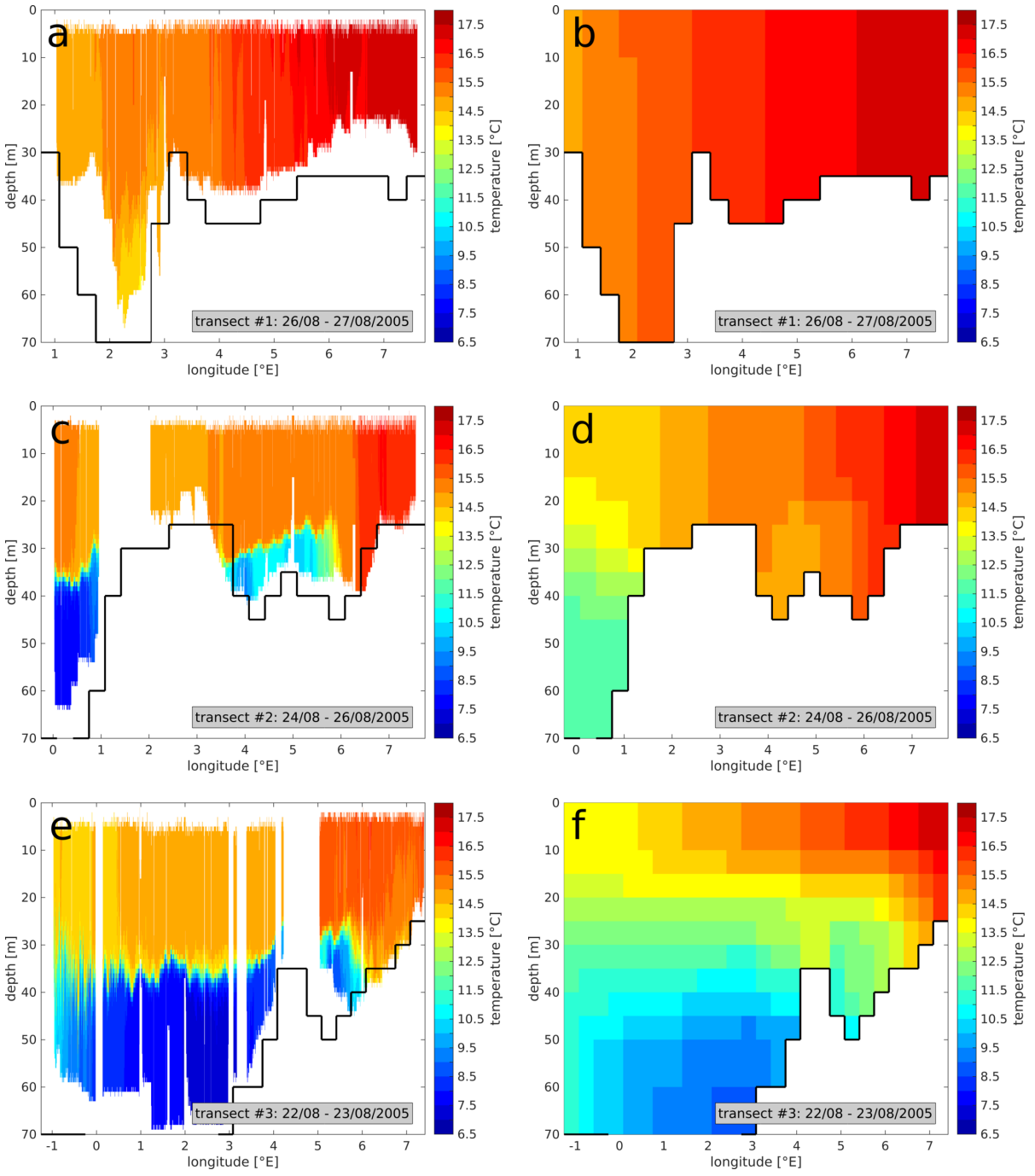

Figure 4.5: Transects of temperature in summer 2005 along the trajectories given in Fig. 4.4 as observed by ScanFish (left) and simulated by HAMSOM (right). Black line indicates HAMSOM bottom topography. HAMSOM results represent averages over observation period (bottom-right corner of each panel) based on daily output. Note different maximum depth and longitudinal range. Transects (a, b) #1 to (e, f) #3.

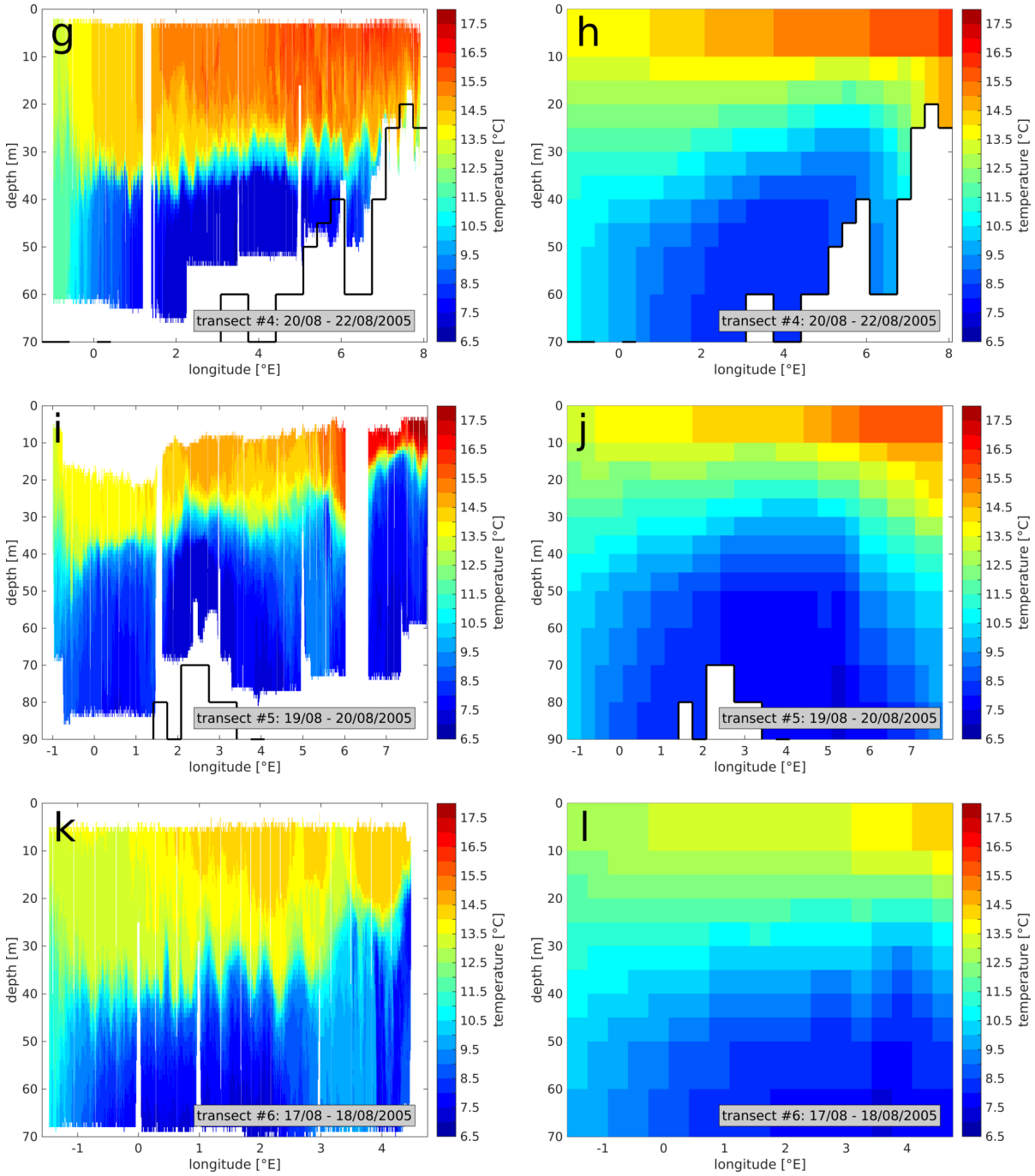

Continued: Transects (g, h) #4 to (k, l) #6.

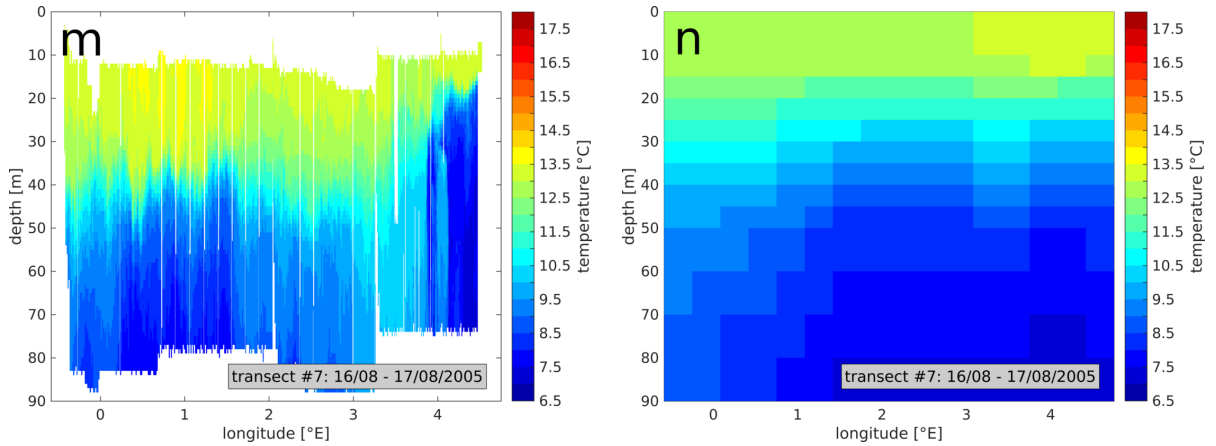

Continued: Transect #7.

7.5 °E, observed T ranges between 14.5 °C and 15 °C throughout the entire water column. The same applies to the simulated T in this area. However, observed T shows values above 15 °C starting east of 2 °E up to 4 °E, while simulated T shows such values from directly east of 1 °E up to only 2 °E. In addition, weak T stratification (T difference: $\Delta T \approx 1$ K between 40 m and bottom) is present in the observations between about 2 °E and 3 °E, where bottom depth exceeds 60 m. This vertical T gradient is not reproduced in the simulations which shows vertically homogeneous T. In the region between 3 °E and 5 °E the simulation shows T consistently by about 0.5 °C–1 °C higher than in the observations. At the eastern edge both, observations and model, show similar values of 17.5 °C–18 °C with no distinct vertical stratification.

At transect #2 (55 °N, 0 °E–7.5 °E; Fig. 4.5c and d), the observations reveal a distinct T stratification in the deeper regions between 0 °E and 1 °E and between 4 °E and 6 °E (data missing from 1 °E to 2 °E). Especially in the first of these two regions, where bottom depth exceeds 60 m a strong vertical T gradient can be seen at about 35 m depth. In the surface layer T lies around 14.5 °C–15.5 °C while in the deeper layers minimum T of below 8.5 °C is reached. In the shallower stratified region further east, surface T is in the same range as in the previously described region, but sub-thermocline T remains higher with minimum values of only slightly less than 9.5 °C in a very limited area at 4 °E. This relates to the shallower bottom depth and thus stronger vertical mixing. In the simulation these low sub-thermocline T are not fully reproduced. In the deep western region, minimum simulated T stays above 11.5 °C and in the shallower eastern stratified region, it even stays above 14.5 °C. Considering the near-surface T, the observations show values between 14.5 °C (0.5 °E–3 °E) and 17 °C (at 6.8 °E). The model results show lower near-surface T (relative to the observations) of 14 °C–14.5 °C west of 2 °E and slightly higher near-surface T east

of 5 °E. Consequently, the vertical ΔT between surface and bottom is less pronounced than in the observations in both stratified regions of transect #2 (Fig. 4.5b). Especially in the western stratified region it can be seen that the vertical mixing between surface and sub-thermocline layers tends to be overestimated, indicated lower surface and higher bottom T and by the less sharp T gradient in the simulation results.

This tendency to overestimate vertical mixing and thus to underestimate vertical T stratification is also present along the transects #3 (56 °N) to #7 (60 °N) in Fig. 4.5e–n. These transects are characterised by bottom depths of more than 70 m over most of each transect's distance, principally favouring the evolution of seasonal stratification due to the separation of the surface mixed layer from the bottom mixed layer. Vertical T stratification is observed along transect #3 (Fig. 4.5e), from its western edge to 6 °E, where the water column is too shallow to allow for seasonal stratification. At the western edge, the ΔT between surface and bottom is less than in the central region around 2 °E–3 °E, with values of below 14.5 °C at the surface and above 10.5 °C near the bottom. In the central region, T results in values above 15.0 °C at the surface and less than 7.5 °C in the deepest layers. HAMSOM is capable of reproducing this tendency for weaker T stratification in the West and highest ΔT in the central region. However, as at transect #2, ΔT is principally underestimated indicating the overestimation of vertical mixing. In HAMSOM, the minimum near-bottom T in the central region of transect #3 (Fig. 4.5f) reaches values less than 9 °C, while surface T is similar to the observations, i.e., ΔT is about 1.5 °C less than in the observations. Besides this, the comparison of observed and simulated vertical T structure along transect #3 shows, that east of 1 °E HAMSOM tends to overestimate T in the uppermost model layer (0 m–10 m) and that the T gradient of the thermocline is significantly less pronounced than in the observations. This first aspect may be related to the fact that all incoming heat is put into this uppermost model layer, i.e., only the surface layer experiences direct heating within HAMSOM. The second aspect may result from the limited spatial resolution of only 5 m between 10 m and 50 m depth in combination with the high numerical diffusion of the applied advection scheme (component upstream) as discussed by Lenhart and Pohlmann (1997).

The spatial patterns of observed T along transect #4 (Fig. 4.5g) only differ slightly from those along transect #3. At its western edge, vertical stratification is very weak with a ΔT of only about 2 K between surface and bottom. Near-surface T reaches about 13 °C–13.5 °C. East of 0 °E distinct T stratification can be observed with bottom T below 7.5 °C between 1.8 °E and 5 °E. At 3.5 °E minimum bottom T even falls below 7 °C. The intensity of the T gradient within the thermocline is already less than at transect #3 which is indicated by lower T difference between the bottom of the surface layer (at around the 14 °C-isotherm) and the top of the deeper layer (indicated by 10.5 °C-isotherm). East of

4 °E near-surface T ranges between 15 °C and 16.5 °C, causing stronger T stratification as indicated by higher T at the bottom of the surface layer (>14.5 °C). At the eastern edge of the transect T stratification is weak due to the low water depth. As for transect #3 the spatial patterns of observed T is principally reproduced by HAMSOM. However, the same shortcomings, namely less strong T stratification accompanied by higher near-bottom T and a less pronounced and shallower thermocline, can be seen.

Transect #5 (Fig. 4.5i and j) is characterised by a bottom depth of at least 50 m (70 m in the model) along the entire longitudinal range (approximately 1 °W–8 °E) allowing for thermal stratification along the entire transect, as shown in the observations (Fig. 4.5i). As for transect #4, stratification is weak at the western edge of the transect (compared to the regions further east), with near-surface T of up to 13.5 °C and T of above 9.5 °C in about 70 m depth. In this area, the maximum vertical T gradient occurs between 20 m and 30 m depth. East of about 0.5 °W thermal stratification intensifies visible in the T increase at around 20 m depth (no observations closer to the surface available). Up to about 2 °E, the thermocline depth ranges from 35 m to 40 m. In the same region, near-bottom T reaches values less than 8 °C in most parts, with minimum T of below 7.5 °C at about 0.6 °E. East of 2 °E near-surface T is consistently higher than 14.5 °C and the thermocline depth ranges from 25 m to 30 m. Between 2 °E and 3 °E, near-bottom T stays consistently below 7.5 °C.

Between 4.5 °E and 5.5 °E, T shows higher values of up to 9.5 °C below the thermocline and down to at least 75 m depth (no deeper data available). A likely cause for this feature is the inflow of NAW along the western slope of the Norwegian Trench. However, it may also relate to eddy activity as a result of the interaction of the Norwegian coastal current in the East (east of 6 °E) with the Atlantic inflow in the West. At 58 °N, 1 ° in zonal direction are about 59 km, i.e., the distance between these two opposed currents is about 90 km to 120 km which is in the same order as the horizontal spatial scale for eddies in that region reported by Johannessen et al. (1989). Such eddy activity would also result in the doming of the thermocline as seen in the observations. East of 5.5 °E, which is directly south of the Norway (see Fig. 4.4), near-surface T clearly increases reaching values of up to 17.5 °C at the eastern edge of the transect. This increase is accompanied by a shallowing of the surface mixed layer (SML) from 15 m to 20 m depth and a decrease in T below the thermocline.

The HAMSOM model is capable of reproducing near-surface T along most parts of transect #5, however, the thermocline depth is too shallow and less pronounced as for transects #3 and #4 (Fig. 4.5f and h, respectively). Like in the observations, T stratification is weakest at the western edge of the transect, but near-bottom T is 0.5 °C to 1 °C higher. Minimum near-bottom T also reaches values less than 7.5 °C, though, only

in a very small area at 5.2 °E, which corresponds to the region of higher near-bottom T in the observations. East of 6 °E, near-surface T is underestimated by the model by about 2 °C, accompanied by an underestimation of T stratification which results in higher T throughout the entire water column relative to the observations.

Along transect #6 the observed T patterns are principally (Fig. 4.5k) similar to transect #5. Stratification is weakest at the western edge at about 1.5 °W and shows an eastward intensification. With respect to near-surface T, an eastward increase can be seen with T being about 0.5 °C less than along transect #5. Maximum near-surface T of above 14 °C are reached in the central region of the transect and near its eastern edge off the Norwegian west coast. These areas of highest near-surface T may relate to the inflow of warm water from the Atlantic and the Norwegian coastal current, respectively. From 1 °W to 0.3 °E the thermocline depth (13 °C-isotherm) ranges between 35 m and 40 m. Between 0.3 °E and 3 °E, thermocline depth shows strong periodic spatial variations with ranges of 20 m to 40 m on a horizontal scale of about 25 km–30 km. These variations may relate to internal baroclinic instabilities as this horizontal scale is in the order of 6 to 8 times the internal Rossby radius of deformation which was found to be in the order of 4 km in the North Sea (van Aken et al., 1987). Another potential cause would be sub-mesoscale eddies. The comparison of T simulated by HAMSOM shows that the model reproduces the basic features relevant for this study. However, in addition to the previously discussed shortcomings, HAMSOM is not capable of resolving these small-scale patterns and slightly underestimates near-surface T in the region between 0 °E and 3 °E.

The observed T distribution along the northernmost transect #7 (Fig. 4.1m) is quite similar to the previous transect, although near-surface T is generally lower and the thermocline is less pronounced along the entire transect. Maximum near-surface T of above 13.5 °C is reached in the region between 0 °E and 1.3 °E, probably related to the inflow of water from the North Atlantic. In the same region low T is observed in the deeper layers, falling below values of 8 °C. Between 1.7 °E and 4 °E T in 40 m to 80 m depth is clearly higher than in the surrounding waters east and west of this region, and shows vertical T variations in zonal direction (e.g., depth variation of 10 °C-isotherm). The causes for this feature may be the same as discussed for transect #5, namely eddy activity in the frontal region between the Norwegian coastal current and the Atlantic inflow. East of 4 °E, thermocline depth decreases to 15 m to 20 m and an intensification of thermal stratification is visible by the low T in deeper layers reaching values of less than 7.5 °C. As for previous transects, HAMSOM reveals some shortcomings in reproducing thermocline depth. In addition, it only shows a very weak increase in T in the deeper layers in the regions between 3 °E to 4 °E, indicated by a slight deepening of the isotherms.

Nevertheless, the basic horizontal and vertical patterns of summer T relevant for this

study are reasonably reproduced by HAMSOM. Shortcomings with respect to meso- and sub-mesoscale features result from the limited horizontal resolution, which also affects indirectly vertical diffusion and thus vertical T stratification. With respect to S, the image provided by the ScanFish observations (Fig. 4.6; left) is slightly different to that for T. All transects show lowest S at their eastern edge which relates to the influence of riverine freshwater discharge along the southern continental coast (transects #1 to #3; Fig. 4.6a, c and e) and the influence of the Baltic inflow of less saline water and riverine freshwater discharge along the Norwegian coast (transects #4 to #7; Fig. 4.6g, i, k and m) as shown in Fig. 4.2. This feature is principally reproduced by HAMSOM, however, as for T with some shortcomings. At transects #1 to #3 (Fig. 4.6b, d and f), no clear stratification in S can be see along the entire length of each transect. Only in the easternmost part of transect #3 weak S stratification can be seen. In contrast, transects #4 to #7 (Fig. 4.6h, j, l and n) show distinct S stratification along large parts of each transect, starting in the East and extending up to 6 ° westward (transect #4).

Along transects #1 to #3 (54 °N, 55 °N and 56 °N, respectively), lowest observed S occurs at the very eastern end of each transect with values of down to 32.5, 32 and 33, respectively. The occurrence of lowest S at transect #2 relates to the fact that this transect is located directly downstream of the Elbe estuary (see Fig. 4.4) which constitutes the largest source of freshwater in that region. In contrast, transect #1 ends west of the Elbe estuary, i.e., is not influenced by the Elbe freshwater discharge due to the eastward flowing continental coastal current. Transect #3 is farther downstream than transect #2, implying a reduced influence of the Elbe freshwater plume. Among these three transects, transect #1 is that with the largest westward extent of the low-S signal. Here, the 34.5-isohaline is located at about 5 °E while at transects #2 (Fig. 4.6c) and #3 (Fig. 4.6e) it is located at 6.2 °E and 5.8 °E, respectively. This relates to the near-shore location of transect #1 and thus the stronger influence of the riverine freshwater discharge from, e.g., the large Dutch tributaries Rhine and Meuse. Despite the apparent influence of riverine freshwater in the eastern part of all three transects, distinct haline stratification cannot evolve due to the intermediate water depth of 40 m and less, and the influence of tidal mixing (e.g., Pingree et al., 1978; Burt et al., 2014; van Leeuwen et al., 2015). In the deeper western parts of the transects, S shows generally higher values up to 35.25 in 30 m to 40 m depth at transect #3 (1 °E to 4 °E). However, observed S does not show any clear northward increase in this deeper western region.

These qualitative differences in the spatial extent and intensity of the low-S plume between the three transects are basically reproduced by HAMSOM, although not to their full extent. The westward propagation of the low-S signal is, similar to the observations, highest at transect #1 (34.25-isohaline at about 4.5 °E; Fig. 4.6b). However, S in the

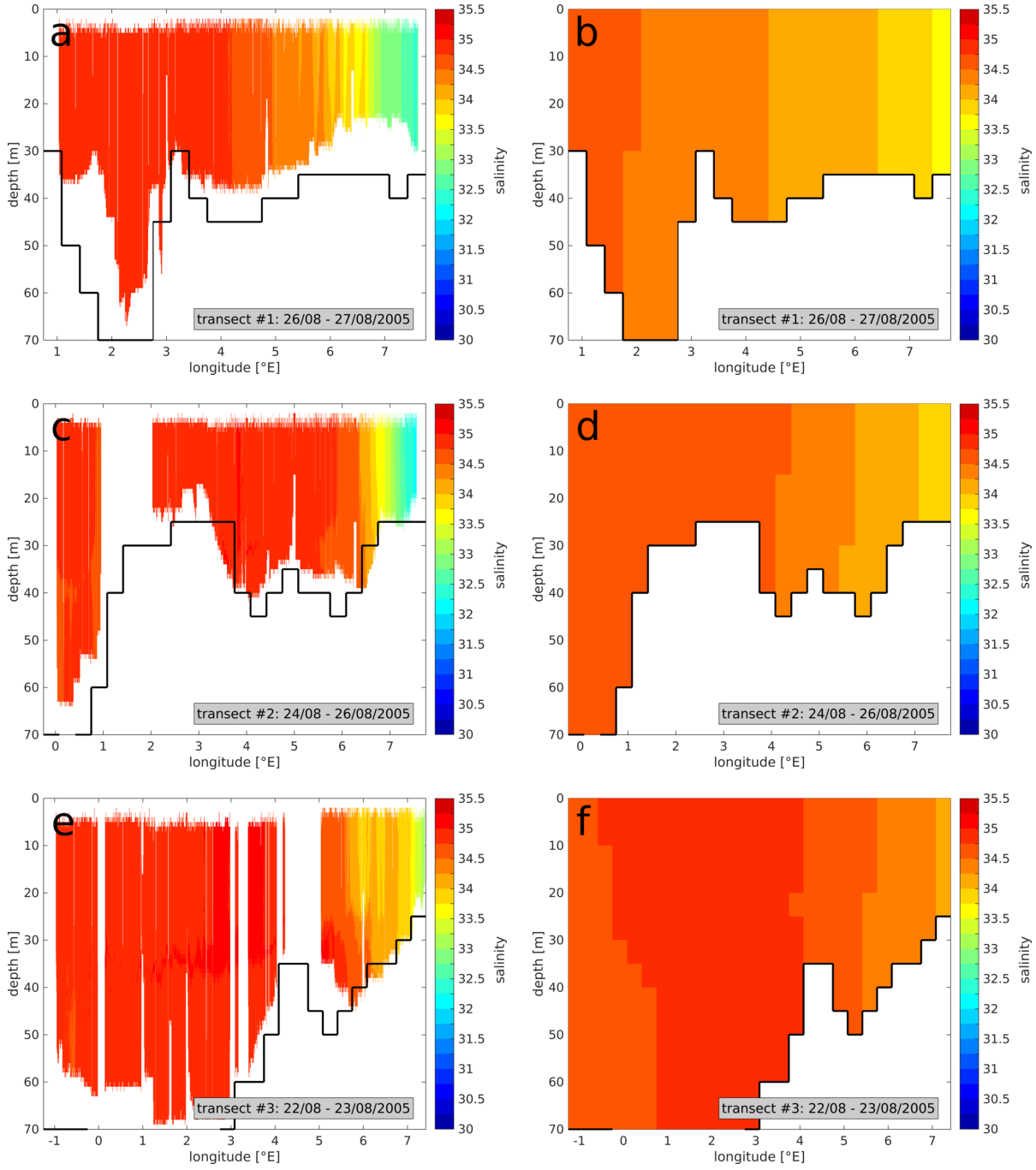

Figure 4.6: Transects of salinity in summer 2005 along the trajectories given in Fig. 4.4 as observed by ScanFish (left) and simulated by HAMSOM (right). Colour scale cut at lower end. Black line indicates HAMSOM bottom topography. HAMSOM results represent averages over observation period (bottom-right corner of each panel) based on daily output. Transects (a, b) #1 to (e, f) #3

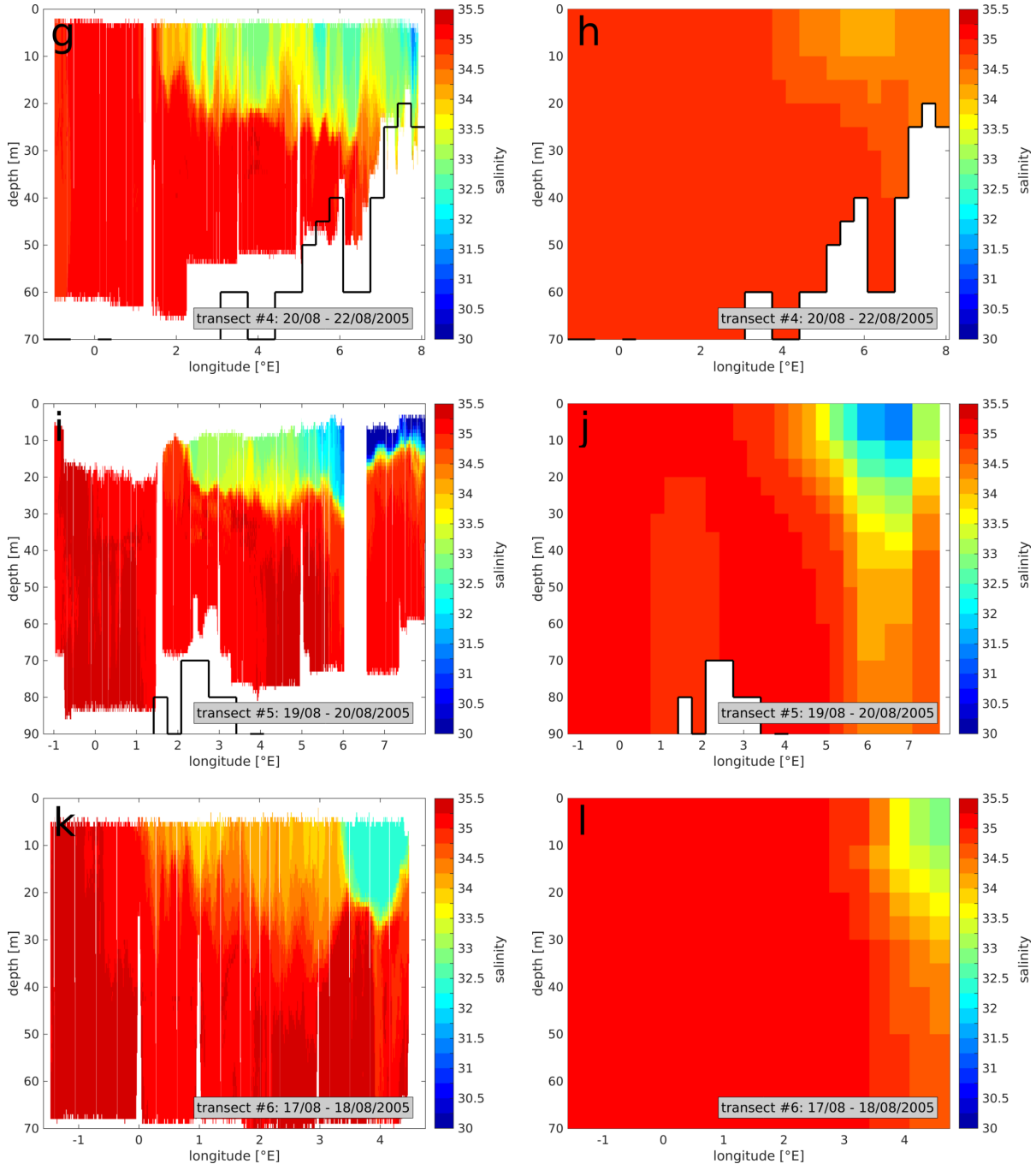

Continued: Transects (g, h) #4 to (k, l) #6.

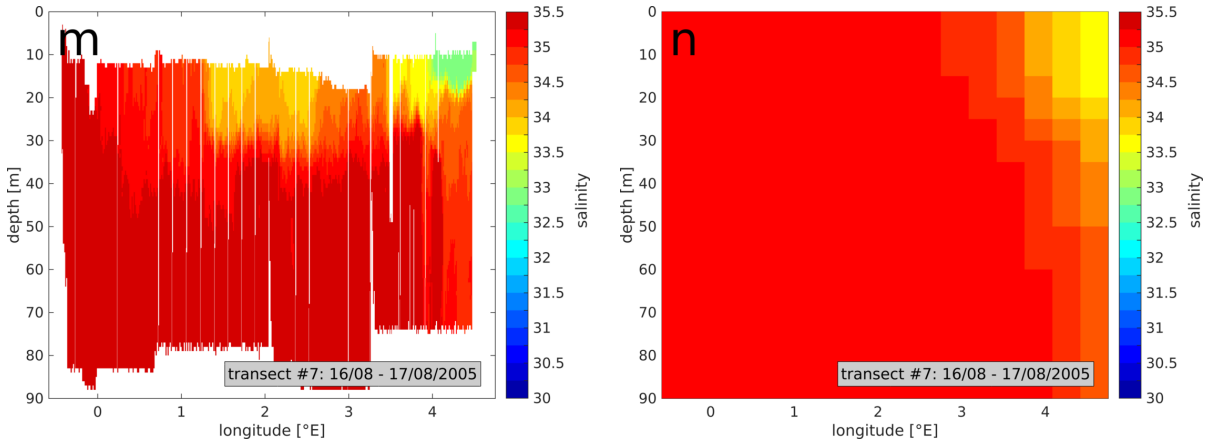

Continued: Transect #7.

eastern parts of each transect is generally higher than in the observations and lowest simulated S occurs at transect #1 with values of down to 33.5. Further west, S stays below 34.75 along the entire distance of transects #1 and #2. At transect #3 (Fig. 4.6f), a region with S higher than 34.75 can be found between 0 °E and 4 °E, while west and east of this area S stays below this value. The general northward increase in water column S, however, is much less pronounced in the observations.

Along transects #4 to #7 (57 °N, 58 °N, 59 °N and 60 °N, respectively), the freshwater signal originating from the East is still present in the observations (Fig. 4.6g, i, k and m) and, due to the greater water column depth, results in haline stratification. The halocline depth ranges between 15 m and 30 m with the tendency to greater depth in the eastern part of the haline-stratified region. Lowest S of less than 30 (colour scale cut at this value) is found at transect #5, east of 6.5 °E, as it is located directly in the Norwegian coastal current characterised by low S due to the Baltic inflow and freshwater from Norwegian rivers. At transect #4, areas of higher (>33.25) and lower near-surface S (<32.5) alternate in the region from 4 °E to 7 °E, which may relate to eddy generation influenced by the Baltic inflow (Røed and Fossum, 2004; Albretsen, 2007). It is worth mentioning that these structures do not occur in the corresponding T observations which emphasises the importance of haline stratification along the Norwegian coast.

Besides these alternations, near-surface S does not show any clear westward gradient until about 2 °E, where near-surface S rapidly increases from values of 33–33.5 to values above 34.75. An even stronger at similar longitude is visible at transect #5, but in addition, a steady increase in near-surface S can be seen within the low-S signal from 8 °E to 2 °E. This may relate to the fact that the region east of 5 °E at transect #5 is dominated by the Norwegian coastal current, while the region west of 5 °E is influenced

by both, the Norwegian coastal current and the Atlantic inflow. This is supported by the observations at transect #6 where a distinct lens of low-S water (32–32.5) can be seen in the upper 15 m to 25 m between 3.5 °E and the eastern end of the transect, while west of 3.5 °E, near-surface S shows higher values of 33.75 to 34.5. As for the thermocline depth (see Fig. 4.5), sub-mesoscale fluctuations of the halocline depth (34.5-isohaline) can be seen between 1 °E to 3 °E, which support the hypothesis that processes such as eddies or internal baroclinic Rossby waves occur in this region.

The low-S lens visible at the eastern edge of transect #6 is still present at transect #7, however, showing slightly higher minimum S (32.5–33 east of 4 °E). Near-surface S between 1.5 °E and 4 °E shows an alternating pattern with lower values around 1.5 °E–2.5 °E and east of 3.5 °E, and higher values in between. The vertical variations in halocline depth on a sub-mesoscale zonal extent cannot be seen. Both aspects suggest, like the corresponding T observations (see Fig. 4.5), that mesoscale eddies generated in the frontal zone between the southward Atlantic inflow and the northward Norwegian coastal current can have a major influence on the spatial T and S structure in this region.

Regarding S in the deeper layers and west of the near-surface, low-S signal a slight increase in S can be seen. At transect #4 most of this region shows S between 34.75 and 35.25, while at transect #7 most of this region is characterised by S higher than 35.25. At transects #5 and #6, regions of S higher than 35.25 can be found in the western part of each transect and around the western slope of the Norwegian Trench (5 °E and 3 °E at transects #5 and #6, respectively). Both patches may be attributed to the inflow of high-saline NAW from the North.

The comparison of simulated S (Fig. 4.6; right) at transects #4 to #7 with the observations reveals that, as for the southern transects #1 to #3, HAMSOM is not capable of fully reproducing all observed features. The relative change in the spatial extent of the near-surface, low-S signal from South to North is partly reproduced. From transect #5 to #7 an increase in minimum near-surface S can be seen similar to the observations, however, absolute simulated values are about 1–2 times higher than observed ones. In addition, transect #4 shows significantly higher minimum S than the other transects which may relate to the fact that the southward extension of the Baltic outflow is not fully reproduced. The spatial extent of the westward propagating low-S signal is underestimated along all four transects, resulting in an overestimation of near-surface S in the centre of the transects. The observed northward increase in S in the western part and deeper layers is also visible in the model results (especially from transect #4 to #5), but simulated S is consistently about 0.5 lower than observed S in this region. However, HAMSOM also reproduces the two pathways of the southward Atlantic inflow, visible at transect #5 where S is less than 35 from 0.8 °E to 2.2 °E and below 20 m, while it is consistently higher

in the surrounding areas indicating the inflow of NAW. It should also be noted that in the vicinity of the Norwegian coastal current, HAMSOM tends to overestimate vertical mixing, especially visible at transects #5 and #6, which results in an underestimation of S in the deeper layers.

With respect to the STD of simulated T and S in 2005 (not shown), most transects show only small values less than <0.15 °C and 0.03, respectively. Higher STD values for T only occur in the eastern parts of transects #2 (up to 0.25 °C) and #3 (up to 0.6 °C) where events of enhanced vertical mixing influence the T distribution in the upper 20 m and even down to 40 m near specific topographic features. For S, highest STDs of up to 0.13 occur in the eastern part of transects #5 and #7, close to the Norwegian coast where the influence of freshwater inflow from the Baltic and Norwegian rivers is highest. In conclusion, HAMSOM is capable of reproducing the basic features of North Sea T and S during summer, namely, distinct thermal stratification in the deeper regions of the central and northern North Sea and weaker thermal stratification in the shallower eastern coastal region and along the British east coast. It furthermore reproduces the west- and northward decrease in near-surface T visible in the observations. With respect to haline stratification, it reproduces the basic structures seen in the observations, i.e., no stratification in the southern and central North Sea (transects #1 to #3), but S stratification in the northeastern North Sea (transects #4 to #7). The westward increase in near-surface S is also principally reproduced.

However, HAMSOM also reveals some shortcomings with respect to summer T and S. Thermal stratification tends to be underestimated in most parts of the North Sea, probably as a result of an overestimation of vertical mixing due to the limited spatial resolution. The same applies to haline stratification in the northeastern North Sea. For the same reason, some meso- and sub-mesoscale structures found in T and S observations cannot be reproduced by the model. In this context, it should be noted that within the observation period 1998–2010, the presented year 2005 constitutes the year with the maximum westward propagation and intensity of this low-S signal – in most years this signal is confined to the region east of 5 °E (other years not shown). Consequently, this can effect the intensity of vertical stratification in individual years in the eastern central and northeastern North Sea. The model additionally tends to overestimate S in the eastern North Sea, while in the western and central North Sea S tends to be underestimated.

4.2.1 A quantitative assessment of model performance with respect to summer hydrography

In order to provide a comprehensive analysis of the model performance with respect to the main aspects of North Sea summer hydrography and stratification, a quantitative assessment of related quantities based on data for multiple years is required. For this purpose, Fig. 4.7 shows the Taylor diagram (Taylor, 2001) for hydrographic and stratification-related quantities for the individual ScanFish transects (see Fig. 4.4; transect locations may slightly differ between years) and for the composite of all transects. The displayed quantities include: T (red), S (blue), potential density anomaly (σ; cyan), and ΔT (magenta). The potential density anomaly, σ, is calculated according to TEOS-10 using software written by McDougall and Barker (2011).

The correlation coefficient (COR) between observation X and simulation Y is calculated as follows for each of the three data sets:

$$\mathrm{COR}(X,Y) = \frac{1}{N \cdot \mathrm{STD}(X) \cdot \mathrm{STD}(Y)} \cdot \sum_{i=1}^{N} (X_i - \overline{X})(Y_i - \overline{Y}). \tag{4.1}$$

Here, N equals the number of observation-simulation pairs. The index i indicates a single value of the considered data set, while $\overline{X}$ and $\overline{Y}$ represent the average values. The unnormalised standard deviation (STD) of a data series Z (observation or simulation) is calculated as:

$$\mathrm{STD}(Z) = \sqrt{\frac{1}{N} \cdot \sum_{i=1}^{N} \left(Z_i - \overline{Z}\right)^2}. \tag{4.2}$$

The unnormalised, centred root-mean-square difference (RMSD) between observation X and simulation Y is calculated as:

$$\mathrm{RMSD}(X,Y) = \sqrt{\frac{1}{N} \cdot \sum_{i=1}^{N} \left[(X_i - \overline{X}) - (Y_i - \overline{Y})\right]^2}. \tag{4.3}$$

For clarity of the Taylor diagram, the STD and the RMSD of each pair of simulation (symbols) and corresponding observation (OBS) are normalised by the STD of the observation. This allows for the presentation of the statistics of all quantities within a single Taylor diagram. In the following, the terms RMSD and STD refer to the corresponding normalised quantities.

The statistics calculated for T confirms that HAMSOM is capable of reproducing well summer T with respect to its spatial (i.e., vertical and horizontal) distribution and year-to-year variability within the entire North Sea. The COR for the entire data set (‘all

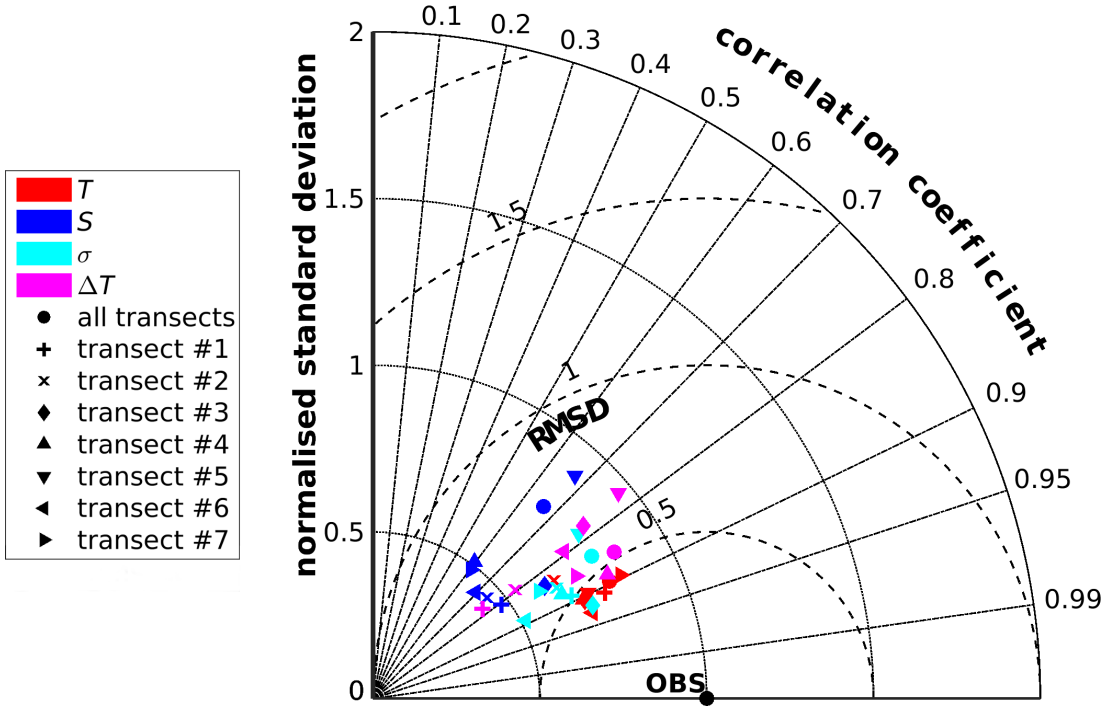

Figure 4.7: Taylor diagram of temperature (T; red), salinity (S; blue), potential density anomaly (σ; cyan), and temperature difference (ΔT; magenta) based on ScanFish data (OBS) and HAM-SOM results (symbols) for the period 1998–2010. Different symbols indicate different transects. Transect numbering according to Fig. 4.4 (transect locations may slightly differ between years).

transects'; filled circle) equals 0.9 and the STD is 0.79, i.e., the overall T variability is slightly underestimated by the model which is also indicated in the qualitative comparison (see Fig. 4.5) by the underestimation of near-surface T and the overestimation of T in the deeper layers in some regions. The corresponding RMSD is 0.46 which confirms the generally good agreement between simulation and observation. Looking at the individual transects it can be seen that along most transects COR for T is high with values around 0.9 or above, except for transect #2 (55 °N) with a COR of only 0.84. This transect also shows the lowest STD and highest RMSD, 0.65 and 0.58, respectively. Along the other transects, STD ranges from 0.7 to 0.83 and RMSD varies between 0.43 and 0.48. This again confirms the generally good model performance with respect to T in most regions of the North Sea, and only minor shortcomings especially in parts of the southern North Sea.

For S, the model performance is less good than for T. Considering the entire data set, COR is only about 0.66, while STD and RMSD are about 0.77 and 0.76, respectively. This relates to the large year-to-year variability in near-surface S in certain regions of the North Sea, especially the regions in the vicinity of the Baltic inflow and Norwegian coastal

current due to the large variations in the intensity and westward propagation of the near-surface, low-S signal (see Sect. 4.2). The statistics of the individual transects confirms this picture. For the southern transects #1 to #3, COR ranges from 0.75 to 0.84, while for the northern transects #4 to #7 COR varies between only 0.6 and 0.69. Transect #4 constitutes the southernmost transect periodically influenced by the Baltic inflow (see Fig. 4.4). This principally better agreement between simulation and observation in the southern North Sea is also shown by the lower RMSD (0.59–0.73) along transects #1 to #3, compared to values from 0.76 to 0.81 for the transects #4 to #7. STD varies between 0.44 and 0.62 for all transects except #5, which shows an STD of 0.9. This good agreement between STD in the simulations and observations in the latter case most likely relates to the fact that the eastern part of transect #5 is located directly in the region of the Baltic inflow (see Fig. 4.4) while its western end is located in the pathway of the Atlantic inflow near the British coast. Thus, zonal S variations along this transect are expected to be consistently the highest among all transects, and to show similar year-to-year variations as the two inflows are the main drivers of near-surface S along the transect. Consequently, simulation and observation have a similar STD.

In order to give insight in a more directly stratification-related quantity, the statistics for σ are also presented in Fig. 4.7. COR of σ derived from simulated T and S with that derived from the observations is 0.84 for the entire data set. The corresponding STD results in 0.78 which implies that the model variability is less than that in the observations, resulting from the lower variability in simulated T and S. RSMD yields 0.55 which confirms the principally good agreement between simulation and observation. This good agreement is confirmed for the individual transects, with minor variations in model performance between the different transects. The lowest COR of 0.78 is calculated for transect #5, while the highest COR of 0.92 results for transect #3. All other transects show CORs between 0.84 and 0.89. The lowest COR for transect #5 differs from the statistics for S, where lowest COR results for transect #4. This indicates, that simulated T and S patterns may balance in such way that patterns in σ get closer to the observations than the patterns in the individual quantities used for its calculation. In addition, this suggests that T is of more importance for σ, i.e., for stratification, in most parts of the northern central North Sea (transects #4 and #5) which relates to the fact that the strong low-S signal from the Baltic inflow is confined to the areas near the Norwegian coast usually.

Transect #5 furthermore shows the highest STD of 0.79, but also the highest RMSD of 0.63. This also applies to the non-normalised quantities (not shown) which constitute the highest among all transects ($\mathrm{STD} = 0.96\,\mathrm{kg\,m^{-3}}$, $\mathrm{RMSD} = 0.76\,\mathrm{kg\,m^{-3}}$). This implies, that although spatial and/or year-to-year variability is highest along transect #5, the spatial

and temporal patterns found in the observations are not fully reproduced, and model performance with respect to σ is worse than along the other transects. With respect to STD the southern transects #1 to #4 show higher values (0.64–0.72) than the two northernmost transects #6 and #7 (0.51 and 0.59, respectively). For RMSD, lower values result for the four southern transects (0.44–0.56) compared to 0.59 for transect #6 and 0.6 for #7. This confirms, that HAMSOM tends to better reproduce the hydrography in the southern and central North Sea (transects #1 to #4) than in the northern North Sea. The overall best statistics for σ results for transect #3 (56 °N) with the highest COR and lowest RMSD, 0.92 and 0.44, respectively, and a high STD of 0.72.

The comparison of the statistics for S and σ along transects #4 and #5 suggests that S is less important for summer stratification than T along these transects. Figure 4.6 furthermore shows that haline stratification is only weak along transects #1 to #3, i.e., in most parts of the southern and southern central North Sea (west of 5 °E). Thus, it can be concluded that T, and more specifically ΔT, is a reliable and simple proxy for summer stratification in the southern and central North Sea. Therefore, the statistics for ΔT derived from simulated T, relative to that derived from the ScanFish data set, is also included in Fig. 4.7. COR for the ΔT along all transects results in 0.85 with a corresponding STD and RMSD of 0.85 and 0.52, respectively. This indicates a principally good agreement between simulation and observation, however, as ΔT is expected to show significant spatial variations, e.g., between the shallow coastal regions of the southern North Sea and the deeper northern North Sea, this high COR does not provide sufficient information about the model performance with respect to ΔT.

Considering the individual transects, COR ranges between 0.77 (transect #5) and 0.88 (transect #4), with most transects yielding CORs slightly below 0.8. The lower CORs – compared to the CORs for T itself – result from the fact that HAMSOM generally tends to underestimate near-surface T, while T in the deeper layers tends to be overestimated. This is especially true for regions where haline stratification plays an additional or even dominant role, e.g., near the Norwegian coast. Consequently, ΔT in the simulations can be very low (or even negligible) in cases of weak observed thermal stratification. In some shallow areas (bottom depth $\leq$40 m) near slopes in the bathymetry (mainly in the southern North Sea), the limited resolution further and the interaction of currents with the topography inhibits the evolution of thermal stratification in the model, while intense thermal stratification with $\Delta T \geq 5$ K is observed during individual years (not shown).

The STD is lowest along the two southernmost transects #1 and #2 (0.42 and 0.54, respectively), which relates to the lower bottom depth and thus none or only weak stratification in the simulation. Along these transects, RMSD is higher with values of 0.73 (transect #1) and 0.66 (transect #2). STD shows the highest values for transects #3 to

#5 (0.79–0.96; non-normalised: 1.78 K–2.27 K), as a result of increasing bottom depth in the offshore regions supporting high summer ΔT in the deeper parts of these transects while it remains low in the shallow coastal zone. RMSD ranges between 0.48 and 0.67, the latter calculated for transect #5. This high RMSD mainly relates to the additional haline stratification in the eastern part of this transect, which constitutes a persistent feature in the observations and supports intensification of thermal stratification, however, is not fully reproduced by HAMSOM (see Fig. 4.6). It should be noted, that the high STD of 0.96 for this transect indicates a good agreement between simulation and observation with respect to the amplitude of ΔT, however, as COR = 0.77 is the lowest among all transects, it appears that some spatial and/or year-to-year variations along this transect are not matched by the model. The two northernmost transects #6 and #7 yield STDs of 0.72 and 0.71, respectively, and low RMSDs of 0.61 (transect #6) and 0.54 (transect #7). This, together with the high CORs, indicates the good model performance along these transects with respect to ΔT.

In summary, the analysis of the model performance with respect to hydrographic quantities (T, S) and stratification-related quantities (σ, ΔT) shows that HAMSOM provides reasonable skill in reproducing the general spatial and year-to-year variability in most parts of the North Sea. Especially in relation to S, some shortcomings are revealed which, however, can be accepted as they only slightly affect the area of interest of this study, namely (the deeper regions of) the southern North Sea and the central North Sea. The analysis furthermore shows that ΔT provides a simple and reliable measure for summer stratification in most regions of the North Sea, including the area of interest. This is supported by previous studies (e.g., Burt et al., 2014; van Leeuwen et al., 2015) demonstrating that in most North Sea regions seasonal stratification is mainly T-driven.

4.3 Thermal stratification in the North Sea

As described in Ch. 1 seasonal stratification during summer plays a key role for the O_2 dynamics of shelf seas and more specifically the North Sea. Section 4 shows that ΔT between surface and bottom provides a reliable proxy for stratification, and that the HAMSOM model is capable of reproducing the main features of summer ΔT. Therefore, this study uses ΔT to describe stratification in the North Sea.

In order to provide a first insight in the annual cycle of stratification, Fig. 4.8a and b, respectively, show the amplitude and phase of the maximum of ΔT derived from daily time series of simulated T during 1998–2014 by applying a Fourier transformation. Thus, it shows amplitude and phase of the annual cycle of ΔT during this period. Due to intense vertical mixing, ΔT tends to be zero during winter in most parts of the North

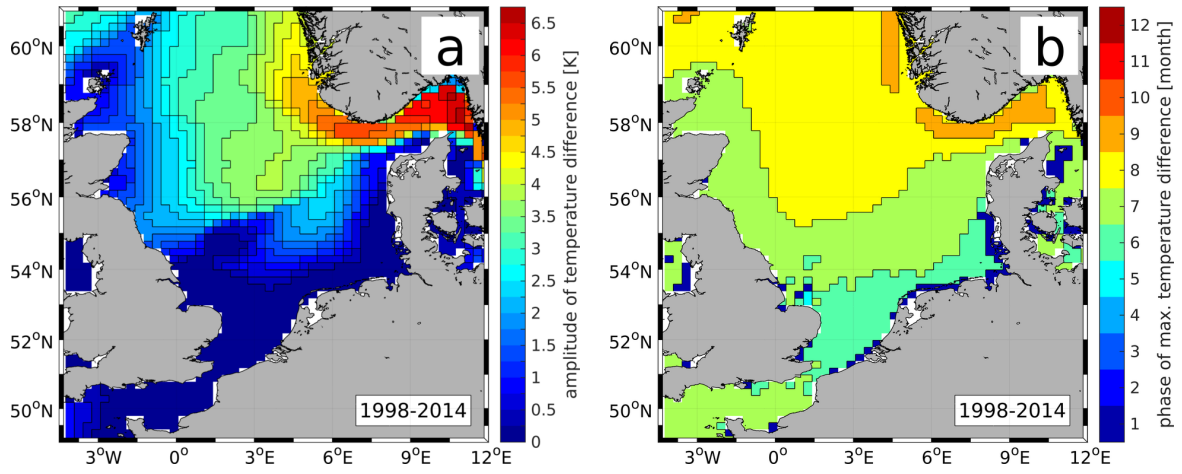

Figure 4.8: Spatial distributions of (a) amplitude and (b) phase (i.e., month) of the maximum of the annual cycle of temperature difference during 1998–2014.

Sea and only slightly negative values ($|\Delta T| < 1\,\mathrm{K}$) may occur in regions of additional haline stratification, i.e., near the Norwegian coast. Therefore, the amplitude of ΔT can be considered to represent the maximum ΔT of the annual cycle of 1998–2014 in most regions of the North Sea. The phase represents the month in which the maximum ΔT occurs during the annual cycle; dark blue areas (phase = 1) indicate water columns with only one model layer, i.e., $\Delta T = 0\,\mathrm{K} = \mathrm{const}$.

The map of the ΔT amplitude indicates that the annual cycle of ΔT shows only very small variation (<0.25 K) in the coastal southern North Sea and in the shallowest part of the Dogger Bank (bottom depth <25 m). In most of these areas, the maximum ΔT occurs during June. Further north and along the east coast of the British Isles maximum ΔT increases, reaching values up to 3 K during June. The part of this region which is located in the southern central North Sea basically represents the area with bottom depths of 25 m–50 m, while in the area along the British east coast bottom depth can reach up to 100 m. In most parts of the northern central and northern North Sea, maximum ΔT occurs in August, except for the deepest parts of the Norwegian Trench and Skagerrak where maximum ΔT occurs in September. In the offshore areas of the central and northern North Sea maximum values reach up to 4 K (at about 56.5 °N, 4 °E). In the eastern Norwegian Trench and Skagerrak maximum values of up to 6.75 K are reached.

The northwest gradient in the timing of maximum ΔT (see Fig. 4.8b) mainly relates to the increase in bottom depth from Southeast to Northwest, as shallower water allows for the earlier onset of water column warming. However, the shallow bottom depth in combination with tidal mixing also prevents the evolution of distinct thermal stratification indicated by the small amplitude. The generally deeper water in the central and northern

North Sea supports the evolution of thermal stratification, although to a later point in time. Only in the northernmost regions near the shelf edge, maximum ΔT again decreases due to the influence of the Atlantic inflow. Furthermore, the annual cycle of ΔT in the northern North Sea is characterised in a zonal gradient in both, amplitude and phase, which relates to the Atlantic inflow, promoting enhanced mixing, in the West and the additional haline stratification along the Norwegian coastal current in the East. Consequently, maximum ΔT in the offshore regions of the North Sea occurs in the central North Sea, where bottom depth $>$50 m supports the evolution of thermal stratification and the influence of the Atlantic inflow is low compared to the northwestern North Sea.

4.3.1 Deriving stratification parameters from simulated temperature

The previous sections showed that T constitutes the major contributor to stratification in most North Sea regions. Therefore, thermal stratification can be considered to play a key role in the temporal evolution of sub-surface O_2 in the North Sea as it inhibits (or clearly reduces) the supply of oxygenated water from the surface into the deeper layers where O_2 consumption exceeds O_2 production. Regional differences in bottom depth, tidal mixing and water masses have a strong influence on thermal stratification in the North Sea. In addition, year-to-year variations in weather as well as in the inflow from adjacent seas can cause strong variations in thermal stratification between different years.

In order to analyse the North Sea O_2 dynamics during seasonal stratification, it is required to define certain parameters characterising stratification. In this study, two such parameters are used: (1) duration of stratification and (2) the MLD. As the spatial and temporal patterns of North Sea T are generally well reproduced by HAMSOM, both parameters can be derived from simulated T, more specifically ΔT and the vertical T gradient ($\partial T/\partial z$), respectively.

The following simple 2-step algorithm describes how stratification period and MLD are derived from simulated T for an individual model water column. First, the stratified period is determined using a T difference criterion:

$$S_{\text{strat}}(x,y,t) = \begin{cases} 1 & \text{for } \Delta T|^{0}_{-H}(x,y,t) \geq 0.05\,\text{K} \\ 0 & \text{otherwise} \end{cases} \tag{4.4}$$

S_{strat} constitutes a switch defining if a water column at location (x, y) and time t is stratified ($S_{\text{strat}} = 1$) or not ($S_{\text{strat}} = 0$) depending on the T difference (ΔT) between the surface and bottom depth H. It should be noted that not the uppermost model layer is used for surface T, but the second layer, in order to elude short-term events only

affecting the uppermost layer. T in the deepest pelagic model layer is used for bottom T. The low critical T difference $\Delta T_{\mathrm{crit}} = 0.05\,\mathrm{K}$ was chosen with special focus on the O_2 dynamics. As lowest O_2 concentrations are expected to occur in the layer directly above the seafloor, it is assumed that O_2 in this layer is replenished only in the case of a complete overturning of the water column, i.e., the vertical homogenisation of T. Furthermore, periods of stratified conditions are only considered as such, if they last for at least five days without any interruption, otherwise bottom waters are considered to be ventilated again. Subsequently, the stratified period (t_{strat}) is calculated as the number of days with $S_{\mathrm{strat}} = 1$.

In the second step, in the case of stratification the MLD of a model water column is determined using the vertical T gradient $\partial T/\partial z$. As the model uses discrete vertical layers the finite difference quotient $\Delta T/\Delta z$ is used:

$$\mathrm{MLD}(x,y,t) = \begin{cases} D(\max(\Delta T/\Delta z)) & \text{for } S_{\mathrm{strat}}(x,y,t) = 1 \\ 0 & \text{otherwise} \end{cases} \tag{4.5}$$

$\Delta T/\Delta z$ is calculated for each grid cell interface within the considered water column. ΔT represents the T difference between two vertically adjacent model layers and Δz represents the distance between the centre points of these two grid cells. The MLD is then defined as the depth level, D, of the interface where $\Delta T/\Delta z$ has its maximum.

4.3.2 Stratification periods in the North Sea

Figure 4.9 provides an overview of the spatial distribution and temporal variability of the stratification period, t_{strat}, in the North Sea during 1998–2014, according to the previously described algorithm. In order to show the spatial distribution during that period, the average duration of the longest continuous t_{strat} per year is displayed (panel a). The corresponding STD (panel b) and minimum and maximum t_{strat} (panels c and d, respectively) during that period provide insight in the temporal variability in (longest continuous) t_{strat}. t_{strat} for individual years was calculated according to Eq. (4.4). Black colour indicates areas where no stratification occurs throughout the entire period 1998–2014.

The spatial distribution of average t_{strat} shows a clear relation to bottom depth. Areas shallower than 25 m, i.e., coastal areas and at the Dogger Bank, do not experience any thermal stratification throughout the entire period. In the regions with bottom depths from 25 m to about 50 m (south of the imaginary line between 54 °N, 0 °E and 57 °N, 8 °E), t_{strat} increases showing average values of up to 160 days in the deepest part of that region at about 55.6 °N, 6 °E. The STD of about 16 days as well as minimum and maximum duration

(120 days and 190 days, respectively) also indicate remarkable year-to-year variations in this deepest part.

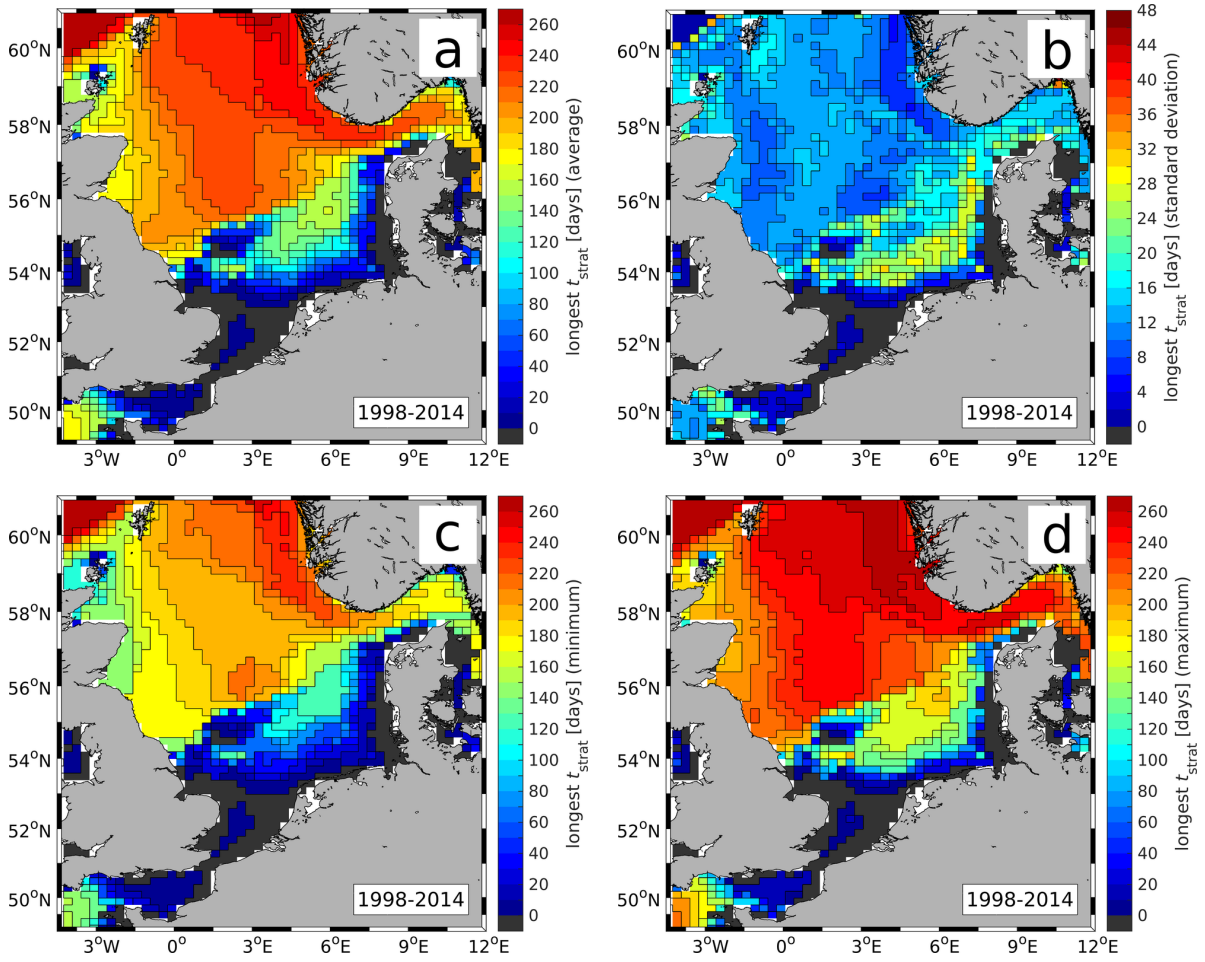

Figure 4.9: Statistics for (longest continuous) stratification period (t_{strat}) per year during 1998–2014: (a) average, (b) STD, (c) minimum, and (d) maximum. Stratification period for individual years calculated according to Eq. (4.4). Black indicates areas where no stratification occurs during 1998–2014. Colour scale for average, minimum and maximum cut at upper limit.

In the transitional zone between the consistently non-stratified coastal areas and the well stratified central North Sea, average t_{strat} ranges between 10 days to 120 days and increases with increasing depth. The high STD in this transitional zone, ranging from 24 days to 34 days, indicates the large year-to-year variability. The minimum and maximum duration of t_{strat} in this region also reveals areas with a range from 20–80 days (minimum) to 100–160 days (maximum).

In the northern North Sea (north of the imaginary line between 54 °N, 0 °E and 57 °N,

8 °E), t_{strat} is generally higher than in the southern North Sea, however, regional differences can be seen. Following the Atlantic inflow along the northeastern British coast, average t_{strat} (Fig. 4.9a) shows a steady increase from 150 days in the Pentland Firth up to 210 days near 55 °N. In the near-shore areas of this region, STD reaches values of 16–20 days while further offshore STD goes down to about 8 days (see Fig. 4.9b). Minimum and maximum t_{strat} (Fig. 4.9c and d)) also indicate a high variation between individual years. In the Pentland Firth, t_{strat} ranges between 100 days and 200 days; at 55 °N at the British coast, values from 170 days to 230 days occur.

In the central northern North Sea, t_{strat} shows high average values of 200 days to 230 days, with an STD of only 6–10 days directly north of the Dogger Bank and values of 14–18 days further northwest. The overall range in t_{strat} is from 190–220 days (minimum) to 230–260 days, i.e., thermal stratification continues for more than 6 months per year in most parts of the central northern North Sea during the period 1998–2014. Longer thermal stratification only occurs along the Norwegian coast where additional haline stratification, driven by the Baltic inflow and freshwater input from Norwegian rivers, and great bottom depth support the evolution and persistence of thermal stratification. Here, average t_{strat} ranges between 210 days at the eastern end of the Norwegian Trench and up to more than 270 days at its northern end. The STD of 16–26 days and minimum-maximum range of 170–200 days to 240–270 days show that at its eastern end, t_{strat} can strongly differ between different years. West of the Norwegian coast, STD is clearly less (<8 days) indicating the generally high t_{strat}. Minimum and maximum t_{strat} show a range from about 230 days to 270 days.

The overall image of t_{strat} provided by Fig. 4.9 shows that the North Sea can be roughly subdivided into three different regimes with respect to seasonal stratification: (1) the shallow, non-stratified southern coastal North Sea, (2) the intermediate-depth, seasonally stratified southern central North Sea (approximately 54 °N–56 °N, 3 °E–7 °N), and (3) the deep, seasonally well-stratified northern North Sea. Among these three regimes, the second one constitutes that with clearly the highest year-to-year variability in t_{strat} ranging between less than one month up to six months. As sufficiently long continuous stratification is considered as a prerequisite for the evolution of O_2 deficiency, this zone is also expected to show highest year-to-year variability in minimum O_2 levels. This will be further discussed in Sect. 5.2.2 and related to other (physical and biological) factors in Sect. 5.2.5.

The here presented algorithm for the determination of t_{strat} (Eq. (4.4)) also yields spatial patterns and stratification periods very similar to those find in the literature. The stratification periods and regimes derived from the HAMSOM results are in good agreement with the different regimes described by Pingree et al. (1978) and van Leeuwen et al.

(2015). The first used a stratification criterion based on tidal energy dissipation and identified three different regimes ('mixed', 'transitional' and 'stratified') very similar to those described above. The latter applied a density-based stratification criterion on model results in order to subdivide the North Sea into areas of different stratification characteristics. They consequently identified five different stratification regimes within the North Sea (see Fig. 2.2): 'permanently stratified', 'seasonally stratified', 'intermittently stratified', 'permanently mixed' and 'region of freshwater influence' (ROFI). The aggregated area of the latter three regimes found by van Leeuwen et al. (2015) basically represents the area the non-stratified areas in Fig. 4.9 and the adjacent parts with only short-lasting stratification (<40 days). They furthermore showed that most regions of the central and northern North Sea can be classified as seasonally stratified with stratification periods of 170 to 230 days, which is in very good agreement with the results of this study. Interestingly, some parts of the North Sea could not be assigned to a distinct type of stratification by van Leeuwen et al. (2015) (white areas in Fig. 2.2). Those parts of these areas located in the southern North Sea match very well the regions of highest variability in t_{strat}, according to (4.4) (see Fig. 4.9b). The only difference relates to the Norwegian Trench area, which was identified as permanently stratified (t_{strat} >345 days) by van Leeuwen et al. (2015), but shows longest stratification periods significantly less than 345 days in the present work. This relates to the use of a density criterion by van Leeuwen et al. (2015), taking haline stratification into account. In contrast, a T-based criterion does not account for this influence. Consequently, t_{strat} is likely to be underestimated in the Norwegian Trench. However, as this region is not in the focus of this study and as the stratification algorithm presented shows a generally good agreement with the spatial distribution and duration of seasonal stratification described by Pingree et al. (1978) and van Leeuwen et al. (2015), it is considered to provide a reliable basis for the analysis of the North Sea O_2 dynamics under stratified conditions.

4.3.3 Evaluation of the stratification algorithm

The algorithm used for the determination of t_{strat} and MLD (see Sect. 4.3.1) deviates clearly from MLD criteria used in earlier studies (see, e.g., Table 1 in Kara et al. (2000)). Therefore, a validation of this new algorithm is required in order to demonstrate that the resulting stratification period and MLD constitute reasonable results. For this purpose, Fig. 4.10 shows Hovmöller diagrams of simulated vertical diffusion (d_v; left), as a proxy for vertical mixing intensity, and T (right), at three different locations in the North Sea for the year 2005: a,b) MARNET station Ems (54 ° 10' N, 6 ° 21' E), and the Cefas stations c,d) Oyster Grounds (54 ° 30' N, 4 ° 30' E), and e,f) North Dogger (55 ° 41' N, 2 ° 16.80' E). The magenta bars at the top of each panel indicate stratified periods according to Eq. (4.4)

and the magenta dashed line marks the corresponding MLD following Eq. (4.5). Depth levels correspond to centre depths of model grid cells.

The first station, MARNET Ems (Fig. 4.10a and b), is characterised by a shallow bottom depth of 35 m and is located in the tidally influenced coastal southern North Sea. Thus, d_v is high throughout the entire year 2005 and thermal stratification remains weak and quite unstable during the spring-autumn period (see Fig. 4.10a), as the intense tidal mixing causes the frequent complete overturning of the water column. ΔT between surface and bottom layer is very low (<0.5 K) throughout the entire year, including the periods of stratification (see Fig. 4.10b). $\Delta T_{\mathrm{crit}} = 0.05\,\mathrm{K}$ is first exceeded in late March, lasting about two weeks, before stratification is again intermittent. This short-term event is also visible by the lower values in d_v during this period, compared to the high values of above $120\,\mathrm{cm^2\,s^{-1}}$ within the entire water column, directly before and after that short period of weak stratification. The period from mid-April to mid-July shows three periods of longer stratification (3–6 weeks), of which the first and the latter show clearly reduced mixing (i.e., lower d_v down to less than $10\,\mathrm{cm^2\,s^{-1}}$) relative to the intermittences between these stratified periods. The latter period also shows the highest ΔT within the entire annual cycle, visible in the slight decrease in T between the uppermost layer and that directly below. From late July until early September, short-lasting events of stratification (1–2 weeks) occur, before the final breakdown of stratification in mid-September. The MLD is quite shallow during all stratified periods, mostly ranging between 10 m and 15 m.

At Cefas station Oyster Grounds, stratification is more pronounced than at MARNET Ems. This relates to the greater bottom depth of 45 m and lower tidal influence which allow for the continuous de-coupling of the bottom mixed layer (BML) from the SML from spring to autumn. Stratification first evolves in late March accompanied by a decrease in d_v in 30 m–40 m depth, which indicates the de-coupling of the SML and BML (see Fig. 4.10c). This region of low d_v ($<10\,\mathrm{cm^2\,s^{-1}}$) persists until early April, when a short-term event of enhanced mixing causes the complete overturning of the water column and the breakdown of stratification. In the T distribution (Fig. 4.10d) it can be seen that thermal stratification remains very weak during this early period, visible only in a slight shift in the 6.5 °C-isotherm. After this short-term intermittence, stratification re-establishes and continues for about 4.5 months until late August when enhanced mixing causes complete water column overturning, prior to new surface warming resulting in two additional weeks of thermal stratification before the final breakdown in mid-September. The breakdown events coincide well with events of high d_v throughout the entire water column, which supports the applicability of the stratification criterion (Eq. (4.4)).

The MLD during the long period of stratification from mid-April to late August mostly ranges between 10 m and 25 m, with a maximum MLD of 30 m in early May. It is shown

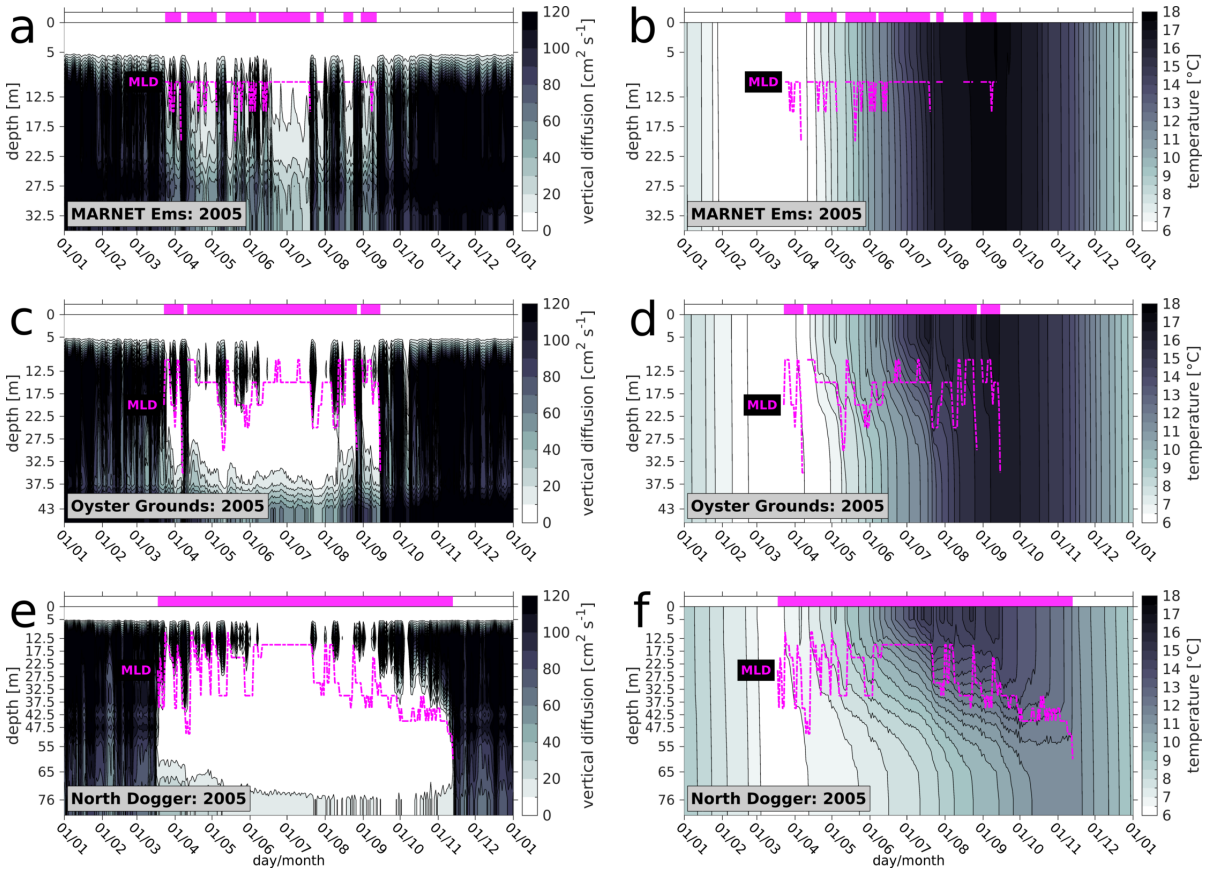

Figure 4.10: Hovmöller diagrams of simulated vertical diffusion (d_v; left) and temperature (T; right) for three stations in 2005: (a, b) MARNET Ems, (c, d) Cefas Oyster Grounds, and (e, f) Cefas North Dogger. Magenta bars at top of each panel indicate stratified periods according to Eq. (4.4), magenta dashed lines indicate corresponding MLD following Eq. (4.5). Colour scales cut at upper end.

that events of enhanced surface mixing correspond with a deepening of the MLD, however, partly with a slight temporal delay of up to five days (e.g., in late May/early June). In general it can be said, that the MLD represents well the lower bound of areas of enhanced surface mixing during the stratified period, which indicates the suitability of the MLD criterion applied (Eq. (4.5)).

The vertical T distribution at Oyster Grounds clearly differs from that at MARNET Ems. As indicated by the clearly lower vertical mixing during most parts of the spring-autumn period, clear thermal stratification can evolve visible by the steeper slope of the isotherms in 10 m to 25 m depth. Strongest thermal stratification occurs in mid-July, just before an event of enhanced surface mixing causing a mixed layer deepening from 15 m to 25 m. Events of enhanced surface warming and those of enhanced surface mixing

alternate periodically from June to August which is nicely represented in T by the sequence of increasing T in the upper 10 m to 15 m, followed by the homogenisation of T from the surface down to the MLD, and recurrent SST increase afterwards. Events of surface warming and events of T homogenisation coincide with low ($<10\,\mathrm{cm^2\,s^{-1}}$) and high near-surface d_v (up to $120\,\mathrm{cm^2\,s^{-1}}$), respectively.

Cefas station North Dogger constitutes the deepest station (model bottom depth = 82 m) among the three presented and, consequently, shows most intense (and longest) thermal stratification indicated by the steep slope of the isotherms in the T distribution (Fig. 4.10f). The onset of thermal stratification occurs in mid-March, visible in the remarkable decrease in d_v between 30 m and 60 m depth (see Fig. 4.10e). Stratification than continues until mid-November without any intermittence, implying a t_{strat} of almost eight months. During this period, the MLD mostly ranges between 10 m and 45 m with high variations from March to May and August/September when both, surface mixing and heating, strongly affect the T distribution in the upper tens of metres, and events of enhanced and reduced mixing alternate. In the earlier period, the MLD again envelops the surface layers showing enhanced vertical mixing. During the period of weakest surface mixing (mid-June to mid-July), the MLD is consistently equal to 15 m, and SST shows a steady increase until an event of enhanced surface mixing in mid-July.

From that point in time until mid-September, the MLD overestimates the actual mixing depth (i.e., the depth until which vertical mixing shows values above $10\,\mathrm{cm^2\,s^{-1}}$). This relates to the fact, that surface mixing during this period only directly affects the upper 15 m to 20 m causing the homogenisation of T down to this depth, but not affecting the $\Delta T/\Delta z$ in the layers below. Consequently, the maximum $\Delta T/\Delta z$ is found in the layers directly below the well-mixed, homogeneous near-surface layer. During the last 1.5–2 months of the stratified period, the MLD represents better the actual mixing depth, which can be seen in the good agreement between MLD and the lower end of both, increased d_v and the vertical progression of the isotherms. The breakdown of stratification also coincides with the onset of the complete overturning of the water column, indicated by the high d_v throughout the entire water column.

The qualitative evaluation of the stratification algorithm presented in Sect. 4.3.1 demonstrates its suitability for the description of the duration of stratification as well as the MLD. The timing of onset and breakdown of stratification according to Eq. (4.4) matches well the end and recurrence of water column overturning indicated by the reduction and increase of d_v, respectively. However, it should be noted that the onset of stratification (according to Eq. (4.4)) may be slightly too early, while the breakdown may be slightly too late, as indicated, e.g., by the existence of still high d_v during the first few days of stratification at Oyster Grounds. This minor temporal mismatch between actual mixing

intensity and the diagnosed onset/breakdown of stratification based on quantities like T or density is a general problem of stratification criteria based on these quantities as their vertical distribution is the result of reduced/enhanced mixing, implying some temporal delay. However, t_{strat} is most likely only slightly overestimated, i.e., by a few days, which is acceptable within the current study.

With respect to the MLD, the use of the maximum $\Delta T/\Delta z$ appears consecutive as the thermocline depth usually defines the lower end of the SML. The evaluation showed that in most cases this approach yields good results, shown by the good agreement between the lower end of areas of enhanced mixing and the MLD. However, at North Dogger a mismatch of up to 15 m between the two can be seen in autumn, which indicates the limitation of this approach in reflecting the actual mixing depth during events of near-surface mixing under principally well-stratified conditions. Despite these minor shortcomings of the stratification and MLD criterion it can be concluded that the algorithm presented (Eqs. (4.4) and (4.5)) reproduces well the vertical extent of surface mixing under stratified conditions as well as the duration of thermal stratification in different parts of the North Sea. This is important as it clearly differs from other commonly used MLD criteria (e.g., Table 1 in Kara et al. (2000)) and, especially, as stratification is considered as the physical prerequisite for the evolution of O_2 deficiency.

4.4 Conclusions on simulated North Sea hydrography and stratification

The results presented in this chapter demonstrate that HAMSOM reproduces well the known spatial and seasonal patterns in SST and SSS in the North Sea (e.g., Otto et al., 1990; Elliott et al., 1991; Janssen et al., 1999). With respect to summer T and S, which is most crucial for seasonal stratification, it shows principally good agreement with the high-resolution ScanFish observations covering the entire North Sea (see Sect. 4.2). HAMSOM reveals some shortcomings for summer S, especially in the northeastern part of the North Sea which, however, are not in the focus of this study. In the southern North Sea, HAMSOM tends to underestimate observed summer S. Though, its effect on vertical stratification is negligible as observed and simulated S do not show haline stratification in these areas. In contrast, observations and simulations of summer T and S clearly show that T constitutes the major contributor to seasonal stratification in the southern and central North Sea (south of 57 °N). Consequently, T can be used for the description of seasonal stratification in most regions of the North Sea, providing the basis for the investigation of the O_2 dynamics.

Focusing on summer ΔT between surface and bottom, as a proxy for seasonal stratification, HAMSOM shows similar tendencies with respect to spatial differences in ΔT in zonal (along the individual transects presented) and meridional direction (between the transects). This is confirmed by the statistics presented in the Fig. 4.7 (magenta markers). Thus, it can be concluded that ΔT derived from simulated T can be used for the derivation of stratification characteristics, providing reliable results. However, the comparison of the observed and simulated T along the ScanFish transects indicates that HAMSOM tends to underestimate thermal stratification, i.e., vertical mixing tends to be overestimated. This likely results – at least partly – from the limited spatial resolution of the model, which is only about 20 km. This also has to be taken into account for the analysis of the O_2 dynamics.

The presented new algorithm for the derivation of stratification duration and MLD (see Sect. 4.3.1) yields stratification periods which are in very good agreement with findings by van Leeuwen et al. (2015) and also represent very well the different stratification-related North Sea zones defined by Pingree et al. (1978). The evaluation of the MLD criterion (Eq. (4.5)) in relation to vertical mixing demonstrates that both, t_{strat} and MLD represent very well the actual vertical mixing conditions. Thus, the results for these two quantities obtained from simulated T provide a reliable basis for the investigation of the North Sea O_2 conditions during seasonal stratification.

Chapter 5

Biogeochemistry and oxygen dynamics of the North Sea

In recent years, several studies focused on the O_2 dynamics of the North Sea (e.g., Greenwood et al., 2010; Meire et al., 2013; Queste et al., 2013, 2016; Rovelli et al., 2016). However, these studies were temporally or spatially confined and do not suffice to provide a general description of the North Sea with respect to O_2. Therefore, this chapter aims for a comprehensive, spatially and temporally consistent description of the North Sea O_2 conditions and the quantitative analysis of the dominant processes controlling the O_2 dynamics. For this purpose, this chapter first provides an overview of the North Sea biogeochemistry during the period 2000–2014, based on a qualitative comparison of observational data and ECOHAM model results. Thereafter, this the focus is put on the O_2 dynamics of the North Sea, by first providing a validation of simulated bottom O_2. Second, a detailed analysis of the North Sea O_2 dynamics during the period 2000–2014 is provided with special focus on both, spatial and year-to-year variability.

5.1 Annual cycle and regional differences in North Sea biogeochemistry

In order to provide a general description of the North Sea biogeochemistry with respect to seasonal and spatial variability and to give insight in the quality of the ECOHAM model, this section presents a qualitative comparison of simulated and observed PO_4^{3-}, NO_3^-, NH_4^+, SiO_4^-, Chl-a (as a proxy for phytoplankton) and O_2 in different areas of the North Sea. For this purpose, the North Sea was first subdivided into a horizontal $1\,^\circ \times 1\,^\circ$-grid (resolution differs near-shore) and one or two vertical boxes, depending on the bottom depth and thus the occurrence of seasonal stratification. In case of no vertical separation, observations are aggregated from surface to bottom, while in case of two vertically adjacent boxes only the uppermost 20 m are considered. As biogeochemical observational data are sparse in most North Sea regions, observations are additionally aggregated over the 15-year period 2000–2014 for each box and monthly averages as well as 17 %- and 83 %-quantiles are calculated

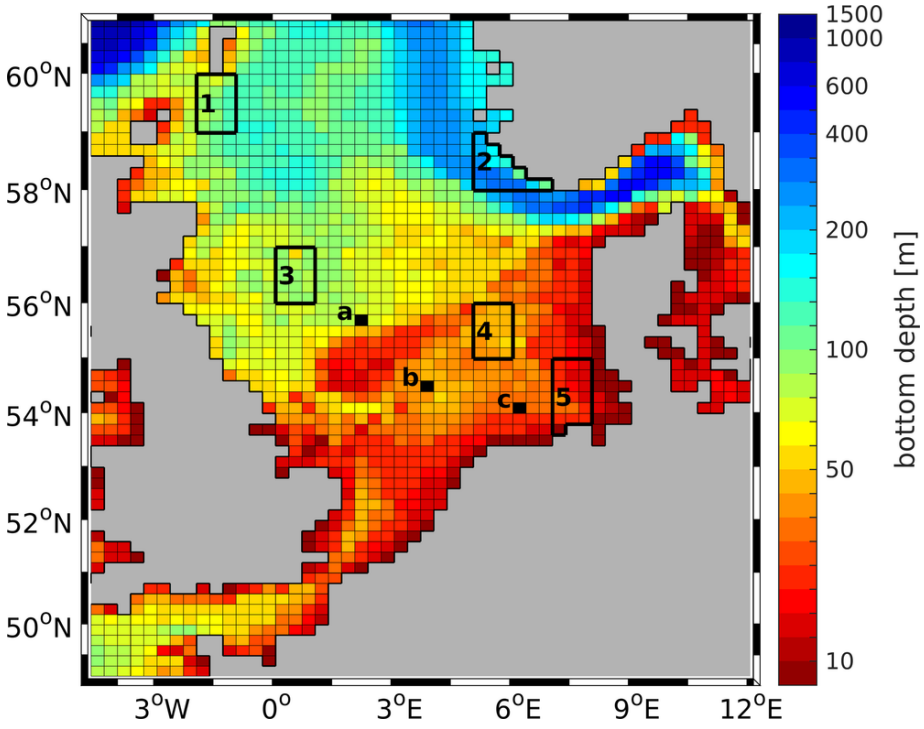

Figure 5.1: North Sea bathymetry as used by ECOHAM (colours) including regions (black-framed boxes) and stations (black-filled cells) used for validation. Regions #1 to #5 are used for validation of ECOHAM biogeochemistry presented in Fig. 5.2. Stations are used for validation of simulated bottom O_2 concentrations presented in Fig. 5.3. For regions #1 to #4 simulation and observation data are averaged over the upper 20 m, for region #5 data are averaged over entire water column. Stations refer to (a) Cefas North Dogger, (b) Cefas Oyster Grounds and (c) MARNET Ems (see Sect. 5.2.1.1). Colour scale increments are equidistant between two labelled depth levels.

and compared against the daily box-averaged model output for the individual years of the observational period. The observation data used for this validation are described in Sect. 3.4.2. The regions used for validation were finally selected with the target of covering different regions of the North Sea, according to highest data availability.

The selected regions are shown in Fig. 5.1 (black-framed). For regions #1 to #4 only the upper 20 m are considered due to regularly occurring seasonal stratification; in case of region #5 the entire water column is considered. Region #1 represents the northwestern North Sea which is strongly influenced by the Atlantic inflow through the Fair Isle Channel, while region #2, located at the southwestern tip of Norway, is influenced by the Norwegian rivers and the northward outflow from the North Sea back into the North Atlantic (see Fig. 2.1). Region #3 is located in the western central North Sea that is still affected by the North Atlantic inflow, however to a lesser extent than region #1. Region #4,

located east of Dogger Bank, represents the southeastern central North Sea, which is less affected by the Atlantic inflow as most of the Atlantic water is recirculated north of the Dogger Bank (Lenhart and Pohlmann, 1997). These four regions have in common that they experience persistent seasonal stratification during the summer period (see Fig. 4.9), which is mainly T-driven in regions #1, #3 and #4, and S-driven in region #2. In contrast, region #5 represents the consistently well-mixed southeastern North Sea with high influence of continental river freshwater discharge and nutrient input.

The annual cycles of PO_4^{3-}, NO_3^-, NH_4^+, SiO_4^-, Chl-a, and O_2 for regions #1 to #5 (see Fig. 5.1, black-framed boxes) are presented in Fig. 5.2. It has to be noted that the observations partly show quite high variability which is a result of the temporal and spatial averaging. Chl-a concentrations are calculated diagnostically within ECOHAM using diatom-C and flagellate-C and a variable Chl-a:C ratio according to Cloern et al. (1995). The average observed concentrations are represented by dots, while 17 %- and 83 %-quantiles are indicated by the error bars. Black-coloured observations indicate at least 15 individual measurements available, grey implies fewer data. Error bars are only displayed in case of more than one measurement available.

In region #1 (Fig. 5.2a), located in the vicinity of the Fair Isle Channel, the simulated nutrient concentrations (PO_4^{3-}, NO_3^-, NH_4^+ and SiO_4^-) show a pronounced annual cycle with high concentrations at the beginning and the end of each year. PO_4^{3-}, NO_3^- and SiO_4^- show a decrease during April/May and low concentrations during summer. In contrast, NH_4^+ steadily decreases until mid-April when it starts to slightly increase. Thereafter, NH_4^+ concentrations stay on stable level throughout summer. All nutrient concentrations start to increase in September/October. The decrease in PO_4^{3-}, NO_3^- and SiO_4^- in April/May is accompanied by an remarkable increase in simulated Chl-a – the so-called spring bloom (Gieskes and Kraay, 1975) – reaching maximum concentrations in late April. After that spring bloom, Chl-a concentrations decrease and stay on a low level during summer. A second, less pronounced increase in Chl-a occurs in September/October, coinciding with the increase in nutrient concentrations. The simulated O_2 concentrations show a maximum in late April/early May, followed by a decrease until late September/early October. O_2 concentrations steadily increase between this minimum and the next year's maximum.

The annual cycles of the different quantities relate to different processes and factors. The decrease in PO_4^{3-}, NO_3^- and SiO_4^- in spring relates to the enhanced NPP due to the onset of stratification, initiating the phytoplankton spring bloom. As a result of increasing zooplankton grazing (not shown) and nutrient limitation Chl-a (and phytoplankton) concentrations start to decrease, i.e., the spring bloom ends. Nutrient limitation is strongly related to the presence of seasonal stratification in that area (see Fig. 4.9), which limits the supply of nutrients from the deeper nutrient-rich layers into the nutrient-depleted,

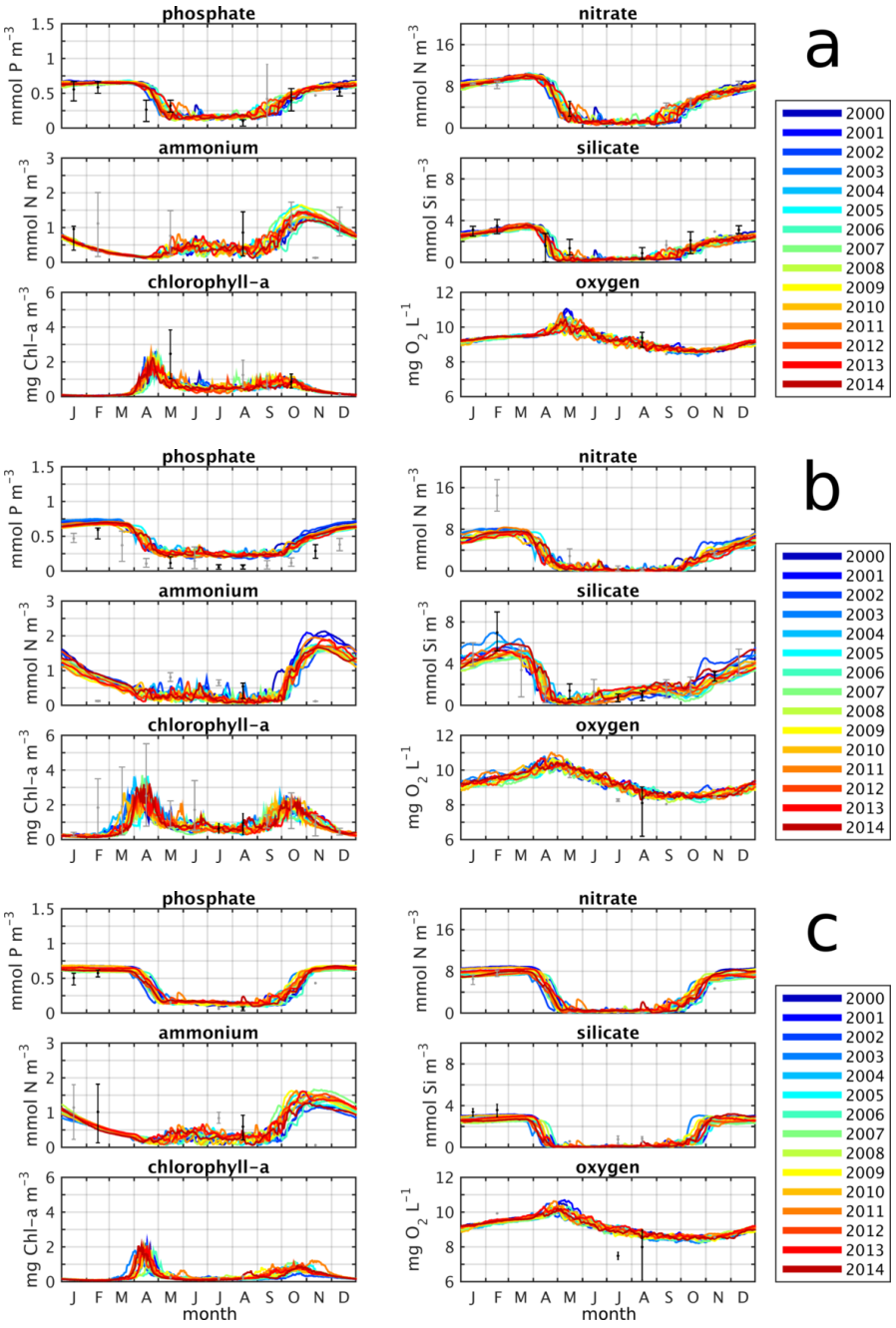

Figure 5.2: Validation of daily, box-averaged ECOHAM results (lines) against 15-year monthly, box-averaged observations (grey/black dots) for nutrients (PO_4^{3-}, NO_3^-, NH_4^+ and SiO_4^-), Chl-a and O_2 for the period 2000–2014 in different regions (see Fig. 5.1). Observation error bars range from 17 %-quantile to 83 %-quantile. Black colour indicates at least 15 individual observations available, grey implies fewer data. Regions (a) #1, (b) #2 and (c) #3.

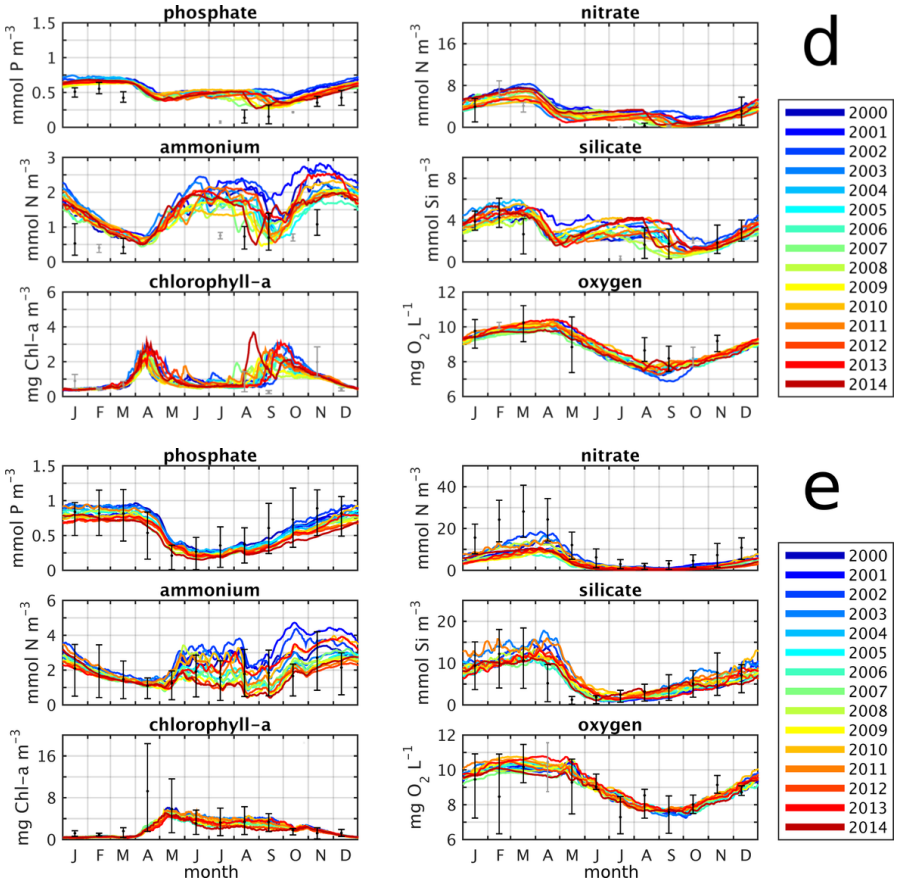

Continued: Regions (d) #4 and (e) #5. Note different y-axis for PO_4^{3-}, NO_3^-, NH_4^+, SiO_4^- and Chl-a for region #5.

euphotic surface layers. In addition, the Chl-a:C ratio decreases due to increasing light availability. Production of organic matter during the spring bloom enhances remineralisation processes, indicated by the increase in NH_4^+ after the Chl-a maximum. The enhanced NPP during the spring bloom also causes the increase in the O_2 concentration, reaching its maximum in May.

During summer, the ongoing stratification causes nutrient concentrations to stay on low levels, except for NH_4^+ which is continuously released by remineralisation and excreted by zooplankton. In case sufficient PO_4^{3-} is available, this NH_4^+ is utilised by flagellates resulting in the maintenance of the so-called summer standing stock (Colebrook, 1979). Short-term events (order of days) of increased nutrient and Chl-a concentrations relate to enhanced, mainly wind-induced mixing, causing the replenishment of the near-surface nutrient pools. Consequently, NPP increases resulting in increased Chl-a concentrations. Subsequent grazing and re-intensification of stratification again lower Chl-a concentrations and limit phytoplankton growth, respectively. These events also affect the Chl-a:C ratio

(not shown) due to changes in T, light and nutrient availability. The summer decrease in near-surface O_2 relates to the T increase, reducing O_2 solubility (Benson and Krause, 1984), as well as continuous biochemical O_2 consumption (zooplankton respiration, remineralisation and nitrification).

The increase in nutrient and Chl-a concentrations in autumn relates to the final breakdown of stratification due to increasing storm activity and reduced solar radiation. The mixing-induced renewal of the near-surface nutrients triggers NPP and results in the minor autumn peak in Chl-a. Thereafter, living organic matter dies and is remineralised resulting in a strong increase in NH_4^+ in October. The subsequent decrease in NH_4^+ relates to ongoing nitrification. The decreases in T and O_2 consumption drive the increase in O_2 concentration.

Considering the individual quantities and years in more detail, it can be seen that the timing of the simulated Chl-a maximum shows only minor year-to-year variability of ±10–15 days. The same applies to the peak concentration which is about 2.2 mg Chl-a m^{-3}–2.9 mg Chl-a m^{-3} in the different years. The O_2 maximum with concentrations of 10.4 mg O_2 L^{-1}–11.1 mg O_2 L^{-1} occurs with a slight temporal of 2–3 weeks relative to the Chl-a maximum. This most likely relates to the balance between biological O_2 consumption and O_2 production. The O_2 concentrations continues to increase until that point when O_2 consumption exceeds O_2 production. This point in time does not coincide with the maximum in Chl-a as PP continues although Chl-a concentrations already started to decrease due to zooplankton grazing.

The fact, that SiO_4^- concentrations reach their minimum concentrations earlier than PO_4^{3-} and NO_3^- nicely illustrates that ECOHAM reproduces well the succession of diatoms and flagellates during the spring bloom, as diatoms require SiO_4^- while the latter do not. The simulated summer nutrient concentrations show values of about 0.17 mmol P m^{-3}, 1 mmol N m^{-3} and 0.3 mmol Si m^{-3} for PO_4^{3-}, NO_3^- and SiO_4^-, respectively. Summer NH_4^+ shows strong fluctuations as its repeatedly utilised by flagellates. Average summer NH_4^+ concentrations are about 0.5 mmol N m^{-3}.

The simulation results in region #1 show a generally good agreement with the observations. The annual cycle of PO_4^{3-}, NO_3^- and SiO_4^- is well reproduced, showing only a slight overestimation of observed summer PO_4^{3-} and NO_3^- concentrations. The observed NH_4^+ concentrations are also well reproduced, despite the slight underestimation of summer concentrations. In November, when the simulation clearly deviates from the observations, only two individual measurements are available, which does not suffice to represent spatial and temporal variability within the region.

For Chl-a, the simulated values underestimate the summer observations, which can relate to differences in phytoplankton-C and Chl-a:C ratio. With respect to the timing of

the spring bloom, the overestimation of PO_4^{3-} and SiO_4^- in April suggests that the spring bloom tends to occur earlier in region #1 than simulated by ECOHAM. However, this cannot be confirmed by the Chl-a observations as no data are available for March/April. The few O_2 observations available suggest that the annual cycle of O_2 is well reproduced.

Box #2 (Fig. 5.2b) is located directly west of the southern tip of Norway and characterised by strong haline stratification. The model shows similar annual cycles for the different quantities as in region #1 with only some differences. The phytoplankton spring bloom already begins in early March, i.e., about one month earlier than in region #1, reaching its peak in late March to mid-April. This most likely relates to the earlier onset of stratification in this region, compared to region #1. Maximum spring concentrations of PO_4^{3-} and NO_3^- are only slightly higher than in region #1, while SiO_4^- concentrations are clearly higher with values of up to $6\,\mathrm{mmol\,Si\,m^{-3}}$. Maximum Chl-a concentrations are also higher than in region #1, reaching $3.2\,\mathrm{mg\,Chl\text{-}a\,m^{-3}}$–$3.7\,\mathrm{mg\,Chl\text{-}a\,m^{-3}}$ due to a higher Chl-a:C ratio. This relates to the lower light availability, due to the earlier onset of the spring bloom, and higher SiO_4^- availability. The latter can be attributed to the riverine input of SiO_4^- by Norwegian rivers entering the North Sea. The increase in NH_4^+ in succession of the Chl-a peak is less strong than in region #1. The O_2 maximum with values similar to region #1 shows a temporal delay of 2–3 weeks relative to the Chl-a maximum, probably for the same reasons as in region #1.

During summer, PO_4^{3-} and NO_3^- concentrations are consistently low with values of about $0.25\,\mathrm{mmol\,P\,m^{-3}}$ and $0.1\,\mathrm{mmol\,N\,m^{-3}}$, respectively. Summer NH_4^+ concentrations stay consistently lower than in region #1. This, in combination with the slightly higher Chl-a concentrations, indicates that summer NPP driven by NH_4^+ is stronger than in region #1. SiO_4^- shows a steady increase until late August and a high year-to-year variability, driven by the Norwegian rivers. This SiO_4^- cannot be utilised completely for NPP by diatoms as low NO_3^- concentrations limit their productivity. Fluctuations in summer nutrient and Chl-a concentrations relate to events of enhanced mixing.

As in region #1, the degradation of stratification in September enables NPP. However, this autumn bloom in Chl-a is more pronounced than in region #1 with maximum concentrations of about $2.5\,\mathrm{mg\,Chl\text{-}a\,m^{-3}}$ (twice as high as in region #1). This autumn increase in Chl-a is driven by enhanced diatom NPP, visible in the decrease in SiO_4^-. Year-to-year variability in the autumn bloom is also higher than in region #1. This may relate to the generally higher SiO_4^- concentrations in region #2, which also show higher variations between the years. The increase in the Chl-a:C ratio due to decreasing light availability additionally increases Chl-a concentrations. PO_4^{3-} and NO_3^- also show autumn increase similar to Chl-a, however, with a temporal delay of 2–3 weeks as they are directly utilised for NPP.

The temporal evolution of O_2 during the summer/autumn period is quite similar to region #1 with a steady decrease after the spring bloom until September/October, when minimum concentrations of about $8.5\,\mathrm{mg\,O_2\,L^{-1}}$ are reached, followed by an increase until the next year's spring bloom.

The comparison of simulated time series with observations shows that the general patterns of the annual cycle of the different quantities are well reproduced. Especially, the annual cycles of SiO_4^- and Chl-a match the observations with respect to the timing of the spring and autumn bloom. This indicates that the simulated annual cycle of diatoms is in good agreement with the actual one. However, the model shows some deviations from the observations in case of PO_4^{3-} and winter/spring NO_3^-, although observation data are very sparse for the latter. Observed PO_4^{3-} concentrations are consistently overestimated by ECOHAM. This likely relates to the applied N:P ratio of 20:1, which is higher than the Redfield ratio of 16:1 (Redfield, 1934). Consequently, the uptake of PO_4^{3-} is reduced relative to the uptake of N, which constitutes the limiting nutrient in this area.

The discrepancies between simulated and observed NO_3^- in February, and NH_4^+ in February and November may relate to sampling confined to a location not representative for the entire region (only four individual measurements per month). With respect to O_2, the average observed concentrations are slightly overestimated by the simulation. The large variability in the August observations most likely results from the fact that measurements were conducted above and below the pycnocline, which was located within the upper 20 m. This implies measurements within the oxygenated SML and the undersaturated deeper layers.

Figure 5.2c shows the annual cycles in region #3, located in the seasonally stratified western central North Sea. The different simulated quantities show similar seasonal patterns as in the previously described regions. Maximum and minimum concentrations of PO_4^{3-} and NO_3^- are comparable to those in region #1. Maximum PO_4^{3-} and NO_3^- concentrations in late winter reach $0.8\,\mathrm{mmol\,P\,m^{-3}}$ and $8.2\,\mathrm{mmol\,N\,m^{-3}}$, respectively. Minimum summer concentrations are about $0.17\,\mathrm{mmol\,P\,m^{-3}}$ and $0.2\,\mathrm{mmol\,N\,m^{-3}}$. The spring bloom starts in mid-March and reaches its peak in mid-April. Maximum Chl-a concentrations during the bloom are about $2\,\mathrm{mg\,Chl\text{-}a\,m^{-3}}$–$2.7\,\mathrm{mg\,Chl\text{-}a\,m^{-3}}$. After the spring bloom, NH_4^+ shows an increase very similar to region #1. This increase is followed by a decline in NH_4^+ concentrations from July until September when the degradation of stratification initiates an autumn bloom in phytoplankton. This bloom is indicated by minor increase in the Chl-a concentration in September/October. Maximum Chl-a concentrations during this autumn bloom stay clearly below the concentrations seen in region #2 and are similar to those in region #1.

SiO_4^- shows generally lower concentrations compared to regions #1 and #2, with min-

imum concentrations of about 0.1 mmol Si m^{-3} throughout the entire summer/autumn period, except for events of enhanced vertical mixing. This likely relates to the absence of riverine sources (like in region #2) and the reduced influence of the Atlantic inflow compared to region #1. The annual O_2 cycle shows maximum and minimum very similar to region #2, and the same temporal delay between Chl-a spring maximum and the subsequent O_2 maximum can be seen.

With respect to model validation in region #3, a clear statement is difficult to make as observational data in this region are very sparse for most of the quantities presented. The annual cycle of PO_4^{3-}, NO_3^- and SiO_4^-, which are those with the most data available, appear to be well reproduced, although summer concentrations of PO_4^{3-} and NO_3^- are slightly overestimated. SiO_4^- concentrations seem slightly underestimated. NH_4^+ concentrations also are in good agreement with the observations. However, January/February observations show high variability, while the November observation (only one value) clearly deviates from the model results.

Box #4 (Fig. 5.2d) is located in the southeastern central North Sea, that region where the lowest bottom O_2 concentrations usually occur (see Sect. 5.2.1.2). The simulated annual cycles of the different quantities reveal quite some differences compared to the previous regions. The onset of the spring bloom occurs in mid-March in all years, i.e., about two weeks earlier than in the other offshore regions #1 and #3. Maximum Chl-a concentrations of 2.6 mg Chl-a m^{-3}–3.3 mg Chl-a m^{-3} are reached in mid-April. Maximum O_2 concentrations of 9.8 mg O_2 L^{-1}–10.3 mg O_2 L^{-1} occur with a temporal delay of about two weeks like in the previous regions. After the spring bloom and the related decrease in PO_4^{3-}, NO_3^- and SiO_4^- concentrations, these nutrients still show high concentrations, compared to the previous regions. PO_4^{3-} and NO_3^- concentrations stay on levels around 0.9 mmol P m^{-3} and 2.7 mmol N m^{-3}, respectively, and show a minor increase during summer. SiO_4^- concentrations also remain high (above 2 mmol Si m^{-3}) and show a remarkable increase during the summer period of individual years (e.g., more than 2 mmol Si m^{-3} in 2014, dark red). This indicates that nutrient limitation on NPP plays a minor role in this region. This likely relates to the advective supply of nutrients from southwestern coastal regions (compare Fig. 2.1) where riverine nutrients enter the marine system.

The annual cycle of NH_4^+ is also quite different to the previous regions. From January to mid-April, NH_4^+ shows a strong decrease reaching minimum concentrations of about 0.5 mmol N m^{-3}. After the spring bloom, NH_4^+ concentrations show a steep increase resulting in maximum summer concentrations of up to 2.8 mmol N m^{-3} during individual years (e.g., in 2001, dark blue). This increase in combination with the non-limiting PO_4^{3-}, NO_3^- and SiO_4^- concentrations suggests that organic matter remineralisation and NH_4^+ excretion by zooplankton is higher than in the previous regions. However, these processes do

not show any distinct regional differences between regions #1 to #4 (not shown). Therefore, it is likely attributable to advective input of NH_4^+ from the Southwest. This raises the question why Chl-a concentrations remain low during summer, except for some events of increasing Chl-a concentrations. In fact, the regional differences are caused by stronger light limitation in region #4 relative to regions #1 to #3. This relates to higher SPM concentrations and a higher attenuation coefficient of the seawater itself in this region (not shown). The stronger light limitation in combination with less strong nutrient limitation results in PP similar to the previous regions. In combination with the advective input of nutrients from adjacent areas this leads to higher nutrient levels, while summer Chl-a concentrations are also similar to the previous regions.

In August/September the autumn phytoplankton bloom occurs, visible in the increase in Chl-a with maximum concentrations similar to the spring bloom. This bloom is driven by both, diatoms and flagellates, indicated by the simultaneous decrease in all nutrients. The autumn bloom also coincides with the onset of the increase in O_2 concentrations. It is worth mentioning that the timing of the onset of the autumn bloom varies remarkably between the years, e.g., showing a very early onset mid-August 2014 (dark red) compared to a late onset in mid-September 2001 (dark blue).

The comparison of the simulation results with the observations in region #4 shows that the autumn and winter concentrations of all presented quantities are well reproduced by ECOHAM. Only PO_4^{3-} and NH_4^+ concentrations tend to be slightly overestimated. This overestimation of PO_4^{3-} most likely results from the high phytoplankton N:P ratio of 20, as seen in region #2. The high NH_4^+ concentrations may result from slightly to high light limitation in that region, due to the climatologic SPM data, which limits the nutrient uptake by PP. For the period from April to July a clear statement about the model quality is difficult as either no or only very few observation data are available. Simulated O_2 is in generally good agreement with the observations.

In the southernmost region #5 (Fig. 5.2e; note different y axes for NO_3^-, NH_4^+, SiO_4^- and Chl-a compared to other regions), located in the German Bight, the simulated annual cycles of the different quantities differ remarkably from those in the previous regions. This applies in particular to the maximum nutrient and Chl-a concentrations. Maximum simulated PO_4^{3-} concentrations of 0.7 mmol P m^{-3}–0.9 mmol P m^{-3} (up to 50 % higher than in regions #1 to #4) occur during January–March. The same applies to winter NO_3^-, NH_4^+ and SiO_4^- concentrations which are about 50 %–100 % higher (and even up to 300 % in case of SiO_4^-). These generally higher winter nutrient concentrations mainly relate to two factors. First, the continuous nutrient supply from continental rivers and, second, the persistently well-mixed water body in this region.

The phytoplankton spring bloom starts in early April, i.e., later than in the offshore

region #4, and maximum Chl-a concentrations of up to 4 mg Chl-a m^{-3}–6 mg Chl-a m^{-3} (50 %–150 % higher than in other regions) are reached in mid-May. Maximum Chl-a concentrations occur in the earlier years (2000/2001) while the more recent years (2012–2014) show lower maximum values. This corresponds to higher, respectively, lower nutrient (PO_4^{3-}, NO_3^- and SiO_4^-) availability at the beginning of the spring bloom. Different to the seasonally stratified regions, maximum O_2 concentrations coincide or even precede the Chl-a maximum, e.g., in mid-February 2014 (dark red). The decreases in PO_4^{3-} and SiO_4^- as well as the minor increase in Chl-a during February 2014 suggest that this is caused by enhanced NPP early during individual years, driving subsequent O_2 consumption. Similar to the other regions, a second maximum in O_2 can be found around the Chl-a maximum, however, without any temporal delay due to the strong vertical mixing.

After the spring increase Chl-a, PO_4^{3-} and SiO_4^- concentrations reach their minimum concentrations in June/July, while NO_3^- continues to decrease until August/September. During the entire summer period, diatom NPP is mainly light-limited, but NO_3^- limitation is also in effect. The former results from the high SPM concentrations in this region. The intra-seasonal variations visible in NH_4^+ concentrations from late May to early August indicate recurrent enhancement of flagellate growth, mainly sustaining the summer phytoplankton stock. This is supported by the increase in SiO_4^- during most of the summer period, i.e., less diatom activity. Events of enhanced diatom productivity, visible in the reduction of SiO_4^- (e.g., in early August and October 2014), also occur during the summer/autumn period. However, less frequently than for flagellates as PO_4^{3-}, NO_3^- and SiO_4^- availability has to be sufficiently high. The summer standing stock shows Chl-a concentrations almost as high as during the spring maximum. Summer NH_4^+ concentrations are up to three times higher and reveal high year-to-year variability, ranging between about 1 mmol N m^{-3} June/July 2014 (dark red) and 3.5 mmol N m^{-3} June/July 2001 (dark blue).

High organic matter production enhances remineralisation and zooplankton respiration, i.e., release of NH_4^+ (as well as PO_4^{3-} and SiO_4^-). Thus, these high year-to-year variations are also present in the summer Chl-a concentrations, which are lowest in 2014 (dark red) and highest in 2001 (blue). The strong decrease in NH_4^+ in mid-August clearly shows that late-summer NPP in the German Bight is dominated by flagellates.

From mid-September to mid-October Chl-a concentrations show a steady decrease, accompanied by an increase in nutrients. Thereafter, a minor increase in Chl-a concentrations can be seen, peaking in about 2.5 mg Chl-a m^{-3} in late October, which is even less than during summer. This minor increase is mainly driven by flagellates, indicated by the decrease in NH_4^+ during all years, however, diatoms also contribute to this bloom during individual years as can be seen by the decrease in SiO_4^-. Thereafter, Chl-a concentrations finally decline and nutrient concentrations continue to increase. Minimum O_2 concentra-

tions of 7.2 mg O_2 L^{-1}–7.9 mg O_2 L^{-1} are reached directly before the onset of the autumn Chl-a increase, as decreasing water T due to surface cooling and enhanced PP increase the O_2 concentrations.

With respect to model validation, the simulated quantities show a generally good agreement with the observations, although it has to be noted that the observations partly show very high variability due to spatial gradients and year-to-year variability in region #5. The simulated nutrient concentrations are well within the range (17 %- to 83 %-quantile) visible in the observations during most times of the simulated period. Only NO_3^- concentrations tend to be underestimated by the model, which most likely relates to the horizontal resolution of ECOHAM of only about 20 km and very high concentrations in the near-shore observations, while observed early winter NH_4^+ concentrations tend to be overestimated indicating a slight overestimation of remineralisation.

Chl-a concentrations in region #5 are also well reproduced by the model, except for the April value which constitutes the highest during the average observed annual cycle. This suggests that the simulated phytoplankton spring maximum occurs with a temporal delay of up to one month, as simulated Chl-a concentrations are highest in May. This delay is also indicated by the decline in PO_4^{3-}, NO_3^- and SiO_4^- concentrations during spring, which also occurs earlier in the observations than in the simulations. The O_2 concentrations are generally well reproduced throughout the entire annual cycle.

In conclusion, the simulated annual cycles of near-surface nutrients, Chl-a and O_2 during the period 2000–2014 showed that ECOHAM reproduces well the main regional and temporal differences of the North Sea's biogeochemistry. Some shortcomings can be seen with respect to absolute PO_4^{3-} levels which tend to be overestimated due to the N:P ratio of 20, relatively high compared to Redfield (1934). However, this underestimation of PO_4^{3-} uptake is considered to have no strong influence on phytoplankton dynamics, as no clear hint for P limitation can be found in the observations.

The simulated differences in the timing of the spring bloom in the offshore regions (boxes #1, #3, and #4) are in good agreement with former studies describing that maximum Chl-a concentrations in the central North Sea are found in mid-April (Greenwood et al., 2010) compared to late April/early May in the northern North Sea (Reid et al., 1990). However, the simulated onset in region #4 occurs about one month later than in the observations, which most likely relates to light limitation due to the use of the daily climatology of SPM. The early onset of the spring bloom in region #2 off the Norwegian coast in late February is also in good agreement with other studies as haline stratification can drive the onset of seasonal stratification in that region earlier than in other North Sea regions (van Leeuwen et al., 2015), promoting the early evolution of a near-surface bloom (Braarud et al., 1958; Skogen et al., 1995).

The succession of phytoplankton species during the spring bloom and summer/autumn period is also well reproduced. The initialisation of the spring bloom by diatoms (Gieskes and Kraay, 1986; Sharples et al., 2006) is nicely illustrated by the decrease in SiO_4^- coinciding with the increase in Chl-a in spring in all regions presented. In contrast, flagellates dominate summer PP in the deeper regions (boxes #1 to #3), indicated by the continuous renewal and reduction of the NH_4^+ stock, as stratification is does not allow for NO_3^- supply from deeper nutrient-rich waters and thus limits PP by diatoms. This so-called summer standing stock, mainly sustained by flagellates in stratified waters, is in good agreement with earlier studies (Colebrook, 1979; Skogen et al., 2004).

In the non-stratified German Bight (box #5), the simulation also shows principally good agreement with the observations. Only the timing and intensity of the phytoplankton spring bloom which occurs about one month delayed relative to the observations and shows lower maximum Chl-a concentrations than found in the observations. The first most likely relates to the use of the SPM climatology which strongly reduces year-to-year variability in the onset of the spring bloom (see Fig. 5.2e). The latter likely results from the limited horizontal resolution which does not allow for the representation of the large spatial gradients in spring Chl-a and nutrient concentrations inside region #5, also indicated by the high range in the observations.

This principally good representation of the annual cycles of the selected biogeochemical quantities, together with the reasonable description of seasonal stratification in most North Sea regions (see Sect. 4.3), demonstrates that the use of the hydrodynamical model HAMSOM in combination with the biogeochemical model ECOHAM provides a reliable basis for the detailed analysis of the O_2 dynamics of the seasonally stratified North Sea during the period 2000–2014.

5.2 Oxygen dynamics of the North Sea

The overview of the North Sea biogeochemistry shows that ECOHAM is capable of reproducing well the annual cycle and spatial differences in of North Sea biogeochemistry near the sea surface. Thus, it provides a reliable basis to investigate the North Sea O_2 dynamics. In order to approach this subject, this section first provides a qualitative and quantitative validation of simulated bottom O_2, with special focus on its annual cycle and spatial patterns during summer. Subsequently, a detailed analysis of the North Sea O_2 dynamics during the period 2000–2014 is provided, first, by a more general analysis of spatial differences in potential key parameters and, second, by a detailed analysis of both, physical and biological drivers of O_2. The first analysis identifies the main drivers and controlling factors for the evolution of O_2 deficiency, while the latter focuses on spatial

and year-to-year variability in the O_2 dynamics and provides a detailed analysis of the processes and interactions leading to O_2 deficiency in the North Sea. In combination, the two analyses provide a consistent and comprehensive image of the current state of the North Sea with respect to its O_2 dynamics and O_2 deficiency. This knowledge will help to describe potential future evolutions of the North Sea O_2 conditions and to optimise the design and setup of studies focusing on their future evolution.

The following sections aim for the description of the dynamics, i.e., physico-biochemical interactions, driving the temporal evolution of bottom O_2 as well as its spatial distribution. For this purpose, potential (physical and biogeochemical) factors influencing the temporal evolution of O_2 in relation to seasonal stratification are evaluated in order to identify the key factors crucial for bottom O_2 dynamics and thus regional and year-to-year differences in minimum bottom O_2 concentrations. Subsequently, an in-depth analysis is presented in order to unveil the physico-biochemical interactions leading to O_2 deficiency (i.e., O_2 concentration $<6\,\mathrm{mg\,O_2\,L^{-1}}$; OSPAR, 2005; Best et al., 2007; Claussen et al., 2009; OSPAR, 2013b).

5.2.1 Temporal variability and spatial patterns of bottom oxygen

Lowest O_2 concentrations in the stratified regions of the North Sea usually occur in the deeper waters below the MLD, due to high O_2 consumption by respiratory processes and the prevention of O_2 supply from the oxygenated surface waters. Consequently, the longer stratification prevails the lower O_2 concentrations below the MLD tend to be, i.e., lowest O_2 concentrations are expected to be found in late summer before the breakdown of seasonal stratification. Furthermore, O_2 concentrations tend to be lowest near the seafloor due to benthic O_2 consumption which directly affects the near-bottom O_2 levels.

Daily time series data for three different locations are used for the validation of the temporal evolution of simulated bottom O_2. These sites are indicated in Fig. 5.1 by black-filled grid cells and represent the following stations: (a) Cefas North Dogger, (b) Cefas Oyster Grounds, and (c) MARNET Ems. The results of this validation are presented in Sect. 5.2.1.1. Additionally, an overview of the spatial patterns of simulated late summer bottom O_2 concentrations in comparison to observations is given in Sect. 5.2.1.2, providing a general image of the spatial distribution of late summer bottom O_2 and insight in the model capabilities in reproducing these spatial variations.

Finally, a quantitative validation of simulated bottom O_2 based on the time series and spatially resolved data is provided in Sect. 5.2.1.3, giving additional insight in the model quality with respect to the representation of seasonal and spatial features in bottom O_2.

5.2.1.1 Seasonal variability

Figure 5.3 shows the comparison of time series of simulated (dotted) and observed (solid) bottom O_2 (Fig. 5.3a, c and e) in relation to the T difference between surface and bottom ($\Delta T_{\mathrm{s-b}}$; Fig. 5.3b, d and f) at the Cefas stations (a, b) North Dogger and (c, d) Oyster Grounds, both for the years 2007 and 2008, and (e, f) the MARNET station Ems for the years 2010 and 2011. Here, observed $\Delta T_{\mathrm{s-b}}$ is defined between the sensor in 1 m depth and that nearest to the bottom for each station. Simulated $\Delta T_{\mathrm{s-b}}$ is defined between the model surface layer and the bottom layer. The indicated t_{strat} (grey-shaded) is derived from simulated T using Eq. (4.4) (i.e., between second model layer and bottom).

At North Dogger, which is characterised by a bottom depth of 82 m in the model, observed and simulated bottom O_2 concentrations show a steady decrease beginning with the onset of stratification in late March 2007. While stratification according to Eq. (4.4) starts a bit earlier compared to that described by Greenwood et al. (2010), the beginning of the decrease in bottom O_2 concentrations coincides well. The simulated and observed O_2 concentrations at this time are in good agreement showing values of $9.4\,\mathrm{mg\,O_2\,L^{-1}}$. The continuous decrease during stratification can be attributed to biochemical O_2 consumption in combination with the significant reduction of downward O_2 supply by vertical mixing.

Some small-scale fluctuations in the observations, like the minimum in the O_2 concentrations on 15 April 2007, are not fully reproduced by the simulation. However, the general evolution is represented well by the model. The average O_2 reduction in the simulation is slightly less than in the observations, visible in the difference between the concentrations at the beginning and the end of the stratified period. The decrease in the observed O_2 concentrations in 2007 suddenly ends with a mixing event between 10 and 12 November. Stratification ends a bit earlier in the simulation, with the result that simulated bottom O_2 starts to recover while the observed concentrations continue to decline, reaching a minimum of $6.4\,\mathrm{mg\,O_2\,L^{-1}}$. The observed O_2 concentration at the end of the stratified period is about $6.8\,\mathrm{mg\,O_2\,L^{-1}}$, while the simulation results in about $7.3\,\mathrm{mg\,O_2\,L^{-1}}$. The beginning increase in simulated bottom O_2 at the end of October coincides well with the end of stratification derived from simulated T.

In 2008, the onset of the decrease in simulated and observed bottom O_2 is in good agreement, although it occurs slightly later in the simulation. Similar to 2007, a slight overestimation of simulated O_2 concentrations during stratification occurs, which is again due to a faster O_2 decline in the observations. Some minor fluctuations visible in the observations in 2007 are also not represented by the model, however, the general evolution of bottom O_2 is represented well. It should be noted, that at station North Dogger, the centre depth of the model bottom layer is equal to 76 m (layer thickness of 12 m, bottom depth of 82 m), while the sampling was conducted in 85 m depth. This may also affect the

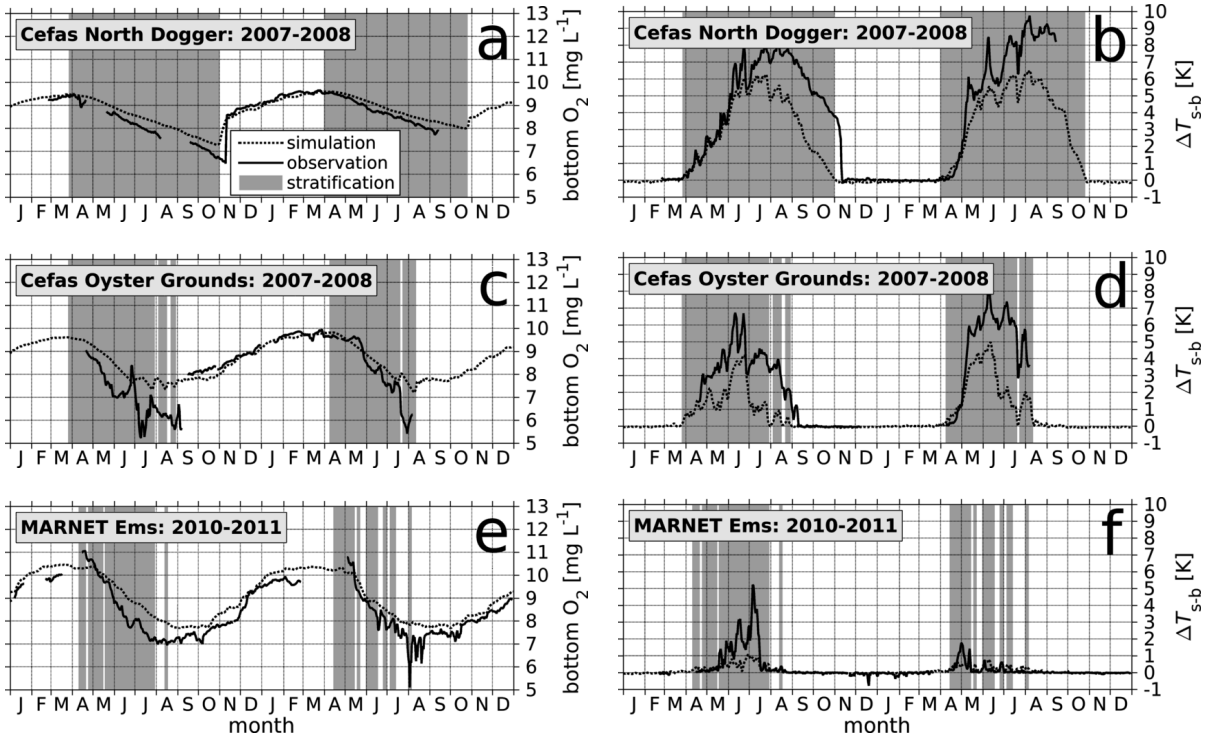

Figure 5.3: Daily time series of (a, c, e) simulated (dotted) and observed (solid) bottom O_2 concentrations and (b, d, f) temperature difference between surface and bottom ($\Delta T_{\mathrm{s-b}}$) at three stations: (a, b) Cefas North Dogger, (c, d) Cefas Oyster Grounds, both in 2007–2008, and (e, f) MARNET Ems in 2010–2011. For geographic positions see Fig. 5.1 (stations a–c). Grey-shaded areas indicate stratification according to Eq. (4.4). Same legend for all panels.

difference between simulated and observed O_2 concentrations.

The simulated $\Delta T_{\mathrm{s-b}}$ at North Dogger underestimates that in the observations during the stratified periods in 2007 and 2008. This is especially true for later summer and autumn (July–October), when differences between simulation and observation reach up to 4 °C in both years. This implies that vertical stratification is clearly underestimated with respect to its strength, although T_{strat} is well reproduced by the model. The good agreement between simulated and observed bottom O_2 most likely relates to the great water column depth which causes that the oxygenated surface waters do not reach the bottom layer, despite the underestimation of stratification.

At Oyster Grounds (model bottom depth of 46 m, bottom layer thickness of 6 m), the observations show clearly higher intra-seasonal variability which is not fully represented by the simulation. Additionally, the observed minimum O_2 concentrations are significantly lower than at North Dogger with values of 5.2 mg O_2 L^{-1} and 5.4 mg O_2 L^{-1} in July 2007 and 2008, respectively. The observed concentration at the beginning of stratification in

April 2008 (no data available for that time in 2007) is higher than at North Dogger. This implies that the decline in observed bottom O_2 during the summer period is clearly faster at Oyster Grounds, which is also visible by the steep negative slope during periods of decreasing bottom O_2 concentrations (e.g., late June to mid-July 2007).

ECOHAM is capable of reproducing the generally faster O_2 decrease relative to North Dogger, however, to a lesser extent than in the observations. Events of strong, short-term declines in bottom O_2 visible in the observations (July 2007, and 2008) are not reproduced by the model. Greenwood et al. (2010) found that the SML and BML at Oyster Grounds were strongly decoupled during the stratified periods in 2007 and 2008 and argued that this decoupling accompanied by strong sheer can trigger episodic events of nutrient injection enhancing PP (Sharples et al., 2007), which finally causes a strong increase in O_2 consumption due to remineralisation of organic matter. These small-scale processes cannot be resolved by the model due to the limited horizontal resolution.

From the end of the stratified period in 2007 until the onset of stratification in 2008, simulated concentrations are in good agreement with the observations which indicates that bottom T during that period is well reproduced by the model. After the onset of stratification in 2008, observation and simulation show a similar decline in O_2 until mid-July. In 2007, the end of stratification derived from simulated T is in good agreement with the beginning increase in simulated bottom O_2. In 2008, simulated O_2 concentrations stay on a stable level for another one and a half months after the final breakdown of stratification in mid-August, which likely relates to high ongoing O_2 consumption, which balances the increase in bottom O_2 concentrations due to vertical mixing.

Similar to North Dogger, simulated $\Delta T_{\mathrm{s-b}}$ at Oyster Grounds clearly underestimates the observed $\Delta T_{\mathrm{s-b}}$ during the summer period. In contrast, to North Dogger this has a visible effect on the evolution of O_2, especially, during July and August in both years, and explains the differences in simulated and observed bottom O_2 during these periods as the overestimation of vertical mixing (indicated by the low simulated $\Delta T_{\mathrm{s-b}}$) balances the biological O_2 consumption. The changes in observed $\Delta T_{\mathrm{s-b}}$ also explain part of the fluctuations in observed bottom O_2 during the summer period, e.g., the increase in bottom O_2 in June 2007, which coincides with a decrease in $\Delta T_{\mathrm{s-b}}$ indicating enhanced vertical mixing. It should be noted that, despite the large differences in the absolute values of simulated and observed $\Delta T_{\mathrm{s-b}}$, the relative changes in both, observations and simulations, are quite similar.

At MARNET Ems (model bottom depth of 35 m, bottom layer thickness of 5 m), the observed bottom O_2 concentrations also show large intra-seasonal fluctuations similar to station Oyster Grounds. This applies to 2010 and 2011, and mainly results from the shallow station depth, i.e., sampling depth (sensor in 30 m). In 2010, the onset of O_2

decline in the observations is in good agreement with the beginning of the decline in the simulated O_2 concentrations. Stratification lasts shorter and is less persistent than at the Cefas stations, especially, compared to North Dogger. From late May to late June, the observed bottom O_2 reveals a steep decrease which is not fully represented in the simulation. The remarkable drop in observed O_2 in the second half of June and the subsequent increase in bottom O_2 is indicated in the simulated O_2 concentration, visible in the slowdown of the decrease and its subsequent speed-up. It has to be noted that the model tends to overestimate bottom O_2 during stratification in 2010, revealing a maximum difference of about $1\,\mathrm{mg\,O_2\,L^{-1}}$.

After the end of stratification in 2010, the simulated O_2 concentration is in good agreement with the observation, however, a slight overestimation of the observed concentrations by up to $0.5\,\mathrm{mg\,O_2\,L^{-1}}$ can be seen. During spring/summer 2011, persistent stratified periods derived from the simulation do not exceed one and a half months in the simulation. Consequently, the temporal evolution of simulated bottom O_2 represents mainly the temporal evolution of the O_2 saturation concentrations. Again large fluctuations of up to $2\,\mathrm{mg\,O_2\,L^{-1}}$ within only a few days can be seen in the observations which are not reproduced by the model. These events may also relate to small-scale processes as described for Oyster Grounds. Besides these short-term changes the difference between simulated and observed bottom concentrations in 2008 is less than $0.7\,\mathrm{mg\,O_2\,L^{-1}}$ with higher summer values in the simulation.

Regarding $\Delta T_{\mathrm{s-b}}$, the two years show a quite different temporal evolution. While in 2007, persistent stratification can evolve between mid-May and mid-July with observed $\Delta T_{\mathrm{s-b}}$ of up to $5\,^{\circ}\mathrm{C}$, the 2008 observations indicate only weak stratification. This may be caused by the influence of freshwater from the continental rivers which can extend to station Ems during individual years. This tendency is also indicated by the model, however, simulated $\Delta T_{\mathrm{s-b}}$ is clearly less, like for the Cefas stations. Consequently, simulated bottom O_2 basically follows the T evolution, as the water column remains well mixed, while distinct T stratification in summer 2007 causes the separation of the surface from the bottom waters and thus gives an explanation for the faster decline in observed bottom O_2, relative to the simulation.

The qualitative validation of bottom O_2 at the stations North Dogger, Oyster Grounds and Ems shows that the ECOHAM model is capable of reproducing the main features and regional differences of the annual cycle of bottom O_2 at these stations, although intra-seasonal variability and stratification strength (indicated by $\Delta T_{\mathrm{s-b}}$) are not fully reproduced by the model. The consistent underestimation of stratification strength causes an overestimation of downward O_2 supply by vertical mixing, which results in an underestimation of O_2 reduction during stratification. Consequently, observed minimum O_2

concentrations at all three stations are significantly lower than simulated ones, especially, at the shallower stations Oyster Grounds and Ems. Differences are largest at Oyster Grounds which is characterised by persistent thermal stratification over a period of 4 to 5 months during the years 2007 and 2008. The model captures t_{strat}, however, simulated $\Delta T_{\mathrm{s-b}}$ is up to 5 °C lower than in the observations. Consequently, observed minimum O_2 concentrations are about $2\,\mathrm{mg\,O_2\,L^{-1}}$ lower than simulated O_2 concentrations.

Besides these discrepancies between simulation and observation, the tendencies shown in the temporal evolution of observed O_2 concentration and $\Delta T_{\mathrm{s-b}}$ at North Dogger and Oyster Grounds are similar in the simulation. This suggests, that the processes affecting the evolution of O_2 concentrations during stratification are principally reproduced by the model, i.e., it provides a reliable basis for the analysis of the O_2 dynamics in these areas of great (North Dogger) and intermediate bottom depth (Oyster Grounds), although specific short-term and small-scale events cannot be reproduced and thus analysed, due to the limited spatial resolution.

The good agreement between the intermittences in simulated stratification in August 2007 and the increase in simulated bottom O_2 concentration confirms that the stratification criterion applied (see Eq. (4.4)) provides a reliable indicator for stratification in relation to bottom O_2. The minor temporal delay between the onset of the temporary increases in bottom O_2 and the temporary breakdowns of stratification results from the fact that bottom T increases (i.e., $\Delta T_{\mathrm{s-b}}$ decreases) with a slight delay relative to the increase in vertical mixing. Consequently, bottom O_2 starts to increase slightly before $\Delta T_{\mathrm{s-b}}$ falls below the critical value defining the end of stratification. This aspect cannot be avoided as long as tracer quantities, such as T or density, are used for the determination of stratification. However, these tracer quantities have a clear benefit compared to more process-related quantities, such as vertical mixing intensity, as they can be determined from both, model simulations and observations.

At station Ems, the model shows only very weak seasonal stratification during summer 2010, while distinct stratification is present in the observations. Consequently, the physico-biochemical interactions driving the O_2 dynamics in this shallow region must be considered to be not reproduced sufficiently and may even differ between simulation and observation. The lack of distinct stratification at this station most likely results from the limited spatial resolution, similar to the Cefas stations. However, independent of the causes for this shortcoming, this implies that the model is not suitable for an in-depth analysis of bottom O_2 dynamics in shallow regions, like station Ems, where seasonal stratification can actually occur, but is not present at all in the model.

5.2.1.2 Spatial and year-to-year variability in late summer

In order to provide an overview of the spatial patterns of late summer bottom O_2 concentrations and to get an insight in the representation of these spatial patterns by ECOHAM, Fig. 5.4 shows the comparison between bottom O_2 observations (circles) and simulations (underlying colours) during three different years: a,b) 2001, c,d) 2005 and e,f) 2008. The period indicated in the bottom-right corner of each panel indicates the period during which the observations were carried out. Observations are gridded to the ECOHAM grid and only those observations are shown which correspond to the deepest pelagic layer of the corresponding model water column. STDs for observations result from this gridding in case of multiple individual measurements corresponding to the same model grid cell. Simulated O_2 are averaged over the entire observation period of each year. Figure 5.4a, c and e show the resulting averaged observed and simulated O_2 concentrations, panels b, e, and f present the corresponding STDs.

In 2001, the observations show the lowest concentrations of all years with minimum values of $5.9\,\mathrm{mg\,O_2\,L^{-1}}$ in the area 54 °N–57 °N, 4.5 °E–7 °E. This minimum is similarly present in the model yielding $6.7\,\mathrm{mg\,O_2\,L^{-1}}$. Maximum observed concentrations were found off the southern tip of Norway ($9.3\,\mathrm{mg\,O_2\,L^{-1}}$) and in the deepest parts of the Norwegian Trench ($8.7\,\mathrm{mg\,O_2\,L^{-1}}$–$8.8\,\mathrm{mg\,O_2\,L^{-1}}$). ECOHAM reproduces well these high values and shows values between $8.4\,\mathrm{mg\,O_2\,L^{-1}}$ and $9\,\mathrm{mg\,O_2\,L^{-1}}$ within the entire Norwegian Trench. Along the British east coast and in the Southern Bight simulated O_2 concentrations show values of $7\,\mathrm{mg\,O_2\,L^{-1}}$ to $8\,\mathrm{mg\,O_2\,L^{-1}}$ which is in good agreement with the observations. The northeastern North Sea shows generally higher bottom O_2 concentrations than the southern and central North Sea representing well the observations.

The STD in 2001 is low for both, observations and simulations. Observed STD is less than $0.1\,\mathrm{mg\,O_2\,L^{-1}}$ at most sampling sites and shows a maximum of $0.5\,\mathrm{mg\,O_2\,L^{-1}}$ near the southern tip of Norway. Directly northeast of the Dogger Bank, the observations also show slightly higher STDs of $0.3\,\mathrm{mg\,O_2\,L^{-1}}$. These few higher values in the observed STD result from fact that at the corresponding sites measurements from above and below the thermocline were gridded into the model bottom grid cell, yielding a high STD. The simulation shows low STDs of less than $0.2\,\mathrm{mg\,O_2\,L^{-1}}$ in most parts of the North Sea. Only some near-shore areas in the southern and northwestern North Sea, and the area in the central North Sea which shows the lowest bottom O_2 concentrations, show higher values. These high STDs indicate that bottom O_2 changes remarkably during the period of observation in these regions, while in the other parts of the North Sea bottom O_2 concentrations stay more or less stable.

In 2005, the observed minimum values are about $0.3\,\mathrm{mg\,O_2\,L^{-1}}$ higher than in 2001 and occur at the northern edge of the 2001 minimum. This relative increase compared to 2001

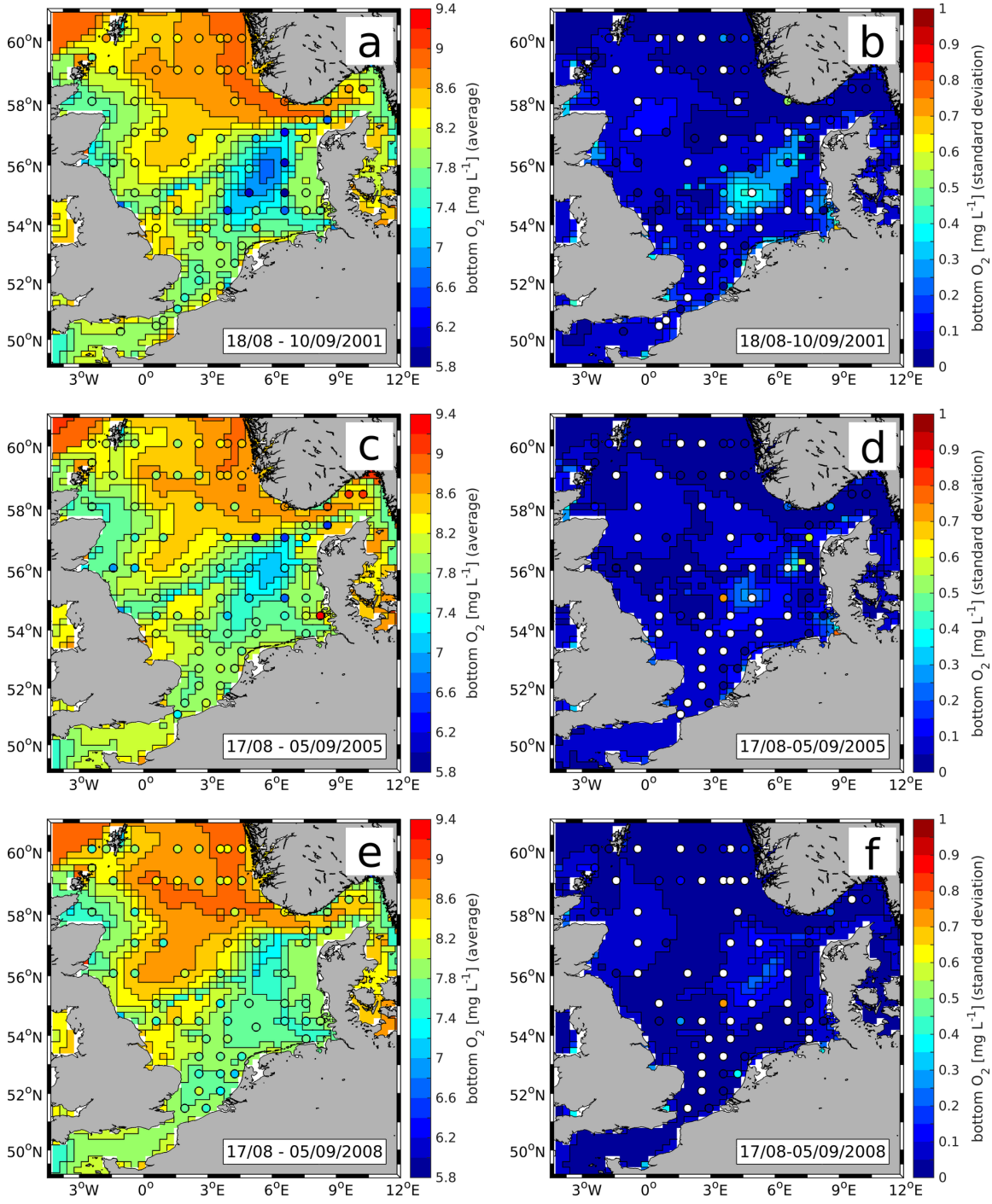

Figure 5.4: Spatial distributions of (a, c, e) observed and simulated average bottom O_2 concentrations and (b, d, f) corresponding STD in late summer (a, b) 2001, (c, d) 2005 and (e, f) 2008. Circles indicate sample sites, underlying colours show simulation results. Averages and standard deviation calculated over entire observation period (bottom-right corner of each panel). White circles in STD panels mark model bottom grid cells with only one observed value (i.e., no STD).

is reproduced well by the simulation showing a similar increase by about $0.4\,\mathrm{mg\,O_2\,L^{-1}}$, although simulated minimum O_2 concentrations occur in basically the same region as in 2001. Observed O_2 concentrations are still low ($7\,\mathrm{mg\,O_2\,L^{-1}}$–$7.4\,\mathrm{mg\,O_2\,L^{-1}}$) in the centre of the simulated minimum. Simulated concentrations in this area are about $7.1\,\mathrm{mg\,O_2\,L^{-1}}$. Highest observed concentrations of $9.3\,\mathrm{mg\,O_2\,L^{-1}}$ are located in the very deep area at the eastern end of the Norwegian Trench, and in the inner German Bight. In both areas the model shows only slightly higher values relative to 2001. In the northeastern North Sea, simulations and observations show lower bottom O_2 concentrations than in 2001, although the relative change between the years is less strong in the simulation. In the Southern Bight the observations show slightly higher O_2 concentrations than in 2001, with values of $7.6\,\mathrm{mg\,O_2\,L^{-1}}$ to $8.2\,\mathrm{mg\,O_2\,L^{-1}}$, which is well reproduced by ECOHAM. Along the British northeast coast, the also model is in good agreement with the observations, both showing lower values than in 2001.

STD in 2005 is quite similar to that for 2001 with respect to the observations. High STDs of $0.75\,\mathrm{mg\,O_2\,L^{-1}}$ and $0.59\,\mathrm{mg\,O_2\,L^{-1}}$ can be seen directly northeast of Dogger Bank and west of the northern tip of Denmark, respectively. In most other areas, the observations show small STDs of less than $0.1\,\mathrm{mg\,O_2\,L^{-1}}$. The simulation also yields lower STDs in most parts of the domain compared to 2001. The highest STD of $0.79\,\mathrm{mg\,O_2\,L^{-1}}$ occurs in the Elbe mouth. In the area of lowest bottom O_2, which shows high STDs in 2001, STDs are clearly lower than in 2001 and stay well below $0.3\,\mathrm{mg\,O_2\,L^{-1}}$ except for the area at around 56 °N, 7 °E, where a high STD of $0.55\,\mathrm{mg\,O_2\,L^{-1}}$ can be seen. These generally low STDs in the simulation show that during the 2005 observations period bottom O_2 concentrations show only minor temporal variability.

In 2008, the observations reveal significantly higher bottom O_2 concentrations in the area of the 2001 minimum, compared to the previous years. This in good agreement with model results which also show higher bottom O_2 concentrations. Lowest observed and simulated concentrations in this region are about $7.7\,\mathrm{mg\,O_2\,L^{-1}}$ and $7.1\,\mathrm{mg\,O_2\,L^{-1}}$, respectively. In most other parts of the North Sea, observed concentrations are lower than in 2001 and 2005. The overall minimum concentration in 2008 of $7.2\,\mathrm{mg\,O_2\,L^{-1}}$ is reached close to the Dutch coast. In the southern North Sea, the simulation also yields lower bottom O_2 concentrations the difference between 2005 and 2008 is less than in the observations.

For the western central and northern North Sea the image is less clear. In the northern Norwegian Trench, the observations show higher values than in 2005, while the simulation results in lower values. Further west, model and observations show higher values, although this increase is less pronounced in the observations. In the western central North Sea, the model shows consistently higher values compared to 2005, while the observations show

partly higher (e.g., at 56 °N, 2 °E) and partly lower bottom O_2 concentrations (e.g., at 57 °N, 1 °E).

The simulated STD in 2008 is lower than in the previous years across the entire domain, with almost all North Sea regions showing values less than $0.1\,mg\,O_2\,L^{-1}$. Slightly higher values of up to $0.25\,mg\,O_2\,L^{-1}$ result for the region of lowest bottom O_2 concentrations; values above this only occur in very few river mouth areas (e.g., Thames and Weser).

In summary, the basin-wide distribution of simulated bottom O_2 represents the observed spatial patterns and their year-to-year variations quite well, although absolute values and relative changes are not always fully reflected. Both observed and simulated bottom O_2 concentrations show that the 50 m-isobath (broadly along 54° N, 0° E to 57° N, 8° E; Thomas et al., 2005) marks the separation line between the northern regions unaffected by low O_2 conditions and the southeastern parts, which are more vulnerable to low O_2 concentrations.

The very small STD in the simulated bottom O_2 concentrations during the observation periods show that the average O_2 concentration provides a reasonable measure for late summer bottom O_2 conditions in most parts of the model domain. In addition, these small values suggest that measurements carried out in late summer (August/September) provide a representative synoptic image of the bottom O_2 conditions in most North Sea regions and thus of the spatial distribution of O_2 deficiency. However, in the eastern central North Sea, bottom O_2 can change significantly during periods of 3–4 weeks (as seen in 2001), e.g., due to the breakdown of stratification and renewal of the bottom O_2 reservoir. This suggests that in these regions the timing of measurements is crucial for the monitoring of O_2 deficiency.

In addition, the observed and simulated time series of simulated bottom O_2 concentrations (see Fig. 5.3) showed that lowest bottom O_2 concentrations can occur remarkably later than in August/September (e.g., at North Dogger), i.e., observations carried out around this time do not necessarily represent the lowest bottom O_2 concentrations and may result in an underestimation of the area of O_2 deficiency.

5.2.1.3 A quantitative assessment of model performance with respect to bottom oxygen

After the qualitative validation of seasonal (Sect. 5.2.1.1) as well as year-to-year and spatial variations in bottom O_2 (Sect. 5.2.1.2), which showed principally good agreement between simulation and observations in most parts of the North Sea, the Taylor diagram (Taylor, 2001) provides a quantitative assessment of the model performance with respect to simulated bottom O_2 concentrations in relation to the validation data used.

For this purpose, observations and the corresponding simulation data of the different

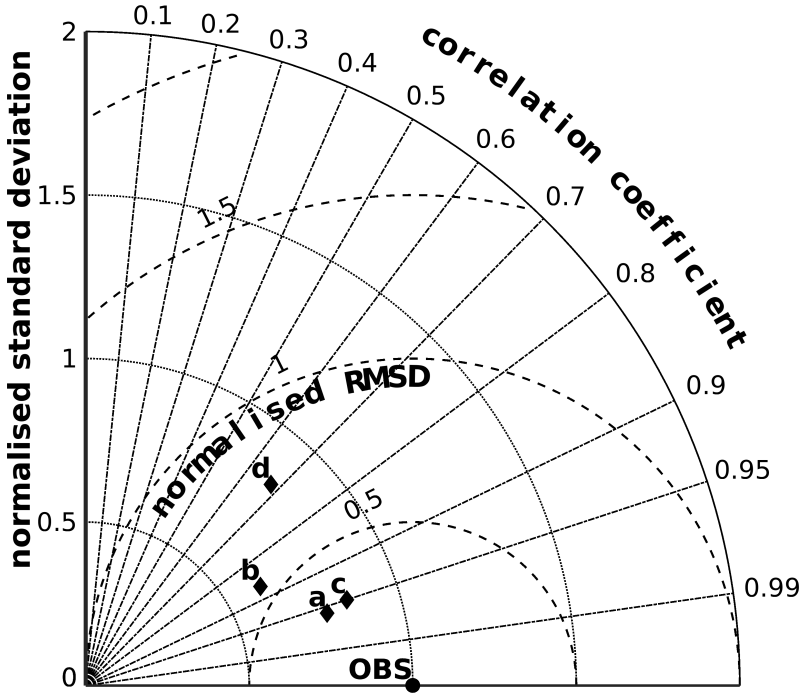

Figure 5.5: Taylor diagram of simulated (a–d) bottom O_2 concentrations compared to observations (OBS) for time series (see Fig. 5.3) at (a) Cefas North Dogger, (b) Cefas Oyster Grounds and (c) MARNET Ems, and (d) spatially resolved data (see Fig. 5.4). Standard deviations and centred root-mean-square differences (RMSD) normalised by the standard deviation of the corresponding observations.

years are merged into a continuous series of data for each of the four data sets (three time series stations and spatially resolved data). The Taylor diagram presents the COR, STD and centred RMSD of the simulation relative to the observation. The statistics for each data set are calculated according to Eqs. (4.1)–(4.3). The STDs of the simulations and RMSDs are finally normalised by the STD of the corresponding observations, facilitating the presentation of the statistics of all four data sets within a single diagram (Fig. 5.5). In the following STD and RMSD refer to the normalised values.

The statistics for the time series data (markers a–c in Fig. 5.5) confirm the principally good agreement between simulation and observation shown in Fig. 5.3. COR is highest for the stations North Dogger (a) and Ems (c) with values of about 0.96 and 0.95, respectively. RMSD is also small yielding 0.34 for North Dogger and 0.33 for Ems. The RMSD values are mainly due to the larger amplitude and higher (seasonal and intra-seasonal) variability in the observed bottom O_2, which is also shown by the normalised STDs of about 0.77 and 0.84 for North Dogger and Ems, respectively. For Oyster Grounds (b), the agreement between simulated and observed bottom O_2 is less good, indicated by a lower COR of

0.87. RMSD for this station is higher with a value of 0.56 while STD is lower, resulting in 0.61. The higher RMSD represents the larger differences between simulated and observed bottom O_2, especially, with respect to intra-seasonal variability and amplitude, both not fully reproduced by the model. This is confirmed by the STD being clearly lower than for the other two stations.

For the spatially resolved data (marker d in Fig. 5.5), COR reaches only about 0.68. This lower correlation is also indicated in Fig. 5.4 by the year-to-year variations in the simulation and observations between year 2008 and the previous years, when the simulation shows a relative change inverse to that in the observations in the northern North Sea. The normalised RMSD is clearly higher than for the time series resulting in 0.75, which can be attributed to the greater regional differences in the observed bottom O_2 concentration with higher maximum and lower minimum values, and partially not matching spatial patterns between simulation and observations. The normalised STD equals 0.84 which also indicates the less strong spatial differences in the simulation. These statistics confirm the picture given by Fig. 5.4, which shows that the spatial distribution of observed bottom O_2 concentration is basically reproduced by the model, with only slight shortcomings with respect to the amplitude of the bottom O_2 concentration and year-to-year variations in some regions of the North Sea.

In summary, the validation based on time series and spatially resolved observations demonstrates that the model is capable of reproducing the main temporal (seasonal and year-to-year) and spatial features of bottom O_2 in most regions of the North Sea. Especially in the deeper regions, with bottom depths of 40 m and more, the HAMSOM-ECOHAM model system can be considered to reasonably reproduce the seasonal dynamics of stratification and bottom O_2 dynamics. Hence, the analysis of the O_2 dynamics in relation to physico-biochemical interactions based on HAMSOM-ECOHAM will provide valuable insight in temporal and spatial differences of the North Sea O_2 dynamics under stratified conditions.

5.2.2 Stratification periods and minimum oxygen concentrations

Continuous seasonal stratification is considered to play a key role in the evolution of O_2 deficiency in the North Sea (Greenwood et al., 2010; Queste et al., 2013, 2016) as it separates the oxygenated surface waters from the deeper layers dominated by respiratory processes. Thus, long t_{strat} principally supports the evolution of low O_2 concentrations below the thermocline as O_2 consumption continues, while O_2 supply from the oxygenated surface waters is still inhibited.

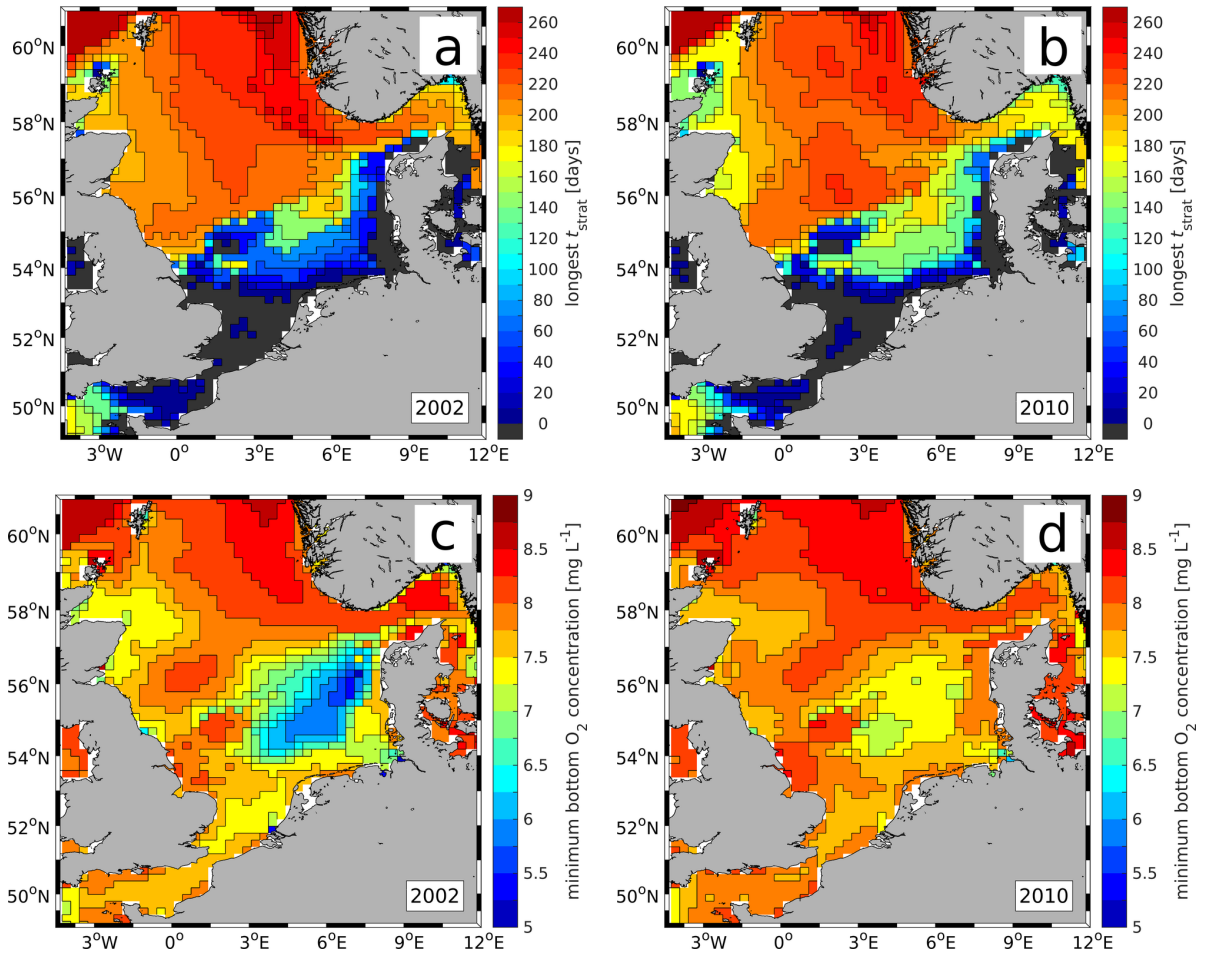

Figure 5.6: Spatial distributions of (a, b) the longest continuous stratified period (t_{strat}), derived from simulated T according to Eq. (4.4), and (c, d) simulated minimum bottom O_2 concentrations for the years (a, c) 2002 and (b, d) 2010. Dark grey areas in top panels indicate areas where no stratification occurred during the year.

In order to illustrate the relation between continuous stratification and bottom O_2 concentration, Fig. 5.6 shows the spatial distributions of (a, b) the longest continuous t_{strat}, derived from simulated T according to Eq. (4.4), and (c, d) simulated minimum bottom O_2 concentrations for the years (a, c) 2002 and (b, d) 2010. Dark grey areas in the t_{strat} panels indicate regions where no stratification occurred.

Along the British northeast coast, t_{strat} in 2010 is up to 50 days shorter than in 2002, which corresponds well with an increase in minimum bottom O_2 concentrations from less than $7.5\,\mathrm{mg\,O_2\,L^{-1}}$ in 2002 to more than $7.75\,\mathrm{mg\,O_2\,L^{-1}}$ in 2010. In the western part of the northern North Sea, the image is similar, also showing a minor reduction in t_{strat} between 2002 and 2010 accompanied by an increase in minimum bottom O_2 levels. Thus,

the conceptual view that extended seasonal stratification supports the evolution of lower O_2 concentrations appears to be valid for the northern North Sea, however, so far based on a rather basic, qualitative consideration.

Focusing on the central North Sea and the deeper regions of the southern North Sea (north of 54 °N), it can be seen that in most parts of this region t_{strat} is longer in 2010 than in 2002. In the southern North Sea between 3 °E and 7 °E, t_{strat} in 2010 is up to two months longer than in 2002, while in the other parts the t_{strat} is only 20 to 40 days longer. Only in the area around 56 °N, 6 °E, t_{strat} is longer in 2002, up to two months compared to 2010. It is furthermore shown that, although t_{strat} lasts longer in the deeper northern North Sea, minimum O_2 concentrations in the central and southern North Sea are clearly lower.

Looking at minimum bottom O_2 in these areas (Fig. 5.6c and d), it can be seen that in the small area around 56 °N, 6 °E–7 °E, where overall lowest concentrations occur, the decrease in t_{strat} between 2002 and 2010 coincides with an increase in minimum bottom O_2. This also meets the concept of longer stratification supporting the evolution of lower bottom O_2 concentrations. However, in the other regions in the central and southern North Sea, e.g., southeast and northeast of Dogger Bank, minimum bottom O_2 is clearly higher in 2010 than in 2002 (e.g., $>7\,mg\,O_2\,L^{-1}$ vs. $<6\,mg\,O_2\,L^{-1}$ at 55 °N, 4 °E), although t_{strat} is remarkably longer in these areas.

This concurrence of longer t_{strat} and lower minimum bottom O_2 concentrations (and vice versa) implies that additional factors have to be taken into account when aiming for the description of bottom O_2 dynamics in the North Sea, especially, in the regions showing a tendency for low bottom O_2 concentrations (southeast to northeast of Dogger Bank). Interestingly, despite the remarkable differences in absolute values of minimum bottom O_2 concentrations between 2002 and 2010 in this area, in both years this area shows the overall lowest O_2 concentrations (except for river mouth locations in non-stratified waters), being a first indicator that this area is generally susceptible to low O_2 conditions.

5.2.3 An oxygen-related characteristic of the North Sea

The exemplary comparison of the t_{strat} and minimum bottom O_2 concentrations in 2002 and 2010 revealed that stratification alone is not sufficient to explain year-to-year variations in North Sea bottom O_2 concentrations. Therefore, this section aims for the identification of key parameters which can be used to describe the basic physico-biochemical interactions affecting bottom O_2 in the North Sea and thus can be used to identify areas susceptible to O_2 deficiency. Finally, those parameters, for which a qualitative relation to bottom O_2 is found, are used for the development of a simple indicator for potential problem areas with respect to O_2 deficiency in the North Sea.

5.2.3.1 Identification of key parameters

For the development of a regional O_2 characteristic, potential controlling factors have to be analysed in relation to O_2. Besides stratification, eutrophication is considered as a major driver for the evolution of low O_2 conditions (e.g., Díaz and Rosenberg, 2008; Kemp et al., 2009). Thus, NPP within the mixed layer and the resulting organic matter export into the layers below the MLD must be considered to be the main source for degradable organic matter. However, in case of sufficient light availability, PP can also occur below the MLD, i.e., NPP taking place within the sub-MLD volume (NPP_{sub}) has to be considered as well. In addition, organic matter can be advected from surrounding waters in the form of phyto- or zooplankton and detritus. The first two can transition into detritus, due to mortality, consequently being remineralised under O_2 consumption. Advective organic matter input is subdivided into inflow and outflow, in order to obtain information about the relative importance of organic matter inflow relative to local organic matter production by PP. Additionally, inflow (and outflow) into the SML and the sub-thermocline volume have to be considered separately, as the latter may directly contribute to O_2 consumption below the MLD, while the former requires the subsequent sinking of the advected organic matter below the MLD (in ECOHAM only in the form of detritus) in order to contribute to O_2 consumption below the MLD.

Another important parameter is the water volume below the thermocline (hereafter 'sub-MLD volume'; Druon et al., 2004). A smaller volume separated from the surface due to stratification holds a lower initial inventory of O_2 than a larger volume even though concentrations can be similar or even higher in the smaller volume. Thus, the set of O_2-related parameters consists of (abbreviations and way of calculation in parentheses):

- surface mixed layer NPP (NPP_{sml}; DIC uptake by diatoms and flagellates),
- sub-MLD NPP (NPP_{sub}; DIC uptake by diatoms and flagellates),
- horizontal advection of organic matter into and out of the SML ($ADH_{org,sml\text{-}in}$ and $ADH_{org,sml\text{-}out}$; incl. detritus, phyto- and zooplankton),
- horizontal advection of organic matter into and out of the sub-MLD volume ($ADH_{org,sub\text{-}in}$ and $ADH_{org,sub\text{-}out}$; incl. detritus, phyto- and zooplankton),
- vertical organic matter export across the MLD (EXP_{org}; vertical mixing of detritus),
- vertical mixing of O_2 across the MLD (MIX_{O_2}), and
- sub-MLD volume (V_{sub}).

In order to detect regional characteristics and identify the key parameters driving the evolution of low O_2 conditions, five different North Sea regions are defined which encompass

4×4 model water columns each (latitude×longitude = 0.8 ° × 1 ° 20') and are selected in relation to differences in t_{strat} and minimum bottom O_2 concentrations. These regions (see Fig. 5.7) can be described as: (#1) southeastern North Sea under strong tidal influence, (#2) southern North Sea with high year-to-year variability in t_{strat} (see Fig. 4.9), (#3) eastern central North Sea with low year-to-year variability in t_{strat}, (#4) northern central North Sea with dominant seasonal stratification each year, and (#5) northern North Sea with dominant seasonal stratification each year and strong influence of the Atlantic inflow.

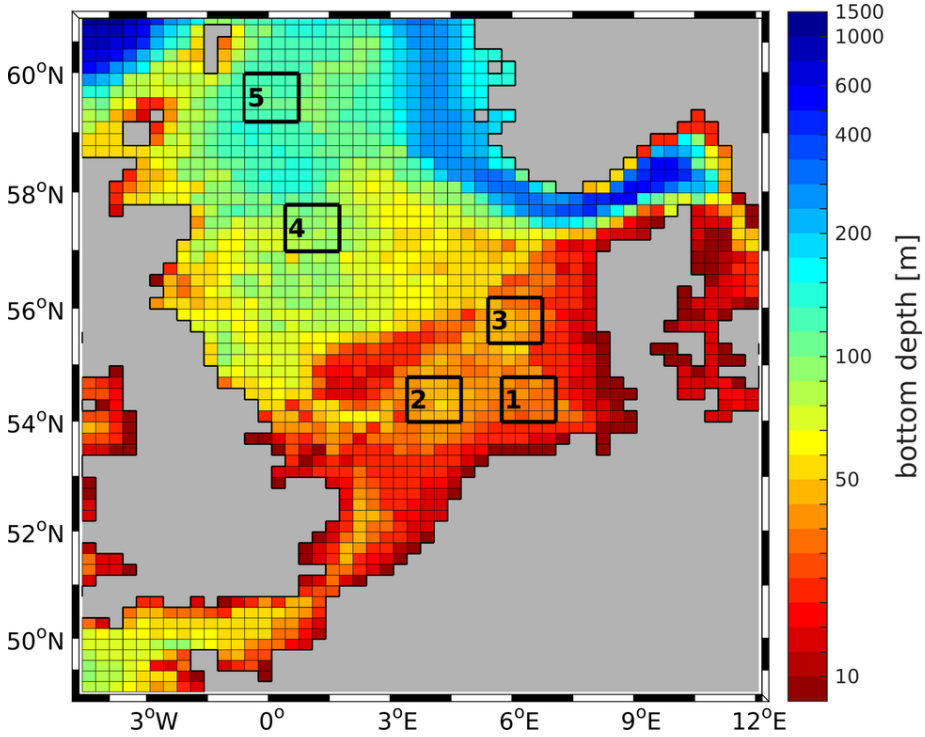

Figure 5.7: North Sea bathymetry as used by ECOHAM (colours) including the five regions (black-framed boxes) used for the development of an oxygen-related characteristic of the North Sea.

The parameters are calculated for all regions for the years 2000–2014 relative to a reference depth D_{ref}, which is defined as the bottom depth of the model layer directly below the annual maximum MLD among all five regions. The D_{ref} >MLD is chosen to ensure all parameters in all regions are determined relative to a comparable depth horizon. This implies that the values for NPP_{sml}, $ADH_{org,sml\text{-}in}$ and $ADH_{org,sml\text{-}out}$ are integrated from the surface to D_{ref}, while $ADH_{org,sub\text{-}in}$ and $ADH_{org,sub\text{-}out}$ are integrated from D_{ref} to the bottom. EXP_{org} and MIX_{O_2} are the vertical fluxes through D_{ref}. The same D_{ref} is applied to all regions and years in order to obtain comparable results.

The annual maximum MLD is determined by first calculating t_{strat} for the regions #2

to #5 using Eq. (4.4). Region #1 is excluded from this calculation as no persistent MLD develops due to tidal mixing. In this context, $S_{\mathrm{strat}}(t)$ of a region is only 1 if $S_{\mathrm{strat}}(x, y, t) = 1$ for all 16 water columns within the considered region. The daily MLD for each water column within a region was calculated by applying $S_{\mathrm{strat}}(t)$ to Eq. (4.5), and subsequently the daily MLD of the region is defined as the median of these 16 daily values. The annual MLD for each region was then determined as the median of this daily time series. The median was used to obtain a D_{ref} corresponding with a model depth level. Subsequently, the maximum of the five median MLDs (one per region) is used to determine the annual maximum MLD. The maximum annual MLD is finally used to set D_{ref} which is defined as the bottom depth of the layer directly below this maximum MLD. This procedure resulted in a D_{ref} of 25 m.

Table 5.1: Average critical quantities (2000–2014) characterising the O_2 dynamics in the five different 4×4-regions (see Fig. 5.7). Fluxes are cumulated from 1 April to 30 September and relate to a surface layer of thickness $D_{\mathrm{ref}} = 25$ m.

region		#1	#2	#3	#4	#5
$\mathrm{NPP_{sml}}$	$\mathrm{g\,C\,m^{-2}}$	176.0	171.9	161.2	151.7	172.2
$\mathrm{NPP_{sub}}$	$\mathrm{g\,C\,m^{-2}}$	0.2	0.3	1.2	1.3	2.4
$\mathrm{ADH_{org,sml\text{-}in}}$	$\mathrm{g\,C\,m^{-2}}$	96.0	85.9	110.6	95.6	104.8
$\mathrm{ADH_{org,sml\text{-}out}}$	$\mathrm{g\,C\,m^{-2}}$	80.7	81.4	108.9	95.7	104.4
$\mathrm{ADH_{org,sub\text{-}in}}$	$\mathrm{g\,C\,m^{-2}}$	17.5	28.6	27.7	17.7	19.6
$\mathrm{ADH_{org,sub\text{-}out}}$	$\mathrm{g\,C\,m^{-2}}$	22.0	21.9	26.5	16.5	17.7
$\mathrm{EXP_{org}}$	$\mathrm{g\,C\,m^{-2}}$	24.7	22.2	18.6	18.0	21.4
$\mathrm{MIX_{O_2}}$	$\mathrm{g\,O_2\,m^{-2}}$	131.9	102.7	67.8	13.5	19.7
$\mathrm{O_{2,ini}}$	$\mathrm{mg\,O_2\,L^{-1}}$	10.1	9.9	9.9	9.6	9.5
$\mathrm{O_{2,end}}$	$\mathrm{mg\,O_2\,L^{-1}}$	7.6	7.7	7.8	8.0	8.3
t_{strat}	days	70	123	153	224	229
MLD	m	11.0	15.4	14.6	23.3	26.4
D_{bot}	m	38.9	46.4	43.5	93.0	124.3
area	$\mathrm{km^2}$	7680.5	7680.5	7454.3	7108.9	6677.2
V_{sub}	$\mathrm{km^3}$	106.5	164.2	138.0	483.3	663.2

The values for the O_2-related quantities are calculated for the individual years 2000–2014 relative to D_{ref} and temporally integrated over the period from 1 April to 30 September (hereafter 'summer'). Consequently, the average values over the entire period are calculated and presented in Table 5.1. Average t_{strat} is also included as it is considered as the prerequisite for the evolution of O_2 deficiency. Additionally, the average O_2 concentrations at the beginning and end of the summer period ($\mathrm{O_{2,ini}}$ on 1 April and $\mathrm{O_{2,end}}$ on 30 September, respectively) are included as a reference to which the different quantities are compared. For the sake of completeness, average bottom depth (D_{bot}) and area of

each region as well as average MLD are added to the table.

NPP_{sml} is strongest in the coastal region #1 and shows decreasing values towards region #4; region #5 again shows higher NPP_{sml} than regions #2 to #4. In the region #2, NPP_{sml} accounts for about 98 % of that in the most productive region #1. The corresponding values for regions #3, #4 and #5 are about 92 %, 86 % and 98 %, respectively. Comparing NPP_{sub} of the different regions, a steady increase from region #1 to #5 can be seen due to lower turbidity, i.e., higher light availability in deeper layers. However, NPP_{sub} is negligible in all regions as its highest contribution to overall NPP (sum of NPP_{sml} and NPP_{sub}) reaches only about 1.4 % in the region #5.

Considering the different terms of advective organic matter transport it can be seen that the SML-related transports are consistently higher than the transports relating to V_{sub} (by factor 4–5), which results from the fact that PP is highest in the upper layers, implying higher amounts of organic matter (phyto-/zooplankton and detritus). In region #1, $ADH_{org,sml\text{-}in}$ exceeds $ADH_{org,sml\text{-}out}$ by $15.3\,g\,C\,m^{-2}$ while $ADH_{org,sub\text{-}in}$ is $4.5\,g\,C\,m^{-2}$less than $ADH_{org,sub\text{-}out}$. In combination with EXP_{org} of $24.7\,g\,C\,m^{-2}$, this indicates that a remarkable share of organic matter transported into the SML is exported into the near-bottom layer (either by vertical mixing or sinking) where it is partly remineralised and partly advected into the adjacent waters.

In region #2, $ADH_{org,sml\text{-}in}$ and $ADH_{org,sub\text{-}in}$ are higher than the corresponding outflows indicating that this regions represents a sink for organic matter implying enhanced O_2 consumption. Especially, the net advective input of $6.7\,g\,C\,m^{-2}$ into V_{sub}, representing the highest among all five regions (5.6 times higher than in regions #3 and #4, 3.5 times higher than in region #5), shows that the deeper layers of this region are characterised by a much stronger loss of organic matter than the other regions. This net advective input into V_{sub} also contributes to about 23 % of the overall net organic matter input (sum of net advective input and EXP_{org}) and thus constitutes an important source of organic matter in that region. In regions #3 to #5 the absolute values of the net differences in $ADH_{org,sml}$ and $ADH_{org,sub}$ are generally less than in regions #1 and #2, i.e., advection plays a less important role for the amount of organic matter being available in these northern regions. EXP_{org} consistently adds up to about 12 %–13 % of NPP_{sml}, indicating the clear link between upper layer PP and the export of organic matter into the deeper layers. The highest EXP_{org} of $24.7\,g\,C\,m^{-2}$is reached in region #1. In region #2, EXP_{org} accounts for about 90 % of that in region #1; in regions #3 to #5 it adds up to 75 %, 73 % and 87 % of that in region #1. The vertical mixing of O_2, MIX_{O_2}, is highest within the coastal region #1 and adds up to $131.9\,g\,O_2\,m^{-2}$, which is due to strong tidal mixing. MIX_{O_2} shows a steady decrease until region #4, where its minimum value of $13.5\,g\,O_2\,m^{-2}$is reached. In region #5, MIX_{O_2} is slightly higher than in region #4 as the used D_{ref} is similar to

the average MLD, i.e., the actual MLD can temporarily exceed D_{ref} resulting in slightly higher $\mathrm{MIX}_{\mathrm{O_2}}$. Interestingly, $\mathrm{MIX}_{\mathrm{O_2}}$ in region #3 is only about 66 % of that in region #2, although region #3 is less deep than region #2. This partly relates to t_{strat}, which is about 24 % longer in region #3 compared to region #2. Further causes may be stronger vertical O_2 gradients between the near-surface and deeper layers which increases the turbulent diffusive transport.

Considering t_{strat} of all regions, a steady increase from 70 days in region #1 to 229 days in region #5 can be seen, which basically corresponds to the northward decrease in $\mathrm{MIX}_{\mathrm{O_2}}$. A similar tendency is shown for the average MLD, although that in region #3 is slightly shallower than in region #2. V_{sub} (Table 5.1) can be calculated as the difference of D_{bot} minus D_{ref} multiplied with the given area. Thus, it decreases from South to North (as the distance per 1 ° in zonal direction decreases) and with decreasing D_{bot}.

The evolution of the O_2 concentrations between the beginning and end of the summer period reveals some interesting aspects in relation to the previously discussed parameters. $O_{2,\mathrm{ini}}$ on 1 April shows significant differences between the regions ranging between 9.5 mg O_2 L^{-1} (region #5) and 10.1 mg O_2 L^{-1} (region #1). On 30 September, $O_{2,\mathrm{end}}$ yields values between 7.6 mg O_2 L^{-1} (region #1) and 8.3 mg O_2 L^{-1} (region #5). This implies a consistently decreasing reduction in sub-MLD O_2 during summer from region #1 to #5. In regions #2 to #5, these reductions are dominated by biochemical O_2 consumption, while in region #1 the increase in T also has a strong effect due to the strong recurrent vertical mixing throughout the entire summer period. The spatial gradient in the decrease in O_2 concentration is opposite to that in t_{strat}, which shows a steady increase from region #1 to #5. The opposing spatial gradients in t_{strat} and O_2 reduction during summer underline that t_{strat} alone is not sufficient to describe spatial differences in the temporal evolution of sub-MLD O_2 concentrations in the North Sea.

In order to give an impression of the impact of $\mathrm{EXP}_{\mathrm{org}}$ on the O_2 dynamics in relation to V_{sub}, the amount of $\mathrm{EXP}_{\mathrm{org}}$ is linked to the amount of O_2 available within V_{sub} for the intermediate-depth region #3 and the deeper region #4. For this purpose, it is assumed that the entire organic matter exported below D_{ref} is remineralised in the area of settlement. Multiplication of $O_{2,\mathrm{ini}}$ on 1 April with V_{sub} yields the total amount of O_2 initially available within $V_{\mathrm{sub.}}$ This product results in 1371 kt O_2 for region #3 and 4617 kt O_2 for region #4. The total amount of exported organic matter is calculated as the product of $\mathrm{EXP}_{\mathrm{org}}$ and the area of the considered region and gives 139 kt C and 128 kt C for the regions #3 and #4, respectively. Conversion to Mmol C using the molar weight of C (12.0107 g mol^{-1}) yields 11.5 Mmol C for region #3 and 10.7 Mmol C for region #4. As O_2 consumption and C release occur with a molar ratio of 1:1 during bacterial remineralisation (Neumann, 2000), the daily O_2 consumption rate is obtained by dividing the amount

of exported organic matter by the duration of the summer period (183 days). Subsequent multiplication with the molar weight of O_2 ($2 \cdot 15.9994\,\mathrm{g\,mol^{-1}}$) gives the average daily O_2 consumption rates of $2\,\mathrm{kt\,O_2\,d^{-1}}$ for region #3 and $1.9\,\mathrm{kt\,O_2\,d^{-1}}$ for region #4.

Assuming the daily O_2 consumption to be constant for each region, division of the total mass of O_2 initially available in V_{sub} by the daily consumption rate provides an estimate of the amount of time required for the consumption of the entire amount of O_2 within $V_{\mathrm{sub.}}$ This calculation yields a period of about 1.9 years for region #3, whereas the corresponding value for region #4 is significantly higher with about 6.8 years. The good agreement of the difference between the resulting periods (factor 3.6) and the difference in the size of V_{sub} (factor 3.5) illustrates the large influence of the extent of V_{sub} on the temporal evolution of the O_2 concentrations below the MLD.

The same estimation for the time required to reach O_2 deficiency ($6\,\mathrm{mg\,O_2\,L^{-1}}$; e.g., OSPAR, 2005) provides a consumption period of 269 days for region #3. Although the average t_{strat} in region #3 is only about half (153 days), this indicates the high potential for O_2 deficiency in this region as the estimation assumes to reach the threshold concentration within the entire $V_{\mathrm{sub.}}$

The analysis of the different parameters for the five different North Sea regions presented in Table 5.1 demonstrates that t_{strat} alone does not suffice to explain the temporal evolution of sub-MLD O_2 concentrations. It emphasises the great importance of $\mathrm{NPP_{sml}}$ constituting the major source for organic matter, which is exported into V_{sub} where it drives the biological O_2 consumption. It further shows that the advective supply of organic matter plays only a minor role in most areas analysed. In addition, the volume below the MLD plays a key role as it governs the amount of O_2 which is available throughout the stratified period, and in combination with the organic matter export defines whether O_2 deficiency may occur or not. Thus, these three quantities (t_{strat}, $\mathrm{NPP_{sml}}$ and V_{sub}) can be considered as the key parameters governing the O_2 dynamics of the seasonally stratified North Sea.

Based on these findings, the North Sea can be subdivided roughly into three different zones in relation to O_2 dynamics: (1) a highly productive, well-mixed coastal zone (region #1), (2) a productive, seasonally stratified zone with a small sub-thermocline volume (regions #2 and #3), and (3) a productive, seasonally stratified zone with a large sub-thermocline volume (regions #4 and #5). While the zones of type 1 and 3 are unlikely to be affected by low O_2 conditions due to either continuously ongoing ventilation (type 1) or the large sub-thermocline volume diluting the effect of O_2 consumption (type 3), type 2 is highly susceptible to low O_2 conditions. This results from the specific combination of high upper layer productivity and small sub-thermocline volume, which causes a strong impact of the consumption processes on the decrease in the sub-MLD O_2 concentrations.

5.2.3.2 The oxygen deficiency index (ODI)

The characteristic presented in the previous section provides sufficient knowledge for the development of a qualitative, spatially resolved indicator for the potential of O_2 deficiency in the North Sea. Such indicator has previously been developed by Druon et al. (2004), who presented a complex approach for the identification of regions susceptible to O_2 deficiency in the North Sea and the Adriatic Sea – the 'eutrophication risk index' (EUTRISK).

This section aims for the definition of a less complex, qualitative indicator which is capable of describing the main spatial patterns in the O_2 conditions in the stratified North Sea. In the following this indicator is referred to as 'oxygen deficiency index' (ODI). In order to find a simple definition of the ODI, the key parameters found in the previous section are further simplified. Near-surface NPP already constitutes a simplified proxy for the organic matter export into deeper layers. The bottom depth can be used as a proxy for V_{sub} assuming only minor fluctuations of the MLD during the summer stratified period. In addition, the bottom depth directly influences the amount of organic matter reaching the bottom layer, relative to the amount being produced near the surface. Consequently, the following key factors are used for the calculation of this index: (longest continuous) t_{strat} (in days), summer surface NPP ($\mathrm{NPP_{sml}}$; in $\mathrm{g\,C\,m^{-2}}$; 1 April to 30 September, 0 m–25 m depth), and bottom depth (D_{bot}; in m).

Before presenting the ODI, some insight is given in the spatial distributions of these quantities used for its definition. With respect to t_{strat} the reader is referred to Fig. 5.6a and b showing the spatial distributions for 2002 and 2010, respectively. The evaluation of t_{strat} in relation to other studies was provided in Sect. 4.3.2. A map of D_{bot} as used by ECOHAM is given in Fig. 5.7.

Figure 5.8 shows the spatial distribution of $\mathrm{NPP_{sml}}$ for the years a) 2002 and b) 2010. It can be seen that in most offshore parts of the North Sea, $\mathrm{NPP_{sml}}$ ranges between $140\,\mathrm{g\,C\,m^{-2}}$ and $200\,\mathrm{g\,C\,m^{-2}}$ in 2002. In 2010, NPP is clearly lower and ranges between $120\,\mathrm{g\,C\,m^{-2}}$ and $170\,\mathrm{g\,C\,m^{-2}}$ in most offshore regions. In the coastal areas of the southern North Sea values of $260\,\mathrm{g\,C\,m^{-2}}$–$300\,\mathrm{g\,C\,m^{-2}}$ (and above) are found in 2002, while in 2010 maximum values are less than $220\,\mathrm{g\,C\,m^{-2}}$ in most coastal regions, except for the inner German Bight. In the Southern Bight $\mathrm{NPP_{sml}}$ is low ($<100\,\mathrm{g\,C\,m^{-2}}$) in both years.

These spatial distributions of simulated $\mathrm{NPP_{sml}}$ are in generally good agreement with earlier studies. Joint and Pomroy (1993) estimated an annual NPP of $119\,\mathrm{g\,C\,m^{-2}}$ in the central and $79\,\mathrm{g\,C\,m^{-2}}$ in the southwestern North Sea. For the German Bight they found average values of $261\,\mathrm{g\,C\,m^{-2}}$, with values higher than $300\,\mathrm{g\,C\,m^{-2}}$ in the inner German Bight. Steele (1956) found annual NPP to be in the range of $54\,\mathrm{g\,C\,m^{-2}}$–$127\,\mathrm{g\,C\,m^{-2}}$ in the northern North Sea. Skogen and Moll (2000) provided model estimates of annual NPP for the 10-year-period 1985–1994 for different regions covering the entire North Sea (see Fig. 3

and Table 1 in Skogen and Moll (2000)). In summary, they found values of 122 g C m^{-2}–180 g C m^{-2} for the northern North Sea, 84 g C m^{-2}–128 g C m^{-2} for the central North Sea, 86 g C m^{-2}–108 g C m^{-2} for the southern North Sea and 129 g C m^{-2}–218 g C m^{-2} for the coastal southern North Sea. The different estimates indicate the large spatial and temporal variability in NPP.

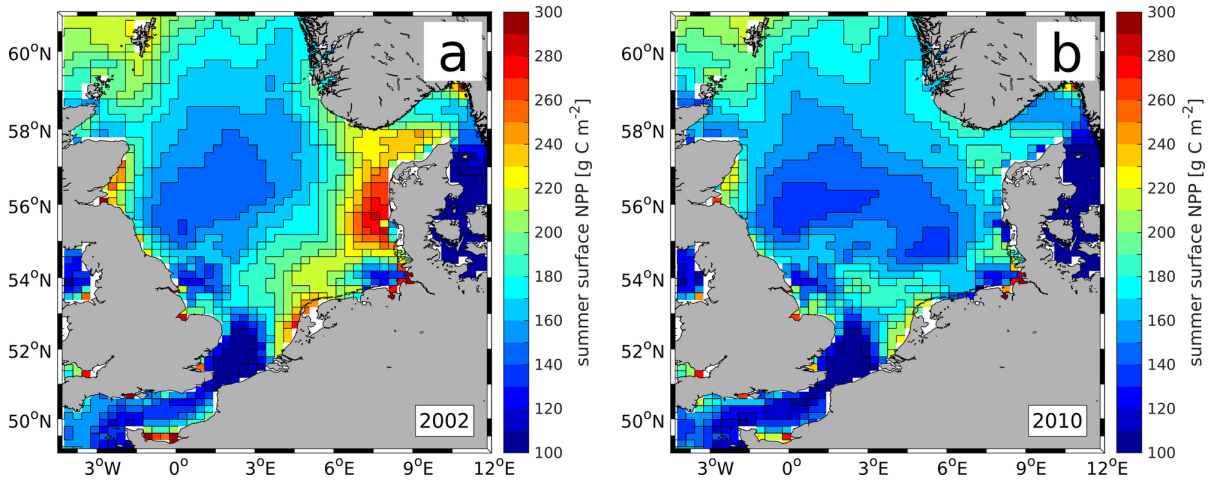

Figure 5.8: Spatial distribution of summer surface NPP (NPP_{sml}; 1 April–30 September, 0 m–25 m) derived from ECOHAM for (a) 2002 and (b) 2010. Colour scale cut at upper and lower limit.

Especially NPP_{sml} in 2010 is in good agreement with the spatial patterns described by previous studies. The 2002 values tend to slightly overestimate these studies, however, are still well within the range provided by Skogen and Moll (2000). Thus, it can be concluded that ECOHAM is capable of reproducing the spatial patterns in NPP. Deviations from the estimates given before can result from the different years considered, and the fact that NPP_{sml} is only calculated for the summer period. Deviations in relation to the limited integration depth (0 m–25 m) can be neglected as Table 5.1 showed that NPP below 25 m contributes to less than 1 % in most parts of the North Sea.

As ECOHAM demonstrated to produce reasonable results for both, t_{strat} and NPP_{sml}, the definition of the ODI can be approached using these quantities and D_{bot}. In the first step, an individual dimensionless index, ranging between 0 and 1, is calculated for each of these three quantities. The calculation of the stratification and NPP indices (I_{strat} and I_{npp}, respectively) is based on the work by Druon et al. (2004) and reads as:

$$I_{Q_i}(x,y) = \min\left(1, \max\left(0, \frac{Q_i(x,y) - Q_{i,\min}}{Q_{i,\max} - Q_{i,\min}}\right)\right), \text{ with } Q_1 = t_{strat},\ Q_2 = I_{npp}. \quad (5.1)$$

$I_{Q_i}(x,y)$ represents the index corresponding to the actual value of the quantity $Q_i(x,y)$

with its defined upper and lower threshold, $Q_{i,\max}$ and $Q_{i,\min}$. For t_{strat} the upper and lower threshold are set to 60 and 150 days, respectively. These values were found by a qualitative comparison of the spatial distributions of simulated t_{strat} and minimum bottom O_2 during the entire period 2000–2014. Minimum t_{strat} in regions with low minimum bottom O_2 concentrations are about 60 days, and areas with t_{strat} of above 150 days are considered as seasonally well-stratified. The lower threshold for NPP_{sml} is set to $120\,\text{g C m}^{-2}$ as NPP_{sml} does not reach lower values in most parts of the North Sea. The upper threshold is set to $200\,\text{g C m}^{-2}$ as such high values and even above can occur in the southeastern North Sea.

For the depth index (I_D) a different definition is chosen as the highest potential for O_2 deficiency occurs in areas of intermediate depth, where seasonal stratification can evolve and the O_2 inventory is limited due to a small volume below the thermocline. Therefore, I_D is defined as follows:

$$I_D(x,y) = \begin{cases} \max\left(0, \frac{D_{\text{bot}}(x,y) - D_{\min}}{D_{\text{peak}} - D_{\min}}\right) & \text{for } D_{\text{bot}}(x,y) < D_{\text{peak}} \\ 1 - \min\left(1, \frac{D_{\text{bot}}(x,y) - D_{\text{peak}}}{D_{\max} - D_{\text{peak}}}\right) & \text{otherwise.} \end{cases} \tag{5.2}$$

D_{bot} represents the actual bottom depth at location (x, y). $D_{\text{peak}} = 40\,\text{m}$ represents the average bottom depth of the regions where lowest O_2 concentrations occur in the simulation. The lower threshold $D_{\min} = 25\,\text{m}$ corresponds to the maximum MLD in the shallower southern North Sea. The upper threshold $D_{\max} = 90\,\text{m}$ is chosen to exclude the areas where the initial O_2 inventory is sufficiently large to prevent O_2 deficiency due to the large volume below the thermocline.

Finally, the ODI combines the three individual indices according to the following equation:

$$\text{ODI}(x,y) = I_D(x,y) \cdot \sum_{i=1}^{2} w_{Q_i}\, I_{Q_i}(x,y), \text{ with } w_{Q_1} = 1/4,\ w_{Q_2} = 3/4. \tag{5.3}$$

Here, I_{Q_i} and w_{Q_i} represent the index for a quantity and the related weight, respectively. The values for t_{strat} are referred to by Q_1 and those for NPP_{sml} by Q_2. The equation for the ODI implies that it is zero in areas where $I_D = 0$. The stronger weighting of NPP_{sml} implies that year-to-year variabilities in the ODI are more strongly affected by variations in summer surface NPP than by t_{strat}. The ODI ranges between 0 (low risk of O_2 deficiency) and 1 (high risk) and is calculated for each water column (x, y) within the model domain to provide a spatially resolved image of the risk of O_2 deficiency in the North Sea.

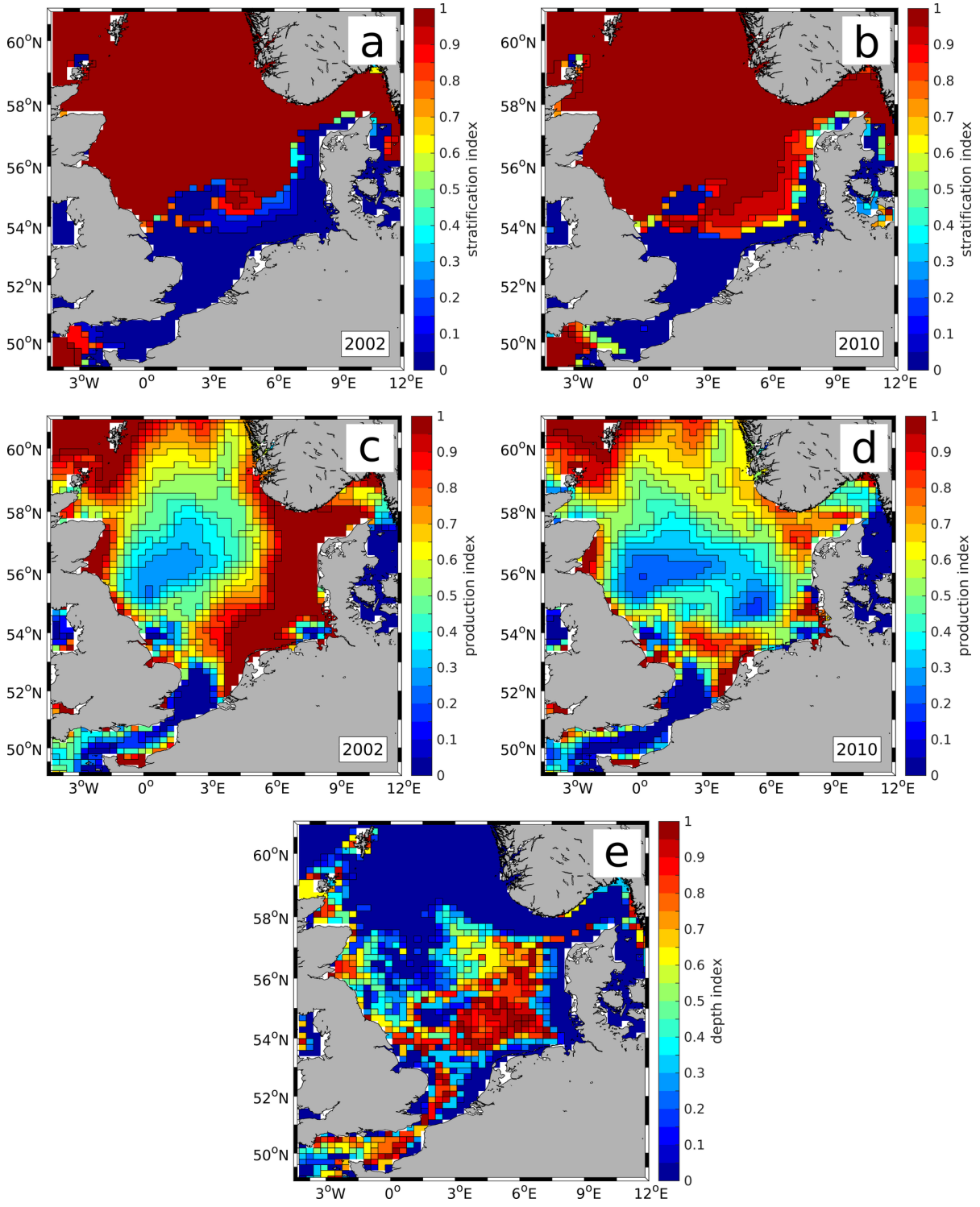

Figure 5.9: Spatial distribution of basic indices used for ODI calculation: (a, b) stratification index (I_{strat}), (c, d) production index (I_{npp}), both according to Eq. (5.1) for (a, c) 2002 and (b, d) 2010, and (e) depth index (I_D; see Eq. (5.2)).

The individual basic indices I_{strat}, I_{prod} and I_D are presented in Fig. 5.9. As the I_{strat} and I_{prod} may vary between years due to variations in NPP and t_{strat}, they are presented for the years 2002 and 2010 (see Fig. 5.9a, c and b, d, respectively) in order to compare the spatial patterns in relation to minimum bottom O_2 concentrations shown in Fig. 5.6c and d. The temporally non-varying I_D is presented in Fig. 5.9e.

Figure 5.9a and b show that I_{strat} basically separates the North Sea into its well-mixed southern part ($I_{\mathrm{strat}} = 0$) and the seasonally well-stratified northern part ($I_{\mathrm{strat}} = 1$). Stronger year-to-year variations only occur in the southern central part between 54 °N–55 °N, 1 °E–7 °E, where t_{strat} can strongly differ between individual years (see Fig. 5.6a and c).

The impact of I_{npp} (see Fig. 5.9c and d) is most dominant in the southeastern and eastern central North Sea, where the variations between the two years are highest. In the southern central North Sea (around 54 °N–56 °N, 5.5 °E–7 °E), I_{npp} shows values of up to 1 in 2002 and below 0.4 in 2010. On the one hand, this shows the high variability between individual years. On the other hand, this illustrates the cause-effect relationship between vertical mixing, i.e., nutrient supply from deeper layers, and NPP, as the higher I_{npp} in 2002 corresponds with a lower I_{strat} compared to 2010. With respect to minimum bottom O_2 concentrations this region also represents that with the largest differences between 2002 and 2010.

The spatial distribution of I_D presented in Fig. 5.9e basically matches the (inverse) general spatial distribution of minimum bottom O_2 concentrations. Values of $I_D = 0$ can be found in the deep northern North Sea and Norwegian Trench and in the shallow coastal areas off Southwest Britain and along the continental coast from the Strait of Dover to Denmark. In the offshore parts of the southern North Sea and in the central North Sea higher values occur, with an I_D between 0.8 and 1 in the region roughly between 54 °N–56 °N, 3 °E–7 °E.

The ODI resulting from the simulated t_{strat}, summer surface NPP ($\mathrm{NPP_{sml}}$) and model bathymetry (D_{bot}) is shown in Fig. 5.10a and b for the years 2002 and 2010, respectively. It can be seen that in 2002 the ODI is clearly higher in the region the O_2 minimum, compared to 2010. This is in very good agreement with the minimum bottom O_2 concentrations of the two years (see Fig. 5.6c and d). Especially in 2002, the highest ODI is located in the direct vicinity of the lowest O_2 concentrations in the entire domain (around 55 °N–57 °N, 6 °E–7 °E).

In 2010, the highest ODI is located a bit south of the minimum O_2 concentrations (at around 54 °N, 4 °E), which is caused by the high $\mathrm{NPP_{sml}}$ and high t_{strat} (relative to 2002) in this region. The ODI also shows slightly higher values in the region directly north of the Dogger Bank which corresponds with the lowered bottom O_2 concentrations in this

region.

Along the northern British coast, the ODI also shows high values for both years which is in good agreement with the slightly lower minimum bottom O_2 in this area, however, ODI values tend to be too high. The ODI also does not represent the slightly lower minimum O_2 concentrations off the eastern Scottish coast around 57 °N–58 °N as the bottom depth in this area exceeds 90 m (i.e., ODI = 0). Directly northwest of Denmark, the ODI also yields high values for both years with higher values in 2002. This corresponds well with the simulated bottom O_2 concentrations in this area, even though ODI values are too high, compared to ODI values in the central North Sea.

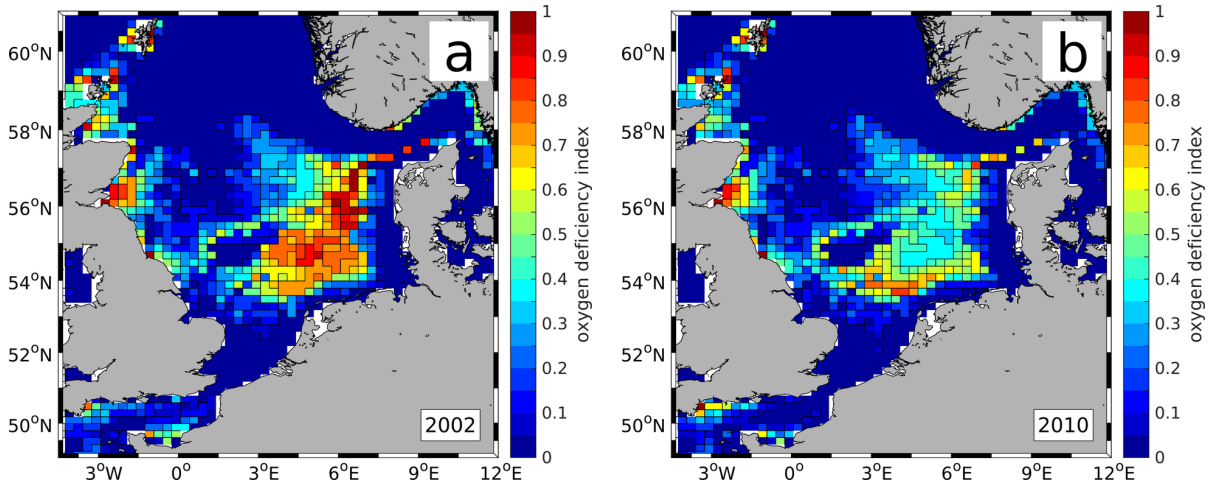

Figure 5.10: Spatial distribution of oxygen deficiency index (ODI) according to Eq. (5.3) for (a) 2002 and (b) 2010.

In summary, the ODI represents well the spatial variations and variations between the two years found in minimum bottom O_2 concentrations, despite the small set of controlling parameters. Although the highest ODI values do not exactly match the lowest bottom O_2 concentrations (compare Fig. 5.6c and d, and Fig. 5.10), this confirms that the basic interactions leading to low bottom O_2 conditions in the seasonally stratified North Sea can be represented by a combination of only t_{strat}, organic matter production and bottom depth. Thus, the findings from Table 5.1 can be applied to most parts of the North Sea.

In comparison to the work by Druon et al. (2004), it is likely that their EUTRISK performs better than the ODI, due the higher complexity of EUTRISK. This may especially apply to small-scale spatial variations as Table 5.1 showed that in some North Sea regions (e.g., region #2) advection may constitute a non-negligible source of organic matter. However, the aim of the ODI is the provision of a simple indicator for the potential for O_2 deficiency in the North Sea. In addition, t_{strat} and $\mathrm{NPP}_{\mathrm{sml}}$, used for the defini-

tion of the ODI, could be derived from operational hydrodynamical models and satellite remote-sensing (e.g., Longhurst et al., 1995; Behrenfeld and Falkowski, 1997). Thus, the ODI may provide a first starting point for the development of an operationally applicable indicator for O_2 deficiency.

Furthermore, the similarity of the ODI inside the regions analysed in Sect. 5.2.3.1 and their surrounding areas shows that these regions can be considered as representative for the different North Sea areas.

5.2.4 Oxygen deficiency in the North Sea

In order to quantify the physico-biochemical interactions contributing to the evolution of O_2 deficiency in the North Sea, this section first provides a more general image of the occurrence of O_2 deficiency. Figure 5.11a and b present the simulated overall minimum bottom O_2 concentrations occurring during the period 2000–2014 and the corresponding longest duration of annual O_2 deficiency (i.e., number of days with bottom O_2 concentration $<6\,\mathrm{mg\,O_2\,L^{-1}}$ per year) during the same period, respectively. Black areas in Fig. 5.11b mark the regions where no O_2 deficiency occurs throughout the entire period 2000–2014.

With respect to the overall minimum bottom O_2 concentration it can be seen that the spatial distribution of areas with less than $6\,\mathrm{mg\,O_2\,L^{-1}}$ is identical to the 2002 distribution (see Fig. 5.6c), i.e., 2002 represents the year with the lowest bottom O_2 concentrations during 2000–2014. Besides this, the spatial distribution shows that the region between approximately 54.5 °N–56.5 °N and 4 °E–7.5 °E is most susceptible to O_2 deficiency (not considering river mouth locations, e.g., Rhine and Elbe, where very low O_2 concentrations can occur due to high water T and remineralisation of organic matter. Lowest O_2 concentrations of less than $5.5\,\mathrm{mg\,O_2\,L^{-1}}$ are simulated at around 56 °N, 7 °E. Low, though non-deficient, bottom O_2 concentrations also occur directly north of Dogger Bank which is in good agreement with the observations by Greenwood et al. (2010) (see also Fig. 5.3a).

Figure 5.11 shows that regions of longest O_2-deficient periods basically match lowest O_2 concentrations, i.e., O_2 deficiency lasts longest where minimum bottom O_2 concentrations are lowest. This results from the fact that in the model the evolution of bottom O_2 under stratified conditions is roughly linear from the onset of stratification until its breakdown (see time series of simulated bottom O_2 and ΔT at the Cefas stations North Dogger and Oyster Grounds shown in Fig. 5.3a–d). Thus, although reduction rates differ regionally, O_2 deficiency tends to be longest where minimum O_2 concentrations are lowest as the concentrations stay below the threshold of $6\,\mathrm{mg\,O_2\,L^{-1}}$ for a longer period due to continuous O_2 reduction.

In these regions of longest O_2 deficiency, bottom O_2 concentrations may stay below $6\,\mathrm{mg\,O_2\,L^{-1}}$ for 35–47 days while in most other regions, where O_2 deficiency occurs during

2000–2014, O_2 deficiency lasts 1–20 days. In other regions, where O_2 deficiency was observed, but not simulated by the model (e.g., Oyster Grounds; see Fig. 5.3c and d), the underestimation of t_{strat} and ΔT by HAMSOM is the likely cause for not reproducing the occurrence of O_2 deficiency. However, as the processes remain the same, it still allows for the quantitative analysis of the physico-biochemical interactions affecting the evolution of O_2 deficiency in this region.

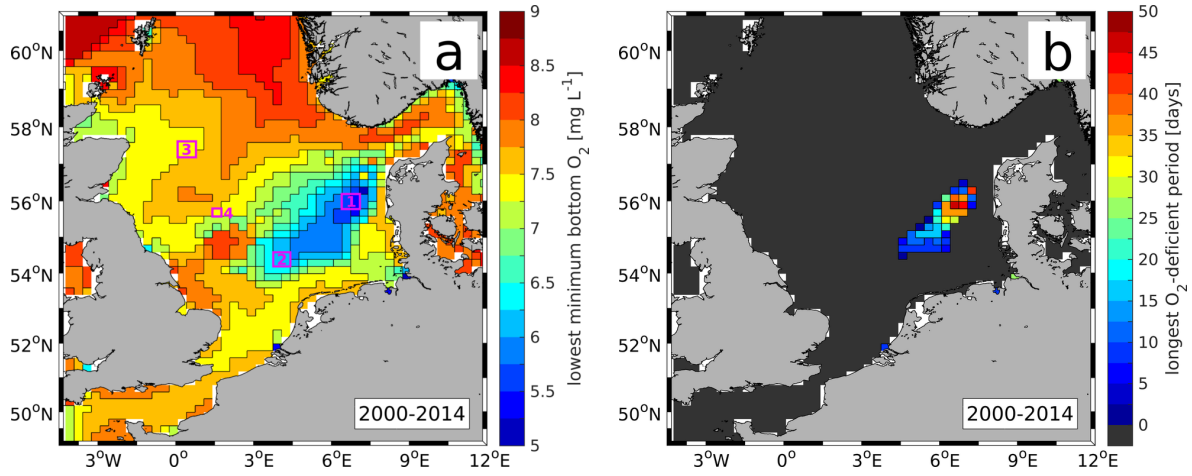

Figure 5.11: Spatial distributions of (a) lowest minimum bottom O_2 concentration and (b) longest O_2-deficient periods per year (O_2 concentration $<6\,mg\,O_2\,L^{-1}$) during the period 2000–2014. Black areas in panel b indicate regions where no O_2 deficiency occurred throughout the entire period. Boxes indicate regions used for analysis presented in Sect. 5.2.5.

Figure 5.11 confirms the findings from Sect. 5.2.3.1 that certain North Sea regions are particularly susceptible to O_2 deficiency, and that the year 2002 represents that year with the largest spatial and temporal extent of O_2 deficiency. Thus, the following analysis of the physico-biochemical interactions leading to O_2 deficiency in the North Sea focuses on these highly susceptible regions and the year 2002, in comparison to other regions and years.

During the following analyses the term 'oxygen deficiency zone' (ODZ) is used. It refers to the study site characterised by lowest O_2 concentrations in the North Sea (see Fig. 5.11, region #1). This is done to avoid confusion with the term 'OMZ', usually used for hypoxic or nearly anoxic conditions in the global ocean (see Ch. 1).

5.2.5 Physico-biochemical controls of oxygen deficiency

In this section, O_2 mass balances are calculated in order to provide a detailed analysis of the processes driving the North Sea O_2 dynamics, potentially leading to O_2 deficiency.

These mass balances are calculated for four different North Sea regions encompassing 2×2 model water columns. The selected regions are marked in Fig. 5.11a by the regions #1 to #3. First, mass balances for the entire volume below the thermocline (V_{sub}) in region #1 are compared with the corresponding bottom layer (i.e., last pelagic model layer) mass balances. This is done since the O_2 dynamics within the entire V_{sub} determine the O_2 supply to the bottom layer. Region #1 is chosen as it is located in the centre of the region with lowest bottom O_2 concentrations within the entire model domain. The analysis is conducted for the years 2002 and 2010 to analyse variations between these years as 2002 represents the year of lowest minimum bottom O_2 and is characterised by higher concentrations in 2010 (see Fig. 5.6c and d).

The mass balances are calculated for the stratified period only (i.e., from very first to very last day of stratification, incl. intermittences). Stratified periods are indicated by grey-shaded areas. The O_2 concentrations (magenta solid) and saturation concentrations ($O_{2,\mathrm{sat}}$; magenta dash-dotted)) shown in the different mass balances represent the average values within the analysed volume. $O_{2,\mathrm{sat}}$ is calculated according to Benson and Krause (1984) using simulated T and S. The processes presented are vertically integrated, cumulative changes in the O_2 concentrations of the considered volume, i.e., the values at the end of the stratified period reflect the total change of O_2 due to the corresponding physical and biological processes. Positive and negative values at the end of the stratification period indicate gain and loss, respectively.

The slope of each process-related line represents the magnitude of the corresponding process at the specific moment in time, i.e., a steep positive (negative) slope implies a strong gain (loss) in O_2. The following processes are included in the mass balances: air-sea flux of O_2 ($\mathrm{ASF}_{\mathrm{O_2}}$; dark blue), vertical mixing of O_2 ($\mathrm{MIX}_{\mathrm{O_2}}$; blue), (sum of horizontal and vertical) advection of O_2 ($\mathrm{ADV}_{\mathrm{O_2}}$; cyan), NPP (green), zooplankton respiration ($\mathrm{RES}_{\mathrm{zoo}}$; yellow), pelagic remineralisation ($\mathrm{REM}_{\mathrm{pel}}$; orange), benthic remineralisation ($\mathrm{REM}_{\mathrm{sed}}$; red), and nitrification (NIT; brown). It should be noted that in the literature, $\mathrm{REM}_{\mathrm{sed}}$ is often referred to as benthic O_2 demand. However, in this study the term 'benthic remineralisation' is used in relation to remineralisation in the pelagic.

The daily resolved MLD defines the upper integration limit for the mass balances within the sub-MLD volume using a time-varying MLD ($V_{\mathrm{sub,var}}$). The daily MLD is defined as the vertical level of the model grid which is closest to the daily average MLD of the 2×2-region according to Eqs. (4.4) and (4.5). As an intermediate step and for better comparability, the mass balances for V_{sub} are additionally calculated for a fixed MLD ($V_{\mathrm{sub,fix}}$) which is calculated as the median of the daily-resolved MLD. In case of an MLD lower than the minimum bottom depth of a water column within a 2×2-region, the MLD set to the model layer depth of the second last pelagic layer in order to ensure that V_{sub} of all four water

columns is taken into account. The bottom layer O_2 mass balances for the regions #2 and #3 in 2002 are compared to that of region #1 to unveil regional differences. It should be noted that in the following, the term 'MLD' refers to the upper end of the integration depth range. In case of $V_{\mathrm{sub,fix}}$, this implies that the term 'MLD' is used even if stratification is intermittent.

5.2.5.1 Sub-thermocline oxygen dynamics

Figure 5.12a–d show the different O_2 mass balances within $V_{\mathrm{sub,var}}$ and $V_{\mathrm{sub,fix}}$ for the ODZ site (region #1 in Fig. 5.11a): (a) for $V_{\mathrm{sub,var}}$ in 2002 and (b) in 2010, and (c) for $V_{\mathrm{sub,fix}}$ below a MLD of 20 m in 2002 and (d) in 2010. The text boxes in the bottom-left corner of each panel provide information about stratification (i.e., integration) period, median MLD, average bottom depth and area of the region, and (average) volume. The average bottom depth in region #1 is about 36.5 m and the area is about 1,840 km^2. The average volume of $V_{\mathrm{sub,var}}$ depends on the temporal evolution of the MLD, showing minor differences between 2002 and 2010 (52.1 km^3 and 53.9 km^3, respectively). For $V_{\mathrm{sub,fix}}$, the volume encompasses 30.5 km^3 for both years.

The comparison of the mass balances for $V_{\mathrm{sub,var}}$ for 2002 and 2010 (Fig. 5.12a and b, respectively) first shows that O_2 and $O_{2,\mathrm{sat}}$ basically decrease from the beginning to the end of stratification in both years. $O_{2,\mathrm{sat}}$ steadily decreases until the final breakdown of stratification. In 2002, t_{strat} lasts longer than in 2010 (187 and 175 days, respectively, including intermittences). However, longest continuous t_{strat} occurs in 2010 (139 days from 8 April to 24 August, compared to 89 days from 4 July to 30 September 2002). At the beginning of stratification, O_2 and $O_{2,\mathrm{sat}}$ concentrations are basically the same, though, the 2010 values of 10.5 mg O_2 L^{-1} are about 0.5 mg O_2 L^{-1} higher than in 2002. Thus, the initial conditions in 2002 favour the evolution of O_2 deficiency compared to 2010.

O_2 shows some stronger fluctuations and temporary increases, especially in 2002. These increases in O_2 coincide either with intermittent stratification (e.g., in early July 2002) or with a shallowing of the MLD. In both cases, near-surface layers characterised by higher O_2 concentrations are included in the integration, resulting in an increase in O_2 concentration presented.

Comparing the temporal evolution of the O_2 concentration against $O_{2,\mathrm{sat}}$ during periods of continuous stratification, it can be seen that O_2 clearly diverges from $O_{2,\mathrm{sat}}$, implying that a decrease in O_2 solubility does not suffice to explain the decrease in O_2 concentration during stratification. At the end of stratification in 2002, O_2 concentration clearly increases and more or less converge with the $O_{2,\mathrm{sat}}$ concentration. In 2010, another 5-day-event of stratification occurs after the temporary breakdown of stratification on 24 August. The convergence of O_2 and $O_{2,\mathrm{sat}}$ already occurs at this latter mentioned breakdown.

The temporal evolutions of O_2 and $O_{2,sat}$ within $V_{sub,var}$ and $V_{sub,fix}$ in 2002 and 2010 (Fig. 5.12c and d, respectively) are very similar. However, O_2 concentrations within $V_{sub,fix}$ show less strong fluctuations, due to the constant MLD. The comparison of the different physical and biochemical processes in $V_{sub,var}$ and $V_{sub,fix}$ between 2002 and 2010 provides valuable insight in the different physico-biochemical interactions affecting O_2 concentrations below the MLD. The values of each process cumulated over the displayed period are presented in Table 5.2 (first and second column for $V_{sub,var}$, third and fourth for $V_{sub,fix}$). The considered integration period (t_{int}) and overall biochemical gross O_2 consumption ($GOC = RES_{zoo} + REM_{pel} + REM_{sed} + NIT$) are additionally included. Values in parentheses represent the relative contributions of individual biochemical O_2-consuming processes to GOC.

The analysis of the physical processes (ASF_{O_2}, MIX_{O_2} and ADV_{O_2}) reveals some differences between the mass balances for $V_{sub,var}$ and $V_{sub,fix}$ which, however, mainly result from the different integration approach. With respect to ASF_{O_2} (dark blue), it has to be noted that this process only affects the O_2 levels in case of no stratification and within $V_{sub,var}$ as it only affects the model surface layer. This is shown in Fig. 5.12a where ASF_{O_2} only changes during the events of intermittent stratification.

ASF_{O_2} adds up to $-10.5\,g\,O_2\,m^{-2}$ in 2002 and $-6.7\,g\,O_2\,m^{-2}$ in 2010. The differences between the two years likely result from the different timing of the intermittences in stratification, and thus different surface T implying different O_2 solubility. The minor negative values for both years indicate that O_2 supply from the atmosphere into the surface waters of the North Sea during spring–autumn is either negligible or can even constitute a sink of O_2 in the surface waters, due to low O_2 solubility and surface NPP. This is in good agreement with the findings by Müller (2008) who found that in most parts of the central North Sea annually integrated ASF_{O_2} is negative (i.e., outgassing) as a result of consistent outgassing from March/April to September/October.

MIX_{O_2} constitutes an important supply process for sub-MLD O_2 in both, $V_{sub,var}$ and $V_{sub,fix}$. However, Fig. 5.12a and b show that stable stratification (e.g., July/August 2002 and May–July 2010) V_{sub} inhibits the mixing-induced supply of O_2 below the MLD. Minor increases in O_2 within $V_{sub,var}$ (e.g., in mid-May 2010) coincide with decreases in MLD and relate to higher near-surface O_2 concentrations. In 2002 and 2010, MIX_{O_2} into $V_{sub,var}$ adds up to $40.7\,g\,O_2\,m^{-2}$ and $16.4\,g\,O_2\,m^{-2}$, respectively. This difference relates to weaker stratification in 2002, indicated by the two intermittences in stratification in late April and early July, but may additionally result from the lower sub-MLD O_2 concentrations implying a stronger vertical gradient and thus increased MIX_{O_2}.

This is confirmed by Fig. 5.12c and d, which also show a consistently steeper increase in MIX_{O_2} in 2002 compared to 2010. In contrast to MIX_{O_2} into $V_{sub,var}$, MIX_{O_2} into

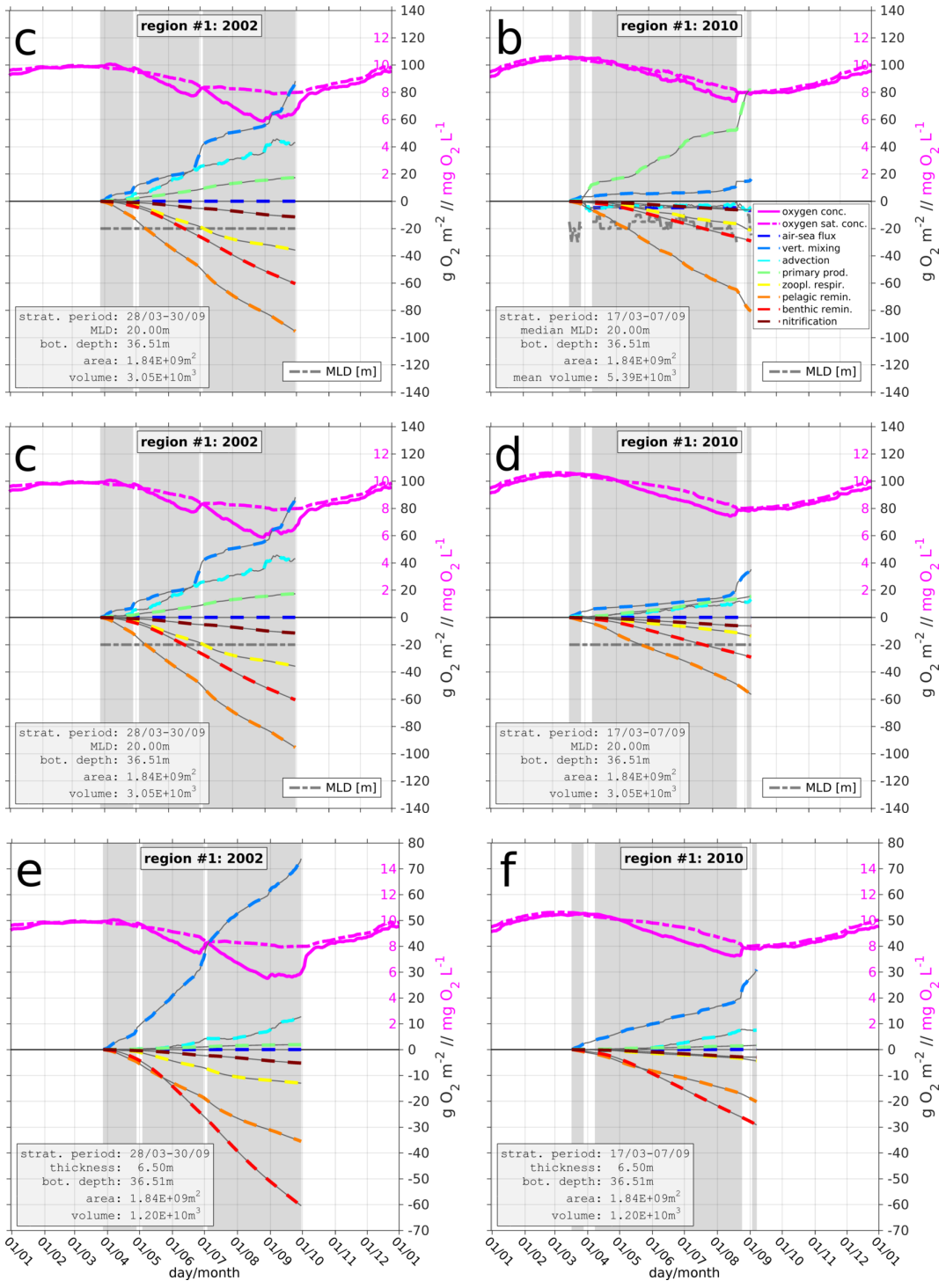

Figure 5.12: Oxygen mass balances for region #1 (see Fig. 5.11a) during stratification (grey shaded) according to Eq. (4.4): (a, b) for V_{sub} using a time-varying MLD (grey, dash-dotted line), (c, d) for V_{sub} using a fixed MLD of 20 m and (e, f) for the model bottom layer; (a, c, e) 2002 and (b, d, f) 2010. Magenta y axes refer to O_2 and $O_{2,\mathrm{sat}}$, black y axes refer to processes. Note different y axes for (e, f). Legend of (b) applies to all panels. Process values in Table 5.2.

Table 5.2: Process values for region #1 (see Fig. 5.11a) cumulated from beginning to end of stratification for the years 2002 and 2010 (compare Fig. 5.12). All process values in $\mathrm{g\,O_2\,m^{-2}}$, negative values imply loss of O_2. Values in parentheses represent relative contributions to overall gross O_2 consumption (GOC; in %).

volume	$V_{\mathrm{sub,var}}$ (variable MLD)				$V_{\mathrm{sub,fix}}$ (fixed MLD)				bottom layer			
year	a) 2002		b) 2010		c) 2002		d) 2010		e) 2002		f) 2010	
t_{int} [days]	187		175		187		175		187		175	
$\mathrm{ASF_{O_2}}$	−10.5		−6.7		0.0		0.0		0.0		0.0	
$\mathrm{MIX_{O_2}}$	40.7		16.4		88.2		35.3		73.9		30.9	
$\mathrm{ADV_{O_2}}$	42.0		−4.4		43.1		13.2		12.7		7.5	
NPP	109.1		81.8		17.3		15.5		1.9		1.6	
GOC	−248.8		−137.3		−203.1		−105.6		−114.2		−56.8	
$\mathrm{REM_{pel}}$	−127.9	(51.4)	−80.5	(58.6)	−95.4	(47.0)	−56.5	(53.5)	−35.5	(31.1)	−20.2	(35.6)
$\mathrm{REM_{sed}}$	−60.5	(24.3)	−29.2	(21.3)	−60.5	(29.7)	−29.2	(27.6)	−60.5	(53.0)	−29.2	(51.4)
$\mathrm{RES_{zoo}}$	−48.7	(19.6)	−21.2	(15.4)	−35.8	(17.6)	−13.7	(13.0)	−13.0	(11.4)	−4.4	(7.7)
NIT	−11.7	(4.7)	−6.4	(4.7)	−11.4	(5.6)	−6.2	(5.9)	−5.2	(4.5)	−3.0	(5.3)

$V_{\mathrm{sub,fix}}$ shows a continuous increase throughout the entire analysed periods. The highest values occur right before events of temporary breakdown of stratification, due to the slight temporal delay between the onset of enhanced mixing and actual change in bottom T (see Sect. 4.3.3). For $V_{\mathrm{sub,fix}}$, $\mathrm{MIX_{O_2}}$ adds up to $88.2\,\mathrm{g\,O_2\,m^{-2}}$ in 2002 and $35.3\,\mathrm{g\,O_2\,m^{-2}}$ in 2010, which is about twice as high as for $V_{\mathrm{sub,var}}$ for both years.

With respect to $\mathrm{ADV_{O_2}}$, the effect on O_2 within $V_{\mathrm{sub,var}}$ is quite different between 2002 and 2010. While in 2002, $\mathrm{ADV_{O_2}}$ similar to $\mathrm{MIX_{O_2}}$ adding up to $42\,\mathrm{g\,O_2\,m^{-2}}$, it is even negative in 2010 resulting in $-4.4\,\mathrm{g\,O_2\,m^{-2}}$. For $V_{\mathrm{sub,fix}}$, a similar tendency can be seen with $\mathrm{ADV_{O_2}}$ of $43.1\,\mathrm{g\,O_2\,m^{-2}}$ in 2002 and $13.2\,\mathrm{g\,O_2\,m^{-2}}$ in 2010. Thus, $\mathrm{ADV_{O_2}}$ can constitute a supply and reduction process for sub-MLD O_2. In this context, it has to be noted that $\mathrm{ADV_{O_2}}$ is mainly affected by spatial gradients in O_2 as the volume of the non-surface model grid cells remains constant. Consequently, $\mathrm{ADV_{O_2}}$ tends to show high positive values in case of low sub-MLD O_2 concentrations within the considered area, and vice versa.

The change in the sign of $\mathrm{ADV_{O_2}}$ between $V_{\mathrm{sub,var}}$ and $V_{\mathrm{sub,fix}}$ in 2010 most likely relates to differences in the spatial gradients within the upper 20 m, as during most times the MLD is less than 20 m deep in 2010 (see Fig. 5.12b). One potential cause could be higher near-surface NPP compared to the surrounding areas, resulting in higher O_2 concentrations and, consequently, in negative $\mathrm{ADV_{O_2}}$ when considering $V_{\mathrm{sub,var}}$.

In general, it can be said that $\mathrm{MIX_{O_2}}$ constitutes the major physical supply of O_2 into V_{sub}. $\mathrm{ADV_{O_2}}$ can be of similar importance, however, can also cause a reduction of sub-MLD O_2, depending on the spatial gradients between the area of interest and the surrounding waters.

The analysis of the biochemical processes affecting O_2 in $V_{\mathrm{sub,var}}$ and $V_{\mathrm{sub,fix}}$ reveals

that, opposite to the physical processes, the integrated effect of these processes results in a net decrease of O_2. NPP constitutes the only potential source for O_2, while all other processes (RES_{zoo}, REM_{pel}, REM_{sed} and NIT) contribute to GOC. In $V_{sub,var}$ in 2002 and 2010 (Fig. 5.12a and b, respectively), NPP shows a generally similar behaviour during the periods of analysis. NPP is high during periods with a shallow MLD, and low during periods of a deeper MLD, resulting in $109.1\,g\,O_2\,m^{-2}$ and $81.8\,g\,O_2\,m^{-2}$ in 2002 and 2010, respectively. This relates to the fact that NPP mainly occurs in the upper 10 m–15 m due to high light availability. Accordingly, NPP in $V_{sub,var}$ increases with a decreasing MLD or in case of intermittences in stratification, due to integration over the entire water column. This is confirmed by the analysis of $V_{sub,fix}$ (Fig. 5.12c and d) in which NPP is significantly lower in both years, adding up to $17.3\,g\,O_2\,m^{-2}$ in 2002 and $15.5\,g\,O_2\,m^{-2}$ in 2010 (5–6 times less than in $V_{sub,var}$).

With respect to GOC, it can first be seen that REM_{pel} (orange) constitutes the largest sink of O_2 within both $V_{sub,var}$ and $V_{sub,fix}$, followed by REM_{sed} (red), RES_{zoo} (yellow) and NIT (brown). This is a consistent image for 2002 and 2010. It has to be noted that, except for REM_{sed}, all these processes occur within the entire water column which explains their steep decreases (i.e., enhanced GOC) in case of a decrease in MLD or intermittences in stratification in the mass balances within $V_{sub,var}$.

The comparison of the individual cumulated processes for $V_{sub,var}$ in 2002 (Fig. 5.12a and Table 5.2, first column) shows that REM_{pel} adds up to $-127.9\,g\,O_2\,m^{-2}$ (51.4 % of GOC) while REM_{sed} accounts for 24.3 % of GOC ($-60.5\,g\,O_2\,m^{-2}$). Thus, the degradation of organic matter in the pelagic and sediment accounts for more than 75 % of GOC. RES_{zoo} and NIT add up to $-48.7\,g\,O_2\,m^{-2}$ (19.6 %) and $-11.7\,g\,O_2\,m^{-2}$ (4.7 %), respectively. Comparing NPP against GOC clearly shows that GOC ($-248.8\,g\,O_2\,m^{-2}$) is more than two times stronger than NPP within $V_{sub,var}$. This relates to the fact that the largest part of NPP occurs within the SML, thus, not directly increasing the O_2 inventory below the MLD.

This becomes even more visible for the biochemical processes within $V_{sub,fix}$ in 2002 (Fig. 5.12c and Table 5.2, third column). Here, GOC adds up to $-203.1\,g\,O_2\,m^{-2}$ which is almost the 12-fold of NPP. With respect to the absolute values of the individual O_2-consuming processes some changes can be seen. REM_{pel} reduces to $-95.4\,g\,O_2\,m^{-2}$(about 75 % of that in $V_{sub,var}$), due to the MLD of 20 m which is deeper than the time-varying MLD during most times. REM_{sed} remains the same as for $V_{sub,var}$ as it only affects the deepest pelagic layer. Like REM_{pel}, RES_{zoo} is clearly reduced in $V_{sub,fix}$ ($-35.8\,g\,O_2\,m^{-2}$, about 74 % of that in $V_{sub,var}$) which also relates to the difference in integration depth. NIT is only slightly less than in $V_{sub,var}$, yielding $-11.4\,g\,O_2\,m^{-2}$. This relates to the light limitation of NIT, favouring higher NIT under low light conditions (see Eq. (3.8)). Thus,

the largest share of NIT occurs in the deeper layers.

Although, the changes in the absolute process values are partly remarkable (REM_{pel} and RES_{zoo}), the relative contributions to GOC show only minor changes. REM_{pel} still constitutes the largest O_2 sink accounting for 47 % of GOC, which is slightly less than in $V_{sub,var}$. The relative contribution of REM_{sed} increased to 29.7 % as its absolute value remains the same, but GOC decreased. RES_{zoo} and NIT account for 17.6 % and 5.6 %, respectively.

The comparison of the processes in 2010 with those of 2002 shows some remarkable differences with respect to their absolute values for $V_{sub,var}$ and $V_{sub,fix}$ (Fig. 5.12b and d and Table 5.2, second and fourth column, respectively). In 2010, GOC adds up to $-137.3\,g\,O_2\,m^{-2}$ in $V_{sub,var}$ and to $-105.6\,g\,O_2\,m^{-2}$ in $V_{sub,fix}$, i.e., GOC is almost half of that in 2002. Interestingly, this difference is much more pronounced than for NPP within the $V_{sub,var}$ which implies that the amount of organic matter being exported from the upper layers into V_{sub} must be significantly higher in 2002 compared to 2010.

This is confirmed by NPP_{sml} and EXP_{org} calculated analogously to Sect. 5.2.3.1, Table 5.1 (not shown). Summer NPP_{sml} within the upper 25 m yields $233.1\,g\,C\,m^{-2}$ and $156.6\,g\,C\,m^{-2}$ for 2002 and 2010, respectively, resulting in EXP_{org} below 25 m of $30.0\,g\,C\,m^{-2}$ and $17.2\,g\,C\,m^{-2}$. Thus, NPP_{sml} is about 1.5 times higher in 2002 than in 2010 which matches well the difference in EXP_{org}, being about 1.7 times higher in 2002. The good agreement between the relative difference in GOC and NPP_{sml}/EXP_{org} between the two years underlines the great importance of near-surface productivity for the sub-MLD O_2 dynamics. Despite the clearly lower GOC in 2010, it can be seen that the relative contributions of the individual processes are quite similar to the 2002 values for $V_{sub,var}$ and $V_{sub,fix}$. REM_{pel} results in $-80.5\,g\,O_2\,m^{-2}$ (58.6 % of GOC) and $-56.5\,g\,O_2\,m^{-2}$ (53.5 %) for $V_{sub,var}$ and $V_{sub,fix}$, respectively. The cumulated effect of REM_{sed} is again identical, however, results in relative contributions of 21.3 % for $V_{sub,var}$ and 27.6 % for $V_{sub,fix}$ due to the different volumes. RES_{zoo} results in $-21.2\,g\,O_2\,m^{-2}$ (15.4 %) and $-13.7\,g\,O_2\,m^{-2}$ (13.0 %) for $V_{sub,var}$ and $V_{sub,fix}$, respectively. Smallest changes in relative contribution occur in NIT, which accounts for 4.7 % in $V_{sub,var}$ (same as in 2002), with a cumulated effect of $-6.4\,g\,O_2\,m^{-2}$, and 5.9 % in $V_{sub,fix}$, yielding $-6.2\,g\,O_2\,m^{-2}$.

The average ($\pm$ STD) relative contributions of the different biochemical O_2-consuming processes to GOC in $V_{sub,fix}$ during the entire period 2000–2014, result in 54.4±3.5 % for REM_{pel}, 23.2±3.8 % for REM_{sed}, and 18.4±2.0 % and 4.0±0.9 % for RES_{zoo} and NIT, respectively. The corresponding average GOC yields $-170.3\pm25.7\,g\,O_2\,m^{-2}$. Thus, the relative importance of the different O_2-consuming processes varies only slightly between the years, independent of overall GOC. This also demonstrates the great importance of REM_{pel} and REM_{sed} account for 77.6±1.4 % of GOC averaged over the entire period.

The more detailed analysis of the temporal evolution of the different O_2-consuming processes within $V_{\mathrm{sub,fix}}$ in 2002 (Fig. 5.12c) reveals some interesting interactions. During and directly after the two events of intermittent stratification in late April/early May and late June/early July, the different consumption processes show a steeper slope than during the well-stratified periods. For $V_{\mathrm{sub,fix}}$ this does not relate to the increase in the integration depth range as in the case of $V_{\mathrm{sub,var}}$, but to an increased supply of organic matter from the surface layers into the deeper layer. Consequently, the temporary replenishment of the sub-MLD O_2 inventory – visible in the steep increase in O_2 concentration in late June/early July – is balanced out about 1–1.5 weeks after the re-formation of stratification, i.e., the O_2 concentration is at the same level as right before the temporary increase in O_2. In the first three weeks after this event, O_2 reduction is even faster than before this event, due to the enhanced GOC directly driven by the increased mixing-induced $\mathrm{EXP_{org}}$. Additionally, the enhanced mixing favours NPP in the upper layers (visible in the minor increase in the slope of NPP) due to nutrient supply from the deeper layers. Consequently, this increase in organic matter production by NPP further increases the $\mathrm{EXP_{org}}$ the MLD with a slight delay after the re-formation of stratification.

This implies that events of intense mixing, causing in a temporary breakdown of stratification and the replenishment of the sub-MLD O_2 inventory, do not necessarily improve sub-MLD O_2 conditions on a time scale in the order of weeks. In fact, the exact opposite can be the case as vertical mixing increases both, the supply of organic matter into the deeper layers and near-surface NPP, which can further increase the organic matter supply. This directly drives $\mathrm{REM_{pel}}$ and $\mathrm{REM_{sed}}$, and indirectly affects NIT as the NH_4^+ release is enhanced by these processes. In addition, enhanced NPP increases food availability for zooplankton, causing an increase in zooplankton biomass and thus $\mathrm{RES_{zoo}}$.

In conclusion, the analysis of the O_2 mass balances in $V_{\mathrm{sub,var}}$ and $V_{\mathrm{sub,fix}}$ demonstrates that downward mixing of O_2 represents the major physical process counteracting the evolution of O_2 deficiency at the ODZ site. However, persistent seasonal stratification strongly limits the mixing-induced supply of O_2 into V_{sub}. Advection may constitute an relevant secondary O_2 supply, but can also have a negative effect on the O_2 concentrations. The air-sea flux of O_2 – although not directly affecting O_2 below the MLD – does not increase summer O_2 concentrations within the surface layers, implying that near-surface NPP constitutes the major source of O_2.

However, the analysis also revealed that the major part of NPP is confined to the upper 10 m–20 m of the water column, only increasing the O_2 inventory in the surface layers. On the downside, the enhanced near-surface NPP causes a subsequent increase in $\mathrm{EXP_{org}}$ into deeper layers, driving biochemical O_2 consumption below the MLD. Furthermore, less intense stratification enhances $\mathrm{EXP_{org}}$, additionally increasing biochemical O_2 consump-

tion. In consequence, on time scales of 1–2 weeks, the effect of enhanced vertical mixing on near-surface NPP and EXP_{org} can fully balance out the effect of MIX_{O_2}, resulting in a net decrease in O_2 concentration.

The analysis of the relative contributions of the individual biochemical processes demonstrates that REM_{pel} and REM_{sed} consistently account for more than three quarters of GOC, independent of the overall consumption. This emphasises the role of near-surface NPP and EXP_{org} as the main driver for the evolution of O_2 deficiency in the North Sea ODZ. The great importance of REM_{pel} for the sub-MLD O_2 inventory is also clearly shown as it consistently contributes to more than 50 % of the overall consumption. Thus, REM_{pel} can be considered as the key process determining the O_2 inventory in the mid-water, which constitutes the main O_2 reservoir available to the near-bottom layers.

5.2.5.2 Bottom layer oxygen dynamics

Minimum O_2 conditions in the North Sea ODZ usually occur directly above the seafloor due to benthic O_2 consumption strongly affecting the O_2 concentrations in this deepest layer. Thus, it is important to investigate the processes in the pelagic bottom layer of the North Sea ODZ. For this purpose, Fig. 5.12e and f show the O_2 mass balances of ECOHAM's pelagic bottom layer within region #1 for the years 2002 and 2010, respectively. The corresponding cumulated process values are presented in Table 5.2 (fifth and sixth column).

The bottom layer volume in region #1 is about $12\,km^3$ defined by an average bottom layer thickness of 6.5 m. In principle, the temporal evolution of O_2 (solid magenta) and $O_{2,sat}$ (dash-dotted magenta) in both years represents that of the $V_{sub,fix}$, although O_2 concentrations are slightly lower while $O_{2,sat}$ concentrations are slightly higher due to lower T near the bottom. The analysis of the physical processes (ADV_{O_2} and MIX_{O_2}) in 2002 reveals that the cumulated effect of ADV_{O_2} on bottom O_2 levels ($12.7\,g\,O_2\,m^{-2}$) is only about 29 %–30 % of that in $V_{sub,var}$ and $V_{sub,fix}$ (Fig. 5.12a and c, respectively) and negligible compared to MIX_{O_2} which adds up $73.9\,g\,O_2\,m^{-2}$. However, the influence of ADV_{O_2} increases during the last two months of stratification (August/September 2002) and counteracts the reduction in O_2 due to biochemical consumption. Consequently, MIX_{O_2} constitutes the only remarkable physical process supplying O_2 to the bottom layer in the ODZ in 2002.

In 2010, MIX_{O_2} also constitutes the main physical supply process for bottom O_2, however, it is only about $30.9\,g\,O_2\,m^{-2}$, which is about 42 % of the 2002 value. This mainly relates to the smaller vertical O_2 gradient due to higher concentrations near the seafloor. ADV_{O_2} is again low, adding up to about $7.5\,g\,O_2\,m^{-2}$.

With respect to NPP, it is clearly shown that its effect is negligible ($1.9\,g\,O_2\,m^{-2}$) com-

pared to V_{sub} as low light availability limits NPP near the bottom. Thus, the biochemical processes basically constitute only a sink of O_2 in the bottom layer. The same applies to 2010, when NPP results in $-1.6\,\mathrm{g\,O_2\,m^{-2}}$.

The overall biochemical O_2 consumption adds up to $-114.2\,\mathrm{g\,O_2\,m^{-2}}$. Among the O_2-consuming processes, $\mathrm{RES_{zoo}}$ and NIT are least important as in V_{sub}, accounting for $-13.0\,\mathrm{g\,O_2\,m^{-2}}$ (4.5 % of GOC) and $-5.2\,\mathrm{g\,O_2\,m^{-2}}$ (11.4 %), respectively. Regarding $\mathrm{REM_{sed}}$ and $\mathrm{REM_{pel}}$, the relative importance for bottom O_2 consumption is opposite to that in $V_{\mathrm{sub.}}$ In the bottom layer of the ODZ, $\mathrm{REM_{sed}}$ constitutes the major O_2 sink accounting for 53 % of GOC in 2002, although the absolute value of $-60.5\,\mathrm{g\,O_2\,m^{-2}}$ is the same as in V_{sub}. This relates to the fact that the influence of $\mathrm{REM_{pel}}$ is notably reduced due to the lower thickness of the bottom layer compared to V_{sub}; $\mathrm{REM_{pel}}$ adds up to $-35.5\,\mathrm{g\,O_2\,m^{-2}}$ (31.1 % of GOC).

The temporal evolution of the individual O_2 consumption processes shows that $\mathrm{REM_{pel}}$ has a stronger effect on O_2 than $\mathrm{REM_{sed}}$ during the first two months of stratification (April/May 2002). Only after that influence of $\mathrm{REM_{sed}}$ increases and stays high until the end of stratification. This relates to the fact that the organic matter which is produced in the upper layers sinks down and is first available to the pelagic bacteria, before it reaches the sediment enhancing $\mathrm{REM_{sed}}$. Besides this, the similar interactions as for $V_{\mathrm{sub,fix}}$ can be seen in relation to intermittent stratification. Especially, $\mathrm{REM_{pel}}$ is enhanced after events of strong mixing due to the increased supply of organic matter, but also $\mathrm{RES_{zoo}}$ slightly increases as a result of downward mixing of phytoplankton allowing for enhanced zooplankton growth and thus respiration.

For the bottom layer of the ODZ, the image is quite similar to $V_{\mathrm{sub,var}}$ and $V_{\mathrm{sub,fix}}$ with respect to year-to-year differences in O_2 consumption. In 2010, GOC results in $-56.8\,\mathrm{g\,O_2\,m^{-2}}$ which is about half of the 2002 value. The analysis of the relative contributions of the different processes shows similar values as for 2002, resulting in 51.4 % for $\mathrm{REM_{sed}}$, 35.6 % for $\mathrm{REM_{pel}}$, and 7.7 % and 5.3 % for $\mathrm{RES_{zoo}}$ and NIT, respectively. This implies that the combined effect of $\mathrm{REM_{sed}}$ and $\mathrm{REM_{pel}}$ on the bottom layer in the North Sea ODZ accounts for 84.1 % and 87 % in 2002 and 2010, respectively. Thus, it is even higher than in V_{sub} which relates to the reduced effect of $\mathrm{RES_{zoo}}$ and NIT, due to lower layer thickness.

As for V_{sub} the relative contributions of the individual processes show only minor variations during the entire period 2000–2014. The averages over the period result in 49.8±1.4 % for $\mathrm{REM_{sed}}$ and 35.1±1.6 % for $\mathrm{REM_{pel}}$. Consequently, $\mathrm{REM_{pel}}$ and $\mathrm{REM_{sed}}$ consistently account for 84.9±0.9 % of the overall GOC. $\mathrm{RES_{zoo}}$ and NIT are clearly less important contributing only 11.2±1.2 % and 3.9±0.6 %, respectively. This confirms the findings of the previous section and emphasises the role of NPP and organic matter export driving

the bottom layer O_2 dynamics.

The mass balance for region #1 clearly shows that vertical mixing is the only efficient gain term for O_2 in the bottom layer. REM_{sed} constitutes the major driver for O_2 deficiency in the North Sea ODZ, although REM_{pel} still has a significant effect on bottom O_2. The simulated average daily REM_{sed} rates during the years 2000–2014 range between $0.17\,g\,O_2\,m^{-2}\,d^{-1}$ ($5.2\,mmol\,O_2\,m^{-2}\,d^{-1}$) and $0.32\,g\,O_2\,m^{-2}\,d^{-1}$ ($10.1\,mmol\,O_2\,m^{-2}\,d^{-1}$) in 2010 and 2002, respectively. These rates are in the same order as those derived from observations ranging from $7\,mmol\,O_2\,m^{-2}\,d^{-1}$ to $25\,mmol\,O_2\,m^{-2}\,d^{-1}$ for a nearby station (station 3 in Upton et al., 1993), however, are rather at the lower end.

5.2.6 Regional differences in the bottom oxygen dynamics

In order to provide insight in spatial differences in the processes and physico-biochemical interactions driving bottom O_2 dynamics, Fig. 5.13a and b show the O_2 mass balances for the regions #2 and #3 (see Fig. 5.11a for locations), respectively. The corresponding cumulated process values are listed in Table 5.3. Both regions show different t_{strat} than region #1. In region #2, the period between the first and last day of stratification results in only 173 days compared to 187 days in region #1. As in region #1, stratification is temporarily intermittent in late April and early July. In region #3, stratification lasts for 216 days without any intermittences. The water depths and bottom layer volumes also differ between the regions. Region #1 has an average water depth of 36.51 m and a bottom layer volume of about $12\,km^3$, while region #2 is characterised by an average depth of 48 m and a bottom layer volume of $10.6\,km^3$. Region #3 has an average bottom depth of 92.5 m and a bottom layer volume of $13.3\,km^3$.

The O_2 concentrations at the beginning of the stratified period in regions #2 and #3 ($9.7\,mg\,O_2\,L^{-1}$ and $9.5\,mg\,O_2\,L^{-1}$, respectively) are lower than in region #1. In contrast, both regions show higher concentrations at the end of stratification compared to region #1. These values reach $6.9\,mg\,O_2\,L^{-1}$ in region #3 and $7.8\,mg\,O_2\,L^{-1}$ in region #3, compared to $6.0\,mg\,O_2\,L^{-1}$ in region #1.

Similar to region #1, intense mixing in late June/early July in region #2, indicated by the steep increase in MIX_{O_2}, causes the temporary breakdown of stratification and the replenishment of bottom O_2. Integrated over the stratified period the effect of MIX_{O_2} is about 30 % lower than in region #1. In region #3, MIX_{O_2} is even 5 times lower. In both regions, this relates to the higher O_2 concentrations in the bottom layer, i.e., a lower vertical gradient in O_2 concentration. The effect of ADV_{O_2} is negligible in regions #2 and #3, resulting in $1.2\,g\,O_2\,m^{-2}$ and $-0.5\,g\,O_2\,m^{-2}$, respectively.

Bottom layer NPP is also in negligible in both regions which relates to the greater bottom depth and thus light limitation. The integrated effect of GOC in region #2

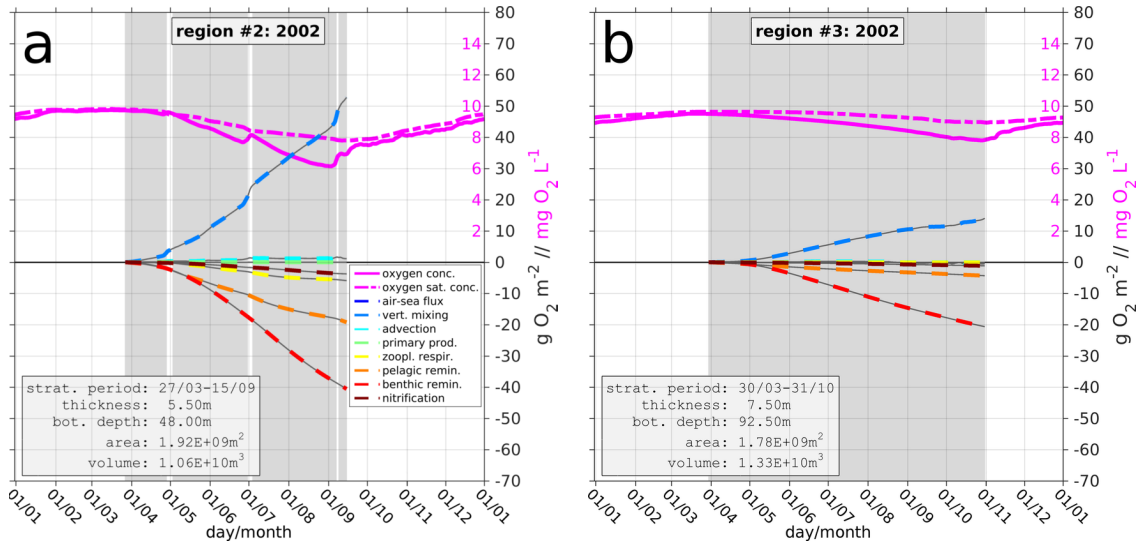

Figure 5.13: Bottom oxygen mass balances for regions (a) #2 and (b) #3 (see Fig. 5.11a) during stratification (grey shaded) according to Eq. (4.4) in 2002. Magenta y axes refer to O_2 and $O_{2,sat}$, black y axes refer to processes. Legend of a) applies to both panels. Process values in Table 5.3.

adds up to $-69.4\,\mathrm{g\,O_2\,m^{-2}}$ (about 61 % of that in region #1). On the one hand, this difference relates to the thinner bottom layer in region #2, and on the other hand, to a 16 % lower export of organic matter below 25 m depth (calculation analogous to Sect. 5.2.3.1). Additionally, the greater water depth results in less organic matter reaching the bottom layer due to $\mathrm{REM_{pel}}$ in the mid-water. In the deep region #3, organic matter export results in only 58 % of that in region #1, while GOC accounts for only 23 % of that in region #1.

Despite these differences in GOC, the relative contributions of the different consumption processes in region #2 are in the same order as in region #1, except for $\mathrm{RES_{zoo}}$. $\mathrm{REM_{sed}}$ represents the largest contributor with about 58.5 % of total GOC, while $\mathrm{REM_{pel}}$ accounts for 27.7 %. Thus, the combined effect of $\mathrm{REM_{sed}}$ and $\mathrm{REM_{pel}}$ accounts for 86.2 % which is similar to region #1. The relative contribution of $\mathrm{RES_{zoo}}$ results in 8.4 % which is less than half of the relative contribution in region #1, related to the greater water depth implying less NPP and thus lower food availability in the bottom layer. NIT contributes about 5.4 % to the overall consumption.

The comparison of the relative contributions of $\mathrm{REM_{pel}}$ and $\mathrm{REM_{sed}}$ in region #3 reveals some changes compared to regions #1 and #2. $\mathrm{REM_{sed}}$ accounts for about 78.8 % of GOC, while $\mathrm{REM_{pel}}$ contributes to only about 16.5 %. This relates to the generally lower amount of exported organic matter reaching the model bottom layer (58 % of that in region #1). On the one hand, this causes lower GOC due to $\mathrm{REM_{pel}}$, and on the other

Table 5.3: Process values for bottom oxygen mass balances for regions #2 and #3 (see Fig. 5.11a) cumulated from beginning to end of stratification for the year 2002 (compare Fig. 5.13). All process values in $g\,O_2\,m^{-2}$, negative values imply loss of O_2. Values in parentheses represent relative contributions to overall biological O_2 consumption (GOC; in %).

region	#2		#3	
t_{int} [days]	173		216	
ASF_{O_2}	0.0		0.0	
MIX_{O_2}	52.8		14.1	
ADV_{O_2}	1.2		−0.5	
NPP	<0.1		<0.1	
GOC	−69.4		−26.1	
REM_{pel}	−19.2	(27.7)	−4.3	(16.5)
REM_{sed}	−40.6	(58.5)	−20.6	(78.8)
RES_{zoo}	−5.9	(8.4)	−0.1	(0.4)
NIT	−3.7	(5.4)	−1.1	(4.3)

hand, enhances REM_{sed} relative to REM_{pel} as more organic matter reaches the bottom. However, absolute REM_{sed} in region #3 is only half of that in region #2 and only about one third of that in region #1.

Considering the combined effect of stratification and GOC in region #2 reveals that the slightly shorter t_{strat}, but more important the clearly lower GOC prevents the evolution of low O_2 conditions. However, the low minimum bottom O_2 of about $6.1\,mg\,O_2\,L^{-1}$ (see Fig. 5.13a) indicates the high potential of O_2 deficiency in the Oyster Grounds. This is in good agreement with the findings by Greenwood et al. (2010), who observed bottom O_2 concentrations less than $6\,mg\,O_2\,L^{-1}$ in this area. The simulated average daily REM_{sed} rates during 2000–2014 range between $0.13\,g\,O_2\,m^{-2}\,d^{-1}$ ($4.2\,mmol\,O_2\,m^{-2}\,d^{-1}$) in 2010 and $0.23\,g\,O_2\,m^{-2}\,d^{-1}$ ($7.3\,mmol\,O_2\,m^{-2}\,d^{-1}$) in 2002. This is in the same order as the average rates found by de Wilde et al. (1984) ($0.18\,g\,O_2\,m^{-2}\,d^{-1}$–$0.28\,g\,O_2\,m^{-2}\,d^{-1}$) during spring and summer 1980 and 1981, although benthic fauna is not included in the model. Compared to more recent studies (Lohse et al., 1996; Weston et al., 2008), this is – as for region #1 – at the lower end of the observed range of $5.6\,mmol\,O_2\,m^{-2}\,d^{-1}$–$30.6\,mmol\,O_2\,m^{-2}\,d^{-1}$, which suggests that the model most likely underestimates REM_{sed} rates.

In region #3, the amount of exported organic matter reaching the bottom layer (i.e., the deepest pelagic model layer) is limited due to the great water depth. Thus, biological consumption in the bottom layer is low, preventing the evolution of O_2 deficiency, even though stratification lasts longer and is more stable than in the other regions. This suggests that region #3 is unlikely to be affected by low bottom O_2 concentrations. However,

Queste et al. (2013) found bottom O_2 concentrations of about $6\,mg\,O_2\,L^{-1}$ near this area in 2010, which indicates that this area can be affected by O_2 deficiency.

5.2.7 Interpreting observed bottom oxygen at North Dogger

The observed bottom O_2 concentrations and ΔT at station North Dogger in 2007 and 2008 (see Fig. 5.3a and b, respectively) are in good agreement with the ECOHAM simulation and show the similar tendency for faster O_2 reduction in 2007 compared to 2008. Thus, the model-derived O_2 mass balances presented in Fig. 5.14 are used to interpret the observed temporal evolution of bottom O_2 in relation to its underlying processes. The corresponding cumulated process values are provided in Table 5.4.

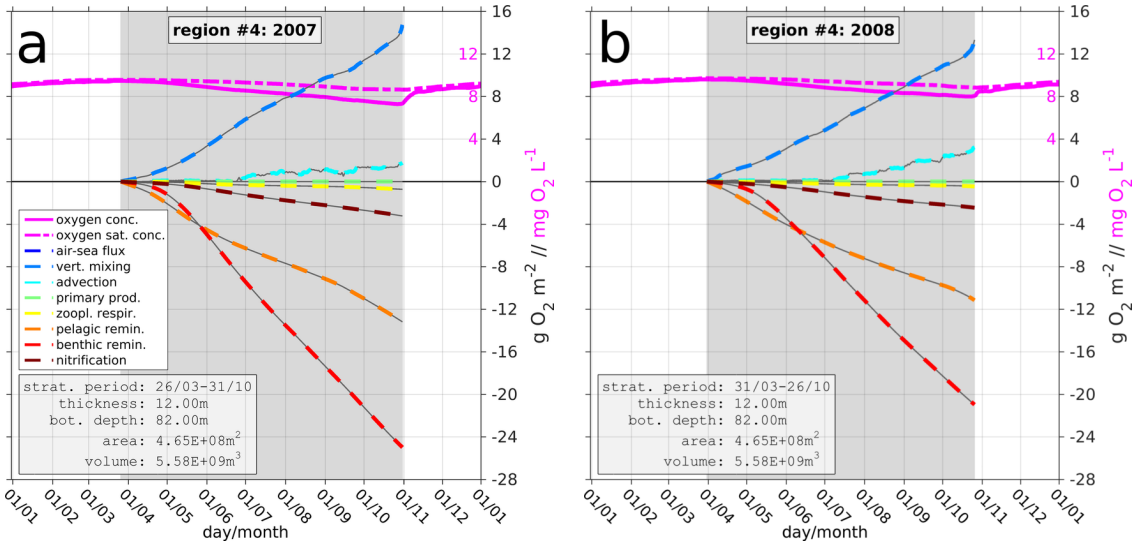

Figure 5.14: Bottom oxygen mass balances for region #4 (North Dogger; see Fig. 5.11a) during stratification (grey shaded) according to Eq. (4.4) in (a) 2007 and (b) 2008. Magenta y axes refer to O_2 and $O_{2,sat}$, black y axes refer to processes. Same legend for (a, b). Process values in Table 5.4.

The first minor differences between the years can be seen in t_{strat} (grey-shaded) which starts on 26 March 2007 lasting 220 days, respectively, on 31 March 2008 lasting 210 days. In both years, stratification is persistent until its breakdown in late October. At the beginning of the stratified period, simulated bottom O_2 concentrations yield $9.5\,mg\,O_2\,L^{-1}$ and $9.6\,mg\,O_2\,L^{-1}$ in 2007 and 2008, respectively, while at the end of stratification concentrations result in $7.3\,mg\,O_2\,L^{-1}$ in 2007 and in $8.1\,mg\,O_2\,L^{-1}$ in 2008. This implies a 1.4 times stronger reduction in O_2 in 2007 which cannot be explained by the only 10 days longer t_{strat}. The average daily O_2 reduction rates (i.e., the combined effect phys-

ical and biochemical processes) during the stratified periods in 2007 and 2008 result in $0.01\,\mathrm{g\,O_2\,m^{-2}\,d^{-1}}$ and $0.007\,\mathrm{g\,O_2\,m^{-2}\,d^{-1}}$, respectively, which implies O_2 reduction being 1.3 times faster in 2007 than in 2008.

The comparison of the physical processes, $\mathrm{MIX_{O_2}}$ and $\mathrm{ADV_{O_2}}$, reveals that physical O_2 supply cumulated over the stratified period results in $16.5\,\mathrm{g\,O_2\,m^{-2}}$ for both years, but the combined daily rate is about 5 % higher in 2008. However, this does not explain the difference in O_2 reduction between the two years. Consequently, these differences must relate to variations in the biochemical O_2 consumption processes.

Table 5.4: Process values for bottom oxygen mass balances for region #4 (North Dogger; see Fig. 5.11a) during stratification in the years 2007 and 2008 (compare Fig. 5.14): cumulated values and rates. Cumulated values in $\mathrm{g\,O_2\,m^{-2}}$, rates in $\mathrm{g\,O_2\,m^{-2}\,d^{-1}}$. Negative values imply loss of O_2. Values in parentheses represent relative contributions to overall gross O_2 consumption (GOC; in %).

year	2007			2008		
t_{int} [days]	220			210		
value	cumulated	rate		cumulated	rate	
$\mathrm{ASF_{O_2}}$	0.0	0.000		0.0	0.000	
$\mathrm{MIX_{O_2}}$	14.7	0.067		13.3	0.063	
$\mathrm{ADV_{O_2}}$	1.8	0.008		3.2	0.015	
NPP	<0.1	$\ll 0.001$		<0.1	$\ll 0.001$	
GOC	-42.1	-0.192		-35.1	-0.167	
$\mathrm{REM_{pel}}$	-13.2	-0.060	(31.3)	-11.2	-0.053	(31.9)
$\mathrm{REM_{sed}}$	-25.0	-0.114	(59.3)	-21.0	-0.010	(59.8)
$\mathrm{RES_{zoo}}$	-0.7	-0.003	(1.7)	-0.5	-0.002	(1.3)
NIT	-3.2	-0.015	(7.7)	-2.5	-0.012	(7.0)

The general temporal evolution of the biological consumption processes is similar in both years, with higher rates in 2007. The integrated effect of all biological sink processes results in $-42.1\,\mathrm{g\,O_2\,m^{-2}}$, which corresponds to an average consumption rate of $0.192\,\mathrm{g\,O_2\,m^{-2}\,d^{-1}}$. For 2008, the simulation yields a $7.1\,\mathrm{g\,O_2\,m^{-2}}$ less strong biological consumption due to a $0.025\,\mathrm{g\,O_2\,m^{-2}\,d^{-1}}$ lower consumption rate. This represents a relative difference of 15 % in GOC between the two years. For organic matter export below 25 m depth during summer (calculation analogous to Sect. 5.2.3.1), a very similar relative difference of 16 % is found.

The relative contribution of the different processes to overall near-bottom GOC shows only minor changes between the two years. $\mathrm{REM_{sed}}$ accounts for 59 %–60 %, while $\mathrm{REM_{pel}}$ accounts for 31 %–32 %. $\mathrm{RES_{zoo}}$ and NIT contribute to about 1.5 % and 7 %–8 %, respectively. This shows that the differences in the O_2 dynamics between 2007 and 2008 are

mainly driven by differences in EXP_{org} and subsequent bacterial degradation. The enhanced release of NH_4^+ due to REM_{pel} and REM_{sed} as well as excretion by zooplankton consequently triggers an increase in NIT.

In contrast to the findings by Greenwood et al. (2010), who argued that strong advection at North Dogger may ventilate the bottom layers in terms of O_2, the mass balance analysis suggests that advection only has a minor positive effect due to the only slightly higher O_2 concentrations in the surrounding waters. The large contribution of bacterial remineralisation (REM_{sed} and REM_{pel}) accounting for more than 90 % of the overall biological consumption at North Dogger confirms that the estimates for C remineralisation rates made by Greenwood et al. (2010) provide reasonable results. However, as NIT also accounts for about 7 %–8 % of GOC, this process should be considered in order to obtain more precise estimates for C remineralisation rates.

5.2.8 Conclusions on the oxygen dynamics

The North Sea is one of the shelf regions regularly experiencing seasonal O_2 deficiency in the bottom water (Díaz and Rosenberg, 2008; Rabalais et al., 2010; Emeis et al., 2015). However, not all areas of the North Sea are similarly affected by low O_2 conditions (e.g., Queste et al., 2013) due to different characteristics with respect to stratification and GOC. Observations and ECOHAM model results suggest that the area between 54 °N–57 °N and 4.5 °E–7 °E shows the highest potential for low O_2 conditions, but also areas around the Doggerbank experience lowered bottom O_2 concentrations.

The small variability in simulated bottom O_2 in most regions during the survey periods further suggests that measurements taken in late summer provide a synoptic image of the North Sea O_2 conditions. This is important for a cost-efficient and informative monitoring by the responsible authorities.

The analysis of different factors affecting O_2 shows that besides sufficiently long continuous t_{strat} (>60 days), surface layer NPP (driving organic matter export) and V_{sub} are the key parameters influencing the bottom O_2 evolution. Based on this, the North Sea can be subdivided into three different zones in terms of O_2 dynamics: (1) a highly productive, non-stratified coastal zone (region #1; see Fig. 5.7), (2) a productive, seasonally stratified zone with a small V_{sub} (regions #2 and #3), and (3) a productive, seasonally stratified zone with a large V_{sub} (regions #4 and #5). While the zones of type 1 and 3 are unlikely to be affected by low O_2 conditions due to either continuously ongoing ventilation (type 1) or the large V_{sub} diluting the effect of O_2 consumption (type 3), type 2 is highly susceptible to low O_2 conditions. This results from the specific combination of high upper layer productivity and small V_{sub}, which causes a strong impact of the consumption processes on the decrease in the bottom O_2 concentrations.

The ODI demonstrates that this regional characterisation, based on only three controlling parameters, can be applied to most parts of the North Sea. However, further in-depth analyses of the applicability of the ODI are required, but are left to future work as the development of the ODI is not the focus of this study. The ODI is rather simple compared to the EUTRISK (Druon et al., 2004) as it is designed to indicate regions with higher risk for O_2 deficiency. Therefore, given the in-depth evaluation of the ODI, it may also allow for an operational use as the information on stratification can be derived from operational hydrodynamical models and information on NPP from satellite data (e.g., Longhurst et al., 1995; Behrenfeld and Falkowski, 1997). This could be worthwhile for the improvement and optimisation of oxygen monitoring in the North Sea.

The model-derived O_2 mass balances show that REM_{pel} constitutes the largest O_2 consuming process within V_{sub}. Near the seafloor, REM_{sed} constitutes the major O_2 sink and consistently contributes more than 50 % to GOC. REM_{pel} consistently contributes to more than 15 % of near-bottom GOC. RES_{zoo} and NIT are less important, however, can contribute up to 12 % and 5 %, respectively. In addition, the results suggest that the relative contributions of the different O_2-consuming processes near the seafloor at a certain location depend on the water column depth, independent of the overall consumption.

The mass balances also show that differences in the surface layer NPP drive variations in the sub-thermocline and bottom O_2 evolution between different years. Increased NPP directly enhances EXP_{org} into the deeper layers. Furthermore, it enhances zooplankton growth enhancing RES_{zoo}, and causing an additional increase in organic matter production and export. The overall increase in EXP_{org} results in stronger bacterial remineralisation which in turn triggers NIT due to the stronger release of NH_4^+.

The analysis further suggests that advection usually has only a minor effect on the bottom O_2 dynamics in most North Sea regions which contradicts the interpretation by other studies (Greenwood et al., 2010; Queste et al., 2013). In addition, the mass balances show that events of strong mixing during summer can cause the replenishment of bottom O_2 to its saturation concentration. However, the enhanced nutrient supply triggers NPP, eventually increasing GOC, which balances or even exceeds the enhanced O_2 supply. Thus, although counter-intuitive, enhanced vertical mixing during seasonal stratification can cause the degradation of O_2 conditions in the North Sea, finally leading to O_2 deficiency.

Chapter 6

The influence of nitrogen inputs on the North Sea

Excess nutrient loads from external sources, such as rivers, are considered the main driver for eutrophication in the North Sea (e.g., Brockmann et al., 1988; Jickells, 1998; Lenhart, 2001; Lenhart et al., 2010), triggering enhanced NPP. Alvarez-Fernandez et al. (2012) show that North Sea NPP is mainly controlled by N availability in the post-1998 period. Due to the strong link between NPP and O_2 consumption, the identification and quantification of the major contributors to TN and N-related NPP constitutes a key aspect to better understand the North Sea O_2 dynamics. Consequently, this is crucial for improving the North Sea O_2 conditions by means of ecosystem management.

Although the freshwater signal of riverine discharge has a limited range within the marine environment, due to gradual mixing with the surrounding waters, organic and inorganic nutrients can be dispersed far beyond boundaries of this freshwater signal, due to mixing processes and – more important – the prevailing currents. However, observational methods for the identification of the origin of nutrients are sparse and very limited with respect to the level of detail needed for a comprehensive analysis.

For instance, the ratio of stable ^{15}N:^{14}N isotopes in sediment cores can be used to determine whether marine or freshwater N sources were dominating at a certain period (e.g., Serna et al., 2010). Still, these methods do not provide information about the exact origin of nutrients (Phillips and Gregg, 2003) and are not available for all nutrients affecting marine ecosystems, e.g., phosphorus (Ehleringer and Rundel, 1989). In the latter case, the ratio of stable $^{18}O_2$:$^{16}O_2$ isotopes can be used (e.g., Longinelli and Nuti, 1973; Blake et al., 1997), however, with the same restrictions in relation to the exact origin. In contrast, numerical biogeochemical models can be expanded to provide such detailed information, allowing for the discrimination between individual sources of nutrients and the quantification of their impact on different areas of the marine environment (e.g., Ménesguen et al., 2006).

This chapter first describes the numerical method used for the tracing of nutrient inputs from multiple sources into the North Sea, and its implementation to the ECOHAM model. Thereafter, a general analysis of the simulated current patterns of the North Sea

is presented as the volume transports play the major role for the dispersal of tracers like nutrients. Consequently, spatial distributions and temporal patterns for TN and N-related NPP are investigated during the period 2000–2014, in relation to the analysis of the O_2 dynamics provided in the previous chapter.

6.1 Tracing nutrient inputs in ecosystem models

Ecosystem models allow for the domain-wide, spatially and temporally consistent quantification of physical and biochemical processes affecting the O_2 dynamics. In addition, they can be used to track the dispersal of tracers within an ecosystem. There are different applications for investigating this spatial displacement of tracers using such models. For instance, passive tracers, like rhodamine, which are not affected by internal source or sink processes can be traced using Lagrangian transport models (e.g., Hainbucher et al., 1987; Lenhart et al., 1995). The modelling of radioactive tracers represents a more complex application as it includes simple decay functions (e.g., Dahlgaard, 1995; Harms, 1997). However, in order to quantify the influence of inorganic and organic nutrients from individual sources on the biochemical processes within an ecosystem, a more sophisticated approach is required.

Ménesguen and Hoch (1997) provided the theoretical basis for the tracing of a selected property (e.g., the source of a N element brought into an ecosystem) throughout the entire biochemical process chain represented by the underlying model (hereafter 'base model'). Since that, several modelling studies made use of their method with various research objectives. For instance, Wijsman et al. (2004) determined the N retention capacity of the Scheldt using this method, while Timmermann et al. (2010) applied it for determining the sources of P inside a Danish estuary. Other studies quantified the amount of N from various riverine sources bound in phytoplankton in French (Ménesguen et al., 2006; Perrot et al., 2014) and Belgian coastal waters (Lacroix et al., 2007). The method was further used for investigating the influence of atmospheric N deposition on the North Sea (Troost et al., 2013) or to determine the dispersal of riverine TN and TP in the Baltic Sea (Neumann, 2007; Radtke et al., 2012). Radtke and Maar (2016) applied the method for the quantification of the TN exchange between the North Sea and the Baltic Sea.

These applications illustrate the versatility of this method, for which – in the meantime – the term 'trans-boundary nutrient transports' (TBNT) was established (Blauw et al., 2006; OSPAR, 2010). This term will also be used throughout this thesis. In the following section the theoretical concept of TBNT is explained.

6.1.1 The concept of trans-boundary nutrient transports

The basic idea of TBNT is that organic and inorganic matter, that contains a certain chemical element (e.g., N), obtains a unique, source-specific label at the moment of its release into the ecosystem. The labelling of matter based on the element implies that all model state variables containing this element must be labelled accordingly. The labelled state variables experience the same biochemical and physical processes as the overall state variables, i.e., the total amount of labelled and unlabelled material, however, proportional to their relative contribution to this overall amount. In the following, the prefixes 'bulk' and 'fraction' are used to refer to the overall state variables and processes, and their labelled counterparts, respectively.

Following the approach by Ménesguen and Hoch (1997), any property p (e.g., origin/source, age etc.) can be attached to any bulk state variable X and can be traced within an ecosystem model by solving an additional differential equation for the product $X \cdot p$ instead of the bulk state variable X. The product $X \cdot p$ then represents that subset of the bulk variable X with the defined property p. Technically, the product $X \cdot p$ is introduced into the base model as a new fraction state variable $X_p = X \cdot p$ and the related processes are introduced according to the differential equation describing the changes in the corresponding bulk state variable X. Each combination of state variables X and properties p_i, $X_p^i = X \cdot p_i$, therefore requires an additional differential equation to be introduced to the model. For easier readability, X_p^i is hereafter denoted as X^i.

In order to show the relation between bulk variables and fraction variables, one has to start with the convection-diffusion equation for the concentration C_X of a bulk state variable X, which reads as:

$$\frac{dC_X}{dt} = \underbrace{\nabla \cdot \left(\overline{\overline{d}} \nabla C_X\right)}_{diffusion} \quad \underbrace{- \nabla \cdot (\vec{v} C_X)}_{convection/advection} \quad \underbrace{+ R_X}_{sources/sinks}. \tag{6.1}$$

The diffusive transport is calculated according to Fick's first law with the second order diffusion tensor (or diffusivity) $\overline{\overline{d}}$. In the convective/advective transport term, $\vec{v}$ represents the 3D velocity vector. R_X represents the sources and sinks of X (i.e., biochemical processes, input from external sources). Assuming that the bulk variable X consists of N fractions $X^i = X \cdot p_i$, with $i = 1, 2, ..., N-1, N$, implies for the concentration C_X:

$$C_X = \sum_{i=1}^{N} C_X^i, \tag{6.2}$$

where C_X^i denotes the concentration of the fraction variable X^i. Dividing Eq. (6.2) by C_X

yields:

$$\sum_{i=1}^{N} \frac{C_X^i}{C_X} = 1, \tag{6.3}$$

with $\frac{C_X^i}{C_X}$ representing the relative contribution of the fraction variable X^i. Multiplication of the right-hand side of Eq. (6.1) with 1 results in:

$$\frac{dC_X}{dt} = \left[\nabla \cdot \left(\overline{\overline{d}} \nabla C_X\right) - \nabla \cdot (\vec{v} C_X) + R_X\right] \cdot 1. \tag{6.4}$$

Combining Eq. (6.4) with Eqs. (6.2) and (6.3) leads to:

$$\frac{d}{dt}\left(\sum_{i=1}^{N} C_X^i\right) = \left[\nabla \cdot \left(\overline{\overline{d}} \nabla C_X\right) - \nabla \cdot (\vec{v} C_X) + R_X\right] \cdot \sum_{i=1}^{N} \frac{C_X^i}{C_X}. \tag{6.5}$$

The summation and differentiation on the left-hand side of Eq. (6.5) can be permuted according to the sum rule in differentiation. Then, the separation of the two sum terms in Eq. (6.5) finally provides the convection-diffusion equation for the concentration of an individual fraction variable, C_X^i:

$$\begin{aligned} \frac{dC_X^i}{dt} &= \left[\nabla \cdot \left(\overline{\overline{d}} \nabla C_X\right) - \nabla \cdot (\vec{v} C_X) + R_X\right] \cdot \frac{C_X^i}{C_X} \\ &= \underbrace{\nabla \cdot \left(\overline{\overline{d}} \nabla C_X\right) \cdot \frac{C_X^i}{C_X}}_{diffusion} \quad \underbrace{-\nabla \cdot (\vec{v} C_X) \cdot \frac{C_X^i}{C_X}}_{convection/advection} \quad \underbrace{+R_X \cdot \frac{C_X^i}{C_X}}_{sources/sinks}. \end{aligned} \tag{6.6}$$

Equation (6.6) implies that all physical (diffusion and transport) and biochemical processes (internal sources/sinks) affecting the concentration of the fraction variable, C_X^i, are calculated as the product of the process based on the concentration of the bulk variable, C_X, and the relative contribution of the fraction variable, C_X^i/C_X. Thus, the major underlying assumption of Eq. (6.6) is that all fraction variables X^i are chemically and physically identical. This in turn means that there is no preference for any fraction variable X^i by any (physical or biochemical) process. Equation (6.6) yields the basis for the application of TBNT in this thesis.

6.1.1.1 The treatment of diffusion

In previous studies (e.g., Ménesguen and Hoch, 1997; Ménesguen et al., 2006; Radtke, 2012; Radtke et al., 2012), the above mentioned major assumption is applied to convective/advective transport and biochemical processes, however, not to diffusive transport.

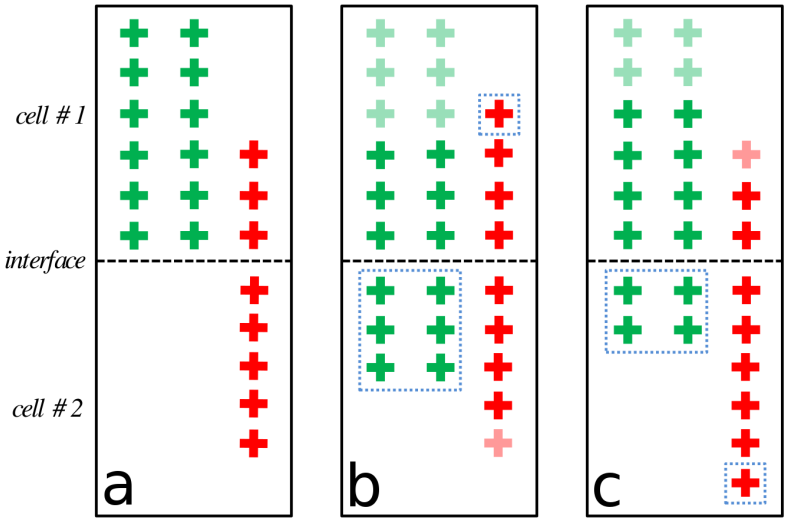

Figure 6.1: Schematic representation of the difference between the treatment of diffusion within the traditional TBNT approach (Ménesguen and Hoch, 1997) and the adapted approach used in this study. The panels show the distribution of two fraction variables of the same species (red/green crosses) at (a) initial state and after instantaneous mixing according to (b) the traditional and (c) the adapted approach. Light-coloured crosses represent the original location of particles which have been diffusively transferred to their target location (blue dotted boxes).

In contrast, these studies calculated an individual diffusive transport for each fraction variable X^i according to Fick's first law:

$$\vec{J}_X^i = \nabla \cdot \left(\overline{\overline{d}} \nabla C_X^i \right), \tag{6.7}$$

with $\vec{J}_X^i$ representing the 3D diffusive net transport. In case of different spatial gradients in C_X and C_X^i, this results in a diffusive transport flux for X^i different from that described by the diffusion term in Eq. (6.6) and, consequently, in different distributions of the fraction variables. Equation (6.7) furthermore implies that the different fraction variables X^i of the same bulk species (e.g., NO_3^- from Rhine and NO_3^- from Elbe) are chemically and/or physically different, i.e., their virtual discriminability implies chemical disparity.

Figure 6.1 illustrates the difference between the two assumptions starting from the same initial distribution (Fig. 6.1a) of two fraction variables of the same species (red and green crosses) in two adjacent water bodies of the same volume. In both cases, the *net* diffusive transport equals five particles from *cell #1* to *cell #2*, i.e., the diffusive net transports of the bulk variable (crosses) are identical. However, according to the traditional approach (Fig. 6.1b; blue dotted boxes) six green particles are transported from *cell #1* to *cell #2* and one red particle is transported from *cell #2* to *cell #1*, while following the approach of this study (Fig. 6.1c; blue dotted boxes) four green and one red

particle are transported from *cell #1* to *cell #2*. Thus, for each spatial dimension the traditional approach results in a bidirectional diffusive transport driven by the distribution of the individual variable fractions (in the case of opposing concentration gradients in the different fraction variables), while the new approach results in a unidirectional diffusive transport in the direction of the concentration gradient of the bulk variable.

As (one-dimensional) diffusion in principle is a bidirectional process, the traditional approach intuitively appears to be exact, while the new approach does not. However, it has to be kept in mind that (1) all fraction variables are of the same species (i.e., chemically and physically identical) and only distinguishable by the 'imaginary' label, and (2) that Fick's first law only provides the diffusive *net* transport which implies that there is no knowledge about the two diffusive gross transports contributing to this net transport. For the example in Fig. 6.1a this means that – considering aspect (1) as valid – aspect (2) allows for any final distribution of the particles of the two fraction variables as long as the diffusive net transport is equal to five particles transported from *cell #1* to *cell #2* and as long as the number of particles (colour-independent) in both cells is balanced. This implies that none of the two different assumptions on the diffusive transport – traditional vs. new approach – does necessarily lead to the actual diffusive gross transports, which are not known. Although the two different approaches result in different distributions of the fraction variables, it should be noted that the differences are expected to be generally small and that noticeable differences may only occur in the case of large differences in the spatial gradients of the fraction and bulk variables, i.e., $|\nabla C_X^i| \gg |\nabla C_X|$ or $|\nabla C_X^i| \ll |\nabla C_X|$.

6.1.2 Application to a numerical biogeochemical model

Equation (6.6) describes the convection-diffusion equation for the concentration of a fraction variable, C_X^i, as it is used in this study, and which represents the basis for the application of TBNT in combination with a biogeochemical model. In order to apply TBNT to a numerical biogeochemical model with a discrete spatial grid and time step, Eq. (6.6) needs to be discretised as well. Additionally, the change in concentration according to Eq. (6.6) has to be transferred into a change in mass as the particles with property p_i are actually labelled. For a given volume $V = const.$ this change in mass reads as:

$$\frac{dM_X^i}{dt} = \frac{dC_X^i}{dt} \cdot V, \tag{6.8}$$

with M_X^i representing the mass of the fraction variable X^i. However, in the case of a model with a free surface – like ECOHAM – $V = const.$ does not apply to the grid cells in the surface layer. Therefore, the change in mass needs to be calculated for a known volume at a given point in time, $V_0 = V(t_0)$, and can afterwards be transferred into a change in

concentration relative to the new volume $V_1 = V(t_1)$. t_0 represents the starting time of the time step of length Δt and $t_1 = t_0 + \Delta t$ represents the ending time of the same time step.

Discretisation of Eq. (6.8) for a given ECOHAM time step $[t_0, t_0 + \Delta t]$ leads to:

$$\frac{\Delta M_X^i}{\Delta t} = \frac{\Delta C_X^i}{\Delta t} \cdot V(t_0). \tag{6.9}$$

According to Eqs. (6.1) and (6.6) the change in mass of a bulk X and fraction variable X^i is calculated as the sum of all transport processes, and source and sink processes. Thus, a model process must be mass-conservative and is either defined as the (physical) **exchange of mass** of a single state variable X between two adjacent grid cells, j and k, or as the (biochemical) **transformation of mass** between two state variables, X and Y, within a single grid cell j. For a certain fraction variable X^i this change in mass over the time step $[t_0, t_0 + \Delta t]$ reads as:

$$\frac{\Delta M_X^i}{\Delta t} = \sum_{n=1}^{N_{\text{ex}}} P_{\text{ex},\,n}^i(\Delta t) + \sum_{n=1}^{N_{\text{tr}}} P_{\text{tr},\,n}^i(\Delta t). \tag{6.10}$$

Here, N_{ex} and N_{tr} represent the numbers of the exchange processes P_{ex}^i and of the transformation processes P_{tr}^i, respectively. These processes on the fraction variable X^i can in principle be calculated as:

$$P_{\text{ex}}^i = P_{\text{ex}} \cdot \frac{M_X^i}{M_X}, \quad P_{\text{tr}}^i = P_{\text{tr}} \cdot \frac{M_X^i}{M_X}, \tag{6.11}$$

with P_{ex} and P_{tr} representing the corresponding bulk processes and the relative fraction $M_X^i/M_X = C_X^i/C_X$ (see Eq. (6.6)) for a known constant volume V. This relation between fraction and bulk process and the related fraction variables is illustrated in Fig. 6.2.

An **exchange process** $P_{\text{ex},\,X}$ reduces the mass of the transferred state variable X in the originating grid cell j and increases its mass in the target grid cell k by the process' value. Advective and diffusive transports are considered as exchange processes. For a time step of length Δt, the changes of mass of a bulk state variable, M_X, in two adjacent grid cells, j and k, due to an exchange process are calculated as:

$$\begin{aligned} M_X(t_0 + \Delta t, j) &= M_X(t_0, j) - P_{\text{ex},\,X}(\Delta t, I_{jk}), \\ M_X(t_0 + \Delta t, k) &= M_X(t_0, k) + P_{\text{ex},\,X}(\Delta t, I_{jk}). \end{aligned} \tag{6.12}$$

Here, M_X refers to the mass of the bulk state variable X being transferred from input grid cell j into output grid cell k. $P_{\text{ex},\,X}$ indicates the bulk exchange process at the interface I_{jk} between the two grid cells j and k.

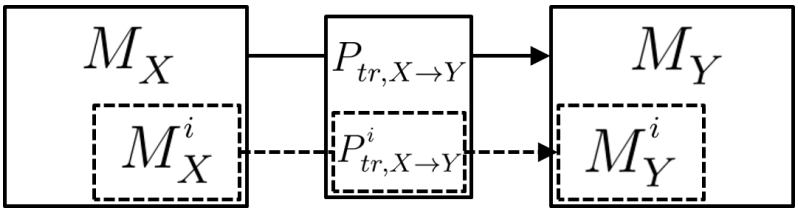

Figure 6.2: Schematic view of relation between model bulk state variables and transformation processes (e.g., NPP) and the corresponding fraction quantities according to the TBNT method. Subscripts indicate bulk quantities, superscript i refers to the corresponding fraction quantities. Process $P_{\mathrm{tr},\,X\to Y}$ transforms mass of state variable M_X into mass of M_Y. The fraction process $P^i_{\mathrm{tr},\,X\to Y}$ is defined as the product of the relative fraction M^i_X/M_X and the bulk process $P_{\mathrm{tr},\,X\to Y}$. Adapted from Wijsman et al. (2004, Appendix D).

A **transformation process** $P_{\mathrm{tr},\,X\to Y}$ reduces the mass of the input variable M_X and increases the mass of the output variable M_Y by its value. Thus, for a time step of length Δt the changes of masses of two bulk state variables, M_X and M_Y, due to a transformation process are calculated as:

$$\begin{aligned} M_X(t_0+\Delta t, j) &= M_X(t_0, j) - P_{\mathrm{tr},\,X\to Y}(\Delta t, j), \\ M_Y(t_0+\Delta t, j) &= M_Y(t_0, j) + P_{\mathrm{tr},\,X\to Y}(\Delta t, j). \end{aligned} \tag{6.13}$$

Here, M_X and M_Y refer to the mass of the bulk input state variable and the bulk output state variable, respectively. $P_{\mathrm{tr},\,X\to Y}$ indicates the bulk transformation process within the grid cell j. t_0 refers to the starting time of the time step of length Δt, i.e., $t_0+\Delta T$ indicates the end of the considered time step.

The definitions of the two types of bulk processes, Eqs. (6.12) and (6.13):, apply accordingly to fraction processes:

$$M^i_X(t_0+\Delta t, j) = M^i_X(t_0, j) - P^i_{\mathrm{ex},\,X}(\Delta t, I_{jk}), \tag{6.14}$$

$$M^i_X(t_0+\Delta t, k) = M^i_X(t_0, k) + P^i_{\mathrm{ex},\,X}(\Delta t, I_{jk}),$$

$$\begin{aligned} M^i_X(t_0+\Delta t, j) &= M^i_X(t_0, j) - P^i_{\mathrm{tr},\,X\to Y}(\Delta t, j), \\ M^i_Y(t_0+\Delta t, j) &= M^i_Y(t_0, j) + P^i_{\mathrm{tr},\,X\to Y}(\Delta t, j). \end{aligned} \tag{6.15}$$

In the first set of equations, Eq. (6.14), M^i_X indicates the mass of the fraction variable transferred from the originating cell j into the target cell k by the fraction exchange process $P^i_{\mathrm{ex},\,X}$. In the second set of equations, Eq. (6.15), M^i_X and M^i_Y refer to the masses of the input and output fraction variables of a transformation process $P^i_{\mathrm{tr},\,X\to Y}$.

Following Eq. (6.11), fraction transformation processes $P^i_{\mathrm{tr},\,X\to Y}$ are proportional to the relative amount R^i_X of mass of the input fraction variable M^i_X compared to the bulk mass

M_X at the beginning of the time step t_0 in the considered grid cell j and the value of the corresponding bulk process $P_{\mathrm{tr},\,X\to Y}$ for the time step Δt. Accordingly, fraction exchange processes $P^i_{\mathrm{ex},\,X}$ are proportional to the relative amount R^i_X of mass of the transferred fraction variable M^i_X compared to the bulk mass M_X at the beginning of the time step t_0 in the originating grid cell j and the value of the bulk process $P_{\mathrm{ex},\,X}$ at the interface I_{jk} between originating cell j and target cell k for the time step Δt. Thus, the two types of fraction processes are calculated as follows:

$$P^i_{\mathrm{ex},\,X}(\Delta t, I_{jk}) = R^i_X(t_0, j) \cdot P_{\mathrm{ex},\,X}(\Delta t, I_{jk}), \tag{6.16}$$

$$P^i_{\mathrm{tr},\,X\to Y}(\Delta t, j) = R^i_X(t_0, j) \cdot P_{\mathrm{tr},\,X\to Y}(\Delta t, j). \tag{6.17}$$

The relative fraction R^i_X is calculated as:

$$R^i_X(t_0, j) = \frac{M^i_X(t_0, j)}{M_X(t_0, j)}, \tag{6.18}$$

with j indicating either the originating grid cell in the case of an exchange process (Eq. (6.16)) or j indicating the grid cell in which the transformation takes place in the case of a transformation process (Eq. (6.17)).

By applying Eqs. (6.14)–(6.18) the fraction processes and state variables can be diagnostically calculated using the corresponding bulk processes and state variables. Technically speaking, an additional set of diagnostic differential equations is introduced for each labelled source and element meaning an increase in the number of model state variables and processes.

6.1.3 A model-independent software for trans-boundary nutrient transports

Existing TBNT studies (Wijsman et al., 2004; Blauw et al., 2006; Ménesguen et al., 2006; Lacroix et al., 2007; Neumann, 2007; Timmermann et al., 2010; Radtke et al., 2012; Troost et al., 2013; Perrot et al., 2014; Radtke and Maar, 2016) are based on the direct implementation of the TBNT method into the biogeochemical base model. That means, additions to the model code were required before being able to calculate TBNT within the model, and consequently, that each application of TBNT is completely model-dependent. In addition, the increasing number of model variables and processes causes an increase in memory usage and computation time. Radtke et al. (2012) circumvented the manual implementation using the so-called 'code generation tool' (`http://www.ergom.net/index.php/code-generation-tool.html`) to automatically generate a model code including labelled quantities. However, this software requires

model-dependent code templates and detailed abstracted descriptions of the processes represented in the base model.

The simple linear relation between fraction processes and state variables and their corresponding bulk quantities (see Eqs. (6.15)–(6.18)) allows for the calculation of fraction processes and state variables using a post-processing software. The only information needed is the initial distribution of the bulk state variables and the magnitude of the bulk processes as well as the input rates of the labelled state variables (e.g., daily rate of riverine NO_3^- input).

This study, for the first time, presents the implementation of the TBNT method as a post-processing approach. The advantage of this approach is that different setups of labelled sources can be applied to the same base model results, providing a flexible method to investigate the impact of different sources depending on the research question which has to be addressed.

6.1.3.1 Data requirements

The TBNT software developed and used during this thesis applies a one-dimensional (1D) indexing scheme, which means that, independent of the base model grid structure, all wet cells of the model domain are sorted into a 1D vector. This would allow for the application to different types of grids, including regular cubic grids as well as unstructured grids, however, it also makes the provision of a list of cell neighbours per grid cell as well as information about whether a cell is a surface or bottom cell inevitable. The software furthermore applies the simple variable-process relations given by Eqs. (6.15) and (6.14). Thus, information about the input and output state variables related to the different model processes is required. By providing this information the software is able to interpret and use the results of the base model.

Besides this model-related information the user has to provide information defining the TBNT setup, i.e., definition of source groups to be labelled including information about the source type (*river*, *atmospheric* or *open boundary*), number of sub-sources (e.g., in case of multiple rivers grouped together), locations of input. If required, so-called *target variables* and *areas* can be defined to obtain some aggregated information from the TBNT calculation. Target variables are defined as state variables which are not explicitly included in the base model but which can be calculated as the sum of existing model state variables (e.g., TN: sum of all N-containing state variables). Target areas are defined as certain sub-regions of the model domain and are described by the model grid cells (according to the 1D indexing) which have to be aggregated to the corresponding target area. Information on the relative fractions of the defined target variables will be produced for each target area.

In order to conduct a TBNT analysis with the described post-processing software, based on the ECOHAM model (see Sect. 3.2), the user has to provide the following information and data:

(a) general user information (mandatory):

- run identifier for TBNT calculation
- year of calculation
- time step on which base model results are stored
- time step on which TBNT calculation shall be conducted
- starting and ending time (of year) of the TBNT calculation
- switch if initialisation file shall be used for fraction variables
- selection of output to be created:
  - relative contributions of fraction variables (incl. output time step)
  - absolute fraction variables and processes (incl. output time step)
  - target variables and areas

(b) bulk process- and variable-related (mandatory):

- list of the names of all model bulk processes and related state variables containing the labelled element (e.g., N)
- data of all model bulk processes and related bulk state variables containing the labelled element

(c) grid-related (mandatory):

- list of indices of neighbours for each grid cell according to 1D indexing scheme
- list of indices of bottom and surface cells according to 1D indexing scheme
- list of all model rivers including name and indices of input cells according to 1D indexing scheme

(d) source-related (mandatory):

- list of all source groups, including names of sub-sources in case of riverine source groups
- list of grid cell indices of open boundaries and – in case of N labelling – atmospheric input

(e) fraction variable-related (optional):

- data of all relative contributions of all fraction variables

(f) target-related (optional):

- list of target variables including contributing model state variables
- list of grid cell indices for all target areas according to 1D indexing scheme

6.1.3.2 Calculation sequence and output

The user-defined input containing the above described information defines the general setup of the TBNT calculation, i.e., areas of interest, source groups etc. The internal sequence of the TBNT software is basically separated into three different phases: (1) initialisation, (2) calculation, and (3) finalisation. During the initialisation phase, the information provided by the user are read and the corresponding setup is generated. With respect to the source groups the software creates the source groups defined by the user, plus one additional group which collects all rivers entering the domain not assigned to any user-defined source group. This additional source group is called *untraced*.

The introduction of this additional source group is necessary as during the TBNT calculation each bulk variable is calculated as the sum of its corresponding fraction variables. Thus, in the likely case of not all rivers being labelled, riverine input of matter would be less than the actual input which would result in a mass deficit relative to the base model. This solution also allows for the labelling, e.g., of only one source, collecting all non-labelled sources in the *untraced* pool.

The additional source group is furthermore required for the generation of the initial distribution of the different fraction variables for the very first year of the TBNT calculation. For this year, only the distribution of the bulk state variables is known as no fraction variables have been put into the model domain. Therefore, the *untraced* source group is initialised with a relative contribution of 100 % within the entire model domain while all user-defined source groups are initialised with 0 %. Accordingly, the initial mass of the fraction variables of the *untraced* source group is identical to the mass of the bulk variables, masses of all other fraction variables are 0.

During the calculation phase, matter assigned to the different user-defined source groups is successively added to the input grid cells of each source group according to the related bulk process (e.g., riverine input, advective transport across open boundaries, atmospheric deposition). Thus, the relative contribution of these fraction variables increases which affects the related fraction processes. Consequently, the signal of a each source group introduced at its input locations propagates through the model domain depending on the advective and diffusive transport (see Eqs. (6.14) and (6.16)). During this propagation, this signal is transferred between fraction variables of different species of the same source group (see Eqs. (6.15) and (6.17)). At the open boundaries, fraction variables of all source groups (user-defined and *untraced*) may leave the model domain depending on their relative contribution and the cross-boundary transport. This guarantees mass conservation relative to the model.

During the calculation the selected output is written with the corresponding output time step, except for the target output which is written with a daily time step. Relative

contributions of all fraction variables are written as instantaneous values into a single file which can later be used as initialisation file for a subsequent TBNT calculation. For absolute fraction variables and processes an individual output file is created for each source group (including the *untraced* group) containing all fraction variables and processes of the corresponding source group. These individual files can then be used, e.g., to calculate mass balances of individual fraction variables etc. The files for the relative contributions and absolute fraction quantities are written in NetCDF (.nc; Unidata, 2016) format, while the target output is written as comma-separated values (.csv).

During the finalisation phase, the created output files are properly closed, and – more important – a mass conservation check is conducted comparing the sum of the masses of all fraction variables of each species (i.e., the calculated bulk variable) at the end of the TBNT calculation with the corresponding bulk mass read from the result file of the base model. By this, the TBNT software provides a quantitative proof that the software ran properly.

6.2 Setup of trans-boundary nutrient transports for the North Sea

In order to apply TBNT to the N cycle of the North Sea, a sub-domain of the ECOHAM model domain is defined in which the TBNT calculations are conducted. Figure 6.3 shows the ECOHAM domain including the boundaries of the TBNT sub-domain (black solid lines). For this study, different sources are defined, including rivers, adjacent seas and the atmosphere (i.e., atmospheric N deposition).

With respect to rivers, a total number of 254 rivers enters the ECOHAM domain, which reduces to 142 within the TBNT sub-domain. As this large number of individual sources would result in a dramatic increase in computation time, 74 of these 142 individual rivers are grouped to eight river groups in relation to the regional grouping by OSPAR (ICG-EMO, 2009; OSPAR, 2010; Los et al., 2014). These eight river groups include all the major North Sea tributaries, e.g., Elbe and Rhine. The untraced 68 smaller rivers are collected in a ninth river group (hereafter referred to as 'others' or 'other rivers'). As some rivers enter the model at the same grid location, the number of river locations in Fig. 6.3 is less than the total number of rivers.

Besides the nine river groups, three inflows from adjacent seas are defined, namely the North Atlantic (entering the North Sea across the northern shelf edge), the English Channel and the Baltic Sea. The inflows are defined by sections which also define the boundaries of the TBNT region (see Fig. 6.3, solid black lines). Finally, one atmospheric

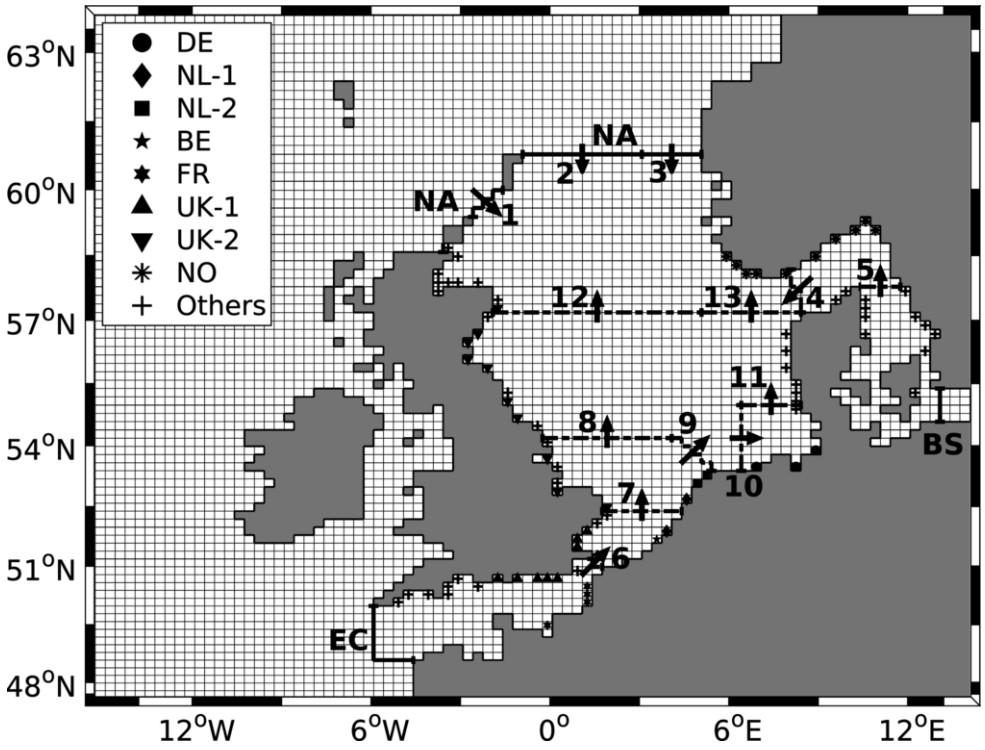

Figure 6.3: Model domain indicating sub-domain used for TBNT analysis, defined by three boundaries (solid black) North Atlantic (NA), English Channel (EC) and Baltic Sea (BS). Different markers indicate river input locations for German (DE), Dutch (NL-1/NL-2), Belgian (BE), French (FR), British (UK-1/UK-2), Norwegian (NO) and other rivers (compare Table 6.1). Dash-dotted lines mark sections #1 to #13 used for the validation of the model hydrodynamics, with arrows indicating the direction of positive net flow. Ticks mark start/end points of sections.

N source is included covering the entire TBNT sub-domain. Table 6.1 provides a list of the 13 source groups defined for the TBNT analysis, including abbreviations used in Fig. 6.3 and individual source group members (in case of rivers).

The TBNT analysis is conducted for the period 2000–2014 (analogous to Ch. 5) and the year 1999 is used for the spin-up of the labelled N variables. The TBNT software uses daily ECOHAM model output including all N-related state variables and processes for the entire model domain. A sensitivity study on the impact of the ECOHAM output time step on the TBNT results is presented in Appendix B. It demonstrates that the impact of the time step on the TBNT results is negligible, which gives confidence that applying TBNT as a post-processing software is feasible.

All labelled variables (except for the 'other rivers') are initialised with a relative contribution of 0 % to the corresponding bulk variables. The 'other rivers' are initialised with a relative contribution of 100 % within the entire TBNT sub-domain. It has to be noted,

that concerning the content there is a difference between the untraced other rivers and this initial distribution of untraced matter within the TBNT sub-domain, as the latter does not originate from these untraced rivers. However, this simplification is done for technical reasons as the former constitute the only sources contributing to the untraced state variables (and processes). Otherwise, an additional 'initial source' would be required which would be negligible after a sufficiently long spin-up, i.e., the overhead would be increased needlessly.

Table 6.1: List of source groups defined for the TBNT analysis, including abbreviations (used in Fig. 6.3 and in-text) and list of individual group members. River groups defined in relation to regional OSPAR river groups (ICG-EMO, 2009; OSPAR, 2010; Los et al., 2014).

source group	abbreviation	(number of) contributing sources
German rivers	DE	(3) Elbe, Weser, Ems
Dutch rivers (group 1)	NL-1	(3) Rhine, Meuse, North Sea Canal
Dutch rivers (group 2)	NL-2	(2) Lake Ijssel West, Lake Ijssel East
Belgian rivers	BE	(1) Scheldt
French rivers	FR	(4) Authie, Canche, Somme, Seine
British rivers (group 1)	UK-1	(22) Avon at Bournemouth, Frome, Itchen, Meon, Stour at Bournemouth, Test, Wallington, Yar (all entering Solent Strait), Adur, Arun, Cuckmere, Ouse at Newhaven, Waller's Haven (all entering Brighton Bay), Thames, Chelmer, Colne, Darent, Deben, Frome, Gipping, Holland Brook, Medway, Stour at Harwich
British rivers (group 2)	UK-2	(27) Babingley, Ouse at King's Lynn, Nene, Welland (all entering The Wash), North Esk, South Esk (both contributing to Esk at Montrose), Almond, Blyth, Dighty Water, Earn, Eden in Scotland, Eye Water, Esk at Edinburgh, Firth of Forth, Humber, Leven in Scotland, Tay, Tees, Tweed, Tyne,Tyne in Scotland, Wansbeck, Water of Leith, Wear, Yare, Ythan
Norwegian rivers	NO	(12) Bjerkreim, Drammen, Glomma, Kvina, Lygna, Mandal, Nidelva, Numedal, Otra, Sira, Skien, Tovdal
Other rivers	Others	(68) remaining smaller rivers: 6 Swedish, 25 Danish, 37 British
North Atlantic	NA	northern and northwestern North Sea boundary (see Fig. 6.3)
English Channel	EC	southwestern end of English Channel (see Fig. 6.3)
Baltic Sea	BS	Baltic Sea boundary (see Fig. 6.3)
Atmosphere	Atmosphere	surface layer of entire TBNT sub-domain

Starting from this initial distribution, the calculation for 1999 is repeated seven times, with iterations 2–7 using the final distributions of the labelled variables of the preceding iteration. The number of seven iterations was found to provide a quasi steady state, i.e., changes in the relative contributions between the final state of sixth and seventh spin-up iteration are negligible. This also gives confidence that the matter attributed to the untraced other rivers in fact originates from these rivers and does not constitute an artefact of the initial labelled variable distribution. The final state of the seventh spin-up

calculation is then used as the initialisation of the TBNT calculation from 2000 to 2014.

This spin-up method was also compared against a different spin-up within which a continuous sequence of seven years (1999–2005) was calculated in order to ensure that the spin-up does not affect the results of the TBNT analysis. The results of the 7-fold calculation of year 2005 yielded qualitatively same results as the 7-year-spin-up run over 1999–2005, with respect to the spatial distribution of the relative variable fractions at the end of the spin-up (not shown).

The TBNT software generates annual files with daily values of the relative contributions of the different sources to the bulk state variables and of the absolute fraction variables and processes related to the individual source groups for the entire TBNT sub-domain (hereafter only 'TBNT domain'). This daily output is subsequently used for the analysis.

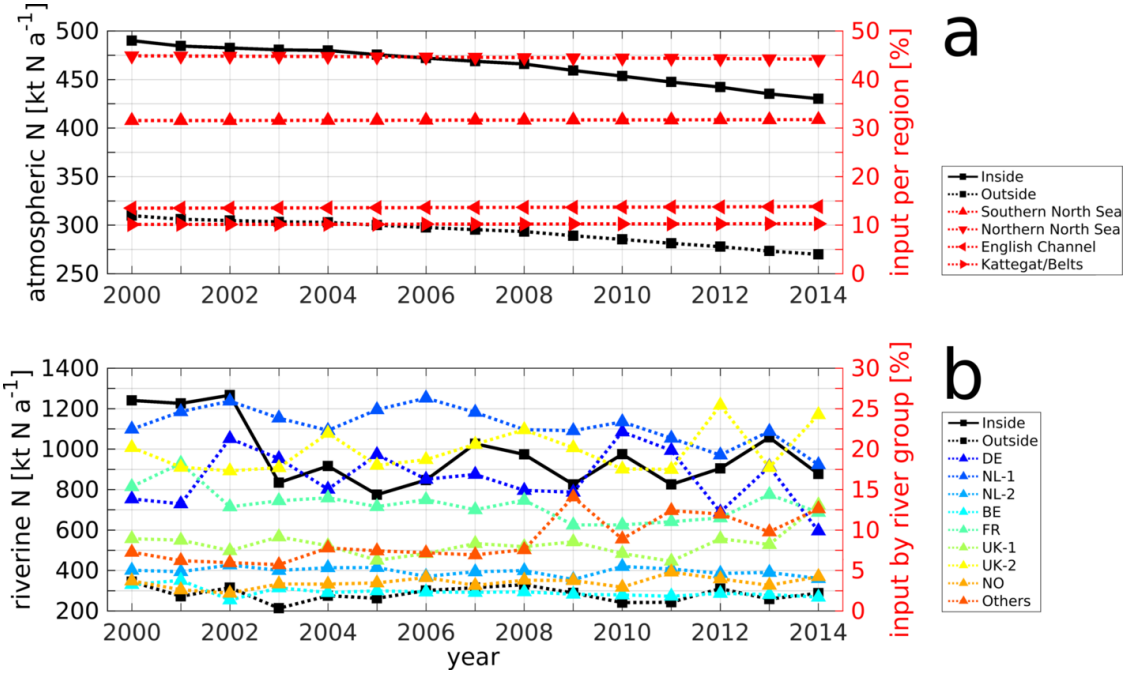

Figure 6.4: Time series of annual (a) atmospheric and (b) riverine TN (black y axes) input into model domain, inside (solid black) and outside (dotted black) the TBNT domain (see Fig. 6.3). Relative contributions (red y axes and coloured dotted lines) represent the share of total input into the TBNT domain by different regions in case of atmospheric deposition and by different river groups (see Table 6.1) in case of riverine input.

In order to give insight in the actual atmospheric and riverine TN loads during the period of analysis Fig. 6.4a and b show time series of annual atmospheric and riverine TN input, respectively, into the model domain. In both cases, the input is separated into total input inside the TBNT domain (solid black) and outside the TBNT domain (dashed black; see Fig. 6.3 for domain boundaries). The black y axes in both panels refer to the

absolute TN input (in $\mathrm{kt\,N\,a^{-1}}$). The red y axes in Fig. 6.4a refer to the contributions of the atmospheric input into different subregions of the TBNT domain, relative to the total input into the TBNT domain: southern North Sea (▲; area of $1.7 \cdot 10^5\,\mathrm{km^2}$), northern North Sea (▼; $3.8 \cdot 10^5\,\mathrm{km^2}$), English Channel (◀; $0.9 \cdot 10^5\,\mathrm{km^2}$) and Kattegat/Belts (▶; $0.5 \cdot 10^5\,\mathrm{km^2}$). The southern North Sea represents the North Sea region south of 56 °N until transport section #6 in the Strait of Dover. The northern North Sea represents the part of the TBNT domain north of 56 °N including the Skagerrak north of the transport section #5 (see Fig. 6.3). The English Channel is the region between the EC boundary of the TBNT domain and transport section #6, while the Kattegat/Belts region is that between the BS boundary and transport section #5. The total area of the TBNT domain is $6.9 \cdot 10^5\,\mathrm{km^2}$ compared to $13.2 \cdot 10^5\,\mathrm{km^2}$ of the areas outside the TBNT domain.

Figure 6.4a shows that the atmospheric input into the TBNT domain is about 1.6 times higher than that outside the TBNT domain, despite its almost 50 % smaller area. This relates to the fact that atmospheric deposition is highest near the continental coast. The annual absolute input (black lines) into both parts of the model domain shows a decrease during the period 2000–2014, with a similar relative change of about 13 % as a result of the preparation of the atmospheric deposition data (see Sect. 3.2.2.1). The input into the TBNT domain is $490\,\mathrm{kt\,N\,a^{-1}}$ in 2000 and stays around $485\,\mathrm{kt\,N\,a^{-1}}$ during 2001–2004. From 2005 on, it shows a steady decrease until 2014 when atmospheric deposition reaches $430\,\mathrm{kt\,N\,a^{-1}}$.

The relative contribution of the absolute atmospheric TN input into the different subregions of the TBNT domain (red lines) is very stable throughout 2000–2014. The largest part of about 44.7 % of atmospheric input is deposited in the northern North Sea. About 31.6 % enter the southern North Sea, which is less than half as large as the northern North Sea region. Considering that the spatial extent of southern North Sea area is less than half of that of the northern North Sea, this emphasises the remarkable spatial differences in atmospheric N deposition, with its largest values near the continental coast. The relative contributions to the English Channel region and the Kattegat/Belts are about 13.6 % and 10.1 %, respectively.

The absolute annual riverine TN input into the TBNT domain (Fig. 6.4b; black solid line) ranges between $775\,\mathrm{kt\,N\,a^{-1}}$ in 2005 and $1266\,\mathrm{kt\,N\,a^{-1}}$ in 2002. A clear decrease can be seen from 2002 to 2003, with consistently lower levels of riverine TN input until 2014. The riverine TN input into the regions outside the TBNT domain (black dotted line) is significantly lower with values between $213\,\mathrm{kt\,N\,a^{-1}}$ and $344\,\mathrm{kt\,N\,a^{-1}}$. The relative contributions of the different river groups to the riverine TN input into the TBNT domain (coloured dotted lines) show that the NL-1 rivers (blue line; incl. Rhine and Meuse; see Table 6.1) are the largest source of TN during most years (excl. 2012 and 2014) with

values between 18.1 % and 26.3 %. The UK-2 rivers (yellow line), located at the British east coast, are of similar importance ranging between 17.3 % and 25.4 %. The DE rivers (dark blue line) constitute the third strongest source during most years with contributions of 9.9 % to 22.1 %. The FR rivers (cyan line) contribute 10.6 % to 18.2 %. The UK-1 (green line) and 'Others' rivers (red line) show values between 6.1 %–13.1 % and 5.7 %–14.1 %, respectively, with higher values in the period after 2008 compared to the earlier period. This indicates that the relative importance of the different rivers on the North Sea system changed during this period. The remaining rivers (NL-2, BE and NO) are less important and contribute 3.9 %–5.7 %, 1.4 %–3.8 % and 2.2 %–4.8 %, respectively.

An interesting feature can be seen for the DE rivers which show high relative contributions in 2002 and 2010 (21.3 % and 22.1 %, respectively). The former value relates to the flood in central Europe in August 2002 (e.g., Ulbrich et al., 2003). In late summer 2010, events of heavy rainfall in the catchment area of Elbe tributaries (e.g., Philipp et al., 2015) resulted in high freshwater discharge (Kienzler et al., 2015) and thus TN input.

6.3 General circulation and volume transports as simulated by HAMSOM

The advective transport of substances, like nutrients, is mainly responsible for their spatial dispersal. Therefore, the reasonable representation of the North Sea general circulation is a prerequisite for a meaningful TBNT analysis. For this reason, this section first provides an overview of the general circulation of the North Sea during 2000–2014 as simulated by HAMSOM. Subsequently, water volume transports across certain sections (see Fig. 6.3, sections #1 to #13) are compared against literature values, providing more detailed information about the model quality.

6.3.1 General circulation

In order to provide a broad overview of the general circulation of the North Sea as simulated by HAMSOM, Fig. 6.5 shows the streamlines (e.g., Stommel, 1948) for the period 2000–2014 derived from 15-year, depth-integrated averages of simulated daily horizontal velocity fields. For better comparability to the current patterns described by Turrell et al. (1992, see Fig. 2.1), Fig. 6.5a shows the streamlines integrated over the entire water depth. Figure 6.5b and c present the streamlines for the near-surface (upper 20 m) and deeper layers (20 m to bottom), respectively, to provide insight in the differences between near-surface currents, strongly affected by wind, and the deeper layers.

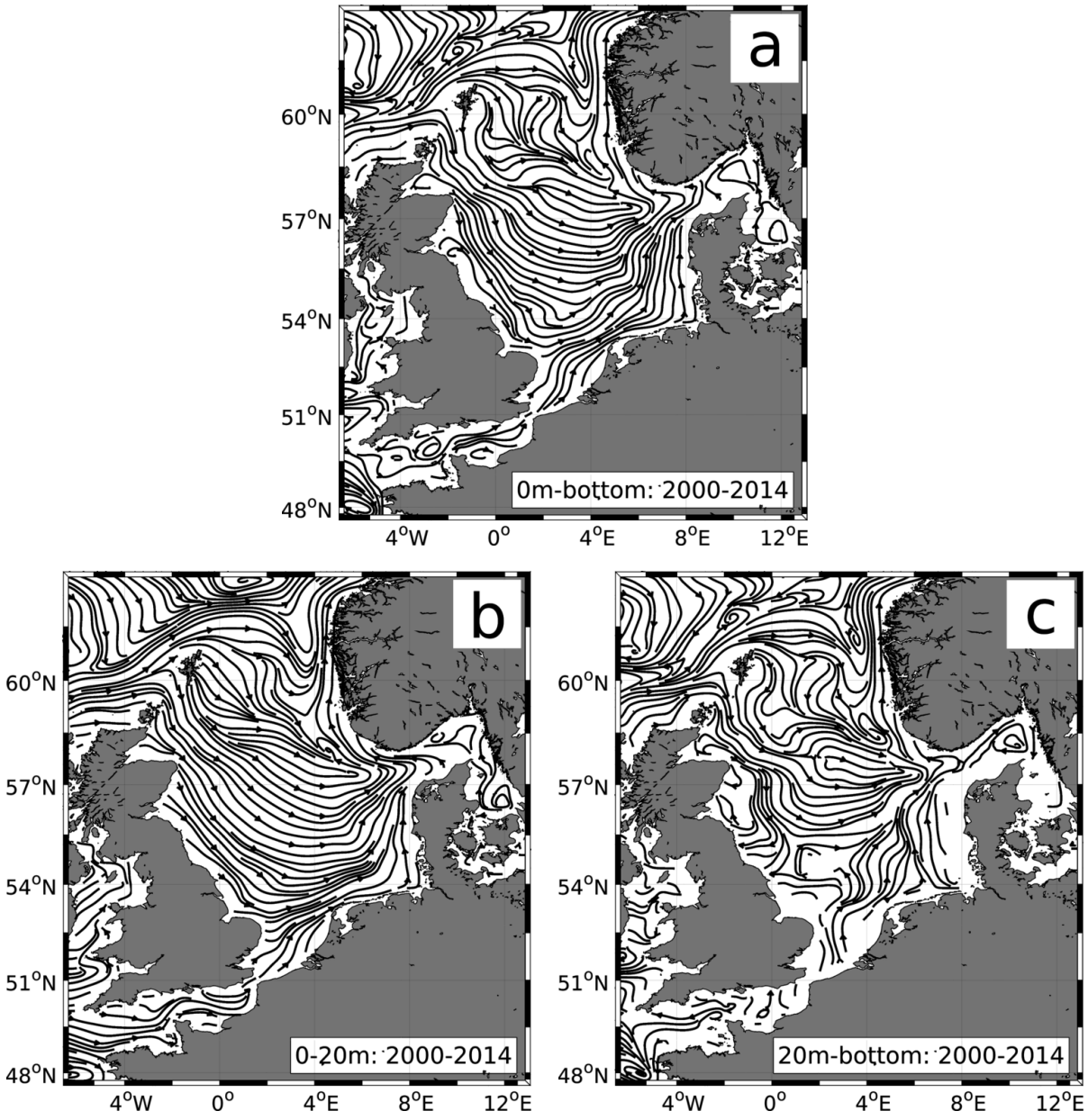

Figure 6.5: Streamline maps for the period 2000–2014 derived from 15-year, depth-integrated averages of daily horizontal velocity fields simulated by HAMSOM: (a) surface to bottom, (b) surface to 20 m and (c) 20 m to bottom.

Figure 6.5a shows that HAMSOM reproduces well the main features of North Sea general circulation. Around the Shetland and Orkney Islands, parts of the North Atlantic Current branch in southward direction and mainly enter the North Sea as the Fair Isle Current between Orkney and Shetland Islands and east of Shetland. Most of the currents entering the North Sea in the West flow southward along the British east coast until about

58 °N. There, parts of the current turn east toward the central northern North Sea (Dooley Current), while the other part continues southward. The currents entering the North Sea directly east of the Shetlands are mainly recirculated in the northern North Sea between 58 °N and 60 °N, however, partly reach latitudes around 57 °N. North Atlantic water entering the North Sea at about 2.5 °E–3 °E flows further south, but strongly interacts with the northward outflow along the Norwegian west coast, indicated by the curvy and interrupted streamlines in this region.

The southward flowing water at the British east coast branches again at around 55 °N–56 °N. In this region, the shallow Dogger Bank causes the offshore part of the southward flow to turn east/southeast entering the central North Sea (Kröncke and Knust, 1995; Lenhart and Pohlmann, 1997), while the other part continues further south. The eastward flow extends to about 54.5 °N and turns north at about 5 °E. The southward branch is recirculated at about 53 °N–54 °N, turning east/northeast and finally flowing north at about 6 °N. South of Norway, both branches first turn east entering the western Skagerrak, where they are recirculated joining the northwestward flow of the Norwegian coastal current.

South of the southern branch (in the Southern Bight), the English Channel inflow through the Strait of Dover can be seen. It continues as the continental coastal current additionally fed by the freshwater discharge from the continental rivers (e.g., Rhine and Meuse). In the simulation this current is clearly separated from the previously described southern branch in the central North Sea, indicated by the intermittent streamlines between the two eastward currents. In the German Bight, the current turns north following the Danish west coast. At the northern tip of Denmark the simulated turns east, entering the Skagerrak where it is recirculated and subsequently joins the Norwegian coastal current, which transports the water masses northward across the northern shelf edge finally joining the North Atlantic Current.

In summary, the 15-year-climatologic currents simulated by HAMSOM represent very well the general North Sea circulation described in Sect. 2.1. Minor deviations can be seen in the Skagerrak region, where the simulated recirculation of northwestward currents occurs slightly farther west. However, the intermittent and curvy streamlines indicate the recirculating currents and interaction between Baltic inflow and eastward flowing water coming from the North Sea.

As HAMSOM reproduces well the water column integrated general circulation of the North Sea, Fig. 6.5b and c show the near-surface (upper 20 m) and deeper layer (20 m to bottom) streamlines, respectively. By this a more differentiated view on the surface and sub-surface currents of the North Sea is provided. The near-surface circulation is strongly affected by wind-driven currents (Lee, 1980), and less influenced by topographic

features such as the Dogger Bank. Consequently, the picture provided for the near-surface circulation of the North Sea (Fig. 6.5a) partly differs from that for the entire water column. Especially in the central and southern North Sea, near-surface currents originating from the Fair Isle Channel propagate further south until 54 °N. In the central North Sea, near-surface currents propagate farther east resulting in a recirculation in the Skagerrak which is also located farther east than that recirculation area of the water column integrated currents.

In some regions, Fig. 6.5c reveals some remarkable differences between the circulation below 20 m depth compared to the water column integrated and near-surface currents. While in the northern North Sea, the current patterns basically represent the patterns visible in Fig. 6.5a, the influence of the Dogger Bank on the deeper layer circulation is illustrated by the diverging streamlines. One branch turns east towards the central North Sea, whereas a second branch turns west towards the British coast. In the Southern Bight south of Dogger Bank, the deeper layer circulation is dominated by the inflow from the English Channel and the bathymetry, visible in the firstly northward flow turning northeast at about 53.5 °N. A smaller part of the simulated currents in this area turns west towards the British coast..

The comparison of near-surface and deeper layer currents along the continental coast between Belgium and Denmark shows that the continental coastal current is mainly confined to the shallow near-shore areas. The northward flow in the deeper layers occurs further west in the central southern North Sea (at about 3 °E–5 °E), indicated by the continuous streamlines in this region.

6.3.2 Volume transports

The streamline maps demonstrate that, qualitatively, HAMSOM reproduces very well the main features of the general circulation of the North Sea. However, for a more quantitative validation of the model performance in relation to horizontal advective transports, it is necessary to consider volume transports into and within the North Sea. For this purpose, certain sections at the North Sea boundaries (northern shelf edge, English Channel and Baltic Sea) as well as in its interior are defined and compared against literature values. The thirteen defined sections are indicated in Fig. 6.3 (arrows indicate direction of positive net flow). Some sections are defined in relation to the work by Winther and Johannessen (2006), others according to the North West Shelf Operational Oceanographic System (NOOS) framework (`http://www.noos.cc/`; Dick, 2013). A subset of these NOOS sections is selected in relation to the work by Ozer (2011). Winther and Johannessen (2006) conducted simulations of the North Sea using a hydrodynamical model and focusing on the in- and outflow into and out of the North Sea across its different outer boundaries.

Ozer (2011) performed a model intercomparison of three operational hydrodynamic models with respect to the general circulation of the interior North Sea for the year 2008. For a more detailed description of the different models, the reader is referred to Winther and Johannessen (2006) and Ozer (2011), respectively. For better comparability, transports across the sections used by Ozer (2011) are calculated for year 2008 only, while transports across the other sections represent statistics over the 15-year period 2000–2014. The comparison of the calculated transports is presented in Table 6.2. The observation data provided in this table were compiled by Winther and Johannessen (2006) and originate from Otto et al. (1990), Rodhe (1996), Rydberg et al. (1996) and Danielssen et al. (1997).

Table 6.2: Volume transports across defined sections (see Fig. 6.3) derived from HAMSOM (mean, minimum and maximum over entire period 2000–2014), compared to values from Winther and Johannessen (2006) and Ozer (2011). Observed literature values compiled by Winther and Johannessen (2006) originate from Otto et al. (1990), Rodhe (1996), Rydberg et al. (1996) and Danielssen et al. (1997). Parentheses in first column indicate how transport is calculated: 'in'/'out' = gross in-/outflow, 'net' = net flow. All values in Sverdrup ($1\,\mathrm{Sv} = 10^6\,\mathrm{m^3\,s^{-1}}$).

section number (flow)	analysis period	this study HAMSOM mean	this study HAMSOM min/max	Winther and Johannessen (2006) model mean	Winther and Johannessen (2006) model min/max	Winther and Johannessen (2006) observation (literature)	Ozer (2011) range of model averages (three different models)
#1 (in)	2000–2014	0.54	$2 \cdot 10^{-5}$/2.66	0.49	0.01/2.36	0.30	–
#2 (in)	2000–2014	1.20	0.14/4.08	0.50	0.02/2.04	0.60	–
#3 (in)	2000–2014	0.41	$9 \cdot 10^{-5}$/3.14	1.23	0.18/2.91	0.70 – 1.11	–
#3 (out)	2000–2014	2.07	0.08/7.00	2.33	0.67/5.73	1.80	–
#4 (in)	2000–2014	0.58	0.08/1.91	1.02	0.44/2.54	0.50 – 1.50	–
#4 (out)	2000–2014	0.56	0.11/2.00	1.04	0.42/2.50	0.50 – 1.50	–
#5 (net)	2000–2014	0.012	−0.46/0.39	0.014	–/–	0.015	–
#6 (in)	2000–2014	0.14	$3 \cdot 10^{-5}$/0.87	0.16	0.00/1.03	0.10 – 0.17	–
#6 (net)	2008	0.09	−0.34/0.71	–	–/–	–	0.080 – 0.121
#7 (net)	2008	0.10	−0.37/0.71	–	–/–	–	0.063 – 0.095
#8 (net)	2008	−0.08	−1.61/0.84	–	–/–	–	−0.085 – −0.027
#9 (net)	2008	0.18	−0.35/1.26	–	–/–	–	0.163 – 0.207
#10 (net)	2008	0.09	−0.28/0.80	–	–/–	–	0.127 – 0.130
#11 (net)	2008	0.09	−0.20/0.78	–	–/–	–	0.105 – 0.122
#12 (net)	2008	−0.43	−4.37/1.56	–	–/–	–	−0.470 – −0.337
#13 (net)	2008	0.53	−0.78/2.92	–	–/–	–	0.362 – 0.421

The comparison of the gross inflow from the North Atlantic into the North Sea across the northern shelf edge (Table 6.2, sections #1, #2 and #3) shows that HAMSOM reproduces well the overall inflow through the three sections. Average gross inflow of the three sections as simulated by HAMSOM adds up to 2.15 Sv which is comparable to the results of Winther and Johannessen (2006) yielding 2.22 Sv and close to the upper range of the observations (1.60 Sv–2.01 Sv). It can be seen that the relative contribution of the inflow through sections #2 and #3 is opposite to that in Winther and Johannessen (2006), which may

partly relate to a different location of the separation point between the two sections (exact position of that in Winther and Johannessen (2006) not known). However, the literature values show a similar tendency as the results by Winther and Johannessen (2006) which suggests that in HAMSOM the inflow of Atlantic water across the northern shelf edge extends further east than it does in reality. Besides this, the simulated minimum and maximum inflow indicate higher variability in the HAMSOM compared to Winther and Johannessen (2006), which most likely relates to the different and significantly longer simulation period of this study. Regarding the outflow in the Norwegian Trench area (section #3), HAMSOM also shows good agreement with the simulations by Winther and Johannessen (2006) and observations.

In the Skagerrak region (section #4), HAMSOM shows consistently lower values than the simulations by Winther and Johannessen (2006) for both, inflow and outflow, however, is still within the observed range of 0.50 Sv–1.50 Sv. The net inflow through section #5 (Kattegat) is in very good agreement with the simulation by Winther and Johannessen (2006) and observations. The same applies to the gross inflow through the English Channel (section #6). The average net inflow through that section in 2008 is also in good agreement with the simulations results of Ozer (2011).

The net transport through section #7, located in the Southern Bight, is only slightly above the range found by Ozer (2011). This may relate to differences in the river forcing, as two major tributaries, Rhine and Meuse, enter the model domain in this region (see Fig. 6.3 and Table 6.1, river group NL-1). For sections #8 and #9 at the northern and northeastern end of the Southern Bight, the net transports are in very good agreement with Ozer (2011), being well in the range simulated by their models. The negative net flow through section #8 implies southward flow in the western part of the southern North Sea, while in the eastern part (section #9) the northwestward coastal current driven by the English Channel inflow and riverine freshwater discharge represents the dominant feature (see also Fig. 6.5). For the net inflow into and outflow out of the German Bight (sections #10 and #11, respectively), HAMSOM yields values of about 0.09 Sv, which are slightly below the range provided by Ozer (2011). This likely relates to the model bathymetry resulting in a northward turn of parts of the currents in the southern North Sea before entering the German Bight (see Fig. 6.5a and c).

The negative net flow across section #12 in the western central North Sea simulated by HAMSOM also indicates the mainly southward flow in this region driven by the North Atlantic inflow in the North, and the average value of -0.43 is well in the range found by Ozer (2011). In the eastern central North Sea (section #13), the positive net flow derived from HAMSOM represents the generally northward flow in this region, however, is slightly above the range simulated by other models (Ozer, 2011). This may relate to a lower inflow

through the Skagerrak (section #4) as indicated by the comparison to observations and the simulations by Winther and Johannessen (2006), though, it cannot be confirmed as simulated transport values through the Skagerrak section are not available for the models used by Ozer (2011).

In summary, despite some minor differences, HAMSOM shows generally good agreement with the results of other hydrodynamical North Sea models and observed inflows across the outer boundaries of the North Sea. The same applies to the interior North Sea, where it is in generally good agreement with other models. Thus, the transport fields simulated by HAMSOM provide a reliable basis for the TBNT analysis of N in the North Sea.

6.4 The influence of nitrogen from different sources on the North Sea

As this thesis focuses on the influence of N from rivers and other external sources (adjacent seas and the atmosphere) on the North Sea O_2 dynamics, this section provides insight in the spatial and temporal patterns of N-related quantities and processes in the North Sea with a special focus on the ODZ site in the eastern central North Sea (see Fig. 5.11a, box #1). More specifically, results for TN, NPP and pelagic and benthic detrital matter are presented. Whenever the term 'contribution' of a certain source is used, this refers to the contribution of N input from the corresponding sources to the considered quantity or process.

6.4.1 Spatial distribution of total nitrogen

In order to provide insight in the influence of N on different North Sea regions in general and of selected sources in particular, first, Fig. 6.6a and b show the annually and vertically averaged (over entire water column end sediment) concentration of overall ('bulk') TN for the years 2002 and 2010, respectively. The years 2002 and 2010 are selected in relation to the analysis of the O_2 dynamics in Sect. 5.2.5. Second, Fig. 6.7 shows the corresponding average relative contributions of selected sources to these TN concentrations. The sources are selected in relation to their relative contribution in the vicinity of the ODZ study site described in Sect. 5.2.5 (see also Fig. 6.6, boxes). Only the five most important sources are presented, namely the North Atlantic (NA), the atmosphere, the first group of Dutch rivers (NL-1), the German rivers (DE) and the second group British rivers (UK-2; along the British east coast).

Daily bulk TN for a single model grid cell is calculated as the sum of all N-containing

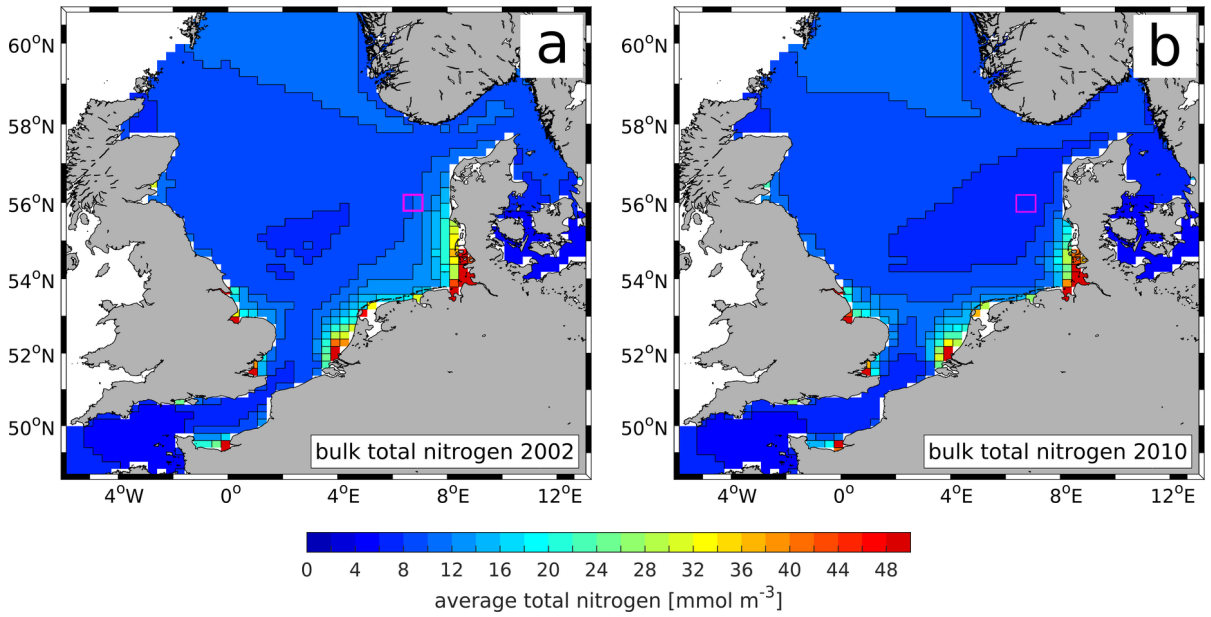

Figure 6.6: Spatial distributions of annually and vertically averaged TN concentration simulated by ECOHAM for (a) 2002 and (b) 2010. Colour scale cut at upper end. Boxes indicate the ODZ study site (see Fig. 5.11a, box #1).

(pelagic and benthic) model state variables, i.e., it includes N bound in inorganic nutrients (NO_3^- and NH_4^+) as well as in organic matter, based on daily model output. The vertically averaged daily TN concentration is calculated as the water column integrated mass of TN divided by the water column volume. Consequently, the annual average concentration is calculated as the average of these daily average water column TN concentrations. The relative contributions of the individual sources (NA, atmosphere, NL-1, DE and UK-2) to TN are calculated as the annually integrated amount of TN from the individual sources divided by the annually integrated amount of bulk TN. As TN includes all N state variables, the annual cycle of organic and inorganic N does not affect the annually averaged TN concentration. Therefore, it provides a good insight in the dispersal of N from different sources within the North Sea, similar to a passive tracer. However, it has to be noted that that part of TN temporarily stored in the sediment is not affected by advection. In addition, atmospheric N deposition affects local TN concentrations as well as REM_{sed} does due to the release of molecular N_2.

The spatial distributions of bulk TN in 2002 and 2010 (Fig. 6.6a and b, respectively; colour scale cut at 50 mmol N m^{-3}) basically show the same spatial patterns. Bulk TN concentrations are low in the central North Sea between 54 °N and 56 °N, east of about 1 °E, yielding minimum concentrations of 7.6 mmol N m^{-3} directly north of the Dogger Bank in

2002. In 2010, minimum TN concentrations of 6.8 mmol N m^{-3} occur a bit southwest of the North Sea ODZ (boxes in Fig. 6.6). In both years, lower concentrations below 5 mmol N m^{-3} only occur in the Belts and in the western English Channel, which are not in the focus of this analysis.

Lowest values occur in the central North Sea in both years. In the northern North Sea values of up to 12 mmol N m^{-3} are present in the region between the Shetlands and Norway. In the coastal regions, TN concentrations are significantly higher than in the offshore regions of the North Sea, showing local maxima at the mouths of major tributaries (e.g., Thames, Rhine and Elbe). Especially around the Rhine/Meuse and Elbe mouths, TN concentrations are significantly elevated. Overall maximum concentrations of 224 mmol N m^{-3} and 215 mmol N m^{-3} are reached at the Elbe mouth in 2002 and 2010, respectively.

Besides these similarities, some distinct differences between TN in 2002 and 2010 can be seen, especially in the southern North Sea. In 2002 (Fig. 6.6a), a band of higher TN concentrations (>12 mmol N m^{-3}) of about 1 ° width follows the continental coastal current, starting from the mouth of Rhine and Meuse up to the northern tip of Denmark. In the area of the ODZ west of Denmark (boxes in Fig. 6.6), TN concentrations in 2002 are almost 50 % higher than in 2010, yielding about 9.5 mmol N m^{-3}–10.5 mmol N m^{-3} compared to 6.9 mmol N m^{-3}–2 mmol N m^{-3} in 2010. In combination with the coastal band of elevated TN concentrations, which extends up to this latitude in 2002, this suggests that the N input from the large continental tributaries (NL-1 and DE rivers) controls the amount of TN in that region.

In order to evaluate this image, Fig. 6.7 shows the spatial distribution of the average relative contributions to TN from the different sources: (a, b) NA, (c, d) atmosphere, (e, f) NL-1 rivers, (g, h) DE rivers and (i, j) UK-2 rivers. Figure 6.7a and b clearly show that the input of N from the North Atlantic dominates the entire northern and most parts of the central North Sea. Its influence is reduced remarkably in the southern North Sea (<50 %), however, still reaches values of up to 25 % in some coastal areas, e.g., at 54 °N, 7 °E in 2002. This spatial distribution of TN from the NA represents very well the current patterns previously shown (Fig. 6.5), as its southernmost extent occurs near the British east coast. In the East, the recirculation limits the southward extension.

With respect to the contribution of the NA to TN in the 2002 ODZ, it can be seen that the relative contribution in 2002 is slightly higher (about 35 %–40 %) than in 2010 (25 %–35 %). The same applies to the southeastern North Sea, where the influence of NA in 2002 is about 10 % higher than in 2010. The southern North Sea is less affected by the North Atlantic inflow. Here, it can be seen that atmospheric N deposition (Fig. 6.7c and d) accounts for 10 %–15 % of the overall amount of TN in most parts of the southern

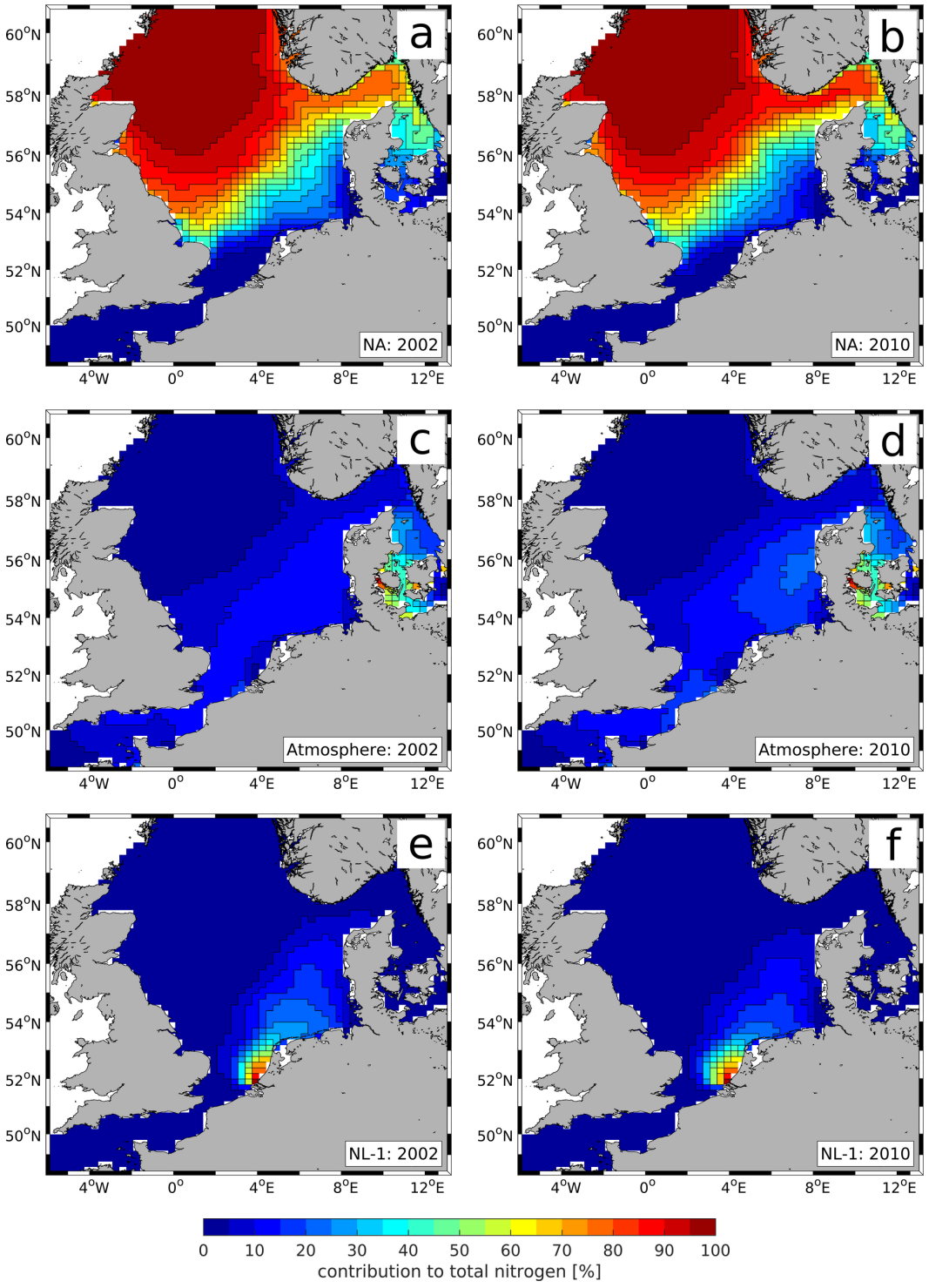

Figure 6.7: Spatial distributions of annual average relative contributions of different N sources to water column integrated TN for (a, c, d) 2002 and (b, d, f) 2010. Sources: (a, b) North Atlantic (NA), (c, d) atmosphere, (e, f) 1st group of Dutch rivers (NL-1). Same scale for all panels.

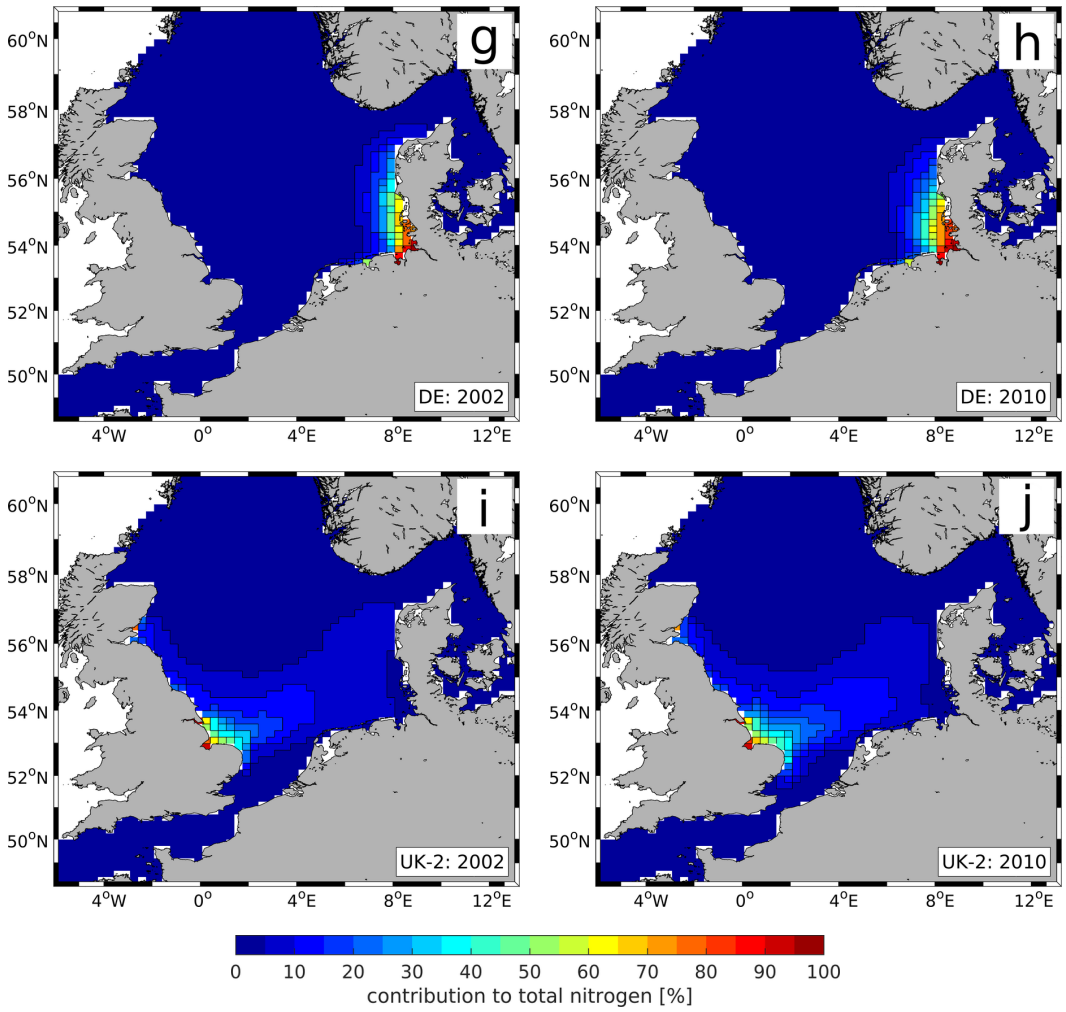

Continued: (g, h) German rivers (DE) and (i, j) 2nd group of British rivers (UK-2) in (g, i) 2002 and (h, j) 2010.

North Sea. This is in good agreement with the TBNT results of Troost et al. (2013), who found a relative contribution of atmospheric deposition to TN of 10 %–20 % in large parts of the southern North Sea in 2002. Besides this, it is shown that in the region of the ODZ its contribution is about 10 % higher in 2010 compared to 2002. In the southern central North Sea, the atmospheric contribution to TN reaches values of up to about 10 %, which is also in good agreement with the results of Troost et al. (2013).

The influence of the NL-1 rivers (Fig. 6.7e and f) on TN in the southern North Sea also shows principally similar patterns in 2002 and 2010. Its influence is highest at the river mouths and gradually decreases offshore. The largest part is spread northeast, due to the continental coastal current and the northward recirculation at about 6 °E–6.5 °E (see

Fig. 6.5). It can be seen that the relative contribution of NL-1 in the eastern North Sea is slightly higher in 2002 than in 2010, reaching values of up to 20 % in the ODZ region in 2002. For the DE rivers (Fig. 6.7g and h) also show very similar spatial patterns for the two years. Their contribution is also highest near the river mouths with values of above 95 % at the mouths of Weser and Elbe. In a narrow band of less than 1 ° width parallel to the Danish west coast, their contribution to TN stays above 40 %, but is clearly reduced further offshore and north of 55.5 °N–56 °N. in 2002, the relative contribution around the northern tip of Denmark is higher than in 2010, however, more confined to the near-shore areas. In the region of the 2002 ODZ, the contribution of the DE rivers stays between 5 %–10 % in 2002, while it reaches up to 15 % in 2010.

Finally, the relative contributions of the UK-2 rivers in 2002 and 2010 are presented in Fig. 6.7i and j, respectively. It is shown that these rivers located at the British east coast north of East Anglia have an expectedly strong influence on the British North Sea coast, with especially high values of more than 90 % near the Wash and the Humber estuaries. However, their influence extends several degrees east towards the central southern North Sea, showing values of above 10 % until about 4 °E in 2002 and even 6 °E in 2010. Thus, the UK-2 rivers play an important role for the TN availability in large parts of the southwestern and southern North Sea. In the region of the North Sea ODZ, they still contribute to more than 5 % in both years. This far eastward extension of their influence relates to the general eastward currents in that region, driven by the recirculated Atlantic water originating from the northern shelf edge as well as the English Channel (see Fig. 6.5). The remarkable atmospheric and riverine (NL-1, DE, UK-2) contributions in the southern North Sea reveal the complexity of this region with respect to N inputs.

The spatial distributions of the relative contributions to TN originating from the NL-1, DE and UK-2 rivers in 2002 (Fig. 6.7e, g and i, respectively) are in good agreement with the spatial patterns found by Painting et al. (2013) (their Fig. 4) during a North Sea TBNT study on TN in 2002. However, it should be noted, that their results are not exactly comparable to the results of this study as they did not include benthic N in TN. They found only minor differences with respect to the NL-1 contribution, which is slightly more confined to the continental coastal current and extends slightly further east in the southern coastal North Sea compared to the results of this study. In the vicinity of the North Sea ODZ they found relative contributions of the NL-1 rivers of about 12 %–18 % which is in the same order as shown in Fig. 6.7e.

For the DE contribution to TN in 2002, Painting et al. (2013) also calculated very similar spatial distributions up to the west coast of northern Denmark. Following an imaginary, meridional line along 7.5 °E starting from the continental coast in the south, the relative contribution of the DE rivers stays above 40 % east of this line until about

55.5 °N in this study (see Fig. 6.7f). This is in very good agreement with the findings by Painting et al. (2013). West of 7.5 °E they found a more rapid decrease in the DE contribution than this study shows, which likely relates to the coarser horizontal resolution of the HAMSOM and ECOHAM models, compared to the model used for their work, and thus higher numerical diffusion. North of 55.5 °N, they found slightly higher contributions of the DE rivers to TN showing values up to about 18 % directly north of Denmark. This is not fully reproduced by this TBNT analysis and, on the one hand, likely relates to enhanced numerical diffusion in the inner German Bight causing a dilution of the DE influence farther north. On the other hand, Sect. 6.3.1 showed that the westward flow of the Jutland current around the northern tip of Denmark is not fully reproduced by HAMSOM, implying a less strong influence of the DE rivers in the coastal waters north of Denmark. For the UK-2 rivers they found a very similar westward extension, although with slightly lower contributions along the continental coast east of Lake Ijssel and also around the North Sea ODZ, as a consequence of a northward dispersal at around 6 °E.

Results from an OSPAR workshop on TBNT (OSPAR, 2010) present the TBNT results of two different models, the one used by Painting et al. (2013) and Delft3D-GEM (Delft Three-Dimensional Generic Ecological Model; `https://oss.deltares.nl/web/delft3d`; e.g., Blauw et al. (2008)). Both models show average contributions to TN of about 65 % from the NL-1 rivers in the coastal area directly northeast of the NL-1 river mouths. This corresponds well with the results of this study yielding contribution of 50 %–80 % in this region (roughly around 52 °N, 4 °E). In the inner German exclusive economic zone the two models yielded ranges of 45 %–48 % of DE contribution and 18 %–23 % of NL-1 contribution to pelagic TN in 2002. In this study, the balance between the two contributions is slightly different resulting in average contributions of about 59 % and 9 % for DE and NL-1 rivers to pelagic TN in the same area (not shown), respectively. Nevertheless, the principally good agreement of the results of this TBNT analysis with previous studies gives confidence for further analyses. OSPAR (2010) (therein Fig. 11) also report an average contribution of the UK-2 rivers of 5 %–12 % to inorganic and organic N in an area in the southern central North Sea, located in the Dutch exclusive economic zone (NL-O2) in 2002. This is in good agreement with the contribution of 12 % to TN in 2002 calculated for the same area.

Unfortunately, existing TBNT studies do not provide detailed information on the NA contribution to TN in the eastern central and southeastern North Sea. Therefore, it is difficult to judge whether the dominance of the NA contribution to TN in the region around the ODZ tends to be overestimated or not. The Delft3D-GEM results given by OSPAR (2010) (therein Fig. 11) provide information on the individual NA contributions to inorganic and organic N. They show that the NA contribution to winter DIN, which

is comparable to pelagic TN as the organic part is quite small during winter, is very low (<2 %) in the coastal German exclusive economic zone. Also during the rest of the year, the combined organic and inorganic N contribution by the North Atlantic is in the same order. For the same area, the TBNT analysis yields an NA contribution of about 9 %. This suggests, that the NA contribution to the southeastern North Sea may be slightly overestimated in the present TBNT analysis. However, the generally good agreement with other TBNT studies (Painting et al., 2013; Troost et al., 2013) in the region around the ODZ site confirms that the TBNT analysis yields reasonable results.

The general image provided for bulk TN (Fig. 6.6) shows that in 2002 a remarkably higher amount of TN was present in the region of the ODZ compared to 2010. The relative contributions of the presented sources (Fig. 6.7) indicate that this higher amount of TN originates from increased TN input from the Dutch and German rivers (about 20 %–25 % joint contribution in 2002), and from the North Atlantic (35 %–40 %). This suggests that these N sources play a key role in the seasonal dynamics of the North Sea ODZ. This is supported by the high relative contributions of the Dutch and German rivers to the TN discharge in 2002 (and also 2010; see Fig. 6.4b).

6.4.2 Total nitrogen in the oxygen deficiency zone

In order to give a deeper insight in the temporal evolution of TN and its contributing sources at the ODZ site (see boxes in Fig. 6.6), Fig. 6.8 shows time series of the volume-averaged, daily TN concentration (black line) derived from the ECOHAM simulation for the years a) 2002 and b) 2010. In addition, daily time series of the relative contributions of the different external N sources (coloured lines; compare Table 6.1) are shown to provide information on changes in the relative importance of the different sources throughout the annual cycle and the different years. The grey areas indicate t_{strat} according to Eq. (4.4). In addition, Table 6.3 provides the averages and STDs of the TN concentration, and the relative contributions of the different sources to annually integrated TN during the two years.

The time series of the TN concentration confirm the image provided by Fig. 6.6 and show that throughout the entire annual cycle TN concentrations at the ODZ site are remarkably higher in 2002 than in 2010. Annual average TN concentrations in 2002 and 2010 result in $10.0 \pm 1.3\,\mathrm{mmol\,N\,m^{-3}}$ and $7.0 \pm 0.5\,\mathrm{mmol\,N\,m^{-3}}$, respectively. In 2002, maximum values of about $12.2\,\mathrm{mmol\,N\,m^{-3}}$ are reached in May, while 2010 maximum concentrations occur in November/December and only reach values of about $7.8\,\mathrm{mmol\,N\,m^{-3}}$. Maximum spring/summer values in 2010 are found in June reaching $7.6\,\mathrm{mmol\,N\,m^{-3}}$. TN concentrations at the beginning of 2002 yield almost $9.8\,\mathrm{mmol\,N\,m^{-3}}$, compared to only $6.3\,\mathrm{mmol\,N\,m^{-3}}$ in 2010.

Table 6.3: Annually averaged TN concentration and relative contributions of different N sources to annually integrated TN in the North Sea ODZ in 2002 and 2010.

	2002	2010
TN	10.0±1.3 mmol N m^{-3}	7.0±0.5 mmol N m^{-3}
Atmosphere	13.1 %	20.0 %
DE	7.9 %	9.7 %
NL-1	14.4 %	11.7 %
NL-2	3.4 %	2.3 %
BE	1.5 %	0.9 %
FR	4.1 %	3.6 %
UK-1	3.1 %	3.1 %
UK-2	7.4 %	7.5 %
NO	<0.1 %	0.2 %
NA	39.4 %	32.5 %
EC	4.3 %	5.9 %
BS	<0.1 %	0.3 %
Others	1.2 %	2.3 %

Besides these differences in the initial and maximum TN concentration between the two years, the temporal evolution of the TN concentration throughout the two annual cycles shows quite some differences. In 2002 (Fig. 6.8a), TN concentration first decreases to about 8.7 mmol N m^{-3} in early February when it starts to increase, showing a very steep increase from mid-February to early March. During this increase, the TN concentration rises from about 9 mmol N m^{-3} to 11.6 mmol N m^{-3} within only two weeks. From March to mid-May 2002, TN concentrations stay on a high level with some fluctuations. Thereafter, concentrations start to continuously decrease (with only minor intermittences) until early December, when minimum concentrations of 7.7 mmol N m^{-3} are reached.

In 2010 (Fig. 6.8b), the temporal evolution of the TN concentration is quite different, showing a steady increase from the beginning of the year until June. Thereafter, TN concentrations decrease until early September when minimum values of 6.1 mmol N m^{-3} are reached. TN concentrations again show a more or less steady increase until the end of the year.

The relative contributions of the different sources given in Table 6.3 confirm that the NA has the strongest influence on the TN concentration in both years, accounting for roughly one third in 2010 and almost 40 % in 2002. In 2002, the input by the Dutch NL-1 rivers and atmospheric input constitute the second and third largest source of TN in the ODZ, contributing to 14.4 % and 13.1 %, respectively. In 2010, the atmosphere has a stronger impact of 20.0 % while that of NL-1 is slightly reduced compared to 2002. The relative

importance of the atmosphere in 2002 slightly underestimates that of 15 %–20 % found by Troost et al. (2013), which may indicate a slight overestimation of the NA influence in that area. Especially, since the atmospheric N deposition used in this study yields values of about 836 mg N m^{-2} a^{-1} in 2002, which is well in the range of 715 mg N m^{-2} a^{-1}–882 mg N m^{-2} a^{-1} reported by Troost et al. (2013) for the deposition data they used for investigating the period 1996–2002.

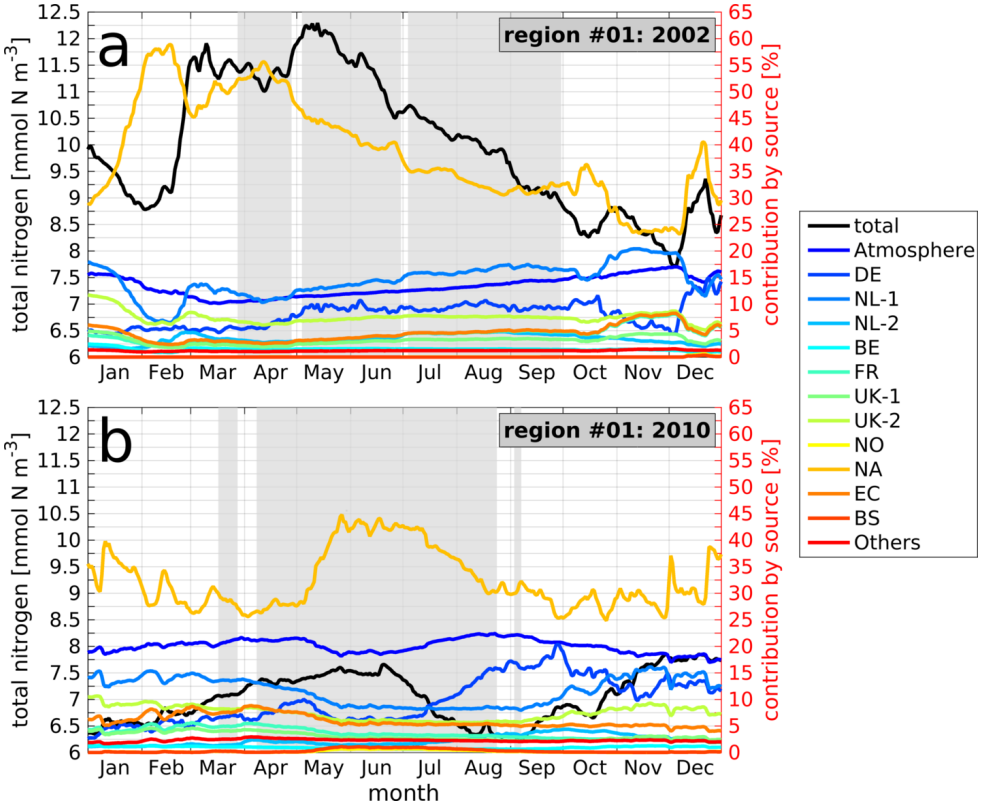

Figure 6.8: Time series of volume-averaged, daily TN concentration (incl. benthic, organic N; black line) and the relative contributions of the different N sources (coloured lines; compare Table 6.1) in the North Sea ODZ (boxes in Fig. 6.6) in (a) 2002 and (b) 2010. Black y axes refer to TN concentration, red y axes refer to relative contributions of different sources. Grey areas indicate stratified periods according to Eq. (4.4). Same legend for both panels.

Among the remaining sources, DE and UK-2 rivers show the strongest influence on TN in the North Sea ODZ with contributions of about 7.5 % for UK-1 in both years and 7.9 % and 9.7 % for the DE rivers in 2002 and 2010, respectively. All other sources show individual contributions of less than 5 % during both years, except for the EC yielding 5.9 % in 2010.

Summation of the relative contributions of the riverine sources and those of the non-

riverine sources (atmosphere, NA, EC and BS) provides insight in the relative importance of sources affected by WFD reduction measures (i.e., rivers; EU, 2000), compared to non-affected sources. For 2002, the riverine contributions add up to 43.1 % compared to 56.9 % of non-riverine TN. In 2010, they result in 41.3 % and 58.7 %, respectively. This shows that the influence of the non-riverine sources on TN in the North Sea ODZ exceeds that of the riverine sources by about 15 %, independent of the high variation in the average TN concentration between the two years. Additionally, this is a strong indicator that the O_2 dynamics in the ODZ are dominated by non-riverine N, especially from the North Atlantic inflow and atmospheric deposition.

The time series of the relative contributions of the different sources (see Fig. 6.8; coloured lines) during 2002 and 2010 provide insight in the seasonal changes in the influence of the different sources on the TN concentration in the North Sea ODZ. Biochemical turnover and exchange of matter across the benthic-pelagic interface are internal processes with respect to TN. Thus, the changes in the relative contributions can be attributed to changes in the lateral (i.e., advective) supply of TN. Atmospheric input constitutes the only exception as N deposition takes place in the entire North Sea region.

The decrease in TN concentration during January 2002 (see Fig. 6.8a) is accompanied by an increase in the NA influence (light orange) from 27 % to 57 % while the riverine sources NL-1 (light blue) and UK-2 (light green) show a clear decrease in their relative contribution. A similar decrease can also be seen in other sources (FR, UK-1 and EC), however, they generally play a less important role on TN in this region. The atmospheric contribution as well as that of the DE and NL-2 rivers remain stable during January. This evolution of the different relative contributions during January 2002 shows that the decrease in TN concentration is mainly driven by only minor advective supply of TN from most riverine sources and the EC, in contrast to a high advective supply of TN from the North Atlantic. However, also the latter is decreasing in terms of absolute TN input (not shown), resulting in a decrease in TN concentration.

The strong increase in TN during the second half of February 2002 coincides with a decrease in the NA contribution from about 58 % to 45 %, while the contributions of the Dutch (NL-1/NL-2) and British (UK-1/UK-2) rivers as well as the EC show a clear increase. Thus, this increase in TN concentration is mainly driven by lateral TN input originating from these river groups and the English Channel. During March/April the fluctuations in the TN concentration are opposite to those in the NA contribution while the DE contribution shows very similar fluctuations (although less pronounced due to the different y axes for TN concentration and relative contributions). The same applies to the fluctuations during the period from mid-May to early July, when the TN concentration is decreasing. This indicates that during this period changes in the TN supply originating

from the German rivers have a strong effect on the fluctuations in the TN concentration in the ODZ. In the later period (late July to October), the variations in TN concentration are more similar to those in the relative contribution of the NL-1 rivers, followed by November when DE fluctuations are again similar to the variations in the TN concentration. In December, the rapid increase in TN concentration corresponds to an increase in the contributions of the North Atlantic and DE rivers while the influence of the atmosphere and EC as well as most other river groups decreases.

The good agreement between fluctuations in the contributions of the DE and NL-1 rivers during long periods of 2002 indicates that short-term (order of days) variability in the TN concentration in the ODZ is mainly driven by variations in the TN loads of the nearest sources with highest riverine TN loads, the German and Dutch rivers (see Fig. 6.4). A similar effect can be expected for the atmosphere in case of atmospheric deposition data with a comparable temporal resolution (only annual data available for this thesis). Furthermore, the opposite behaviour of the NA contribution compared to the DE and NL-1 contribution the summer/autumn period shows that the balance between riverine TN loads from the DE and NL-1 rivers and the supply from the North Atlantic drive the general evolution of the TN concentration in the North Sea ODZ. In turn, the atmospheric N input as well as the more remote and less strong sources (English Channel and other river groups) only have a strong integrated effect on the base level of TN, but have a less strong effect on short-term variations. This is visible in the very small variations in their contributions during most parts of the year.

This general image is supported by the temporal evolution of the relative contributions in 2010 (Fig. 6.8b). The NA influence from January to mid-March shows a decrease with some strong fluctuations. The TN concentrations shows an increase during this period with variations corresponding to those in the NA contribution (e.g., in early January and February). The DE rivers show similar fluctuations although less pronounced, while most other riverine sources and the EC show variations opposite to those in TN concentration. The increase in TN concentration during that period is accompanied by increasing contributions from the atmosphere EC as well as the DE, FR and UK-1 rivers. This likely relates to a stronger inflow through the Strait of Dover in late 2009, resulting in this increase of their contributions and TN (delayed in time due to the distance from the ODZ).

From late March to early May, fluctuations in the TN concentrations are similar to those in the EC and DE contributions, while the patterns in the NA contribution are opposed. However, in April TN concentrations remain stable around 7.2 $\mathrm{mmol\,N\,m^{-3}}$, although only NA and DE (and NL-2 to a minor extent) show increasing contributions. This implies that NA and DE drive the TN evolution during this period. The TN concentrations continues to increase during May which is accompanied by a steep increase in the NA contribution,

while most other sources – except for the Baltic inflow (BS; red) and the Norwegian rivers (NO; yellow) – show decreasing contributions. Thus, the increase in TN during this period is dominated by strong TN supply originating from the North Atlantic. Although only of minor importance the increases in the BS and NO contributions is worth mentioning as they indicate the southwestward advection of TN from these sources around the northern tip of Denmark (compare Fig. 6.6).

The decrease in TN concentration from mid-June to September is accompanied by a decrease in the NA contribution and increases in the atmospheric and, even stronger, the DE contribution. The other sources show more or less stable contributions during this period. This implies that the decrease in the TN supply from the North Atlantic cannot be balanced by the enhanced supply from the atmosphere and the German rivers. From mid-September until the end of the year, the TN concentrations shows a general increase with some intermittent decreases. During this period the fluctuations in the NA and DE contributions are mainly opposite to the TN evolution, while those in the NL-1 and UK-2 contribution are quite similar to the TN fluctuations. Thus, this increase in TN is mainly driven by the enhanced supply of TN from the latter two riverine sources. The minor decrease in TN concentration in late December results from the decreasing TN supply from basically all sources, except for the NA which shows a steep increase. However, the TN supply by the NA cannot balance the reduced supply of the other sources.

In summary, the time series of TN concentration and the relative contributions of the different sources show that the North Atlantic inflow across the northern shelf constitutes the main controlling factor for the base level of the TN concentration and its long-term (order of months and longer) evolution in the North Sea ODZ. This implies that years with a strong TN supply from the NA, like 2002, are potentially more susceptible to low O_2 conditions as the N availability (in combination with P, Si and light availability) controls NPP, i.e., organic matter availability in the North Sea ODZ. However, it has to be kept in mind that TN entering the North Sea across the northern shelf edge needs some time before it reaches the southern central North Sea where the ODZ is located (e.g., Otto et al., 1990).

In case that years, preconditioned with high TN levels due to the North Atlantic inflow, coincide with high TN supply from the Dutch (NL-1) or German (DE) rivers (Fig. 6.8a, February and December, respectively) this can lead to particularly high TN levels like in spring/summer 2002. In consequence, this can result in strongly enhanced NPP over an entire summer period, potentially driving the evolution of O_2 deficiency.

6.4.3 Net primary production and organic nitrogen in the North Sea

The production of organic matter during NPP constitutes the key factor for biochemical O_2 consumption. In contrast to TN which is affected by only very few processes (advection, atmospheric deposition loss of N_2 due to REM_{sed}), NPP constitutes exactly such a process. Consequently, NPP is influenced by additional factors like light limitation or limitation due to other inorganic nutrients (PO_4^{3-}, SiO_4^-). Hence, differences between the spatial patterns and the annual cycle of NPP can be expected compared to TN.

For this reason, this section provides an overview of annual water column integrated NPP in the North Sea and the relative contributions of the different N sources (see Fig. 6.3 and Table 6.1). For consistency reasons NPP is calculated in N units as the sum of the uptakes of NO_3^- and NH_4^+ by diatoms and flagellates as these two processes are the actual fraction processes which are traced. The values can be translated into C units using a molar ratio of C:N = 6.625 (Redfield, 1934) and the molar weights of C and N. In addition, daily time series of water column NPP and the relative contributions of the different N sources are presented for the ODZ study site. Finally, the daily time series of pelagic and benthic organic matter as well as the corresponding source contributions are provided for the ODZ as they constitute the direct link to aerobic remineralisation, the dominant process in O_2 consumption.

6.4.3.1 Spatial distribution of net primary production

Figure 6.9a and b show the spatial distributions of annual water column integrated NPP in 2002 and 2010, respectively. The spatial patterns and differences between the two years are basically the same as in the C-bases upper layer summer (April to September) NPP shown in Fig. 5.8, due to the fact that most NPP takes place during summer and in the upper euphotic layers. In most parts of the domain, NPP is generally higher in 2002 compared to 2010. In 2002, maximum values of up to $78\,g\,N\,m^{-2}\,a^{-1}$ occur at the mouth of river Seine (49.5 °N, 0 °E). At the river mouth locations of the German rivers Weser and Elbe NPP also reaches high values of about $60\,g\,N\,m^{-2}\,a^{-1}$. Around the mouths of Rhine and Meuse (and downstream the continental coastal current) enhanced NPP of up $45\,g\,N\,m^{-2}\,a^{-1}$ occurs. In the eastern North Sea, maximum annual NPP also reaches $45\,g\,N\,m^{-2}\,a^{-1}$ southeast of the North Sea ODZ (boxes in Fig. 6.9). In the ODZ, NPP ranges between $30\,g\,N\,m^{-2}\,a^{-1}$–$36\,g\,N\,m^{-2}\,a^{-1}$. In general, large parts of the southern and eastern North Sea show NPP values of more than $25\,g\,N\,m^{-2}\,a^{-1}$, while in the central North Sea around 56 °N–58 °N, 0 °E–3 °E NPP stays below $20\,g\,N\,m^{-2}\,a^{-1}$.

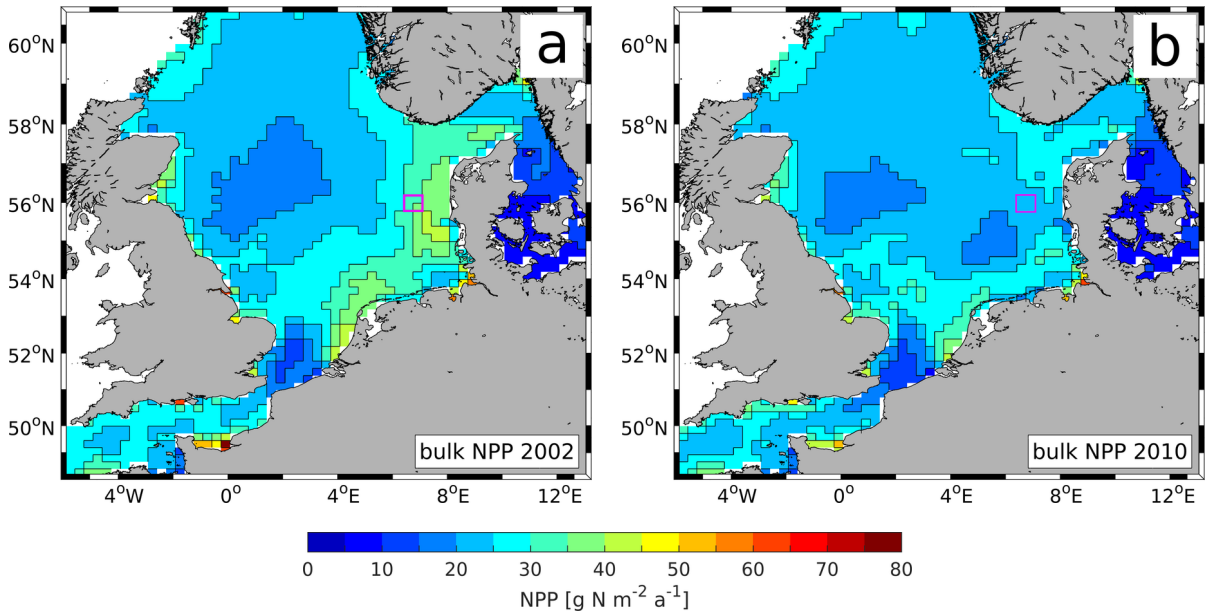

Figure 6.9: Spatial distributions of annual, water column integrated NPP (in N units) as simulated by ECOHAM for (a) 2002 and (b) 2010. Boxes indicate the ODZ site (see Fig. 5.11a, box #1).

In 2010, highest NPP occurs at the Elbe mouth reaching values of 65 g N m^{-2} a^{-1}. NPP of above 25 g N m^{-2} a^{-1} only occurs in the southern coastal North Sea, in the western Skagerrak and along the British coast. In the southeastern central North Sea, NPP is significantly lower in 2010 yielding values of less than 20 g N m^{-2} a^{-1} around 54 °N–56 °N, 4 °E–6 °E. NPP is also clearly reduced in and around the ODZ showing values of about 25 g N m^{-2} a^{-1}.

Figure 6.10 shows he spatial distributions of the relative contributions to NPP in 2002 and 2010 due to N from the North Atlantic (NA), atmosphere as well as Dutch (NL-1), German (DE) and east British (UK-2) rivers. The spatial distributions of the NA contributions (Fig. 6.10a and b) show similar patterns to the NA contributions to TN (see Fig. 6.7a and b). The northern North Sea north of 58 °N is clearly dominated by the NA influence, however, in the central North Sea, the influence of N from the North Atlantic on NPP is less than the NA contribution to TN. The same applies to the Norwegian Trench region where the NA contribution to NPP is clearly less than that to TN.

The analysis of the atmospheric contribution to NPP (Fig. 6.10c and d) provides the explanation for these differences in the NA contribution between NPP and TN. It can be seen that in both years the atmospheric contribution to NPP in the central North Sea and in the Norwegian Trench is higher than that to TN, reaching values of up to 13 %. This increase in the relative contribution of atmospheric N to NPP, compared to its influence on TN, can be explained by the fact that atmospheric N enters the marine system in the

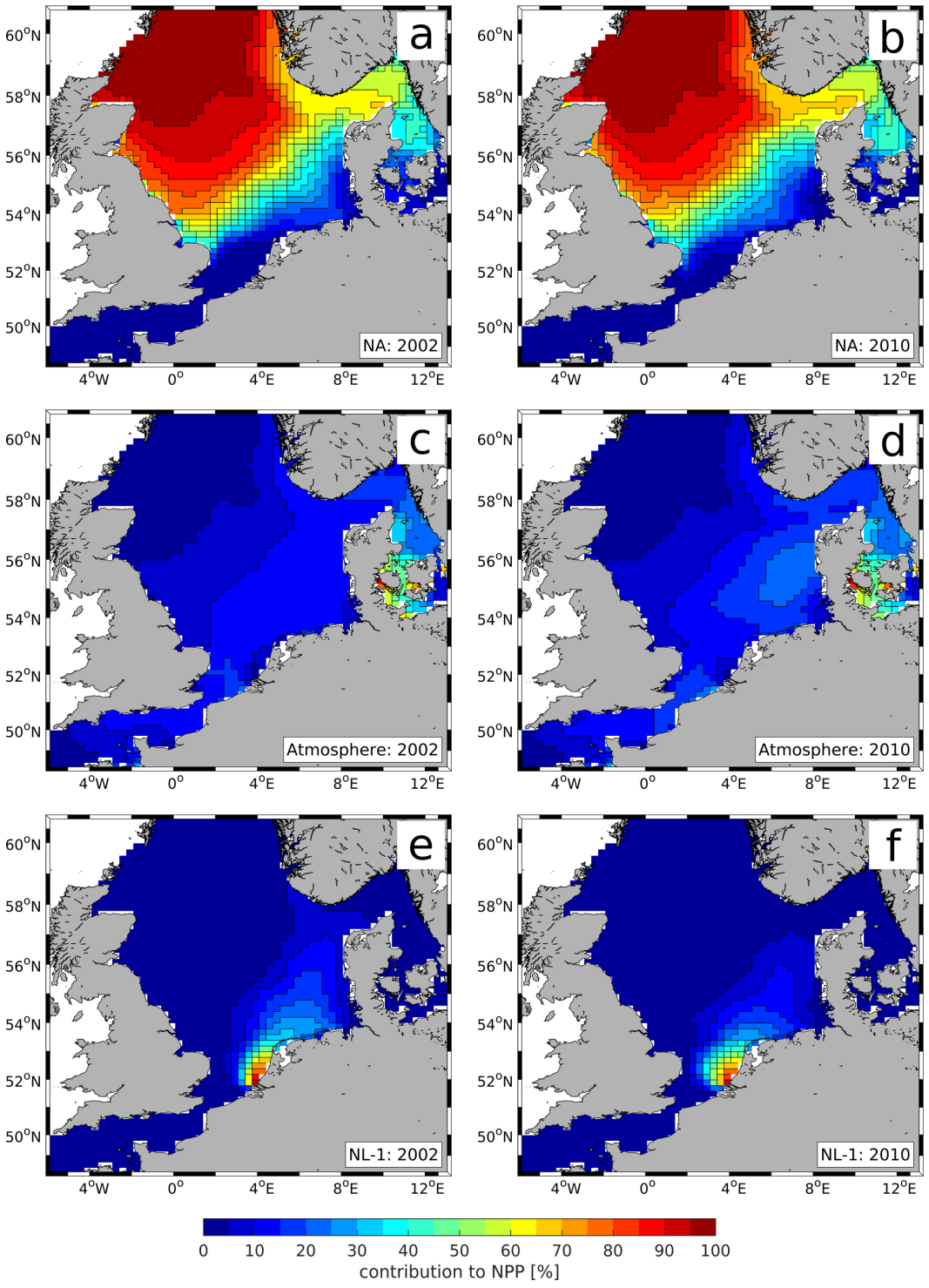

Figure 6.10: Spatial distributions of relative contributions of different N sources to annual, water column integrated NPP for (a, c, d) 2002 and (b, d, f) 2010. Sources: (a, b) North Atlantic (NA), (c, d) atmosphere, (e, f) 1st group of Dutch rivers (NL-1).

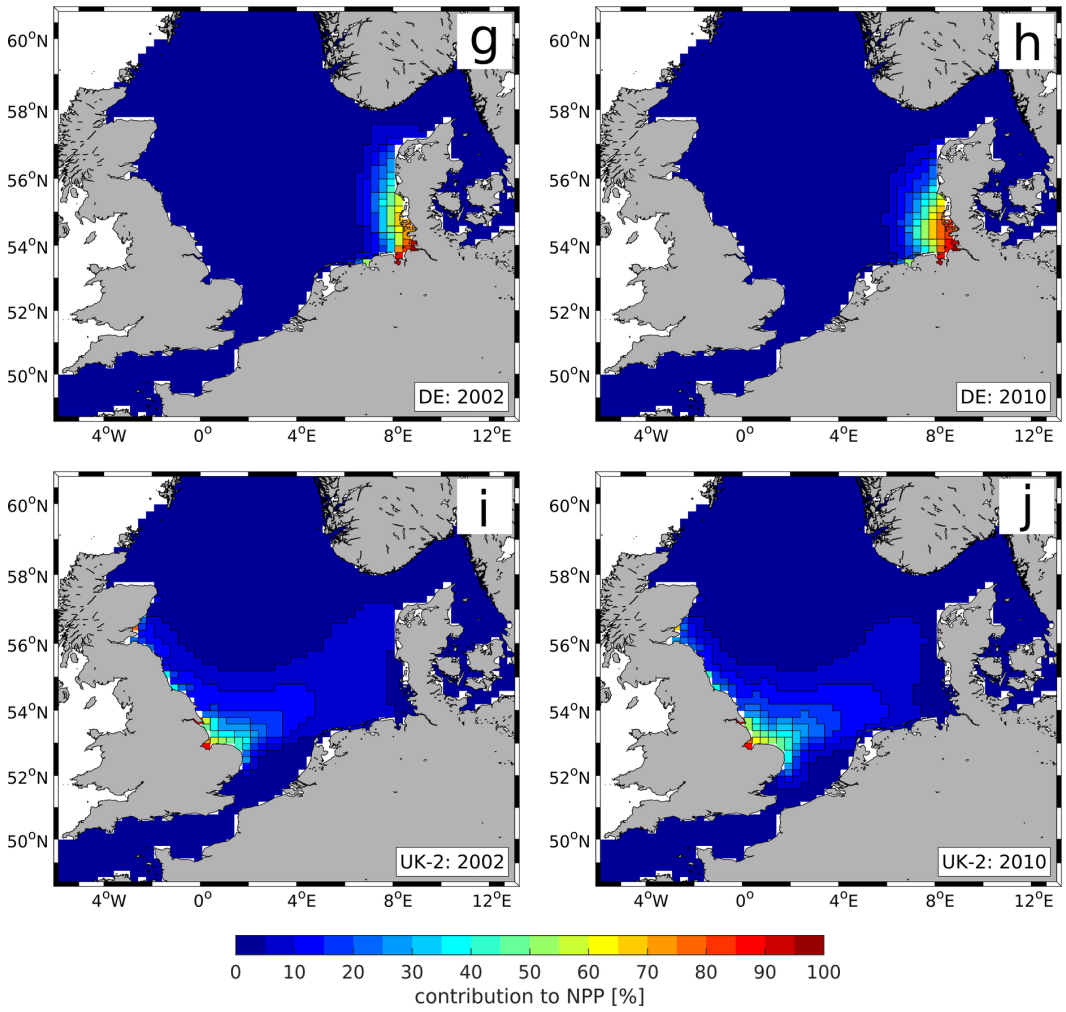

Continued: (g, h) German rivers (DE) and (i, j) 2nd group of British rivers (UK-2) in (g, i) 2002 and (h, j) 2010.

euphotic surface layer and as inorganic N. Thus, it can be utilised immediately by primary producers (assuming no P or Si limitation). In contrast, the NA influence is reduced as much of the TN originating from the North Atlantic enters the North Sea (and partly remains) also in deeper layers, where light limitation inhibits PP.

The influence of atmospheric N on NPP in the southern North Sea is consistently higher than 10 % with values up to 15 % in the vicinity of the North Sea ODZ. In 2010, the relative contribution of atmospheric N on NPP is enhanced compared to 2010, similar to the its higher contribution to TN in 2010. Maximum contributions of up to 23 % occur in the vicinity of the ODZ. In addition, a slightly higher impact of atmospheric N on NPP relative to TN can be found in the southern North Sea, although to a lesser extent than

in the central North Sea due to lower bottom depths.

Troost et al. (2013) found a relative contribution of atmospheric N to NPP in 2002 ranging between 20 %–30 % in most parts of the southern North Sea and a maximum contribution of almost 50 % near the British southeast coast. For the southern central North Sea they report contributions of up to 20 %. In contrast, Spokes and Jickells (2005) attributed only 2 % (in June 1998) to 6 % (in August 1999) of southern North Sea NPP to atmospheric N, but to about 13 % in the Kattegat region in May 2001. Thus, the results of this study are well in the range provided by earlier studies and match the relative spatial gradients between the southern North Sea and the Kattegat found by observational studies (Spokes and Jickells, 2005).

For the Dutch NL-1 rivers (Fig. 6.10e and f) the spatial patterns and differences between the two years are also quite similar to the image provided for TN (Fig. 6.7e and f). In the coastal southern North Sea its influence in 2002 is slightly higher than that on TN, with values above 20 % until slightly west of the Jade Bight. In the vicinity of the ODZ, the 2002 contribution of NL-1 rivers to NPP is slightly lower than that to TN with values of 10 %–15 %. In 2010, the NL-1 contribution to NPP shows values of about 10 % at the ODZ site.

The DE rivers (Fig. 6.10g and h) also show contributions very similar to those to TN in both years. The inner German Bight is clearly dominated by the Elbe and Weser N, which influence stays above 65 % in the coastal grid cells until about 55 °N. Farther offshore and north their influence on NPP steadily decreases reaching values of 8-12 % in the ODZ in both years. As for TN (Fig. 6.7g and h) the influence of the DE rivers on NPP extends farther offshore compared to 2002, while in 2002 it reaches farther north showing values of above 5 % northwest of Denmark.

Interestingly, the DE contribution to NPP in the inner German Bight in 2002 is quite similar to that to TN, while in 2010 the contribution to NPP is visibly higher than to TN. Locally, differences of up to 30 % can be seen. This likely relates to the fact that in 2002 Elbe N inputs were quite high, however, especially after end of August (Ulbrich et al., 2003). Consequently, the contribution to NPP is less than to TN as most parts of the summer growing season were not affected by these high N loads. In contrast, Elbe N input in 2010 occurred in large amounts throughout the entire summer period, positively affecting NPP during the growing season.

Finally, the UK-2 rivers' contributions to NPP in 2002 and 2010 (Fig. 6.10i and j, respectively) show very similar patterns as for TN. Only directly at the British east coast and within the westward extension between 53 °N–54 °N they show slightly higher contributions to NPP than to TN. This likely relates to the fact that the riverine nutrients (including N) are added to the model surface layer within ECOHAM (for the sake of

mass conservation in relation to volume change by riverine freshwater discharge), where they can be used directly for PP due to sufficient light availability. In the vicinity of the ODZ they contribute to more than 5 % of overall NPP, similar to TN. Thus, it can be expected that the UK-2 rivers also effect the O_2 dynamics in the ODZ as they constitute a non-negligible contributing source to organic matter production in that area.

6.4.3.2 Net primary production in the oxygen deficiency zone

In order to get a more quantitative insight in the differences in NPP in the North Sea ODZ between 2002 and 2010, Table 6.4 lists the annual, water column integrated NPP for the North Sea ODZ and the corresponding relative contributions of the different sources. It can be seen that overall NPP in 2002 is almost 1.5 times higher than in 2010, yielding 33.3 g N m^{-2} a^{-1} compared to 22.9 g N m^{-2} a^{-1} in 2010. With respect to the relative contributions of the different N sources to overall NPP, the 2002 values are quite similar to those for TN (see Table 6.3). Maximum differences in the relative contributions to NPP and TN in 2002 can be found for the atmosphere which contributes 13.8 % to NPP and only 13.1 % to TN. This again relates to the atmospheric input entering the marine system in the euphotic surface layer where it can be used directly for PP. As for TN, the NA influence is strongest contributing about 39.7 % to NPP. The NL-1 rivers contribute 14.1 %, which constitutes a slightly lower influence than on TN, while the influence of the DE rivers is increased (relative to its TN contribution) by the same percentage, resulting in 8.2 %.

In 2010, the relative contributions show stronger deviations from the contributions to TN. Maximum differences of 1.9 % can be found for the atmospheric influence (21.9 % for NPP, 20 % for TN) and the NL-1 rivers (9.8 % for NPP, 11.7 % for TN). The NA contribution also shows a 1.4 % higher value of 33.9 % (relative to its contribution to TN), while the UK-2 contribution is 1.1 % lower yielding 6.4 %. This could relate to the different timing of the availability of inorganic N (NH_4^+ and NO_3^-) originating from the different sources.

The integrated relative contributions of the riverine and non-riverine (atmosphere, NA, EC and BS) sources to NPP in 2002 result in 42.7 % and 57.3 %, respectively, compared to 38.2 % and 61.8 % in 2010. Thus, the contribution of the non-riverine sources to NPP in the North Sea ODZ is even slightly higher than that to TN (56.9 % in 2002, 58.7 % in 2010). Local organic matter production constitutes the most dominant driver of organic matter supply to the deeper layers in the vicinity of the North Sea ODZ (see Sect. 5.2.3.1, region #3). Consequently, the results suggest that the non-riverine, i.e., those sources not affected by riverine N reductions, play an even more important role for O_2 in the ODZ. However, as atmospheric N deposition also constitutes a predominantly anthropogenically

Table 6.4: Annual, water column integrated NPP and relative contributions of different N sources in the North Sea ODZ in 2002 and 2010.

	2002	2010
NPP	$33.3\,\mathrm{g\,N\,m^{-2}\,a^{-1}}$	$22.9\,\mathrm{g\,N\,m^{-2}\,a^{-1}}$
Atmosphere	13.8 %	21.9 %
DE	8.2 %	10.2 %
NL-1	14.1 %	9.8 %
NL-2	3.5 %	2.4 %
BE	1.4 %	0.8 %
FR	3.9 %	3.3 %
UK-1	2.9 %	2.7 %
UK-2	7.1 %	6.4 %
NO	<0.1 %	0.3 %
NA	39.7 %	33.9 %
EC	4.1 %	5.5 %
BS	<0.1 %	0.5 %
Others	1.2 %	2.3 %

affected process, future reductions in atmospheric N input will likely reduce NPP.

The temporal evolution of NPP and the influence of its contributing sources on NPP is shown in Fig. 6.11a and b for the years 2002 and 2010, respectively, including the stratified periods according to Eq. (4.4) (grey areas). At first, it is clearly visible that fluctuations in NPP (black) in both years are much stronger than variations in TN (see Fig. 6.8). This can be attributed to the fact that NPP is affected by more controlling factors (light limitation, limitation due to other nutrients than N) than TN, which is only affected by variations in TN advection and atmospheric N input.

The comparison of NPP during the productive seasons (March–November) of the two years shows that NPP is clearly higher in 2002 compared to 2010. In 2002, very high daily NPP rates of $240\,\mathrm{g\,N\,m^{-2}\,d^{-1}}$–$270\,\mathrm{g\,N\,m^{-2}\,d^{-1}}$ are reached in early April and May as well as in late June. In 2010, maximum values of $175\,\mathrm{g\,N\,m^{-2}\,d^{-1}}$ are reached during the spring and autumn bloom in mid-April and late-August, respectively. The comparison of the average rates during summer (excl. the events of very high NPP in 2002) shows that average summer NPP is about 1.5 times higher in 2002, which matches the annually integrated NPP values (see Table 6.4).

Regarding the seasonal succession of the contributions of the different sources a principally similar evolution can be seen as for TN (see Fig. 6.8. During January/February 2002, when NPP is low the NA influence (light orange) shows an increase up to 75 % in early February, before it starts to decrease until late August, with some fluctuations

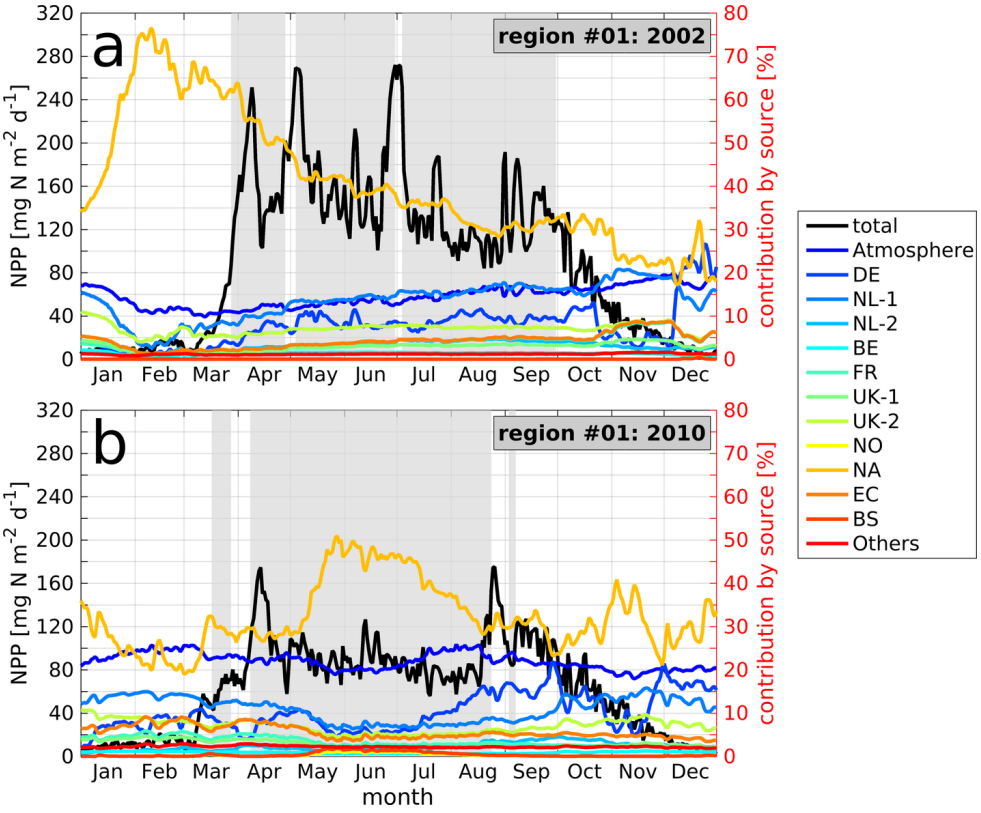

Figure 6.11: Daily time series of water column integrated NPP (black line) and relative contributions of the different N sources (coloured lines; compare Table 6.1) in the North Sea ODZ (boxes in Fig. 6.9) in (a) 2002 and (b) 2010. Black y axes refer to detritus-N concentration, red y axes refer to relative contributions of different sources. Grey areas indicate stratified periods according to Eq. (4.4). Same legend for both panels.

in-between. It can be seen that the very steep spring increase (spring bloom) in March 2002 first coincides with an increase in the NA contribution in late March, before this contribution decreases and that of the DE and NL-1 rivers increases. The drop in NPP after this first spring maximum relates to a combination of nutrient limitation setting in and stronger light limitation due to increased self-shading. Consequently, increasing zooplankton grazing reduces phytoplankton biomass, which additionally lowers NPP.

The second NPP maximum in early May 2002 is supported by an increase NO_3^- availability reducing NO_3^- limitation. The increase in NPP from mid-April to early May is first accompanied by an increase in the NA contribution, followed by an increase in the NL-1 (blue) and UK-2 (green) contributions in late April and finally by an increase in the DE contribution in early April. This event of enhanced NPP in late April coincides with an event of strong vertical mixing, indicated by the temporary breakdown of stratification.

Thus, the upward mixing of inorganic N from these sources (and other nutrients) drives the evolution of the second NPP maximum in the described sequence. The same applies to the event in late June, only the contributing sources differ. First, the NA and DE influence increase, before the atmospheric and NL-1 contributions show an increase. Some other sources (UK-1/-2 and EC) also show minor increases during this latter event, however, to a lesser extent.

The steady decrease of the NA contribution during summer is accompanied by an increase of the atmospheric contribution and that of most riverine sources. Only the DE contribution stays on a basically stable level of around 10 % (with some fluctuation). This could relate to the comparably short distance between the DE river mouths and the ODZ compared to other rivers, implying that their supply of N available for NPP is less affected by changes in the circulation, e.g., upstream the continental coastal current or in the recirculation of the Atlantic water around the Dogger Bank. This is also supported by the good agreement in TN fluctuations and fluctuations in the DE contribution to TN (see Fig. 6.8). The less good agreement between NPP fluctuations and the corresponding DE contribution relates to the fact that additional factors such as stratification, light limitation or limitation by other nutrients have an additional influence on NPP.

From October to December 2002, the different relative contributions evolve quite similar to those of TN as stratification has ended and NPP is strongly light limited (visible in the decline in NPP), implying that the distribution of the source contributions in NPP basically represents the distribution of inorganic N in the euphotic near-surface layer.

In 2010, overall NPP is significantly lower than in 2002. The temporal evolution of the contributions of the different sources principally show similar patterns as for TN (see Fig. 6.8b), however, as for 2002 stronger fluctuations throughout the entire annual cycle. This again relates to the different processes and factors controlling NPP, compared to TN being only affected by advection and atmospheric deposition. The onset of enhanced NPP in early March 2010 coincides with an increase in the NA contribution (light orange) to NPP from 20 % to about 32 % and in the DE contribution (blue) from 5 % to 11 %. During the increase in NPP in mid-March, both contributions drop, while most other riverine contributions as wells as the atmospheric and EC contributions show increases. The spring maximum in NPP in mid-April coincides with an increase in the DE river contribution, indicating in increasing influence of inorganic N supply originating from the German rivers during this phase of the spring bloom. This is in good agreement with the maxima of the 2002 NPP time series (see Fig. 6.11a), which coincides with increases in the DE contribution to NPP.

During the summer period (late April to mid-August), NPP is dominated by the NA influence contributing 30 %–50 % to overall NPP during that period. The atmosphere also

plays an important role during that time contributing 18 %–25 %. In contrast, the different river groups show very low contributions compared to the spring and autumn periods. Only during the minor NPP maximum in mid-June all river group contributions show a minor increase while the NA contributions drops. The same applies to another minor increase in NPP in mid-July. From late May to mid-August, the relative contribution of the NA steadily decreases reaching values of about 30 % when NPP starts to rapidly increase in mid-August. This decrease in the NA contribution during July and August is accompanied by increases, especially, in the DE and atmospheric contributions, but also to a lesser extent in the other riverine sources.

The autumn NPP maximum in late April is dominated by contributions from the North Atlantic, the atmosphere and the DE rivers. This is different to the spring bloom when the Dutch NL-1 rivers has a stronger influence on NPP than the DE rivers, and also to the spring and autumn blooms in 2002, when again the Dutch NL-1 contributions are higher than those of the DE rivers (see Fig. 6.11a). Together with the high NA contributions in the first half of 2002, this underlines that the enhanced production of organic matter in the ODZ in spring 2002 can be attributed to the strong influence of the North Atlantic and the NL-1 rivers. After the NPP maximum in August, the NPP shows a general decrease, due to light limitation setting in, with many fluctuations. These fluctuations partly match the variations in the DE contribution, to which the NA contribution shows an exactly opposed behaviour. This indicates that towards the end of 2010, the balance between the DIN supply originating from the German rivers and the North Atlantic control the N limitation of NPP, although light limitation constitutes the major controlling factor during that time.

The time series of NPP and its contributing sources during 2002 and 2010 clearly demonstrate that the high NPP in 2002 is driven by high N availability originating from the North Atlantic, but, especially during summer, also from the Dutch, German and also British river sources. Atmospheric deposition has a slightly stronger effect on NPP than on TN as atmospheric N enters the system in the euphotic surface layer where it can be used immediately, assuming no other limitation on phytoplankton growth. However, the minor decrease trend in atmospheric N deposition between 2002 and 2010 (see Fig. 6.4a) cannot explain the strong reduction in NPP between the two years. Thus, it can be concluded that variations in the N supply from the North Atlantic, the large continental rivers and also the UK-2 rivers (at the British east coast) control year-to-year variations in NPP, and thus on the O_2 dynamics in the North Sea ODZ.

6.4.3.3 Particulate organic nitrogen in the oxygen deficiency zone

REM_{sed} and REM_{pel} constitute the major O_2-consuming processes in the North Sea ODZ, consistently accounting for more than 75 % of GOC in the sub-MLD volume and for about 85 % in the bottom layer (see Sect. 5.2.5). Therefore, it is important to analyse which sources of N have the largest contributions to organic N in the North Sea ODZ. For this purpose, this section provides insight in the seasonal evolution of pelagic and benthic organic matter (in N units) in the North Sea ODZ, and the relative contributions of the different contributing sources.

Table 6.5 provides an overview of the average concentration of pelagic organic matter (detritus-N; in $\mathrm{mmol\,N\,m^{-3}}$) and the amount of organic matter in the sediment (sediment-N; in $\mathrm{mmol\,N\,m^{-2}}$) for the years 2002 and 2010. Sediment-N is given in units per area as ECOHAM uses a simple sediment module with no vertical extent (see Sect. 3.2.1). It can be seen that detritus-N and sediment-N show higher values in 2002 compared to 2010. The average detritus-N concentration in 2010 ($0.6\pm0.3\,\mathrm{mmol\,N\,m^{-3}}$) is only about three quarters of that in 2002 ($0.8\pm0.6\,\mathrm{mmol\,N\,m^{-3}}$). The average amount of sediment-N in 2010 ($22.0\pm11.0\,\mathrm{mmol\,N\,m^{-2}}$) represents only about two thirds of that in 2002 ($33.7\pm21.0\,\mathrm{mmol\,N\,m^{-2}}$) which matches the difference in NPP between the two years.

Despite these minor differences in the ratio between the absolute values in 2002 and 2010 for detritus-N and sediment-N, respectively, it can be seen that the relative contributions of the individual sources during the two years are quite similar for both quantities. This likely results from the fact that sediment-N basically constitutes detritus-N which sank to the bottom. Consequently, the amount of sediment-N from a certain sources is strongly linked to the amount of detritus-N from a certain source in the water column. Minor differences between the relative contributions of individual sources to detritus-N and sediment-N probably relate to the slight temporal shift between the two variables.

The relative contributions of the different sources to the two variables are also quite similar to those for TN (see Table 6.3). Largest differences can be found for the DE rivers with relative contributions to detritus-N of 8.9 % and 11.4 % in 2002 and 2010, respectively, 9.1 % and 11.5 % to sediment-N (compared to 7.9 % in 2002 and 9.7 % in 2010 to TN). In 2002, these slightly higher contributions by the DE rivers are accompanied by slightly lower contributions from the North Atlantic (NA), while the NA contribution to organic matter in 2010 is higher than that to TN. Instead, the Dutch NL-1 rivers have a visibly lower relative contribution (9.9 % and 10 % to detritus-N and sediment-N, respectively) than for TN (11.7 %). This underlines that the North Sea ODZ is controlled mainly by the balance between the varying influences of the NL-1 and DE rivers and the North Atlantic. The atmosphere has a stronger influence during years of lower contributions from these three sources.

Table 6.5: Annually averaged detritus-N concentration and sediment-N amount per unit area, and relative contributions of different N sources to annually integrated detritus-N and sediment-N mass in the North Sea ODZ in 2002 and 2010.

	detritus-N [mmol N m^{-3}]		sediment-N [mmol N m^{-2}]	
	2002	2010	2002	2010
bulk	0.8±0.6	0.6±0.3	33.7±21.0	22.0±11.0
Atmosphere	13.5 %	20.8 %	13.2 %	20.7 %
DE	8.9 %	11.4 %	9.1 %	11.5 %
NL-1	14.3 %	9.9 %	14.5 %	10.0 %
NL-2	3.5 %	2.4 %	3.6 %	2.5 %
BE	1.4 %	0.8 %	1.5 %	0.8 %
FR	4.1 %	3.1 %	4.0 %	3.2 %
UK-1	3.0 %	2.6 %	3.0 %	2.6 %
UK-2	7.1 %	6.4 %	7.3 %	6.6 %
NO	<0.1 %	0.4 %	<0.1 %	0.3 %
NA	38.7 %	34.2 %	38.3 %	33.7 %
EC	4.2 %	5.3 %	4.2 %	5.4 %
BS	<0.1 %	0.5 %	<0.1 %	0.5 %
Others	1.2 %	2.2 %	1.2 %	2.2 %

The annual cycles of detritus-N in the North Sea ODZ in 2002 and 2010 are shown in Fig. 6.12a and b, respectively. It is nicely shown that the temporal evolution of detritus-N (black line) follows the annual cycle of NPP (see Fig. 6.11) with a slight temporal delay of about one week. This minor delay results from the fact that first phytoplankton growth has to be initiated resulting in higher amounts of living organic matter (i.e., phytoplankton). This phytoplankton either dies or is eaten by zooplankton, which subsequently dies, causing an increase in detrital matter. This good agreement between the annual cycles of NPP and detritus-N emphasises that most of the organic matter at the ODZ site originates from local production, while advection of organic matter has only a minor effect on the detritus-N concentrations.

From January to mid-March 2002 (see Fig. 6.12a) detritus-N concentrations remain low due to low NPP rates as a result of light limitation. The onset of enhanced spring NPP in 2002 occurs in early March and results in an increase in detritus-N starting in mid-March (see Fig. 6.12a). The spring increase in detritus-N represents the strongest increase within the entire annual cycle and results in maximum concentrations of 1.7 mmol N m^{-3} in mid-April, again about one week delayed after maximum NPP rates occur. This first peak in detritus-N is followed by a decrease in detritus-N due to reduced NPP. A second increase in detritus-N occurs in early May reaching the annual maximum concentration

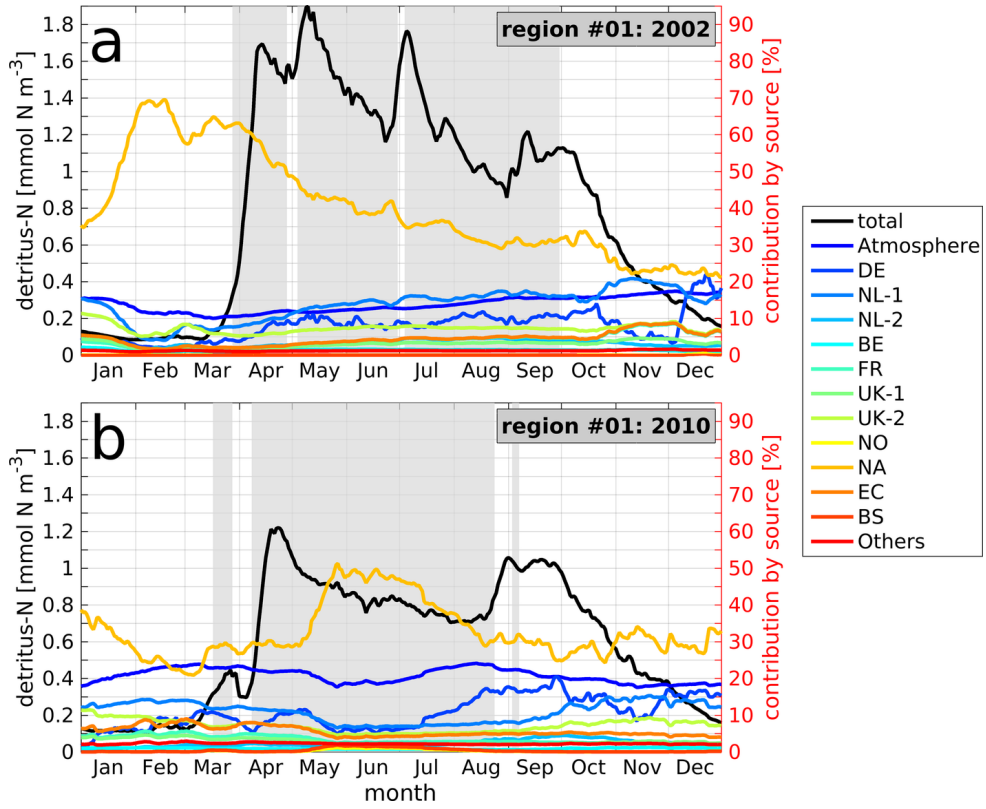

Figure 6.12: Daily time series of volume-averaged (pelagic) detritus-N concentration (black line) and relative contributions of the different N sources (coloured lines; compare Table 6.1) in the North Sea ODZ (boxes in Fig. 6.9) in (a) 2002 and (b) 2010. Black y axes refer to detritus-N concentration, red y axes refer to relative contributions of different sources. Grey areas indicate stratified periods according to Eq. (4.4). Same legend for both panels.

of 1.9 mmol N m^{-3}. Again this increase in detritus-N is caused by the strongly enhanced NPP. In the succession of this peak, detritus-N concentration shows a steady decrease with only minor fluctuations until late June. Then another event of high NPP (see Fig. 6.11a) causes another remarkable increase in detritus-N reaching a maximum concentration of 1.75 mmol N m^{-3} in early July. This maximum is followed by a steady decrease until end of August when enhanced NPP (initiated by nutrient supply from deeper layers due to the breakdown of stratification) causes an increase in detritus-N concentration up to 1.2 mmol N m^{-3}. After the autumn bloom period ending in late September, detritus-N concentrations decrease due to reduced NPP and ongoing remineralisation.

The annual cycle of detritus-N in 2010 (see Fig. 6.12b) also represents well the annual cycle of NPP in 2010 (see Fig. 6.11b). As for 2002, detritus-N concentrations increase with a slight temporal delay of about one week relative to NPP. In 2010, the first increase

in detritus-N due to enhanced NPP occurs about two weeks earlier than in 2010, starting in early March. In consequence, the increase in zooplankton grazing, as a response to increasing phytoplankton concentrations, in combination with lower light availability compared to 2002 results in a minor decrease in detritus-N concentration in late March. In early April, when light availability has increased the actual spring bloom is initiated (see NPP maximum in Fig. 6.11b) resulting in a maximum detritus-N concentration of about 1.2 mmol N m^{-3}. Maximum spring detritus-N concentrations in 2002 are about 1.5 times higher than in 2010 which matches the difference in maximum spring NPP rates between 2002 and 2010, underlining the great influence of local NPP on the amount of organic matter in the ODZ.

After the spring maximum, the detritus-N concentration steadily decreases until early August reaching minimum concentrations of 0.8 mmol N m^{-3}. Throughout the entire summer period, detritus-N concentrations are significantly lower than in 2002. This relates to the fact that NPP within the summer surface mixed layer is strongly controlled by the nutrients released by remineralisation. Consequently, higher initial nutrient levels at the beginning of the growing season (as indicated by the clearly higher TN levels in spring 2002 compared to 2010; see Fig. 6.8) allow for higher spring NPP, and consequently, higher remineralisation and release inorganic nutrients.

In mid-August, the onset of wind-induced mixing causes the renewal of the surface layer nutrient pool enhancing NPP, which triggers the evolution of the autumn detritus-N maximum with values of 1.05 mmol N m^{-3}. The detritus-N concentrations during this autumn maximum are only slightly lower than those in 2002, which is different to the spring maximum. This relates to the fact that during this time of the year, nutrient limitation is less dominant than during and after the spring bloom, but increasing light limitation constitutes the main controlling factor. After the autumn maximum, the detritus-N concentration steadily decreases reaching values of less than 0.2 mmol N m^{-3} at the end of the year, which is similar to 2002.

Like the detritus-N concentration, the temporal evolution of the relative contributions of the different sources to detritus-N in the ODZ in the two years basically follows the temporal evolution of the different contributions to NPP (see Fig. 6.12). This again underlines the great importance of local NPP on the amount of detrital matter inside the ODZ. As for NPP, the NA contribution (light orange) dominates detritus-N throughout the annual cycle in both years. After the 2002 spring bloom, the NA contribution steadily decreases while the contributions of N and from the atmosphere (dark blue) and the Dutch NL-1 rivers (light blue) show a steady increase. The same applies to most other river groups, except for the DE rivers (blue) which only show a clear increase during April followed by varying contributions of 8 %–13 % until mid-October. The NO and 'Others'

rivers' contributions (yellow and red, respectively) are negligible throughout most of the year.

As for NPP, the contributions of the NA as well as the DE and NL-1 rivers show the strongest fluctuations during 2002, compared to the other N sources, which indicates that the balance between these three sources mainly controls fluctuations in detritus-N in the ODZ during the annual cycle. This also applies for the year 2010 which confirms this image.

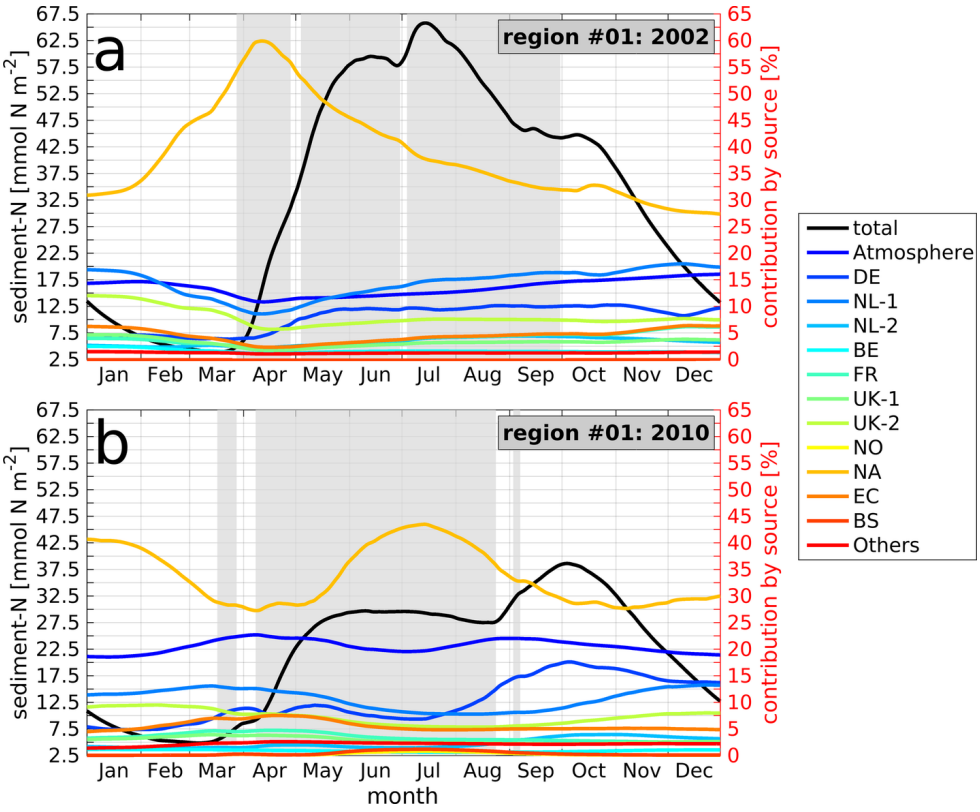

Figure 6.13: Daily time series of amount of benthic organic matter per unit area (sediment-N; black line) and relative contributions of the different N sources (coloured lines; compare Table 6.1) in the North Sea ODZ (boxes in Fig. 6.9) in (a) 2002 and (b) 2010. Black y axes refer to sediment-N, red y axes refer to relative contributions of different sources. Grey areas indicate stratified periods according to Eq. (4.4). Same legend for both panels.

The daily time series of sediment-N in the ODZ in 2002 and 2010 (Fig. 6.13a and b, respectively) show some differences compared to the detritus-N time series in Fig. 6.12. First, it can be seen that the time series of the absolute amount of sediment-N per unit area (black line; hereafter also referred to as 'concentration') in both years shows almost no short-term variability comparable to that visible in the detritus-N or NPP time series.

On the one hand, this relates to the fact that advection does not affect sediment-N concentrations. On the other hand, sediment-N is only controlled by two processes, namely the sedimentation of detritus-N as a source of sediment-N and REM_{sed} as a sink. As ECOHAM uses constant sinking velocities for slowly and fast sinking detritus ($0.4\,m\,d^{-1}$ and $10\,m\,d^{-1}$, respectively), sedimentation rates mainly depend on the detritus concentrations in the pelagic bottom layer. Similarly, REM_{sed} mainly depends on the concentration of sediment-N, applying a constant remineralisation rate of $0.0333\,d^{-1}$ to sediment-N. Besides this less variable temporal evolution of sediment-N relative to detritus-N, a temporal delay of varying magnitude relative to the temporal evolution of detritus-N can be seen. This temporal delay is due to the sinking of detritus-N and its magnitude depends on the location of maximum detritus-N concentrations within the water column and intensity of vertical mixing influencing the sedimentation speed. In 2002, the lowest sediment-N concentration of about $4\,mmol\,N\,m^{-2}$ occurs in mid-March, before it starts to increase in late March with a temporal of about two weeks relative to the increase in detritus-N concentration (see Fig. 6.12a). In 2010, the increase in sediment-N starts with a similar delay relative to the increase in detritus-N (see Fig. 6.12b), indicating higher amounts of detritus-N in the layers closer to the seafloor compared to 2002.

The steep spring increase in detritus-N in March and April 2002 results in a strong increase in sediment-N concentration, although less steep than in detritus-N. This relates to the fact that spring NPP is mainly confined to the euphotic near-surface layer, where light availability is highest. Consequently, the distance between the depth of production and the seafloor is highest and the effect of REM_{pel} on the 'removal' of organic matter from the water column is maximal. Thus, the amount of detrital matter being sedimented is small relative to the locally produced amount of organic matter. As a result, the minor peak in sediment-N concentration ($60\,mmol\,N\,m^{-2}$) in June 2002, which is caused by the phytoplankton spring bloom (and subsequent sinking of dead organic matter), occurs with a temporal delay of about one month relative to the spring maximum in detritus-N in May 2002. In 2010, an even longer temporal delay of about one and a half months between the April maximum in detritus-N and the minor sediment-N maximum in June 2010 can be found.

While the sediment-N concentration in 2010 stays on a stable level of $27.7\,mmol\,N\,m^{-2}$–$30\,mmol\,N\,m^{-2}$ during summer (May to August), sediment-N concentration in 2002 shows a second maximum in mid-July reaching a concentration of $66\,mmol\,N\,m^{-2}$. This maximum relates to the NPP and detritus-N maximum in early July 2002, which is driven by the renewal of the near-surface nutrient pool due to strong vertical mixing causing the temporary breakdown of stratification. Consequently, organic matter production is enhanced as well as the downward transport of organic matter as a result of the intensi-

fied vertical mixing. The latter also is the reason for the shorter temporal delay of less than two weeks between the increases in detritus-N and sediment-N. The average summer sediment-N concentration in 2002 is about two times higher than that in 2010. This corresponds very well with the two times higher cumulated O_2 consumption due to REM_{sed} during the stratified period in 2002 compared to 2010.

After the summer maximum in sediment-N concentration in July 2002, sediment-N shows a steady decrease until early September which corresponds to the decrease in detritus-N concentration. From then until mid-October, sediment-N concentration stays on a stable level of about $45\,\mathrm{mmol\,N\,m^{-2}}$ related to the autumn bloom causing enhanced production of organic matter, which is sedimented and balances the loss in sediment-N due to REM_{sed}. In 2010, the autumn bloom results in a distinct maximum in sediment-N yielding a concentration of $38\,\mathrm{mmol\,N\,m^{-2}}$ in early October. As for the sediment-N maximum in July 2002, sediment-N concentrations in both years start to decrease with a temporal delay of only about one week after detritus-N concentrations start to decrease. This is for the same reason for the in July 2002 maximum, namely the enhanced mixing after the breakdown of stratification, which first drives the autumn phytoplankton bloom, but also enhances the downward transport of organic matter produced in the euphotic upper layers.

It should be noted that the sediment-N concentrations at the end of the two years are quite similar to the initial concentrations at the beginning of the two years. This results from the simple sediment module used for this study, which does not allow for storage of sedimented organic matter over longer periods, and basically applies a direct temporally delayed (depending on the remineralisation rate) return of sedimented organic matter in the form of inorganic nutrients (and molecular N_2).

The annual cycles of the relative contributions of the different N sources to sediment-N show principally the same long-term (order of months) patterns as detritus-N. However, a clear temporal delay relative to the source contributions to detritus-N (see Fig. 6.12) and less strong short-term (days to weeks) fluctuations can be seen. This temporal delay is about one month during spring, e.g., between the second peak in the NA contribution to detritus-N in mid-March and the peak in the corresponding contribution to sediment-N in mid-April. In autumn, the response in the relative contributions to sediment-N is more direct to the contributions to detritus-N (e.g., about one week between the minor autumn maxima in detritus-N and sediment-N from NA). This relates to the enhanced mixing-induced, downward transport of organic matter within the pelagic.

Regarding the individual contributions of the different sources to sediment-N, it can be seen that the NA contribution dominates the evolution of sediment-N throughout the entire annual cycle of both years with minimum contributions of 27.5 %.. This is different

from the NA contribution to detritus-N in the two years, which yield minimum values of about 20 %. On the one hand, this relates to the temporal delay between detritus-N production and sedimentation. On the other hand, contributions of individual sources to detritus-N may vary within the water column. Thus, the contributions of the different sources to the vertically averaged detritus-N do not necessarily represent the contributions to detritus-N in the pelagic bottom layer. However, only this affects sediment-N. The NA contribution to sediment-N during May to August 2002 shows quite similar values as the corresponding contribution to detritus-N (taking into account the temporal delay of about two weeks). The decrease in the NA contribution to sediment-N after mid-April 2002 coincides well with the increase in overall sediment-N and with increases in the relative contributions of the atmosphere (dark blue) and, especially, the Dutch (NL-1; light blue) and German rivers (DE; blue). Most other river groups and the English Channel (EC; orange) also show an increasing influence during that period. This indicates that most of the newly sedimented organic matter was produced during NPP using larger amounts of N originating from these sources, relative to N from the North Atlantic (compare also Fig. 6.11a). In contrast to 2002, the maximum NA contribution to sediment-N in summer 2010 is about 5 % less than the maximum NA contribution to detritus-N. This relates to the slightly higher influences of the atmosphere as well as the NL-1 and DE rivers compared to detritus-N.

The increase in sediment-N in autumn 2010 is accompanied by increasing contributions of the German, Dutch (NL-1 and NL-2) and UK-2 (light green) rivers indicating that this high amount of N originating from these sources is bound in the newly sedimented organic matter. In September/October 2002, only the atmospheric contribution shows a clear increase (and later that from the NA), underlining the differences in the N supply from the large continental rivers between the two years.

In general, the analysis of the time series of NPP (Fig. 6.11), detritus-N (Fig. 6.12) and sediment-N (Fig. 6.13), and their contributing sources, clearly illustrates the direct link between local NPP and the amount of detritus-N and sediment-N in the North Sea ODZ. This confirms the findings of Sect. 5.2 that near-surface NPP and subsequent REM_{pel} and REM_{sed} below the MLD constitute the main controlling factors of GOC. This strong link in combination with the relative importance of the different N sources (see also Tables 6.4 and 6.5) further allow for the conclusion that the N supplies from the North Atlantic, the atmosphere and the large Dutch and German rivers dominate the N dynamics in the ODZ.

6.5 Conclusions on the trans-boundary nutrient transport analysis of nitrogen

This chapter presented a newly developed software which allows for the calculation of TBNT on the basis of the biogeochemical model ECOHAM. The design of TBNT as a post-processing software principally allows for the future application to models other than ECOHAM. This constitutes the major technical difference to existing TBNT studies, which required either the implementation of the TBNT method to the applied model (e.g., Blauw et al., 2006; Ménesguen et al., 2006; Lacroix et al., 2007; Neumann, 2007; Timmermann et al., 2010; Troost et al., 2013; Perrot et al., 2014) or in-depth knowledge of the program code of the base model (Radtke et al., 2012; Radtke and Maar, 2016). In contrast, the here described software only needs information about the model grid structure and a description which state variables interact via which model processes in order to enable the calculation of TBNT. Despite this post-processing approach the presented software provides results very similar to previous TBNT studies on the North Sea (OSPAR, 2010; Painting et al., 2013; Troost et al., 2013). Though, the North Atlantic influence in the southeastern North Sea might be slightly overestimated.

The results for TN provide information on the spatial dispersal of N from non-atmospheric sources, as TN is only affected by advection, atmospheric deposition and the loss of molecular N_2 due to REM_{sed}. In contrast, NPP is influenced by additional factors (light/P/Si limitation). Despite these differences in complexity, the spatial distributions of the source-related, average relative contributions to TN and NPP in 2002 and 2010 are quite similar for all analysed sources. This is an important insight as it suggests that TN can be used as a proxy for the impact of N on NPP in most regions. However, differences of up to 30 % can occur locally, e.g., for the DE contributions in the German Bight. Besides this, minor differences (<2 %) between the contributions to TN and NPP only occur for the atmospheric contribution with a higher contribution to NPP.

The spatial distributions of the source-related contributions to TN and NPP show that the North Atlantic inflow of N dominates the entire northern and most parts of the central North Sea. The NA contribution to N is still high in the offshore regions of the southern North Sea, with relative contributions of above 25 %. In the central North Sea, the atmosphere and partly the rivers at the British east coast (UK-2) constitute additional relevant sources. The atmosphere contributes 5 %–12 % to TN and slightly higher values to NPP, which relates to the input of atmospheric N into the euphotic surface layer. In the southern central North Sea, the UK-2 rivers also contribute to more than 5 % of TN and NPP. In the central part of the southern North Sea, the Dutch NL-1 rivers (Rhine and Meuse) and atmospheric deposition constitute the main contributing sources to TN

and NPP. Here, the analysis yields a 10 %–15 % atmospheric contribution to NPP, and 10 %–25 % by the NL-1 rivers.

For the southeastern North Sea, the analysis clearly shows the dominance of the German rivers (DE; Elbe, Ems, Weser) on TN and NPP. However, although the Elbe constitutes one of the largest North Sea tributaries, the DE influence is strongly confined to the inner German Bight and the Danish west coast. In the inner German Bight the DE contribution to TN and NPP exceeds 50 % during the considered years, which emphasises the great importance of these rivers for the biochemistry of that area.

The TN time series at the ODZ study site shows that advection of nutrient-rich water is essential for the preconditioning of the pool of N (and other nutrients). In 2002, the large N supply originating from the NA and the Dutch rivers caused remarkably high N levels at the end of the winter period (1.5 times higher than in 2010), enabling very high spring and summer NPP.

The good agreement between the temporal evolution of detritus-N and sediment-N relative to NPP, and between the evolution of the individual contributions by the different sources, also demonstrates the strong link between local NPP and the amounts of detrital matter in the pelagic and sediment. This supports the use of NPP as an indicator for organic matter for the definition of the ODI (see Sect. 5.2.3.2). As REM_{pel} and REM_{sed} constitute the major O_2 consuming processes it can be concluded that the major sources of organic N in the ODZ control the O_2 dynamics in the North Sea ODZ.

Among the traced N sources, the NA contribution constitutes the major contributing source to NPP in the ODZ (30 %–40 %). The second most important source is the atmosphere (13 %–22 %) followed by the large Dutch (NL-1; 10 %–15 %), German (8 %–10 %) and UK-2 (6 %–7 %). The analyses show that the other large, but more remote sources (English Channel, French and southern British rivers) also have a relevant influence to the NPP in the ODZ, adding up to about 10 %–12 %.

The comparison of the riverine against the non-riverine N sources showed that the relative contribution of non-riverine sources to NPP in the ODZ results in roughly 60 %, while that of the riverine sources accounts for only about 40 %. This suggests that N reduction measures in the catchment areas of the main contributing rivers, e.g., according to the WFD (EU, 2000), will only have a limited effect on NPP and thus the O_2 conditions of the ODZ. However, the atmospheric contribution to detritus-N and sediment-N at the ODZ site yields about 13 % in 2002 and almost 21 % in 2010. This suggests that future reductions in atmospheric N deposition, as agreed on by the so-called Gothenburg Protocol (UNESC, 1999), will have an additional positive effect on the O_2 conditions in the ODZ.

Chapter 7

The influence of nitrogen inputs on the North Sea oxygen dynamics

In this chapter the O_2 consumption related to N input from riverine and non-riverine (see Table 6.1) as well as anthropogenically affected and non-affected sources will be investigated in a quantitative way. For this purpose, an extension of the TBNT method (Sect. 6.1) is presented which enables the link of biochemical processes affecting O_2 to the N originating from different sources. This approach, for the first time, allows for the quantification of the influence of N from different sources on the O_2 dynamics of the North Sea under recent environmental conditions. The presented analyses focus on the dynamics of the ODZ study site, but the Oyster Grounds region is additionally considered as it is well known to be susceptible to O_2 deficiency (e.g., Greenwood et al., 2010). Finally, an N reduction exercise is conducted and the effects on the North Sea O_2 dynamics in relation to the individual N sources are discussed.

7.1 Linking oxygen dynamics to labelled nitrogen

To date, the TBNT method allows for the tracing of elements (and related state variables) from individual external sources, such as rivers or the atmosphere, within biogeochemical models. However, the described methodology implies that the element, that is labelled, does not change, i.e., information about its source cannot be passed from one element to another (e.g., from N to O_2). Therefore, the investigation of the influence of N input from selected sources on the O_2 dynamics requires, first, the labelling and tracing of the N state variables (and connecting processes) from these sources and, second, the establishment of a link between the labelled N variables and processes with the processes affecting O_2.

For biogeochemical processes within the O_2 cycle whose formulation within the underlying model is based on a state variable containing the labelled element, this state variable can be used to create the link to the O_2 cycle, analogous to the description in Sect. 6.1.2. For processes whose formulation is based on a different element than the labelled one (e.g., C instead of N), a different approach has to be chosen for creating the link between the

labelled element and the O_2 cycle.

As shown in Fig. 3.1 the O_2 cycle within ECOHAM is linked to the cycles of C, N and P by different processes. NPP provides a link to the elemental cycles of C, N and P. The same applies to RES_{zoo}, REM_{pel} and REM_{sed}, while NIT and pelagic denitrification are only linked to the N cycle. However, the latter is not considered in ECOHAM as it only takes place under anoxic conditions which do not occur in the pelagic of the North Sea (compare Sect. 3.2.1).

In the case of N labelling NIT has to be considered. According to ECOHAM's process formulation of NIT (see Eq. (3.8)), the O_2 consumption related to NIT is proportional to the available amount of dissolved NH_4^+. Thus, the O_2 consumption due to NIT of NH_4^+ from a selected N source i is calculated as:

$$P^i_{O_2,\mathrm{nit}}(\Delta t, j) = R^i_{NH_4^+}(t_0, j) \cdot P_{O_2,\mathrm{nit}}(\Delta t, j). \tag{7.1}$$

Here, $R^i_{NH_4^+}(t_0, j)$ represents the relative fraction of NH_4^+ from source i according to Eq. (6.18), and $P_{O_2,\mathrm{nit}}$ represents the NIT process on bulk NH_4^+ as calculated by ECOHAM.

The other biogeochemical processes affecting the O_2 dynamics are formulated based on C: NPP, RES_{zoo}, REM_{pel} and REM_{sed} (see Sect. 3.2.1). Thus, for these processes no N-based model state variable exists which provides a direct link from the N cycle to the O_2 cycle. However, within ECOHAM all these processes – except REM_{sed} – are conducted by organisms (phytoplankton, zooplankton, bacteria) which contain C as well as N (and also P). Therefore, these organisms act as some kind of 'mediator' and can be used for establishing the link between labelled N and the O_2 cycle. The same applies to the linking of the O_2 cycle to labelled P which is, however, not part of this study.

The TBNT method described in Sect. 6.1.2 allows for the calculation of the relative fractions of these mediators containing N from a selected source (see Eqs. (6.15), (6.17) and (6.18)). These relative fractions represent that portion of the mediator containing N from a specific source. Therefore, these relative fractions in combination with the corresponding bulk processes of the O_2 cycle can be used to calculate the O_2 consumption or production (in case of NPP) similar to Eq. (7.1). Accordingly, the change in O_2 by a specific process and due to N input from a selected source i is calculated as follows:

$$P^i_{O_2}(\Delta t, j) = R^i_{X_M}(t_0, j) \cdot P_{O_2}(\Delta t, j). \tag{7.2}$$

P_{O_2} represents the bulk process affecting O_2 and $R^i_{X_M}$ represents the relative fraction of the mediator state variable X_M from source i according to Eq. (6.18). In the here presented case of N labelling, X_M refers to the following ECOHAM state variables: diatom-N and flagellate-N for NPP, micro- and mesozooplankton-N for RES_{zoo} and bacteria-N for REM_{pel}. In the case of P labelling, the corresponding P state variables need to be used.

The major underlying assumption of Eq. (7.2) is, that (besides light limitation) the build-up of organic matter by NPP is limited by the availability of nutrients (e.g., N). This implies that the uptake and thus the amount of C in organic matter is proportional to the uptake and amount of, e.g., N. The relation between the two is not necessarily linear, e.g., in case of temporally varying stoichiometry. Nevertheless, the assumption that higher amounts of N bound in organic matter allow for higher amounts of C in that organic matter remains valid. This can be applied analogously to bacteria.

For REM_{sed} (i.e., benthic O_2 consumption) no real mediator state variable exists within ECOHAM as the process only depends on the concentration of POC in the sediment and a fixed C remineralisation rate (see Eq. (3.18)). However, the above described assumption can also be applied as the organic matter was initially produced by NPP, i.e., the amount of POC is related to that of PON. Therefore, the calculation of REM_{sed} also follows Eq. (7.2), with X_M representing sediment-N in the case of N labelling (i.e., sediment-P in case of P labelling).

7.2 The influence of nitrogen inputs on biochemical oxygen consumption

Nutrients from different sources influence both, O_2 production due to NPP and O_2 consumption due to biochemical processes (REM_{pel}, REM_{sed}, RES_{zoo}, NIT). Therefore, this section first provides an overview of the spatial patterns in O_2 consumption in the North Sea and the contributions related to N from the different riverine and non-riverine sources (see Table 6.1). For this purpose, first O_2 consumption is considered in an integrated manner using the net O_2 consumption (NOC) and GOC. The former is calculated as the sum of the biochemical O_2-consuming processes minus O_2 production by NPP, while the latter represents the sum of the O_2 consumption processes only.

7.2.1 Spatial distributions of oxygen consumption

In order to provide an overview on the general spatial patterns in biochemical O_2 production and consumption in the North Sea, Fig. 7.1 shows the annual NOC integrated over different depths ranges for the years 2002 and 2010.

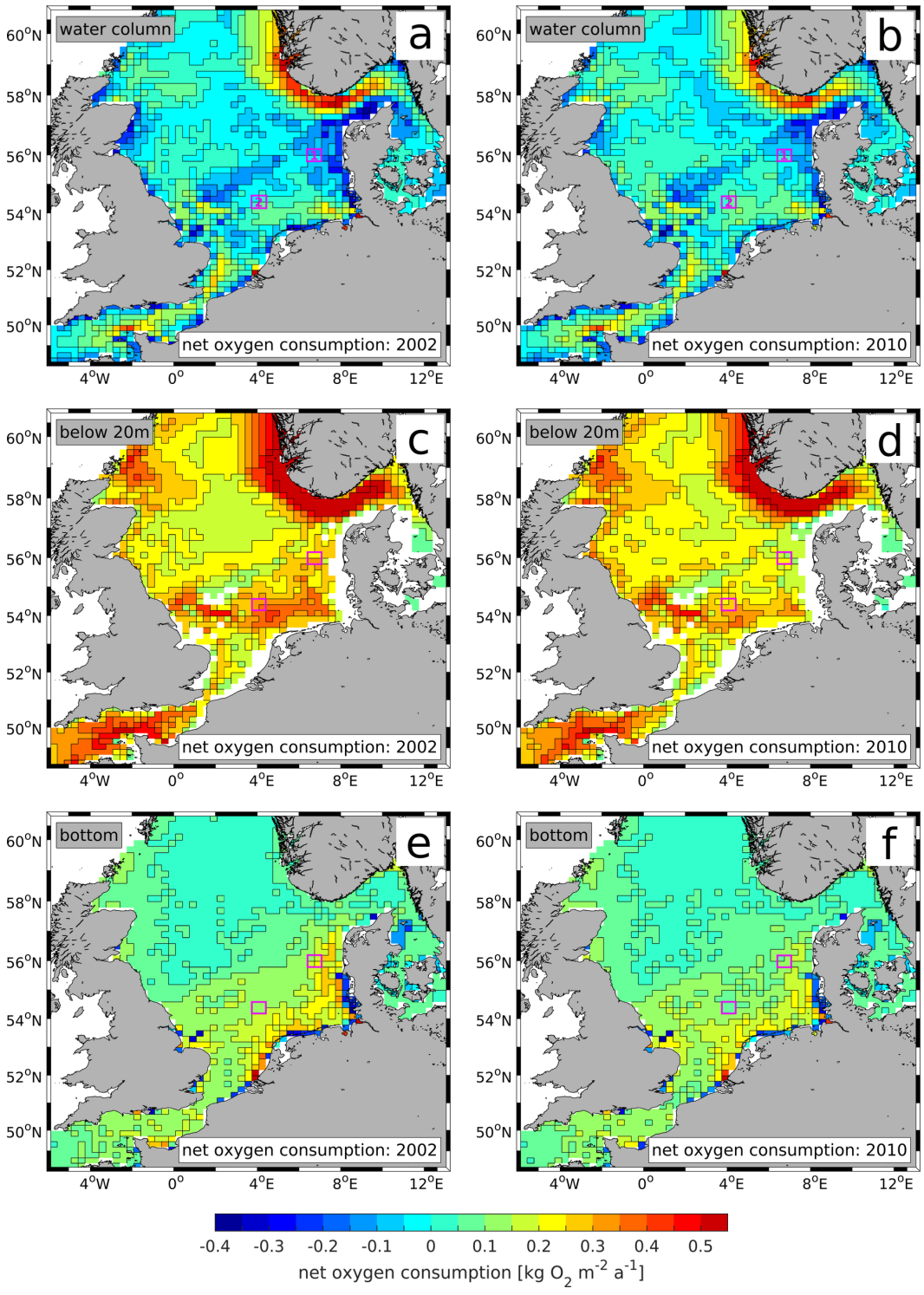

Figure 7.1: Spatial distributions of annual net O_2 consumption (NOC) integrated (a, b) over the entire water column, (c, d) from 20 m to bottom and (e, f) in the model bottom layer, in (a, c, e) 2002 and (b, d, f) 2010. Colour scale cut at upper end. Box #1: ODZ site, box #2: Oyster Grounds. White areas in (c, d) shallower than 20 m.

The NOC integrated over the entire water column (Fig. 7.1a and b) indicates whether a region constitutes a source (negative NOC) or sink (positive NOC) of O_2. However, as shown in Sect. 5.2, NPP mainly takes place in the euphotic near-surface layers. Therefore, Fig. 7.1c and d show the NOC integrated over the entire depth range below a fixed MLD of 20 m ($V_{\mathrm{sub,fix}}$), and as lowest O_2 concentrations occur closest to the bottom, Fig. 7.1e and f show the NOC within the model bottom layer.

Figure 7.1a and b show that the principal spatial patterns in water column integrated annual NOC are quite similar for both years, 2002 and 2010. Negative NOC, i.e., net production of O_2 occurs in most of the shallow coastal regions, over the Dogger Bank and also southwest of the Norwegian Trench. The lowest values of about $-0.37\,\mathrm{kg\,O_2\,m^{-2}\,a^{-1}}$ occur northeast of the Wash at about 53.3 °N, 1 °E. In contrast, NOC is very high in the Norwegian Trench, due to the great water depth implying high O_2 consumption within the pelagic, and in the river mouths of Elbe as well as Rhine and Meuse, where maximum values up to $0.52\,\mathrm{kg\,O_2\,m^{-2}\,a^{-1}}$ are reached. The latter results from the input of large amounts of detrital matter by the rivers, resulting in enhanced O_2 consumption. In the northwestern and southern North Sea, NOC is slightly positive with values up to $0.15\,\mathrm{kg\,O_2\,m^{-2}\,a^{-1}}$. A local maximum with values up to $0.45\,\mathrm{kg\,O_2\,m^{-2}\,a^{-1}}$ can be seen in the English Channel near the French coast.

At the ODZ site (see box #1 in Fig. 7.1a and b). NOC is slightly negative and further decreases in northern direction, i.e., NPP exceeds GOC in that region. In the Oyster Grounds region (see box #2 in Fig. 7.1a and b), which was found to be susceptible to O_2 deficiency, e.g., by Greenwood et al. (2010), NOC is positive with values around $0.1\,\mathrm{kg\,O_2\,m^{-2}\,a^{-1}}$.

The NOC in the water column between 20 m depth and the bottom (Fig. 7.1c and d) shows similar relative spatial differences as the NOC within the entire water column (white areas indicate regions shallower than 20 m). However, with the major difference that it is consistently positive, due to very low NPP below 20 m in most regions. The spatial patterns found in NOC below 20 m basically represent the patterns of near-surface NPP (i.e., organic matter production; see Fig. 5.8). The highly productive, but shallow regions of the southern and in the northwestern North Sea show high NOC values up to $0.4\,\mathrm{kg\,O_2\,m^{-2}\,a^{-1}}$ in both years. The same applies to the Norwegian Trench, where maximum values above $0.55\,\mathrm{kg\,O_2\,m^{-2}\,a^{-1}}$ occur in most parts, as a result of high near-surface NPP and great water column depth implying high O_2 consumption in the pelagic.

In the southern North Sea the NOC below 20 m is clearly higher in 2002 than in 2010 (Fig. 7.1c and d, respectively), with values above $0.25\,\mathrm{kg\,O_2\,m^{-2}\,a^{-1}}$ in most regions. In contrast, values are higher in the central North Sea in 2010 compared to 2002. These relative changes between the two years in the two regions correspond to the changes in

near-surface NPP (see Fig. 5.8).

At the ODZ site, the NOC below 20 m yields $0.2\,\mathrm{kg\,O_2\,m^{-2}\,a^{-1}}$–$0.35\,\mathrm{kg\,O_2\,m^{-2}\,a^{-1}}$ in 2002, compared to values of only $0.1\,\mathrm{kg\,O_2\,m^{-2}\,a^{-1}}$–$0.25\,\mathrm{kg\,O_2\,m^{-2}\,a^{-1}}$ in 2010. In the vicinity of the ODZ, the 2002 values are also clearly higher than in 2010, due to the higher NPP in 2002 in that area. The same holds for the Oyster Grounds region, where 2002 values yield $0.3\,\mathrm{kg\,O_2\,m^{-2}\,a^{-1}}$–$0.4\,\mathrm{kg\,O_2\,m^{-2}\,a^{-1}}$, compared to only $0.2\,\mathrm{kg\,O_2\,m^{-2}\,a^{-1}}$–$0.3\,\mathrm{kg\,O_2\,m^{-2}\,a^{-1}}$ in 2010. The higher values in the Oyster Grounds area relative to those in the ODZ result from the greater bottom depth in the Oyster Grounds region.

The NOC in the bottom layer for the years 2002 and 2010 are shown in Fig. 7.1e and f, respectively. Different to the NOC below 20 m, it shows negative values in some shallow coastal regions, which simply relates to the fact that these regions were not taken into account due to the low bottom depth. Except for these few coastal areas, bottom layer NOC is positive due to decreasing NPP with increasing depth as a result of light limitation. For the same reason, the NOC in the bottom layer is higher in coastal regions, compared to the regions farther offshore, as NPP is high and large amounts of organic matter reach the bottom due to shallower bottom depth.

One interesting aspect can be seen in the vicinity of the mouths of Rhine/Meuse and Elbe. In both cases bottom layer NOC is very high ($0.52\,\mathrm{kg\,O_2\,m^{-2}\,a^{-1}}$) directly at the river mouth due to the large input of detrital matter. In the former case NOC also shows high values further downstream the continental coastal current, while in the case of the Elbe, NOC is strongly negative ($-0.2\,\mathrm{kg\,O_2\,m^{-2}\,a^{-1}}$ to $-0.35\,\mathrm{kg\,O_2\,m^{-2}\,a^{-1}}$) in the very near-shore areas north of the Elbe mouth. This implies that in these regions NPP, driven by nutrient input from the Elbe (see Fig. 6.10g and h), exceeds GOC. Farther offshore, NOC clearly increases, showing positive values of $0.2\,\mathrm{kg\,O_2\,m^{-2}\,a^{-1}}$–$0.35\,\mathrm{kg\,O_2\,m^{-2}\,a^{-1}}$ and $0.15\,\mathrm{kg\,O_2\,m^{-2}\,a^{-1}}$–$0.3\,\mathrm{kg\,O_2\,m^{-2}\,a^{-1}}$ in 2002 and 2010, respectively. Consequently, bottom layer NOC in the ODZ in 2002 is also higher than in 2010 as discussed in Sect. 5.2.5. In the offshore regions of the southern North Sea, bottom layer NOC is only slightly higher in 2002 than in 2010, with an average difference of about $0.05\,\mathrm{kg\,O_2\,m^{-2}\,a^{-1}}$ between the two years. This also holds for the Oyster Grounds region where NOC in 2002 yields $0.1\,\mathrm{kg\,O_2\,m^{-2}\,a^{-1}}$–$0.15\,\mathrm{kg\,O_2\,m^{-2}\,a^{-1}}$, compared to $0.05\,\mathrm{kg\,O_2\,m^{-2}\,a^{-1}}$–$0.1\,\mathrm{kg\,O_2\,m^{-2}\,a^{-1}}$ in 2010. In the deeper central and northern North Sea, bottom layer NOC is generally lower than in the shallower southern and coastal North Sea, with slightly higher values in 2010 than in 2002 similar to NOC below 20 m.

As seasonal stratification separates the NPP-dominated near-surface layers from the deeper layers below the MLD, where GOC clearly exceeds NPP (see Fig. 7.1c and d), Fig. 7.2 shows the annual, vertically integrated GOC for the water column below 20 m depth and the model bottom layer in years 2002 and 2010. In both years NPP below 20 m

is less than $0.005\,\mathrm{kg\,O_2\,m^{-2}\,a^{-1}}$ within the entire southern North Sea (including Oyster Grounds) and below $0.015\,\mathrm{kg\,O_2\,m^{-2}\,a^{-1}}$ in the vicinity of the ODZ; NPP is negligible in the bottom layer of the entire offshore North Sea (both not shown).

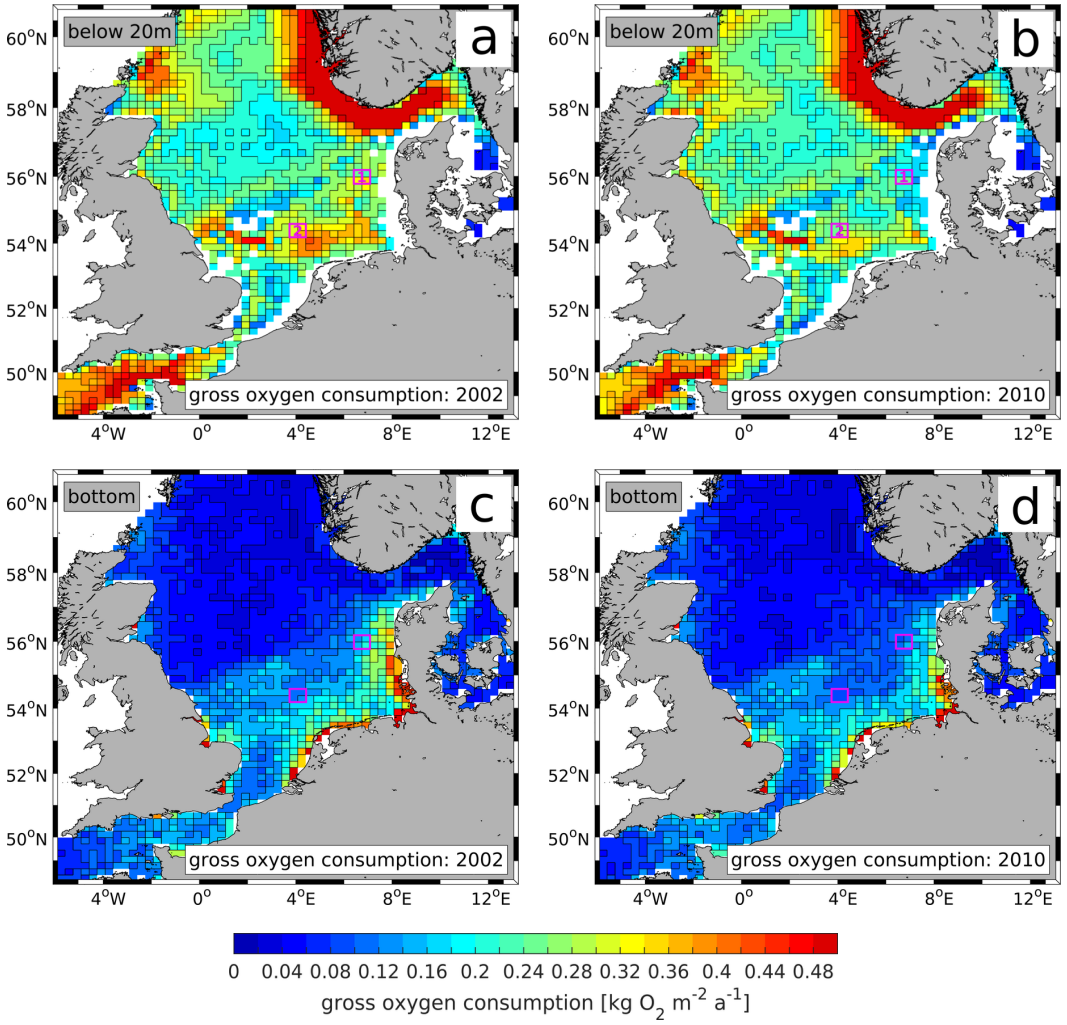

Figure 7.2: Spatial distributions of annual gross O_2 consumption (GOC) integrated (a, b) from 20 m to bottom and (c, d) in the model bottom layer, in (a, c) 2002 and (b, d) 2010. Colour scale cut at upper end. Box #1: ODZ site, box #2: Oyster Grounds. White areas in (a, b) shallower than 20 m.

Figure 7.2a and b show the GOC below 20 m in the years 2002 and 2010, respectively. Similar to the NOC, the GOC integrated over the entire water column below 20 m illustrates the combined effect of organic matter availability (mainly originating from near-surface NPP) and water column depth. The spatial patterns are very similar to those in the corresponding NOC (Fig. 7.1c and d, respectively), with very high values in the

Norwegian Trench (>0.5 kg O_2 m^{-2} a^{-1}), in the northwestern North Sea and in the highly productive southern North Sea. Low values of less than 0.016 kg O_2 m^{-2} a^{-1} occur in the central North Sea due to low near-surface NPP as well as on and northeast of the Dogger Bank due to the shallow water column depth.

As for NOC, the 2002 values in GOC are higher than in 2010 in the southern North Sea with maximum values of about 0.4 kg O_2 m^{-2} a^{-1} southeast of the Oyster Grounds area (see box #2 in Fig. 7.2a). In 2010, GOC is higher in the areas directly south and west of the Dogger Bank and also in the northern North Sea. In the Southern Bight (north of the Strait of Dover) GOC is generally low as a result of low NPP in this area (see Fig. 6.10).

In the vicinity of the ODZ (box #1 in Fig. 7.2a and b), GOC yields 0.26 kg O_2 m^{-2} a^{-1}–0.36 kg O_2 m^{-2} a^{-1} in 2002 and 0.12 kg O_2 m^{-2} a^{-1}–0.24 kg O_2 m^{-2} a^{-1} in 2010. This implies that annual GOC in the ODZ in 2002 is 1.5–2 times higher than in 2010 which is in good agreement with the results for O_2 consumption during the summer stratified period (see Sect. 5.2.5.1, Table 5.2).

The GOC in the model bottom layer is shown in Fig. 7.2c and d for the years 2002 and 2010, respectively. Bottom layer GOC basically represents bottom layer NOC (see Fig. 7.1e and f; different colour scale than Fig. 7.2), except for the very shallow coastal areas dominated by NPP (i.e., positive NOC). In the shallow southern North Sea, bottom layer GOC basically matches the spatial patterns and temporal differences between the two years, although it is positively modulated in the very near-shore areas affected by riverine input of detrital matter. Consequently, GOC is highest in the inner German Bight due to high inorganic nutrient loads driving NPP and additional organic loads especially from the Elbe and Weser. In the coastal strip (with a width of about 20 km) from the mouths of Rhine and Meuse until the mouth of river Ems, GOC also shows clearly elevated values compared to the regions farther offshore. At the mouths of Rhine/Meuse and Elbe, maximum GOC values of 1.9 kg O_2 m^{-2} a^{-1} and 1.4 kg O_2 m^{-2} a^{-1} are reached in 2002 and 2010, respectively.

Although GOC in these regions is much higher than in the regions farther offshore, simulated O_2 concentrations around these river mouths are clearly higher than in the central southern North Sea (see Fig. 5.6c and d), due to the shallow water depth resulting in strong vertical mixing. Only directly at the river mouth locations of Rhine/Meuse, Elbe and Weser, minimum O_2 concentrations are similarly low as in the ODZ due to the remineralisation of detrital matter from the rivers and high summer SST reducing O_2 solubility. Near the major British tributaries, GOC is also significantly higher than in the offshore areas as a result of riverine organic matter input.

At the ODZ site (box #1 in Fig. 7.2c), bottom layer GOC results in 0.12 kg O_2 m^{-2} a^{-1}–0.2 kg O_2 m^{-2} a^{-1} in 2002, compared to only 0.06 kg O_2 m^{-2} a^{-1}–0.14 kg O_2 m^{-2} a^{-1} in 2010.

This corresponds well with the about 2 times higher O_2 consumption during the summer stratified period in 2002 relative to 2010 (see Sect. 5.2.5.1, Table 5.2). In the Oyster Grounds area (box #2), bottom layer GOC reaches values of $0.1\,kg\,O_2\,m^{-2}\,a^{-1}$–$0.14\,kg\,O_2\,m^{-2}\,a^{-1}$, while in 2010 only slightly lower values of about $0.09\,kg\,O_2\,m^{-2}\,a^{-1}$ are shown.

In the northern and central North Sea – north of the imaginary line between Dogger Bank and the northern tip of Denmark – both years show generally low bottom layer GOC of less than $0.06\,kg\,O_2\,m^{-2}\,a^{-1}$ and decreasing values with increasing depth as less detrital matter reaches the bottom, and RES_{zoo} being negligible due to low zooplankton biomass. The latter results from the fact that zooplankton constitute the highest trophic species and closure term of the trophic pyramid in ECOHAM and are directly linked to phytoplankton biomass.

In summary, the spatial distributions of annual, water column integrated NOC (Fig. 7.1a and b) show that most shallow coastal regions constitute a net source of O_2, while in most offshore regions GOC exceeds O_2 production. In fact, GOC surmounts O_2 production in all North Sea regions as soon as only the deeper layers (below a fixed depth horizon of 20 m) are considered (see Fig. 7.1c and d). This confirms that seasonal stratification in the North Sea (with an average MLD of 15 m–20 m) separates the productive surface layers from the O_2 consuming sub-MLD volume. In the bottom layer, NOC (Fig. 7.1e and f) and GOC (Fig. 7.2c and d) are very similar as bottom layer NPP is very small in most regions due to low light availability. The good agreement between the spatial patterns of summer surface NPP (see Fig. 5.8) and bottom layer NOC and GOC also confirms the strong link between surface productivity and sub-surface O_2 consumption.

7.2.2 Spatial distributions related to different nitrogen sources

As this thesis focuses on O_2 deficiency in the North Sea, which usually evolves near the bottom, where NPP (i.e., O_2 production) is negligible relative to GOC in most regions, Fig. 7.3 shows the relative contributions of the major N sources to bottom layer GOC in the North Sea. The selected sources are the same as in Sect. 6.4.1, namely: North Atlantic (NA), Atmosphere, Dutch NL-1 rivers, German rivers (DE) and British UK-2 rivers (see Fig. 6.3 for NA boundary and river locations). It should be noted that the spatial patterns in the different contributions are very similar for both bottom layer GOC and GOC below 20 m depth.

Figure 7.3a and b show the relative contributions of N originating from the NA to annual bottom layer GOC in 2002 and 2010, respectively. The basic spatial patterns and differences between the two years are similar to those shown for the NA contributions to annually and water column averaged TN (see Fig. 6.7a and b) and annual, water

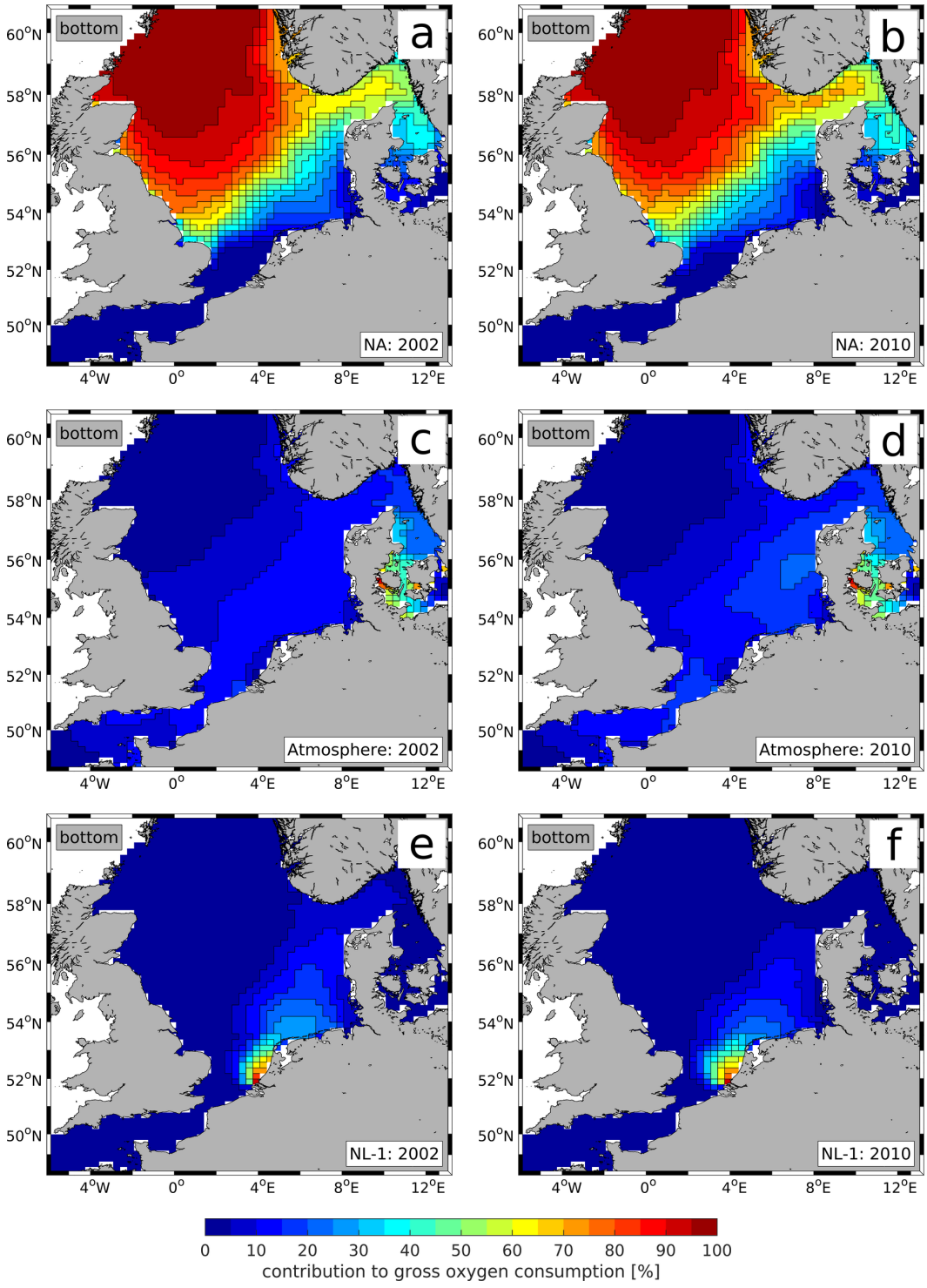

Figure 7.3: Spatial distributions of relative contributions of different N sources to annual bottom layer gross O_2 consumption for (a, c, d) 2002 and (b, d, f) 2010. Sources: (a, b) North Atlantic (NA), (c, d) atmosphere, (e, f) 1st group of Dutch rivers (NL-1). Same scale for all panels.

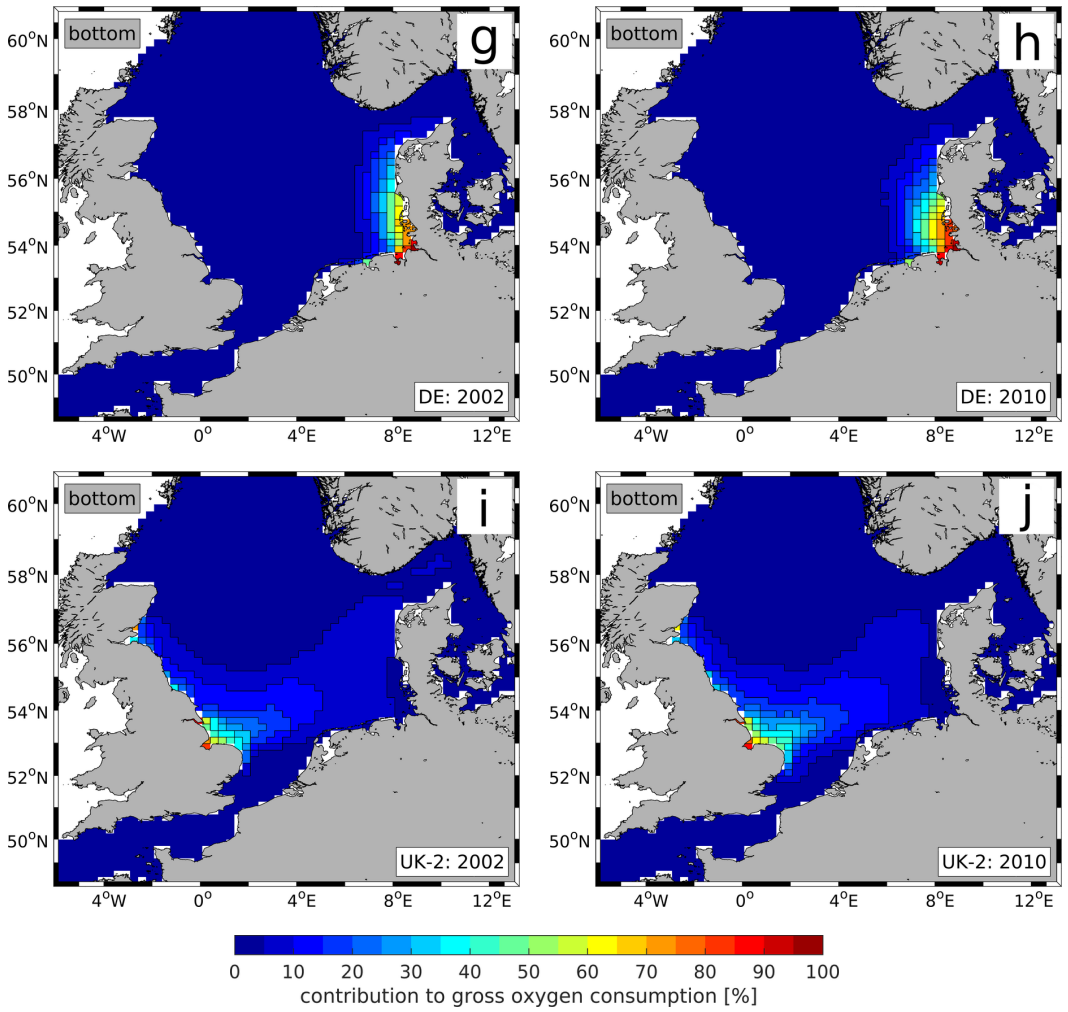

Continued: (g, h) German rivers (DE) and (i, j) 2nd group of British rivers (UK-2) in (g, i) 2002 and (h, j) 2010.

column integrated NPP (see Fig. 6.10a and b). However, the spatial patterns in the NA contributions to NPP are in slightly better agreement with those to bottom layer GOC. On the one hand, this is somehow surprising as one could expect that the contribution to TN within the entire water column is more representative for the O_2 consumption linked to N from an individual source than NPP, which only occurs in the upper tens of metres of the water column. On the other hand, this underlines the great importance of local near-surface NPP on GOC near the seafloor.

As for NPP, the NA contribution to GOC is highest in the entire northwestern North Sea (north of 57 °N), with contributions of above 95 %. In the eastern Norwegian Trench, it also shows high values (>60 % in 2002, 65 %–75 % in 2010). In southeastern direction

its contribution is gradually decreasing and is less than 60 % southeast of the imaginary line between Dogger Bank and northern Denmark. In the Southern Bight its influence is lowest with values of consistently less than 5 %. In the German Bight its contribution decreases from about 40 % at 55 °N, 6 °E to less than 5 % near the mouths of Elbe and Weser. Variations between 2002 and 2010 are small, except for the difference in the eastern Norwegian Trench and Skagerrak.

The relative contributions of atmospheric N deposition to GOC in 2002 and 2010 are shown in Fig. 7.3c and d, respectively. Here, the spatial patterns are also similar to those for TN and NPP, however, the agreement between the atmospheric contribution to TN and that to GOC is better, which relates to the fact that atmospheric N has a stronger impact on near-surface NPP than on processes in the bottom layer.

Highest atmospheric contributions of 40 %–90 % occur in the Belt Sea east of Denmark, where the amount of riverine N from other sources is low. In the North Sea region, the atmospheric contribution to GOC reaches values of above 15 % in the eastern North Sea in 2010. In most parts of the southern North Sea its contribution ranges between 10 % and 15 %, except for the coastal areas influenced by the large continental rivers (e.g., Seine, Rhine/Meuse and Elbe). In 2002, its contribution to GOC in the southern North Sea is slightly less than in 2010, however, still reaches values of above 10 % in most areas. As for NPP and TN, the atmospheric contribution to bottom layer GOC steadily decreases towards the northwestern North Sea, where values stay consistently below 5 %. The GOC related to N from the Dutch NL-1 rivers (see Fig. 7.3e and f) also shows similar patterns as for the NL-1 contributions to TN (Fig. 6.7e and f) and NPP (Fig. 6.10e and f). Similar to the NA contribution, the agreement with its contribution to NPP is slightly better, e.g., in the eastern Norwegian Trench, where it contributes to more than 5 % of bottom GOC, while its contribution to TN is less than 5 % in that region. The generally higher influence of N from the NL-1 rivers on GOC in the southeastern North Sea in 2002, relative to 2010, corresponds with the differences between the two years seen in TN and NPP.

Interestingly, the NL-1 contribution to bottom GOC in the coastal regions northeast of the mouths of Rhine and Meuse is a bit less than that to TN and NPP. This relates to the fact that N originating from these rivers directly affects the contribution to TN and (in case of inorganic N input) the contribution to NPP in the vicinity of the river mouths. In contrast, the riverine input of organic matter only directly influences GOC around the river mouth, while farther away riverine inorganic and organic N affect GOC with a slight temporal delay relative to NPP due to sinking. In addition, the ratio between inorganic and organic N originating from the rivers can change, while it is advected downstream the continental coastal current, due to the biochemical overturning.

The spatial distributions of the relative contribution to GOC related to N from the

DE rivers in 2002 and 2010 (Fig. 7.3g and h, respectively) are very similar to both, the DE contributions to TN (Fig. 6.7g and h) and NPP (Fig. 6.10g and h). This relates to the shallow water depth in the regions affected by the DE rivers, which implies that NPP occurs within the entire water column. The relative contributions in both years are highest in the inner German Bight with values above 95 % near the mouths of Elbe and Weser. In 2002, the high-contribution region is more confined to the Danish west coast, due to higher contributions from the North Atlantic, atmospheric deposition and NL-1 rivers, compared to 2010. For the same reason, the DE influence on GOC is less in the inner German Bight with values of above 80 % in the grid cells directly neighbouring the input locations of Elbe and Weser, while such high contributions are reached in a larger area in 2010. This also corresponds well with the differences between 2002 and 2010 regarding the DE contribution to TN and NPP. In general, the relative contribution of the DE rivers to GOC tends to be slightly lower than those to TN and NPP, for the same reason as discussed for the NL-1 rivers.

The contribution of the UK-2 rivers to GOC in the North Sea (Fig. 7.3g and h) also shows spatial patterns very similar to the corresponding contributions to TN (Fig. 6.7g and h) and NPP (Fig. 6.10g and h). Contributions are highest in the vicinity of the large rivers at the British east coast (tributaries to The Wash, Humber and Tees). Interestingly, their contribution to GOC in the offshore regions of the southwestern North Sea is slightly less compared to their contributions to TN and NPP, while it is slightly higher in the southeastern North Sea (visible in the extension slightly farther east). This likely relates to the different depth ranges considered (entire water column for TN and NPP, bottom layer for GOC) and the influence of sediment-N left over from the year prior to the considered year (i.e., 2001 and 2009, respectively) and whose remineralisation continues until January/February of the considered year (see, e.g., Fig. 6.13).

In summary, the relative contributions of the different N sources to bottom layer GOC in 2002 and 2010 are very similar to the corresponding contributions to TN and NPP. This results from the direct link between N-containing model state variables and the O_2-consuming processes introduced in this thesis (see Eqs. (7.1) and (7.2)). However, although the general patterns and differences between the presented years 2002 and 2010 are quite similar, the spatial distributions also revealed some differences compared to those provided for TN and NPP, which partly relate to the differences regarding the considered depth range (in regions of greater depth), but effects of biochemical overturning of organic and inorganic matter in the vicinity of rivers.

Despite these minor differences, the presented qualitative analysis suggests that TN and NPP can be used as proxies for GOC in most regions related to N input from the individual sources. In the following, this question will be further analysed with respect to

the temporal variability at the ODZ site and in the Oyster Grounds region (see Fig. 7.2, boxes #1 and #2, respectively). Additionally, a quantitative analysis of the influence of the different N sources on the O_2 dynamics in these regions is provided. The Oyster Ground area is analysed as O_2 deficiency was observed in this region in July/August 2007 and 2008 (see Fig. 5.3c; Greenwood et al., 2010).

7.2.3 Sources of oxygen consumption in the oxygen deficiency zone

The annually integrated bottom layer GOC in the ODZ for the years 2002 and 2010 is provided in Table 7.1, together with the relative contributions of the different N sources for the two years. The average bottom layer thickness in the ODZ is 6.5 m. GOC in 2002 results in 164.9 g O_2 m^{-2} a^{-1} compared to only 115.0 g O_2 m^{-2} a^{-1} in 2010. Thus, GOC in 2002 is more than 1.4 times higher than in 2010. This smaller factor compared to the factor of about 2 between summer GOC of the two years (see Table 5.2) relates to the fact that winter GOC is generally low and quite similar for both years, while the largest differences occur during the productive summer period.

The relative contributions of the individual sources to GOC are similar to those of TN, NPP and pelagic and benthic organic matter presented in the previous chapter. The NA influence is the largest and contributes 37.4 % and 31.6 % in 2002 and 2010, receptively. The atmospheric contribution adds up to 13.1 % in 2002 and 20.3 % in 2010. The Dutch NL-1 and German rivers are the major riverine contributing sources. The former contribute 14.7 % and 10.7 % in 2002 and 2010, respectively, while the latter account for 9.3 % in 2002 and 12.2 % in 2010. The UK-2 rivers also constitute a relevant source with a contribution of roughly 7 % in both years.

Interestingly, the North Atlantic influence on bottom layer GOC is about 1 %–2 % less than its influence on detritus-N and sediment-N in the ODZ (see Table 6.5). This indicates that the influence of the NA on RES_{zoo} and NIT is less than on REM_{pel} and REM_{sed}.

Summation of the influences of the riverine and non-riverine N sources on GOC yields 45.1 % and 54.9 %, respectively, in 2002. For 2010, the same calculation results in 42.1 % for the riverine sources and 57.9 % for the non-riverine sources. Thus, the bottom layer GOC due to riverine N input is 1 %–2 % higher than the riverine contribution to water column TN and even 2 %–4 % higher than to NPP.

In addition to the relative contributions during 2002 and 2010, Table 7.1 shows the average contributions of the individual sources over the entire period 2000–2014. The contributions of the individual sources show that the NL-1 contribution in 2002 is extraordinarily high compared to the average contribution of 11.7 % during 2000–2014. Most

Table 7.1: Annually integrated bottom layer gross oxygen consumption and relative contributions of different N sources in the North Sea ODZ in 2002, 2010 and averaged over 2000–2014.

	2002	2010	2000–2014
GOC	$164.9\,\mathrm{g\,O_2\,m^{-2}\,a^{-1}}$	$115.0\,\mathrm{g\,O_2\,m^{-2}\,a^{-1}}$	$141.1\pm14.1\,\mathrm{g\,O_2\,m^{-2}\,a^{-1}}$
Atmosphere	13.1 %	20.3 %	16.8 %
DE	9.3 %	12.2 %	10.2 %
NL-1	14.7 %	10.7 %	11.7 %
NL-2	3.7 %	2.7 %	3.2 %
BE	1.5 %	0.9 %	1.1 %
FR	4.2 %	3.3 %	3.0 %
UK-1	3.1 %	2.8 %	2.6 %
UK-2	7.4 %	7.0 %	7.5 %
NO	<0.1 %	0.2 %	0.1 %
NA	37.4 %	31.6 %	38.0 %
EC	4.3 %	5.7 %	4.2 %
BS	<0.1 %	0.3 %	0.1 %
Others	1.2 %	2.3 %	1.5 %

other sources show deviations of less than 1 % from the average contribution, except for the atmosphere whose contribution in 2002 is about 3 % less than the average value.

The average contributions of the riverine sources add up to 40.9 %, i.e., on average the non-riverine sources account for 59.1 % of overall bottom layer GOC in the North Sea ODZ. This also means that the overall riverine contribution to GOC in 2002 is clearly above the average riverine contribution which mainly relates to the high NL-1 contribution. In 2010, the NA contribution is very small relative to the average contribution of 38 %.

The daily time series of bottom layer GOC in the ODZ in 2002 and 2010 are shown in Fig. 7.4a and b, respectively. The GOC time series (black lines) of both years basically represent a superposition of the time series of detritus-N and sediment-N (see Fig. 6.12 and Fig. 6.13, respectively), which relates to the fact that $\mathrm{REM_{pel}}$ and $\mathrm{REM_{sed}}$ constitute the major O_2-consuming processes in that region (see Sect. 5.2.5.2).

In 2002, GOC decreases from January to March as organic matter concentrations decrease. In late March, GOC starts to increase, which corresponds well with the increasing sediment-N concentrations (see Fig. 6.13a). The daily GOC rates continue to increase until early May, with a minor slowdown in mid-April. The latter coincides with a decrease in detritus-N as a result of reduced NPP (see Fig. 6.11a and Fig. 6.12a).

During May and June, GOC rates stay on a stable level with values of $0.65\,\mathrm{g\,O_2\,m^{-2}\,d^{-1}}$–$0.75\,\mathrm{g\,O_2\,m^{-2}\,d^{-1}}$. During and after the temporary breakdown of stratification in late June/early July, GOC shows a strong increase. This relates to the mixing-induced nutrient

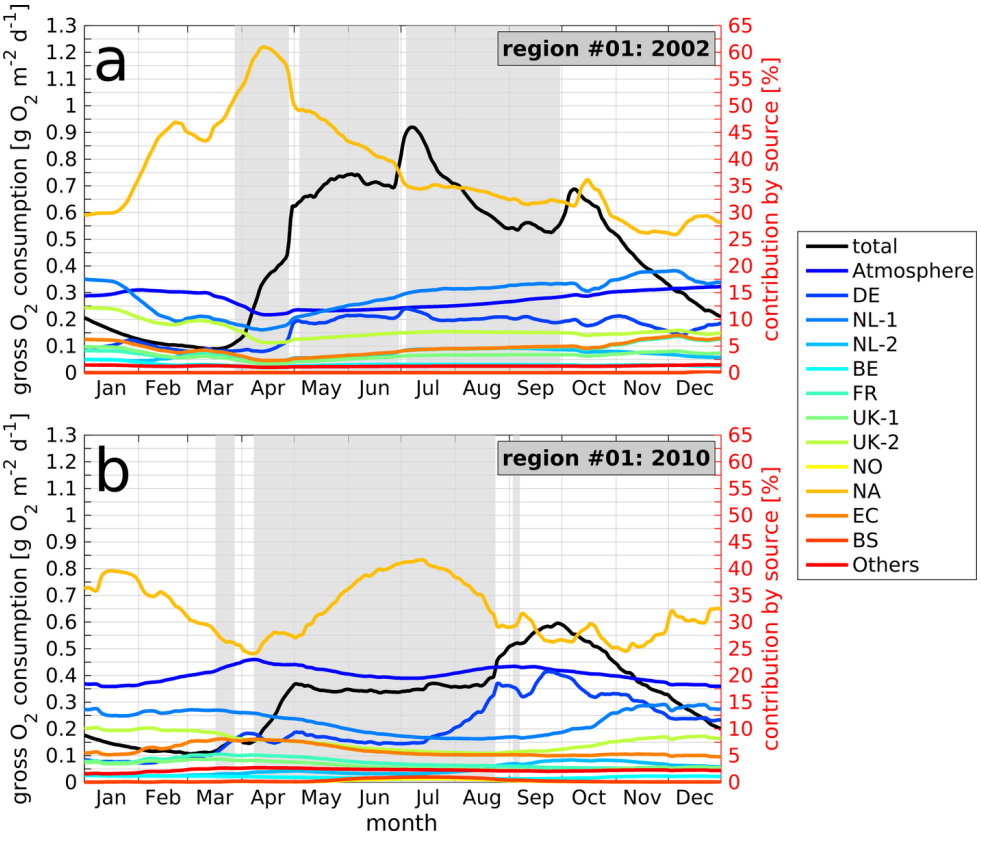

Figure 7.4: Daily time series of bottom layer gross O_2 consumption (black line) and relative contributions of the different N sources (coloured lines; compare Table 6.1) in the North Sea ODZ (box #1 in Fig. 7.2a) in (a) 2002 and (b) 2010. Black y axes refer to gross O_2 consumption, red y axes refer to relative contributions of different sources. Same legend for both panels. Grey areas indicate stratification.

supply from the deeper layers to the surface which enhances NPP causing an increase in EXP_{org} and thus GOC in the bottom layer. Maximum GOC rates of $0.92\,g\,O_2\,m^{-2}\,d^{-1}$ area reached during that period.

After this summer maximum in GOC, a continuous decrease can be seen until early September, this corresponds with the decreasing detritus-N and sediment-N concentrations. The minor increase in GOC in September coincides with an increase in detritus-N, which also causes an increase in sediment-N. After the breakdown of stratification in late September, GOC rates again increase as a result of phytoplankton autumn bloom and enhanced vertical mixing, implying enhanced organic matter production and downward export by turbulent mixing. Maximum GOC rates during that autumn maximum reach about $0.68\,g\,O_2\,m^{-2}\,d^{-1}$. After the maximum, GOC rates steadily decrease until the end of the year.

For the relative contributions of the individual sources to bottom layer GOC (Fig. 7.4a), the same applies as for the overall GOC, i.e., their temporal evolution basically represents a superposition of the annual cycles of the contributions to detritus-N and sediment-N. The NA contribution (light orange) constitutes the major source throughout the entire annual cycle, with a maximum contribution of 61 % in mid-April. This maximum occurs with a temporal delay of about one week relative to the maximum in the NA contribution to sediment-N (see Fig. 6.13a), which underlines the strong influence of REM_{sed} on O_2 consumption. The minor delay results from the fact that the amount of sediment-N from a specific source has to increase first, before the related benthic O_2 consumption increases.

Interestingly, the steep increases in GOC during the temporary breakdowns of stratification in early May and early July coincide with a reduction of the NA contribution and increases in most other contributions, especially in the DE (blue) and NL-1 (light blue) ones. This suggests that organic matter produced in the upper layers under utilisation of N from these sources is mixed downward, consequently enhancing bottom layer GOC.

During the autumn increase in GOC in October 2002 the image is opposed, i.e., the NA contribution increases from 31 % to 36 %, which corresponds to a decrease in the most riverine contributions.

The temporal evolution of GOC in 2010 (Fig. 7.4b; black line) basically corresponds with the combined annual cycles of detritus-N and sediment-N. The minor increase in late-March results from the increase in detritus-N (see Fig. 6.12b) and the subsequent increase in sediment-N (see Fig. 6.13b). The following stronger increase during April also coincides with increases in detritus-N and sediment-N. Maximum daily GOC rates at the end of this increase yield $0.37\,g\,O_2\,m^{-2}\,d^{-1}$.

After that increase, GOC rates stay at roughly $0.35\,g\,O_2\,m^{-2}\,d^{-1}$ until mid-August. This relates to a decrease in detritus-N implying reduced REM_{pel}, while sediment-N and thus REM_{sed} continue to increase until mid-June. The release of NH_4^+ by REM_{pel} and REM_{sed} also enhances GOC due to pelagic NIT, which additionally balances the reduction in GOC due to lower remineralisation.

The autumn increase in GOC, which starts in mid-August and reaches its peak of $0.6\,g\,O_2\,m^{-2}\,d^{-1}$ in late September, is strongly linked to the breakdown of stratification in mid-August, enforcing surface production and vertical mixing of organic matter. As for the other quantities shown in Ch. 6, the GOC rates during the autumn maximum in 2010 are comparable to those in 2002, while spring and summer GOC is only about half of that in 2002. These lower GOC rates in combination with the longer stratified period in 2002 explain the lower minimum O_2 concentrations in the ODZ in 2002.

With respect to the relative contributions of the individual sources to GOC in 2010, the annual cycle again represents a combination of the annual cycles of detritus-N and

sediment-N (see Fig. 6.12b and Fig. 6.13b, respectively). The major temporal patterns in the individual GOC contributions correspond with the patterns in sediment-N (e.g., the maxima in the NA contribution in mid-January and mid-July). After the final breakdown of stratification in September, minor fluctuations, e.g., in the NA contribution to GOC in mid-October coincide with similar fluctuations in the NA contribution to detritus-N.

As for 2002, the NA contribution represents the major influence on bottom layer GOC in the North Sea ODZ throughout the entire annual cycle. Its contribution is higher than 25 % during most of the year and reaches maximum values of 42 % in mid-July. The atmosphere constitutes the second largest contribution with values of 18 %–23 %. The DE contribution is less than 10 % until end of July, when it shows a clear increase reaching maximum values of 21 % in late September. However, this increase is less relevant for the actual bottom O_2 concentrations as stratification has ceased and vertical mixing causes a steady supply of O_2 from the surface into the deeper layers.

7.2.4 Year-to-year variability in the oxygen deficiency zone

As bottom O_2 concentrations only decrease during stratification it is important to analyse GOC and its contributing sources during the stratified periods. With respect to the North Sea ODZ, it is furthermore important to compare multiple years with each other in order to obtain a more general image of the major contributors to GOC. For this reason, Fig. 7.5 shows the average daily GOC rates during the stratified periods of the individual years 2000 to 2014, and the average value over the entire period 2000–2014. Each (stacked) bar represents the overall daily-averaged GOC rate, while the differently coloured parts of one bar represent the absolute contribution related to an individual N source. The average daily GOC rates during the stratified period are calculated as they constitute comparable values independent of differences in t_{strat} between individual years. t_{strat} is defined from the very first day of stratification until the very last day of stratification, including potential intermittences. In addition, Table 7.2 provides the values of daily GOC during stratification, t_{strat} and the relative contributions of individual sources to daily GOC for the individual years and averaged over the entire period.

Figure 7.5 and Table 7.2 show that 2002 represents an exceptional year during the period 2000–2014 with the highest daily GOC during stratification ($0.61\,\mathrm{g\,O_2\,m^{-2}\,d^{-1}}$) and the longest $t_{\mathrm{strat}} = 187$ days. This explains why minimum O_2 concentrations in the ODZ in 2002 are significantly lower than in all other years. In 2010, t_{strat} yields 175 days, which is also longer than the average t_{strat} of 160 days, however, daily GOC ($0.32\,\mathrm{g\,O_2\,m^{-2}\,d^{-1}}$) is about half of that in 2002 and the lowest among all years.

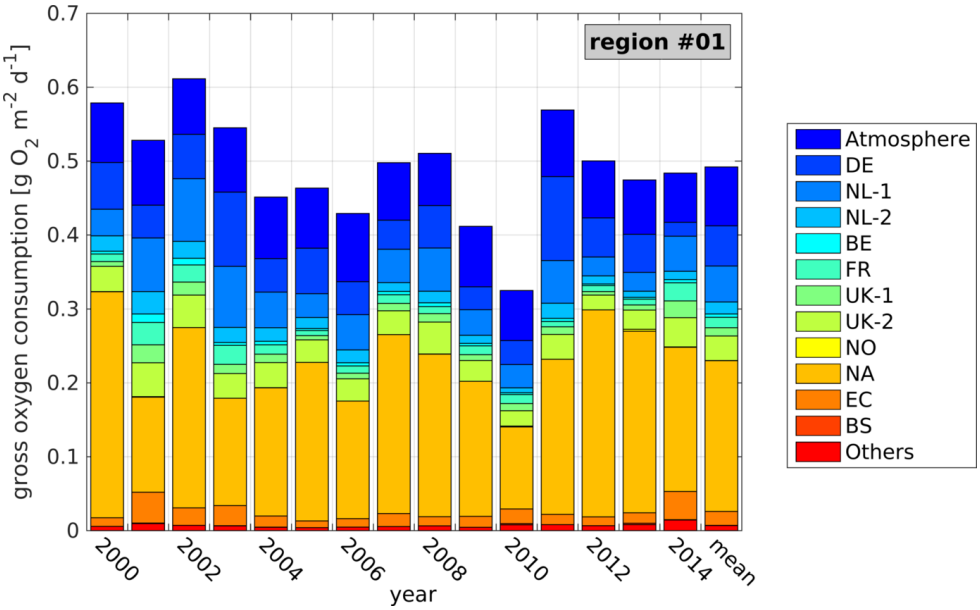

Figure 7.5: Average daily gross O_2 consumption during seasonal stratification and contributions of the different N sources (colours; compare Table 6.1) in the North Sea ODZ (box #1 in Fig. 7.2a) during the individual years 2000–2014, and averaged over the entire period. For corresponding values see Table 7.2.

The comparison of the relative contributions of the different sources during t_{strat} of the two years clearly shows that in 2002, N originating from the Dutch NL-1 rivers (Rhine and Meuse) has a high impact on GOC in the ODZ (13.9 %). In 2010, the NL-1 contribution of 9.7 % is very similar to the average contribution of 9.8 %. Further remarkable differences can be seen for the atmospheric contribution, which is the lowest in 2002 (12.3 %) and very high in 2010 (20.8 %), relative to the average contribution of 16.5 %. In 2010, the NA contribution of 34.1 % is also quite low compared to its average influence of 41.4 %.

Considering the GOC of the individual years, it can be seen that 2000 and 2011 constitute the years with the second and third highest daily GOC ($0.58\,\mathrm{g\,O_2\,m^{-2}\,d^{-1}}$ and $0.57\,\mathrm{g\,O_2\,m^{-2}\,d^{-1}}$, respectively). However, due to the much shorter t_{strat} of 151 days in 2000 and 134 days in 2011, O_2 deficiency did not evolve during these years in the simulation. Interestingly, the main contributing sources are quite different between these two years. In 2000, the NA contribution accounts for 52.8 % of overall consumption, and the non-riverine contributions add up to 68.8 %. The very high NA contribution in year 2000 may relate to high inflow of water and thus N (and other nutrients) in early 2000. Most riverine sources, especially that of the NL-1 rivers are clearly below the average contribution during 2000–2014.

In contrast, the riverine contributions in 2011 account for 44.8 % of the overall daily

Table 7.2: Average daily gross O_2 consumption during seasonal stratification and relative contributions of the different N sources in the North Sea ODZ (box #1 in Fig. 7.2a) during the individual years 2000–2014, and averaged over the entire period. Stratification period (t_{strat}; first to last day) in days, GOC in $g\,O_2\,m^{-2}\,d^{-1}$, contributions by sources in %. Deviations in sum of relative contributions from 100 % due to rounding.

	2000	2001	2002	2003	2004	2005	2006	2007	2008	2009	2010	2011	2012	2013	2014	average (±STD)
t_{strat}	151	152	187	181	168	166	159	154	124	145	175	136	166	164	176	160±17
GOC	0.58	0.53	0.61	0.55	0.45	0.46	0.43	0.50	0.51	0.41	0.32	0.57	0.50	0.47	0.48	0.49±0.07
Atmosphere	14.0	16.6	12.3	16.0	18.5	17.5	21.5	15.6	13.8	19.8	20.8	15.9	15.4	15.5	13.7	16.5±2.7
DE	10.9	8.4	9.8	18.4	10.0	13.3	10.4	7.9	11.3	7.5	10.0	19.9	10.6	10.9	3.9	10.9±4.0
NL-1	6.2	13.7	13.9	15.1	10.7	6.9	11.1	9.0	11.5	8.4	9.7	10.1	5.1	5.4	9.8	9.8±3.1
NL-2	3.6	5.8	3.8	3.7	4.1	3.2	4.1	2.4	3.1	2.7	2.0	3.6	2.2	1.7	2.3	3.2±1.0
BE	0.7	2.2	1.5	0.7	1.1	0.6	1.0	0.9	1.0	0.8	0.8	0.8	0.4	0.5	0.9	0.9±0.4
FR	1.8	5.7	3.8	4.7	2.8	1.5	2.3	2.3	1.9	2.9	3.8	1.3	1.7	1.6	5.1	2.9±1.4
UK-1	1.1	4.6	2.9	2.3	2.6	1.3	1.8	2.0	2.2	1.9	3.0	1.8	1.0	1.5	4.7	2.3±1.1
UK-2	5.9	8.7	7.2	6.1	7.5	6.6	7.0	6.5	8.5	6.9	6.4	5.9	4.0	5.5	8.2	6.7±1.2
NO	<0.1	0.1	<0.1	<0.1	<0.1	<0.1	<0.1	<0.1	<0.1	<0.1	0.4	<0.1	<0.1	0.6	0.1	0.1±0.2
NA	52.8	24.4	39.9	26.6	38.4	46.3	37.1	48.6	43.1	44.4	34.1	36.9	55.9	51.8	40.4	41.4±9.1
EC	2.0	7.9	3.9	5.0	3.4	1.9	2.6	3.5	2.4	3.5	6.1	2.5	2.4	3.0	7.9	3.9±2.0
BS	<0.1	0.1	<0.1	<0.1	<0.1	<0.1	<0.1	<0.1	<0.1	<0.1	0.6	<0.1	<0.1	0.4	0.1	0.1±0.2
Others	1.0	1.8	1.2	1.2	1.0	0.9	1.1	1.1	1.2	1.1	2.4	1.4	1.3	1.7	2.9	1.4±0.6
riverine	31.2	51.0	43.9	52.3	39.7	34.3	38.8	32.2	40.6	32.2	38.4	44.8	26.2	29.4	37.9	38.2±7.6
non-riverine	68.8	49.0	56.1	47.7	60.3	65.7	61.2	67.8	59.4	67.8	61.6	55.2	73.8	70.6	62.1	61.8±7.6

GOC, with an particularly high contribution of 19.9 % by the DE rivers (highest during entire period). The latter likely relates to the Elbe flood in January 2011 (e.g., Kienzler et al., 2015; Mudersbach et al., 2016). This is supported by the results of a cross-correlation calculated between the de-trended daily time series of TN loads by the DE rivers and the mass of TN originating from the DE rivers in the ODZ for the entire period 2000–2014 (not shown). This cross-correlation yields the maximum correlation coefficient of 0.67 (95 % confidence level) for a time lag of 152 days. Significance was tested using a t-test with the number of degrees of freedom dependent on the de-correlation scales of both variables. This suggests that the N loads from the German rivers increase the N availability in the ODZ during summer 2011, when nutrients are usually depleted in the euphotic surface layer. Consequently, summer GOC due to N from the DE rivers is significantly increased.

In 2002, when a severe flooding occurred at the Elbe in late August (Ulbrich et al., 2003; Kienzler et al., 2015; Mudersbach et al., 2016), no increased contribution of the DE rivers to GOC is visible as the loads originating from the Elbe arrived in the ODZ in spring 2003 (not shown). This also explains the high DE contribution in 2003 yielding 18.4 %. The same applies to the increased loads resulting from the Elbe flood in August 2010 (Kienzler et al., 2015), which is also expressed in the highest DE contribution (19.9 %) of all years.

Considering the temporal evolution of GOC in the North Sea ODZ during 2000–2014, no clear trend can be found. From 2000 to 2010, average daily GOC tends to decrease, before GOC again shows high values in 2011. From 2012 to 2014, average GOC rates during seasonal stratification are very similar to the average rate during the entire period 2000–2014, and range between $0.47\,\mathrm{g\,O_2\,m^{-2}\,d^{-1}}$ in 2013 and $0.5\,\mathrm{g\,O_2\,m^{-2}\,d^{-1}}$ in 2012. For the contributions of the individual sources no clear trend can be found. Distinct changes in the riverine and non-riverine contributions relate to specific events of increased riverine discharge, e.g., in the German rivers as described above, and to variations in the inflow through the English Channel (EC contribution) and across the northern shelf edge (NA contribution). With respect to the influence of N on GOC in the ODZ, that entered the North Sea through these two sections, no clear connection to large scale patterns such as the North Atlantic Oscillation (NAO; e.g., NCAR, 2016) can be found.

In summary, it can be said that the North Atlantic (NA) and atmospheric contribution constitute the major non-riverine contributions to GOC in the North Sea ODZ, while the Dutch NL-1, German and British UK-2 rivers represent the most important riverine sources during the period 2000–2014. High GOC rates may relate to both strong N input from the North Atlantic (e.g., in 2000) and from these two riverine sources (e.g., NL-1 in 2002 and DE in 2011). This suggests that substantial improvements in the O_2 conditions in the North Sea ODZ can be achieved by reducing N loads in these rivers. The combined

effect of all riverine sources can add up to more than 50 % during individual years (2001 and 2003), while on average the non-riverine sources have a clearly larger impact on bottom layer GOC in the ODZ, adding up to 61.8 %. This indicates that the impact of riverine N reductions on GOC at the ODZ site is limited as non-riverine sources account for most of GOC during most years. However, it also indicates that substantial reductions in the major riverine contributions could have a noticeable, positive effect on the O_2 conditions as they account for more than 25 % (DE, NL-1 and UK-2) of GOC. The high atmospheric contribution of 16.5±2.7 % further shows that the anthropogenic influence (riverine and atmospheric) on the O_2 dynamics at the ODZ site is quite relevant. In addition, the analysis of the daily GOC rates in relation to t_{strat} also emphasises the importance of the duration of stratification as the essential prerequisite for the evolution of O_2 deficiency in the ODZ.

7.2.5 Oxygen consumption due to different processes and sources

In order to provide more information on the differences between the individual processes contributing to GOC in the North Sea ODZ, Fig. 7.6 shows the histograms of average daily O_2 consumption due to the different biochemical processes during seasonal stratification and the contributions of individual sources for the individual years 2000–2014 and averaged over the entire period. The presented processes are: (a) REM_{sed}, (b) REM_{pel}, (c) RES_{zoo} and (d) NIT. In addition, Table 7.3 shows the absolute rates and relative contributions of the most relevant sources (atmosphere, DE and NL-1 rivers, and NA) for these four processes.

Figure 7.6 reveals that the contributions of the different O_2-consuming processes to GOC during the stratified period vary between the years. It also shows that the relative contributions to the individual processes also vary between the different processes. For instance, daily GOC in 2002 is the highest among all years (see Fig. 7.5), which also applies to REM_{sed} and NIT (see Fig. 7.6a and d, respectively) with values of $0.324\,g\,O_2\,m^{-2}\,d^{-1}$ for REM_{sed} and $0.028\,g\,O_2\,m^{-2}\,d^{-1}$ for NIT. In contrast, REM_{pel} (Fig. 7.6b) and RES_{zoo} (Fig. 7.6c) are highest in 2011 showing values of $0.198\,g\,O_2\,m^{-2}\,d^{-1}$ and $0.073\,g\,O_2\,m^{-2}\,d^{-1}$, respectively. Similarly, lowest consumption rates due to individual processes do not necessarily correspond to lowest GOC rates, e.g., in the case of NIT which is lowest in 2007 (of $0.014\,g\,O_2\,m^{-2}\,d^{-1}$) and not in 2010.

Despite these minor variations, the relative contributions of the individual processes to GOC during stratification are stable throughout the entire period 2000–2014. Average relative contributions (± STD) of the individual processes to daily GOC result in 49.8±1.4 % for REM_{sed}, 35.1±1.6 % for REM_{pel}, 11.2±1.2 % for RES_{zoo} and 3.9±0.6 % for NIT.

With respect to the relative contributions of the different N sources to the O_2-consuming

Table 7.3: Average daily O_2 consumption due to benthic remineralisation (REM_{sed}), pelagic remineralisation (REM_{pel}), zooplankton respiration (RES_{zoo}) and nitrification (NIT) during seasonal stratification and relative contributions of the most relevant N sources in the North Sea ODZ (box #1 in Fig. 7.2a) during the individual years 2000–2014, and averaged over the entire period. Daily process rates in $g\,O_2\,m^{-2}\,d^{-1}$, contributions by sources in %.

	2000	2001	2002	2003	2004	2005	2006	2007	2008	2009	2010	2011	2012	2013	2014	average (±STD)
REM_{sed}	0.292	0.266	0.324	0.275	0.223	0.230	0.210	0.235	0.251	0.198	0.167	0.277	0.245	0.239	0.246	0.245±0.039
Atmosphere	14.1	17.1	12.5	16.3	18.8	17.7	21.9	15.5	14.0	19.8	20.9	15.9	15.4	15.6	13.8	16.6±2.7
DE	10.0	7.8	9.2	17.7	9.2	12.1	9.7	6.7	10.2	6.4	8.9	18.5	9.5	9.6	3.8	10.0±3.8
NL-1	5.9	13.2	13.7	14.8	10.4	6.7	10.6	8.7	11.5	8.0	9.2	9.2	4.8	5.2	9.7	9.4±3.0
NA	54.4	25.9	40.8	28.0	39.5	48.0	38.4	51.5	44.5	46.8	36.7	40.2	57.7	53.6	41.7	43.2±9.2
REM_{pel}	0.196	0.179	0.190	0.183	0.162	0.164	0.157	0.186	0.180	0.154	0.116	0.198	0.181	0.167	0.166	0.172±0.021
Atmosphere	13.8	16.2	12.1	15.8	18.2	17.4	21.2	15.7	13.7	19.9	20.8	15.9	15.4	15.4	13.7	16.3±2.7
DE	11.6	8.9	10.2	18.7	10.6	14.2	10.9	8.9	12.1	8.6	11.2	21.0	11.4	11.9	3.9	11.6±4.1
NL-1	6.5	14.1	13.9	15.5	10.9	7.1	11.6	9.3	11.4	8.8	10.2	11.0	5.3	5.6	9.9	10.1±3.1
NA	51.7	23.1	39.5	25.7	37.5	44.9	35.8	46.3	42.0	42.3	31.2	34.0	54.6	50.3	39.2	39.9±9.1
RES_{zoo}	0.069	0.060	0.070	0.065	0.049	0.051	0.046	0.063	0.060	0.045	0.025	0.073	0.059	0.052	0.052	0.056±0.012
Atmosphere	13.9	16.1	12.0	15.6	18.1	17.3	21.0	15.9	13.8	19.9	20.7	15.9	15.5	15.3	14.0	16.3±2.6
DE	12.6	9.7	11.3	20.8	12.0	15.5	11.6	9.8	13.8	9.4	12.8	22.3	12.3	12.3	4.2	12.7±4.4
NL-1	6.6	14.6	14.2	15.5	11.1	7.3	11.7	9.7	11.6	8.9	9.8	11.4	5.3	5.5	10.3	10.2±3.2
NA	50.2	21.7	37.9	24.2	36.2	43.2	35.3	44.5	40.0	41.3	31.0	32.2	53.6	50.3	37.1	38.6±9.2
NIT	0.022	0.023	0.028	0.022	0.018	0.018	0.017	0.014	0.020	0.015	0.017	0.020	0.015	0.017	0.020	0.019±0.004
Atmosphere	13.8	16.1	12.2	15.6	18.0	17.2	21.1	15.4	13.3	19.4	20.4	15.8	15.5	16.1	12.9	16.2±2.7
DE	11.2	8.3	9.8	18.4	9.2	13.3	10.5	7.3	9.8	7.2	9.2	20.8	11.6	13.6	3.5	10.9±4.4
NL-1	6.8	14.0	14.5	16.1	10.7	7.1	10.9	8.8	11.3	8.6	10.1	10.3	5.8	6.2	9.9	10.1±3.1
NA	51.2	23.6	38.2	24.8	39.2	45.8	37.1	49.6	45.3	44.3	33.5	35.5	53.1	45.5	41.7	40.6±8.7

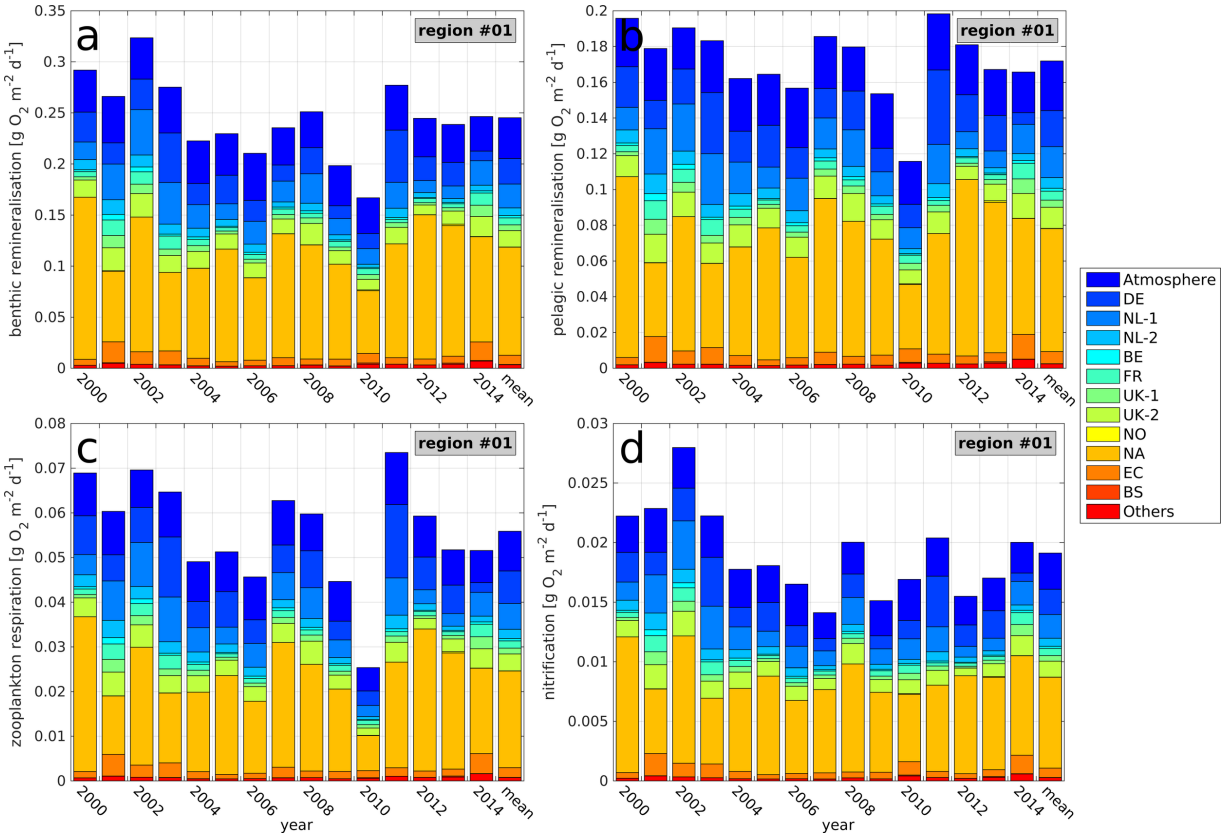

Figure 7.6: Average daily O_2 consumption due to (a) benthic remineralisation (REM_{sed}), (b) pelagic remineralisation (REM_{pel}), (c) zooplankton respiration (RES_{zoo}) and (d) nitrification (NIT) during seasonal stratification and contributions of the different N sources (colours; compare Table 6.1) in the North Sea ODZ (box #1 in Fig. 7.2a) during the individual years 2000–2014, and averaged over the entire period. Average values for most relevant sources provided in Table 7.3.

processes, Table 7.3 shows that the source-related contributions to the different processes are in the same order. However, for individual years and sources quite some differences can be found between the four processes. For instance, during most years the NA contribution to REM_{sed} is higher than the NA contributions to the other processes. Only during 2008 and 2014 the NA contribution to NIT is the same or higher than to REM_{sed}, while the NA contributions to REM_{pel} and RES_{zoo} are generally lower. This indicates that the amount of benthic organic matter containing N from the NA, that is remineralised during the stratified period, is generally higher than in pelagic organic matter. Consequently, the NA contribution to NIT is between those to REM_{pel} and REM_{sed} as both processes constitute the main sources for NH_4^+ in the bottom layer.

The NA contribution to RES_{zoo} is consistently lower than for the other processes, which relates to the fact that NPP and thus zooplankton grazing during summer are

highest around the thermocline due to the highest availability of both light and nutrients. In addition, N (and other nutrients) originating from the DE and NL-1 play a more important role on NPP during summer, consequently increasing their contributions to RES_{zoo}. This is also consistent with the tendentially higher DE and NL-1 contributions to REM_{pel}, relative to REM_{sed} and NIT, which are also directly linked to the NPP dynamics during summer. In principle, the minor differences between the relative contributions to the individual processes relate to temporal delays between the different processes (e.g., in case of REM_{pel} and REM_{sed}) or to additional factors (e.g., light limitation in case of NIT). However, the basically similar relative contributions underline the strong link between the different processes.

In general, it has to be noted that the minor differences between the relative contributions of the individual sources to GOC (and its contributing processes) during stratification and those described in the analyses and results of Ch. 6 are not contradictory. For the sake of better comparability to earlier studies (OSPAR, 2010; Painting et al., 2013; Troost et al., 2013), the analyses in Ch. 6 consider the entire year. In contrast, the here presented analysis focuses on the O_2 dynamics during the relevant period of the year, i.e., seasonal stratification. Consequently, slightly different relative contributions are mainly attributable to these different periods of analysis.

7.2.6 Year-to-year variability in the Oyster Grounds

Although this study could not identify the Oyster Grounds (see box #2 in Fig. 7.2a) as a region susceptible to O_2 deficiency due to an underestimation of seasonal stratification (see Fig. 5.3c and d), Greenwood et al. (2010) observed O_2 deficiency in the Oyster Grounds during late summer 2007 and 2008. Despite these discrepancies, the basic dynamics controlling O_2 remain the same. Especially, the daily GOC is only indirectly affected by stratification, namely by potentially stronger near-surface NPP due to enhanced upward mixing of nutrients in case of less intense stratification. However, NPP simulated by ECOHAM shows realistic values in this region (see Sect. 5.2.3.2) and the TBNT results of Ch. 6 are in good agreement with existing studies. Thus, this section aims for the identification of the different N sources contributing to GOC in the Oyster Grounds area, analogous to Sect. 7.2.4. Figure 7.7 and Table 7.4 show the average daily bottom layer GOC rates during the stratified periods of the individual years 2000–2014 and the corresponding average over the entire period, and the contributions attributable to the individual N sources. First, it can be seen that the daily GOC rates are roughly 1.5–2 times lower in the Oyster Grounds than in the ODZ (see Fig. 7.5), with maximum values of $0.40\,g\,O_2\,m^{-2}\,d^{-1}$ in 2002 and minimum rates of $0.23\,g\,O_2\,m^{-2}\,d^{-1}$ in 2010. This only partly relates to the differences in bottom layer thickness between the two regions, as the

ODZ has a bottom layer of 6.5 m thickness compared to 5.5 m in the Oyster Grounds.

Different to the ODZ, second highest GOC rates do not occur in 2000, but in 2001 yielding $0.38\,\mathrm{g\,O_2\,m^{-2}\,d^{-1}}$. This difference in year-to-year variability in daily GOC relates to the differences in the influence of the individual sources on GOC in the Oyster Grounds, compared to the North Sea ODZ. Although the average riverine contribution of 39.8±6.1 % (see Table 7.4) is very similar to that in the ODZ, the relative contributions of the individual sources are quite different. The DE contribution is negligible in most years (except for 2013), while that of the UK-2 rivers of 12.7±2.6 % is clearly higher than in the ODZ. These changes relate to the geographical location of the Oyster Grounds relative to the DE and UK-2 river mouths. While the former are located downstream of the Oyster Grounds relative to the general circulation of the North Sea, the latter are located upstream and are closer to the Oyster Grounds than to the ODZ.

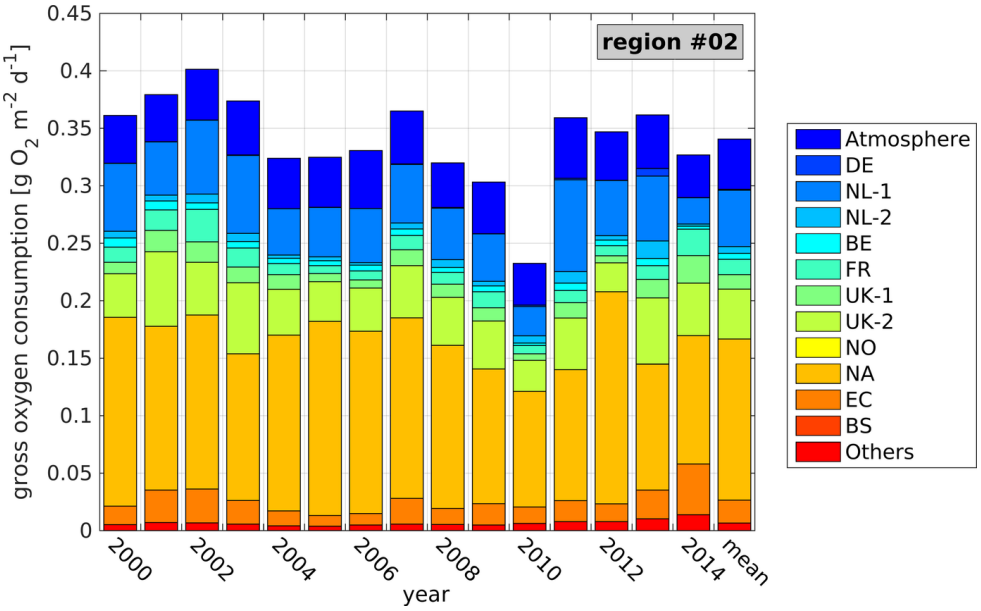

Figure 7.7: Average daily gross O_2 consumption during seasonal stratification and contributions of the different sources (colours; compare Table 6.1) in the Oyster Grounds (box #2 in Fig. 7.2a) during the individual years 2000–2014, and averaged over the entire period. For corresponding values see Table 7.4.

The NL-1 rivers also show a higher average contribution of 14.3±3.4 % compared to the ODZ, which also relates to the lower distance between the NL-1 river mouths and the Oyster Grounds and the upstream location of the former. Except for the NL-2 and NO rivers, all riverine sources have a higher influence on GOC during stratification in the Oyster Grounds than in the ODZ. The same applies to the EC contribution, while the atmospheric contribution is less, contributing 13.0±1.6 % on average. Like for the NO

Table 7.4: Average daily gross O_2 consumption during seasonal stratification and relative contributions of the different N sources in the Oyster Grounds (box #2 in Fig. 7.2a) during the individual years 2000–2014, and averaged over the entire period. Dashes indicate zero contributions. Stratification period (t_{strat}; first to last day) in days, GOC in $g\,O_2\,m^{-2}\,d^{-1}$, contributions by sources in %. Deviations in sum of relative contributions from 100 % due to rounding.

	2000	2001	2002	2003	2004	2005	2006	2007	2008	2009	2010	2011	2012	2013	2014	average (±STD)
t_{strat}	166	149	173	165	169	175	158	158	127	157	160	166	168	162	180	163±13
GOC	0.36	0.38	0.40	0.37	0.32	0.32	0.33	0.37	0.32	0.30	0.23	0.36	0.35	0.36	0.33	0.34±0.04
Atmosphere	11.5	10.8	11.0	12.6	13.5	13.4	15.3	12.6	12.1	14.9	15.6	14.7	12.2	12.9	11.4	13.0±1.6
DE	<0.1	<0.1	0.1	0.1	<0.1	0.1	<0.1	0.1	0.2	0.1	0.5	0.3	<0.1	1.8	<0.1	0.2±0.5
NL-1	16.3	12.2	16.0	18.1	12.4	13.2	14.2	14.0	14.0	13.6	11.0	22.2	13.8	15.6	7.0	14.3±3.4
NL-2	1.6	1.3	1.9	1.9	0.8	1.0	0.6	1.4	2.1	1.3	2.7	2.8	1.1	4.2	0.6	1.7±1.0
BE	2.2	2.1	1.4	1.5	1.4	1.3	1.5	1.6	1.4	1.7	0.9	1.8	1.4	1.7	0.8	1.5±0.4
FR	3.7	4.7	7.0	4.4	3.0	2.1	2.4	3.4	3.2	4.6	3.1	2.9	2.5	3.3	7.0	3.8±1.5
UK-1	2.8	4.9	4.4	3.7	3.9	2.2	2.1	3.8	3.6	3.8	2.5	3.7	1.8	4.4	7.3	3.7±1.4
UK-2	10.5	17.1	11.5	16.5	12.3	10.6	11.4	12.4	13.1	13.7	11.6	12.5	7.2	15.9	14.0	12.7±2.6
NO	–	–	–	–	–	–	–	–	–	–	–	–	–	–	–	–
NA	45.5	37.6	37.7	34.1	47.2	52.0	47.9	43.0	44.3	38.7	43.3	31.8	53.2	30.3	34.1	41.4±7.2
EC	4.5	7.4	7.3	5.5	4.0	2.8	3.0	6.1	4.4	6.1	6.1	5.1	4.4	6.9	13.5	5.8±2.6
BS	–	–	–	–	–	–	–	–	–	–	–	–	–	–	–	–
Others	1.5	1.9	1.7	1.5	1.3	1.2	1.5	1.6	1.7	1.6	2.7	2.2	2.3	2.9	4.2	2.0±0.8
riverine	38.6	44.2	44.0	47.8	35.2	31.7	33.8	38.3	39.1	40.4	34.9	48.5	30.2	49.9	41.0	39.8±6.1
non-riverine	61.4	55.8	56.0	52.2	64.8	68.3	66.2	61.7	60.9	59.6	65.1	51.5	69.8	50.1	59.0	60.2±6.1

rivers, the BS contribution to GOC in the Oyster grounds is zero throughout the entire period.

Interestingly, the years with high GOC in the Oyster Grounds region correspond to high riverine contributions, either by the Dutch NL-1 rivers (e.g., 2002, 2003, 2011 and 2013) or by the British UK-2 rivers (e.g., 2001, 2003 and 2013), and low NA contributions. This indicates that these two riverine sources play a key role in the O_2 dynamics in the Oyster Grounds region, and that high loads from these rivers can considerably deteriorate O_2 conditions in this region. This constitutes an important information with respect to the O_2-related management of eutrophication by river N reduction measures as it suggests that substantial improvements in the O_2 conditions in the Oyster Grounds area can only be achieved by reductions in the N inputs in the NL-1 and UK-2 rivers.

7.3 The effect of nitrogen reductions in rivers on the oxygen dynamics

In order to evaluate the conclusions drawn from the relative contributions of the different N sources on GOC at the two study sites, a N reduction scenario in alignment with riverine N reductions according to the WFD and OSPAR is presented in the following. For this purpose, N reduction numbers agreed on by the national representatives of the OSPAR member states neighbouring the North Sea, namely France, Belgium, the Netherlands, Germany and UK (OSPAR, 2016), are implemented to an ECOHAM simulation over the period 2000–2014. This reduction scenario uses the final state of the year 1999 of the previously analysed standard run as initialisation.

Besides the reductions in riverine N input, the same physical and biochemical forcing (e.g., atmospheric N deposition) is applied (see Sect. 3.2.2). In addition, a TBNT analysis is conducted on the results of the ECOHAM reduction scenario, using the same setup as described in Sect. 6.2. The initial state of the labelled model state variables is also identical to that of the TBNT calculation analysed in the previous sections (hereafter 'reference run').

7.3.1 Definition of riverine nitrogen reductions

The riverine N reductions implemented to ECOHAM in alignment with the WFD basically represent political targets defined by the North Sea neighbouring OSPAR member states. In the case of the German N rivers an annual average target concentration of $2.8\,\mathrm{mg\,N\,L^{-1}}$ is defined for TN (BLMP, 2011). In order to translate this target concentration into a percentage of TN reduction, the actual annual average TN concentrations

for the three German rivers Elbe, Ems and Weser are calculated for the years 2006–2012. Consequently, the required percentage of TN reduction for each year and river is calculated as:

$$\mathrm{red_{TN}} = 100 \cdot (1 - f_{\mathrm{red,TN}}) \quad [\%], \tag{7.3}$$

with the reduction factor $f_{\mathrm{red,TN}}$ calculated as:

$$f_{\mathrm{red,TN}} = \frac{C_{\mathrm{TN,tar}}}{C_{\mathrm{TN}}}. \tag{7.4}$$

Here, C_{TN} represents the actual annual, discharge-weighted average TN concentration of the considered river and $C_{\mathrm{TN,tar}}$ constitutes the TN target concentration of $2.8\,\mathrm{mg\,N\,L^{-1}}$. ECOHAM applies riverine input of both, DIN and PON (see Sect. 3.2.2.2). Therefore, the resulting TN reduction is translated into a reduction in DIN and PON by calculating the target concentrations of the two using the discharge-weighted average DIN:PON ratio during 2006–2012, derived from the actual river load data, and $C_{\mathrm{TN,tar}}$. Finally, Eqs. (7.3) and (7.4) are analogously applied to PON and DIN. The resulting DIN reduction is applied to both NO_3^- and NH_4^+.

For the other OSPAR member states, percentages of N reduction are taken from different documents. For the French rivers, DIN reductions of 50 % are taken from an OSPAR questionnaire on DIN reductions (document ID: HASEC15/04/Info.01-E; collected by Hermann Lenhart, Universität Hamburg), in agreement with the range of DIN reduction of 39 %–83 % reported by Desmit et al. (2015). For the Belgian river Scheldt a DIN reduction of 37 % is obtained from Desmit et al. (2015). A DIN reduction of 5 % in the Dutch rivers is taken from Loos et al. (2014), and for the British rivers the DIN reduction is considered to be zero according to an official OSPAR statement (OSPAR, 2016).

As the German reduction target for TN implies reductions in both DIN and PON, PON reductions are also defined for the other states. For the sake of simplicity, in this study the same reduction percentages are applied to PON in these rivers as for DIN. This implies that the DIN:PON ratios in these rivers remain the same as in the original load data. Another problem with respect to the percentages of N reduction for all states, but Germany, is that no reference period is defined. Consequently, it is not possible to define an actual target state as it is done for the German rivers. Therefore, the provided percentages of N reduction are translated into reduction factors using Eqs. (7.3) and (7.4) and the actual river loads of the individual rivers for the years 2000–2014 are multiplied with these factors. The percentages of DIN and PON reductions used for the N reduction scenario are summarised in Table 7.5. For all countries and rivers not included in Table 7.5 no reductions are applied. Time series of the reduced annual riverine TN loads inside and outside the TBNT domain (see Fig. 6.3) and the relative contribution by the different river groups (see Table 6.1) are shown in Fig. 7.8.

Table 7.5: Overview on percentages of dissolved inorganic (DIN) and particulate organic N (PON) reductions in major North Sea tributaries under WFD measures. All numbers in %. Adapted from Gade (2016); OSPAR (2016).

country	river	DIN	ON
France	Authie	50	50
France	Canche	50	50
France	Seine	50	50
France	Somme	50	50
Belgium	Scheldt	37	37
The Netherlands	Rhine	5	5
The Netherlands	Meuse	5	5
The Netherlands	North Sea Canal	5	5
The Netherlands	Lake Ijssel (East and West)	5	5
Germany	Elbe	29	9
Germany	Ems	50	37
Germany	Weser	35	15

As no river reductions are applied to the British, Irish and Northern Irish rivers outside the TBNT domain, the time series of the N input outside the TBNT domain (black dotted line) is identical to that of the reference run (see Fig. 6.4b). In contrast, the riverine N input inside the TBNT domain (black solid line) is clearly less than that of the reference run, although the year-to-year variations are similar to the reference run, which relates to the use of constant reduction factors for the individual years. Maximum overall N inputs of $1084\,\mathrm{kt\,N\,a^{-1}}$ occur in 2002 and minimum values of $665\,\mathrm{kt\,N\,a^{-1}}$ in 2005 (14.4 % and 14.2 % lower than in the reference run, respectively). Cumulated over the entire period 2000–2014, the overall riverine N input inside the TBNT domain is 13.5 % less than in the reference run. Considering individual years, the reduction in the overall riverine N input varies between 10.7 % in 2014 and 15.5 % in 2001, relative to the reference run.

These year-to-year variations in the reductions in overall riverine N input result from the different reductions by the individual members states and from the year-to-year variations in the individual river loads indicated by the varying relative contributions of the different river groups (coloured dashed lines). For instance, the high reduction in 2001 relates to the originally very high FR contribution of 18.2 % (second highest; see Fig. 6.4b) and the strong N reduction of 50 % in the French rivers. Consequently, the FR contribution (light green line) to overall N input in 2001 is remarkably less than in the reference run, yielding only 11.1 %. Cumulated over the entire period 2000–2014, the relative contribution of the FR rivers to riverine N input is reduced from 13.3 % in the reference run to 7.7 % in the reduction scenario.

Similar to the FR rivers, the DE and BE contributions (dark blue and cyan line,

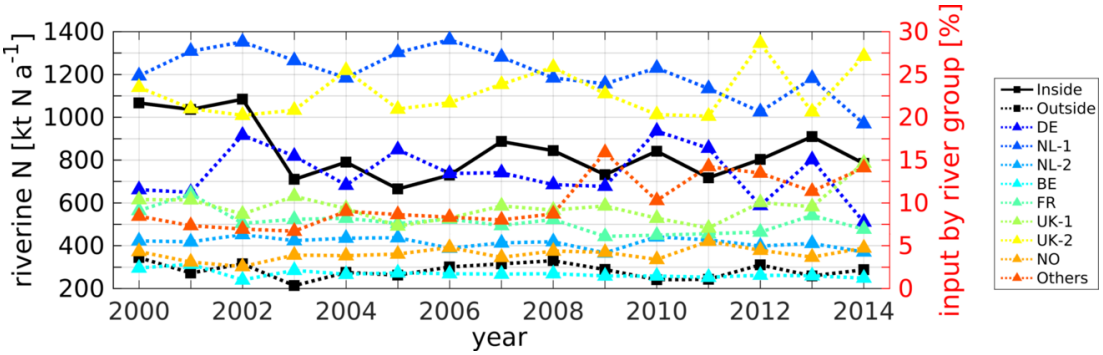

Figure 7.8: Time series of WFD-compliant annual riverine TN input (black y axes; see Table 7.5) into the model domain, inside (solid black) and outside (dotted black) the TBNT domain (see Fig. 6.3). Relative contributions (red y axes and coloured dotted lines) represent the share of total input into the TBNT domain by different river groups (see Table 6.1).

respectively) to overall riverine N input are clearly reduced as both countries also aim for high N reductions (see Table 7.5). Although the BE contribution to riverine N input during 2000–2014 is already low in the reference run, its cumulated contribution is further reduced from 2.3 % to 1.7 %. The DE contribution to riverine N input, which is among the four highest in the reference run, is reduced from 16.4 % to 13.5 %.

Consequently, the relative contributions of the Dutch (NL-1/-2; blue/light blue line) and British (UK-1/-2; green/yellow line) are clearly higher than in the reference run, due to the very low (5 %) or zero reductions, respectively. The NL-1 contribution has increased from 23.0 % to 25.3 % (cumulated over 2000–2014) from the reference to the reduction scenario. The cumulated NL-2 contribution results in 5.4 % in the reduction run, compared to 4.9 % in the reference run. The UK-1 and UK-2 rivers also show increases in the cumulated contributions from 8.3 % to 9.6 % and from 19.7 % to 22.8 %, respectively, compared to the reference run. As zero reductions are also applied to the NO and other rivers, these two groups also show minor increases in their relative contributions (NO: 3.4 % to 4.0 %; Others: 8.6 % to 9.9 %).

7.3.2 Bottom oxygen concentrations and periods of oxygen deficiency

In order to provide a first insight in the impacts of reduced riverine N inputs on O_2 deficiency in the North Sea, Fig. 7.9a shows the spatial distribution of overall minimum bottom O_2 concentrations simulated during the period 2000–2014 under WFD-compliant N reductions. The spatial distribution of the corresponding longest periods of annual O_2 deficiency (O_2 concentration $<6\,\mathrm{mg\,O_2\,L^{-1}}$) are shown in Fig. 7.9b, with the light grey

areas indicating the regions that are affected by O_2 deficiency in the reference run, but not in the reduction run. In addition, Fig. 7.9c shows the spatial distribution of relative change in the minimum bottom O_2 concentration between the reference and the reduction run calculated for each grid point as:

$$\Delta_{O_2} = 100 \cdot \left(\frac{C^{\min}_{O_2,\mathrm{red}}}{C^{\min}_{O_2,\mathrm{ref}}} - 1 \right) \quad [\%], \tag{7.5}$$

with simulated minimum O_2 concentrations of the reference and the reduction run, $C^{\min}_{O_2,\mathrm{ref}}$ and $C^{\min}_{O_2,\mathrm{red}}$, respectively. Consequently, a positive (negative) relative change implies an increase (decrease) in the minimum bottom O_2 concentration. Finally, Fig. 7.9d shows the spatial distribution of the reduction in the duration of O_2 deficiency in the North Sea from reference run to reduction run, i.e., positive values imply shorter O_2-deficient periods in the reduction run.

Figure 7.9a and c show that O_2 concentrations show negligible changes in the northern and western central North Sea (minor positive/negative relative changes $< \pm 0.5\,\%$ due to numerical differences). In the O_2-deficient region of the reference run (see coloured and light grey area in Fig. 7.9b) in the southeastern central North Sea, minimum O_2 concentrations are clearly higher in the reduction run, i.e., bottom O_2 conditions are improved. Minimum O_2 concentrations in the reduction run reach about $5.5\,\mathrm{mg\,O_2\,L^{-1}}$ in this region (56.3 °N, 7.0 °E), compared to $5.0\,\mathrm{mg\,O_2\,L^{-1}}$ in the reference run which implies a relative increase of almost 9.2 % (highest in the entire region). In the vicinity of this region, minimum O_2 concentrations also show an increase due to riverine N reductions by 5 %–8 %.

In the ODZ (box #1 in Fig. 7.9a), the increase in minimum bottom O_2 concentration varies between 3 % in the northern part (northern two grid cells of box #1) and 6 % in the southern part (southern two grid cells). Increases of only 0.5 %–1 % are reached in the Oyster Grounds region (box #2 in Fig. 7.9a) This likely relates to the strong influence of the North Atlantic as wells as the UK-1 and NL-1 rivers, to which none or only minor N reductions are applied. North of Denmark and in the eastern Skagerrak/Kattegat, bottom O_2 concentrations also show slight increases by up to 2 %, which likely relate to the reductions in the N reductions in the German and – to a lesser extent – Dutch rivers, as no N reductions are applied to the Norwegian rivers.

In the southeastern North Sea and in the inner German Bight, bottom O_2 conditions also improved slightly by 1 %–4 % in most regions. Interestingly, minimum O_2 concentrations even show minor reductions (up to 1 % less than in the reference run) along the Danish west coast (see Fig. 7.9c). Different to the northern North Sea these reductions do not relate to numerical differences, but represent actual O_2 reductions as a result of changes in biogeochemistry in the inner German Bight.

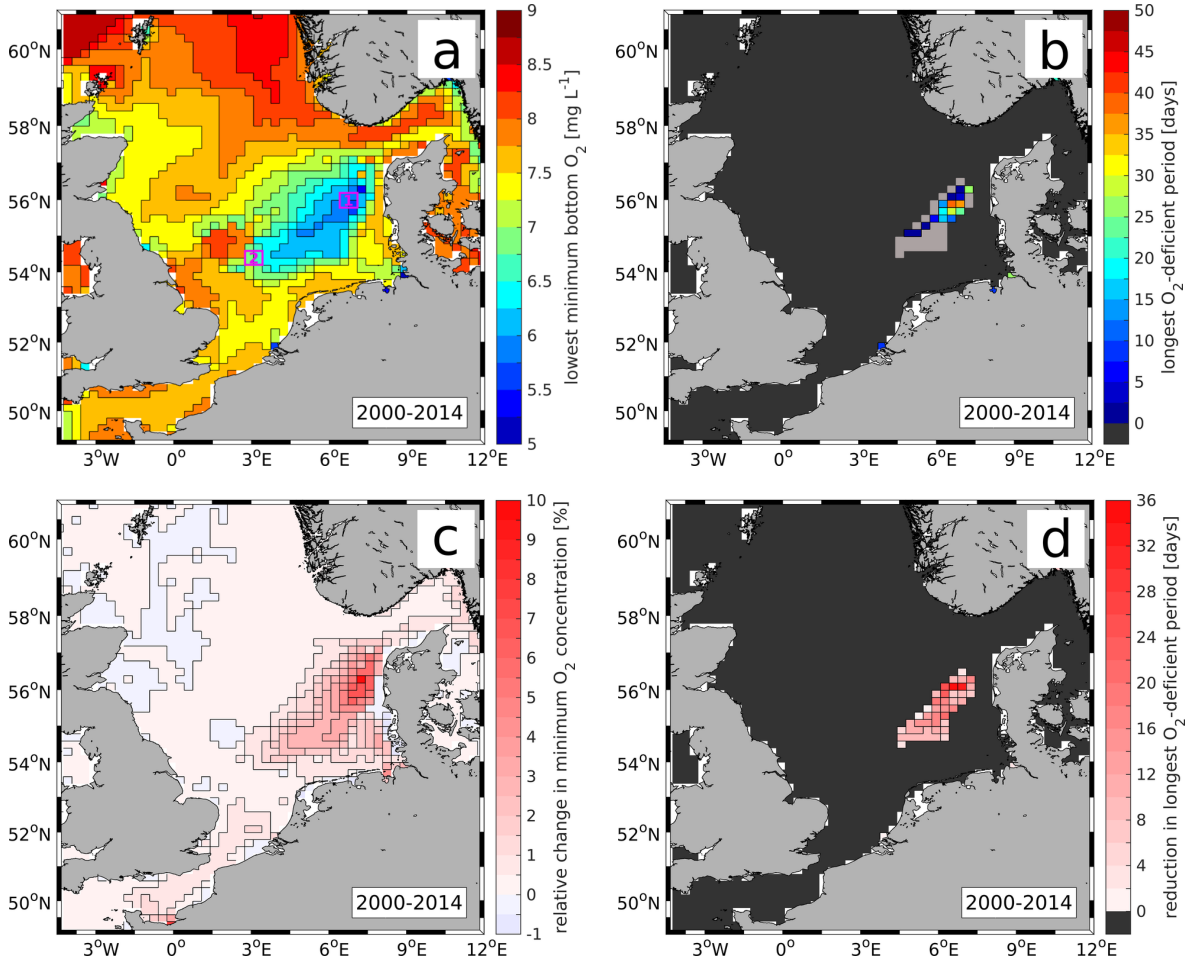

Figure 7.9: Spatial distributions of (a) lowest minimum bottom O_2 concentration, (b) longest O_2-deficient periods per year (O_2 concentration $<6\,\mathrm{mg\,O_2\,L^{-1}}$) under WFD-compliant river N reductions during the period 2000–2014, (c) relative change in minimum bottom O_2 concentrations between reference and reduction run (according to Eq. (7.5)), and (d) reduction in the duration of the O_2-deficient period between reference and reduction run. Black areas in panels b and d indicate regions where no O_2 deficiency occurred throughout the entire period in both simulations. Light grey areas in panel b indicate the additional areas of O_2 deficiency in the reference run (see Fig. 5.11b). Boxes #1 and #2 in panel a indicate North Sea ODZ and Oyster Grounds, respectively.

The riverine N reductions in the German rivers cause reduced NPP in the vicinity of the river mouths resulting in slightly higher nutrient (e.g., PO_4^{3-} and SiO_4^-) availability in the downstream regions along the Danish west coast, which in turn increase NPP and thus GOC in these areas. A similar change can be seen in the Southern Bight, which

is dominated by improved bottom O_2 conditions due to high N reductions in the French rivers, but shows minor reductions in minimum bottom O_2 concentrations in the vicinity of the Scheldt mouth (51.4 °N, 3.5 °E).

The reduction run also shows improvements with respect to the maximum duration of annual O_2 deficiency during 2000–2014. First, a clear decrease in the spatial extent of the O_2-deficient area in the southeastern central North Sea by about two thirds can be seen in Fig. 7.9b (grey area incl. coloured area represents O_2-deficient area in reference run). It is further shown that annual O_2 deficiency persists for a maximum period of 36 days in the reduction run, compared to a maximum duration of 45 days in the reference run.

Interestingly, the decrease in the duration of O_2 deficiency is quite different in the northern and southern part of the ODZ site (northern and southern two grid cells, respectively), although the relative change in minimum O_2 concentration is very similar. In the northern part, the O_2-deficient period is reduced by 36 and 33 days, while the reduction is only 6 and 9 days in the southern ODZ. This shows that a clear increase in minimum O_2 concentration does not necessarily result in clearly shorter period of O_2 deficiency. These differences inside the ODZ correspond to differences in the bathymetry. The southern two grid cells of the ODZ are deeper than the surrounding bathymetry and only connected to deeper regions in the West (see Fig. 3.2). Thus, these deeper regions are likely stronger affected by the Atlantic and UK river influences from the West than by the German riverine influences from the South.

This may cause spatial variations inside the ODZ with respect to the seasonal succession of the contributions of the individual N sources to GOC (see, e.g., Fig. 7.4a). Consequently, minimum bottom O_2 concentrations may increase remarkably as one of the major contributions during the period of lowest O_2 concentration (e.g., DE) is reduced. In contrast, the O_2-deficient period is only slightly reduced as most other major contributions (NL-1, UK-1, NA, atmosphere) remain high.

In the following the changes in the O_2 dynamics in the North Sea ODZ and in the Oyster Grounds region (box #1 and #2 in Fig. 7.9a) are analysed in more detail, with special focus on changes in minimum bottom O_2 concentrations and changes in GOC due to N reductions in the different N sources during the period 2000–2014.

7.3.3 The effect on the oxygen deficiency zone

In order to provide a deeper insight in the effects of WFD-compliant river N reductions on the O_2 conditions in the North Sea ODZ (box #1 in Fig. 7.9a), Fig. 7.10 shows the time series of the annual minimum of the daily volume-averaged bottom O_2 concentration in the ODZ during the period 2000–2014 for both the reference run (solid line) and the WFD-compliant reduction run (dotted line). It is shown that the minimum O_2 concentrations in

the reduction run are generally higher than in the reference run, with the largest difference of $0.30\,\mathrm{mg\,O_2\,L^{-1}}$ in 2002 which corresponds to a relative change of 5.5 % (according to Eq. (7.5)). During the others years, the absolute differences in minimum O_2 concentration vary between $0.04\,\mathrm{mg\,O_2\,L^{-1}}$ in 2007 and $0.25\,\mathrm{mg\,O_2\,L^{-1}}$ in 2014 (average during over entire period: $0.14\pm0.07\,\mathrm{mg\,O_2\,L^{-1}}$). The relative change during the other years varies between 0.5 % in 2007 and 4.0 % in 2003, with an average value of 2.1±1.3 % for the entire period.

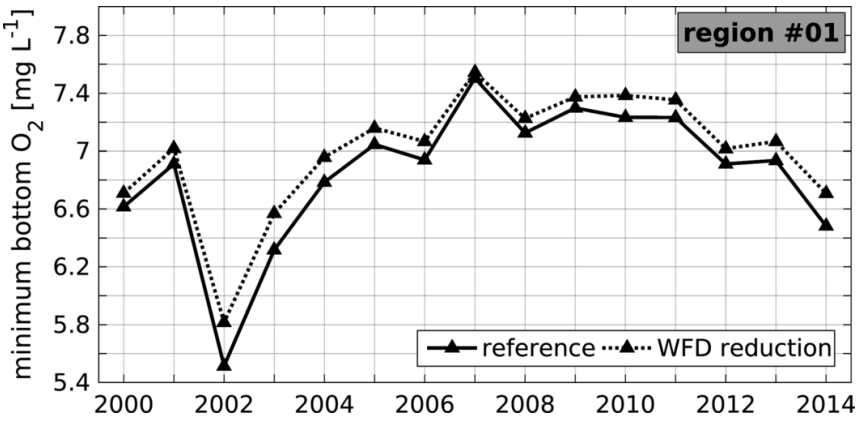

Figure 7.10: Time series of annual minimum O_2 concentrations in the bottom layer of the North Sea ODZ (see box #1 in Fig. 7.9a): reference run (solid line) and WFD-compliant N reduction run (dotted line).

With respect to O_2 deficiency in the ODZ, it is shown that 2002 constitutes the only year during the entire period, in which O_2 deficiency occurs. This applies to both reference and reduction run. The increase in the volume-averaged bottom O_2 concentration in the ODZ in 2002 also implies an almost 50 %-reduction in the duration of O_2 deficiency from 44 days in the reference run to 23 days in the reduction run.

The evolution of bottom O_2 concentrations in the ODZ during summer is controlled mainly by biochemical O_2 consumption and – in response to the evolution of a biochemically induced, spatial O_2 gradients – by vertical mixing and advection of O_2 (see Sect. 5.2.5.2). Therefore, the average daily GOC rate during stratification due to N from different sources under WFD-compliant riverine N reductions (see Table 7.5) in the bottom layer of the ODZ is presented in Fig. 7.11. The corresponding values are presented in Table 7.6, including the relative reduction in daily GOC compared to the reference run calculated as:

$$\mathrm{red_{GOC}} = 100 \cdot \left(1 - \frac{\mathrm{GOC_{red}}}{\mathrm{GOC_{ref}}}\right) \quad [\%], \tag{7.6}$$

with $\mathrm{GOC_{red}}$ and $\mathrm{GOC_{ref}}$ representing the daily GOC rate of the reduction run and reference run, respectively.

Table 7.6: Average daily gross O_2 consumption during seasonal stratification and relative contributions of the different N sources in the North Sea ODZ (box #1 in Fig. 7.2a) under WFD-compliant river N reductions during the individual years 2000–2014, and averaged over the entire period. Stratification period (t_{strat}; first to last day) in days, GOC in $g\,O_2\,m^{-2}\,d^{-1}$, reductions (red_{GOC}; according to Eq. (7.6)) and contributions by sources in %. Deviations in sum of relative contributions from 100 % due to rounding.

	2000	2001	2002	2003	2004	2005	2006	2007	2008	2009	2010	2011	2012	2013	2014	average (±STD)
t_{strat}	151	152	187	181	168	166	159	154	124	145	175	136	166	164	176	160±17
GOC	0.56	0.49	0.56	0.48	0.41	0.43	0.40	0.47	0.47	0.38	0.30	0.52	0.47	0.45	0.45	0.46±0.07
red_{GOC}	3.0	7.8	7.9	12.6	8.3	7.3	7.2	6.2	7.0	6.5	6.8	9.1	6.7	6.0	7.6	7.3±1.9
Atmosphere	14.4	18.0	13.3	18.0	19.9	18.8	23.1	16.5	14.8	21.1	22.4	17.4	16.4	16.3	14.6	17.7±3.0
DE	8.3	5.6	7.0	13.8	6.7	9.2	7.0	5.2	7.7	5.2	7.1	14.6	7.4	7.5	2.7	7.7±3.1
NL-1	6.3	14.2	14.2	16.0	10.8	7.0	11.0	9.0	11.6	8.3	9.7	10.3	5.0	5.3	9.9	9.9±3.3
NL-2	3.5	6.0	3.9	4.0	4.1	3.3	4.1	2.4	3.1	2.7	2.1	3.7	2.2	1.7	2.3	3.3±1.1
BE	0.6	1.5	1.0	0.5	0.7	0.4	0.7	0.6	0.6	0.5	0.5	0.5	0.3	0.3	0.6	0.6±0.3
FR	1.8	3.2	1.5	1.9	1.1	0.6	0.9	0.9	0.8	1.1	1.6	0.5	0.7	0.7	2.0	1.3±0.7
UK-1	1.1	4.9	2.9	2.4	2.6	1.3	1.8	2.1	2.3	1.9	3.1	1.9	1.0	1.5	4.8	2.4±1.2
UK-2	6.1	9.5	7.8	6.9	8.1	7.0	7.6	6.8	9.0	7.2	7.0	6.5	4.2	5.8	8.8	7.2±1.3
NO	<0.1	0.1	<0.1	<0.1	<0.1	<0.1	<0.1	<0.1	<0.1	<0.1	0.4	<0.1	<0.1	0.6	0.1	0.1±0.2
NA	54.7	26.9	43.8	30.3	41.7	49.7	40.0	51.8	46.4	47.4	37.1	40.7	59.4	55.1	43.6	44.6±9.0
EC	2.1	8.1	3.5	4.8	3.2	1.8	2.5	3.4	2.3	3.3	6.0	2.4	2.3	2.9	7.5	3.7±2.0
BS	<0.1	0.1	<0.1	<0.1	<0.1	<0.1	<0.1	<0.1	<0.1	<0.1	0.6	<0.1	<0.1	0.4	0.2	0.1±0.2
Others	1.0	1.9	1.2	1.2	1.0	0.9	1.2	1.1	1.3	1.1	2.5	1.5	1.3	1.7	2.9	1.5±0.6
riverine	28.8	46.9	39.4	46.9	35.2	29.7	34.3	28.2	36.5	28.2	33.9	39.4	22.0	25.2	34.1	33.9±7.2
non-riverine	71.2	53.1	60.6	53.1	64.8	70.3	65.7	71.8	63.5	71.8	66.1	60.6	78.0	74.8	65.9	66.1±7.2

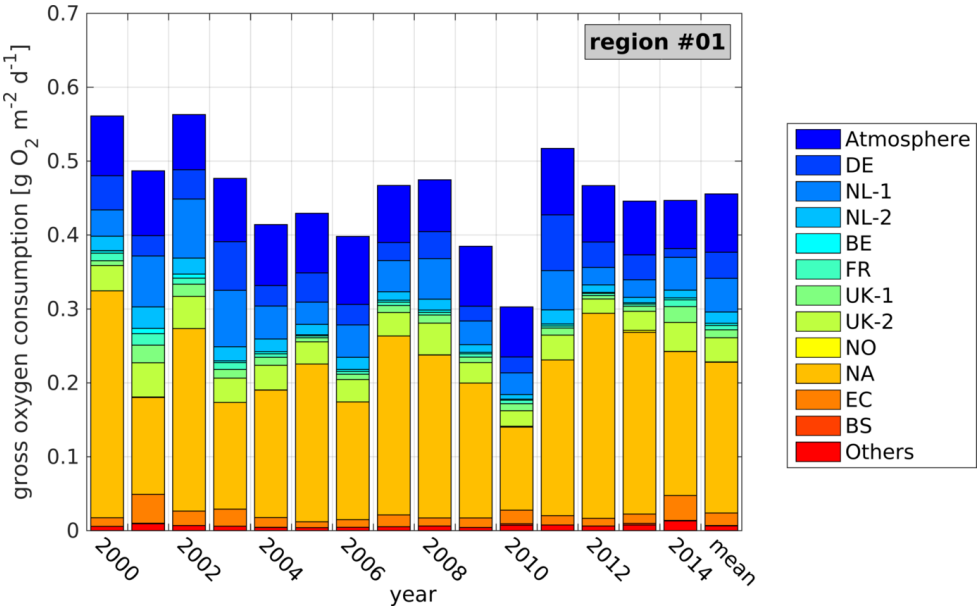

Figure 7.11: Average daily gross O_2 consumption during seasonal stratification and contributions of the different N sources (colours; compare Table 6.1) in the North Sea ODZ (box #1 in Fig. 7.2a) under WFD-compliant river N reductions during the individual years 2000–2014, and averaged over the entire period. For corresponding values see Table 7.6.

Figure 7.11 and Table 7.6 show that in the reduction run, GOC in the bottom layer of the ODZ is consistently less than in the reference run, with a maximum reduction of 12.6 % in 2003 and an average reduction of 7.3±1.9 % during the entire period 2000–2014. The low reduction of only 3 % in 2000 relates to the fact that the results for year 2000 are still strongly influenced by the initial conditions, which are the same as for the reference run. In the later years, the lowest reduction in GOC occurs in 2013, yielding 6.0 %. The reduction in GOC in 2003 is so strong that the resulting daily GOC rate of $0.48\,\mathrm{g\,O_2\,m^{-2}\,d^{-1}}$ is in the same order as in 2007 and 2008 (both about $0.47\,\mathrm{g\,O_2\,m^{-2}\,d^{-1}}$), while it is clearly higher in the reference run ($0.55\,\mathrm{g\,O_2\,m^{-2}\,d^{-1}}$, $0.50\,\mathrm{g\,O_2\,m^{-2}\,d^{-1}}$ and $0.51\,\mathrm{g\,O_2\,m^{-2}\,d^{-1}}$, respectively). This strong decrease in 2003 relates to the very high DE contribution of 18.4 % in the reference run (see Table 7.2). As the DE rivers are those with the highest N reductions (see Table 7.5) among the rivers with a strong influence on GOC in the ODZ, the achieved GOC reductions are highest in years with high DE contributions (2003 and 2011). The reduction in GOC in 2003 also coincides with a strong reduction in the DE contribution, yielding a contribution of 13.8 % in the reduction run (see Table 7.6). The average DE contribution results in 7.7±3.1 % (10.9±4.0 % in the reference run).

The BE and FR contributions in 2003 are also slightly reduced (from 0.7 % to 0.5 % and from 4.7 % to 1.9 %, respectively), which relates to the high N reductions in these

rivers. The decrease in the BE and FR contributions is consistent over the entire period.

The Dutch NL-1 and NL-2 rivers show either minor increases or decreases in their contributions to GOC in individual years. This relates to the only minor reductions in N input by these rivers and also depends on the reductions in the other riverine sources. The same applies to the UK-1 and 'other' rivers, which show either no or only very minor changes in their contributions. Averaged over the entire period, these riverine contributions show increases by 0.1 % relative to the reference run. The UK-2 contribution is consistently higher in the reduction run than in the reference run, with an average contribution 7.2 %±1.3 % in the reduction run compared to 6.7±1.2 % in the reference run. This also relates to the high contribution of the UK-2 rivers to GOC and the zero reduction. The contribution by the Norwegian rivers has not changed.

The non-riverine sources (atmosphere, NA, EC and BS) show different changes relative to the reference run. While the BS contribution remained basically the same, the EC contribution is slightly lower in the reduction run. The latter likely relates to changes in the biochemistry in the English Channel and Southern Bight, due to reductions in the French rivers. Relative to the overall available N in these regions, more N originating from the EC is utilised for NPP implying higher sedimentation of organic N from the EC in these regions (in relative terms). Consequently, less N from the EC reaches the ODZ. This is a consistent image for the entire period, except for the first two years, which may relate to the influence of the initial conditions during these first years. On average, the EC contribution is 0.2 % lower than in the reference run.

The atmospheric and NA contribution are consistently higher in the reduction run than in the reference run. This relates to the fact that the input of N into the TBNT domain by these two sources is the same in the reference and the reduction run. Although regional changes in N uptake during NPP and thus sedimentation of organic matter, may modulate the atmospheric and NA signal in the ODZ (similar to the EC contribution), this effect is less pronounced in the two contributions. On the one hand, this relates to the generally higher atmospheric and NA contributions. On the other hand, the most of the N originating from the NA comes from the West and Northwest, where no or only minor riverine reductions (UK-2, NL-1) are applied, i.e., changes in biochemistry in these regions are less strong (see Fig. 7.9c). Consequently, the modulation of the NA contribution 'upstream' of the ODZ can be considered to be small. For the atmospheric contribution, the strong reduction in the DE contribution is the most important influence, as it can be assumed that most of the atmospheric N contributing to GOC in the ODZ entered the system in the vicinity of the ODZ and upstream the Jutland Current, i.e., regions dominated by the DE rivers in the reference run. Finally, the N reductions in some rivers result in a shift in the overall riverine and non-riverine contributions, yielding

a riverine contribution of 33.9±7.2 % compared to 38.2±7.6 % in the reference run.

In order to illustrate the influence of the decreased GOC as a result of the WFD-compliant riverine N reductions on the physico-biochemical interactions controlling the O_2 dynamics in the North Sea ODZ (see Sect. 5.2.5.2), the change in daily GOC in 2002 is put in context with the findings on these interactions. According to Table 5.2, the integrated effect of vertical mixing and advection on O_2 in the bottom layer of the ODZ adds up to about 76 % of GOC, i.e., about three quarters of GOC are compensated by physical O_2 supply to the bottom layer. The difference between GOC in 2002 in the reference run and in the reduction is about $0.05\,g\,O_2\,m^{-2}\,d^{-1}$. This corresponds to a difference in O_2 between the two simulations by $9.1\,g\,O_2\,m^{-2}$ integrated over the stratified period (187 days). Dividing this value by the average bottom layer thickness of 6.5 m yields a difference in O_2 concentration by $1.4\,g\,O_2\,m^{-3}$. The inclusion of the compensation effect of the physical processes finally results in a difference in the O_2 concentration at the end of stratification of $0.34\,mg\,O_2\,L^{-1}$. This value corresponds very well with the difference in the minimum O_2 concentration in 2002 between the reference and the reduction run ($0.30\,mg\,O_2\,L^{-1}$). The minor differences between these values likely relate to the fact that the minimum O_2 concentrations do not occur exactly at the end of stratification (see Fig. 5.12e) and to changes in the spatial gradients influencing vertical mixing and advection of O_2. This is also indicated by the lower compensation effect of the physical processes in 2010 (68 %) due to weaker spatial gradients.

For 2010, the difference in the O_2 concentrations between the reference and reduction run based on the differences in GOC results in $0.19\,mg\,O_2\,L^{-1}$, compared to $0.15\,mg\,O_2\,L^{-1}$ using the simulated minimum concentrations. Despite these minor deviations, the generally good agreement between the two differently calculated changes in O_2 concentration from the reference run to the reduction run for the two years suggests that the daily GOC provides a useful measure for the analysis of the implications of riverine N reductions on the O_2 dynamics of the ODZ.

In general, it can be said that even the high N reductions applied to the German rivers as well as the Belgian and French rivers (see Table 7.5) result in only minor improvements in the bottom O_2 conditions in the ODZ, with maximum changes of 5.5 % in 2002. This mainly relates to the fact that on average these rivers only account for about 15 % of overall GOC in the ODZ in the reference run. Considering that the Dutch NL-1 and British UK-2 rivers account for 16.5 % of overall GOC averaged over 2000–2014, it is likely that additional reductions in these rivers would result in a further improvement of the O_2 conditions in the North Sea ODZ. The atmospheric contribution of almost 18 % on average also suggests a relevant impact of future reductions in atmospheric deposition (UNESC, 1999) on the O_2 conditions.

7.3.4 The effect on the Oyster Grounds

As Greenwood et al. (2010) found the Oyster Grounds region to be susceptible to O_2 deficiency, this section presents the changes in minimum bottom O_2 concentrations and GOC in the Oyster Grounds region (box #2 in Fig. 7.9a) analogously to the previous section. Figure 7.12 shows the time series of the annual minimum of the daily volume-averaged bottom O_2 concentration in the Oyster Grounds during the period 2000–2014 for both the reference run (solid line) and the WFD-compliant reduction run (dotted line).

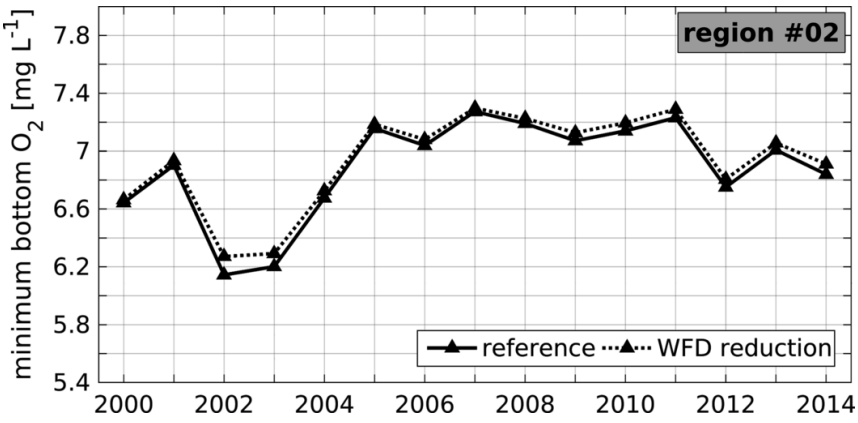

Figure 7.12: Time series of annual minimum O_2 concentrations in the bottom layer of the Oyster Grounds (see box #2 in Fig. 7.9a): reference run (solid line) and WFD-compliant N reduction run (dotted line).

As for the ODZ it can be seen that minimum O_2 concentrations are generally higher in the reduction run than in the reference run, however, to a clearly lesser extent than in the ODZ. Maximum differences in minimum bottom O_2 concentration result for 2002 with a value of $0.13\,\mathrm{mg\,O_2\,L^{-1}}$ (about 2.4 times less than in the ODZ), corresponding to a relative change of 2.1 % which also represents the highest relative change of the entire period. On average, the minimum O_2 concentrations in the reduction run is only $0.05\pm0.03\,\mathrm{mg\,O_2\,L^{-1}}$ higher than in the reference corresponding to an average relative change of 0.8 ± 0.5 %. These generally smaller changes in minimum O_2 concentrations in the Oyster Grounds, compared to the ODZ, likely result from the zero or only minor reductions in the most dominating riverine sources (NL-1 and UK-2).

In order to further elucidate the effects of the N reductions on the Oyster Grounds, Fig. 7.13 shows the time series of the average daily GOC for the reduction run for the individual years 2000–2014 and averaged over the entire period, including the contributions by the different N sources. The corresponding values and the changes in GOC relative to the reference run (according to Eq. (7.6)) are provided in Table 7.7.

Table 7.7: Average daily gross O_2 consumption during seasonal stratification and relative contributions of the different N sources in the Oyster Grounds (box #2 in Fig. 7.2a) under WFD-compliant river N reductions during the individual years 2000–2014, and averaged over the entire period. Dashes indicate zero contributions. Stratification period (t_{strat}; first to last day) in days, GOC in $\mathrm{g\,O_2\,m^{-2}\,d^{-1}}$, reductions in GOC ($\mathrm{red_{GOC}}$; according to Eq. (7.6)) and contributions by sources in %. Deviations in sum of relative contributions from 100 % due to rounding.

	2000	2001	2002	2003	2004	2005	2006	2007	2008	2009	2010	2011	2012	2013	2014	average (±STD)
t_{strat}	166	149	173	165	169	175	158	158	127	157	160	166	168	162	180	163±13
GOC	0.36	0.37	0.38	0.36	0.32	0.32	0.32	0.36	0.31	0.29	0.23	0.35	0.34	0.35	0.32	0.33±0.04
$\mathrm{red_{GOC}}$	0.8	1.8	4.2	2.5	2.3	1.8	2.2	2.6	2.7	3.7	3.1	3.7	2.6	3.3	3.3	2.7±0.8
Atmosphere	11.7	11.2	11.6	13.1	14.0	13.7	15.7	13.1	12.5	15.5	16.2	15.3	12.5	13.5	11.9	13.4±1.6
DE	<0.1	<0.1	<0.1	0.1	<0.1	<0.1	<0.1	0.1	0.1	<0.1	0.3	0.2	<0.1	1.1	<0.1	0.1±0.3
NL-1	16.0	12.2	16.7	18.4	12.2	12.9	13.9	13.8	13.9	13.6	10.8	22.2	13.6	15.5	7.0	14.2±3.5
NL-2	1.6	1.3	2.0	1.9	0.8	1.0	0.6	1.4	2.0	1.3	2.6	2.8	1.1	4.2	0.6	1.7±1.0
BE	1.6	1.3	0.9	1.0	0.9	0.8	1.0	1.0	0.9	1.1	0.6	1.2	0.9	1.1	0.5	1.0±0.3
FR	3.7	2.4	2.8	1.8	1.2	0.9	1.0	1.4	1.3	1.8	1.2	1.2	1.0	1.4	3.1	1.7±0.9
UK-1	2.8	5.2	4.6	3.8	4.0	2.2	2.1	3.9	3.7	3.9	2.5	3.8	1.8	4.6	7.8	3.8±1.5
UK-2	10.7	17.9	12.4	17.4	12.9	11.0	11.8	13.1	13.7	14.5	12.1	13.1	7.6	16.9	14.9	13.3±2.7
NO	–	–	–	–	–	–	–	–	–	–	–	–	–	–	–	–
NA	46.0	39.0	40.5	35.8	49.0	53.6	49.5	44.7	46.2	40.7	45.1	33.3	55.0	32.0	36.1	43.1±7.1
EC	4.6	7.6	6.8	5.2	3.8	2.7	2.8	6.0	4.1	5.9	5.9	4.8	4.2	6.9	13.7	5.7±2.7
BS	–	–	–	–	–	–	–	–	–	–	–	–	–	–	–	–
Others	1.5	1.9	1.7	1.6	1.3	1.2	1.5	1.6	1.7	1.7	2.7	2.2	2.3	2.9	4.4	2.0±0.8
riverine	37.8	42.3	41.1	45.8	33.3	30.0	31.9	36.2	37.2	37.9	32.8	46.6	28.3	47.7	38.2	37.8±6.0
non-riverine	62.2	57.7	58.9	54.2	66.7	70.0	68.1	63.8	62.8	62.1	67.2	53.4	71.7	52.3	61.8	62.2±6.0

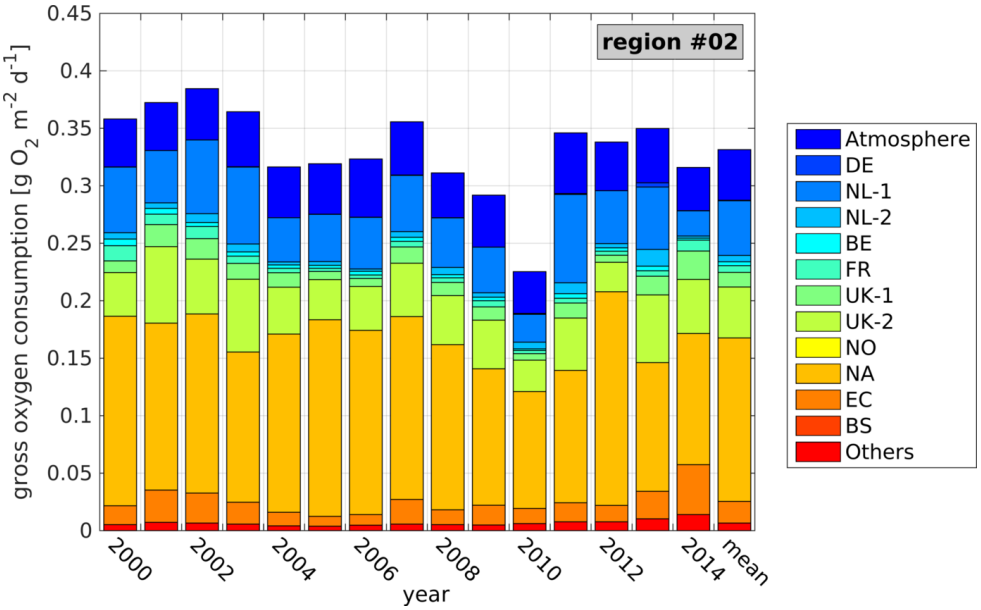

Figure 7.13: Average daily gross O_2 consumption during seasonal stratification and contributions of the different N sources (colours; compare Table 6.1) in the Oyster Grounds (box #2 in Fig. 7.2a) under WFD-compliant river N reductions during the individual years 2000–2014, and averaged over the entire period. For corresponding values see Table 7.7.

Figure 7.13 reveals a general reduction in daily GOC rates between 0.8 % in 2000 and 4.2 % in 2002. On average, the GOC reduction results in 2.7±0.8 %, i.e., the reduction the Oyster Grounds is about 2.7 times less than in the ODZ. This is in good agreement with the difference in the absolute changes in minimum O_2 concentration from the reference to the reduction run between the two regions. Different to the ODZ, the year-to-year differences in GOC in the reduction run are very similar to those in the reference run. This relates to the only minor reductions in the most dominant riverine sources (NL-1 and UK-2 add up to an average contribution of about 27 % in the reference run) implying only minor year-to-year variations in the GOC reductions due to these rivers.

As for the ODZ, only the BE, FR and DE rivers show consistently lower contributions to GOC in the Oyster Grounds in the reduction run, although the latter generally have only small influence on the Oyster Grounds. The average French contribution shows the strongest reduction from 3.8±1.5 % in the reference run to 1.7±0.9 % in the reduction run (see Tables 7.4 and 7.7, respectively). The Belgian rivers also show a reduction from 1.5±0.4 % to 1.0±0.3 % in the reduction run, averaged over the entire period 2000–2014. Strong year-to-year variations can be seen in the relative contributions of the Dutch (NL-1/-2) and British rivers (UK-1/-2) to GOC, with both increases and decreases compared to the reference run. These variations relate to the contributions of the BE and – more

important – of the FR rivers. In years of high relative contributions from these rivers in the reference run (e.g., combined contribution of 8.4 % in 2002) the Dutch and British rivers tend to show increased relative contributions in the reduction run, while in years of minor FR and BE contributions in the reference run (e.g., 2005) the NL-1 rivers show a lower contribution due to the increased UK-2 contribution.

With respect to the non-riverine sources the image provided for the Oyster Grounds is also similar to that for the ODZ. The atmospheric and NA contributions in the reduction run are consistently higher than in the reference run as a result of the reduced riverine contributions. The former shows an increase from 13.0±1.6 % to 13.4±1.6 %, while latter increased from 41.4±7.2 % to 43.1±7.1 %. The EC contributions shows varying changes in its relative contribution to GOC in the Oyster Grounds. While its contribution is increased in 2000, 2001 and 2014, it shows similar or lower relative contributions for all other years, which is also represented in a reduction of the average contribution by 0.1 % compared to the reference run. This most likely also relates to the changes in biochemistry in the English Channel and Southern Bight regions due to changes in N limitation in these regions as a result of the French and Belgian riverine N reductions. This is supported by the fact that the EC contributions is increased in years when the FR contribution is highest in the reference run (2002 and 2014; see Table 7.4).

Considering the integrated effect of riverine and non-riverine N sources on bottom layer GOC in the Oyster Grounds, it can be seen that the average riverine contribution is reduced by only 2 % resulting in 37.8±6.0 % in the reduction run. Thus, the average reduction in the riverine contribution is less than half of that in the ODZ, which relates to the zero reductions in the British rivers and the only minor reductions in the Dutch rivers. This suggests, that the improvement of the O_2 conditions in the Oyster Grounds would require strong reductions in the British rivers along the east coast of Great Britain (UK-2) and in the large Dutch rivers, Rhine and Meuse (NL-1).

Analogous to Sect. 7.3.3, an decrease in GOC of 0.53 mg O_2 L^{-1} during stratification in 2002 (173 days) can be derived from the difference in daily GOC between the reference run and the reduction run (Tables 7.4 and 7.7, respectively) and the average bottom layer thickness of 5.5 m. Including the physical compensation effect of 78 % due to mixing and advection (derived from Table 5.3) finally yields an increase in the O_2 concentration at the end of stratification by 0.12 mg O_2 L^{-1} from the reference to the reduction run. This is in very good agreement with the difference in the minimum O_2 concentration of 0.13 mg O_2 L^{-1} between the two simulations. This underlines that GOC constitutes a reliable indicator for changes in O_2 dynamics in relation to N from different sources (in water bodies not directly affected by NPP).

7.4 Constraints of the presented approach

The here presented quantitative analysis of the North Sea O_2 dynamics in relation to N from riverine and non-riverine sources represents the first approach for creating a direct link between the N input from specific sources and its influence on the O_2 dynamics on the level of O_2-affecting processes. Consequently, there are only very few comparable studies available in the literature. Therefore, this sections focuses for the discussion of the results in the context of the general constraints of biogeochemical models and the TBNT method, after a brief discussion in the relation to existing literature.

In fact, there have been earlier North Sea studies on the relationship between river nutrient loads and O_2 deficiency in the North Sea (e.g., Brockmann et al., 1988; Topcu and Brockmann, 2015). However, these studies rely on statistical analyses and the qualitative description of the interactions controlling the evolution of O_2 deficiency. Other studies investigated the effect of river nutrients on the North Sea biochemistry by conducting nutrient reduction scenarios (e.g., Skogen et al., 2004; Lenhart et al., 2010; Emeis et al., 2015). Though, only Lenhart et al. (2010) considered the implications for the O_2 conditions in the North Sea based on a model comparison study. The other studies were confined to the effects on nutrient (N and P) and Chl-a levels. Lenhart et al. (2010) found that riverine N and P reductions of 50 % relative to 1985 resulted in an increase in minimum bottom O_2 in the Oyster Grounds region in 2002 by about $0.2\,\mathrm{mg\,O_2\,L^{-1}}$ to $0.3\,\mathrm{mg\,O_2\,L^{-1}}$ (range of three different models). This represents a stronger increase than in shown in Sect. 7.3.4, which likely relates to the significantly higher reductions in NO_3^- in the Dutch and British rivers (both 50 %).

Troost et al. (2013) used a biogeochemical model for the quantification of the impact of atmospheric N deposition on bottom O_2 concentrations in the Oyster Grounds region by comparing two different model scenarios. They found that atmospheric N causes summer bottom O_2 concentrations to be about $0.5\,\mathrm{mg\,O_2\,L^{-1}}$ lower than in a simulation not taking into account atmospheric deposition. Combining the results for GOC in the Oyster Grounds in 2002 and the corresponding atmospheric contribution (see Table 7.4) with the physical compensation due to advection and mixing of 78 % (derived from Table 5.3), the atmospheric contribution causes a reduction in bottom O_2 concentration during stratification of $0.31\,\mathrm{mg\,O_2\,L^{-1}}$. This is in the same order as the results of Troost et al. (2013), however, the deviation may relate to various aspects such as differences in t_{strat}, atmospheric deposition data used as forcing etc., which makes the direct comparison difficult.

Besides the work by Lenhart et al. (2010) and Troost et al. (2013), no other results comparable to those of this study could be found in the literature. For this reason, in the following the general constraints of biogeochemical models and the TBNT method

are discussed. In principle, the outcome of biogeochemical model simulations depends on three key factors: (1) the model intrinsics (e.g., process parameterisations, stoichiometry), (2) the model forcing (including the open boundary conditions) and (3) the model grid (e.g., spatial resolution).

With respect to the model intrinsics, Sect. 5.2.5 already showed that REM_{sed} tends to be slightly underestimated. In addition, the rather simple sediment module implemented to ECOHAM does not allow for a long-term burial of organic matter in the sediment. However, this is in good agreement with observational studies that found that burial of N and also C in the North Sea sediment is negligible (e.g., Wirth and Wiesner, 1988; de Haas et al., 1997; Brion et al., 2004).

It should further be mentioned that benthic fauna is not included in the model, i.e., the effect of respiration by benthic species is neglected. However, de Wilde et al. (1984) reported a great influence of benthic species on near-bottom O_2 consumption. In addition, they can affect the release and storage of nutrients due to bioturbation and life spans of several months up to years (e.g., of polychaetes; de Wilde et al., 1984; Künitzer et al., 1992; Thompson and Schaffner, 2001). The latter may have an influence on the temporal delay between organic matter sedimentation and the release of inorganic nutrients by the sediment, and thus on the relative contribution by individual N sources to O_2 consumption in specific regions. Therefore, benthic fauna should be considered in future studies in order to obtain a more precise image of the O_2 dynamics and the cycling of N from the different sources.

The stoichiometry applied to phytoplankton, but also zooplankton, bacteria and organic matter constitutes another factor, that may strongly affect the overall results of this study. As already mentioned, the N:P ratio of 20:1 applied to phytoplankton deviates from the corresponding Redfield ratio of 16:1 (Redfield, 1934). Furthermore, it is known that elemental ratios vary between different phytoplankton species (e.g., Geider and La Roche, 2002; Quigg et al., 2003; Malzahn et al., 2010) as well as under varying environmental conditions (e.g., Rhee, 1978; Goldman et al., 1979). However, the model validation and comparison to existing literature (see Ch. 5) showed that ECOHAM reproduces the main features of the North Sea biogeochemistry and NPP are in the range of other modelling and observation studies.

In fact, simulations conducted with different elemental ratios would result in different phytoplankton growth, e.g., by stronger P limitation in case of a lower N:P ratio. Consequently, these changes in phytoplankton growth would also affect the entire ecosystem dynamics, including the O_2-affecting processes and thus the O_2 concentrations as well as the contributions by the individual N sources. In order to assess these impacts of different stoichiometry, a comprehensive sensitivity analysis would be required, which is beyond the

scope of this thesis.

With respect to the influence of the different N sources on the ecosystem, the biochemical forcing data also play an important role. The quality of the river discharge and nutrient load data is crucial for both, the model hydrodynamics due to haline stratification in coastal regions, and the model biochemistry, due to the amount of nutrients being provided to the ecosystem. Although this data is compiled to the best knowledge (see Sect. 3.2.2.2), it underlies various assumptions as a result of limited data availability. For instance, processes like retention of N and P in estuaries, such as the Elbe estuary, were found to be non-negligible (e.g., Behrendt, 1996). However, nutrient retention is not included in the river data used for this study, implying a potential source of error. Furthermore, for many rivers only monthly data are available on a long-term basis (i.e., over time spans of decades). In order to obtain daily time series, that are required for running a simulation with HAMSOM and ECOHAM, temporal (linear) interpolation is applied, which most likely does not fully represent the actual river loads and discharges. Despite these restrictions, the here applied data set – to my knowledge – constitutes the most comprehensive data set, with respect to the number of rivers included and the amount of underlying data, for the North Sea.

For atmospheric N deposition, the situation is somehow similar. At first, it is necessary to provide deposition data for the entire simulation period and the entire model domain. This can be obtained by temporal extrapolation (see Sect. 3.2.2.1) and spatial interpolation to the model grid, based on the original deposition data from EMEP. However, with respect to the quality of these original data one has to rely on the model used by EMEP. EMEP provides deposition data sets with different temporal resolutions, e.g., monthly or annual. Interestingly, the annual sum of the monthly EMEP deposition data (used, e.g., by Desmit et al. (2015)) is not identical to the annual data used in this study. In individual regions of the North Sea, differences in the order of $10\,\mathrm{kt\,N\,a^{-1}}$ between the two data sets can occur (not shown), which indicates a large uncertainty in the available atmospheric deposition data sets. However, the EMEP data constitutes the only spatially and temporally consistent data that is currently available. Therefore, one has to rely on this product for the inclusion of atmospheric N deposition in ecosystem models.

Considering further potential nutrient sources such as point sources (e.g., sewage treatment plants), it should be mentioned that these are not included in ECOHAM (except for the British river data). However, this can be assumed to be a reasonable constraint as Kemp et al. (2009) reported that their influence on O_2 dynamics of deeper seasonally stratified shelf seas appears to be of only minor importance. Also, the exchange of organic matter or nutrients between North Sea and the Wadden Sea is not included in ECOHAM. Postma (1981) reported that the outgoing tide in the Dutch Wadden Sea contains about

18 % less organic matter than the incoming tide, and a correspondingly higher amount of inorganic matter. The Marsdiep basin (also in the Dutch Wadden Sea) also constituted a source of organic and inorganic P during most of the years 1950–1985 (van Raaphorst and van der Veer, 1990). Several studies also report the (Dutch and German) Wadden Sea to be an important sink of N due to benthic denitrification (e.g., Kieskamp et al., 1991; van Beusekom and de Jonge, 1998; van Beusekom et al., 1999). Thus, the inclusion of the exchange of organic and inorganic nutrients with the Wadden Sea could additionally influence the model results especially in the coastal North Sea off the Wadden Sea. Hoppema (1991) further showed that the Marsdiep constitutes an O_2 sink for the North Sea, i.e., exchange of oxygenated and de-oxygenated waters between North Sea and Wadden Sea may additionally impact O_2 in the coastal southeastern North Sea. Therefore, the mass exchange between the open North Sea and the adjacent Wadden Sea should be considered in future studies.

Although Sect. 6.4 shows that the overall agreement with other TBNT studies (OSPAR, 2010; Painting et al., 2013; Troost et al., 2013) on N is good and the general spatial features are similar to the features found in these studies, the contributions of individual sources to N and NPP in different North Sea regions showed variations of up to about 5-10 %. For instance, the influence of the North Atlantic on the southeastern North Sea appears to be slightly overestimated. This likely relates to the high numerical diffusion of the HAMSOM model (Lenhart and Pohlmann, 1997). In addition, the model revealed some shortcomings with respect to the representation of the intensity of seasonal stratification. This tendency for underestimating stratification intensity can be related to both, the coarse horizontal resolution (20 km) of the model and the high numerical diffusion (Lenhart and Pohlmann, 1997).

This underestimation implies enhanced vertical mixing, which affects both, the O_2 dynamics itself and the contributions of individual sources to GOC in the bottom layer. Consequently, the use of a higher resolution model (e.g., Pohlmann, 2006; Mathis and Pohlmann, 2014) is highly recommended for future studies on the North Sea O_2 dynamics. Furthermore, a more sophisticated advection scheme may improve the model performance. However, as the processes controlling O_2 remain the same, the interactions described in this thesis would also principally be the same, although absolute values of individual processes will probably change. The contributions of the individual N sources on GOC in the different North Sea regions will also likely change. However, due to the generally good agreement with earlier TBNT studies on TN and NPP (OSPAR, 2010; Painting et al., 2013; Troost et al., 2013) and the strong link between NPP and GOC shown in this thesis, it can be expected that the overall image will not change. Nevertheless, future studies on the North Sea O_2 dynamics and riverine contributions should base on an improved

representation of the North Sea hydrography and hydrodynamics.

Another important aspect for the interpretation of the results of this study is the influence of non-linearities in biogeochemistry. Lenhart et al. (2010) already showed that even a 50 %-reduction in riverine DIN in the major North Sea tributaries results in only minor improvements in the O_2 conditions in the Oyster Grounds. On the one hand, this relates to changes in biogeochemistry in regions in the vicinity of the rivers with reduced nutrient inputs, as indicated by the decrease in the contribution of the English Channel inflow in the Oyster Grounds area (see Sect. 7.3.4). On the other hand, additional aspects such as seasonal and year-to-year variations, e.g., in river nutrient loads, play an important role as shown in this chapter. Consequently, the river nutrient reductions relative contribution of the individual sources cannot be translated linearly into actual improvements in the O_2 conditions (i.e., 'riverine reduction' $\times$ 'riverine contribution' $\neq$ 'increase in O_2 concentration').

In contrast, reduction scenarios similar to the presented one are still required and need to be analysed with respect to O_2 in order to determine the optimal setup of N reductions for improving the North Sea O_2 conditions. The linear optimisation method proposed by Los et al. (2014) could be expanded by the application to GOC based on the method described in this chapter. Consequently, it could be used for speeding up the iterative process of running multiple reduction scenarios in order to find the optimal setup of river nutrient reductions. However, it has to be kept in mind that even those optimised reductions obviously do not guarantee the attainment of the actual target state due to the underlying non-linearities.

It should further be mentioned that the application of the here presented approach for linking the O_2 dynamics to N from individual riverine and non-riverine sources would yield different results in case of the tracing of another element (P, C or Si) from the individual sources. For instance, atmospheric deposition of P is not implemented to the current version of ECOHAM, although it has been reported to play a role in the North Sea (Maenhaut et al., 1997; Maenhaut and Cafmeyer, 1998; Mahowald et al., 2008). Thus, its implementation should be considered for future North Sea studies. Tréguer et al. (1995) also report that atmospheric Si deposition (i.e., silicic acid aeolian input) contributes about $0.5 \pm 0.5\,\mathrm{Tmol\,Si\,a^{-1}}$ to the Si budget of the global ocean, representing roughly 10 % of the riverine contribution. Although, no actual values of atmospheric Si deposition could be found for the North Sea, it can be assumed that it is negligible for the North Sea as Prospero et al. (1996) (their Table 9) showed that only a very small proportion of aeolian dust entering the North Atlantic is deposited in the North Sea.

Besides this, NIT only affects N and does not influence other nutrients, i.e., it is not possible to create a link of O_2 consumption by NIT to P, Si or C using the here presented

approach. In this context, it has to be mentioned that this approach requires a process-based link between the O_2 cycle and the considered nutrient cycle (e.g., N). This also implies that it cannot be applied to empirical process formulations that only base on, e.g., O_2 concentrations, but not on other nutrients (e.g., REM_{sed} according to Eq. (1) in Hetland and DiMarco (2008)).

Furthermore, different REM_{sed} rates for different labelled elements may influence the relative contributions of individual sources during the annual cycle, relative to those of N. Finally, the relative contributions of the different North Sea tributaries to overall P, Si or C input into the North Sea may differ from those for N (see Fig. 6.4b), which could additionally affect the results of a similar application to one of these elements. However, these studies are beyond the scope of this thesis.

Despite the discussed constraints of the here presented work, the general image of the North Sea physics and biochemistry as well as the influence of individual N sources on TN and NPP is consistent with existing studies. Therefore, it can be concluded that the TBNT analysis of the O_2 dynamics also provides reasonable results. However, absolute values, e.g., of GOC or individual source contributions to GOC, will likely show minor variations in case of a different model setup, e.g., with an improved representation of the North Sea physics. Therefore, it is first recommended applying the here presented approach to a HAMSOM-ECOHAM setup with an improved advection scheme. The validation and analysis tools developed during this thesis can be applied easily to such new simulation. Second, a comparative application to other North Sea ecosystem models would be worthwhile for better estimating the uncertainties in the presented results. An intercomparison of the results from different models would exhibit the bandwidth of the contributions of the individual N sources on the O_2 dynamics of the different North Sea regions. This would provide a more reliable basis for the proposed iterative procedure for the determination of optimised N reduction targets. Third, additional relevant factors, such as mass exchange with the Wadden Sea and atmospheric P deposition, should be included in the model in order to achieve a more realistic representation of the North Sea ecosystem.

7.5 Conclusions on the influence of nitrogen on oxygen consumption

The here presented study, for the first time, proposes an approach for directly linking the O_2 dynamics of the North Sea to N inputs from various external sources (rivers, the atmosphere and adjacent seas). This is done by expanding the TBNT method applied

on N by a process-based link to the O_2 cycle implemented to ECOHAM. By this, the impact of individual N sources on the O_2 dynamics can be quantified in different North Sea regions and on different time scales, ranging from days to multiple years.

The analyses of the spatial distributions of annual NOC and GOC show that GOC provides a reliable proxy for the detailed analysis of the impact of individual N sources on the near-bottom O_2 dynamics in the deeper North Sea regions. The good agreement between the spatial distributions of the relative contributions of the individual sources to bottom layer GOC with those to water column integrated NPP based on N labelling underlines the strong link between local NPP and O_2 consumption in the North Sea. This is also supported by the annual cycles of GOC and its contributing N sources in the ODZ during 2002 and 2010. This gives additional confidence in using NPP for the definition of the ODI (see Sect. 5.2.3.2).

The analysis of GOC in the ODZ further shows that, on average, atmospheric N deposition (17 %), the North Atlantic inflow (NA; 41 %) and the riverine contributions by the large Dutch (NL-1; incl. Rhine and Meuse; 10 %), German (DE; Elbe, Weser, Ems; 11 %) and British rivers (UK-2; along the east coast; 7 %) constitute the main N sources affecting GOC in the ODZ. In total, almost 62 % of GOC during seasonal stratification are controlled by non-riverine contributions. However, the riverine contribution can add up to more than 50 % during individual years. Furthermore, years of high GOC tend to coincide with such high riverine contributions, especially from the Dutch and German rivers.

Flood events in these rivers can significantly increase GOC at the ODZ site. However, this strongly depends on the timing of these events. For instance, the Elbe floods in August 2002 (e.g., Ulbrich et al., 2003) and April 2006 (e.g., Pinto et al., 2007) did not affect GOC during summer as the excess loads of N (and other nutrients) arrived in the ODZ after the end of the growing season. In contrast, the Elbe flood in January 2011 (e.g., Kienzler et al., 2015; Mudersbach et al., 2016) resulted in both, high daily GOC rates in summer 2011 and a high German contribution to summer GOC of 19.9 %. However, the only short t_{strat} of 136 days (compared to 185 days in 2002) prohibited the evolution of O_2 deficiency. This underlines the great importance of seasonal stratification as a prerequisite for the evolution of O_2 deficiency in the North Sea ODZ.

For the Oyster Grounds – for which O_2 deficiency has been reported in recent years (Greenwood et al., 2010) – the analysis revealed that the average contribution of non-riverine sources to GOC during stratification is similar to that in the ODZ, yielding about 60 %, i.e., the riverine contributions results in about 40 %. However, the contribution by the individual sources is different to the ODZ. The contribution from the DE rivers can be neglected, while, the NL-1 and UK-2 rivers provide the major contributions to GOC, with a combined effect of about 27 % averaged over the period 2000–2014. During individual

years, the French rivers discharging into the English Channel also contribute up to 7 %. The atmospheric contribution results in about 13 % and the NA accounts for 41 %.

At the ODZ site and in the Oyster Grounds, the riverine contributions to GOC can reach about 50 % during individual years. This underlines the basic potential of river N reductions for improving the O_2 conditions in the ODZ and the southeastern North Sea. However, it also suggests that riverine N reductions, especially in the DE, NL-1 and UK-2 rivers are required to improve the O_2 conditions at the ODZ site and in the Oyster Grounds. This is confirmed by the results of the WFD-compliant N reduction scenario, which showed only minor improvements in the minimum O_2 concentrations (less than 4 % in most North Sea regions). In the vicinity of the ODZ strongest increases in minimum bottom O_2 occurred and reached values up to about 9 %, mainly due to the reductions in the DE rivers. In the Oyster Grounds, the strongest increase in minimum O_2 resulted in about 2 %, which can be attributed to the zero or only small reductions in the British and Dutch rivers, respectively, planned under WFD measures.

The comparison of the reduction and the reference runs also revealed very strong differences in the response of bottom O_2 and O_2-deficient periods to N reductions in adjacent model grid cells. This suggests that reductions in river loads can have very different impacts even inside small regions. This likely relates to particularities in the bathymetry affecting the currents and thus the influence of individual N sources. This demonstrates that the assessment and analysis of the O_2 conditions in the North Sea requires temporally and spatially consistent, high-resolution approaches which can only be provided by biogeochemical models, as such monitoring would be very costly.

In summary, the results suggest that, although GOC is dominated by non-riverine N sources in most North Sea regions, river N reductions constitute a means with principally high potential for improving the O_2 conditions in the North Sea. However, the results clearly show that significant improvements in the O_2 conditions in most parts of the southern North Sea can only be achieved by reductions in the large Dutch rivers and in the rivers along the British east cost.

In this context, it should further be mentioned that the basic definition of reduction targets should be reconsidered. First, a meaningful implementation of reduction percentages into biogeochemical models can only be done, when reference periods are defined, or if the reductions are calculated on the basis of actual target concentrations. Second, N reductions under the WFD are only defined as reductions in DIN according to the OSPAR approach on which this study is based. Only the German rivers constitute and exception as TN targets are defined for these rivers. The assumptions made for PON reductions in this study may not reflect the actual reductions in PON induced by the applied DIN reductions. With respect to the incorporation of reduction targets for organic matter,

Kemp et al. (2009) also highlighted the importance of organic nutrient reductions for the improvement of O_2 conditions in shallow coastal systems. In accordance with this, river N reduction targets should include information on both, DIN and PON.

Chapter 8

Concluding summary

This chapter provides a final summary of the presented work including the main conclusions drawn from this thesis. Furthermore, the research questions formulated at the beginning of this work (see Sect. 1.2, **Q1**–**Q6**) are addressed.

The present work investigates the North Sea O_2 dynamics in recent years (2000–2014) with a special focus on the physico-biochemical interactions driving the evolution of O_2 concentrations during seasonal stratification, and the influence of N sources on the O_2 dynamics. For this purpose, a model system consisting of the physical model HAMSOM (Backhaus, 1985; Pohlmann, 1991, 1996) and the biogeochemical model ECOHAM (Moll, 1998; Pätsch and Kühn, 2008; Kühn et al., 2010; Lorkowski et al., 2012; Große et al., 2016) was applied to the North Sea.

First, the validation of the simulated North Sea hydrography, with particular focus on summer T and S as well as seasonal stratification, showed that HAMSOM reproduces the main features of the annual cycle of SST and SSS (e.g., Otto et al., 1990; Elliott et al., 1991; Janssen et al., 1999). The qualitative and quantitative validation of summer T and S confirmed that HAMSOM also represents well the spatial patterns of summer North Sea hydrography. Some shortcomings were revealed with regard to summer S, that, however, were not relevant in the regions in the focus of this thesis. It was also shown that thermal stratification is slightly underestimated by the model in some North Sea regions, which slightly affects the O_2 dynamics due to an overestimation of vertical mixing.

Observed and simulated T and S showed that stratification in most North Sea regions is T-driven, which is in good agreement with earlier studies (e.g., Janssen et al., 1999; van Leeuwen et al., 2015). With the focus on the O_2 dynamics, a new stratification criterion using a critical $\Delta T_{\mathrm{crit}} = 0.05\,\mathrm{K}$ between sea surface and bottom was applied, in order to determine the stratification periods from simulated T. The maximum vertical T gradient was used for the identification of the MLD. Despite the remarkable difference to existing stratification criteria (e.g., Kara et al., 2000), the results are in very good agreement with recent work by van Leeuwen et al. (2015). It was furthermore shown that the stratification period and MLD resulting from the new criterion encompass very well the temporal evolution of vertical mixing, which is crucial for the analysis of the O_2 dynamics.

In the second step, a qualitative validation the near-surface biochemistry simulated by ECOHAM was conducted, based on nutrients (PO_4^{3-}, NO_3^-, NH_4^+ and SiO_4^-), Chl-a and O_2. The comparison of the simulated and observed annual cycles demonstrated that ECOHAM reproduces the relevant features of the annual cycles of the selected quantities in different North Sea regions. Minor shortcomings were found with respect to maximum Chl-a concentrations during the spring bloom, which are slightly underestimated by ECOHAM, and summer nutrient concentrations, which slightly overestimate the observations.

As the HAMSOM-ECOHAM model system showed reasonable skill in representing the North Sea ecosystem, the first major objective of this thesis was addressed – the analysis of the O_2 dynamics of the North Sea with respect to the physico-biochemical interactions controlling O_2 during stratification. The validation of simulated bottom O_2 concentrations, based on continuous time series measurements and spatially resolved late summer measurements, revealed that HAMSOM-ECOHAM reproduces well the basic spatial and seasonal patterns of bottom O_2. Though, it was also shown that the model slightly overestimates late summer bottom O_2 concentrations in regions of lowest observed O_2 concentrations.

The analysis of the standard deviation of the simulated bottom O_2 concentrations during the observation periods of summer surveys additionally illustrated that in most North Sea regions, O_2 measurements taken during late August/early September provide a synoptic image of the late summer O_2 conditions. However, in some regions stratification and thus the O_2 decline prevail longer than late August/early September, i.e., surveys carried out at this time of the year may not represent the minimum O_2 levels (see Sect. 5.2.1.2).

Research question Q1: The analysis of the spatial differences in the factors controlling the O_2 dynamics showed that sufficiently long continuous stratification ($t_{\mathrm{strat}} > 60$ days) constitutes the prerequisite for the evolution of low O_2 conditions. However, near-surface NPP and the size of V_{sub} are the key parameters influencing the bottom O_2 evolution. Consequently, the North Sea can be subdivided into three different zones in terms of O_2 dynamics: (1) a highly productive, non-stratified (due to tidal mixing) coastal zone, (2) a productive, seasonally stratified zone with a small V_{sub}, and (3) a productive, seasonally stratified zone with a large V_{sub}. The analysis revealed that the type-1 and type-3 zones are unlikely to be affected by low O_2 conditions due to either continuously ongoing ventilation (type 1) or the large V_{sub} buffering the effect of O_2 consumption (type 3). In contrast, type 2 is highly susceptible to low O_2 conditions, which results from the specific combination of high upper layer productivity and small V_{sub}. Type 1 is found mainly in the coastal southern North Sea, while large parts of the offshore regions of the southern and southern central North Sea can be classified as type 2. Type 3 dominates the northern central and northern North Sea.

These findings were combined in the development of the so-called oxygen deficiency

index (ODI), which showed that the regional characterisation of the North Sea, in terms of its O_2 conditions, can be addressed by using only three controlling parameters: water depth (as a proxy for the V_{sub}), t_{strat} and near-surface NPP. Consequently, the ODI is much simpler than the EUTRISK index by Druon et al. (2004) and could provide the basis for an operational use as the information on stratification can be derived from operational hydrodynamical models and information on NPP from satellite data (e.g., Longhurst et al., 1995; Behrenfeld and Falkowski, 1997). This could be worthwhile for the improvement and optimisation of O_2 monitoring in the North Sea. However, further in-depth analyses of the applicability of the ODI are required.

Research question Q2: The model simulations showed that lowest bottom O_2 concentrations generally occur in the eastern central North Sea at about 55.5 °N–56.5 °N, 6 °E–7 °E, due to sufficiently long stratification, high NPP and a thin V_{sub}. Overall lowest O_2 concentrations of about 5.2 mg O_2 L^{-1} occurred in 2002. The O_2 mass balances at the ODZ site showed that REM_{pel} constitutes the largest O_2-consuming process within V_{sub}, with a contribution of about 50 % to GOC. In contrast, REM_{sed} constitutes the major O_2 sink near the seafloor and accounts for about half of the near-bottom GOC in the ODZ, averaged over the entire period 2000–2014. REM_{pel} contributes about 35 % during 2000–2014. Thus, REM_{pel} and REM_{sed} account for roughly 85 % of GOC in the bottom layer of the North Sea ODZ, while RES_{zoo} and NIT are less important. The mass balances further suggest that the relative contributions of the different O_2-consuming processes in the bottom layer at a certain location depend on the water column depth, independent of the overall GOC.

The analysis also showed that advection is usually of only minor importance for the bottom O_2 dynamics in most North Sea regions. This also applies to the region north of Dogger Bank which contradicts the interpretation of O_2 observations in that area by Queste et al. (2013). In addition, the mass balances show that events of strong mixing during summer can cause the complete replenishment of bottom O_2 to its saturation concentration. However, the enhanced nutrient supply triggers NPP, eventually increasing the GOC, which balances or even exceeds the physical O_2 supply. Thus, enhanced vertical mixing during seasonal stratification can cause the degradation of O_2 conditions in the North Sea, finally leading to O_2 deficiency.

Research question Q3: Year-to-year variability in bottom layer O_2 dynamics in the ODZ is controlled by variations in the near-surface NPP. Increased NPP directly enhances the EXP_{org} into the deeper layers. Furthermore, it enhances zooplankton growth which causes an additional increase in organic matter production and export. In addition, RES_{zoo} increases. The overall increase in EXP_{org} results in stronger bacterial remineralisation which in turn triggers NIT due to the stronger release of NH_4^+.

In order to address the second major objective of this thesis – the quantification of the influence of riverine and non-riverine external sources of N on the O_2 dynamics of the North Sea – the numerical method of so-called 'trans-boundary nutrient transports' (TBNT Ménesguen et al., 2006) was applied to the N cycle implemented to ECOHAM. This method allows for the tracing of nutrients from individual sources (e.g., rivers) throughout the entire biochemical cycle and the entire ecosystem. By this, it meets the requirements of the 'integrated target-oriented and source-oriented approach' intended by OSPAR (1999).

In a first step, a TBNT post-processing software was designed and applied to N from various sources. The implementation of the TBNT method as a post-processing software provides the additional potential for applying the software to other biogeochemical models, not restricted to marine models only. For instance, it could also be applied to limnic ecosystem models or atmospheric models. However, this would require additional minor adaptations which could not be finished during this thesis.

The new software utilises the daily, 3D output of the model state variables and process rates calculated by ECOHAM and enables the simultaneous tracing of nutrient inputs from multiple sources. In order to keep the computational costs and time effort on a reasonable level, the rivers entering the North Sea domain were sorted into 8 different groups according to OSPAR (ICG-EMO, 2009; OSPAR, 2010; Los et al., 2014). Four additional groups were defined for tracing the inputs from adjacent seas (North Atlantic, English Channel, Baltic Sea) and atmospheric N deposition.

The spatial distributions of TN and NPP related to individual sources based on the reference run showed good agreement with existing studies. The northern North Sea and most central regions are dominated by the North Atlantic inflow. In contrast, the large Dutch (Rhine and Meuse) and German (Elbe, Ems, Weser), but also the British rivers at the British east coast have a strong impact on the southern and partly on the southern central North Sea. Here, atmospheric N deposition constitutes an additional relevant source.

The daily time series of NPP and (benthic and pelagic) organic matter at the ODZ site showed that the North Atlantic also dominates this region. However, the integrated riverine contribution to NPP and organic matter can be of similar importance during individual years. The time series also confirmed that near-surface NPP is the major controlling factor for the amount of organic matter in the bottom layer of the ODZ. This supports the use of NPP as a proxy for organic matter within the ODI. They further suggested that the preconditioning of the N pool before the spring bloom is strongly affected by the North Atlantic inflow.

In a second step, the TBNT method was expanded by a direct link of nutrient input to the biochemical processes affecting O_2. This expansion of TBNT – to my knowledge –

constitutes the first approach to directly link the O_2 dynamics of a marine ecosystem to the input of nutrients (here, N) in a quantitative way, that does not depend on different model scenarios (e.g., Lenhart et al., 2010; Troost et al., 2013; Laurent and Fennel, 2014) or statistical analyses (e.g., Pokryfki and Randall, 1987; Brockmann et al., 1988; Malone, 1991; Justić et al., 1993, 1997; Dauer et al., 2000; Hagy et al., 2004; Turner et al., 2008; Topcu and Brockmann, 2015).

The TBNT analysis on O_2 was first conducted for the ECOHAM simulation on which the previously described results are based ('reference run'). The spatial distributions of the individual source contributions to bottom layer GOC showed basically the same patterns as TN and NPP. The daily time series of bottom layer GOC in the ODZ confirmed the strong link between organic matter availability and O_2 consumption, providing additional confidence in the basic concept of the ODI.

Research question Q4: The analysis of annual bottom layer GOC during stratification in the ODZ showed that, averaged over 2000–2014, about 60 % can be attributed to non-riverine sources (i.e., adjacent seas and atmosphere). Consequently, only about 40 % are linked to riverine N input. Among the non-riverine sources, the North Atlantic input across the northern shelf edge could be identified as the most relevant influencing factor accounting for about 42 % of daily GOC. However, this contribution is probably slightly overestimated. The atmosphere constitutes the second strongest non-riverine source, contributing almost 17 %. The German rivers (Elbe, Ems, Weser) account for about 11 %, representing the strongest riverine contribution. However, the large Dutch rivers (Rhine and Meuse) also account for about 10 % and even the rivers along the British east coast (including, e.g., the Humber) contribute to almost 7 %. During individual years, the Dutch and German rivers can contribute up to 15 % and 20 %, respectively. Thus, these five sources of N dominate the evolution of O_2 deficiency in that region most susceptible to low O_2 conditions.

The ODZ analysis also revealed that years of particularly high GOC rates correspond to years with a strong influence of either the German (e.g., 2011) or the Dutch rivers (e.g., 2002). Though, it also underlined the importance of sufficiently long stratification as a basic requirement for the evolution of O_2 deficiency, as high GOC rates did not necessarily lead to O_2 deficiency in case of only short-lasting stratification (e.g., in 2011). It was further shown that the timing of events of increased riverine N discharge, e.g., as a result of river floods, is crucial for their impact on the O_2 dynamics. For instance, the Elbe flood in August 2002 (Ulbrich et al., 2003) did not affect summer GOC in the ODZ in 2002, but in 2003 as the N loads arrived in the ODZ during the spring bloom period. The same applies to the Elbe floods in August 2010 and January 2011 (Kienzler et al., 2015; Mudersbach et al., 2016), which affected the GOC in the ODZ during the growing

season 2011 and resulted in the highest German contribution to GOC (19.9 %) of the entire period of analysis.

The large contribution of the North Atlantic suggests that its input of N (and probably also other nutrients) is essential for the preconditioning of the North Sea ODZ with respect to the amount of DIN available for primary production during spring–autumn. This implies that the likeliness of the evolution of O_2 deficiency is strongly increased during years of high N loads originating from the North Atlantic. In this context, it would be helpful to further investigate the time span needed for N (and other nutrients), that enter the North Sea across the northern shelf edge, to reach the ODZ. This would provide valuable information on the influence of the general circulation of the North Sea, also in relation to large-scale phenomena, like the North Atlantic oscillation (e.g., Winther and Johannessen, 2006), on the O_2 dynamics of the North Sea. This subject could be addressed with the implementation of the so-called 'age' (Ménesguen and Hoch, 1997; Delhez et al., 1999) into the here presented TBNT software as done for the Baltic Sea by Radtke et al. (2012). With respect to the Oyster Grounds, a region well known for its susceptibility to O_2 deficiency (de Wilde et al., 1984; Peeters et al., 1995; Weston et al., 2008; Greenwood et al., 2010), the analysis of the reference run showed that this region is also dominated by the North Atlantic inflow (about 41 %). However, about 13 % can be attributed to atmospheric deposition. In addition, the individual riverine contributions to GOC add up to about 40 % on average, with contributions of the Dutch (Rhine and Meuse) and British (east coast) rivers of about 14 % and 13 %, respectively. Thus, these rivers strongly affect the O_2 dynamics of the Oyster Grounds region.

Research question Q5: In the reference run, the relative contributions of the riverine sources to GOC in the North Sea ODZ add up to roughly 40 %. This indicates that the potential of riverine N reductions for improving the O_2 conditions in the ODZ is limited. However, it also suggests that a substantial reduction in the main contributing riverine sources (German, Dutch and British rivers) will likely result in a clear improvement in the O_2 conditions of the ODZ.

In order to evaluate this insight, a second model scenario was conducted, applying WFD-compliant (EU, 2000) riverine N reductions (Gade, 2016; OSPAR, 2016). In addition, this scenario provided on the effects of N reductions on North Sea O_2 as most nutrient reduction do not consider O_2 levels, but focus only on the concentrations of nutrients (N and P) and Chl-a (e.g., Lenhart, 2001; Skogen et al., 2004; Lenhart et al., 2010). The reduction scenario supports that riverine N can have a remarkable, positive impact on the North Sea O_2 conditions, although it resulted in only small increases in the minimum O_2 concentrations of at most $0.3\,\mathrm{mg\,O_2\,L^{-1}}$ in 2002 (5.5 % change). However, this represents a surprisingly strong response, keeping in mind that reductions in the Dutch rivers were

very small (5 % in DIN and PON) and British reductions were even zero. Among the main riverine sources, only to the German rivers strong reductions were applied (29 %–50 % in DIN, 9 %–37 % in PON). Taking into account that the German rivers added up to only about 10 % of overall GOC in the ODZ in 2002, this constitutes a remarkable improvement. This suggests that additional reductions in the Dutch and British rivers could significantly improve the O_2 conditions in the ODZ. Assuming additional reductions in the predominantly anthropogenically controlled atmospheric N deposition (e.g., Paerl, 1997; Schöpp et al., 2003), as adopted within the so-called Gothenburg Protocol (UNESC, 1999), a further improvement can be expected.

The relative contributions to GOC in the Oyster Grounds suggest that carefully defined riverine N reduction targets can also have a substantial, positive effect. However, here reductions in the Dutch and British rivers are likely to have the strongest influence. This is supported by the analysis of the WFD-compliant reduction scenario, which showed only a minor increase in minimum O_2 concentration of at most $0.13\,\mathrm{mg\,O_2\,L^{-1}}$ (4.2 % increase). Due to the large contributions of the Dutch and British rivers, the only small or zero reductions in the rivers have limited influence on the O_2 conditions in the Oyster Grounds. Consequently, the achieved reductions can mainly be attributed to the strong reductions in the French (50 % for DIN and PON) and in the Belgian river Scheldt (37 % for DIN and PON), although these are of only minor importance (3.8±1.5 % and 1.5±0.4 %, respectively, averaged over 2000–2014). As for the ODZ, it can be expected that future reductions in atmospheric N deposition will have a positive effect on the O_2 conditions.

The results of the TBNT analysis of O_2 in combination with the results of the eduction run suggest that reductions in riverine N inputs constitute a reasonable and promising approach for improving the O_2 conditions of the North Sea. However, currently defined reduction targets, especially, for the Dutch and British rivers may require re-consideration due to the strong influence of these rivers on the southern and southern central North Sea.

In this context it should further be mentioned, that the here presented methodology (and software) should also be applied to P in order to evaluate the influence of the different P sources on the North Sea. Especially, since there is a discussion going on for decades whether N (e.g., Ryther and Dunstan, 1971; Howarth and Marino, 2006) or P (e.g., Smith, 1984; Tyrrell, 1999) reductions should be in the focus of eutrophication management of coastal marine ecosystems. More recent studies suggest that reductions in both, N and P, are required for a successful management (Conley et al., 2009; Paerl, 2009). For the North Sea, Peeters and Peperzak (1990) suggested that the Dutch coastal waters are likely P limited while the offshore parts of the southern North Sea are dominated by N limitation. This is also in agreement with the findings by Skogen et al. (2004), Lenhart et al. (2010) and Emeis et al. (2015). Thus, considering low O_2 conditions as the ultimate ecosystem

perturbation related to eutrophication, a quantitative assessment of the influence of P under current environmental conditions is required.

Research question Q6: With respect to potential future changes in the North Sea O_2 conditions, this study added valuable new pieces to the overall image. However, this image is still not complete, as future changes in the environmental conditions are partly uncertain. Díaz and Rosenberg (2008) argue that future changes in O_2 conditions will strongly depend on the effects of climate change on stratification and riverine nutrient supply. This is clearly supported by the results of this thesis. It put emphasis on the role of seasonal stratification as a prerequisite for the evolution of O_2 deficiency, however, it also showed that events of high riverine N loads (and other nutrients) have a strong impact on the O_2 conditions of large parts of southern North Sea during individual years.

However, while most studies predict an increase in North Sea T (Lowe et al., 2009; Meire et al., 2013; Mathis and Pohlmann, 2014; Wakelin et al., 2015), the implications for stratification vary between different studies. Most of these studies project an intensification of thermal stratification (Lowe et al., 2009; Meire et al., 2013; Wakelin et al., 2015), though, Mathis and Pohlmann (2014) predict a decrease in stratification intensity. However, the estimation of the implications of both potential scenarios on O_2 remains difficult. On the one hand, continuous stratification enables the evolution of O_2 deficiency. On the other hand, this study showed that even enhanced mixing can negatively impact the O_2 conditions due to enhanced nutrient supply to the surface layers and thus higher NPP. For the same reason, surface NPP could increase as a result of increasing storm frequency and wind-induced mixing (Rabalais et al., 2010) as prognosticated for the North Sea (e.g., Ulbrich and Christoph, 1999; Beniston et al., 2007). The predicted increase in T would furthermore lower O_2 solubility (Benson and Krause, 1984; Weston et al., 2008) and increase metabolic rates (van der Molen et al., 2013). This would imply a reduced initial O_2 inventory and accelerated NPP, respectively. The former would generally increase the potential for O_2 deficiency, while the latter would result in higher amounts of organic matter being exported below the thermocline. Both in combination would result in a reduction of the time needed for reaching O_2-deficient conditions. Thus, O_2 deficiency may evolve even during shorter periods of stratification.

All this suggests that eventually the amount of locally available inorganic nutrients will be the crucial factor for the evolution of O_2 deficiency during seasonal stratification. This study demonstrated that the North Atlantic inflow, atmospheric deposition and the riverine inputs from the German, Dutch (Rhine and Meuse) and British (east coast) rivers dominate the nutrient availability and the O_2 dynamics in wide parts of the southern North Sea. Thus, the future changes in these nutrient sources will be vital for the O_2 conditions of the North Sea. While atmospheric deposition is anthropogenically controlled (Paerl, 1997;

Schöpp et al., 2003), the North Atlantic inflow constitutes a natural source of nutrient for the North Sea. Ulbrich and Christoph (1999) projected a slight increase in the NAO. This could cause an increase in the North Atlantic inflow into the North Sea as it is partly controlled by the NAO (Winther and Johannessen, 2006). However, Gröger et al. (2013) predict a reduction in the nutrient supply from the North Atlantic, resulting in a North Sea wide reduction of NPP by about 30 % until the end of the 21st century. This could substantially improve the O_2 conditions in large parts of the southern and central North Sea.

The riverine nutrient inputs to the North Sea are human-manageable, as shown in the past (Artioli et al., 2008; OSPAR, 2013a). However, they are also affected by natural hazards such as floods, e.g., in consequence of events of heavy rainfall (e.g. Ulbrich et al., 2003). This thesis showed, that such flood events can have remarkable impact on GOC during the seasonal stratification. While some future climate projections indicate a decrease in annual river discharges (e.g., Arnell, 1999) or a decrease in the frequency of flood over Europe (e.g., Lehner et al., 2006), others suggest an increase in such extreme events over central (Beniston et al., 2007) as well as northern and eastern Europe (Frei et al., 2006), especially during winter. The former two potential changes would imply principally lower riverine nutrient inputs, i.e., a potential improvement of the O_2 conditions. However, the latter suggest temporary, strong increases in nutrient loads from the continental rivers (particularly the Elbe which rises in eastern Europe) and would negatively affect the O_2 conditions in the North Sea ODZ during individual years.

In this context, Wakelin et al. (2015) explicitly analysed the relative importance of climate change induced impacts on the North Sea ecosystem compared to impacts induced by changes in anthropogenic pressures (i.e., riverine and atmospheric nutrient inputs). They found that, especially in the eastern central North Sea (including the ODZ site), NPP may increase or decrease in the near future (2030–2040) due to climate change effects, depending on the nutrient abatement policies in the future. They concluded that reduced anthropogenic nutrient inputs are likely to mitigate the effects of climate change, especially in the southern and eastern central North Sea. This is in good agreement with the results of this thesis, clearly showing that riverine N inputs have a strong influence on this North Sea region highly susceptible to O_2 deficiency.

The high susceptibility of this region to O_2 deficiency shown in this thesis puts additional emphasis on the consideration of carefully defined (riverine and atmospheric) nutrient reduction measures (Los et al., 2014) for mitigating the potential aggravation of the North Sea O_2 conditions. Therefore, it is highly recommended following the precautionary principle with respect to future nutrient reductions: Prevention is better than cure.

Appendix A

North Sea hydrography

A.1 Error analysis of the equation of state used in HAMSOM

Very shortly before the submission of this thesis a bug was found in the application of the equation of state in HAMSOM, used for the calculation of density as a function of S, T and pressure. More precisely, the equation of state after Jackett and McDougall (1995), that is formulated for potential temperature (θ), was applied on *in situ* T. Technically, this bug affects the entire results presented in this study. Unfortunately, due to the limited time left, it was not possible to repeat the entire analysis. However, it is definitely necessary to provide some insight in the impact of this bug on the simulated North Sea physics as they play an important role in both, the evolution of O_2 concentrations and the dispersal of tracer quantities such as T or O_2. For this purpose, a sensitivity run for the year 2000 was conducted with HAMSOM, that applied the equation of state by Fofonoff and Millard (1983) using T. The sensitivity run was initialised with the spatial distributions of T and S for 1st January calculated by the reference simulation, i.e., that used for this thesis. The calculation time step of the sensitivity run was identical to that of the reference run ($\Delta t = 10\,\mathrm{min}$).

As the differences in density resulting from the bug in the application of the equation of state only directly affect the vertical mixing (see Eq. (3.1)), Fig. A.1a shows a scatter plot of the vertical diffusion coefficients (A_v) calculated by the sensitivity run (y axis) against A_v calculated by the reference run (x axis) for the year 2000. As this thesis focusses on the North Sea, more specifically on the shallower regions, only the values in regions with a maximum bottom depth of 200 m inside the TBNT domain (see Fig. 6.3) are considered. In addition, It should be noted that the analysis of one year can be assumed to be sufficient, as winter mixing results in a complete overturning, i.e., homogenisation, of the water column in the North Sea region. The plotted data represent the matching pairs of the daily HAMSOM output of the two simulations and encompass the entire year 2000 and each grid location, to which the previously mentioned criteria apply. For a more detailed analysis, the simulated A_v values are colour-coded according to their location

within the water column.

Figure A.1a shows that in general the simulated A_v are close to one-to-one agreement (black diagonal line) between the reference run and the sensitivity run. This is especially true for the values in water depths of 50 m and more (green, brown and yellow markers). In these depths, the difference between the two simulations is less than 0.00125 $m^2 s^{-1}$ (i.e., half of the distance between two minor ticks, which equals 0.0025 $m^2 s^{-1}$) corresponding to relative differences of clearly less than 5 % in the vast majority of data pairs.

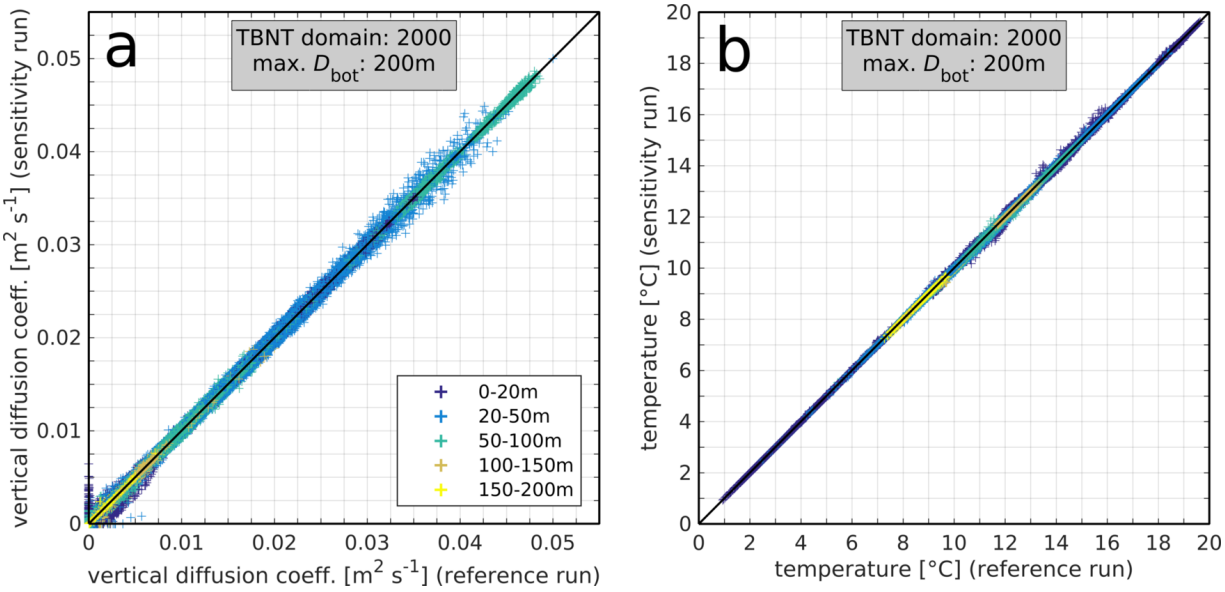

Figure A.1: Scatter plots of a) vertical diffusion coefficient (A_v) and b) *in situ* temperature (T) in 2000 in regions with a maximum bottom depth of 200 m inside the TBNT domain (see Fig. 6.3) calculated by the HAMSOM reference run (x axis) and sensitivity run (y axis). The values are grouped according to their location within the water column (see different colours). Same legend for both panels.

For A_v in the upper layers down to 50 m (dark blue and blue) the image is slightly different. While most A_v values in this depth range show similarly low deviations between the two simulations as A_v below 50 m, some stronger deviations can be found at very low A_v values (<0.005 $m^2 s^{-1}$) in depths of less than 20 m (dark blue), and for A_v values between 0.03 $m^2 s^{-1}$–0.045 $m^2 s^{-1}$ in depths between 20 and 50 unitm (blue). In the former case, the sensitivity run tends to yield slightly lower A_v values between 0.00125 $m^2 s^{-1}$ and 0.01 $m^2 s^{-1}$, while it yields higher values in cases of A_v <0.00125 $m^2 s^{-1}$ in the reference run. This suggests that the vertical mixing in the upper 20 m, i.e., inside the surface mixed layer is different between the two simulations as a result of the different equations of state In the latter case, both simulations show partly higher and partly lower A_v values. This

suggests that during periods of relatively strong vertical mixing, the mixing in intermediate depths shows some variations between the two simulations. However, the corresponding relative differences between the reference and sensitivity run are still less than 10 % in all of these cases.

Despite these differences, the comparison of A_v of the reference run and the sensitivity run indicates clearly that the implications on tracer quantities such as T or O_2, because of two major aspects. First, the overall agreement between A_v of the two simulations is very good. Second, stronger differences in A_v between the two simulation occur during periods and regions, which are less relevant for the analysis of the O_2 dynamics: 1) during periods of weakest mixing within the summer surface mixed layer (see, e.g., Sect. 4.3.3, Fig. 4.10c and e), and 2) in intermediate depths during periods of strong mixing, i.e., in autumn/winter or during events of strong mixing during seasonal stratification (see, e.g., Sect. 4.3.3, Fig. 4.10a and e).

In fact, the latter aspect may slightly influence the O_2 dynamics as simulated by ECOHAM in cases of events of strong vertical mixing during seasonal stratification. However, the analysis of the O_2 dynamics in the North Sea ODZ (see Sect. 5.2.5.1, Fig. 5.12) shows that events of strong mixing cause a remarkable increase in bottom O_2, but also enhance near-surface NPP (due to nutrient supply from deeper layers) and bottom O_2 consumption due to increases in organic matter biomass in the deeper layers). As A_v is uniformly applied to all tracer quantities (T, O_2, nutrients etc.) – having in mind the influence of the vertical gradients of these quantities – it can be concluded the O_2-controlling, physico-biochemical interactions discussed in this thesis remain qualitatively the same. Thus, the conclusions drawn with respect to the O_2 dynamics of the North Sea do not change.

In order to demonstrate that the impact of the differences in A_v on tracer quantities is very small and that also quantitatively only very minor changes in these quantities have to be expected, Fig. A.1b shows the comparison of simulated T between the reference and sensitivity run, analogous to the comparison of A_v. It is clearly shown that the general agreement between the two simulations is very good as the vast majority of value pairs is on or close to the one-to-one line. Only very few deviations of maximal 0.55 °C occur at T values between 13.5 °C and 16.5 °C in the upper 20 m. The maximum relative difference between the two simulations results in 4.7 % (corresponding to an absolute difference of 0.5 °C. However, most deviations are less than 2 % which illustrates the only small influence on the absolute values of tracer quantities such as T. It further has to be noted, that NPP constitutes a T-dependent process in ECOHAM (see Eq. (3.6)), though, even the maximum differences in T between the two simulations result in maximum changes in NPP rates of 2 %. As the difference is much less in most cases, it can be concluded that the impact on the phytoplankton dynamics is also negligible.

As different formulations of the equation of state also influence the horizontal density distribution, the simulated current fields can also change due to changes in the geostrophic balance. As the volume transports play a key role in the dispersal of tracer quantities within the model domain and, thus, strongly affect the results of the TBNT analysis, a comparison of the monthly averaged net volume transports across the sections used in Sect. 6.3.2 (see Fig. 6.3) of the reference run and the sensitivity run was conducted for the year 2000. The results of this comparison are not shown as the differences between the two simulations are very small in most cases. The maximum absolute difference of 0.018 Sv results for the section #3 at the northern end of the Norwegian Trench and corresponds to a relative difference of only 1.2 %. The relative differences are very small (<1 %) in most cases and yield an average over all sections and months of 0.9±2.6 %. The comparably large standard deviation results from very few higher relative differences of maximal 28.1 % for the Skagerrak section #5. However, all these higher relative differences correspond to very small absolute differences of clearly less than 0.01 Sv. Thus, it can be concluded that the impact of the bug in the application of the equation of state in HAMSOM on the volume transports is negligible.

Considering the generally small differences between the HAMSOM simulations presented in this sensitivity study, and keeping in mind the general uncertainties in numerical models, it can be concluded that the findings of this thesis are not affected by the incorrect application of the equation of state. Despite this good news with respect to this thesis, the model developers should consider a revision of the equation of state in HAMSOM, as McDougall et al. (2003) already argued that the UNESCO equation of state (Fofonoff and Millard, 1983) is no longer the most accurate.

A.2 Standard deviations of the monthly climatologies of simulated sea surface temperature and salinity

Figure A.2 shows the standard deviation (STD) of the 17-year monthly climatology of SST in the North Sea region corresponding to the monthly climatology of SST presented in Fig. 4.1. During most months highest variations of up to 2.1 °C occur in the Danish straits and in the Kattegat/Skagerrak region, the areas strongly influenced by the Baltic inflow. In the shallow areas of the continental North Sea coast, STDs also reach values of up to about 1.8 °C in the German Bight. In this shallow region highest STDs occur in April and October (Fig. 4.1d and j, respectively) and are likely controlled by year-to-year variability of air temperature as in the water body remains well-mixed throughout the entire year due to water depths of less than 15 to 20 m and the relatively coarse vertical

resolution resulting in only 2 to 3 vertical layers.

From late spring to summer (May to August; Fig. 4.1e–h) the eastern central North Sea shows highest STDs within the North Sea (up to 1.4 °C, which may also relate to year-to-year variations in solar radiation and air temperature as this period basically represents the period of seasonal stratification in this area. At the northern edge of this area the Baltic inflow may also cause part of these variations. Along the east coast of the British Isles STDs are generally lower as in the previously discussed regions. This relates to the greater depths and weaker seasonal stratification, which dampens the effect of surface heating on the SST. Lowest STDs in the entire region can be seen at the northwestern edge of the North Sea which is strongly influenced by the Atlantic inflow characterised by only minor year-to-year variations in SST.

The STD of the 17-year monthly climatologic SSS is presented in Fig. A.3. In contrast to SST, spatial patterns are similar throughout the entire annual cycle showing only small variations of below 0.25 in most parts of the North Sea. Slightly higher STDs of above 0.5 and up to 1.6 only occur near the mouths of the major tributaries along the continental coast (e.g., Rhine/Meuse and Elbe) and in the Moray Firth at the east coast of Scotland. Remarkable variations of up to 4 only occur in the Danish straits, Kattegat and Skagerrak which are strongly affected by the inflow of less saline water from the Baltic Sea. Thus, the high STD in these regions can most likely be attributed to variations in the volume transport of this less saline water from the Baltic Sea.

This is supported by the fact that highest variations occur in autumn and winter when precipitation (rainfall/snowfall) is higher than during summer causing direct and indirect (by rivers) freshwater discharge into the Baltic Sea. This results in higher inflow into the North Sea having a stronger effect on the SSS in this region. From the Skagerrak, this tongue of increased STD – although it stays well below 1.5 – extends west until about 4.5 °E spreading into the western central North Sea. West of 4.5 °E and south of 55 °N STD stays below 0.25 in the offshore regions.

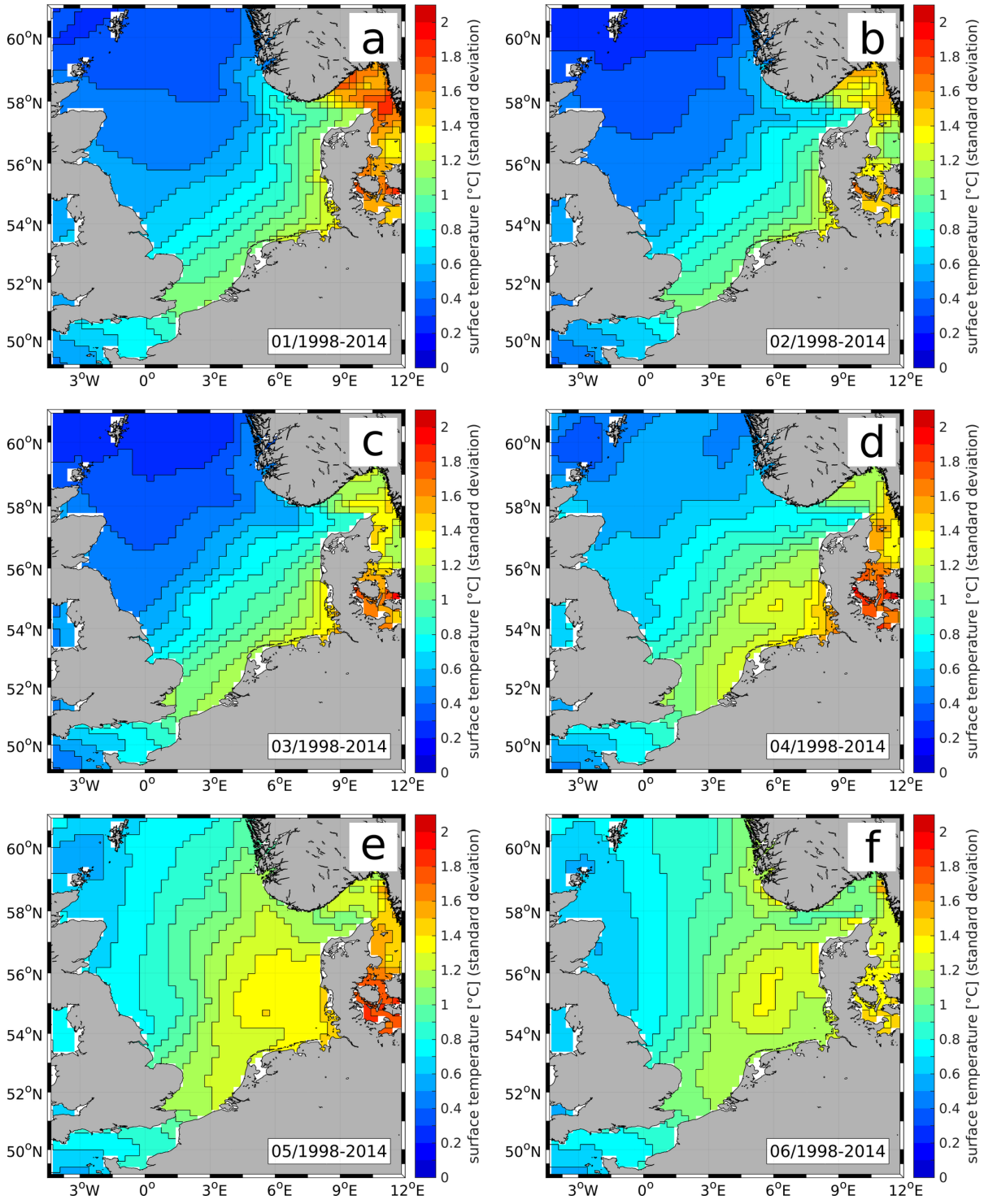

Figure A.2: Standard deviation of monthly climatology of simulated sea surface temperature over the 17-year period 1998–2014 (see average values in Fig. 4.1). Months are indicated by numbers in bottom-right corner of each panel: (a) January to (f) June.

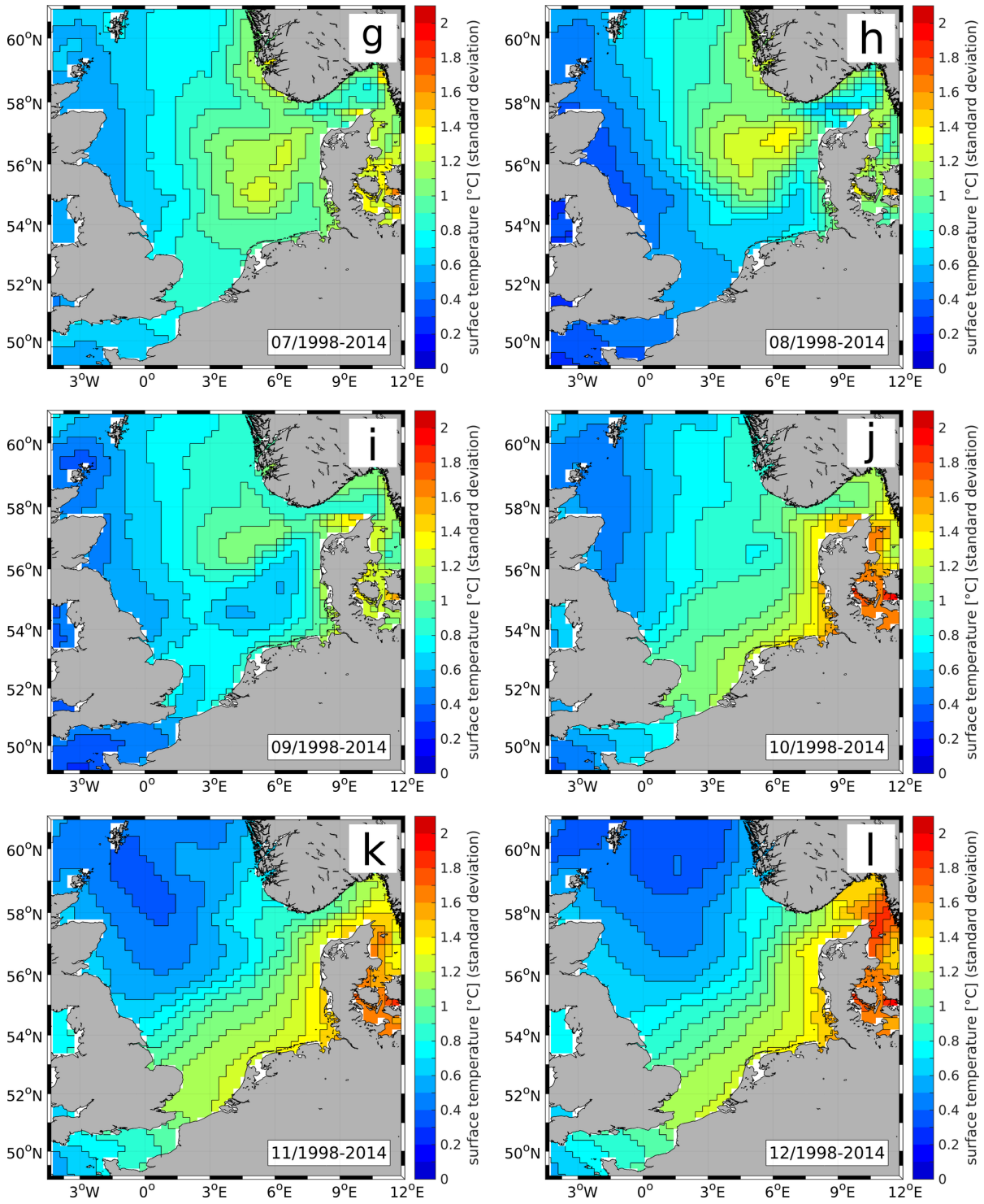

Continued: (g) July to (l) December.

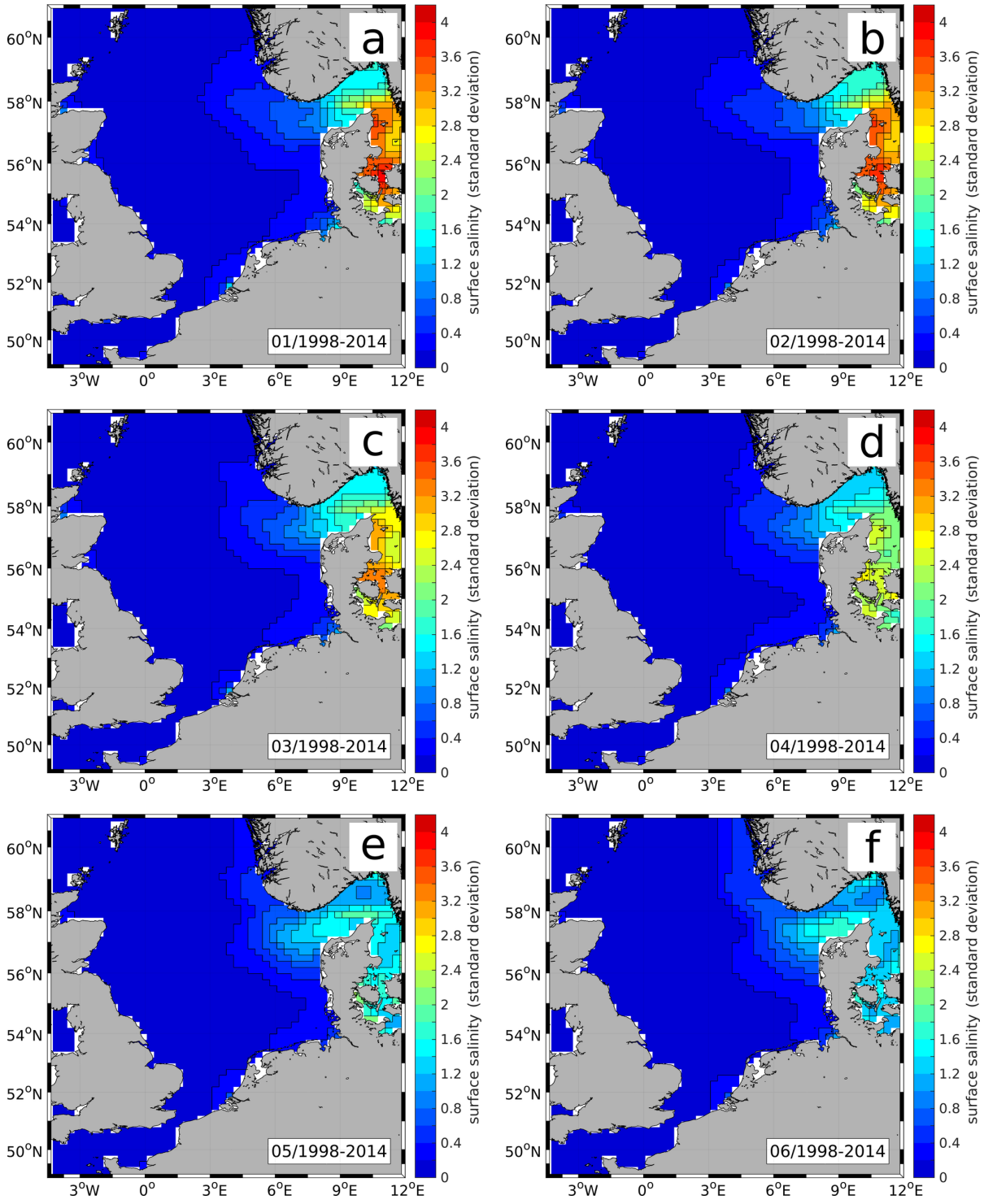

Figure A.3: Standard deviation of monthly climatology of simulated sea surface salinity over the 17-year period 1998–2014 (see average values in Fig. 4.2). Months are indicated by numbers in bottom-right corner of each panel: (a) January to (f) June.

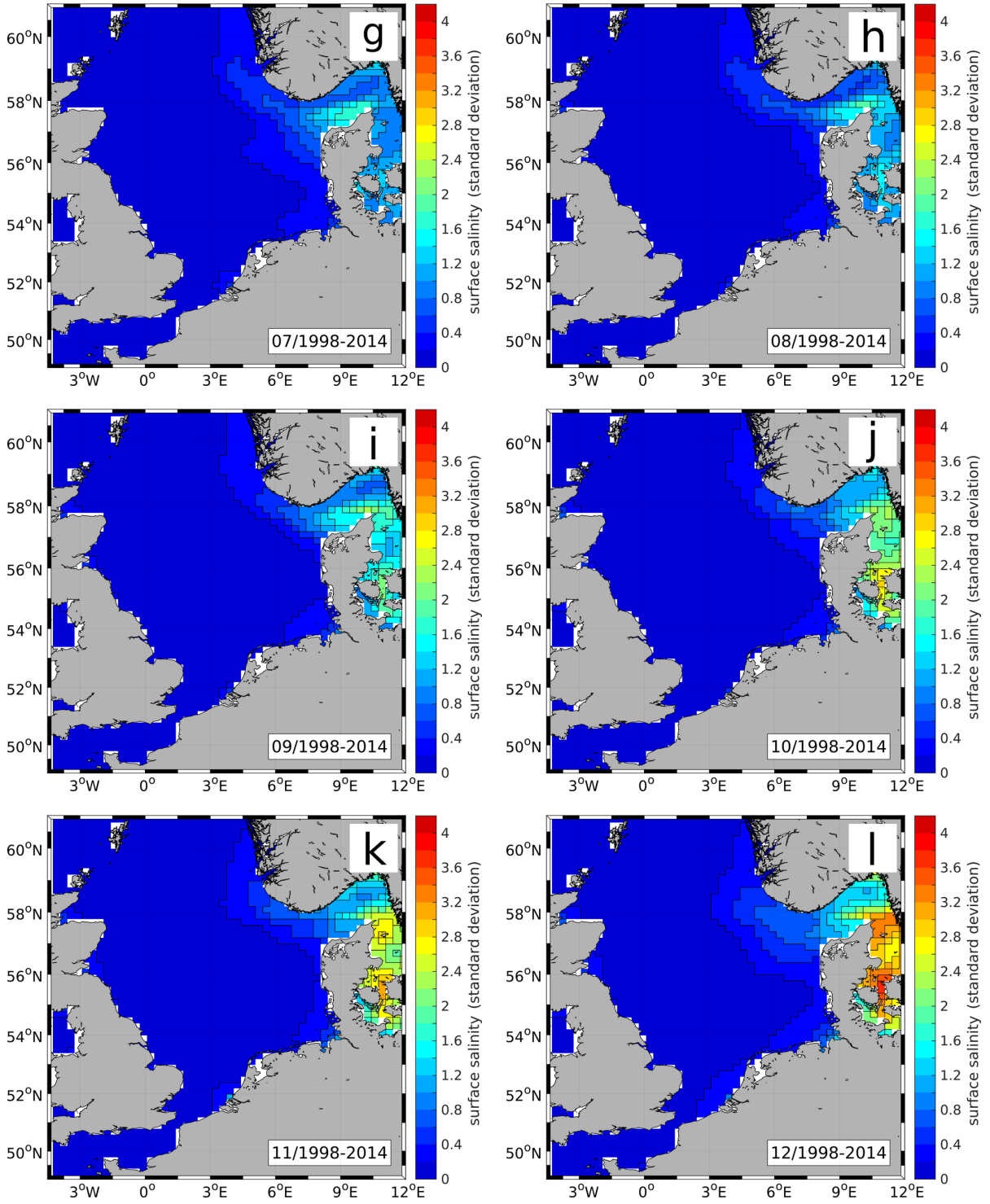

Continued: (g) July to (l) December.

Appendix B

Sensitivity of trans-boundary nutrient transports to the output time step

The TBNT analysis conducted during this thesis is based on ECOHAM results written with an output time step of $\Delta t = 1$ day (hereafter 'TBNT reference run'). This implies that linearity of the different processes is assumed over the duration of one day. In fact, the processes simulated by ECOHAM are only linear over the duration of an ECOHAM calculation time step, which is 30 minutes (not considering dynamic time step subdivision). Thus, it is important to investigate the effect of a time step remarkably smaller than one day on the TBNT results.

For this purpose, an ECOHAM simulation with an output time step of $\Delta t = 2\,\mathrm{h}$ was conducted for the year 2000. The output time step of 2 h was chosen for the sake of data manageability. The simulation was initialised with the same data as the ECOHAM reference run (i.e., the spatial distribution of all state variables on 1 January 2000, 12:00 a.m.). The simulated state variable concentrations at the end of each day are are not affected by the output time step. The same applies to the daily cumulated process values. The only difference occurs in the intra-daily evolution of the processes, which is only linear over the time step of 2 h in this simulation.

For the TBNT calculation of year 2000 based on this 2-hourly ECOHAM output (hereafter 'TBNT sensitivity run') the same initial spatial distribution of the relative contributions of the individual sources is used as for the previously described TBNT analysis. This implies that the initial states of both, the TBNT reference and sensitivity runs, are identical. The TBNT sensitivity run is than calculated based on the 2-hourly ECOHAM results and the relative contributions of the individual state variables to the bulk variables are stored on a daily basis. By this, results comparable to those of the TBNT reference run are obtained.

In order to provide a comparable measure for the influence of $\Delta t = 2\,\mathrm{h}$ compared to $\Delta t = 1\,\mathrm{d}$ on the TBNT results, first, the mass of each labelled state variable is calculated by multiplying its relative contribution with the mass of the corresponding bulk state variable. This is done for each day and each grid cell inside the TBNT domain (see Fig. 6.3). Second, the mass of each labelled state variable of each water column is vertically integrated over

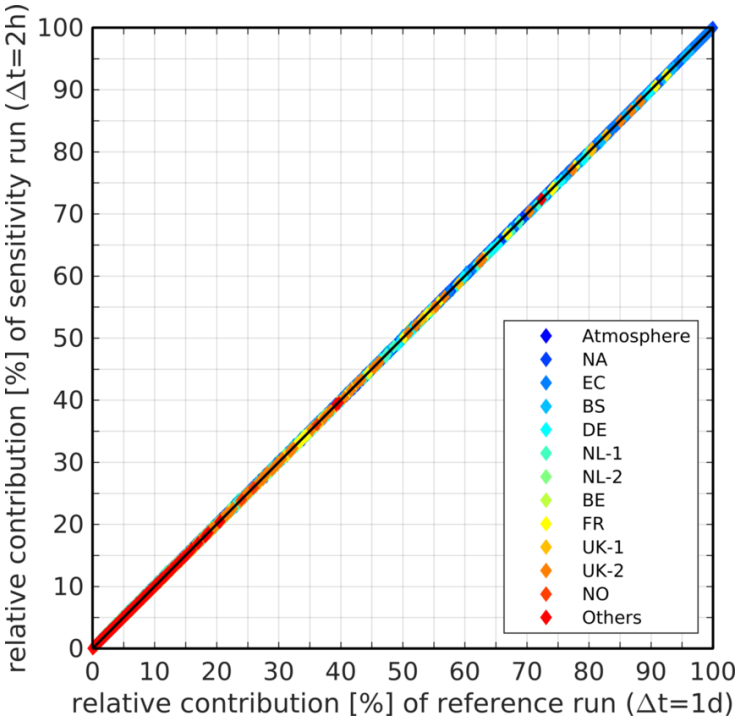

Figure B.1: Scatter plots of TBNT reference vs. sensitivity run. Each marker represents the relative contribution of an individual labelled state variable to the corresponding vertically integrated, cumulated bulk state variable of an individual water column inside the TBNT domain (see Fig. 6.3). Colours indicate the source of the labelled state variables (see Table 6.1). Black line marks one-to-one agreement between TBNT reference and sensitivity runs.

the entire depth range. Third, this mass is cumulated over the entire year 2000. This is done for the TBNT reference and sensitivity run. Finally, these cumulated values are divided by the corresponding bulk state variable mass calculated accordingly. By this, the annual average relative contribution of each labelled state variable to the bulk state variable within each individual water column of the TBNT domain is obtained for both TBNT scenarios.

Although the final values are expected to be most affected by a potential drift in the relative fractions due to the different time step, the comparison of the final values only would not provide a representative image as relative contributions at individual time steps (at any point of the year) may show higher differences. Furthermore, the overall influence of the different sources is more important than minor day-to-day fluctuations. Therefore, the annually averaged relative contributions provide a comparable measure for the influence of the time step on the TBNT results, as they represent the cumulative difference between the two calculations in the different parts of the TBNT domain.

Table B.1: Maximum differences between relative contributions (in %) of TBNT sensitivity run and TBNT reference run for the individual state variables and sources according to Eq. (2.1). Maximum differences are defined as those with the largest magnitude. Numbers in parentheses represent the corresponding relative difference calculated according to Eq. (2.2).

variable\source	Atmosphere		NA		EC		BS		DE	
nitrate	0.34	(1.0 %)	0.21	(1.3 %)	0.13	(0.5 %)	0.35	(0.7 %)	0.33	(1.0 %)
ammonium	0.18	(0.6 %)	0.25	(0.3 %)	0.10	(0.1 %)	0.15	(0.2 %)	0.33	(0.4 %)
diatom-N	0.21	(0.5 %)	0.19	(1.3 %)	0.12	(0.2 %)	0.25	(0.3 %)	0.27	(0.6 %)
flagellate-N	0.21	(0.5 %)	0.19	(1.3 %)	0.15	(1.2 %)	0.33	(0.4 %)	0.33	(0.4 %)
microzooplankton-N	0.20	(0.5 %)	0.22	(1.0 %)	0.14	(0.2 %)	0.36	(0.4 %)	0.34	(0.4 %)
mesozooplankton-N	0.21	(0.5 %)	0.21	(0.2 %)	0.13	(0.2 %)	0.36	(0.4 %)	0.34	(0.4 %)
slow-sinking detritus-N	0.22	(0.5 %)	0.20	(1.3 %)	0.14	(0.2 %)	0.33	(0.4 %)	0.33	(0.4 %)
fast-sinking detritus-N	0.22	(0.5 %)	0.20	(1.3 %)	0.14	(0.8 %)	0.34	(0.4 %)	0.33	(0.6 %)
dissolved organic N	0.19	(0.5 %)	0.21	(1.3 %)	0.15	(0.2 %)	0.30	(0.4 %)	0.34	(0.4 %)
benthic organic N	0.23	(0.5 %)	0.20	(0.2 %)	0.14	(0.2 %)	0.29	(0.4 %)	0.31	(0.4 %)
bacteria-N	0.19	(0.4 %)	0.22	(0.3 %)	0.14	(0.2 %)	0.29	(0.4 %)	0.34	(0.4 %)
molecular N (N_2)	0.15	(0.4 %)	0.14	(0.2 %)	0.09	(0.1 %)	0.15	(0.5 %)	0.19	(0.3 %)
variable\source	NL-1		NL-2		BE		FR		UK-1	
nitrate	0.50	(2.1 %)	0.08	(1.1 %)	0.23	(2.1 %)	0.11	(0.4 %)	0.21	(1.1 %)
ammonium	0.24	(1.4 %)	0.05	(6.5 %)	0.04	(0.6 %)	0.13	(0.1 %)	0.19	(0.3 %)
diatom-N	0.41	(4.0 %)	0.20	(0.6 %)	0.23	(0.4 %)	0.12	(0.4 %)	0.29	(0.5 %)
flagellate-N	0.34	(1.7 %)	0.21	(0.7 %)	0.41	(0.8 %)	0.17	(1.5 %)	0.26	(0.5 %)
microzooplankton-N	0.28	(1.5 %)	0.17	(0.8 %)	0.12	(0.3 %)	0.16	(0.2 %)	0.29	(0.5 %)
mesozooplankton-N	0.28	(1.3 %)	0.17	(0.9 %)	0.13	(0.3 %)	0.15	(0.2 %)	0.27	(0.5 %)
slow-sinking detritus-N	0.32	(1.4 %)	0.16	(0.6 %)	0.15	(0.3 %)	0.16	(0.2 %)	0.33	(0.5 %)
fast-sinking detritus-N	0.34	(1.5 %)	0.18	(0.2 %)	0.09	(0.1 %)	0.20	(0.3 %)	0.30	(0.5 %)
dissolved organic N	0.25	(3.3 %)	0.07	(5.8 %)	0.06	(0.8 %)	0.14	(0.2 %)	0.30	(0.5 %)
benthic organic N	0.30	(1.1 %)	0.07	(0.4 %)	0.06	(0.7 %)	0.13	(0.5 %)	0.31	(0.5 %)
bacteria-N	0.29	(1.4 %)	0.12	(0.4 %)	0.06	(0.2 %)	0.14	(0.2 %)	0.29	(0.5 %)
molecular N (N_2)	0.28	(3.0 %)	0.08	(0.3 %)	0.07	(0.7 %)	0.08	(0.3 %)	0.26	(0.5 %)
variable\source	UK-2		NO		Others					
nitrate	0.22	(0.4 %)	0.05	(0.2 %)	0.16	(0.8 %)				
ammonium	0.23	(0.3 %)	0.06	(0.2 %)	0.08	(0.2 %)				
diatom-N	0.21	(0.7 %)	0.09	(0.3 %)	0.22	(0.4 %)				
flagellate-N	0.22	(0.3 %)	0.06	(0.5 %)	0.25	(0.6 %)				
microzooplankton-N	0.24	(0.3 %)	0.06	(0.2 %)	0.12	(0.3 %)				
mesozooplankton-N	0.23	(0.3 %)	0.06	(0.2 %)	0.12	(0.3 %)				
slow-sinking detritus-N	0.24	(0.3 %)	0.06	(0.2 %)	0.13	(0.3 %)				
fast-sinking detritus-N	0.24	(0.3 %)	0.13	(0.3 %)	0.14	(0.3 %)				
dissolved organic N	0.24	(0.3 %)	0.06	(0.2 %)	0.11	(0.3 %)				
benthic organic N	0.23	(0.3 %)	0.05	(0.3 %)	0.09	(0.2 %)				
bacteria-N	0.24	(0.3 %)	0.06	(0.2 %)	0.12	(0.3 %)				
molecular N (N_2)	0.16	(0.3 %)	0.02	(0.1 %)	0.08	(0.1 %)				

Figure B.1 shows a scatter plot of the relative contributions resulting from the TBNT sensitivity run compared to the TBNT reference run, providing a qualitative overview of the results of the sensitivity analysis, . Each marker represents an individual relative contribution of to an individual water column, different colours indicate different input sources according to Table 6.1. For better clarity of the plot, no additional visual separation related to the different state variables is applied. The results presented in Fig. B.1 clearly

show that the calculations of the TBNT reference and sensitivity run are in very good agreement with each other and show only very minor deviations from on-to-on agreement (black line). Furthermore, no differences can be seen for the different sources.

In addition to this qualitative comparison, a more quantitative analysis is provided by calculating the maximum absolute difference between the relative contributions of the TBNT sensitivity run and the reference run:

$$\Delta^{\max}_{|\mathrm{S-R}|} = \max\left(|\mathrm{S-R}|\right) \quad [\%]. \tag{2.1}$$

Here, S and R represent the relative contribution (in %) of a specific source to a certain model state variable for an individual water column calculated from the results of the TBNT sensitivity and reference run, respectively. Furthermore, the relative difference is calculated in order to evaluate the maximum absolute difference in comparison to the overall relative contribution of a source to a certain state variable:

$$\Delta^{\max,\mathrm{rel}}_{|\mathrm{S-R}|} = \frac{\Delta^{\max}_{|\mathrm{S-R}|}}{\mathrm{R}_{\Delta^{\max}_{|\mathrm{S-R}|}}}. \tag{2.2}$$

Here, $\mathrm{R}_{\Delta^{\max}_{|\mathrm{S-R}|}}$ represents the relative contribution of the TBNT reference run (in %) that corresponds to the maximum difference between sensitivity and the reference run, $\Delta^{\max}_{|\mathrm{S-R}|}$.

Table B.1 lists the maximum difference of the relative contributions shown in Fig. B.1 for each source and state variable according to Eq. (2.1), and the corresponding relative differences (values in parentheses) according to Eq. (2.2).

The values of $\Delta^{\max}_{|\mathrm{S-R}|}$ presented in Table B.1 (values without parentheses) confirm the image provided by Fig. B.1. The differences in the relative contributions of the different sources to the individual state variables are very small between the reference and sensitivity run. The overall largest difference results in 0.5 % for nitrate from the NL-1 river group, for almost all other state-variable-source combinations the values are less than 0.4 %. The corresponding relative differences ($\Delta^{\max,\mathrm{rel}}_{|\mathrm{S-R}|}$; values in parentheses) are also very small ($\leq$1.0 %) for most variables and sources. Only for the Dutch NL-1 rivers the relative differences for the different variables are consistently larger than 1 %. However, the absolute difference between the relative contributions of the reference and sensitivity run are still very low with maximum differences of 0.5 % nitrate. This demonstrated that the overall results of the two different TBNT calculations are in very good agreement, and that the time step of the ECOHAM output used for the TBNT calculation only has a minor effect on the TBNT results and does not affect the general image obtained from the TBNT analysis.

References

J. Albretsen. The impact of freshwater discharges on the ocean circulation in the Skagerrak/northern North Sea area. Part II: energy analysis. *Ocean Dynamics*, 57(4-5): 287–304, 2007. doi: 10.1007/s10236-007-0121-6.

J. Alheit, C. Möllmann, J. Dutz, G. Kornilovs, P. Loewe, V. Mohrholz, and N. Wasmund. Synchronous ecological regime shifts in the central Baltic and the North Sea in the late 1980s. *ICES Journal of Marine Science: Journal du Conseil*, 62(7):1205–1215, 2005. doi: 10.1016/j.icesjms.2005.04.024.

S. Alvarez-Fernandez, H. Lindeboom, and E. Meesters. Temporal changes in plankton of the North Sea: community shifts and environmental drivers. *Marine Ecology Progress Series*, 462:21–38, 2012. doi: 10.3354/meps09817.

A. Arakawa and V.R. Lamb. Computational Design of the Basic Dynamical Processes of the {UCLA} General Circulation Model. In J. Chang, editor, *General Circulation Models of the Atmosphere*, volume 17 of *Methods in Computational Physics: Advances in Research and Applications*, pages 173–265. Elsevier, 1977. doi: 10.1016/B978-0-12-460817-7.50009-4.

N.W. Arnell. The effect of climate change on hydrological regimes in Europe: a continental perspective. *Global Environmental Change*, 9(1):5–23, 1999. doi: 10.1016/S0959-3780(98)00015-6.

Y. Artioli, J. Friedrich, A.J. Gilbert, A. McQuatters-Gollop, L.D. Mee, J.E. Vermaat, F. Wulff, C. Humborg, L. Palmeri, and F. Pollehne. Nutrient budgets for European seas: a measure of the effectiveness of nutrient reduction policies. *Marine Pollution Bulletin*, 56(9):1609–1617, 2008. doi: 10.1016/j.marpolbul.2008.05.027.

M.J. Attrill, J. Wright, and M. Edwards. Climate-related increases in jellyfish frequency suggest a more gelatinous future for the North Sea. *Limnology and Oceanography*, 52 (1):480–485, 2007. doi: 10.4319/lo.2007.52.1.0480.

F. Azam, T. Fenchel, J.G. Field, J.S. Gray, L.A. Meyer-Reil, and F. Thingstad. The ecological role of water-column microbes in the sea. *Marine Ecology Progress Series. Oldendorf*, 10(3):257–263, 1983. URL http://www.int-res.com/articles/meps/10/m010p257.pdf. Last accessed: 17-01-2017.

J.O. Backhaus. A three-dimensional model for the simulation of shelf sea dynamics. *Ocean Dynamics*, 38(4):165–187, 1985. doi: 10.1007/BF02328975.

J.O. Backhaus and D. Hainbucher. A finite difference general circulation model for shelf seas and its application to low frequency variability on the North European Shelf. *Elsevier Oceanography Series*, 45:221–244, 1987. doi: 10.1016/S0422-9894(08)70450-1.

J.W. Baretta, W. Ebenhöh, and P. Ruardij. The European regional seas ecosystem model, a complex marine ecosystem model. *Netherlands Journal of Sea Research*, 33(3-4):233–246, 1995. doi: 10.1016/0077-7579(95)90047-0.

H. Behrendt. Inventories of point and diffuse sources and estimated nutrient loads – a comparison for different river basins in Central Europe. *Water Science and Technology*, 33(4):99–107, 1996. doi: 10.1016/0273-1223(96)00219-3.

M.J. Behrenfeld and P.G. Falkowski. Photosynthetic rates derived from satellite-based chlorophyll concentration. *Limnology and oceanography*, 42(1):1–20, 1997. doi: 10.4319/lo.1997.42.1.0001.

M. Beniston, D.B. Stephenson, O.B. Christensen, C.A.T. Ferro, C. Frei, S. Goyette, K. Halsnaes, T. Holt, K. Jylhä, B. Koffi, J. Palutikof, R. Schöll, T. Semmler, and K. Woth. Future extreme events in European climate: an exploration of regional climate model projections. *Climatic change*, 81(1):71–95, 2007. doi: 10.1007/s10584-006-9226-z.

B. Benson and D. Krause. The concentration and isotopic fractionation of oxygen dissolved in freshwater and seawater in equilibrium with the atmosphere. *Limnology and Oceanography*, 29:620–632, 1984. doi: 10.4319/lo.1984.29.3.0620.

M.A. Best, A.W. Wither, and S. Coates. Dissolved oxygen as a physico-chemical supporting element in the Water Framework Directive. *Marine Pollution Bulletin*, 55(1):53–64, 2007. doi: 10.1016/j.marpolbul.2006.08.037.

R.E. Blake, J.R. O'Neil, and G.A. Garcia. Oxygen isotope systematics of biologically mediated reactions of phosphate: I. Microbial degradation of organophosphorus compounds. *Geochimica et Cosmochimica Acta*, 61(20):4411–4422, 1997. doi: 10.1016/S0016-7037(97)00272-X.

A.N. Blauw, K. van de Wolfshaar, and H. Meuwese. Transboundary nutrient transports in the North Sea. *WL|Delft Hydraulics Reports*, Z4188, 2006. URL http://publicaties.minienm.nl/download-bijlage/17327/

wl-report-z4188-transboundary-nutrient-transorts-in-the-north-sea.pdf. Last accessed: 16-09-2016.

A.N. Blauw, H.F.J. Los, M. Bokhorst, and P.L.A. Erftemeijer. GEM: a generic ecological model for estuaries and coastal waters. *Hydrobiologia*, 618(1):175–198, 2008. ISSN 1573-5117. doi: 10.1007/s10750-008-9575-x.

BLMP. Konzept zur Ableitung von Nährstoffreduzierungszielen in den Flussgebieten Ems, Weser, Elbe und Eider aufgrund von Anforderungen an den ökologischen Zustand der Küstengewässer gemäß Wasserrahmenrichtlinie. Ad hoc-AG Nährstoffreduzierung des BLMP, 2011. URL http://www.blmp-online.de/PDF/WRRL/WRRL_Papier_Naehrstoffe.pdf. German only.

Y. Bozec, H. Thomas, K. Elkalay, and H.J.W. de Baar. The continental shelf pump for CO_2 in the North Sea – evidence from summer observation. *Marine Chemistry*, 93(2–4): 131–147, 2005. doi: 10.1016/j.marchem.2004.07.006.

Y. Bozec, H. Thomas, L.-S. Schiettecatte, A.V. Borges, K. Elkalay, and H.J.W. de Baar. Assessment of the processes controlling the seasonal variations of dissolved inorganic carbon in the North Sea. *Limnology and Oceanography*, 51(6):2746–2762, 2006. doi: 10.4319/lo.2006.51.6.2746.

T. Braarud, K.R. Gaarder, and O. Nordli. Seasonal changes in the phytoplankton at various points off the Norwegian West Coast: Observations at the permanent oceanographic stations, 1945–46). 1958. URL http://hdl.handle.net/11250/114724. Last accessed: 05-10-2016.

N. Brion, W. Baeyens, S. de Galan, M. Elskens, and R.W.P.M. Laane. The North Sea: source or sink for nitrogen and phosphorus to the Atlantic Ocean? *Biogeochemistry*, 68 (3):277–296, 2004. doi: 10.1023/B:BIOG.0000031041.38663.aa.

U. Brockmann, G. Billen, and W.W.C. Gieskes. North Sea Nutrients and Eutrophication. In W. Salomons, B.L. Bayne, E.K. Duursma, and U. Förstner, editors, *Pollution of the North Sea: An Assessment*, pages 348–389. Springer, Berlin, Heidelberg, 1988. ISBN 978-3-642-73709-1. doi: 10.1007/978-3-642-73709-1_20.

U.H. Brockmann and K. Eberlein. River input of nutrients into the German Bight. In *The role of freshwater outflow in coastal marine ecosystems*, pages 231–240. Springer, 1986. doi: 10.1007/978-3-642-70886-2_15.

W.J. Burt, H. Thomas, J. Paetsch, A. M. Omar, C. Schrum, U. Daewel, H. Brenner, and H.J.W. de Baar. Radium isotopes as a tracer of sediment-water column exchange in the North Sea. *Global Biogeochemical Cycles*, 28(8):786–804, 8 2014. ISSN 0886-6236. doi: 10.1002/2014GB004825.

H.-R. Buser, M.D. Müller, and N. Theobald. Occurrence of the pharmaceutical drug clofibric acid and the herbicide mecoprop in various Swiss lakes and in the North Sea. *Environmental Science & Technology*, 32(1):188–192, 1998. doi: 10.1021/es9705811.

J. Carstensen, J.H. Andersen, B.G. Gustafsson, and D.J. Conley. Deoxygenation of the Baltic Sea during the last century. *Proceedings of the National Academy of Sciences*, 111(15):5628–5633, 2014a. doi: 10.1073/pnas.1323156111.

J. Carstensen, D.J. Conley, E. Bonsdorff, B.G. Gustafsson, S. Hietanen, U. Janas, T. Jilbert, A. Maximov, A. Norkko, J. Norkko, D.C. Reed, C.P. Slomp, K. Timmermann, and M. Voss. Hypoxia in the Baltic Sea: Biogeochemical Cycles, Benthic Fauna, and Management. *Ambio*, 43(1):26–36, 2014b. ISSN 1654-7209. doi: 10.1007/s13280-013-0474-7.

P. Chapman and L.V. Shannon. The Benguela ecosystem – Part II. Chemistry and related processes. *Oceanogr. Mar. Biol. Ann. Rev.*, 23:183–251, 1985. URL https://www.researchgate.net/profile/Piers_Chapman/publication/256803781_The_Benguela_Ecosystem_Part_II_Chemistry_and_related_processes/links/55cdfdb408ae6a881381ecdb.pdf. Last accessed: 04-01-2017.

X. Chen, C. Liu, K. O'Driscoll, B. Mayer, J. Su, and T. Pohlmann. On the nudging terms at open boundaries in regional ocean models. *Ocean Modelling*, 66:14–25, 2013. doi: 10.1016/j.ocemod.2013.02.006.

X. Chen, S. Dangendorf, N. Narayan, K. O'Driscoll, M.N. Tsimplis, J. Su, B. Mayer, and T. Pohlmann. On sea level change in the North Sea influenced by the North Atlantic Oscillation: local and remote steric effects. *Estuarine, Coastal and Shelf Science*, 151: 186–195, 2014. doi: 10.1016/j.ecss.2014.10.009.

R.A. Clark, C.J. Fox, D. Viner, and M. Livermore. North Sea cod and climate change–modelling the effects of temperature on population dynamics. *Global Change Biology*, 9(11):1669–1680, 2003. doi: 10.1046/j.1365-2486.2003.00685.x.

U. Claussen, W. Zevenboom, U. Brockmann, D. Topcu, and P. Bot. Assessment of the eutrophication status of transitional, coastal and marine waters within OSPAR. *Hydrobiologia*, 629(1):49–58, 2009. doi: 10.1007/s10750-009-9763-3.

J.E. Cloern, C. Grenz, and L. Vidergar-Lucas. An empirical model of the phytoplankton chlorophyll:carbon ratio – the conversion factor between productivity and growth rate. *Limnology and Oceanography*, 40(7):1313–1321, 1995. ISSN 1939-5590. doi: 10.4319/lo.1995.40.7.1313.

J.M. Colebrook. Continuous plankton records: seasonal cycles of phytoplankton and copepods in the North Atlantic Ocean and the North Sea. *Marine Biology*, 51(1):23–32, 1979. doi: 10.1007/BF00389027.

M.E. Conkright, R.A. Locarnini, H.E. Garcia, T.D. O'Brien, T.P. Boyer, C. Stephens, and J.I. Antonov. World Ocean Atlas 2001: Objective analyses, data statistics, and figures: CD-ROM documentation, 2002. URL ftp://ftp.nodc.noaa.gov/pub/WOA01/readme.pdf. Last accessed: 16-11-2016.

D.J. Conley, H.W. Paerl, R.W. Howarth, D.F. Boesch, S.P. Seitzinger, K.E. Havens, C. Lancelot, and G.E. Likens. Controlling eutrophication: nitrogen and phosphorus. *Science*, 123:1014–1015, 2009. doi: 10.1126/science.1167755.

S.R. Cooper and G.S. Brush. A 2,500-year history of anoxia and eutrophication in Chesapeake Bay. *Estuaries*, 16(3):617–626, 1993. doi: 10.2307/1352799.

H. Dahlgaard. Transfer of European coastal pollution to the Arctic: radioactive tracers. *Marine Pollution Bulletin*, 31(1):3–7, 1995. doi: 10.1016/0025-326X(95)00003-6.

D.S. Danielssen, L. Edler, S. Fonselius, L. Hernroth, M. Ostrowski, E. Svendsen, and L. Talpsepp. Oceanographic variability in the Skagerrak and northern Kattegat, May–June, 1990. *ICES Journal of Marine Science: Journal du Conseil*, 54(5):753–773, 1997. doi: 10.1006/jmsc.1996.0210.

D.M. Dauer, J.A. Ranasinghe, and S.B. Weisberg. Relationships between benthic community condition, water quality, sediment quality, nutrient loads, and land use patterns in Chesapeake Bay. *Estuaries*, 23(1):80–96, 2000. doi: 10.2307/1353227.

H. de Haas, W. Boer, and T.C.E. van Weering. Recent sedimentation and organic carbon burial in a shelf sea: the North Sea. *Marine Geology*, 144(1):131–146, 1997. doi: 10.1016/S0025-3227(97)00082-0.

P.A.W.J. de Wilde, E.M. Berghuis, and A. Kok. Structure and energy demand of the benthic community of the oyster ground, central north sea. *Netherlands Journal of Sea Research*, 18(1-2):143–159, 1984. doi: 10.1016/0077-7579(84)90029-2.

E.J.M. Delhez, J.-M. Campin, A.C. Hirst, and E. Deleersnijder. Toward a general theory of the age in ocean modelling. *Ocean Modelling*, 1(1):17–27, 1999. doi: 10.1016/S1463-5003(99)00003-7.

X. Desmit, G. Lacroix, V. Dulière, C. Lancelot, N. Gypens, A. Ménesguen, B. Thouvenin, M. Dussauze, G. Billen, J. Garnier, V. Thieu, M. Silvestre, P. Passy, Lassaletta L., G. Guittard, S. Théry, R. Neves, F. Campuzano, C. Garcia, L. Pinto, J. Sobrinho, M. Mateus, and I. Ascione Kenov. Ecosystem Models as Support to Eutrophication Management in the North Atlantic OCean (EMoSEM): Final report, 2015. URL http://odnature.naturalsciences.be/downloads/publications/emosem_final_report.pdf. Last accessed: 11-01-2017.

R.J. Díaz. Overview of hypoxia around the world. *Journal of environmental quality*, 30(2): 275–281, 2001. URL http://search.proquest.com/docview/197377300?accountid=104421. Last accessed: 04-01-2017.

R.J. Díaz and R. Rosenberg. Marine benthic hypoxia: a review of its ecological effects and the behavioural responses of benthic macrofauna. *Oceanography and marine biology. An annual review*, 33:245–03, 1995. URL https://www.researchgate.net/profile/Robert_Diaz5/publication/236628341_Marine_benthic_hypoxia_A_review_of_its_ecological_effects_and_the_behavioural_response_of_benthic_macrofauna/links/02e7e526a7c717396d000000.pdf. Last accessed: 17-12-2016.

R.J. Díaz and R. Rosenberg. Spreading dead zones and consequences for marine ecosystems. *Science*, 321(5891):926–929, 2008. doi: 10.1126/science.1156401.

S. Dick. NOOS Activity: Exchange of computed water, salt, and heat transports across selected transects, 2013. URL http://noos.bsh.de/download/exch_transports_NOOS-BOOS_2013-08-30.pdf. Last accessed: 04-11-2016.

A.T. Doodson. Meteorological Perturbations of Sea-Level and Tides. *Geophysical Journal International*, 1(s4):124–147, 1924. doi: 10.1111/j.1365-246X.1924.tb05363.x.

H.D. Dooley. Hypotheses concerning the circulation of the northern North Sea. *Journal du Conseil*, 36(1):54–61, 1974. doi: 10.1093/icesjms/36.1.54.

J.-N. Druon, W. Schrimpf, S. Dobricic, and A. Stips. Comparative assessment of large-scale marine eutrophication: North Sea area and Adriatic Sea as case studies. *Marine Ecology Progress Series*, 272:1–23, 2004. doi: 10.3354/meps272001.

J.P. Ducrotoy, M. Elliott, and V.N. de Jonge. The North Sea. *Marine Pollution Bulletin*, 41(1-6):5–23, 2000. doi: 10.1016/S0025-326X(00)00099-0.

R.C. Dugdale, J.J. Goering, R.T. Barber, R.L. Smith, and T.T. Packard. Denitrification and hydrogen sulfide in the Peru upwelling region during 1976. *Deep Sea Research*, 24 (6):601–608, 1977. doi: 10.1016/0146-6291(77)90530-6.

G.C.A. Duineveld, A. Künitzer, U. Niermann, P.A.W.J. de Wilde, and J.S. Gray. The macrobenthos of the North Sea. *Netherlands Journal of Sea Research*, 28(1-2):53–65, 1991. doi: 10.1016/0077-7579(91)90004-K.

S.R. Dye, S.L. Hughes, J. Tinker, D.I. Berry, N.P. Holliday, E.C. Kent, K. Kennington, M. Inall, T. Smyth, G. Nolan, K. Lyons, O. Andres, and A. Beszczynska-Möller. Impacts of climate change on temperature (air and sea). *MCCIP Science Review*, 2013:1–12, 2013. URL https://www.researchgate.net/profile/Stephen_Dye/publication/259679111_Impacts_of_climate_change_on_temperature_(air_and_sea)/links/0c96053a7f0dcc79b1000000.pdf.

J.R. Ehleringer and P. Rundel. *1. Stable Isotopes: History, Units and Instrumentation*, volume 68, pages 1–16. Springer-Verlag New York Inc., 1989. URL http://www.ehleringer.net/uploads/3/1/8/3/31835701/094.pdf. Last accessed: 01-11-2016.

A.J. Elliott, T. Clarke, and Z. Li. Monthly distributions of surface and bottom temperatures in the northwest European shelf seas. *Continental Shelf Research*, 11(5):453–466, 1991. doi: 10.1016/0278-4343(91)90053-9.

K.-C. Emeis, J. van Beusekom, U. Callies, R. Ebinghaus, A. Kannen, G. Kraus, I. Kröncke, H. Lenhart, I. Lorkowski, V. Matthias, C. Möllmann, J. Pätsch, M. Scharfe, H. Thomas, R. Weisse, and E. Zorita. The North Sea – A shelf sea in the Anthropocene. *Journal of Marine Systems*, 141:18–33, 2015. ISSN 0924-7963. doi: 10.1016/j.jmarsys.2014.03.012.

EU. Directive 2000/60/EC of the European Parliament and of the Council of 23 October 2000 establishing a framework for Community action in the field of water policy. 43:1–72, 2000. URL http://eur-lex.europa.eu/resource.html?uri=cellar:5c835afb-2ec6-4577-bdf8-756d3d694eeb.0004.02/DOC_1&format=PDF. Last accessed: 04-01-2017.

EU. Directive 2008/56/EC of the European Parliament and of the Council of 17 June 2008 establishing a framework for community action in the field of marine environmental pol-

icy (Marine Strategy Framework Directive). 51:19–40, 2008. URL http://eur-lex.europa.eu/legal-content/EN/TXT/PDF/?uri=CELEX:32008L0056&from=EN. Last accessed: 04-01-2017.

P.G. Falkowski, T. Algeo, L. Codispoti, C. Deutsch, S. Emerson, B. Hales, R.B. Huey, W.J. Jenkins, L.R. Kump, L.A. Levin, T.W. Lyons, N.B. Nelson, O.S. Schofield, R. Summons, L.D. Talley, E. Thomas, F. Whitney, and C.B. Pilcher. Ocean deoxygenation: Past, present, and future. *Eos, Transactions American Geophysical Union*, 92(46):409–410, 2011. ISSN 2324-9250. doi: 10.1029/2011EO460001.

K. Fennel, J. Wilkin, J. Levin, J. Moisan, J. O'Reilly, and D. Haidvogel. Nitrogen cycling in the Middle Atlantic Bight: Results from a three-dimensional model and implications for the North Atlantic nitrogen budget. *Global Biogeochemical Cycles*, 20(3), 2006. doi: 10.1029/2005GB002456.

N.P. Fofonoff and R.C. Millard. Algorithms for computation of fundamental properties of seawater. 1983. URL http://hdl.handle.net/1912/2470. Last accessed: 16-11-2016.

C. Frei, R. Schöll, S. Fukutome, J. Schmidli, and P.L. Vidale. Future change of precipitation extremes in Europe: Intercomparison of scenarios from regional climate models. *Journal of Geophysical Research: Atmospheres*, 111(D6), 2006. doi: 10.1029/2005JD005965.

J. Friedrich, F. Janssen, D. Aleynik, H.W. Bange, N. Boltacheva, M.N. Çagatay, A.W. Dale, G. Etiope, Z. Erdem, M. Geraga, A. Gilli, M.T. Gomoiu, P.O.J. Hall, D. Hansson, Y. He, M. Holtappels, M.K. Kirf, M. Kononets, S. Konovalov, A. Lichtschlag, D.M. Livingstone, G. Marinaro, S. Mazlumyan, S. Naeher, R.P. North, G. Papatheodorou, O. Pfannkuche, R. Prien, G. Rehder, C.J. Schubert, T. Soltwedel, S. Sommer, H. Stahl, E.V. Stanev, A. Teaca, A. Tengberg, C. Waldmann, B. Wehrli, and F. Wenzhöfer. Investigating hypoxia in aquatic environments: diverse approaches to addressing a complex phenomenon. *Biogeosciences*, 11(4):1215–1259, 2014. doi: 10.5194/bg-11-1215-2014.

T.L. Frölicher, F. Joos, G.-K. Plattner, M. Steinacher, and S.C. Doney. Natural variability and anthropogenic trends in oceanic oxygen in a coupled carbon cycle-climate model ensemble. *Global Biogeochemical Cycles*, 23(1):15pp., 2009. ISSN 1944-9224. doi: 10.1029/2008GB003316.

G.K. Furnes, B. Hackett, and R. Sætre. Retroflection of Atlantic water in the Norwegian Trench. *Deep Sea Research Part A. Oceanographic Research Papers*, 33(2):247–265, 1986. doi: 10.1016/0198-0149(86)90121-4.

R. Gade. Reduzierung der Nährstoffeinträge aus Sicht des Meeresschutzes, 2016. URL http://www.lbeg.niedersachsen.de/download/107321/Reduzierung_der_Naehrstoffeintraege_aus_Sicht_des_Meeresschutzes_MR_Rudolf_Gade.pdf. Presentation slides. German only. Last accessed: 28-12-2016.

R. Geider and J. La Roche. Redfield revisited: variability of C:N:P in marine microalgae and its biochemical basis. *European Journal of Phycology*, 37(1):1–17, 2002. doi: 10.1017/S0967026201003456.

W.W.C. Gieskes and G.W. Kraay. The phytoplankton spring bloom in Dutch coastal waters of the North Sea. *Netherlands Journal of Sea Research*, 9(2):166–196, 1975. doi: 10.1016/0077-7579(75)90014-9.

W.W.C. Gieskes and G.W. Kraay. Dominance of Cryptophyceae during the phytoplankton spring bloom in the central North Sea detected by HPLC analysis of pigments. *Marine Biology*, 75(2):179–185, 1983. ISSN 1432-1793. doi: 10.1007/BF00406000.

W.W.C. Gieskes and G.W. Kraay. Analysis of phytoplankton pigments by HPLC before, during and after mass occurrence of the microflagellate Corymbellus aureus during the spring bloom in the open northern North Sea in 1983. *Marine Biology*, 92(1):45–52, 1986. doi: 10.1007/BF00392744.

D. Gilbert, N.N. Rabalais, R.J. Díaz, and J. Zhang. Evidence for greater oxygen decline rates in the coastal ocean than in the open ocean. *Biogeosciences*, 7(7):2283–2296, 2010. doi: 10.5194/bg-7-2283-2010.

J.C. Goldman, J.J. McCarthy, and D.G. Peavey. Growth rate influence on the chemical composition of phytoplankton in oceanic waters. *Nature*, 279(2):1, 1979. doi: 10.1038/279210a0.

J.S. Gray, R.S. Wu, and Y.Y. Or. Effects of hypoxia and organic enrichment on the coastal marine environment. *Marine Ecology Progress Series*, 238:249–279, 2002. doi: 10.3354/meps238249.

N. Greenwood, E.R. Parker, L. Fernand, D.B. Sivyer, K. Weston, S.J. Painting, S. Kröger, R.M. Forster, H.E. Lees, D.K. Mills, and R.W.P.M. Laane. Detection of low bottom water oxygen concentrations in the North Sea; implications for monitoring and assessment of ecosystem health. *Biogeosciences*, 7(4):1357–1373, 2010. doi: 10.5194/bg-7-1357-2010.

M. Gröger, E. Maier-Reimer, U. Mikolajewicz, A. Moll, and D. Sein. NW European shelf under climate warming: implications for open ocean-shelf exchange, primary production, and carbon absorption. *Biogeosciences*, 10(6):3767–3792, 2013. doi: 10.5194/bg-10-3767-2013.

F. Große, N. Greenwood, M. Kreus, H.-J. Lenhart, D. Machoczek, J. Pätsch, L. Salt, and H. Thomas. Looking beyond stratification: a model-based analysis of the biological drivers of oxygen deficiency in the North Sea. *Biogeosciences*, 13(8):2511–2535, 2016. doi: 10.5194/bg-13-2511-2016.

J.D. Hagy, W.R. Boynton, C.W. Keefe, and K.V. Wood. Hypoxia in Chesapeake Bay, 1950–2001: long-term change in relation to nutrient loading and river flow. *Estuaries*, 27(4):634–658, 2004. doi: 10.1007/BF02907650.

D. Hainbucher and J.O. Backhaus. Circulation of the eastern North Atlantic and northwest European continental shelf–a hydrodynamic modelling study. *Fisheries Oceanography*, 8(s1):1–12, 1999. doi: 10.1046/j.1365-2419.1999.00009.x.

D. Hainbucher, T. Pohlmann, and J.O. Backhaus. Transport of conservative passive tracers in the North Sea: first results of a circulation and transport model. *Continental Shelf Research*, 7(10):1161–1179, 1987. doi: 10.1016/0278-4343(87)90083-5.

I.H Harms. Modelling the dispersion of ^{137}Cs and ^{239}Pu released from dumped waste in the Kara Sea. *Journal of Marine Systems*, 13(1):1–19, 1997. doi: 10.1016/S0924-7963(96)00117-0.

B. Haurwitz, H. Stommel, and W.H. Munk. On the thermal unrest in the ocean. In B. Bolin, editor, *The atmosphere and the sea in motion: Scientific contributions to the Rossby memorial volume*, pages 74–94. Rockfeller Institute Press New York, 1959. ISBN 978-0-874-70033-6. URL http://books.rupress.org/catalog/book/atmosphere-and-sea-motion. Last accessed: 13-01-2017.

M.R. Heath, A.C. Edwards, J. Pätsch, and W.R. Turrell. Modelling the behaviour of nutrients in the coastal waters of Scotland, 2002. URL https://core.ac.uk/download/pdf/9026812.pdf. Last accessed: 28-11-2016.

K.P. Helm, N.L. Bindoff, and J.A. Church. Observed decreases in oxygen content of the global ocean. *Geophysical Research Letters*, 38(23):6pp, 2011. ISSN 1944-8007. doi: 10.1029/2011GL049513.

R.D. Hetland and S.F. DiMarco. How does the character of oxygen demand control the structure of hypoxia on the Texas–Louisiana continental shelf? *Journal of Marine Systems*, 70(1):49–62, 2008. doi: 10.1016/j.jmarsys.2007.03.002.

J. Hofmann, H. Behrendt, A. Gilbert, R. Janssen, A. Kannen, J. Kappenberg, H. Lenhart, W. Lise, C. Nunneri, and W. Windhorst. Catchment–coastal zone interaction based upon scenario and model analysis: Elbe and the German Bight case study. *Regional Environmental Change*, 5(2-3):54–81, 2005. doi: 10.1007/s10113-004-0082-y.

N.P. Holliday, S.L. Hughes, and A. Beszczynska-Möller. ICES report on Ocean Climate 2008. *ICES Cooperative Research Report*, 298:66pp., 2009. URL http://epic.awi.de/22807/1/Hol2009c.pdf. Last accessed: 05-01-2017.

J.M.J. Hoppema. The oxygen budget of the western Wadden Sea, The Netherlands. *Estuarine, Coastal and Shelf Science*, 32(5):483–502, 1991. doi: 10.1016/0272-7714(91)90036-B.

R.W. Howarth and R. Marino. Nitrogen as the limiting nutrient for eutrophication in coastal marine ecosystems: evolving views over three decades. *Limnology and Oceanography*, 51(1part2):364–376, 2006. doi: 10.4319/lo.2006.51.1_part_2.0364.

J.M. Huthnance. Physical oceanography of the North Sea. *Ocean and Shoreline Management*, 16(3-4):199–231, 1991. doi: 10.1016/0951-8312(91)90005-M.

J.M. Huthnance, R. Weisse, T. Wahl, H. Thomas, J. Pietrzak, A.J. Souza, S. van Heteren, N. Schmelzer, J. van Beusekom, F. Colijn, I. Haigh, S. Hjøllo, J. Holfort, E.C. Kent, W. Kühn, P. Loewe, I. Lorkowski, K.A. Mork, J. Pätsch, M. Quante, L. Salt, J. Siddorn, T. Smyth, A. Sterl, and P. Woodworth. Recent Change – North Sea. In *North Sea Region Climate Change Assessment*, pages 85–136. Springer, 2016. doi: 10.1007/978-3-319-39745-0_3.

D.J. Hydes, B.A. Kelly-Gerreyn, A.C. Le Gall, and R. Proctor. The balance of supply of nutrients and demands of biological production and denitrification in a temperate latitude shelf sea – a treatment of the southern North Sea as an extended estuary. *Marine Chemistry*, 68(1):117–131, 1999. doi: 10.1016/S0304-4203(99)00069-9.

IAPWS. *Release on the IAPWS Formulation 2008 for the Thermodynamic Properties of Seawater*. The International Association for the Properties of Water and Steam, Berlin, Germany, September 2008. URL http://www.teos-10.org/pubs/IAPWS-10.pdf. Last accessed: 16-09-2016.

ICES. Flushing times of the North Sea, 1983.

ICG-EMO. ICG-EMO 3rd OSPAR Workshop User Guide, 2009. Intersessional Correspondence Group on Eutrophication Modelling.

ICNS-2. Second International Conference on the Protection of the North Sea: Ministerial Declaration calling for Reduction of Pollution. *International Legal Materials*, 27(3):835–848, 1988. ISSN 00207829, 19306571. URL http://www.jstor.org/stable/20693232. Last accessed: 04-01-2017.

IOC, SCOR, and IAPSO. *The international thermodynamic equation of seawater - 2010: Calculation and use of thermodynamic properties*, volume 56 of *Manuals and Guides*. UNESCO, 2010. URL http://www.teos-10.org/pubs/TEOS-10_Manual.pdf. Last accessed: 16-09-2016.

D.R. Jackett and T.J. McDougall. Minimal adjustment of hydrographic profiles to achieve static stability. *Journal of Atmospheric and Oceanic Technology*, 12(2):381–389, 1995. doi: 10.1175/1520-0426(1995)012<0381:MAOHPT>2.0.CO;2.

F. Janssen, C. Schrum, and J.O. Backhaus. A climatological data set of temperature and salinity for the Baltic Sea and the North Sea. *Deutsche Hydrografische Zeitschrift*, 51 (9):5–245, 1999. doi: 10.1007/BF02933676.

T.D. Jickells. Nutrient biogeochemistry of the coastal zone. *Science*, 281(5374):217–222, 1998. doi: 10.1126/science.281.5374.217.

J.A. Johannessen, S. Sandven, K. Lygre, E. Svendsen, and O.M. Johannessen. Three-dimensional structure of mesoscale eddies in the Norwegian Coastal Current. *Journal of Physical Oceanography*, 19(1):3–19, 1989. doi: 10.1175/1520-0485(1989)019<0003:TDSOME>2.0.CO;2.

I. Joint and A. Pomroy. Phytoplankton biomass and production in the southern North Sea. *Marine Ecology-Progress Series*, 99:169–182, 1993. URL http://www.int-res.com/articles/meps/99/m099p169.pdf. Last accessed: 20-10-2016.

D. Justić, N.N. Rabalais, R.E. Turner, and W.J. Wiseman. Seasonal coupling between riverborne nutrients, net productivity and hypoxia. *Marine Pollution Bulletin*, 26(4): 184–189, 1993. doi: 10.1016/0025-326X(93)90620-Y.

D. Justić, N.N. Rabalais, and R.E. Turner. Effects of climate change on hypoxia in coastal waters: A doubled CO_2 scenario for the northern Gulf of Mexico. *Limnology and Oceanography*, 41:992–1003, 1996. doi: 10.4319/lo.1996.41.5.0992.

D. Justić, N.N. Rabalais, and R.E. Turner. Impacts of climate change on net productivity of coastal waters: implications for carbon budgets and hypoxia. *Climate Research*, 8(3): 225–237, 1997. doi: 10.3354/cr008225.

D. Justić, R.E. Turner, and N.N. Rabalais. Climatic influences on riverine nitrate flux: Implications for coastal marine eutrophication and hypoxia. *Estuaries*, 26(1):1–11, 2003. doi: 10.1007/BF02691688.

E. Kalnay, M. Kanamitsu, R. Kistler, W. Collins, D. Deaven, L. Gandin, M. Iredell, S. Saha, G. White, J. Woollen, Y. Zhu, M. Chelliah, W. Ebisuzaki, W. Higgins, J. Janowiak, K.C. Mo, C. Ropelewski, J. Wang, A. Leetmaa, R. Reynolds, R. Jenne, and D. Joseph. The NCEP/NCAR 40-year reanalysis project. *Bulletin Of The American Meteorological Society*, 77(3):437–471, 1996. doi: 10.1175/1520-0477(1996)077<0437:TNYRP>2.0.CO;2.

A.B. Kara, P.A. Rochford, and H.E. Hurlburt. An optimal definition for ocean mixed layer depth. *Journal of Geophysical Research*, 105(C7):16803–16821, 2000. doi: 10.1029/2000JC900072.

W.M. Kemp, J.M. Testa, D.J. Conley, D. Gilbert, and J.D. Hagy. Temporal responses of coastal hypoxia to nutrient loading and physical controls. *Biogeosciences*, 6(12): 2985–3008, 2009. doi: 10.5194/bg-6-2985-2009.

S. Kienzler, I. Pech, H. Kreibich, M. Müller, and A.H. Thieken. After the extreme flood in 2002: changes in preparedness, response and recovery of flood-affected residents in Germany between 2005 and 2011. *Natural Hazards and Earth System Sciences*, 15(3): 505–526, 2015. doi: 10.5194/nhess-15-505-2015.

W.M. Kieskamp, L. Lohse, E. Epping, and W. Helder. Seasonal variation in denitrification rates and nitrous oxide fluxes in intertidal sediments of the western Wadden Sea. *Marine Ecology Progress Series. Oldendorf*, 72(1):145–151, 1991. URL http://www.int-res.com/articles/meps/72/m072p145.pdf. Last accessed: 03-01-2017.

R. Kistler, W. Collins, S. Saha, G. White, J. Woollen, E. Kalnay, M. Chelliah, W. Ebisuzaki, M. Kanamitsu, V. Kousky, H. van den Dool, R. Jenne, and M. Fiorino. The NCEP-NCAR 50-year reanalysis: Monthly means CD-ROM and documentation. *Bulletin of the American Meteorological Society*, 82(2):247–267, 2001. doi: 10.1175/1520-0477(2001)082<0247:TNNYRM>2.3.CO;2.

V.P. Kochergin. Three-dimensional prognostic models. In N.S. Heaps, editor, *Three-Dimensional Coastal Ocean Models*, pages 201–208. American Geophysical Union, 1987. ISBN 978-1-118-66504-6. doi: 10.1029/CO004.

M. Krause and G. Radach. On the relations of vertical distribution, diurnal migration and nutritional state of herbivorous zooplankton in the northern North Sea during FLEX 1976. *Internationale Revue der gesamten Hydrobiologie und Hydrographie*, 74(4):371–417, 1989. doi: 10.1002/iroh.19890740403.

I. Kröncke and R. Knust. The Dogger Bank: a special ecological region in the central North Sea. *Helgoland Marine Research*, 49(1):335–353, 1995. doi: 10.1007/BF02368361.

W. Kühn, J. Pätsch, H. Thomas, A.V. Borges, L.-S. Schiettecatte, Y. Bozec, and A.E.F. Prowe. Nitrogen and carbon cycling in the North Sea and exchange with the North Atlantic–A model study, Part II: Carbon budget and fluxes. *Continental Shelf Research*, 30(16):1701–1716, 2010. doi: 10.1016/j.csr.2010.07.001.

A. Künitzer, D. Basford, J.A. Craeymeersch, J.M. Dewarumez, J. Dörjes, G.C.A. Duineveld, A. Eleftheriou, C. Heip, P. Herman, P. Kingston, U. Niermann, E. Rachor, H. Rumohr, and P.A.J. de Wilde. The benthic infauna of the North Sea: species distribution and assemblages. *ICES Journal of Marine Science: Journal du Conseil*, 49(2):127–143, 1992. doi: 10.1093/icesjms/49.2.127.

G. Lacroix, K. Ruddick, N. Gypens, and C. Lancelot. Modelling the relative impact of rivers (Scheldt/Rhine/Seine) and Western Channel waters on the nutrient and diatoms/Phaeocystis distributions in Belgian waters (Southern North Sea). *Continental Shelf Research*, 27(10):1422–1446, 2007. doi: 10.1016/j.csr.2007.01.013.

H. Lamb. The equations of motion. In H. Lamb, editor, *A treatise on the mathematical theory of Motion of Fluids*, pages 1–17. Cambridge University Press, 1879. URL https://ia600500.us.archive.org/17/items/atreatiseonmath00lambgoog/atreatiseonmath00lambgoog.pdf. Last accessed: 13-01-2017.

C. Lancelot, V. Rousseau, G. Billen, and D. van Eeckhout. Coastal eutrophication of the southern bight of the North Sea: assesment and modelling. In *Sensitivity to Change: Black Sea, Baltic Sea and North Sea*, pages 439–453. Springer, 1997. doi: 10.1007/978-94-011-5758-2_33.

K.M.H. Larsen, C. Gonzalez-Pola, P. Fratantoni, A. Beszczynska-Möller, and S.L. Hughes. ICES report on Ocean Climate 2015. *ICES Cooperative Research Re-*

port, 331:79pp., 2016. URL http://www.ices.dk/sites/pub/PublicationReports/CooperativeResearchReport(CRR)/crr331/CRR331.pdf. Last accessed: 05-01-2017.

P.D. Latinopoulos, Y.N. Krestenitis, and L.A. Valioulis. A decision analysis approach to a coastal pollution problem: the sewage system of the City of Thessaloniki (Greece). *WIT Transactions on Ecology and the Environment*, 15, 1970. URL https://www.witpress.com/Secure/elibrary/papers/CENV96/CENV96002FU.pdf. Last accessed: 17-01-2017.

A. Laurent and K. Fennel. Simulated reduction of hypoxia in the northern Gulf of Mexico due to phosphorus limitation. *Elementa: Science of the Anthropocene*, 2(1):000022, 2014. doi: 10.12952/journal.elementa.000022.

A.J. Lee. North Sea: Physical Oceanography. *Elsevier Oceanography Series*, 24:467–493, 1980. doi: 10.1016/S0422-9894(08)71359-X.

B. Lehner, P. Döll, J. Alcamo, T. Henrichs, and F. Kaspar. Estimating the impact of global change on flood and drought risks in Europe: a continental, integrated analysis. *Climatic Change*, 75(3):273–299, 2006. doi: 10.1007/s10584-006-6338-4.

H.-J. Lenhart and T. Pohlmann. The ICES-boxes approach in relation to results of a North Sea circulation model. *Tellus A*, 49(1):139–160, 1997. doi: 10.1034/j.1600-0870.1997.00010.x.

H.-J. Lenhart, D.K. Mills, H. Baretta-Bekker, S.M. van Leeuwen, J. van der Molen, J.W. Baretta, M. Blaas, X. Desmit, W. Kühn, G. Lacroix, H.J. Los, A. Ménesguen, R. Neves, R. Proctor, P. Ruardij, M.D. Skogen, A. Vanhoutte-Brunier, M.T. Villars, and S.L. Wakelin. Predicting the consequences of nutrient reduction on the eutrophication status of the North Sea. *Journal of Marine Systems*, 81(1):148–170, 2010. doi: 10.1016/j.jmarsys.2009.12.014.

H.J. Lenhart. Effects of river nutrient load reduction on the eutrophication of the North Sea, simulated with the ecosystem model ERSEM. *Senckenbergiana maritima*, 31(2):299–311, 2001. doi: 10.1007/BF03043038.

H.J. Lenhart, G. Radach, J.O. Backhaus, and T. Pohlmann. Simulations of the North Sea circulation, its variability, and its implementation as hydrodynamical forcing in ERSEM. *Netherlands Journal of Sea Research*, 33(3-4):271–299, 1995. doi: 10.1016/0077-7579(95)90050-0.

L.A. Levin, W. Ekau, A.J. Gooday, F. Jorissen, J.J. Middelburg, W. Naqvi, C. Neira, N.M. Rabalais, and J.Z. Zhang. Effects of natural and human-induced hypoxia on coastal benthos. *Biogeosciences*, 6(10):2063–2098, 2009. doi: 10.5194/bg-6-2063-2009.

E.L. Lewis and R.G. Perkin. Salinity: its definition and calculation. *Journal of Geophysical Research: Oceans*, 83(C1):466–478, 1978. doi: 10.1029/JC083iC01p00466.

J. Liebig. *Die organische Chemie in ihrer Anwendung auf Agricultur und Physiologie*. 1841.

L. Lohse, H.T. Kloosterhuis, W. van Raaphorst, and W. Helder. Denitrification rates as measured by the isotope pairing method and by the acetylene inhibition technique in continental shelf sediments of the North Sea. *Marine Ecology Progress Series*, 132: 169–179, 1996. doi: 10.3354/meps132169.

A. Longhurst, S. Sathyendranath, T. Platt, and C. Caverhill. An estimate of global primary production in the ocean from satellite radiometer data. *Journal of Plankton Research*, 17(6):1245–1271, 1995. doi: 10.1093/plankt/17.6.1245.

A. Longinelli and S. Nuti. Revised phosphate-water isotopic temperature scale. *Earth and Planetary Science Letters*, 19(3):373–376, 1973. doi: 10.1016/0012-821X(73)90088-5.

S. Loos, T. Troost, N. Goorden, M. Weeber, and H. Los. Stikstof scenario met KRW-Verkenner en koppeling met het Nordzee model, 2014. Dutch only.

I. Lorkowski, J. Pätsch, A. Moll, and W. Kühn. Interannual variability of carbon fluxes in the North Sea from 1970 to 2006 – Competing effects of abiotic and biotic drivers on the gas-exchange of CO_2. *Estuarine, Coastal and Shelf Science*, 100:38–57, 2012. doi: 10.1016/j.ecss.2011.11.037.

F.J. Los, T.A. Troost, and J.K.L. van Beek. Finding the optimal reduction to meet all targets – applying Linear Programming with a nutrient tracer model of the North Sea. *Journal of Marine Systems*, 131:91–101, 2014. doi: 10.1016/j.jmarsys.2013.12.001.

J. Lowe, T. Howard, A. Pardaens, J. Tinker, J. Holt, S. Wakelin, G. Milne, J. Leake, J. Wolf, K. Horsburgh, T. Reeder, G. Jenkins, J. Ridley, S. Dye, and S. Bradley. UK Climate Projections Science Report: Marine and Coastal Projections. Technical report, Met Office Hadley Centre, Exeter, UK, 2009. URL http://ukclimateprojections.metoffice.gov.uk/media.jsp?mediaid=87905&. Last accessed: 01-11-2016.

W. Maenhaut and J. Cafmeyer. Long-term atmospheric aerosol study at urban and rural sites in Belgium using multi-elemental analysis by particle-induced x-ray emission spectrometry and short-irradiation instrumental neutron activation analysis. *X-Ray Spectrometry*, 27(4):236–246, 1998. doi: 10.1002/(SICI)1097-4539(199807/08)27:4<236::AID-XRS292>3.0.CO;2-F.

W. Maenhaut, F. Francois, J. Cafmeyer, C. Gilot, and J. Hanssen. Long-term aerosol study in southern Norway, and the relationship of aerosol components to source regions. In *EUROTRAC Symposium 96: Transport and transformation of pollutants in the troposphere*, pages 277–280. Computational Mechanics, 1997. ISBN 978-1-853-12496-9.

N. Mahowald, T.D. Jickells, A.R. Baker, P. Artaxo, C.R. Benitez-Nelson, G. Bergametti, T.C. Bond, Y. Chen, D.D. Cohen, B. Herut, N. Kubilay, R. Losno, C. Luo, W. Maenhaut, K.A. McGee, G.S. Okin, R.L. Siefert, and S. Tsukuda. Global distribution of atmospheric phosphorus sources, concentrations and deposition rates, and anthropogenic impacts. *Global Biogeochemical Cycles*, 22(4), 2008. doi: 10.1029/2008GB003240.

T.C. Malone. River flow, phytoplankton production and oxygen depletion in Chesapeake Bay. *Geological Society, London, Special Publications*, 58(1):83–93, 1991. doi: 10.1144/GSL.SP.1991.058.01.06.

A.M. Malzahn, F. Hantzsche, K. L. Schoo, M. Boersma, and N. Aberle. Differential effects of nutrient-limited primary production on primary, secondary or tertiary consumers. *Oecologia*, 162(1):35–48, 2010. ISSN 1432-1939. doi: 10.1007/s00442-009-1458-y.

M. Mathis and T. Pohlmann. Projection of physical conditions in the North Sea for the 21st century. *Climate Research*, 61(1):1–17, 2014. doi: 10.3354/cr01232.

T.J. McDougall and P.M. Barker. *Getting started with TEOS-10 and the Gibbs Seawater (GSW) oceanographic toolbox*, volume 127. SCOR/IAPSO WG, 2011. ISBN 978-0-646-55621-5. URL http://www.teos-10.org/pubs/Getting_Started.pdf. Last accessed: 16-09-2016.

T.J. McDougall, D.R. Jackett, D.G. Wright, and R. Feistel. Accurate and computationally efficient algorithms for potential temperature and density of seawater. *Journal of Atmospheric and Oceanic Technology*, 20(5):730–741, 2003. doi: 10.1175/1520-0426(2003)20<730:AACEAF>2.0.CO;2.

A. McQuatters-Gollop, D.E. Raitsos, M. Edwards, and M.J. Attrill. Spatial patterns of diatom and dinoflagellate seasonal cycles in the NE Atlantic Ocean. *Marine Ecology Progress Series*, 339:301–306, 2007. doi: 10.3354/meps339301.

L Mee. Reviving dead zones. *Scientific American*, 295(5):78–85, 2006. doi: 10.1038/scientificamerican1106-78.

L. Meire, K.E.R. Soetaert, and F.J.R. Meysman. Impact of global change on coastal oxygen dynamics and risk of hypoxia. *Biogeosciences*, 10(4):2633–2653, 2013. doi: 10.5194/bg-10-2633-2013.

G.L. Mellor and T. Yamada. A hierarchy of turbulence closure models for planetary boundary layers. *Journal of the Atmospheric Sciences*, 31(7):1791–1806, 1974. doi: 10.1175/1520-0469(1974)031<1791:AHOTCM>2.0.CO;2.

F. Melzner, J. Thomsen, W. Koeve, A. Oschlies, M.A. Gutowska, H.W. Bange, H.P. Hansen, and A. Körtzinger. Future ocean acidification will be amplified by hypoxia in coastal habitats. *Marine Biology*, 160(8):1875–1888, 2013. doi: 10.1007/s00227-012-1954-1.

A. Ménesguen and T. Hoch. Modelling the biogeochemical cycles of elements limiting primary production in the English Channel. I. Role of thermohaline stratification. *Marine Ecology Progress Series*, 146(1):173–188, 1997. doi: 10.3354/meps146173.

A. Ménesguen, P. Cugier, and I. Leblond. A new numerical technique for tracking chemical species in a multi-source, coastal ecosystem, applied to nitrogen causing Ulva blooms in the Bay of Brest (France). *Limnology and Oceanography*, 51(1.2):591–601, 2006. doi: 10.4319/lo.2006.51.1_part_2.0591.

D.K. Mills, R.W.P.M. Laane, J.M. Rees, M.R. van der Loeff, J.M. Suylen, D.J. Pearce, D.B. Sivyer, C. Heins, K. Platt, and M. Rawlinson. Smartbuoy: a marine environmental monitoring buoy with a difference. *Elsevier Oceanography Series*, 69:311–316, 2003. doi: 10.1016/S0422-9894(03)80050-8.

Mississippi River Gulf of Mexico Watershed Nutrient Task Force. Reassessment 2013: Assessing Progress Made Since 2008, 2013. URL https://www.epa.gov/sites/production/files/2015-03/documents/hypoxia_reassessment_508.pdf.

A. Moll. Regional distribution of primary production in the North Sea simulated by a three-dimensional model. *Journal of Marine Systems*, 16(1–2):151–170, 1998. doi: 10.1016/S0924-7963(97)00104-8.

C. Mudersbach, J. Bender, and F. Netzel. An analysis of changes in flood quantiles at the gauge Neu Darchau (Elbe River) from 1875 to 2013. *Stochastic Environmental Research and Risk Assessment*, pages 1–13, 2016. doi: 10.5194/piahs-373-193-2016.

L. Müller. Sauerstoffdynamik der Nordsee – Untersuchungen mit einem drei-dimensionalen Ökosystemmodell. *Berichte des BSH*, 43:1–171, 2008. URL http://www.bsh.de/de/Produkte/Buecher/Berichte_/Bericht43/Bericht43.pdf.

S.W.A. Naqvi, D.A. Jayakumar, P.V. Narvekar, H. Naik, V.V.S.S. Sarma, W. D'Souza, S. Joseph, and M.D. George. Increased marine production of N_2O due to intensifying

anoxia on the Indian continental shelf. *Nature*, 408(6810):346–349, 2000. doi: 10.1038/35042551.

NCAR. The Climate Data Guide: Hurrell North Atlantic Oscillation (NAO) Index (PC-based), 2016. URL https://climatedataguide.ucar.edu/climate-data/hurrell-north-atlantic-oscillation-nao-index-pc-based. Last modified: 16-08-2016. Last accessed: 25-12-2016.

T. Neumann. Towards a 3D-ecosystem model of the Baltic Sea. *Journal of Marine Systems*, 25:405–419, 2000. doi: 10.1016/S0924-7963(00)00030-0.

T. Neumann. The fate of river-borne nitrogen in the Baltic Sea–An example for the River Oder. *Estuarine, Coastal and Shelf Science*, 73(1):1–7, 2007. doi: 10.1016/j.ecss.2006.12.005.

T. Neumann. Climate-change effects on the Baltic Sea ecosystem: A model study. *Journal of Marine Systems*, 81(3):213–224, 2010. doi: 10.1016/j.jmarsys.2009.12.001.

Shane O'Boyle and Glenn Nolan. The influence of water column stratification on dissolved oxygen levels in coastal and shelf waters around Ireland. In *Biology and Environment: Proceedings of the Royal Irish Academy*, pages 195–209, 2010. doi: 10.3318/BIOE.2010.110.3.195.

K. O'Driscoll, B. Mayer, T. Ilyina, and T. Pohlmann. Modelling the cycling of persistent organic pollutants (POPs) in the North Sea system: fluxes, loading, seasonality, trends. *Journal of Marine Systems*, 111:69–82, 2013. doi: 10.1016/j.jmarsys.2012.09.011.

I. Orlanski. A simple boundary condition for unbounded hyperbolic flows. *Journal of Computational Physics*, 21(3):251–269, 1976. doi: 10.1016/0021-9991(76)90023-1.

OSPAR. *Convention for the Protection of the Marine Environment of the North-East Atlantic*. OSPAR Commission, London, 1992. URL http://www.ospar.org/site/assets/files/1290/ospar_convention_e_updated_text_in_2007_no_revs.pdf. Last accessed: 04-01-2017.

OSPAR. *Strategy to Combat Eutrophication, Reference number: 1998–18*. OSPAR Commission, London, 1999. URL http://www.bmub.bund.de/fileadmin/bmu-import/files/pdfs/allgemein/application/pdf/ospar_strategy3_eut.pdf. Last accessed: 23-01-2017.

OSPAR. *Quality Status Report 2000, Region II – Greater North Sea*. OSPAR Commission, London, 2000. URL http://qsr2010.ospar.org/media/assessments/QSR_2000_Region_II.pdf. Last accessed: 04-01-2017.

OSPAR. *OSPAR Integrated Report 2003 on the Eutrophication Status of the OSPAR Maritime Area Based Upon the First Application of the Comprehensive Procedure*. OSPAR Commission, London, 2003. ISBN 1-904426-25-5. URL http://www.ospar.org/documents?d=6962. Last accessed: 05-01-2017.

OSPAR. *Revised Common Procedure for the identification of the Eutrophication status of the OSPAR Maritime area*, volume 2005-3. OSPAR Commission, London, 2005.

OSPAR. *Results of the 2009 ICG-EMO Workshop on transboundary nutrient transport*, volume 540/2011. OSPAR Commission, London, 2010. ISBN 978-1-907390-81-4. HASEC 11/6/Info.1-E.

OSPAR. *Riverine Inputs and Direct Discharges to Convention Waters – Contracting Parties' RID 2009 Data Report*, volume 540/2011. OSPAR Commission, London, 2011. ISBN 978-1-907390-81-4. URL http://www.ospar.org/documents?d=7276. Last accessed: 29-11-2016.

OSPAR. *MSFD Advice Manual and Background document on Good environmental status – Descriptor 5: Eutrophication*. OSPAR Commission, London, 2012. URL http://www.ospar.org/documents?d=7288. Last accessed: 04-01-2017.

OSPAR. *Riverine Inputs and Direct Discharges to Convention Waters – Contracting Parties' RID 2011 Data Report*, volume 598/2013. OSPAR Commission, London, 2013a. ISBN 978-1-909159-31-0. URL http://www.ospar.org/ospar-data/p00598_rid_2011_data_report.pdf. Last accessed: 04-01-2017.

OSPAR. *Common Procedure for the identification of the Eutrophication status of the OSPAR Maritime area*, volume 2013-8. OSPAR Commission, London, 2013b. URL http://mcc.jrc.ec.europa.eu/documents/201606235331.pdf. Last accessed: 13-10-2016.

OSPAR. *Renewed terms of references for ICG-EMO on WFD reduction study*. OSPAR Commission, London, 2016. HASEC 16/8/7-E.

L. Otto, J.T.F. Zimmerman, G.K. Furnes, M. Mork, R. Saetre, and G. Becker. Review of the physical oceanography of the North Sea. *Netherlands Journal of Sea Research*, 26 (2-4):161–238, 1990. doi: 10.1016/0077-7579(90)90091-T.

J. Ozer. Model to model comparison of transports through North Sea transects, 2011. URL http://noos.bsh.de/download/working_group_reports/Comparison_of_transports_bm1.pdf. Last accessed: 04-11-2016.

H.W. Paerl. Coastal eutrophication and harmful algal blooms: Importance of atmospheric deposition and groundwater as "new" nitrogen and other nutrient sources. *Limnology and Oceanography*, 42(2):1154–1165, 1997. doi: 10.4319/lo.1997.42.5_part_2.1154.

H.W. Paerl. Assessing and managing nutrient-enhanced eutrophication in estuarine and coastal waters: Interactive effects of human and climatic perturbations. *Ecological Engineering*, 26(1):40–54, 2006. doi: 10.1016/j.ecoleng.2005.09.006.

H.W. Paerl. Controlling eutrophication along the freshwater–marine continuum: dual nutrient (N and P) reductions are essential. *Estuaries and Coasts*, 32(4):593–601, 2009. doi: 10.1007/s12237-009-9158-8.

S. Painting, J. Foden, R. Forster, J. van der Molen, J. Aldridge, M. Best, P. Jonas, D. Hydes, P. Walsham, L. Webster, M. Gubbins, M. Heath, E. McGovern, C. Vincent, R. Gowen, and S. O'Boyle. Impacts of climate change on nutrient enrichment. *Marine Climate Change Impacts Partnership: Science Review*, pages 219–235, 2013. doi: 10.14465/2013.arc23.219-235.

J. Pätsch and W. Kühn. Nitrogen and carbon cycling in the North Sea and exchange with the North Atlantic–A model study. Part I. Nitrogen budget and fluxes. *Continental Shelf Research*, 28(6):767–787, 2008. doi: 10.1016/j.csr.2007.12.013.

J. Pätsch, W. Kühn, A. Moll, and H. Lenhart. ECOHAM4 – User Guide "Ecosystem Model, Hamburg, Version 4", 2009. URL https://dx.doi.org/10.2312/zmk-2009_1.

J. Pätsch, H.-J. Lenhart, and M. Schütt. Daily Loads of Nutrients, Total Alkalinity, Dissolved Inorganic Carbon and Dissolved Organic Carbon of the European Continental Rivers for the Years 1977–2014, 2016. URL https://wiki.zmaw.de/ifm/ECOHAM/DATA_RIVER?action=AttachFile&do=view&target=RIVER_feb_2016.pdf. Last accessed: 28-09-2016.

J.C.H. Peeters and L. Peperzak. Nutrient limitation in the North Sea: A bioassay approach. *Netherlands Journal of Sea Research*, 26(1):61–73, 1990. doi: 10.1016/0077-7579(90)90056-M.

J.C.H. Peeters, F.J. Los, R. Jansen, H.A. Haas, L. Peperzak, and I. de Vries. The oxygen dynamics of the Oyster Ground, North Sea. Impact of eutrophication and environmental conditions. *Ophelia*, 42(1):257–288, 1995. doi: 10.1080/00785326.1995.10431508.

M.A. Peña, S. Katsev, T. Oguz, and D. Gilbert. Modeling dissolved oxygen dynamics and hypoxia. *Biogeosciences*, 7(3):933–957, 2010. doi: 10.5194/bg-7-933-2010.

L. Peperzak. Climate change and harmful algal blooms in the North Sea. *Acta Oecologica*, 24:S139–S144, 2003. doi: 10.1016/S1146-609X(03)00009-2.

T. Perrot, N. Rossi, A. Ménesguen, and F. Dumas. Modelling green macroalgal blooms on the coasts of Brittany, France to enhance water quality management. *Journal of Marine Systems*, 132:38–53, 2014. doi: 10.1016/j.jmarsys.2013.12.010.

A. Philipp, F. Kerl, and U. Müller. Ansprüche potenzieller Nutzer an ein Hochwasser-Frühwarnsystem für Sachsen. *Hydrologie und Wasserbewirtschaftung*, 1:4–22, 2015. doi: 10.5675/HyWa_2015,1_1. German only.

D.L. Phillips and J.W. Gregg. Source partitioning using stable isotopes: coping with too many sources. *Oecologia*, 136(2):261–269, 2003. doi: 10.1007/s00442-003-1218-3.

R.D. Pingree, P.M. Holligan, and G.T. Mardell. The effects of vertical stability on phytoplankton distributions in the summer on the northwest European Shelf. *Deep Sea Research*, 25(11):1011–1016, 1978. doi: 10.1016/0146-6291(78)90584-2.

J.G. Pinto, T. Brücher, A.H. Fink, and A. Krüger. Extraordinary snow accumulations over parts of central Europe during the winter of 2005/06 and weather-related hazards. *Weather*, 62(1):16–21, 2007. doi: 10.1002/wea.19.

T. Pohlmann. Untersuchung hydro- und thermodynamischer Prozesse in der Nordsee mit einem dreidimensionalen numerischem Modell. *Berichte aus dem Zentrum für Meeres- und Klimaforschung*, Reihe B(Nr. 23):116pp., 1991. Ph.D. thesis. German only.

T. Pohlmann. Predicting the thermocline in a circulation model of the North Sea - Part I: model description, calibration and verification. *Continental Shelf Research*, 16(2): 131–146, 1996. doi: 10.1016/0278-4343(95)90885-S.

T. Pohlmann. A meso-scale model of the central and southern North Sea: Consequences of an improved resolution. *Continental Shelf Research*, 26(19):2367–2385, 2006. doi: 10.1016/j.csr.2006.06.011.

L. Pokryfki and R.E. Randall. Nearshore hypoxia in the bottom water of the northwestern Gulf of Mexico from 1981 to 1984. *Marine Environmental Research*, 22(1):75–90, 1987. doi: 10.1016/0141-1136(87)90081-X.

H. Postma. Exchange of materials between the North Sea and the Wadden Sea. *Marine Geology*, 40(1):199–213, 1981. doi: 10.1016/0025-3227(81)90050-5.

J.M. Prospero, K. Barrett, T. Church, F. Dentener, R.A. Duce, J.N. Galloway, H. Levy Ii, J. Moody, and P. Quinn. Atmospheric deposition of nutrients to the North Atlantic Basin. *Biogeochemistry*, 35(1):27–73, 1996. doi: 10.1007/BF02179824.

B.Y. Queste, L. Fernand, T.D. Jickells, and K.J. Heywood. Spatial extent and historical context of North Sea oxygen depletion in August 2010. *Biogeochemistry*, 113(1):53–68, 2013. ISSN 1573-515X. doi: 10.1007/s10533-012-9729-9.

B.Y. Queste, L. Fernand, T.D. Jickells, K.J. Heywood, and A.J. Hind. Drivers of summer oxygen depletion in the central North Sea. *Biogeosciences*, 13(4):1209–1222, 2016. doi: 10.5194/bg-13-1209-2016.

A. Quigg, Z.V. Finkel, A.J. Irwin, Y. Rosenthal, T.-Y. Ho, J.R. Reinfelder, O. Schofield, F.M.M. Morel, and P.G. Falkowski. The evolutionary inheritance of elemental stoichiometry in marine phytoplankton. *Nature*, 425(6955):291–294, 2003. doi: 10.1038/nature01953.

N.N. Rabalais and R.E. Turner. *Hypoxia in the Northern Gulf of Mexico: Description, Causes and Change*, pages 1–36. Coastal and Estuarine Studies. American Geophysical Union, Washington, D.C., 2001. ISBN 978-1-118-66410-0. doi: 10.1029/CE058.

N.N. Rabalais, R.E. Turner, and D. Scavia. Beyond Science into Policy: Gulf of Mexico Hypoxia and the Mississippi River. *BioScience*, 52(2):129–142, 2002a. URL https://search.proquest.com/docview/216469517?accountid=104421. Last accessed: 17-01-2017.

N.N. Rabalais, R.J. Díaz, L.A. Levin, R.E. Turner, D. Gilbert, and J. Zhang. Dynamics and distribution of natural and human-caused hypoxia. *Biogeosciences*, 7(2):585–619, 2010. doi: 10.5194/bg-7-585-2010.

E Rachor and H Albrecht. Sauerstoffmangel im Bodenwasser der Deutschen Bucht. *Veröffflichungen des Instituts für Meeresforschung in Bremerhaven*, 19:209–227, 1983. doi: 10.2312/reports-ifm-bhv.1983.19.2.209. German only.

G. Radach and H.-J. Lenhart. Nutrient dynamics in the North Sea: fluxes and budgets in the water column derived from ERSEM. *Netherlands Journal of Sea Research*, 33(3):301–335, 1995. doi: 10.1016/0077-7579(95)90051-9.

H. Radtke. Einfluss biologischer Prozesse auf die Ausbreitungswege von Nährstoffen in der Ostsee, 2012. URL http://rosdok.uni-rostock.de/file/rosdok_disshab_0000000981/rosdok_derivate_0000005088/Dissertation_Radtke_2013.pdf. Ph.D. thesis. In German only. Last accessed: 16-09-2016.

H. Radtke and M. Maar. Estimating the effective nitrogen import: An example for the North Sea-Baltic Sea boundary. *Journal of Geophysical Research: Biogeosciences*, pages 1–14, 2016. ISSN 2169-8961. doi: 10.1002/2016JG003516.

H. Radtke, T. Neumann, M. Voss, and W. Fennel. Modeling pathways of riverine nitrogen and phosphorus in the Baltic Sea. *Journal of Geophysical Research: Oceans (1978–2012)*, 117(C9), 2012. doi: 10.1029/2012JC008119.

A.C. Redfield. *On the proportions of organic derivatives in sea water and their relation to the composition of plankton*. University Press of Liverpool, 1934. URL http://faculty.uml.edu/david_ryan/84.653/CourseMaterial/lecture15/Redfield1934.pdf. Last accessed: 17-01-2017.

P.C. Reid, C. Lancelot, W.W.C. Gieskes, E. Hagmeier, and G. Weichart. Phytoplankton of the North Sea and its dynamics: a review. *Netherlands Journal of Sea Research*, 26 (2-4):295–331, 1990. doi: 10.1016/0077-7579(90)90094-W.

T. Reinthaler, K. Bakker, R. Manuels, J. van Ooijen, and G.J. Herndl. Fully automated spectrophotometric approach to determine oxygen concentrations in seawater via continuous-flow analysis. *Limnology and Oceanography: Methods*, 4(10):358–366, 2006. ISSN 1541-5856. doi: 10.4319/lom.2006.4.358.

G.-Y. Rhee. Effects of N:P atomic ratios and nitrate limitation on algal growth, cell composition, and nitrate uptake. *Limnology and Oceanography*, 23(1):10–25, 1978. URL http://m.aslo.net/lo/toc/vol_23/issue_1/0010.pdf. Last accessed: 02-01-2017.

F.A. Richards. Anoxic basins and fjords. In J.P. Ripley and G. Skirrow, editors, *Chemical Oceanography*, volume 1, chapter 13, pages 611–643. Academic Press, New York, USA, 1965.

J. Rodhe. On the dynamics of the large-scale circulation of the Skagerrak. *Journal of Sea Research*, 35(1):9–21, 1996. doi: 10.1016/S1385-1101(96)90731-5.

L.P. Røed and I. Fossum. Mean and eddy motion in the Skagerrak/northern North Sea: insight from a numerical model. *Ocean Dynamics*, 54(2):197–220, 2004. doi: 10.1007/s10236-003-0076-1.

R. Rosenberg. Eutrophication – the future marine coastal nuisance? *Marine Pollution Bulletin*, 16(6):227–231, 1985. doi: 10.1016/0025-326X(85)90505-3.

R. Rosenberg, B. Hellman, and B. Johansson. Hypoxic tolerance of marine benthic fauna. *Marine Ecology Progress Series*, 79(1):127–131, 1991. URL http://www.int-res.com/articles/meps/79/m079p127.pdf. Last accessed: 09-01-2017.

L. Rovelli, M. Dengler, M. Schmidt, S. Sommer, P. Linke, and D.F. McGinnis. Thermocline mixing and vertical oxygen fluxes in the stratified central North Sea. *Biogeosciences*, 13 (5):1609–1620, 2016. doi: 10.5194/bg-13-1609-2016.

L. Rydberg, J. Haamer, and O. Liungman. Fluxes of water and nutrients within and into the Skagerrak. *Journal of Sea Research*, 35(1):23–38, 1996. doi: 10.1016/S1385-1101(96)90732-7.

J.H. Ryther and W.M. Dunstan. Nitrogen, phosphorus, and eutrophication in the coastal marine environment. *Science*, 171(3975):1008–1013, 1971. doi: 10.1126/science.171.3975.1008.

L.A. Salt, H. Thomas, A.E.F. Prowe, A.V. Borges, Y. Bozec, and H.J.W. de Baar. Variability of North Sea pH and CO_2 in response to North Atlantic Oscillation forcing. *Journal of Geophysical Research: Biogeosciences*, 118(4):1584–1592, 2013. ISSN 2169-8961. doi: 10.1002/2013JG002306.

E.W. Sanderson, M. Jaiteh, M.A. Levy, K.H. Redford, A.V. Wannebo, and G. Woolmer. The Human Footprint and the Last of the Wild: The human footprint is a global map of human influence on the land surface, which suggests that human beings are stewards of nature, whether we like it or not. 52(10):891–904, 2002. doi: 10.1641/0006-3568(2002)052[0891:THFATL]2.0.CO;2.

W. Schöpp, M. Posch, S. Mylona, and M. Johansson. Long-term development of acid deposition (1880–2030) in sensitive freshwater regions in Europe. *Hydrology and Earth System Sciences*, 7(4):436–446, 2003. doi: 10.5194/hess-7-436-2003.

B. Schuchardt and M. Schirmer. Seasonal and Spatial Patterns of the Diatom Actinocyclus Normanii in the Weser Estuary (NW-Germany) in Relation to Environmental Factors. In W. Michaelis, editor, *Estuarine Water Quality Management: Monitoring, Modelling and Research*, volume 36, pages 385–388. Springer, Berlin, Heidelberg, 1990. ISBN 978-3-642-75413-5. doi: 10.1007/978-3-642-75413-5_56.

S.P. Seitzinger and A.E. Giblin. Estimating denitrification in North Atlantic continental shelf sediments. *Biogeochemistry*, 35(1):235–260, 1996. doi: 10.1007/BF02179829.

A. Serna, J. Pätsch, K. Dähnke, M.G. Wiesner, H.C. Hass, M. Zeiler, D Hebbeln, and K.-C. Emeis. History of anthropogenic nitrogen input to the German Bight/SE North Sea as reflected by nitrogen isotopes in surface sediments, sediment cores and hindcast models. *Continental Shelf Research*, 30(15):1626–1638, 2010. doi: 10.1016/j.csr.2010.06.010.

J. Sharples, O.N. Ross, B.E. Scott, S.P.R. Greenstreet, and H. Fraser. Inter-annual variability in the timing of stratification and the spring bloom in the North-western North Sea. *Continental Shelf Research*, 26(6):733–751, 2006. ISSN 0278-4343. doi: 10.1016/j.csr.2006.01.011.

J. Sharples, J.F. Tweddle, J.A. Mattias Green, M.R. Palmer, Y.-N. Kim, A.E. Hickman, P.M. Holligan, C.M. Moore, T.P. Rippeth, J.H. Simpson, and V. Krivtsov. Spring-neap modulation of internal tide mixing and vertical nitrate fluxes at a shelf edge in summer. *Limnology and Oceanography*, 52(5):1735–1747, 2007. doi: 10.4319/lo.2007.52.5.1735.

J.H. Simpson and J.R. Hunter. Fronts in the Irish sea. *Nature*, 250:404–406, 1974. doi: 10.1038/250404a0.

M.D. Skogen and A. Moll. Interannual variability of the North Sea primary production: comparison from two model studies. *Continental Shelf Research*, 20(2):129–151, 2000. doi: 10.1016/S0278-4343(99)00069-2.

M.D. Skogen, E. Svendsen, J. Berntsen, D. Aksnes, and K.B. Ulvestad. Modelling the primary production in the North Sea using a coupled three-dimensional physical-chemical-biological ocean model. *Estuarine, Coastal and Shelf Science*, 41(5):545–565, 1995. doi: 10.1016/0272-7714(95)90026-8.

M.D. Skogen, E. Svendsen, and H. Søiland. Environmental status of the Skagerrak and North Sea 2000, 2002. URL http://www.imr.no/Dokumenter/Rapporter/Fisken_havet_3_2002.pdf. Last accessed: 17-01-2017.

M.D. Skogen, H. Søiland, and E. Svendsen. Effects of changing nutrient loads to the North Sea. *Journal of Marine Systems*, 46(1):23–38, 2004. ISSN 0924-7963. doi: 10.1016/j.jmarsys.2003.11.013.

J.A. Smith, P.E. Damm, M.D. Skogen, R.A. Flather, and J. PÄtsch. An investigation into the variability of circulation and transport on the North-West European shelf using three hydrodynamic models. *Ocean Dynamics*, 48(3):325–348, 1996. doi: 10.1007/BF02799377.

S.V. Smith. Phosphorus versus nitrogen limitation in the marine environment. *Limnology and Oceanography*, 29(6):1149–1160, 1984. doi: 10.4319/lo.1984.29.6.1149.

L.J. Spokes and T.D. Jickells. Is the atmosphere really an important source of reactive nitrogen to coastal waters? *Continental Shelf Research*, 25(16):2022–2035, 2005. doi: 10.1016/j.csr.2005.07.004.

J.H. Steele. Plant production on the Fladen Ground. *Journal of the Marine Biological Association of the United Kingdom*, 35(1):1–33, 1956. doi: 10.1017/S0025315400008948.

J.H. Steele. Environmental control of photosynthesis in the sea. *Limnology and Oceanography*, 7(2):137–150, 1962. doi: 10.4319/lo.1962.7.2.0137.

R.W. Sterner and J.J. Elser. *Ecological Stoichiometry: The Biology of Elements from Molecules to the Biosphere*. Princeton University Press, 2002. ISBN 978-0-691074-91-7.

A. Stigebrandt and B.G. Gustafsson. Response of the Baltic Sea to climate change – theory and observations. *Journal of Sea Research*, 49(4):243–256, 2003. doi: 10.1016/S1385-1101(03)00021-2.

H. Stommel. The westward intensification of wind-driven ocean currents. *Eos, Transactions American Geophysical Union*, 29(2):202–206, 1948. doi: 10.1029/TR029i002p00202.

L. Stramma, G.C. Johnson, J. Sprintall, and V. Mohrholz. Expanding oxygen-minimum zones in the tropical oceans. *Science*, 320(5876):655–658, 2008. doi: 10.1126/science.1153847.

L. Stramma, S. Schmidtko, L.A. Levin, and G.C. Johnson. Ocean oxygen minima expansions and their biological impacts. *Deep Sea Research Part I: Oceanographic Research Papers*, 57(4):587–595, 2010. doi: 10.1016/j.dsr.2010.01.005.

K.E. Taylor. Summarizing multiple aspects of model performance in a single diagram. *Journal of Geophysical Research: Atmospheres*, 106(D7):7183–7192, 2001. ISSN 2156-2202. doi: 10.1029/2000JD900719.

H. Thomas and A. Borges. Carbon Dioxide, Hydrographic, and Chemical Data Obtained During the R/V Pelagia Cruise 64PE239 in the North Sea (17 August–6 September, 2005), 2012. URL http://cdiac.ornl.gov/ftp/oceans/North_Sea/Pelagia_2005/.

H. Thomas, Y. Bozec, K. Elkalay, H.J.W. de Baar, A.V. Borges, and L.-S. Schiettecatte. Controls of the surface water partial pressure of CO_2 in the North Sea. *Biogeosciences*, 2(4):323–334, 2005. doi: 10.5194/bg-2-323-2005.

H. Thomas, A. Borges, J. Derksen, and K. Bakker. Carbon Dioxide, Hydrographic, and Chemical Data Obtained During the R/V Pelagia CANOBA Cruises in the North Sea (2001–2002), 2012. URL http://cdiac.ornl.gov/ftp/oceans/North_Sea/Pelagia_CANOBA/.

M.L. Thompson and L.C. Schaffner. Population biology and secondary production of the suspension feeding polychaete Chaetopterus cf. variopedatus: Implications for benthic-pelagic coupling in lower Chesapeake Bay. *Limnology and Oceanography*, 46(8):1899–1907, 2001. doi: 10.4319/lo.2001.46.8.1899.

K. Timmermann, S. Markager, and K.E. Gustafsson. Streams or open sea? Tracing sources and effects of nutrient loadings in a shallow estuary with a 3D hydrodynamic–ecological model. *Journal of Marine Systems*, 82(3):111–121, 2010. doi: 10.1016/j.jmarsys.2010.04.008.

D. Topcu, U. Brockmann, and U. Claussen. Relationship between eutrophication reference conditions and boundary settings considering OSPAR recommendations and the Water Framework Directive – examples from the German Bight. *Hydrobiologia*, 629(1):91–106, 2009. doi: 10.1007/s10750-009-9778-9.

H.D. Topcu and U.H. Brockmann. Seasonal oxygen depletion in the North Sea, a review. *Marine Pollution Bulletin*, 99(1):5–27, 2015. doi: 10.1016/j.marpolbul.2015.06.021.

P. Tréguer, D.M. Nelson, A.J. van Bennekom, D.J. DeMaster, A. Leynaert, and B. Queguiner. The silica balance in the world ocean: a reestimate. *Science*, 268(5209):375, 1995. URL http://www.academia.edu/download/39100471/09e415005626a88209000000.pdf. Last accessed: 02-01-2017.

T.A. Troost, M. Blaas, and F.J. Los. The role of atmospheric deposition in the eutrophication of the North Sea: a model analysis. *Journal of Marine Systems*, 125:101–112, 2013. doi: 10.1016/j.jmarsys.2012.10.005.

T.A. Troost, A. de Kluijver, and F.J. Los. Evaluation of eutrophication variables and thresholds in the Dutch North Sea in a historical context – a model analysis. *Journal of Marine Systems*, 134:45–56, 2014. doi: 10.1016/j.jmarsys.2014.01.015.

R.E. Turner, N.N. Rabalais, and D. Justić. Gulf of Mexico hypoxia: Alternate states and a legacy. *Environmental Science & Technology*, 42(7):2323–2327, 2008. doi: 10.1021/es071617k.

W.R. Turrell, E.W. Henderson, G. Slesser, R. Payne, and R.D. Adams. Seasonal changes in the circulation of the northern North Sea. *Continental Shelf Research*, 12(2-3):257–286, 1992. doi: 10.1016/0278-4343(92)90032-F.

T. Tyrrell. The relative influences of nitrogen and phosphorus on oceanic primary production. *Nature*, 400(6744):525–531, 1999. doi: 10.1038/22941.

R.V. Tyson and T.H. Pearson. Modern and ancient continental shelf anoxia: an overview. *Geological Society of London Special Publications*, 58(1):1–24, 1991. doi: 10.1144/GSL.SP.1991.058.01.01.

U. Ulbrich and M. Christoph. A shift of the NAO and increasing storm track activity over Europe due to anthropogenic greenhouse gas forcing. *Climate dynamics*, 15(7):551–559, 1999. doi: 10.1007/s003820050299.

U. Ulbrich, T. Brücher, A.H. Fink, G.C. Leckebusch, A. Krüger, and J.G. Pinto. The central European floods of August 2002: Part 1 – Rainfall periods and flood development. *Weather*, 58(10):371–377, 2003. doi: 10.1256/wea.61.03A.

UNESC. Protocol to the 1979 Convention on Long-range Transboundary Air Pollution to Abate Acidification, Eutrophication and Ground-level Ozone, 1999. URL https://treaties.un.org/doc/Publication/UNTS/Volume2319/v2319.pdf. Last accessed: 09-01-2017.

Unidata. Network Common Data Form (NetCDF), 2016. URL http://www.unidata.ucar.edu/software/netcdf/. Last accessed: 20-07-2016.

A.C. Upton, D.B. Nedwell, R.J. Parkes, and S.M. Harvey. Seasonal benthic microbial activity in the southern North Sea; oxygen uptake and sulphate reduction. *Marine Ecology Progress Series*, 101:273–281, 1993. doi: 10.3354/meps101273.

H.M. van Aken, G.J.F. van Heijst, and L.R.M. Maas. Observations of fronts in the North Sea. *Journal of Marine Research*, 45(3):579–600, 1987. doi: 10.1357/002224087788326830.

J.E.E. van Beusekom and V.N. de Jonge. Retention of phosphorus and nitrogen in the Ems estuary. *Estuaries*, 21(4):527–539, 1998. doi: 10.2307/1353292.

J.E.E. van Beusekom, U.H. Brockmann, K.-J. Hesse, W. Hickel, K. Poremba, and U. Tillmann. The importance of sediments in the transformation and turnover of nutrients and organic matter in the Wadden Sea and German Bight. *Deutsche Hydrografische Zeitschrift*, 51(2-3):245–266, 1999. doi: 10.1007/BF02764176.

J. van der Molen, J.N. Aldridge, C. Coughlan, E.R. Parker, D. Stephens, and P. Ruardij. Modelling marine ecosystem response to climate change and trawling in the North Sea. *Biogeochemistry*, 113(1-3):213–236, 2013. doi: 10.1007/s10533-012-9763-7.

H. van Haren, D.K. Mills, and L.P.M.J. Wetsteyn. Detailed observations of the phytoplankton spring bloom in the stratifying central North Sea. *Journal of Marine Research*, 56(3):655–680, 1998. doi: 10.1357/002224098765213621.

S. van Leeuwen, P. Tett, D. Mills, and J. van der Molen. Stratified and nonstratified areas in the north sea: Long-term variability and biological and policy implications. *Journal of Geophysical Research: Oceans*, 120(7):4670–4686, 2015. ISSN 2169-9291. doi: 10.1002/2014JC010485.

S.M. van Leeuwen, J. van der Molen, P. Ruardij, L. Fernand, and T. Jickells. Modelling the contribution of deep chlorophyll maxima to annual primary production in the North Sea. *Biogeochemistry*, 113(1-3):137–152, 2013. doi: 10.1007/s10533-012-9704-5.

W. van Raaphorst and H.W. van der Veer. The phosphorus budget of the Marsdiep tidal basin (Dutch Wadden Sea) in the period 1950–1985: importance of the exchange with the North Sea. *Hydrobiologia*, 195(1):21–38, 1990. doi: 10.1007/BF00026811.

R. Vaquer-Sunyer and C.M. Duarte. Thresholds of hypoxia for marine biodiversity. *Proceedings of the National Academy of Sciences*, 105(40):15452–15457, 2008. doi: 10.1073/pnas.0803833105.

H. von Westernhagen and V. Dethlefsen. North Sea Oxygen Deficiency 1982 and Its Effects on the Bottom Fauna. *Ambio*, 12(5):264–266, 1983. URL http://www.jstor.org/stable/4312934. Last accessed: 04-01-2017.

S.L. Wakelin, Y. Artioli, M. Butenschön, J.I. Allen, and J.T. Holt. Modelling the combined impacts of climate change and direct anthropogenic drivers on the ecosystem of the northwest European continental shelf. *Journal of Marine Systems*, 152:51–63, 2015. doi: 10.1016/j.jmarsys.2015.07.006.

R. Wanninkhof. Relationship between wind speed and gas exchange over the ocean. *Journal of Geophysical Research: Oceans*, 97(C5):7373–7382, 1992. doi: 10.1029/92JC00188.

K. Weston, L. Fernand, D. K. Mills, R. Delahunty, and J. Brown. Primary production in the deep chlorophyll maximum of the central North Sea. *Journal of Plankton Research*, 27(9):909–922, 2005. doi: 10.1093/plankt/fbi064.

K. Weston, L. Fernand, J. Nicholls, A. Marca-Bell, D. Mills, D. Sivyer, and M. Trimmer. Sedimentary and water column processes in the Oyster Grounds: a potentially hypoxic region of the North Sea. *Marine Environmental Research*, 65(3):235–249, 2008. doi: 10.1016/j.marenvres.2007.11.002.

J. Wijsman, H. Los, and J. van Beek. The filtering capacity of an estuary for nutrients. *WL/Delft Hydraulics Reports*, Z2836:51pp., 2004.

K.H. Wiltshire, A. Malzahn, W. Greve, K. Wirtz, S. Janisch, P. Mangelsdorf, B.F.J. Manly, and M. Boersma. Resilience of North Sea phytoplankton spring blooms dynamics: an analysis of long term data at Helgoland Roads. *Limnology and Oceanography*, 53:1294–1302, 2008. doi: 10.4319/lo.2008.53.4.1294.

N.G. Winther and J.A. Johannessen. North Sea circulation: Atlantic inflow and its destination. *Journal of Geophysical Research: Oceans*, 111(C12), 2006. doi: 10.1029/2005JC003310.

H. Wirth and M.G. Wiesner. Sedimentary facies in the North Sea. *Mitteilungen des Geologisch-paläontologischen Instituts der Universität Hamburg*, 65:269–287, 1988.

K. Woth, R. Weisse, and H. von Storch. Climate change and North Sea storm surge extremes: an ensemble study of storm surge extremes expected in a changed climate projected by four different regional climate models. *Ocean Dynamics*, 56(1):3–15, 2006. doi: 10.1007/s10236-005-0024-3.

H. Zemmelink. Cruise Report of the cruise 64PE294, Texel, NL – Texel, NL, 19.08.2008–11.09.2008, 2008. URL http://melia.nioz.nl/public/dmg/rpt/crs/64pe294.pdf. Last accessed: 26 April 2016.

L. Zillén, D.J. Conley, T. Andrén, E. Andrén, and S. Björck. Past occurrences of hypoxia in the Baltic Sea and the role of climate variability, environmental change and human impact. *Earth-Science Reviews*, 91(1):77–92, 2008. doi: 10.1016/j.earscirev.2008.10.001.

A.R. Zimmerman and E.A. Canuel. Sediment geochemical records of eutrophication in the mesohaline Chesapeake Bay. *Limnology and Oceanography*, 47(4):1084–1093, 2002. doi: 10.4319/lo.2002.47.4.1084.

List of Figures

List of Tables

List of Abbreviations

General abbreviations

1D/3D	one-dimensional/three-dimensional
AAAS	American Association for the Advancement of Science
BED	Baltic Environmental Database
BNI	Baltic Nest Institute
BSH	Bundesamt für Seeschifffahrt und Hydrographie (English: Federal Maritime Agency)
Cefas	Centre of Environment, Fisheries and Aquaculture Science
CMEMS	Copernicus Marine Environment Monitoring Service
COR	correlation coefficient
CTD	sensor for conductivity, temperature and depth measurement
Delft3D-GEM	Delft Three-Dimensional Generic Ecological Model
DMU	Danmarks Miljøundersøgelser (English: National Environmental Research Institute of Denmark)
ECOHAM	Ecosystem Model, Hamburg
EMEP	European Monitoring and Evaluation Programme
EU	European Union
EUTRISK	eutrophication risk index
HAMSOM	Hamburg Shelf Ocean Model
ICNS-2	2nd International Conference on the Protection of the North Sea
MARNET	Marine Monitoring Network
MSFD	Marine Strategy Framework Directive (of the European Union)
MUDAB	Meeresumweltdatenbank (English: Marine Environment Data Base)
NAW	North Atlantic water
NIOZ	Koninklijk Nederlands Instituut voor Onderzoek der Zee (English: Royal Netherlands Institute for Sea Research)
NOOS	North West Shelf Operational Oceanographic System
NPZD	nutrients-phytoplankton-zooplankton-detritus
NRFA	National River Flow Archive
OSPAR	Oslo-Paris (Convention for the Protection of the Marine Environment of the North-East Atlantic)
PSS-78	practical salinity scale from 1978
RMSD	root-mean-square difference
ROFI	region of freshwater influence
R/V	research vessel
STD	standard deviation
TBNT	trans-boundary nutrient transports
UBA	Umweltbundesamt (English: German Federal Environment Agency)
WFD	Water Framework Directive (of the European Union)

Abbreviations related to biochemical and physical processes and quantities

$\mathbf{ADH_{org,sml\text{-}in/\text{-}out}}$	horizontal advection of organic matter into/out of the surface mixed layer
$\mathbf{ADH_{org,sub\text{-}in/\text{-}out}}$	horizontal advection of organic matter into/out of the volume below the mixed layer depth
$\mathbf{ADV_{O_2}}$	(sum of horizontal and vertical) advection) of oxygen
$\mathbf{ASF_{O_2}}$	air-sea flux of oxygen
Chl-a	chlorophyll-a
BML	bottom mixed layer
$\boldsymbol{D_{bot}}$	bottom depth
DIC/**DIN**	dissolved inorganic carbon/nitrogen
DOC/**DON**/**DOP**	dissolved organic carbon/nitrogen/phosphorus
$\mathbf{EXP_{org}}$	turbulent vertical export of organic matter into the volume below the mixed layer depth
GOC	gross oxygen consumption
$\mathbf{MIX_{O_2}}$	vertical mixing of oxygen into the the volume below the mixed layer depth
MLD	mixed layer depth
NIT	nitrification
NOC	net oxygen consumption
NPP	net primary production
$\mathbf{NPP_{sml}}$/$\mathbf{NPP_{sub}}$	net primary production in the surface mixed layer/the volume below the mixed layer depth
$\mathbf{O_{2,ini}}$/$\mathbf{O_{2,end}}$	oxygen concentration on 1 April/30 September
ODI	oxygen deficiency index
ODZ	oxygen deficiency zone
OMZ	oxygen minimum zone
POC/**PON**/**POP**	particulate organic carbon/nitrogen/phosphorus
PP	primary production
$\mathbf{REM_{pel}}$/$\mathbf{REM_{sed}}$	pelagic/benthic remineralisation
$\mathbf{RES_{zoo}}$	zooplankton respiration
SPOC	sedimented particulate organic carbon
SML	surface mixed layer
SPM	suspended particulate matter
SSS/**SST**	sea surface salinity/temperature
$\boldsymbol{t_{strat}}$	stratification period
TN/**TP**	total nitrogen/phosphorus
$\boldsymbol{V_{sub}}$	volume below the mixed layer depth
$\boldsymbol{V_{sub,var}}$/ $\boldsymbol{V_{sub,fix}}$	volume below time-varying/fixed mixed layer depth

Contributions to the published manuscript

Parts of the methods applied in this thesis were recently published in a peer-reviewed journal:

Große, F., Greenwood, N., Kreus, M., Lenhart, H.-J., Machoczek, D., Pätsch, J., Salt, L., and Thomas, H.: Looking beyond stratification: a model-based analysis of the biological drivers of oxygen deficiency in the North Sea, Biogeosciences, 13, 2511-2535, doi:10.5194/bg-13-2511-2016, 2016.

More specifically, this applies to the algorithm used for the determination of the stratification-related parameters (Sect. 4.3.1) and the analysis methods used in Sect. 5.2 (and sub-sections). These methods were developed by me, in cooperation with Hermann-Josef Lenhart, co-author of the above mentioned manuscript and co-supervisor of this thesis. The technical implementation and execution of the analyses was done by myself. The results obtained from these methods and presented in this thesis differ slightly from the results published as a revised model setup was used.

Furthermore, some text passages of the above mentioned manuscript are used in this thesis (and adapted, if necessary). Most of the manuscript was written by myself. Contributions to the Introduction and Conclusions were provided by Hermann-Josef Lenhart. The following co-authors contributed to the technical description of the observation data: Naomi Greenwood, Detlev Machoczek, Lesley A. Salt and Helmuth Thomas. A technical description of the atmospheric and open boundary conditions was provided by Markus Kreus. Johannes Pätsch contributed to the model description.

All co-author contributions were reviewed (and revised, if necessary) by myself before submitting the original manuscript (and its revised versions) to the journal.

Software overview

The TBNT software developed during this thesis was programmed in Fortran. All post-processing, analysis and visualisation of output from the HAMSOM and ECOHAM models, the TBNT software and observation data was conducted with MATLAB®. The GNU Image Manipulation Program was used adapting Fig. 1.2 and Fig. 2.2. The word processing was done with LaTeX.

Acknowledgements

I am grateful to Dr. habil. Thomas Pohlmann for supervising and reviewing this thesis. In particular, I would like to thank him for keeping me aligned and focused on the scientific questions of this study.

Special thanks go to my co-supervisor Dr. Hermann-Josef Lenhart for his guidance and support, but also his confidence in my work. I learned a lot during these past years, and much of this is owed to him. He enabled my stay in the Netherlands and introduced me to many people in the ecosystem modelling community. He also always ensured my funding – which often was not easy. Besides this, you always had an open ear for my concerns and questions – personal and professional ones – and I appreciated our open communication. All in all, I can only say: Thank you very much for all this, Hermann!

I would like to thank Prof. Dr. Myron Peck for reviewing this thesis.

Many thanks go to the institutions and people who provided me with resources used in this work. Without their willingness for sharing, this work would not have been possible. These thanks go to: Dr. Naomi Greenwood (Cefas) for the time series data of North Dogger and Oyster Grounds; Dr. Detlev Machoczek (BSH) for the time series data of MARNET Ems; Prof. Dr. Helmuth Thomas (Department of Oceanography, Dalhousie University) for the O_2 survey data; Monika Schütt, Dr. Dilek Topcu and Dr. Uwe Brockmann (all Institute for Geology, Universität Hamburg) for their collection of biochemical North Sea data and for allowing the use of Fig. 1.2; Rita Kramer and Dr. Sieglinde Weigelt-Krenz (both BSH) for bottom O_2 maps used for updating Fig. 1.2; Sonja van Leeuwen (Cefas) for the river forcing data and for allowing the use of Fig. 2.2; Dr. Anne Che-Bohnenstengel, Dr. Khosro Motamedi, Dr. Friedrich Nast and Frank Oestereich (all BSH) for providing biochemical data from the MUDAB data base (now 'Deutsches Ozeanographisches Datenzentrum'); the AAAS and the OSPAR Secretariat for allowing the use of Fig. 1.1 and Fig. 2.1, respectively; CMEMS for access to the ScanFish data; Deutsches Klimarechenzentrum for compute time on its main frame HLRE-3 'Mistral'.

I thank the German Federal Environment Agency (UBA; projects: UFO-12, -13 and -16) and the German Academic Exchange Service for funding this work.

I would like to thank my colleagues Markus Kreus and Dr. Johannes Pätsch. They taught me a lot about the various aspects of modelling and its constraints, and contributed substantially to the conception of the TBNT software. I really enjoyed the teamwork in our small ECOHAM family – colleagues like you make working life much easier!

I am also grateful to my '7-months colleagues' at Deltares in the Netherlands, particularly, Dr. Tineke Troost and Dr. Hans Los. First, simply for enabling my stay at Deltares.

Second, for being very supportive in any sense and critical about the post-processing concept of TBNT. Hartelijk bedankt voor de erg leuke tijd in Nederland!

I thank Annika Grage, Dr. Wera Leujak and Dr. Onur Kerimoglu for the interesting and fruitful cooperation crossing the science-policy interface.

Further thanks to my colleagues at Scientific Computing. I really enjoyed the time with you and got valuable insights in the world of high performance computing. Cheers to you!

Many thanks to Julia Köhler for proof-reading this thesis. Especially, since it helped to shorten the original version at least a little bit. My reviewers can be thankful to you.

What shall I say about my friends here in Hamburg? Thank you all for your open ears in any situation of life, for joint brunches, dinners, drinks, board game parties, nights on the town, concerts, holidays and great/serious/amusing/honest conversations – just for being there. Special thanks to my dearest 'Deers' – the 'majupper' of the past few years – only deer love is peer love! Thank you, Marc, for weekly squash (yes, the sports) sessions. Simon, some extra thanks to you for being a great flatmate and friend for years. And Mathias, thank you for providing me a roof over my head for the last couple of months – I appreciate that a lot, and really enjoy(ed) this time.

Julia, my Italian is a bit rusty ... therefore, I am tempted to re-use the same dedication as for my last thesis – I hope you can live with that. You know it is still wholehearted:
Ti ringrazio per gli anni ad Amburgo e per le molte serate con la nostra musica preferita: Ho avuto dubbi sui dettagli, ma mai sul dono grande. Grazie mille per un'amicizia grandiosa, in quanto non potrebbe essere più semplice. E la cosa più importante: è molto bello sapere che anche gli altri non possono leggere tra le righe – non siamo soli!
And if I may add some non-Italian words: thank you for the (non-)scientific discussions during lunch time, in bars over a beer, wine or basil smash – it was always a great help to share experiences with you, especially, as you were at a similar stage of professional life. Last but not least, thank you for making me the (unbaptised) godfather of Emil!

Abschließend möchte ich meinen Eltern und meiner Schwester Juliane aus tiefstem Herzen danken. Eure immerwährende, (quasi) bedingungslose Unterstützung und Euer Vertrauen in das, was ich tue, war und ist seit jeher die Basis für das, was aus mir geworden ist. Zudem gebt Ihr mir immer wieder die Gewissheit, dass dieses ‚was' wohl auch ganz in Ordnung ist. Weiterhin danke ich Euch sehr dafür, dass ihr in allen Lebenslagen für mich da seid. Ich bin mir nicht sicher, ob diese Dissertation (und der Weg dahin) ohne Euch überhaupt möglich gewesen wäre – wahrscheinlich nicht –, aber Ihr habt es mir in jedem Falle erheblich erleichtert. Auch wenn am Ende ich diese Seiten zu Papier gebracht habe – einen großen Teil davon verdanke ich Euch. Vielen, vielen Dank für alles!

Statutory declaration

I hereby declare, on oath, that I have developed and written the enclosed dissertation completely by myself, and have not used sources or means without declaration in the text. Any thoughts from others or literal quotations are clearly marked. This dissertation was not used in the same or in a similar version to achieve an academic grading or is being published elsewhere.

Hamburg, 25 January, 2017

Fabian Große